frontiers | Research Topics

Microbial involvement in biogeochemical cycling and contaminant transformations at land-water ecotones

Edited by
Yizhi Sheng, Xiangfeng Zeng, Linduo Zhao and Yongbin Li

Coordinated by
Min Zhang

Published in
Frontiers in Microbiology

ISSN 1664-8714
ISBN 978-2-8325-5794-5
DOI 10.3389/978-2-8325-5794-5

About Frontiers

Frontiers is more than just an open access publisher of scholarly articles: it is a pioneering approach to the world of academia, radically improving the way scholarly research is managed. The grand vision of Frontiers is a world where all people have an equal opportunity to seek, share and generate knowledge. Frontiers provides immediate and permanent online open access to all its publications, but this alone is not enough to realize our grand goals.

Frontiers journal series

The Frontiers journal series is a multi-tier and interdisciplinary set of open-access, online journals, promising a paradigm shift from the current review, selection and dissemination processes in academic publishing. All Frontiers journals are driven by researchers for researchers; therefore, they constitute a service to the scholarly community. At the same time, the *Frontiers journal series* operates on a revolutionary invention, the tiered publishing system, initially addressing specific communities of scholars, and gradually climbing up to broader public understanding, thus serving the interests of the lay society, too.

Dedication to quality

Each Frontiers article is a landmark of the highest quality, thanks to genuinely collaborative interactions between authors and review editors, who include some of the world's best academicians. Research must be certified by peers before entering a stream of knowledge that may eventually reach the public - and shape society; therefore, Frontiers only applies the most rigorous and unbiased reviews. Frontiers revolutionizes research publishing by freely delivering the most outstanding research, evaluated with no bias from both the academic and social point of view. By applying the most advanced information technologies, Frontiers is catapulting scholarly publishing into a new generation.

What are Frontiers Research Topics?

Frontiers Research Topics are very popular trademarks of the *Frontiers journals series*: they are collections of at least ten articles, all centered on a particular subject. With their unique mix of varied contributions from Original Research to Review Articles, Frontiers Research Topics unify the most influential researchers, the latest key findings and historical advances in a hot research area.

Find out more on how to host your own Frontiers Research Topic or contribute to one as an author by contacting the Frontiers editorial office: frontiersin.org/about/contact

Microbial involvement in biogeochemical cycling and contaminant transformations at land-water ecotones

Topic editors

Yizhi Sheng — China University of Geosciences, China

Xiangfeng Zeng — Institute of Applied Ecology, Chinese Academy of Sciences (CAS), China

Linduo Zhao — Illinois Sustainable Technology Center. University of Illinois at Urbana-Champaign, United States

Yongbin Li — Dalian University of Technology, China

Topic coordinator

Min Zhang — Institute of Hydrogeology and Environmental Geology, Chinese Academy of Geological Sciences, China

Citation

Sheng, Y., Zeng, X., Zhao, L., Li, Y., Zhang, M., eds. (2024). *Microbial involvement in biogeochemical cycling and contaminant transformations at land-water ecotones*. Lausanne: Frontiers Media SA. doi: 10.3389/978-2-8325-5794-5

Table of contents

frontiers | Frontiers in Microbiology

TYPE Editorial
PUBLISHED 05 December 2024
DOI 10.3389/fmicb.2024.1525521

OPEN ACCESS

EDITED AND REVIEWED BY
David Emerson,
Bigelow Laboratory for Ocean Sciences,
United States

*CORRESPONDENCE
Yizhi Sheng
✉ shengyz@cugb.edu.cn
Xiangfeng Zeng
✉ zengxf@iae.ac.cn

RECEIVED 09 November 2024
ACCEPTED 21 November 2024
PUBLISHED 05 December 2024

CITATION
Sheng Y, Zeng X, Zhao L and Li Y (2024) Editorial: Microbial involvement in biogeochemical cycling and contaminant transformations at land-water ecotones. *Front. Microbiol.* 15:1525521. doi: 10.3389/fmicb.2024.1525521

Editorial: Microbial involvement in biogeochemical cycling and contaminant transformations at land-water ecotones

Yizhi Sheng[1]*, Xiangfeng Zeng[2]*, Linduo Zhao[3] and Yongbin Li[4]

[1]Center for Geomicrobiology and Biogeochemistry Research, State Key Laboratory of Biogeology and Environmental Geology, China University of Geosciences, Beijing, China, [2]Key Laboratory of Pollution Ecology and Environmental Engineering, Institute of Applied Ecology, Chinese Academy of Sciences, Shenyang, Liaoning, China, [3]Prairie Research Institute-Illinois Sustainable Technology Centre/Illinois State Water Survey, University of Illinois at Urbana Champaign, Champaign, IL, United States, [4]Key Laboratory of Industrial Ecology and Environmental Engineering (Ministry of Education), School of Environmental Science and Technology, Dalian University of Technology, Dalian, China

KEYWORDS

microbial biogeochemistry, microbial ecology, contaminant transformation, land-water ecotones, bioremediation

Editorial on the Research Topic
Microbial involvement in biogeochemical cycling and contaminant transformations at land-water ecotones

Microorganisms, including bacteria, archaea, and fungi, play pivotal roles in facilitating energy and matter exchange, promoting mineral weathering, cycling nutrients, and transforming contaminants (Shi et al., 2016; Dong et al., 2022). Land-water ecotones, such as coastal areas, wetlands, riverine zones, and aquifer recharge regions, are characterized by intensive mass and energy exchanges, dynamic redox processes and varying geochemical conditions. These environments serve as critical transitional zones that support complex biogeochemical interactions between terrestrial and aquatic ecosystems. For instance, the complex interactions between organic matter and iron-bearing minerals at redox interfaces across diverse environments can either enhance or inhibit microbial and extracellular enzyme activity, thereby controlling the carbon budget in those transition zones (Dong et al., 2023; Sheng et al., 2022). In wetland transition zones between groundwater and lakes, processes such as dissimilatory nitrate reduction to ammonia are enriched, exhibiting seasonal variations in microbial activity (Chen et al., 2024). In the continental shelf sediments of China, denitrification is the primary pathway for dinitrogen gas production, followed by anaerobic ammonium oxidation (anammox; Sun et al., 2021). In tropical oceans, biological nitrogen fixation is limited by iron-to-nitrogen ratios, with iron primarily sourced from land and mineral dust deposition (Wen et al., 2022). To counteract metal nutrient limitations, microorganisms have evolved strategies such as producing siderophores to acquire essential metals (e.g., Fe, Mo) from minerals for their growth (Sheng et al., 2023a; Zhou et al., 2024). Understanding how microbial communities and biogeochemical processes respond to both natural variations and human-induced disturbances in these environments is crucial.

The 10 published articles in this Research Topic provide valuable insights into two main themes: (1) microbial community distribution responses to environmental variations, and (2) the impacts of anthropogenic activities on microbial processes, along with potential bioremediation and sustainable development strategies.

The assembly of microbial communities demonstrates remarkable adaptability to fluctuating environmental conditions, including changes in temperature, pH, salinity, oxygen levels, nutrient availability, moisture, hydrodynamic disturbances, and contaminant stress (Sheng et al., 2016; Ruff et al., 2023; Chen et al., 2022; Shu and Huang, 2022). Liu et al. investigated bacterial community dynamics in oligosaline lakes, revealing that temporal succession was the primary driver of community assembly, with temperature, pH, and nitrate significantly influencing microbial structure and function across seasons. Shi et al. explored the effects of environmental gradients on microbial diversity and co-occurrence networks at various depths in Hulun lake, providing insights into nitrogen-cycling taxa and their habitat-specific adaptations in grassland lakes. Xian et al. highlighted the significant impact of water masses, identifiable body of water with a common formation history which has physical properties distinct from surrounding water, on the bacterial composition, topological characteristics and assembly process in the Yangtze River Estuary. These findings offer a theoretical foundation for predicting alterations in microbial communities within estuarine ecosystems under the influence of water masses. Brooks and Field studied responses of microbial communities in freshwater iron mats to hydrocarbon exposure and found that hydrocarbon pollution affects diversity, community structure, and resilience in contaminated ecotones. Guo et al. examined the effects of mining-induced soil fissures on microbial communities, showing that varying fissure conditions impacted soil moisture, pH, and nutrient availability, with rare species playing critical roles in maintaining microbial network stability.

Nutrient and contaminant transformation through microbial degradation, redox reactions, and related processes can either intensify or mitigate their ecological effects. As mobile contaminants cross ecosystem boundaries, the role of microbial communities in detoxification and stabilization becomes crucial for sustaining ecological balance (Sheng et al., 2023b). Li et al. examined the hydrocarbon degradation capabilities of a facultative anaerobic bacterium *Shewanella putrefaciens* CN32 under both aerobic (using O_2 as an electron acceptor) and anaerobic [using Fe (III) as an electron acceptor] conditions, emphasizing its potential for bioremediation in fluctuating redox environments. Zhan et al. identified the zinc resilience of *Chlamydomonas* sp. 1710, with the half-maximal inhibitory concentration (IC50) values of 225.4 mg/L, suggesting its potential in phytoremediation for metal-contaminated waters. Aké et al. identified microbial strains with high Cr (VI) adsorption capacities, offering insights for Cr-laden wastewater treatment or similar contaminated environments. Feng et al. explored the application of phosphate-solubilizing microorganisms (PSMs) to enhance soil fertility and plant resilience in urban areas, offering a sustainable alternative to chemical fertilizers. Wang et al. reviewed microbial biosorption techniques for radioactive nuclides, highlighting microbial approaches as sustainable alternatives for nuclear waste management in geological environments.

Taken together, this Research Topic advances our understanding of microbial metabolism, distribution, and the key underlying drivers of microbial functions in both pristine and contaminated ecotones and similar environments. By integrating these findings, we will gain a better understanding of global nutrient cycles, contaminant bioremediation, and microbial-environment interactions.

Author contributions

YS: Writing – original draft, Writing – review & editing. XZ: Writing – original draft, Writing – review & editing. LZ: Writing – original draft, Writing – review & editing. YL: Writing – original draft, Writing – review & editing.

Acknowledgments

We would like to extend our sincere gratitude to all the authors, reviewers, and editorial team for their distinguished contributions to our Research Topic in Frontiers in Microbiology.

Conflict of interest

The authors declare that the research was conducted in the absence of any commercial or financial relationships that could be construed as a potential conflict of interest.

The author(s) declared that they were an editorial board member of Frontiers, at the time of submission. This had no impact on the peer review process and the final decision.

Publisher's note

References

Chen, X., Sheng, Y., Wang, G., Zhou, P., Liao, F., Mao, H., et al. (2024). Spatiotemporal successions of N, S, C, Fe, and as cycling genes in groundwater of a wetland ecosystem: enhanced heterogeneity in wet season. *Water Res.* 251:121105. doi: 10.1016/j.watres.2024.121105

Chen, Y. J., Leung, P. M., Cook, P. L., Wong, W. W., Hutchinson, T., Eate, V., et al. (2022). Hydrodynamic disturbance controls microbial community assembly and biogeochemical processes in coastal sediments. *ISME J.* 16, 750–763. doi: 10.1038/s41396-021-01111-9

Dong, H., Huang, L., Zhao, L., Zeng, Q., Liu, X., Sheng, Y., et al. (2022). A critical review of mineral-microbe interaction and co-evolution: mechanisms and applications. *Natl. Sci. Rev.* 9:nwac128. doi: 10.1093/nsr/nwac128

Dong, H., Zeng, Q., Sheng, Y., Chen, C., Yu, G., and Kappler, A. (2023). Coupled iron cycling and organic matter transformation across redox interfaces. *Nat. Rev. Earth Environ.* 4, 659–673. doi: 10.1038/s43017-023-00470-5

Ruff, S. E., Humez, P., de Angelis, I. H., Diao, M., Nightingale, M., Cho, S., et al. (2023). Hydrogen and dark oxygen drive microbial productivity in diverse groundwater ecosystems. *Nat. Commun.* 14:3194. doi: 10.1038/s41467-023-38523-4

Sheng, Y., Baars, O., Guo, D., Whitham, J., Srivastava, S., and Dong, H. (2023a). Mineral-bound trace metals as cofactors for anaerobic biological nitrogen fixation. *Environ. Sci. Technol.* 57, 7206–7216. doi: 10.1021/acs.est.3c01371

Sheng, Y., Bibby, K., Grettenberger, C., Kaley, B., Macalady, J. L., Wang, G., et al. (2016). Geochemical and temporal influences on the enrichment of acidophilic iron-oxidizing bacterial communities. *Appl. Environ. Microbiol.* 82, 3611–3621. doi: 10.1128/AEM.00917-16

Sheng, Y., Dong, H., Coffin, E., Myrold, D., and Kleber, M. (2022). The important role of enzyme adsorbing capacity of soil minerals in regulating β-glucosidase activity. *Geophys. Res. Lett.* 49:e2021GL097556. doi: 10.1029/2021GL097556

Sheng, Y., Jiang, W., and Zhang, M. (2023b). Mobilization, speciation, and transformation of organic and inorganic contaminants in soil-groundwater ecosystems. *Appl. Sci.* 13:11454. doi: 10.3390/app132011454

Shi, L., Dong, H., Reguera, G., Beyenal, H., Lu, A., Liu, J., et al. (2016). Extracellular electron transfer mechanisms between microorganisms and minerals. *Nat. Rev. Microbiol.* 14, 651–662. doi: 10.1038/nrmicro.2016.93

Shu, W. S., and Huang, L. N. (2022). Microbial diversity in extreme environments. *Nat. Rev. Microbiol.* 20, 219–235. doi: 10.1038/s41579-021-00648-y

Sun, L., Wang, C., Yu, H., Liu, D., Houlton, B. Z., Wang, S., et al. (2021). Biotic and abiotic controls on dinitrogen production in coastal sediments. *Glob. Biogeochem. Cycl.* 35:e2021GB007069. doi: 10.1029/2021GB007069

Wen, Z., Browning, T. J., Cai, Y., Dai, R., Zhang, R., Du, C., et al. (2022). Nutrient regulation of biological nitrogen fixation across the tropical western North Pacific. *Sci. Adv.* 8:eabl7564. doi: 10.1126/sciadv.abl7564

Zhou, X., Sheng, Y., Zheng, Y., Jiang, M., Wang, M., Zhu, Z., et al. (2024). Bioavailability of molybdenite to support nitrogen fixation on early Earth by an anoxygenic phototroph. *Earth Planet. Sci. Lett.* 647:119056. doi: 10.1016/j.epsl.2024.119056

frontiers | Frontiers in Microbiology

TYPE Original Research
PUBLISHED 20 September 2023
DOI 10.3389/fmicb.2023.1261079

OPEN ACCESS

EDITED BY
Yizhi Sheng,
China University of Geosciences, China

REVIEWED BY
Xiaofeng Cao,
Tsinghua University, China
Yucheng Wu,
Chinese Academy of Sciences (CAS), China

*CORRESPONDENCE
Xiangming Tang
✉ xmtang@niglas.ac.cn
Hang Wang
✉ wanghang39@scu.edu.cn

RECEIVED 24 July 2023
ACCEPTED 04 September 2023
PUBLISHED 20 September 2023

CITATION
Liu H, Dai J, Fan Z, Yang B, Wang H, Hu Y, Shao K, Gao G and Tang X (2023) Bacterial community assembly driven by temporal succession rather than spatial heterogeneity in Lake Bosten: a large lake suffering from eutrophication and salinization. *Front. Microbiol.* 14:1261079. doi: 10.3389/fmicb.2023.1261079

Bacterial community assembly driven by temporal succession rather than spatial heterogeneity in Lake Bosten: a large lake suffering from eutrophication and salinization

Hao Liu[1,2,3], Jiangyu Dai[2], Ziwu Fan[2], Bei Yang[4], Hang Wang[1]*, Yang Hu[3], Keqiang Shao[3], Guang Gao[3] and Xiangming Tang[3]*

[1]State Key Laboratory of Hydraulics and Mountain River Engineering, Sichuan University, Chengdu, China, [2]Key Laboratory of Taihu Basin Water Resources Management, Ministry of Water Resources, Nanjing Hydraulic Research Institute, Nanjing, China, [3]State Key Laboratory of Lake Science and Environment, Nanjing Institute of Geography and Limnology, Chinese Academy of Sciences, Nanjing, China, [4]Key Laboratory of Agricultural Environment of the Lower Reaches of the Yangtze River, Institute of Agricultural Resources and Environment, Jiangsu Academy of Agricultural Sciences, Nanjing, China

Oligosaline lakes in arid and semi-arid regions play a crucial role in providing essential water resources for local populations. However, limited research exists on the impact of the environment on bacterial community structure in these lakes, co-occurrence patterns and the mechanisms governing bacterial community assembly. This study aims to address this knowledge gap by examining samples collected from five areas of Lake Bosten over four seasons. Using the 16S rRNA gene sequencing method, we identified a total of 510 to 1,005 operational taxonomic units (OTUs) belonging to 37 phyla and 359 genera in Lake Bosten. The major bacterial phyla were Proteobacteria (46.5%), Actinobacteria (25.9%), Bacteroidetes (13.2%), and Cyanobacteria (5.7%), while the major genera were *hgcI_clade* (12.9%), *Limnohabitans* (6.2%), and *Polynucleobacter* (4.7%). Water temperature emerged as the primary driver of these community structure variations on global level. However, when considering only seasonal variations, pH and nitrate were identified as key factors influencing bacterial community structures. Summer differed from other seasons in aspects of seasonal symbiotic patterns of bacterial communities, community assembly and function are different from other seasons. There were notable variations in bacterial community structures between winter and summer. Deterministic processes dominated community assembly, but there was an increase in the proportion of stochastic processes during summer. In summer, the functions related to photosynthesis, nitrogen fixation, and decomposition of organic matter showed higher abundance. Our findings shed light on the response of bacterial communities to environmental changes and the underlying mechanisms of community assembly in oligosaline lakes in arid regions.

KEYWORDS

Lake Bosten, oligosaline, bacterial community structure, cooccurrence network, assembly mechanism

1. Introduction

Arid and semi-arid regions, characterized by average annual precipitation between 25 and 500 mm, encompass approximately one-third of the world's land area and are inhabited by nearly 400 million people. Freshwater lakes in these regions serve as vital water resources on which local populations depend for their survival (Williams, 1999). However, the distribution of rainfall and temperature has been altered due to the effects of global climate change, resulting in a significant reduction in the water surface area of inland northwest China (Li et al., 2007). Moreover, the discharge of pollutants into these water bodies has led to increased salinity and eutrophication, posing threats not only to the livelihoods of local residents but also to the ecological environment within the lake basin (Wang and Qin, 2017; Fang et al., 2018). Consequently, lakes situated in arid and semi-arid regions are considered early indicators of regional and global environmental changes, with their resident bacteria recognized as highly responsive to these alterations (Adrian et al., 2009; Williamson et al., 2009; Tang et al., 2015).

Heterotrophic bacteria play a crucial role in biogeochemical processes within aquatic ecosystems (Cotner and Biddanda, 2002). As decomposers, they are involved in micro-pollutant degradation (Johnson et al., 2015) and contribute to the maintenance of ecosystem stability (Awasthi et al., 2014). Therefore, understanding the composition, structure, and response of bacterial communities in water bodies to environmental changes becomes imperative. Numerous studies have focused on the composition, structure, and response of bacterial communities in lakes, particularly in shallow eutrophic lakes such as Lake Taihu (Niu et al., 2015; Kong et al., 2018; Xie et al., 2020). Additionally, research has been conducted on lakes in the Qinghai-Tibet Plateau (Liu et al., 2014, 2017; Ren et al., 2022), dammed or stepped reservoirs (Chen et al., 2020; Xie et al., 2021), and temperate or cold lakes (Yannarell et al., 2003; Daniel et al., 2016).

In recent years, there has been a growing interest in studying the mechanisms of community assembly, driven by the recognition that stochastic processes may significantly influence community dynamics. The balance between community succession based on niche theory and neutral theory is currently a central research focus in microbial ecology (Dini-Andreote et al., 2015). While studies have explored community assembly processes in eutrophic lakes on different scales of time and space (Zhao et al., 2017; Liu et al., 2020), and under different environmental gradients (Aguilar and Sommaruga, 2020), fewer investigations have been conducted in oligosaline lakes with less trophic levels.

Lake Bosten, situated in the central Tianshan Mountains, is the largest inland freshwater lake in China, covering an area of 1,064 km^2 (1,047 m a.s.l.) with an average water depth of 8 m. The annual evaporation in the Lake Bosten area is 1881 mm (Bai et al., 2011). Over the past 50 years, Lake Bosten has undergone significant changes due to climate shifts and human activities (Yao et al., 2018). Salinity has increased from 0.38 g/L to 1.46 g/L, and nutrient levels have transitioned from oligotrophic to mesotrophic (Tang et al., 2015). These ongoing transformations provide a unique opportunity to study the response of microbial communities to salinization and eutrophication.

While progress has been made in understanding the seasonal changes in bacterial community structure in the sediment of Lake Bosten (Zhang et al., 2020), surface water studies have been limited to single-season investigations (Tang et al., 2012, 2015). Furthermore, there is a scarcity of research on the temporal and spatial variations in bacterial communities in the surface water column, which represents the interface layer between the water body and the external environment (Song et al., 2018). Additionally, little is known about the mechanisms of bacterial community assembly in oligosaline water habitats in arid regions. In this study, we employed high-throughput sequencing technology, redundancy analysis, co-occurrence network analysis, and neutral community models to explore the spatiotemporal changes in bacterial communities in Lake Bosten, their relationship with environmental factors, and the mechanisms governing bacterial assembly. Our specific objectives are as follows: (1) to identify the key environmental factors driving the spatiotemporal heterogeneity of bacterial communities in the surface water of Lake Bosten under the pressures of eutrophication and salinization, and (2) to investigate the potential bacterial community assembly mechanisms, community stability, and ecological function.

2. Materials and methods

2.1. Study area and sampling procedures

A total of 20 surface water samples were collected from Lake Bosten between 2010 and 2011. These samples were obtained from five different sampling sites, as illustrated in Figure 1. The collection of water samples followed a seasonal schedule, with undisturbed duplicate water columns being collected in August 2010 (summer), October 2010 (fall), January 2011 (winter), and May 2011 (spring). To preserve the integrity of the samples, they were transferred to sterile containers immediately after collection. Subsequently, subsamples of 500–1,000 mL from each water column were filtered through 0.2 μm polycarbonate filters (Millipore) in the laboratory, using a vacuum pump. The filtered samples were carefully stored at −80°C until DNA extraction for 16S rRNA gene analysis. The remaining water samples were transported to the laboratory for chemical analysis.

2.2. Physicochemical analysis

Water depth (WD) and transparency (SD) were measured *in situ* using a water depth meter (Uwitec, Austria) and a Secchi disk (BP21-SD-20), respectively. Water temperature (WT), pH, turbidity (TUB), total dissolved solids (TDS), salinity (Sal) and dissolved oxygen (DO) were measured *in situ* with a multiparameter water quality probe (YSI 6600 v2, Yellow Springs Instruments Inc., United States). Concentrations of total nitrogen (TN), total nitrate-nitrogen (NO_3^-), ammonia-nitrogen (NH_4^+), total phosphorus (TP), chlorophyll a (Chl-*a*), chloride (Cl^-), sulfate (SO_4^{2-}), and total organic carbon (TOC) were determined in the laboratory using standard methods (Jin and Tu, 1990). Bacterial abundance (BA) was enumerated using epifluorescence microscopy, following the method outlined by Tang et al. (2015).

2.3. DNA extraction purification and PCR amplification

DNA extraction from the collected water samples was performed using the FastDNA® Spin Kit for Soil (MP Biomedicals). The integrity

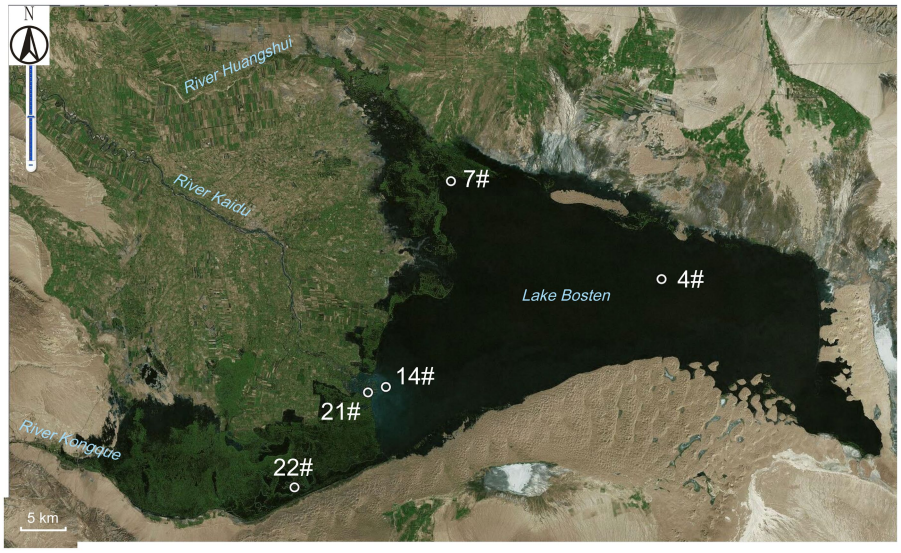

FIGURE 1
The sampling sites within Lake Bosten. The specific coordinates and descriptions of each site are as follows: Site 4# (87.1333° E, 42.0000° N): Located in the middle of Lake Bosten. Site 7# (86.8417° E, 42.1000° N): This site is situated in the estuary of River Huangshui, which is a seasonal river affected by agricultural pollution and other human activities. Site 14# (86.7417° E, 41.8889° N): Found at the estuary of River Kaidu, the largest perennial river with the highest annual volume of water. Site 21# (86.7269° E, 41.8836° N): Positioned near the boundary between the lake and the swamp area. Site 22# (86.6247° E, 41.7858° N): Located within the swamp area of Lake Bosten. These sampling sites were chosen to capture different environmental conditions and potential sources of influence within the lake.

of the extracted DNA was assessed by subjecting it to 0.8% agarose gel electrophoresis. Gel electrophoresis was conducted at a voltage of 120 V for approximately 30 min.

For PCR amplification, the V1-V3 region of the bacterial 16S rRNA gene was targeted using universal primers 8 F (5'-AGAGTTTGATCCTGGCTCAG-3′) and 533 R (5'-TTACCGCGGCTGCTGGCAC-3′) (Bai et al., 2012). Duplicate PCR products were purified and concentrated using the E.Z.N.A.® Cycle-Pure Kit. The purified products from each sample were then combined in equimolar ratios to create a mixed sample for 454 pyrosequencing.

2.4. 454 pyrosequencing and data analysis

Amplicon pyrosequencing was carried out on a Roche Genome Sequencer GS FLX Titanium platform using a 454/Roche A sequencing primer kit. High-quality sequences were obtained by removing the primers, and labels, and performing quality control procedures. The resulting sequences were then subjected to clustering using UCLUST, implemented in QIIME2 2018.11 software, with a minimum identity threshold of 97% to generate operational taxonomic units (OTUs) (Caporaso et al., 2010). Representative sequences for each OTU were trimmed and compared against the Bacterial Silva database (version 138) using QIIME.

Statistical analyses and data visualization were performed using *ggplot2* package in R 4.1.3.[1] Non-metric multidimensional scaling (nMDS) was performed using the metaMDS function based on the Bray-Curtis distance calculated by the vegdist function after Hellinger transformation. Analysis of similarity (ANOSIM) was used to assess the significance of temporal and spatial differences in bacterial communities (Clarke, 1993). Redundancy analysis (RDA) was carried out by the *vegan* package (Borcard et al., 2011). The relationship between OTUs, functional community compositions, and each environmental factor was examined using partial (geographic distance corrected) mantel tests, performed with the *ggcor* package (Sunagawa et al., 2015). Kruskal-Wallis tests was used to calculate the significant differences between groups.

The functional prediction analysis was performed on the Tutools platform[2] based on the FAPROTAX database, an online data analysis website that provides free access to its services. The Tutools platform was also used to generate a bubble chart visualizing the functions.

2.5. Co-occurrence network analysis of bacterial communities

To analyze the co-occurrence patterns of bacterial communities in Lake Bosten, Spearman's correlation coefficients (r) were calculated using the *psych* package in R 4.1.3 (Barberan et al., 2014; Codello et al., 2023). The resulting correlation coefficients were used to construct co-occurrence networks. The topological properties of the networks, such as robustness and vulnerability, were evaluated using the *igraph* package in R 4.1.3 (Yuan et al., 2021; Shen et al., 2022). To identify key species in the co-occurrence network, thresholds based on degree,

1 https://www.r-project.org

2 http://www.cloudtutu.com

closeness centrality, and betweenness centrality were used. Species with a degree greater than 40, closeness centrality greater than 0.44, and betweenness centrality less than 0.12 are considered key species in the network (Banerjee et al., 2019). The resulting networks were visualized using Gephi v0.9, an interactive platform for network visualization.

2.6. Neutral community model

In the study, Sloan's community model was utilized to examine the potential influence of stochastic processes on the phytoplankton community (Sloan et al., 2006). This model provides insights into the relationship between observed species abundance in local communities and their relative abundance in the larger metacommunity. It is based on neutral theory and can be applied to large microbial populations. The neutral model was implemented using the *MicEco* package, which provides tools for ecological analysis in R 4.1.3.

2.7. Deposition of nucleotide sequence accession numbers

The raw bacterial 16S rRNA gene sequences determined in the present study have been deposited in the Genome Sequence Archive of the BIG Data Center[3] under the accession number CRA011126.

3. Results

3.1. Spatial and temporal variation in physicochemical parameters

WT ranged widely across the four seasons, from 1.23°C to 23.96°C, indicating significant seasonal fluctuations. The average DO concentration in winter (12.1 ± 4.7 mg/L) was significantly higher than that in summer, suggesting a seasonal difference in DO levels. The concentration of TOC in spring (17.8 ± 4.2 mg/L) was significantly higher than that in fall and winter, where it remained below 10 mg/L. Chl-*a* concentration was higher in fall (4.0 ± 2.3 μg/L) compared to winter (1.7 ± 0.7 μg/L), indicating a significant seasonal variation. The mean TP concentration in spring (0.06 mg/L) was higher compared to the other three seasons.

The highest SD was observed in the center of Lake Bosten (4#), reaching 3.65 ± 0.68 m, which was significantly higher than other sampling sites. SD in the estuary of River Huangshui (7#) and the swamp area of Lake Bosten (22#) were also significantly higher compared to the estuary of River Kaidu (14#) and the boundary between lake and swamp area (21#). The variation pattern of turbidity was similar to SD, with higher levels observed in the center of the lake (4#) and in the estuary of River Huangshui (7#) and swamp area (22#). pH at sites 21# and 22# was lower compared to other sites. DO at site 21# was extremely low (1.5 ± 1.7 mg/L), while the concentration of NH_4^+ at this site was higher than at other sites (0.59 ± 0.31 mg/L), especially compared to site 4#. TN concentration at site 22# was notably lower than at site 21# (Supplementary Table S1, Supplementary Figure S1).

3.2. Profiles of bacterial communities in Lake Bosten

The number of high-quality sequences obtained varied from 14,323 to 23,593 across different samples, with an average of 18,051. The number of OTUs varied from 510 to 1,005, with an average of 742. The rarefaction curves reached a plateau after the sequencing depth of 15,000, indicating that the sequencing depth was sufficient to capture a robust diversity of bacterial communities (Supplementary Figure S2).

Bacterial community in Lake Bosten contained a total of 37 phyla. The major phyla in Lake Bosten were Proteobacteria (46.5%), Actinobacteria (25.9%), Bacteroidetes (13.2%), and Cyanobacteria (5.7%). The relative proportions of these dominant phyla varied across seasons and sampling sites. Proteobacteria accounted for a higher proportion (more than 60%) of the bacteria at sites 22# and 14# in spring but was lower (approximately 40%) at sites 4# and 7#. The relative proportion of cyanobacteria increased at site 7# compared to other sites. In summer, there was an increase in the proportion of Firmicutes at sites 7# and 14#, potentially due to their locations at the estuary of River Huangshui and River Kaidu, respectively. The proportion of Bacteroidetes increased in winter.

A total of 359 genera were identified in Lake Bosten. The major genera were *hgcI_clade* (12.9%), *Limnohabitans* (6.2%), *Polynucleobacter* (4.7%), *Flavobacterium* (3.5%), *Arcobacter* (3.3%), and *CL500-29 Marine group* (3.3%). The dominant genus, *hgcI_clade*, was present in most sites but varied in relative abundance over time and space. In spring, *Limnohabitans* and *Polynucleobacter* occupied a significant proportion, except at site 4#. The dominance of *hgcI_clade* was more consistent across sites, with less apparent variation among locations in summer. *Arcobacter* became the dominant genus at site 7# in fall and winter. These findings highlight the dynamic nature of the bacterial community composition in Lake Bosten, with variations observed across seasons and sampling sites (Figure 2).

3.3. Diversity of bacterial communities in Lake Bosten

The α-diversity of the bacterial communities in Lake Bosten is summarized in Figure 3. The Simpson and Shannon indices showed slightly higher values in spring and summer compared to fall and winter, while the Chao1 index was lowest in fall and highest in spring. No significant differences were found in the alpha diversity indices among the four seasons ($p > 0.05$), suggesting that the diversity of bacterial communities did not vary significantly throughout the year.

The Simpson and Shannon indices exhibited the highest values at site 22# and the lowest values at site 7#. The Chao1 index showed the highest value at site 21# and the lowest value at site 4#. There were no significant differences in the alpha diversity indices among the different sampling sites ($p > 0.05$), indicating that the diversity of bacterial communities did not significantly differ spatially.

3 http://bigd.big.ac.cn/gsa

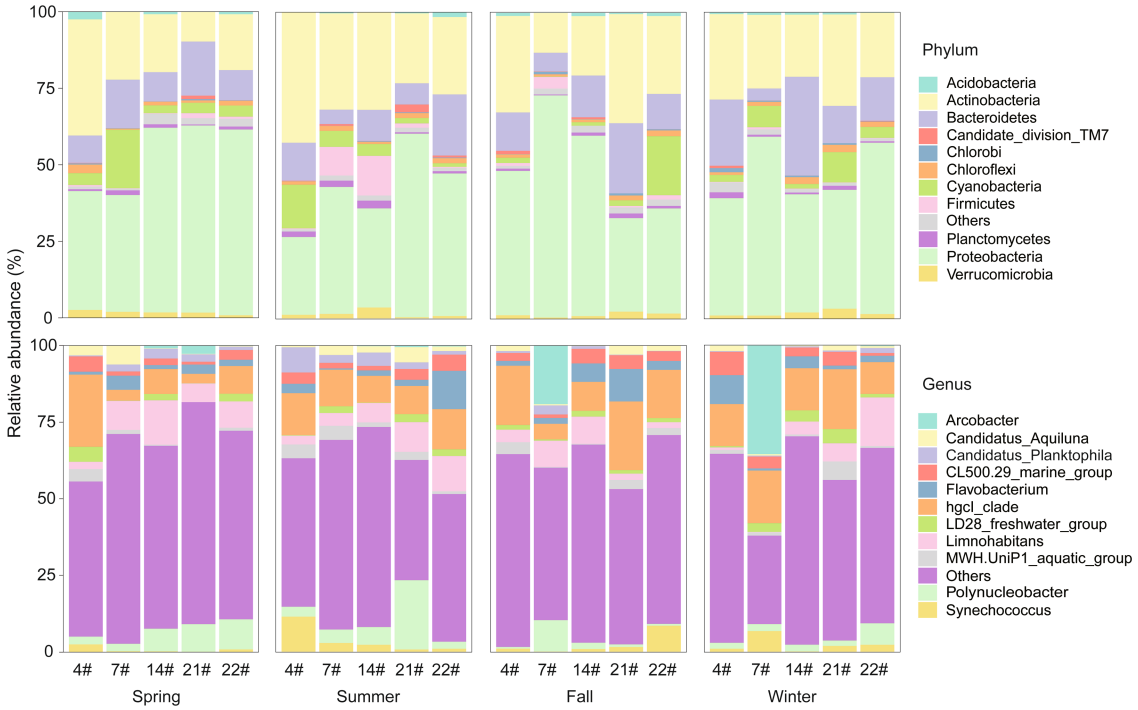

FIGURE 2
Relative abundance of bacterial taxonomy at the phylum and genus levels in Lake Bosten. The top 11 phyla/genera with relative abundance were selected to draw the percentage accumulation map, and the remaining phyla/genera were classified into others.

The nMDS plot (Figure 4) indicates a significant separation in the bacterial community structure between summer and winter. The separation suggests distinct microbial compositions during these seasons. The separation between summer and winter communities was found to be statistically significant ($p < 0.05$), indicating that the bacterial communities in Lake Bosten undergo seasonal shifts. The nMDS analysis did not reveal an obvious separation between different spatial locations. The bacterial community structure at the various sampling sites (spatial locations) appear to be more similar to each other compared to the temporal variations. The lack of separation between spatial locations suggests that there were no significant differences in bacterial community structure among the sampled sites, as supported by the available data (Supplementary Figure S3). These findings suggest that temporal factors, such as seasons, play a more prominent role in shaping the bacterial community structure in Lake Bosten compared to spatial factors.

3.4. Relationship between bacteria community and environmental factors in Lake Bosten

The results of the RDA indicated that Axis 1 and Axis 2 were significantly associated with the variation in bacterial communities in Lake Bosten, explaining 16.5% and 10.1% of the observed variation, respectively. The analysis revealed that water temperature (WT) was the most significant environmental factor ($p < 0.05$) influencing the spatial and temporal variation in bacterial community structure at the OTU level (Figure 5).

Additionally, the Mantel test analysis, which assessed the correlation between the bacterial community structure and environmental factors, suggested that different factors drove the community variation in each season. Specifically, in summer, pH and NO_3^- were identified as the main driving factors shaping the bacterial community structure.

3.5. Co-occurrence network analysis of Lake Bosten

The co-occurrence network analysis revealed interesting patterns in the bacterial community of Lake Bosten. All co-occurrence networks in different seasons showed non-randomly structured patterns and high "small-world" properties. The network varied in terms of the number of nodes (bacterial taxa) and edges (connections between taxa) across different seasons. In spring, the network consisted of 505 nodes and 4,367 edges, while in summer, it had 430 nodes and 2,669 edges. Fall had 521 nodes and 2,874 edges, and winter had 481 nodes and 4,100 edges (Supplementary Table S2). These variations in network size indicate differences in the complexity and connectivity of the bacterial community structure throughout the year.

Some topology parameters were displayed that the community structure of Lake Bosten exhibited a similar symbiotic pattern in spring and winter (Supplementary Table S3), suggesting some consistency in the interactions between bacterial taxa during these seasons. However, the network structure differed in summer and fall, particularly in summer, where network showed that the highest modularity and the lowest average degree, indicating a possibly less

10.3389/fmicb.2023.1261079

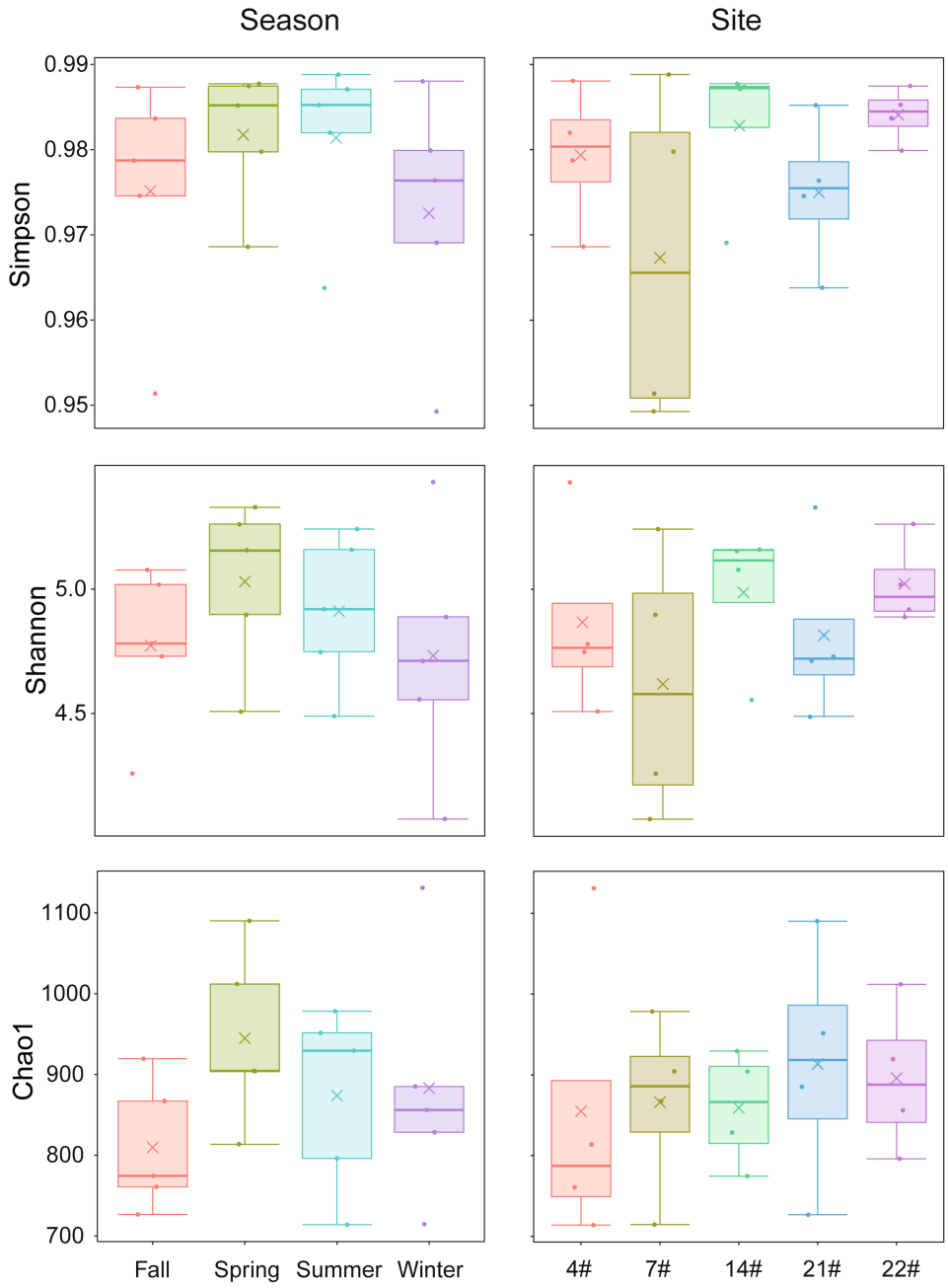

FIGURE 3
Seasonal and spatial variations of α-diversity indices in Lake Bosten. The symbol "×" in the figure represents the mean data of each group. Kruskal-Wallis test was used to analyze differences between groups.

cohesive and more fragile community structure during summer(Shi et al., 2020; Shen et al., 2022) (Supplementary Table S2, Figure 6). At the phylum level, the bacterial networks remained relatively stable, primarily consisting of Proteobacteria, Bacteroidetes, Actinobacteria, and Firmicutes (Supplementary Figure S4). These phyla consistently played important roles in the bacterial community dynamics throughout the seasons.

The analysis of robustness and vulnerability, which are topological properties related to network stability, revealed interesting patterns. The robustness index was higher in spring than in to the other seasons, indicating a more resilient network during that time. On the other hand, the vulnerability index was low in winter but high in fall, with spring and summer falling somewhere in between (Figure 7). These results highlight the dynamic nature of network stability across different seasons.

The identification of keystone species, which are taxa with high importance in maintaining community structure and stability, showed that all seasons except summer contained a certain number of keystone species. Spring, fall, and winter had 10 phyla and 67 genera, 10 phyla and 49 genera, and 11 phyla and 53 genera, respectively (Supplementary Table S4). These keystone species likely play crucial roles in shaping the network structure and functioning of the bacterial community in Lake Bosten.

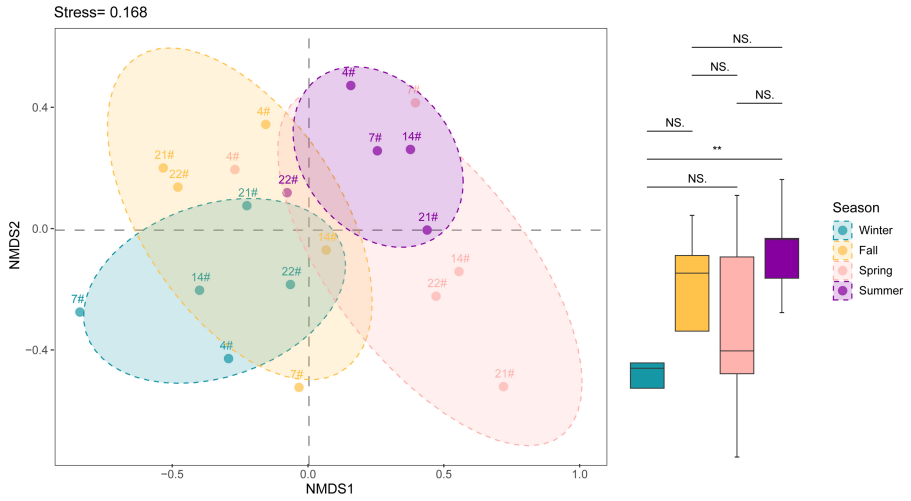

FIGURE 4
NMDS analysis showing the variation of beta diversity in Lake Bosten. ANOSIM analysis was used to estimate the differences between groups and *p* value indicated significant levels (**$p < 0.01$; NS., non-significant).

3.6. Stochastic and deterministic assembly assessment

The assessment of stochastic processes in shaping the bacterial community in Lake Bosten provides valuable insights into the assembly mechanisms of the community. The overall analysis indicated that stochastic processes accounted for 54.2% of the community assembly, suggesting that randomness played a dominant role in structuring the bacterial community in the lake. However, when considering seasonal differences and the succession rate of bacterial communities, the proportion of stochastic processes varied across seasons. In spring, fall, and winter, the proportion of stochastic processes was relatively small, ranging from 23.1% to 37.8% (see Figure 8). This indicates that deterministic processes, such as environmental filtering or species interactions, played a more significant role in shaping the community during these seasons. Interestingly, in summer, the proportion of stochastic processes increased by approximately 10% compared to the other seasons. This suggests that during the summer season, random factors and chance events had a more pronounced influence on the assembly of the bacterial community in Lake Bosten. These stochastic processes may include dispersal limitation, ecological drift, or random colonization events. The observed seasonal differences in the proportion of stochastic processes highlight the dynamic nature of community assembly and the varying importance of deterministic and random factors in different seasons. This implies that environmental conditions, resource availability, and biological interactions may differ throughout the year, leading to variations in the mechanisms governing bacterial community assembly.

3.7. Functional analysis

The functional analysis of dominant bacteria in Lake Bosten revealed that the main functional groups were chemoheterotrophic and oxyheterotrophic bacterial communities. These functional groups are commonly associated with the utilization of organic compounds as energy sources and the consumption of oxygen in their metabolic processes (Supplementary Figure S5). Interestingly, there were no significant spatiotemporal differences observed in functional predictions, indicating that the functional composition of the bacterial community remained relatively stable across different sites and seasons. This suggests that the functional potential of the bacterial community in Lake Bosten is relatively consistent and not strongly influenced by spatial or temporal factors. However, when specifically comparing the functional differences between summer and other seasons, certain variations were observed. In summer, the functions related to photosynthesis, nitrogen fixation, and decomposition of organic matter showed higher abundance compared to other seasons. This suggests that during the summer season, there may be increased metabolic activities associated with photosynthetic bacteria, nitrogen-fixing bacteria, and decomposers, potentially driven by the availability of light, nutrients, and organic matter inputs. On the other hand, the function of nitrate respiration was found to be lowest in summer compared to other seasons. Figure 9 visually represents the differences in functional predictions between summer and other seasons, highlighting the specific functions that exhibit variation during the summer season.

4. Discussion

4.1. The main driving factors of the bacterial community structure in Lake Bosten

The bacterial community composition of Lake Bosten is characterized by the predominance of Proteobacteria, Actinobacteria, Bacteroidetes, Cyanobacteria, and Firmicutes at the phylum level. These findings align with previous studies conducted by Tang et al. (2012) and Zhang et al. (2020). Proteobacteria and Actinobacteria are commonly found in freshwater lakes worldwide (Spain et al., 2009; Tang et al., 2015; Kong et al., 2018). *Limnohabitans* and

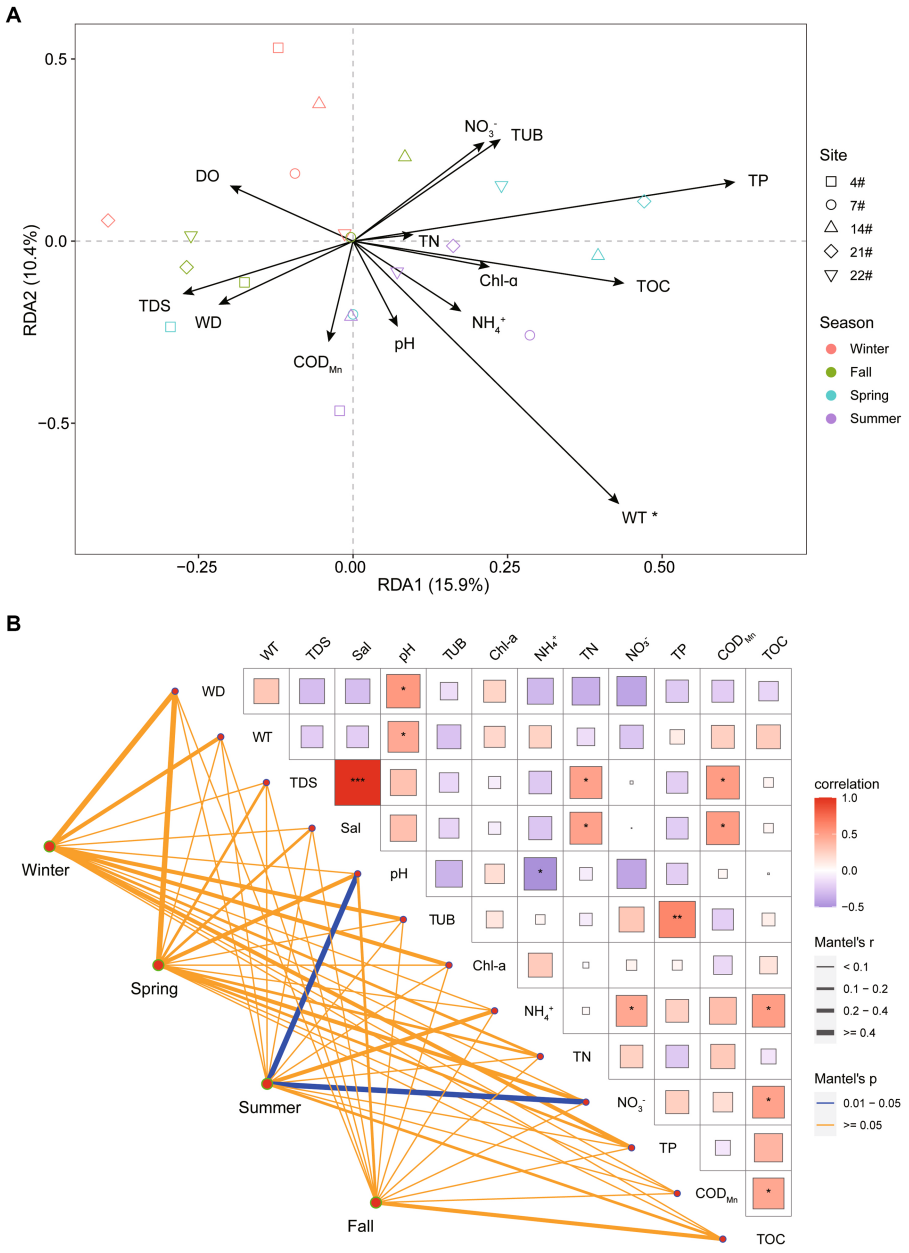

FIGURE 5
(A) Redundancy analysis (RDA) illustrating the relationship between bacterial communities and the environmental parameters in Lake Bosten. The collinear factors were removed by variance inflation factor analysis (VIF analysis). **(B)** Pearson's correlation coefficients of the main 13 environmental parameters (Euclidean distance), seasons (Bray-Curtis distance), and sites (Bray-Curtis distance) of bacterial communities using Mantel permutation tests. The edge width corresponds to the correlation coefficient, and the edge color indicates statistical significance.

Polynucleobacter, both belonging to the Proteobacteria phylum, are particularly abundant in freshwater surface waters and are considered key players in freshwater ecosystems (Nuy et al., 2020). It is also one of the most studied bacterial communities (Newton et al., 2006). *HgcI_clade*, associated with Actinobacteria, has been widely detected in various freshwater environments, including lakes of different trophic states, reservoirs, rivers, and even oligosaline water (Liu et al., 2015; Aguilar et al., 2018; Camara dos Reis et al., 2019; Cruaud et al., 2019; Mohapatra et al., 2019). Firmicutes, Bacteroidetes, and Cyanobacteria are predominant phyla in the planktonic prokaryote communities of lakes, with Cyanobacteria often reflecting eutrophication status due to nitrogen and phosphorus inputs (Qin et al., 2019; Chakraborty et al., 2020), while Firmicutes and Bacteroidetes are commonly associated with the human intestinal environment (Fan and Pedersen, 2021; Zahran et al., 2021).

The seasonal WT was identified as a crucial factor driving the variation in the bacterial community structure of Lake Bosten (Figure 5A). The species diversity estimators, including Chao1 richness and Shannon indices, exhibited seasonal variations (Figure 3). Unlike previous studies on sediment bacterial communities in Lake Bosten, which indicated that WT variations weakened interspecific competition and increased the relative

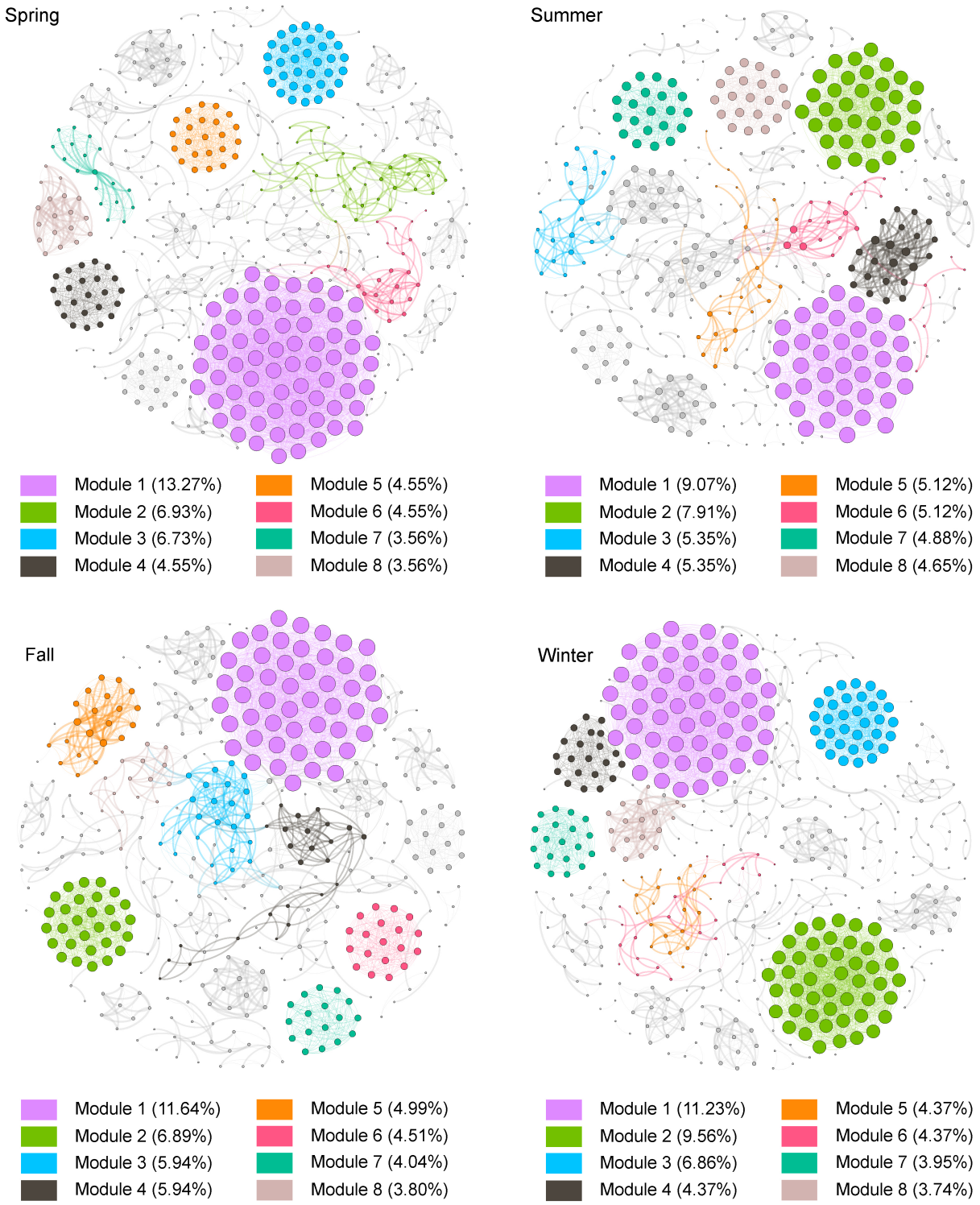

FIGURE 6
Co-occurrence networks and their topological properties for bacterial communities in Lake Bosten. OTUs were selected by their relative abundance (≥ 0.05%) among the total bacterial sequences. A connection represents a significant abs(r) > 0.85 ($p < 0.01$). The nodes in the networks were organized based on the number of nodes in each module, sorted from largest to smallest and filled with color. The size of the nodes in the network was determined by the value of degree, with larger nodes representing higher degrees.

abundance of certain bacteria (Zhang et al., 2020), the microbial communities in the water were more influenced by WT fluctuations. Surface water, in particular, is highly susceptible to environmental factors due to its direct exposure to the external environment at the water-air interface (Pilla et al., 2021). Significant changes in atmospheric temperature can have cascading effects on plankton

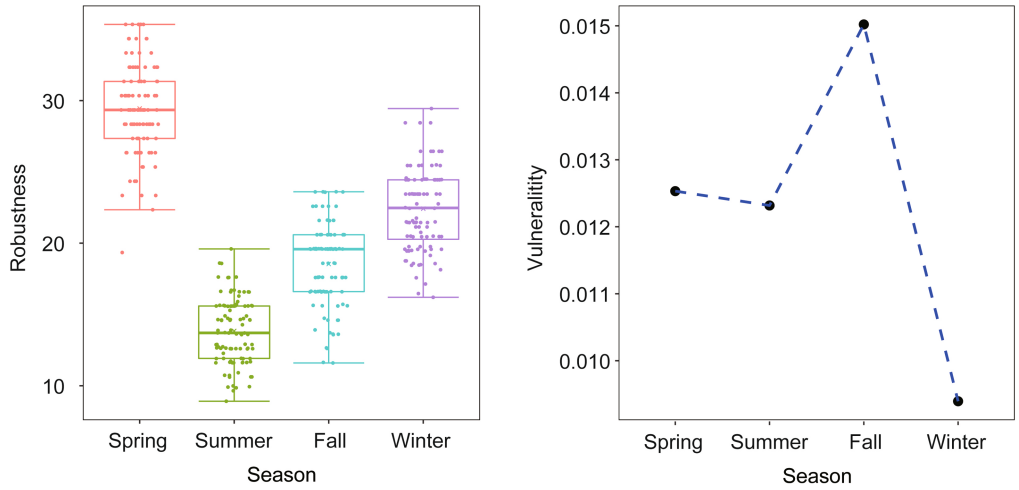

FIGURE 7
Comparison of network topological properties among networks of different seasons. Robustness is measured as the proportion of remaining taxa in a network after random node (50%) removal. Vulnerability is measured by the maximum node vulnerability in each network.

growth rates, lake primary productivity, and the physical and chemical environment of the lake (Lewandowska et al., 2012). Cyanobacteria, as primary producers, can stimulate the growth of heterotrophic bacteria through the release of organic matter produced via photosynthesis and respiration, consequently affecting water quality parameters such as dissolved oxygen (Zhu et al., 2013).

Furthermore, different bacterial species exhibit varying adaptations to WT. Cyanobacteria, although having an optimal growth temperature range of 25–35°C, can survive in water temperatures lower than 10°C. On the other hand, Bacteroidetes display higher growth rates at lower temperatures, making them more abundant during cold seasons such as winter (Arandia-Gorostidi et al., 2017).

Moreover, the influence of WT on the bacterial community structure is also influenced by seasonal variations in exogenous inputs. Lake Bosten receives inflows from the River Kaidu and the River Huangshui, as well as surrounding agricultural drainages (Tang et al., 2012). These inflows exhibit seasonal differences, with the River Kaidu mainly relying on glacier melt and accounting for the majority of the lake's external inflow. In contrast, agricultural activities in the vicinity of Lake Bosten and the River Huangshui result in the discharge of high-salinity agricultural wastewater. The increase in inflow and river input during summer may explain the higher abundance of Firmicutes observed during this season. Additionally, the dominant bacterial genus at the River Kaidu estuary shifts from *hgcI_clade* to *Limnohabitans* during spring and summer, consistent with previous studies (Hu et al., 2018). The presence of *Arcobacter* dominating the estuary during fall and winter aligns with its association with animal diseases and livestock manure (Chinivasagam et al., 2007), thus reflecting the impact of agricultural practices.

4.2. Bacterial assembly mechanism and community stability in Lake Bosten

Based on the information provided, it appears that the community assembly of the bacterial community in Lake Bosten is influenced by both stochastic and deterministic processes, depending on the season. Overall, stochastic processes account for a significant portion (54.2%) of the community assembly, which can be attributed to the severe environmental disturbance in Lake Bosten (Guo et al., 2015; Li et al., 2021), such as extreme temperature variations and low annual planktonic microorganism numbers (Rose and Caron, 2007; Bakermans and Skidmore, 2011; Manna et al., 2019). These factors weaken interspecific competition and indirectly increase the influence of stochastic processes such as ecological drif—the bacterial abundance is only 10^5 orders of magnitude in fall and winter (Supplementary Table S1), which is close to the critical level of ecological drift (Louca et al., 2018).

However, within each season, deterministic processes seem to play a more prominent role in shaping the bacterial community structure. The composition of the bacterial community in different seasons shows clear patterns, indicating that environmental selection and species relationships play a crucial role in community structure (Dini-Andreote et al., 2015). This observation aligns with similar studies focusing on single environmental stresses, such as lake elevation (Aguilar and Sommaruga, 2020), salinity gradient (Liu et al., 2022), geographic scale (Xiao et al., 2022), and nutrient concentration (Zeng et al., 2019).

The presence of driving factors in Lake Bosten contributes to an increase in stochastic community assembly. While randomness tends to dominate the initial phase of community succession, as community succession progresses, deterministic processes become more dominant (Dini-Andreote et al., 2015). The adaptability of microorganisms allows community succession to occur rapidly, typically within 2 weeks for certain processes (Hu et al., 2018). Therefore, from a global perspective, the community assembly mechanism may indicate that the bacterial community in Lake Bosten is in a changing and unstable state for a long time. This may have something to do with changing environmental factors (Geng et al., 2022). The driving factors—nitrate and pH—are present in Lake Bosten only in summer, indicating a certain degree of nitrogen limitation in Lake Bosten, which shows the improvement of nitrogen

10.3389/fmicb.2023.1261079

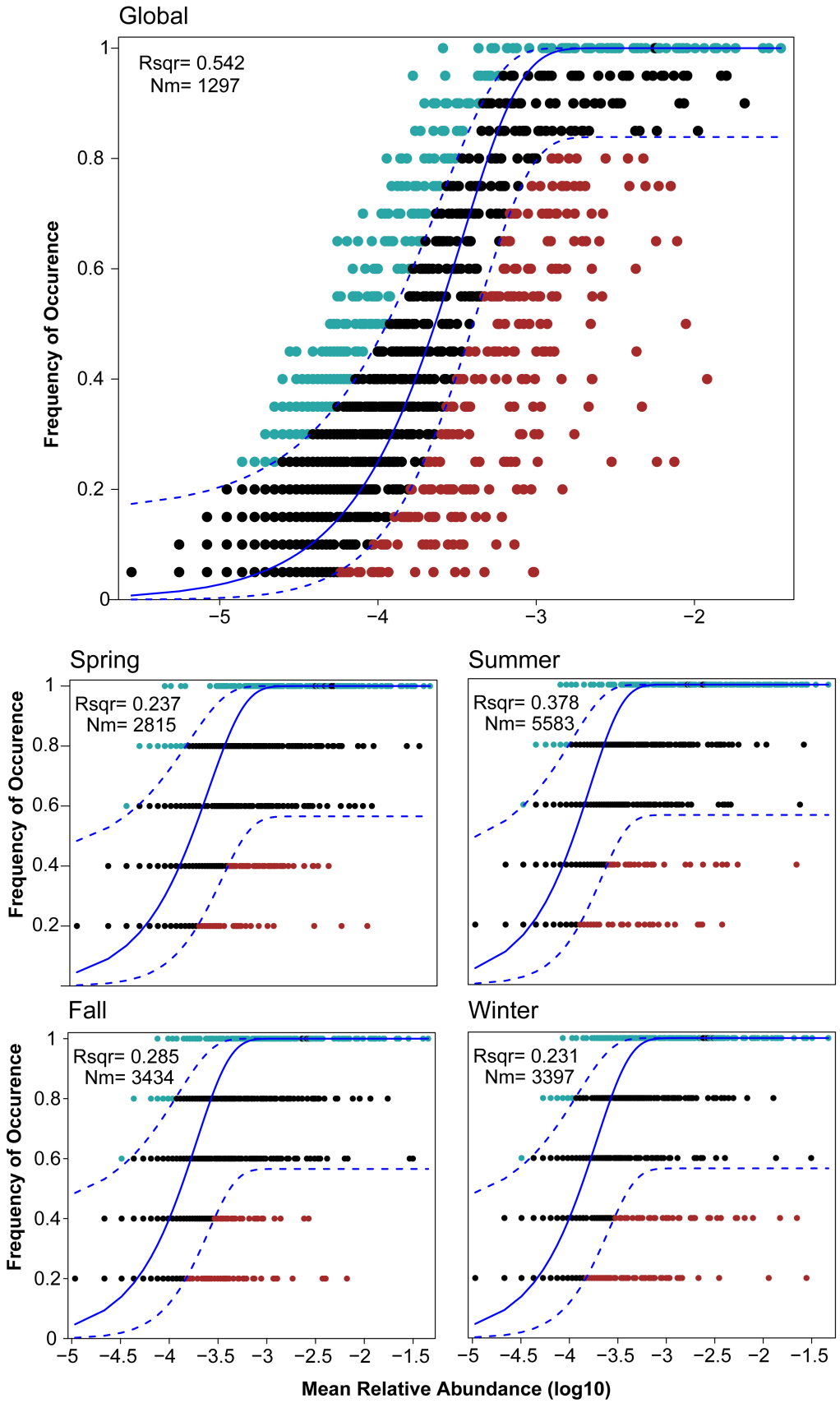

FIGURE 8
Fit of Sloan's neutral model for analysis of bacterial community assembly globally and seasonally. The solid blue line represented the best-fitting neutral model. The dashed line represented the 95% confidence intervals (CIs) around the best-fitting neutral model. OTUs within the CIs (black points)

(Continued)

FIGURE 8 (Continued)
followed the neutral process. OTUs that occur more frequently than predicted by the model were shown in red, whereas those that occur less frequently than predicted were shown in blue. *m* quantified the estimated migration rate, *N* described meta-community size, which was the total abundance of all OTUs in each sample and r^2 indicated the fit to the neutral model.

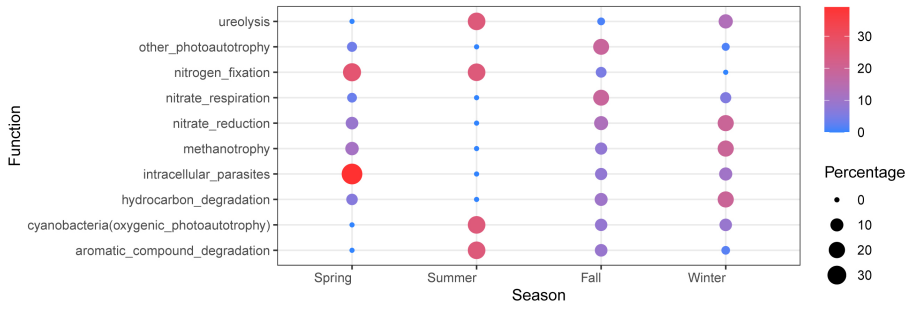

FIGURE 9
Bubble chart of OTU function in Lake Bosten. The seasonal values of each function are normalized and functions with a summer value of 1 or 0 and relative abundance in the top 20 will be retained.

fixation by plankton and nitrate assimilation; and a higher pH means an increase in plankton like cyanobacteria. The network analysis indicates less cohesive and more fragile network, smaller nodes and edges, and the absence of key species in summer. This can be attributed to the variations and fluctuations of ecological effects in dominant environmental factors' combinations, increasing the complexity and variability of interspecific relationships, weakening the status and role of key or constructive species(Banerjee et al., 2018), and making the stochastic effects of microbial communities in Bosten Lake water higher in summer.

For the other seasons, there is a hypothesis suggesting that niche assembly applies in areas with low migration rates, while diffusion assembly applies in regions with high migration rates (Loke and Chisholm, 2023). In the case of Lake Bosten, the migration rate of species entering or leaving the lake is low during spring, fall, and winter due to decreased incoming water. This observation aligns with the dominance of deterministic processes in those seasons.

5. Conclusion

The study conducted on Lake Bosten confirmed that the bacterial community structure exhibited spatio-temporal patterns. The major bacterial phyla identified across various sampling sites and seasons were Proteobacteria, Actinobacteria, Bacteroidetes, and Cyanobacteria. The dominant genera observed were *HgcI_clade*, *Limnohabitans*, and *Polynucleobacter*. Water temperature (WT) emerged as the most influential factor driving the spatio-temporal variations in bacterial communities. However, pH and nitrate (NO_3^-) levels were also identified as key factors influencing the bacterial community structure, particularly when considering only seasonal variations. The bacterial communities exhibited distinct seasonal symbiotic patterns, especially during summer. Deterministic processes primarily governed the community structure, but the role of deterministic processes decreased in summer. The functions related to photosynthesis, nitrogen fixation, and decomposition of organic matter showed higher abundance compared to other seasons.

Data availability statement

The datasets presented in this study can be found in online repositories. The names of the repository/repositories and accession number(s) can be found at: http://bigd.big.ac.cn/gsa, CRA011126.

Author contributions

HL: Data curation, Formal analysis, Methodology, Writing – original draft, Writing – review & editing, Visualization. JD: Resources, Writing – original draft, Data curation. ZF: Supervision, Writing – review & editing. BY: Visualization, Writing – original draft. HW: Supervision, Writing – review & editing. YH: Writing – original draft, Investigation. KS: Writing – original draft, Investigation. GG: Writing – review & editing, Conceptualization, Supervision, Validation. XT: Conceptualization, Writing – review & editing, Methodology, Resources, Supervision.

Funding

The author(s) declare financial support was received for the research, authorship, and/or publication of this article. This work was supported by the National Key R&D Program of China (2022YFC3203902 and 2022YFC3202104), the National Natural Science Foundation of China (grant number: 41971062) and the National Natural Science Foundation of China (U2003205).

Conflict of interest

The authors declare that the research was conducted in the absence of any commercial or financial relationships that could be construed as a potential conflict of interest.

Publisher's note

All claims expressed in this article are solely those of the authors and do not necessarily represent those of their affiliated organizations, or those of the publisher, the editors and the reviewers. Any product that may be evaluated in this article, or claim that may be made by its manufacturer, is not guaranteed or endorsed by the publisher.

Supplementary material

The Supplementary material for this article can be found online at: https://www.frontiersin.org/articles/10.3389/fmicb.2023.1261079/full#supplementary-material

References

Adrian, R., O'Reilly, C. M., Zagarese, H., Baines, S. B., Hessen, D. O., Keller, W., et al. (2009). Lakes as sentinels of climate change. *Limnol. Oceanogr.* 54, 2283–2297. doi: 10.4319/lo.2009.54.6_part_2.2283

Aguilar, P., Dorador, C., Vila, I., and Sommaruga, R. (2018). Bacterioplankton composition in tropical high-elevation lakes of the Andean plateau. *FEMS Microbiol. Ecol.* 94:fiy004. doi: 10.1093/femsec/fiy004

Aguilar, P., and Sommaruga, R. (2020). The balance between deterministic and stochastic processes in structuring lake bacterioplankton community over time. *Mol. Ecol.* 29, 3117–3130. doi: 10.1111/mec.15538

Arandia-Gorostidi, N., Huete-Stauffer, T. M., Alonso-Sáez, L., and Morán, X. A. G. (2017). Testing the metabolic theory of ecology with marine bacteria: different temperature sensitivity of major phylogenetic groups during the spring phytoplankton bloom. *Environ. Microbiol.* 19, 4493–4505. doi: 10.1111/1462-2920.13898

Awasthi, A., Singh, M., Soni, S. K., Singh, R., and Kalra, A. (2014). Biodiversity acts as insurance of productivity of bacterial communities under abiotic perturbations. *ISME J.* 8, 2445–2452. doi: 10.1038/ismej.2014.91

Bai, J., Chen, X., Li, J., Yang, L., and Fang, H. (2011). Changes in the area of inland lakes in arid regions of Central Asia during the past 30 years. *Environ. Monit. Assess.* 178, 247–256. doi: 10.1007/s10661-010-1686-y

Bai, Y., Shi, Q., Wen, D., Li, Z., Jefferson, W. A., Feng, C., et al. (2012). Bacterial communities in the sediments of Dianchi Lake, a partitioned eutrophic waterbody in China. *PLoS One* 7:e37796. doi: 10.1371/journal.pone.0037796

Bakermans, C., and Skidmore, M. (2011). Microbial respiration in ice at subzero temperatures (−4 degrees C to-33 degrees C). *Environ. Microbiol. Rep.* 3, 774–782. doi: 10.1111/j.1758-2229.2011.00298.x

Banerjee, S., Schlaeppi, K., and van der Heijden, M. G. A. (2018). Keystone taxa as drivers of microbiome structure and functioning. *Nat. Rev. Microbiol.* 16, 567–576. doi: 10.1038/s41579-018-0024-1

Banerjee, S., Walder, F., Buchi, L., Meyer, M., Held, A. Y., Gattinger, A., et al. (2019). Agricultural intensification reduces microbial network complexity and the abundance of keystone taxa in roots. *ISME J.* 13, 1722–1736. doi: 10.1038/s41396-019-0383-2

Barberan, A., Bates, S. T., Casamayor, E. O., and Fierer, N. (2014). Using network analysis to explore co-occurrence patterns in soil microbial communities. *ISME J.* 8:952. doi: 10.1038/ismej.2013.236

Borcard, D., Gillet, F., and Legendre, P., *Numerical ecology with R*, (2011). New York: Springer.

Camara dos Reis, M., Lacativa Bagatini, I., Vidal, L., Bonnet, M.-P., Marques, D., and Sarmento, H. (2019). Spatial heterogeneity and hydrological fluctuations drive bacterioplankton community composition in an Amazon floodplain system. *PLoS One* 14:e0220695. doi: 10.1371/journal.pone.0220695

Caporaso, J. G., Kuczynski, J., Stombaugh, J., Bittinger, K., Bushman, F. D., Costello, E. K., et al. (2010). QIIME allows analysis of high-throughput community sequencing data. *Nat. Methods* 7, 335–336. doi: 10.1038/nmeth.f.303

Chakraborty, J., Sapkale, V., Rajput, V., Shah, M., Kamble, S., and Dharne, M. (2020). Shotgun metagenome guided exploration of anthropogenically driven resistomic hotspots within Lonar soda lake of India. *Ecotoxicol. Environ. Saf.* 194:110443. doi: 10.1016/j.ecoenv.2020.110443

Chen, J., Wang, P. F., Wang, C., Wang, X., Miao, L. Z., Liu, S., et al. (2020). Distinct assembly mechanisms underlie similar biogeographic patterns of rare and abundant bacterioplankton in cascade reservoirs of a large river. *Front. Microbiol.* 11:158. doi: 10.3389/fmicb.2020.00158

Chinivasagam, H. N., Corney, B. G., Wright, L. L., Diallo, I. S., and Blackall, P. J. (2007). Detection of Arcobacter spp. in piggery effluent and effluent-irrigated soils in Southeast Queensland. *J. Appl. Microbiol.* 103, 418–426. doi: 10.1111/j.1365-2672.2007.03275.x

Clarke, K. R. (1993). Non-parametric multivariate analyses of changes in community structure. *Aust. J. Ecol.* 18, 117–143. doi: 10.1111/j.1442-9993.1993.tb00438.x

Codello, A., Hose, G. C., and Chariton, A. (2023). Microbial co-occurrence networks as a biomonitoring tool for aquatic environments: a review. *Mar. Freshw. Res.* 74, 409–422. doi: 10.1071/MF22045

Cotner, J. B., and Biddanda, B. A. (2002). Small players, large role: microbial influence on biogeochemical processes in pelagic aquatic ecosystems. *Ecosystems* 5, 105–121. doi: 10.1007/s10021-001-0059-3

Cruaud, P., Vigneron, A., Fradette, M.-S., Dorea, C., Culley, A., Rodriguez, M., et al. (2019). Annual bacterial community cycle in a seasonally ice-covered river reflects environmental and climatic conditions. *Limnol. Oceanogr.* 65, 1–17. doi: 10.1002/lno.11130

Daniel, A. D. C., Pedros-Alio, C., Pearce, D. A., and Alcami, A. (2016). Composition and interactions among bacterial, microeukaryotic, and T4-like viral assemblages in lakes from both polar zones. *Front. Microbiol.* 7:337. doi: 10.3389/fmicb.2016.00337

Dini-Andreote, F., Stegen, J. C., van Elsas, J. D., and Salles, J. F. (2015). Disentangling mechanisms that mediate the balance between stochastic and deterministic processes in microbial succession. *Proc. Natl. Acad. Sci. U. S. A.* 112, E1326–E1332. doi: 10.1073/pnas.1414261112

Fan, Y., and Pedersen, O. (2021). Gut microbiota in human metabolic health and disease. *Nat. Rev. Microbiol.* 19, 55–71. doi: 10.1038/s41579-020-0433-9

Fang, L., Tao, S., Zhu, J., and Liu, Y. (2018). Impacts of climate change and irrigation on lakes in arid Northwest China. *J. Arid Environ.* 154, 34–39. doi: 10.1016/j.jaridenv.2018.03.008

Geng, Y., Li, M., Yu, R., Sun, H., Zhang, L., Sun, L., et al. (2022). Response of planktonic diversity and stability to environmental drivers in a shallow eutrophic lake. *Ecol. Indic.* 144:109560. doi: 10.1016/j.ecolind.2022.109560

Guo, M. J., Zhou, X. D., Li, J., Wu, W., and Chen, Y. M. (2015). Assessment of the salinization processes in the largest inland freshwater lake of China. *Stoch. Env. Res. Risk A.* 29, 1823–1833. doi: 10.1007/s00477-014-0995-z

Hu, Y., Bai, C., Cai, J., Dai, J., Shao, K., Tang, X., et al. (2018). Co-occurrence network reveals the higher fragmentation of the bacterial community in Kaidu river than its tributaries in northwestern China. *Microbes Environ.* 33, 127–134. doi: 10.1264/jsme2.ME17170

Hu, Y., Bai, C., Cai, J., Shao, K., Tang, X., and Gao, G. (2018). Low recovery of bacterial community after an extreme salinization-desalinization cycle. *BMC Microbiol.* 18:195. doi: 10.1186/s12866-018-1333-2

Jin, X. C., and Tu, Q. Y. (1990). *Investigation specifications for lake eutrophication. 2nd Edn*. Beijing, China: China Environmental Science Press.

Johnson, D. R., Helbling, D. E., Lee, T. K., Park, J., Fenner, K., Kohler, H.-P. E., et al. (2015). Association of biodiversity with the rates of micropollutant biotransformations among full-scale wastewater treatment plant communities. *Appl. Environ. Microbiol.* 81, 666–675. doi: 10.1128/AEM.03286-14

Kong, Z. Y., Kou, W. B., Ma, Y. T., Yu, H. T., Ge, G., and Wu, L. (2018). Seasonal dynamics of the bacterioplankton community in a large, shallow, highly dynamic freshwater lake. *Can. J. Microbiol.* 64, 786–797. doi: 10.1139/cjm-2018-0126

Lewandowska, A. M., Breithaupt, P., Hillebrand, H., Hoppe, H.-G., Jürgens, K., and Sommer, U. (2012). Responses of primary productivity to increased temperature and phytoplankton diversity. *J. Sea Res.* 72, 87–93. doi: 10.1016/j.seares.2011.10.003

Li, Y., Hu, L., Zhao, Y. T., Wang, H. P., Huang, X. Z., Chen, G. J., et al. (2021). Meltwater-driven water-level fluctuations of Bosten Lake in arid China over the past 2,000 years. *Geophys. Res. Lett.* 48:2020GL090988. doi: 10.1029/2020GL090988

Li, X. Y., Xu, H. Y., Sun, Y. L., Zhang, D. S., and Yang, Z. P. (2007). Lake-level change and water balance analysis at Lake Qinghai, West China during recent decades. *Water Resour. Manag.* 21, 1505–1516. doi: 10.1007/s11269-006-9096-1

Liu, M. K., Han, X., Tong, J., Zhu, H. F., and Bai, X. H. (2020). Mutual environmental drivers of the community composition, functional attributes and co-occurrence patterns

of bacterioplankton in the composite aquatic ecosystem of Taihu watershed in China. *FEMS Microbiol. Ecol.* 96:fiaa137. doi: 10.1093/femsec/fiaa137

Liu, K. S., Liu, Y. Q., Jiao, N. Z., Xu, B. Q., Gu, Z. Q., Xing, T. T., et al. (2017). Bacterial community composition and diversity in Kalakuli, an alpine glacial-fed lake in Muztagh Ata of the westernmost Tibetan plateau. *FEMS Microbiol. Ecol.* 93:138398. doi: 10.1093/femsec/fix085

Liu, Y. Q., Priscu, J. C., Yao, T. D., Vick-Majors, T. J., Michaud, A. B., Jiao, N. Z., et al. (2014). A comparison of pelagic, littoral, and riverine bacterial assemblages in Lake Bangongco, Tibetan plateau. *FEMS Microbiol. Ecol.* 89, 211–221. doi: 10.1111/1574-6941.12278

Liu, C. Q., Wu, F., Jiang, X. Y., Hu, Y., Shao, K. Q., Tang, X. M., et al. (2022). Salinity is a key determinant for the microeukaryotic community in lake ecosystems of the inner Mongolia plateau, China. *Front. Microbiol.* 13:841686. doi: 10.3389/fmicb.2022.841686

Liu, L., Yang, J., Yu, Z., and Wilkinson, D. M. (2015). The biogeography of abundant and rare bacterioplankton in the lakes and reservoirs of China. *ISME J.* 9, 2068–2077. doi: 10.1038/ismej.2015.29

Loke, L. H. L., and Chisholm, R. A. (2023). Unveiling the transition from niche to dispersal assembly in ecology. *Nature* 618, 537–542. doi: 10.1038/s41586-023-06161-x

Louca, S., Polz, M. F., Mazel, F., Albright, M. B. N., Huber, J. A., O'Connor, M. I., et al. (2018). Function and functional redundancy in microbial systems. *Nat. Ecol. Evol.* 2, 936–943. doi: 10.1038/s41559-018-0519-1

Manna, V., Fabbro, C., Cerino, F., Bazzaro, M., Del Negro, P., and Celussi, M. (2019). Effect of an extreme cold event on the metabolism of planktonic microbes in the northernmost basin of the Mediterranean Sea. *Estuar. Coast. Shelf Sci.* 225:106252. doi: 10.1016/j.ecss.2019.106252

Mohapatra, M., Behera, P., Kim, J. Y., and Rastogi, G. (2019). Seasonal and spatial dynamics of bacterioplankton communities in a oligosaline water coastal lagoon. *Sci. Total Environ.* 705:134729. doi: 10.1016/j.scitotenv.2019.134729

Newton, R. J., Kent, A. D., Triplett, E. W., and McMahon, K. D. (2006). Microbial community dynamics in a humic lake: differential persistence of common freshwater phylotypes. *Environ. Microbiol.* 8, 956–970. doi: 10.1111/j.1462-2920.2005.00979.x

Niu, Y., Yu, H., and Jiang, X. (2015). Within-lake heterogeneity of environmental factors structuring bacterial community composition in lake Dongting, China. *World J. Microbiol. Biotechnol.* 31, 1683–1689. doi: 10.1007/s11274-015-1917-z

Nuy, J. K., Hoetzinger, M., Hahn, M. W., Beisser, D., and Boenigk, J. (2020). Ecological differentiation in two major freshwater bacterial taxa along environmental gradients. *Front. Microbiol.* 11:154. doi: 10.3389/fmicb.2020.00154

Pilla, R. M., Mette, E. M., Williamson, C. E., Adamovich, B. V., Adrian, R., Anneville, O., et al. (2021). Global data set of long-term summertime vertical temperature profiles in 153 lakes. *Sci. Data* 8:200. doi: 10.1038/s41597-021-00983-y

Qin, B., Paerl, H. W., Brookes, J. D., Liu, J., Jeppesen, E., Zhu, G., et al. (2019). Why Lake Taihu continues to be plagued with cyanobacterial blooms through 10 years (2007–2017) efforts. *Sci. Bull.* 64, 354–356. doi: 10.1016/j.scib.2019.02.008

Ren, Z., Zhang, C., Li, X., Ma, K., and Cui, B. S. (2022). Abundant and rare bacterial taxa structuring differently in sediment and water in thermokarst lakes in the yellow river source area, Qinghai-Tibet Plateau. *Front. Microbiol.* 13:774514. doi: 10.3389/fmicb.2022.774514

Rose, J. M., and Caron, D. A. (2007). Does low temperature constrain the growth rates of heterotrophic protists? Evidence and implications for algal blooms in cold waters. *Limnol. Oceanogr.* 52, 886–895. doi: 10.4319/lo.2007.52.2.0886

Shen, Z., Xie, G., Zhang, Y., Yu, B., Shao, K., Gao, G., et al. (2022). Similar assembly mechanisms but distinct co-occurrence patterns of free-living vs. particle-attached bacterial communities across different habitats and seasons in shallow, eutrophic Lake Taihu. *Environ. Pollut.* 314:120305. doi: 10.1016/j.envpol.2022.120305

Shi, Y., Delgado-Baquerizo, M., Li, Y., Yang, Y., Zhu, Y.-G., Peñuelas, J., et al. (2020). Abundance of kinless hubs within soil microbial networks are associated with high functional potential in agricultural ecosystems. *Environ. Int.* 142:105869. doi: 10.1016/j.envint.2020.105869

Sloan, W. T., Lunn, M., Woodcock, S., Head, I. M., Nee, S., and Curtis, T. P. (2006). Quantifying the roles of immigration and chance in shaping prokaryote community structure. *Environ. Microbiol.* 8, 732–740. doi: 10.1111/j.1462-2920.2005.00956.x

Song, J., Qu, B., Li, X., Yuan, H., Li, N., and Duan, L. (2018). Carbon sinks/sources in the yellow and East China seas—air-sea interface exchange, dissolution in seawater, and burial in sediments. *Sci. China Earth Sci.* 61, 1583–1593. doi: 10.1007/s11430-017-9213-6

Spain, A. M., Krumholz, L. R., and Elshahed, M. S. (2009). Abundance, composition, diversity and novelty of soil Proteobacteria. *ISME J.* 3, 992–1000. doi: 10.1038/ismej.2009.43

Sunagawa, S., Coelho, L. P., Chaffron, S., Kultima, J. R., Labadie, K., Salazar, G., et al. (2015). Tara oceans, structure and function of the global ocean microbiome. *Science* 348:1261359. doi: 10.1126/science.1261359

Tang, X., Xie, G., Shao, K., Bayartu, S., Chen, Y., and Gao, G. (2012). Influence of salinity on the bacterial community composition in Lake Bosten, a large oligosaline lake in arid northwestern China. *Appl. Environ. Microbiol.* 78, 4748–4751. doi: 10.1128/AEM.07806-11

Tang, X., Xie, G., Shao, K., Dai, J., Chen, Y., Xu, Q., et al. (2015). Bacterial community composition in oligosaline Lake Bosten: low overlap of betaproteobacteria and bacteroidetes with freshwater ecosystems. *Microbes Environ.* 30, 180–188. doi: 10.1264/jsme2.ME14177

Wang, Y. J., and Qin, D. H. (2017). Influence of climate change and human activity on water resources in arid region of Northwest China: an overview. *Adv. Clim. Chang. Res.* 8, 268–278. doi: 10.1016/j.accre.2017.08.004

Williams, W. D. (1999). Salinisation: a major threat to water resources in the arid and semi-arid regions of the world. *Lakes Reserv.* 4, 85–91. doi: 10.1046/j.1440-1770.1999.00089.x

Williamson, C. E., Saros, J. E., Vincent, W. F., and Smol, J. P. (2009). Lakes and reservoirs as sentinels, integrators, and regulators of climate change. *Limnol. Oceanogr.* 54, 2273–2282. doi: 10.4319/lo.2009.54.6_part_2.2273

Xiao, Z., Li, H., Li, X. C., Li, R. H., Huo, S. L., and Yu, G. L. (2022). Geographic pattern of phytoplankton community and their drivers in lakes of middle and lower reaches of Yangtze River floodplain, China. *Environ. Sci. Pollut. Res.* 29, 83993–84005. doi: 10.1007/s11356-022-21657-1

Xie, G. J., Tang, X. M., Gong, Y., Shao, K. Q., and Gao, G. (2020). How do planktonic particle collection methods affect bacterial diversity estimates and community composition in oligo-, meso- and eutrophic lakes? *Front. Microbiol.* 11:593589. doi: 10.3389/fmicb.2020.593589

Xie, G. J., Tang, X. M., Shao, K. Q., Zhu, G. W., and Gao, G. (2021). Bacterial diversity, community composition and metabolic function in Lake Tianmuhu and its dammed river: effects of domestic wastewater and damming. *Ecotoxicol. Environ. Saf.* 213:112069. doi: 10.1016/j.ecoenv.2021.112069

Yannarell, A. C., Kent, A. D., Lauster, G. H., Kratz, T. K., and Triplett, E. W. (2003). Temporal patterns in bacterial communities in three temperate lakes of different trophic status. *Microb. Ecol.* 46, 391–405. doi: 10.1007/s00248-003-1008-9

Yao, J., Chen, Y., Zhao, Y., and Yu, X. (2018). Hydroclimatic changes of Lake Bosten in Northwest China during the last decades. *Sci. Rep.* 8:9118. doi: 10.1038/s41598-018-27466-2

Yuan, M. M., Guo, X., Wu, L. W., Zhang, Y., Xiao, N. J., Ning, D. L., et al. (2021). Climate warming enhances microbial network complexity and stability. *Nat. Clim. Chang.* 11, 343–348. doi: 10.1038/s41558-021-00989-9

Zahran, S. A., Ali-Tammam, M., Ali, A. E., and Aziz, R. K. (2021). Compositional variation of the human fecal microbiome in relation to azo-reducing activity: a pilot study. *Gut Pathog.* 13:58. doi: 10.1186/s13099-021-00454-0

Zeng, J., Lin, Y. Q., Zhao, D. Y., Huang, R., Xu, H. M., and Jiao, C. C. (2019). Seasonality overwhelms aquacultural activity in determining the composition and assembly of the bacterial community in Lake Taihu, China. *Sci. Total Environ.* 683, 427–435. doi: 10.1016/j.scitotenv.2019.05.256

Zhang, L., Shen, T., Cheng, Y., Zhao, T., Li, L., and Qi, P. (2020). Temporal and spatial variations in the bacterial community composition in Lake Bosten, a large, oligosaline lake in China. *Sci. Rep.* 10:304. doi: 10.1038/s41598-019-57238-5

Zhao, D. Y., Cao, X. Y., Huang, R., Zeng, J., Shen, F., Xu, H. M., et al. (2017). The heterogeneity of composition and assembly processes of the microbial community between different nutrient loading lake zones in Taihu Lake. *Appl. Microbiol. Biotechnol.* 101, 5913–5923. doi: 10.1007/s00253-017-8327-0

Zhu, M., Zhu, G., Zhao, L., Yao, X., Zhang, Y., Gao, G., et al. (2013). Influence of algal bloom degradation on nutrient release at the sediment–water interface in Lake Taihu, China. *Environ. Sci. Pollut. Res.* 20, 1803–1811. doi: 10.1007/s11356-012-1084-9

frontiers | Frontiers in Microbiology

TYPE Original Research
PUBLISHED 22 November 2023
DOI 10.3389/fmicb.2023.1305345

OPEN ACCESS

EDITED BY
Yizhi Sheng,
China University of Geosciences, China

REVIEWED BY
Yuying Li,
Nanyang Normal University, China
Alain Isabwe,
University of Michigan, United States

*CORRESPONDENCE
Wenbao Li
✉ tianshiTD@126.com

RECEIVED 01 October 2023
ACCEPTED 10 November 2023
PUBLISHED 22 November 2023

CITATION
Shi Y, Li W and Guo X (2023) Composition, interaction networks, and nitrogen metabolism patterns of bacterioplankton communities in a grassland type Lake: a case of Hulun Lake, China.
Front. Microbiol. 14:1305345.
doi: 10.3389/fmicb.2023.1305345

Composition, interaction networks, and nitrogen metabolism patterns of bacterioplankton communities in a grassland type Lake: a case of Hulun Lake, China

Yujiao Shi[1], Wenbao Li[1,2]* and Xin Guo[1]

[1]Water Conservancy and Civil Engineering College, Inner Mongolia Agricultural University, Hohhot, China, [2]Inner Mongolia Key Laboratory of Protection and Utilization of Water Resources, Hohhot, China

The composition of bacterial communities in freshwater ecosystems is influenced by numerous factors including environmental conditions and biological interactions. In grassland inland closed lakes, factors affecting lake ecosystems are either exogenous or endogenous, contributing to the formation of distinct habitats in the surface and bottom waters of the bacterial communities. However, the extent to which environmental factors selectively shape the bacterial communities in aquatic systems remains unclear. Therefore, we sampled the surface, middle, and bottom waters at 13 sampling points in each layer. High-throughput sequencing techniques were employed to examine the spatial heterogeneity of the bacterial community structure during summer in Hulun Lake, the largest grassland-type lake in Inner Mongolia, China, to determine the microbial community dynamics and symbiosis patterns under different habitat conditions. Our results revealed a decrease in the diversity and heterogeneity of the bacterioplankton community, influenced by changes in the environment from exogenous inputs to endogenous releases. Furthermore, this alteration in community structure was concomitant with enhanced co-occurrences among microorganisms in the bottom water layers. This finding suggests that endogenous release promotes heightened symbiotic interactions, thereby facilitating the development of more complex modular structures. Symbiotic networks in different layers were differentiated by key species, with the ecological clustering modules of these species demonstrating dissimilar environmental preferences. The microbial communities were highly habitat-specific, mimicking responses to total nitrogen (TN) in the surface layer, pH in the middle layer, and chemical oxygen demand (COD) in the bottom layer. Bacterioplankton functions were assessed using Tax4Fun, indicating exogenous inputs and endogenous release increased the relative abundance of genes with nitrogen-fixing and nitrification potential nitrogen metabolism functions in surface and bottom waters, respectively. With Planctomycetota and Proteobacteria phyla as potential key groups for regulating nitrogen metabolic processes, Proteobacteria may facilitate the depletion of nitrate in surface and bottom waters, while the close contact of surface waters with the atmosphere accelerated Planctomycetota-dominated nitrogen fixation into the lake. Our findings contribute to the understanding of vertical microbial diversity and its network patterns in grassland type lakes, underscoring the potential role of environmental factors (exogenous inputs and endogenous releases) in bacterioplankton community formation.

KEYWORDS

water ecosystems, co-occurrence network, potential function, community structure, environmental preferences

1 Introduction

Among the diverse life forms on Earth, bacteria are characterized by their taxonomic diversity, ubiquitous distribution, and intricate interaction networks. They play a crucial role in mediating metabolic processes within biogeochemical cycles, thereby significantly contributing to ecosystem stability and ecological functionality (Liu et al., 2021; Wu et al., 2021). Bacterioplankton serve not only as an integral component of lake ecosystems but also as a key indicator for water quality assessment (van de Graaf et al., 1995; Karpowicz et al., 2012; Shang et al., 2022). They facilitate the efficient functioning of lake ecosystems by participating in the cycling of chemical elements, such as nitrogen, within the water column (Tammert et al., 2015; Grover, 2017; Gu et al., 2020; Wang Y. B. et al., 2020). Various studies have demonstrated that bacterioplankton community structure is affected by different environmental indicators. De Menezes et al. (2015) discovered a relationship between community composition and variables such as moisture, and nitrogen. Zhang L. Y. et al. (2021) suggested that community diversity significantly affects total nitrogen (TN). Wahdan et al. (2023) identified a correlation between the relative abundance of microorganisms and chemical composition. These findings indicate that the use of bacteria as indicators for monitoring the evolution of aquatic environments is highly sensitive to environmental changes and has substantial implications for the health of lake ecosystems (Swift et al., 1979; Bertilsson et al., 2007; Dumbrell et al., 2010).

Lakes in Inner Mongolia serve as critical water resources in the ecologically vulnerable regions of northern China, fulfilling essential roles in economic development, ecological balance, and environmental conservation (Li et al., 2019). Hulun Lake, the largest lake in Inner Mongolia, is representative of grassland-type lakes in the high-latitude, cold, and arid regions. It is vital for climate regulation, water resource protection, desertification prevention, and the maintenance of grassland ecosystem equilibrium (Zhang et al., 2020). Because of its unique geographical location, the primary nutrient sources for the lake are dried grass from the expansive Hulunbeier grassland, municipal wastewater, and animal feces, mainly from cattle and sheep (Chen et al., 2021). These nutrients are transported into the lake by rivers and winds, resulting in what is known as exogenous inputs, and these exogenous inputs lead to increased levels of organic pollutants in the surface waters. It documented that Hulun Lake has been in a state of eutrophication since the 1980s (Wang, 2006; Michael and Jörg, 2008; Chuai et al., 2012; Quiza et al., 2014). In addition, extensive research has indicated that sediments act as a "source" of nutrients in the water column. Nutrients stored in sediments are continuously released into upper water layers (Nikolai and Dzialowski, 2014; Zhang H. G. et al., 2021). This endogenous release of sediments makes the environment stratified between the bottom and surface layers (Zhang et al., 2016; Dong et al., 2019; Khabouchi et al., 2020; Wang et al., 2023). Therefore, these aquatic ecosystems provide an optimal option for investigating environmental sensitivities and habitat preferences of bacterial communities.

Although incremental progress has been made in studies concerning the distribution patterns of elements and bacterioplankton in eutrophic grassland-type lakes, such as Hulun Lake (Wang et al., 2018; Zhang et al., 2019; Shang et al., 2020), existing research largely lacks mechanistic explanations for how the bacterioplankton community responds to variations in the aquatic environment attributable to exogenous inputs and endogenous releases. This gap presents a considerable challenge for ecologists aiming to establish ecological criteria for lakes, particularly with respect to interactions between nutrients and microorganisms. Therefore, an in-depth analysis of the dynamics and structure of the bacterioplankton community in Hulun Lake, as an integral component of the aquatic ecosystem, would yield valuable insights for more effective freshwater lake management (Dimitry et al., 2014).

To address these knowledge gaps, in this study, we investigated bacterial diversity, environmental drivers, and nitrogen functioning patterns in aquatic systems influenced by both exogenous inputs and endogenous releases. Moreover, we examined the symbiotic relationships within bacterial communities. Specifically, within the context of grassland-confined inland lakes affected by both exogenous inputs and endogenous releases, three research questions were posed. (1) Do bacterial communities in the surface, middle, and bottom water columns exhibit differences in diversity and structure? (2) Do different environmental drivers affect the structure and nitrogen metabolism patterns of the coexisting bacterial communities? (3) Do symbiotic relationships and associated environmental preferences among these bacterial communities vary across different water layers?

Building on the aforementioned knowledge gaps, this study focused on Hulun Lake as the study area. Using high-throughput sequencing technology, we investigated the response relationships between environmental shifts caused by both exogenous inputs and endogenous releases, and the micro-ecological system of the lake. Employing a stratified sampling approach during the summer months, we combined changes in typical physicochemical indicators and nutrient elements across the surface, middle, and bottom water layers. This facilitated examination of the structural evolution of the dominant phyla and genera in the bacterioplankton community at varying depths. Additionally, we explored variations in the ecological structure of these bacterioplankton communities. The aim was to promote limited micro-ecological studies on Hulun Lake while providing a theoretical foundation for understanding its environmental evolution.

2 Materials and methods

2.1 Study lake

Hulun Lake (116°58′–117°48′E, 48°33′–49°20′N) is located in Hulunbeier City in northern China and southern Mongolia, across

Beier Lake. It lies 57 km from the China–Mongolia western border and 15 km from Russia to the north, which is at the junction of China, Mongolia, and Russia. Recognized as the premier freshwater lake in northern China, Hulun Lake is a unique natural asset with biodiversity and ecological multifunctionality unparalleled globally in cold and arid regions (Zhang et al., 2017; Li et al., 2020). Its topography is irregularly sloping and elongated, flanked by expansive grasslands and a flat terrain. It covers an approximate surface area of 2,043 km^2 and exhibits climatic characteristics such as a multi-year average temperature of −0.60°C, precipitation of 352.30 mm, evaporation of 1549.80 mm, and wind speed of 3.45 m/s (Li et al., 2019; Wang W. L. et al., 2020). Influenced primarily by the mid-temperate continental monsoon climate, the region experiences pronounced seasonal variability, including short spring and summer seasons and prolonged winter. Precipitation is concentrated from late June to early August (Zhao et al., 2017). Regarding water recharge, the lake primarily receives inflows from the Kelulun River, Wuerxun River, and Hailaer River, in addition to precipitation (Figure 1). The water supply is crucial for the preservation of grassland biodiversity and ecological integrity (Li et al., 2019).

2.2 Sample collection

Prior to the main study, a preliminary survey was conducted to identify 13 sampling sites (H1–H13) arranged from north to south for summer water sample collection in August 2021 covering the entire lake. Water samples were collected at three different depths: upper (0–15 cm below the water surface), middle (half the depth of the water column), and lower (10–50 cm above the sediment–water interface). The samples were collected using a water extraction device with a 1 L sterile polyethylene bottle employed as the collection device. Pre-disinfected with ultrapure water and alcohol, each bottle was rinsed three times with water from the respective sampling point before sample collection. Three bottles were secured from each point, refrigerated, and promptly transported to the laboratory for analysis. Concurrent with sample collection, a multi-parameter water quality monitor was used to measure various physicochemical indicators. These examples were used for the determination of nutrients in the water column and collection of bacterioplankton.

2.3 Measurement of environmental factors

At each sampling site, key physicochemical parameters, namely water temperature (WT), electrical conductivity (EC), pH, dissolved oxygen (DO), salinity (SAL), oxidation–reduction potential (ORP), and total dissolved solids (TDS), were measured using a multi-parameter water quality monitor. Laboratory analyses were conducted to quantify nutrient concentrations, including free-state ammonia nitrogen (NH_4^+-N), TN, chlorophyll-a (Chla), total phosphorus (TP), dissolved inorganic phosphorus (DIP), total dissolved phosphorus (TDP), and total organic matter (COD), in accordance with standard methods.

2.4 Sample processing, DNA extraction, and PCR amplification

Genomic DNA from microbial communities was extracted from water samples using a DNA Kit (Omega Bio-tek, Norcross, GA, United States) according to the manufacturer's instructions. DNA quality and concentration were assessed using a 1% agarose gel and quantified using a NanoDrop 2000 UV–Vis spectrophotometer (Thermo Scientific, Wilmington, United States). The V3–V4 hypervariable region of the bacterial 16S rRNA gene was amplified using primers 338F (5′-ACTCCTACGGGAGGCAGCAG-3′) and 806R (5′-GGACTACHVGGGTWTCTAAT-3′) on an ABI GeneAmp® 9700 PCR thermocycler (ABI, CA, United States) (Walters et al., 2016). PCR amplification of the 16S rRNA gene was performed using the following thermal profile: initial denaturation at 95°C for 3 min, followed by 27 cycles of denaturation at 95°C for 30 s, annealing at

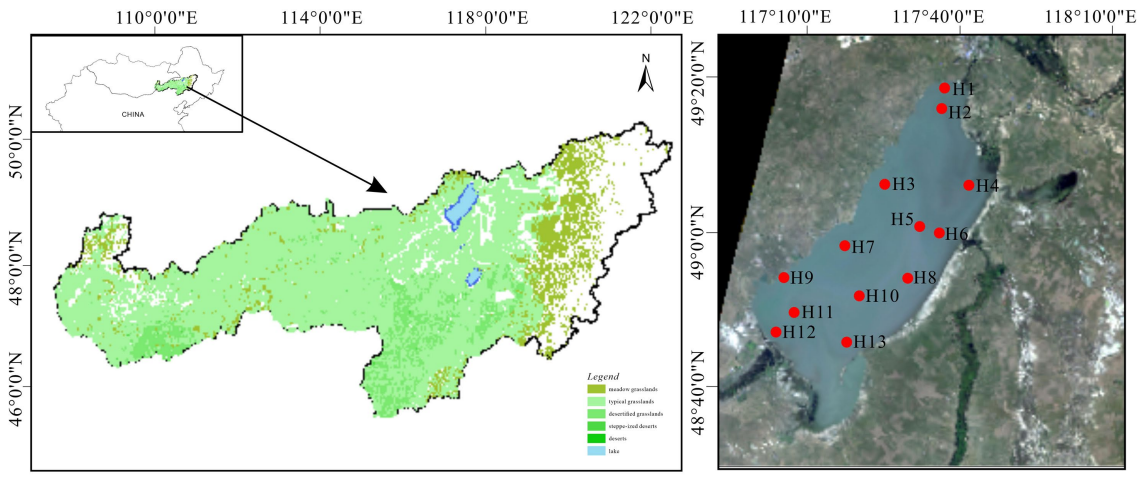

FIGURE 1
Geographical location of Hulun Lake and sampling site distribution.

55°C for 30 s, and extension at 72°C for 45 s, followed by a final extension at 72°C for 10 min, and termination at 4°C. The PCR mixture was composed of 4 μL of 5 × TransStart FastPfu buffer, 2 μL of 2.5 mM dNTPs, 0.8 μL each of 5 μM forward and reverse primers, 0.4 μL of TransStart FastPfu DNA Polymerase, 10 ng of template DNA, and ddH_2O to achieve a final volume of 20 μL. The reactions were performed in triplicates. After amplification, the PCR products were extracted from a 2% agarose gel, purified using an AxyPrep DNA Gel Extraction Kit (Axygen Biosciences, Union City, CA, United States) according to the manufacturer's instructions, and quantified using a Quantus™ Fluorometer (Promega, United States).

2.5 Illumina MiSeq sequencing

Purified amplicons were pooled in equimolar ratios and subjected to paired-end sequencing on an Illumina MiSeq PE300 or NovaSeq PE250 platform (Illumina, San Diego, CA, United States), based on the standard protocols provided by Majorbio Bio-Pharm Technology Co. Ltd. (Shanghai, China).

2.6 Processing of sequencing data

Raw 16S rRNA gene sequencing reads were demultiplexed and quality-filtered using fastp version 0.20.0 (Chen et al., 2018), and subsequently merged with FLASH version 1.2.7 (Mago and Salzberg, 2011). The quality filtering and merging criteria were as follows: (i) reads of 300 bp were truncated if any site displayed an average quality score lower than 20 across a 50 bp sliding window, if truncated reads were shorter than 50 bp, or if reads containing ambiguous characters, they were discarded; (ii) only overlapping sequences exceeding 10 bp were assembled based on their overlapping regions, with a maximum mismatch ratio set at 0.2. Unassembled reads were discarded; and (iii) samples were distinguished by barcode and primer sequences, with sequence direction adjusted accordingly, employing exact barcode matching and allowing for a two-nucleotide mismatch in primer matching.

Operational taxonomic units (OTUs) were clustered using UPARSE version 7.1 (Edgar, 2013) with a 97% similarity cut-off (Stackebrandt and Goebel, 1994; Edgar, 2013), and chimeric sequences were removed. Taxonomic analysis for each representative OTU sequence was performed using the RDP Classifier version 2.2 (Wang et al., 2007) against the 16S rRNA database (e.g., Silva v138), using a confidence threshold of 0.7.

2.7 Data analysis and statistics

Alpha diversity indices, including Good's coverage, Chao1, Shannoneven, Shannon and phylogenetic diversity, were evaluated at a 97% OTU similarity level using mothur (version v.1.30.2). Venn diagram analysis was performed using R language (version 3.3.1) for statistical analysis and graphing. Community composition differences were assessed using the Kruskal-Wallis rank sum test, while beta diversity distance matrices were computed using Qiime. NMDS plots based on Bray-Curtis distances were generated using the R language (version 3.3.1) vegan package. Distance redundancy analysis (RDA) and Mantel tests were conducted for variance classification and genus abundance data assessment, respectively. These analyses were performed using the "vegan" package in R. The genus and environmental variables were fitted to ordination plots to assess the relative significance of each environmental factor in elucidating community variation using the goodness-of-fit statistic (R^2) ($p < 0.05$). To reduce the complexity of the ecological network, only the top 500 genera were selected based on their relative abundance across different water depths. Network metrics, such as mean node degree, clustering coefficient, mean path length, modularity, network density, and network diameter, were calculated and visualized using Gephi (version 0.9.2). Subsequent analyses were conducted to identify the microbial modules in the underlying water and their association with water quality metrics. Following log-transformation and normalization of the environmental variables, Spearman correlations were calculated, considering $p < 0.05$, as indicative of a valid relationship. Taxonomic profiling was performed by converting 16S rRNA sequences based on the Silva database into the corresponding prokaryotic profiles in the KEGG database. The normalization of prokaryotic abundance in the corresponding KEGG database was performed using the 16S copy numbers. Finally, we employed homogenized abundance data and combined the correspondence between the prokaryotes in the KEGG database and the 16S taxonomic profiles in the Silva database to identify and quantify the different functional genes involved in nitrogen metabolism within the microbial communities. To assess the impact of dominant phyla on these functional genes, correlation analyses were conducted to determine the correlation between both using *p*-values. All statistical analyses were performed using Origin version 2023.

3 Results

3.1 Environmental characterization

Figure 2 presents the comprehensive environmental parameters of Hulun Lake water sampled at various depths. Owing to the influence of multiple factors, the physicochemical properties of the surface, middle, and bottom water samples from the Hulun Lake varied to some extent. By measuring seven indicators, including physicochemical and nutrient elements, the results revealed that pH and TN concentrations were the highest in the surface water of the lake (mean values of approximately 9.12 and 3.37 mg/L, respectively) and the lowest in the middle water of the lake (mean values of approximately 9.11 and 3.19 mg/L, respectively). The ORP levels increased from the surface to the bottom, reaching a peak mean value of approximately −223.93 mV in the bottom layer. Conversely, DO and COD demonstrated a declining trend from surface to bottom, with minimum mean values of 5.58 mg/L and 88.41 mg/L, respectively, in the bottom layer. The SAL remained relatively stable in the middle and bottom layers, but was lowest in the surface layer, with a mean value of approximately 0.81 mg/L. Overall, horizontal variations were observed in the physicochemical indicators. Specifically, NH_4^+-N in the middle water column exhibited significant fluctuations and outlier values, whereas the remaining indicators exhibited relatively stable distributions (Figure 2).

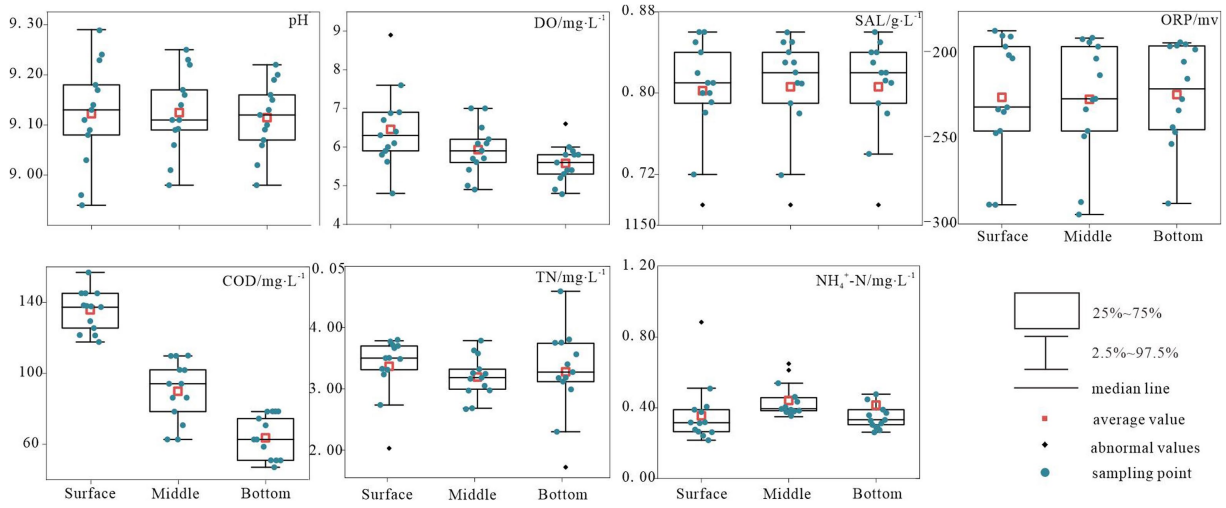

FIGURE 2
Variation characteristics of typical physicochemical indices in Hulun Lake.

3.2 Abundance and α-diversity of bacterioplankton in Hulun Lake

To elucidate the variations in bacterial communities across different depths in the water column of Hulun Lake, we employed NMDS maps to depict species composition similarities. Additionally, the Chao, Shannoneven, and Shannon indices were utilized to rigorously examine community richness, evenness, and diversity in alpha diversity. These analyses provided insights into the distribution characteristics of bacterioplankton communities in the surface, middle, and bottom water layers of Hulun Lake.

NMDS analysis utilizing the Bray-Curtis distance algorithm demonstrated depth-dependent horizontal heterogeneity in water samples. Notably, variations within bacterioplankton communities decreased along a gradient from the surface layer to the bottom layer. Furthermore, community dispersion was significantly lower in the bottom layer than in the other two layers, accompanied by an increase in both community similarity and overall structure with increasing depth. The vertical variability in the structure of the bacterioplankton community indicated that the water depth had a profound influence on the structure of the bacterioplankton communities (Figure 3A).

The Coverage index values for all sample libraries exceeded 99%, indicating that the generated sequences adequately represented microbial communities at the study sites. Higher values of the Chao, Shannoneven, and Shannon indices, representing alpha diversity characteristics, demonstrated higher abundance, homogeneity, and diversity within the bacterioplankton communities. As depicted in Figure 3D, a depth-dependent increase in the Chao index was observed, indicating the lowest bacterioplankton abundance in surface water and the highest abundance in bottom water. Conversely, the lowest Shannoneven and Shannon indices were recorded in the bottom and middle water, respectively. These results suggest that while the bottom layer exhibited high bacterial abundance but an uneven distribution, the middle layer demonstrated the lowest diversity. Interestingly, phylogenetic diversity indices exhibited minor depth-dependent variations and shared OTUs constituted 42.5% of the total OTUs (Figures 3B,D).

Our analysis revealed a notable depth-dependent evolution of the environmental factors affecting bacterioplankton diversity. Specifically, microbial diversity in the surface layer exhibited a strong negative correlation with DO, whereas COD positively influenced the diversity in the bottom layer (Figure 3C; Supplementary Table S1).

3.3 Variation in the response of bacterioplankton composition to lake depth and environmental drivers

The bacterial community composition plays a pivotal role in nutrient cycling and energy transfer in water. Upon collecting and analyzing samples from the surface, middle, and bottom water layers, 10 dominant bacterial phyla were detected in samples where the relative abundance exceeded a 1% threshold. Proteobacteria and Actinobacteria constituted the majority of bacterioplankton OTUs, accounting for a combined relative abundance exceeding 50% across all depths (approximately 42.00 and 21.20% in surface water, 44.70 and 27.50% in midwater, and 49.20 and 30.80% in bottom water, respectively). In contrast, the relative abundance of other dominant phyla, such as Verrucomicrobiota, Bacteroidetes, and Planctomycetota, declined progressively from 11.20, 6.61, and 10.60% in the surface layer to 3.40, 3.13, and 6.26% in the bottom layer, respectively (Figure 4A). Patescibacteria emerged as the most dominant bacterial group, demonstrating a significant depth-dependent variability (Supplementary Table S1).

The dominant bacterial phylum was primarily dominated by five phylotypes with high relative abundance: *hgcI_clade* (attributed to Actinobacteriota), *norank_f__Clade_III* (attributed to Proteobacteria), *CL500-29_marine_group* (attributed to Actinobacteriota), *unclassified_f__Comamonadaceae* (attributed to Proteobacteria), and *norank_f__Pirellulaceae* (attributed to Planctomycetota). Although their relative abundance consistently changed with the depth of the lake, *hgcI_clade*, *norank_f__Clade_III*, *Rhodobacter*, and *Pseudomonas* exhibited the most pronounced changes. Specifically, the relative abundances of *hgcI_clade* and *norank_f__Clade_III* in the surface

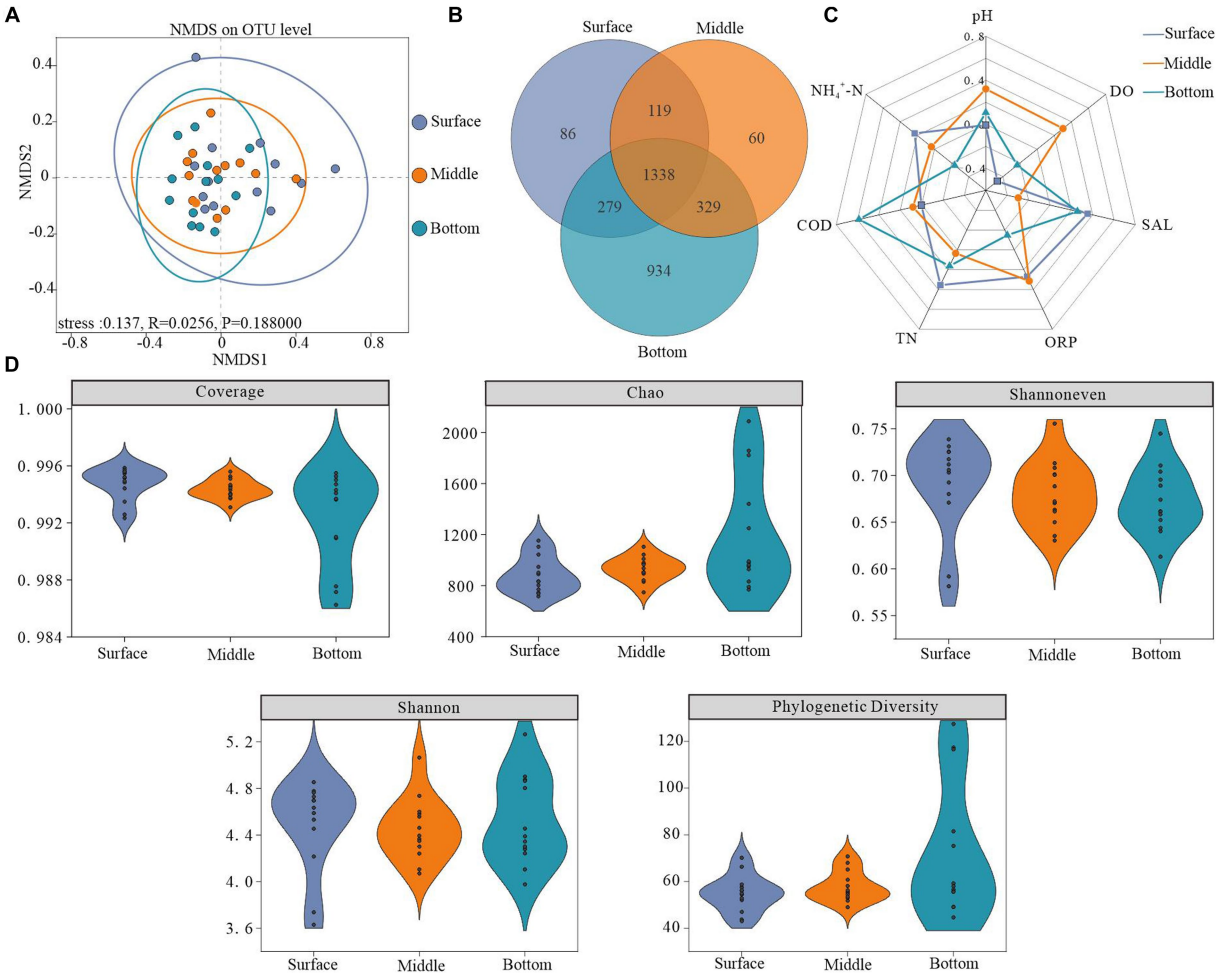

FIGURE 3
Microbial diversity across different depths. **(A)** Non-metric multidimensional scaling analysis (NMDS) based on surface, midwater, and bottom bacterioplankton communities at the OTU level (using the Bray–Curtis dissimilarity matrix), **(B)** number of shared and unique OTUs at different depths, **(C)** radar plot showing factors significantly correlated with bacterioplankton diversity (Pearson's rank correlation, $p < 0.05$), and **(D)** bacterioplankton diversity indices.

waters were 8.43 and 3.97%, respectively, which were significantly lower than those in the middle (13.09 and 6.22%, respectively) and bottom waters (14.66 and 8.46%, respectively). The relative abundance of *hgcI_clade* and *norank_f__Clade_III* increased with water depth, whereas the relative abundance of *norank_f__Pirellulaceae* declined from 6.42 to 2.33% in the surface layer. *CL500-29_marine_group* and *unclassified_f__Comamonadaceae* demonstrated minimal variation and peaked in the middle layer with approximate values of 6.16 and 5.80%, respectively (Figure 4B; Supplementary Table S2). Additionally, we observed that the highest OTUs in relative sequence abundance exhibited considerable variation with increasing lake depth. According to the cumulative relative abundance of the top 20 OTUs, the bacterioplankton community was predominantly characterized by OTU3163 and OTU286. Notably, dominant OTUs exhibited depth-related shifts. For instance, the third most dominant OTU in surface waters shifted from OTU1070 to OTU1425 and OTU996 in middle waters (Figure 4C; Supplementary Table S3).

The relative abundance of dominant microbial species across various layers is closely associated with the trophic status of the lake. In the surface and midwater layers, the dominant phyla, genera, and OTUs exhibited similar environmental responses. pH and TN were the primary factors affecting surface bacterioplankton, whereas pH, SAL, and DO were key determinants of midwater bacterioplankton (Supplementary Figure S1). Conversely, the environmental responsiveness of species at different taxonomic levels in the bottom layer exhibited greater variability. Specifically, the relative abundance of the dominant phyla was primarily influenced by pH, NH_4^+-N, and COD. The dominant genera and OTUs were mainly influenced by pH, NH_4^+-N, ORP, and SAL (Supplementary Figure S1).

The dominant species exhibited similar environmental responsiveness in both the surface and midwater layers. However, in the bottom layer, COD was positively correlated with Verrucomicrobiota, whereas ORP and NH_4^+-N were negatively correlated with the dominant genera. Additionally, pH and SAL were positively correlated with *unclassified_f__Comamonadaceae* and *hgcI_clade* (Supplementary Figure S1). These findings suggest that both external inputs and internal releases influenced not only the

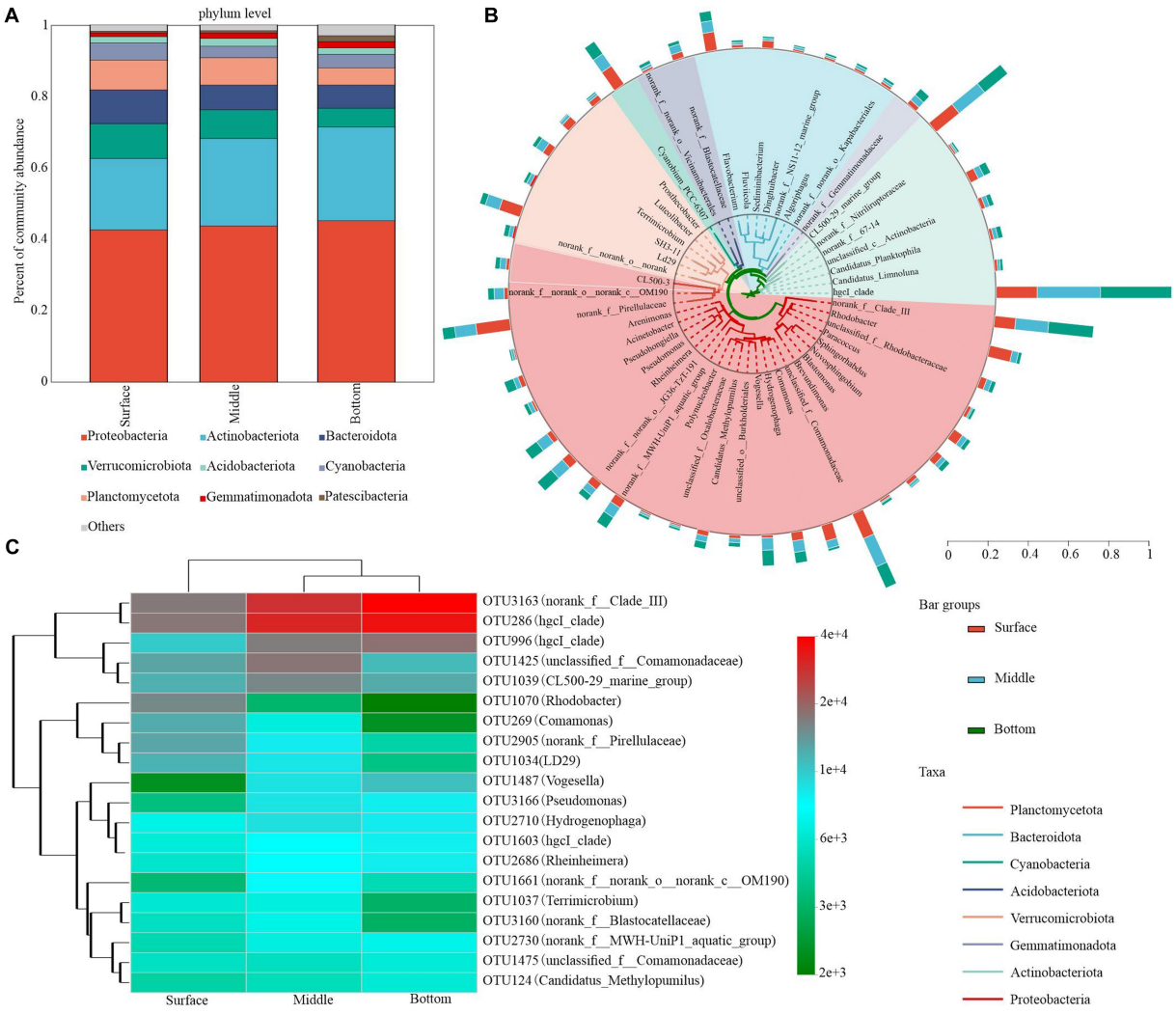

FIGURE 4
Bacterial community composition in water at different depths. **(A)** Phylum level (relative abundance >1%). **(B)** Phylogenetic tree showing the top 50 genera with the highest relative abundances. Taxonomic affiliations of each genus at the phylum level were determined by the color range within the tree. **(C)** Heatmap depicting the dynamics of the top 20 asv species classified at the genus level in the bottom water column of the table.

composition of the bacterioplankton community but also its interaction with environmental factors.

3.4 Vertical shifts in the ecological network structure of bacterioplankton

Network analysis not only provides an excellent exploration of potential interactions among microbial communities but also elucidates the complexities of community structure. Therefore, in this study, the ecosystem network structures of bacterioplankton in the surface, midwater, and benthic layers were constructed based on the top 500 genera and their relative abundances. The results revealed that the surface water network comprised 12,241 edges, with a graph density of 0.098. In contrast, the bottom water network contained 23,093 edges, with a higher graph density of 0.184. However, the middle water network had 10,078 edges and a lower graph density of 0.08, indicating less interconnectivity among the bacterioplankton communities (Supplementary Table S4).

In the surface water samples, Nanoarchaeota (*g_norank_f_GW2011_GWC1_47_15*) exhibited the highest structural contribution and decreased structural contribution in the middle and bottom samples, indicating its pivotal role in stabilizing the bacterial community structure in the surface water (Figure 5A). In the middle water, other phyla, such as Actinobacteriota and Verrucomicrobiota, had greater network contributions than those in the bottom water. In particular, despite their low relative abundances in the bottom water, both Aenigmarchaeota (*g_norank_f_norank_o_Aenigmarchaeales*) and Patescibacteria (*g_norank_f_norank_o_norank_c_WWE3*) made substantial contributions to the ecological network structure (Figures 5B,C).

Subsequent modularization of all network nodes revealed a gradual increase in the number of modules from the surface to the bottom layers, along with variations in the keystone genera across different network structures. From the positions of the modules where

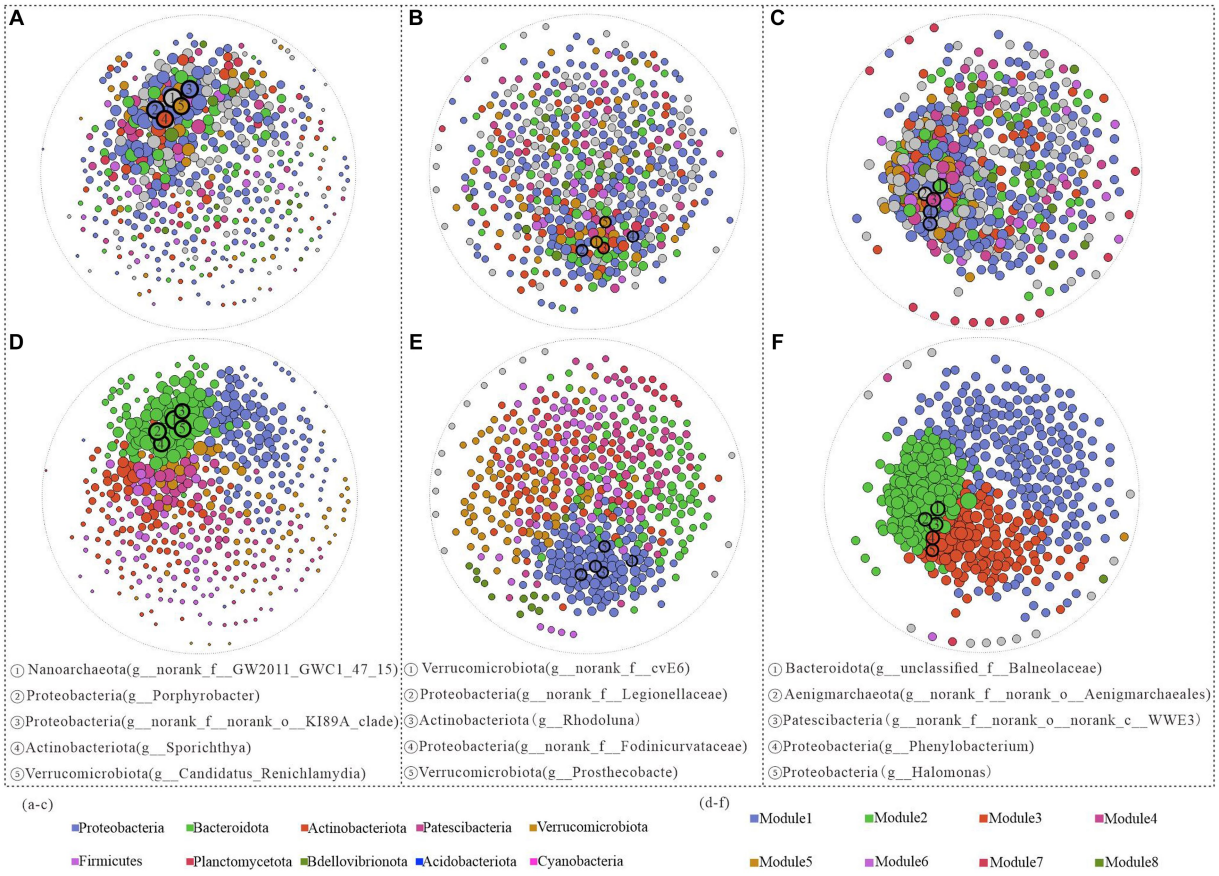

FIGURE 5
Network structure analysis of Hulun Lake based on genus level at different depths. Surface **(A)**, middle **(B)**, and bottom **(C)** water nodes are colored by phylum taxa, and surface **(D)**, middle **(E)**, and bottom **(F)** nodes are colored by module.

all keystone genera were located in both the surface and midwater layers, the top five keystone genera were situated within the same module, but exhibited stronger interactions with each other in the surface layer than in the midwater network (Figures 5D,E). In contrast, the bottom water keystone genera were distributed across distinct modules. Specifically, Bacteroidota (*g_unclassified_f_Balneolaceae*), Aenigmarchaeota (*g_norank_f_norank_o_Aenigmarchaeales*), and Patescibacteria (*g_norank_f_norank_o_norank_c_WWE3*) were located on Module2, while Proteobacteria (*g_Phenylobacterium* and *g_Halomonas*) were situated in Module3. These patterns potentially reflect differences in ecological functionality among these genera (Figure 5F).

As observed in Figure 6, the correlation strength between the network structure and environmental variables was lower in the bottom water of the lake than in the surface and middle waters. In summary, bacterioplankton network modules at varying depths in Hulun Lake exhibited distinct associations with surveyed environmental factors. In the surface layer, Module1 was predominantly influenced by pH and DO, Module2 was significantly affected only by pH, and Module3 was notably impacted by pH, DO, and TN (Figure 6A). In the midwater layer, pH and DO emerged as principal factors shaping the network modules (Figure 6B). In the bottom water, only Module3 was significant correlated with the pH and SAL (Figure 6C).

3.5 Observations on nitrogen function of bacterioplankton at various depths in water

Utilizing KEGG Ortholog groups (KOs) and Tax4Fun, we predicted potential nitrogen metabolism functional profiles for bacterial communities based on the 16S rRNA genes of the retrieved bacterial taxa. Our analysis focused on functional genes associated with nitrification, denitrification, nitrogen fixation, and nitrate reduction. We identified 23 potential nitrogen-related genes, with nitrate reduction genes, particularly K00362 and K00372, demonstrating the highest relative abundance across all functional pathways, followed by denitrification genes (Figure 7A). The surface layer exhibited a significantly higher relative abundance of potential genes for nitrogen fixation than did the bottom layer (Figure 7B). Conversely, potential genes for nitrification were less abundant in the surface layer than in the bottom layer (Figure 7C). The relative abundance of genes associated with denitrification and nitrate reduction remained relatively consistent across different water depths (Figures 7D,E).

In the surface water, the variation in the relative abundance of genes related to potential nitrogen metabolic functions in bacterioplankton was negatively correlated with the phyla Verrucomicrobiota and Planctomycetota and positively correlated

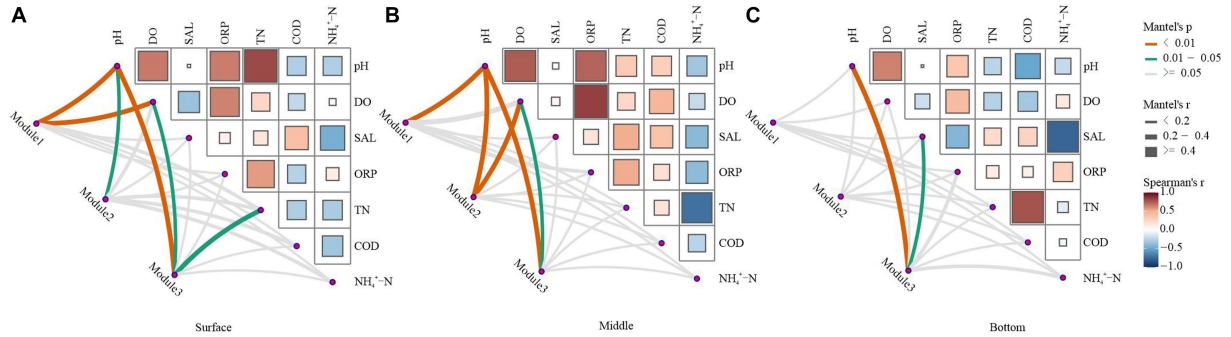

FIGURE 6
Environmental drivers of ecological network modules in water. The top three modules in the ecological network structure, which accounted for over 60% of the total number of modules, were selected and used as key modules to characterize the ecological network structure. Relationships between the surface **(A)**, middle **(B)**, and bottom **(C)** bacterial network modules and the physicochemical properties of water were calculated by Mantel test analysis. The edge width corresponds to the *R*-value, and the edge color indicates statistical significance. Color gradients indicate Pearson correlation coefficients between water physicochemical properties.

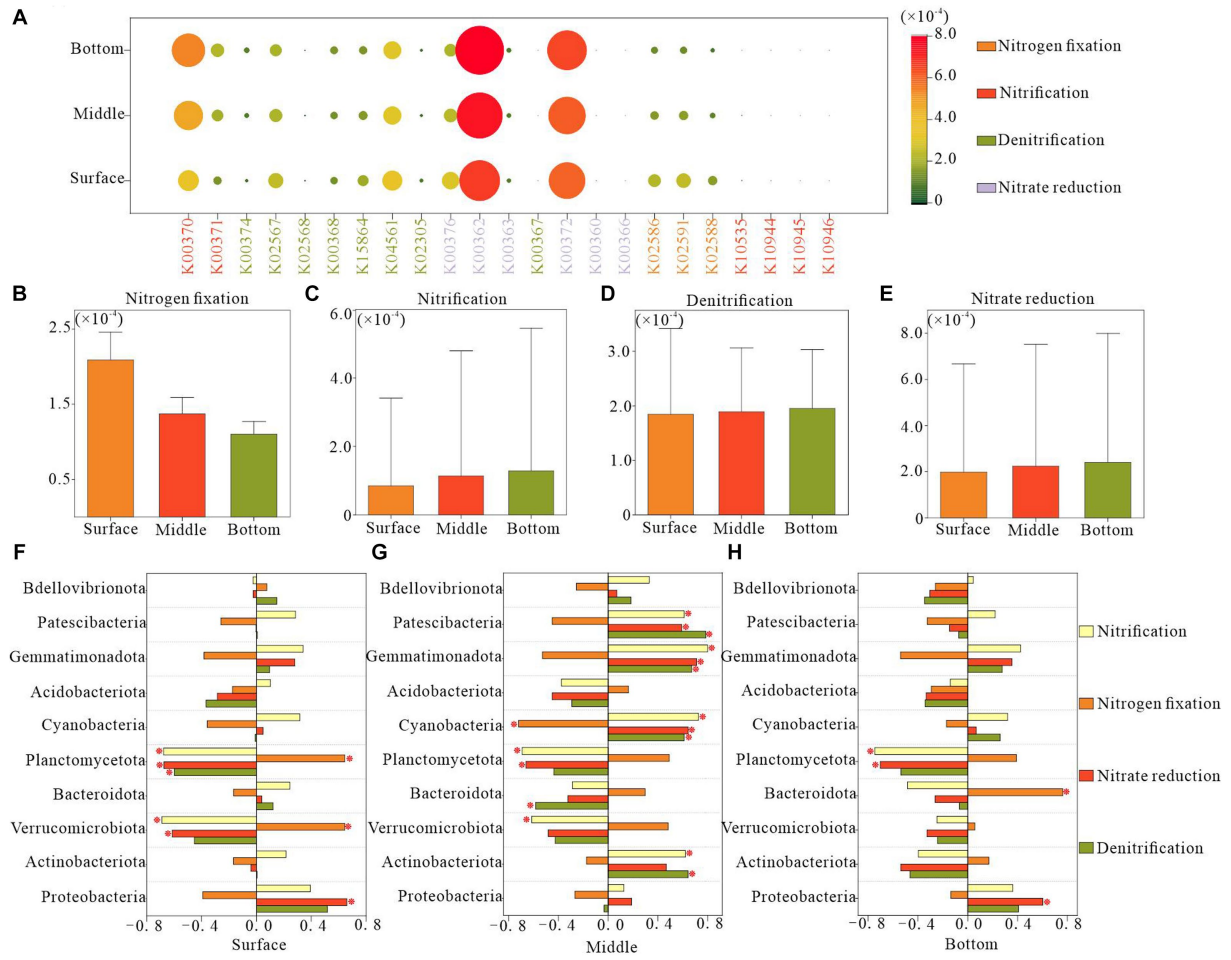

FIGURE 7
Functional genes of nitrogen metabolic pathways in bacterioplankton at different depths of the water column. **(A)** Relative abundance of various nitrogen functional genes, **(B–E)** relative abundance of different nitrogen metabolic process genes, and **(F–H)** correlation between the abundance of nitrogen functional genes and the dominant phyla in bacterioplankton.

with Proteobacteria. In the bottom layer, such correlations were primarily observed for Planctomycetota and Proteobacteria. The midwater bacterioplankton community exhibited the strongest association with nitrogen metabolic functions, specifically involving the phyla Planctomycetota, Cyanobacteria, Gemmatimonadota, and Patescibacteria. These findings indicated the pivotal role of these

bacterioplankton taxa in the regulation of nitrogen metabolism (Figures 7F–H).

4 Discussion

Hulun Lake, a typical grassland inland lagoon, primarily receives recharge from atmospheric precipitation, groundwater, and rivers. During summer, increased rainfall contributes to more urban wastewater, animal manure, and hay entering the lake via rivers. In contrast, rising temperatures enhance the primary productivity of the lake, facilitating the release of bottom sediments. These seasonal variations have significantly altered the environmental conditions of the lake. In this study, we conducted a comprehensive analysis of the vertical variations in bacterioplankton community structure across different depths in Hulun Lake. Both exogenous inputs and endogenous releases affected the nutrient dynamics of the lake surface and bottom water environment, with the microbial community structure demonstrating variability at smaller taxonomic units, such as bacterial genera and OTUs. In addition, these alterations also affected the complexity of microbial network interactions. Our findings advanced the understanding of the ecological processes shaping this lake ecosystem.

4.1 Effects of exogenous inputs and endogenous releases on nutrient dynamics, microbial community composition, and function in the water

In this study, key environmental parameters such as pH, DO, COD, and various nitrogen forms exhibited significant depth-dependent variations. Surface water in direct contact with the atmosphere had higher DO levels, whereas exogenous inputs led to higher COD concentrations in surface water (Figure 2), which is consistent with our previous research (Wang, 2006; Zhao et al., 2007; Kumar et al., 2019; Nevers et al., 2020). The microbial community exhibited an evident depth-related succession pattern. Proteobacteria and Actinobacteriota emerged as the most dominant bacterial phyla in Hulun Lake, with the lowest relative abundances of 42.63 and 19.99% in surface water, and peak abundances of 45.17 and 26.25% in middle water, consistent with findings from other freshwater lakes (Christina et al., 2018) (Figure 4A; Supplementary Table S1). These shifts in bacterial community composition across water depths were attributed to inherent water characteristics.

Our study revealed that the bottom water possessed a higher diversity of bacterioplankton taxa (Figure 3B), which was likely influenced by two primary factors. First, the release of bottom sediments enriched the nutrient content of the bottom water, supporting bacterioplankton survival. Second, numerous studies have indicated that bottom sediments usually contain more abundant biological taxa than the water column, and frequent material-energy exchanges between these compartments further increase bacterioplankton diversity in bottom water (Perkins et al., 2014; Fang et al., 2015; Kumar et al., 2019; Sun et al., 2019; Khabouchi et al., 2020; Gao et al., 2022). Simultaneously, the spatial distribution of the sampling sites varied notably across different depths (Figure 3A). Surface water, influenced by factors such as atmospheric precipitation, wind speed, and river confluence, exhibits greater environmental instability and looser bacterioplankton distributions (Mesbah et al., 2007; Dong et al., 2019). In addition, the bacterioplankton community composition demonstrated significant variations in α-diversity across the surface, middle, and bottom layers (Figure 3D). We identified that physicochemical indicators, including pH and SAL, along with nutrient elements, such as TN, COD, and NH_4^+-N, were the key drivers of these microbial community changes (Supplementary Figure S1). However, TN and NH_4^+-N had stronger effects on the bacterioplankton community structure in the surface and benthic layers, respectively. pH was consistently correlated with bacterial communities at various depths, suggesting that both surface and bottom bacterioplankton communities were highly sensitive to nitrogen fluctuations, and slight variations in pH significantly affected the structure of the bacterial communities in Hulun Lake (Glassman et al., 2018; Wahdan et al., 2023).

The dominant bacterial taxa across different water depths remained consistent, predominantly Proteobacteria, Actinobacteriota, Verrucomicrobiota, and Bacteroidota at the phylum level. Additionally, *hgcI_clade*, *norank_f_Clade_III*, *CL500-29_marine_group*, *unclassified_f_Comamonadaceae*, and *norank_f_Pirellulaceae* were the most dominant at the genus level (Figures 4A,B), which is consistent with findings from other freshwater ecosystems (Newton et al., 2011; Shang et al., 2020). Nevertheless, notable variations in the relative abundances of these dominant genera were observed at different water depths, which are likely attributed to nutrient element fluctuations (Mesbah et al., 2007). A comparison of the NH_4^+-N content and the relative abundance of *norank_f_Pirellulaceae* revealed contrasting trends (Figure 2; Supplementary Table S2). RDA analysis confirmed a mutually inhibitory relationship between these variables across different depths (Supplementary Figure S1), suggesting that nutrient variations are key factors in bacterioplankton community structure (Feng et al., 2009; Fang et al., 2015; Qu et al., 2015). In the case of other dominant phyla such as *CL500-29_marine_group*, although their relative abundance changes paralleled those of NH_4^+-N, the relationship transitioned from mutual promotion to inhibition (Supplementary Figure S1). This indicated that the effects of nutrients on bacterial communities differ under different habitat conditions (Xiong et al., 2014; Liang et al., 2016; Huang et al., 2018).

Microbial community dynamics are crucial factors of community function and offer insights into ecophysiological responses to depth-dependent changes. Consistent with our expectations, strong correlations were observed between the nitrogen metabolic processes and microbial communities. Specifically, the relative abundance of genes related to nitrate reduction exhibited a positive correlation with Proteobacteria in both the surface and bottom layers but was negatively correlated with Planctomycetota. In contrast, Planctomycetota in the surface layer demonstrated a positive correlation with genes associated with nitrogen fixation and a negative correlation with nitrification-related genes in the middle and bottom layers (Figures 7F–H). This suggests that Proteobacteria promoted the depletion of NO_3^--N in surface and bottom waters, as influenced by exogenous inputs and endogenous releases. Alternatively, sufficient contact between surface waters and the atmosphere facilitated an ample supply of N_2, enabling microorganisms to promote nitrogen fixation, a process mainly dominated by Planctomycetota. In addition,

we observed positive correlations between surface and bottom Proteobacteria and Planctomycetota with NH_4^+-N, whereas the middle-layer Planctomycetota was negatively correlated with NH_4^+-N (Supplementary Figure S1). These close associations between the dominant phyla and nitrogen suggest that the predominant phyla in the surface and bottom layers may promote nitrogen fixation and nitrate reduction. Conversely, the dominant phylum in the midwater may inhibit nitrification processes, thereby affecting NH_4^+-N levels at various depths in Hulun Lake (Figure 2). In a previous study, Fisher et al. (2000) reported that nutrient availability not only influenced microbial growth rates and productivity, but also significantly affected community composition and function, which is applicable to our study.

4.2 Influence of microbial interactions across depth-varying water masses and their environmental significance

Microorganisms exhibit complex ecological interactions that can be synergistic, reciprocal, or antagonistic (Shang et al., 2020). Recent studies have indicated a strong correlation between microbes in Hulun Lake and its rivers, driving distinct ecological functions (Shang et al., 2020). Our results suggest that increased lake depth corresponds to heightened complexity within the microbial network. Notably, the network structure of the mesocosm was more stable than those of the surface and bottom layers (Supplementary Table S4). This may be due to the frequent exchange of species energy between the surface and bottom bacterioplankton, which are more susceptible to environmental perturbations due to exogenous inputs and endogenous releases. In contrast, the midwater environment remains relatively stable (Jiao et al., 2016). Similar observations have been made in soil microbial communities, where improved microhabitat conditions influence the interactions between organisms (Li et al., 2013). Our results are supported by studies highlighting how environmental heterogeneity can engender variations in ecological network structure (Mitchell et al., 2010; Prober and Wiehl, 2011).

Proteobacteria, Bacteroidetes, and Actinobacteria were predominant in the microbial network structures across water samples at various depths (Supplementary Table S5). However, variations in the relative abundances of these dominant phyla across different samples and modules suggest diverse ecological roles they may play (Newman, 2006; Shang et al., 2020). Specifically, all modules in the surface water network were dominated by Proteobacteria, indicating their primary role in organic matter degradation (Chun et al., 2019; Shang et al., 2020; Zhang Y. H. et al., 2021). Moreover, our analysis revealed that environmental changes affected the bacterioplankton network structure not only at the phylum level but also significantly influenced key genera. Nanoarchaeota (*g_norank_f_GW2011_GWC1_47_15*), Verrucomicrobiota (*g_norank_f_cvE6*), and Bacteroidota (*g__unclassified_f_Balneolaceae*) emerged as the key bacterial taxa on the surface, mesopelagic, and bottom layers, respectively (Figures 5A–C). Despite their low abundance, these key taxa can substantially influence the biometabolic networks within the microbial community of the lake. Notably, the distribution of these keystone genera shifted from a single module in the surface waters to two modules in the bottom layer, suggesting potential fragmentation in their ecological interactions and functions (Figures 5D–F).

Significant differences were observed in the microbial communities across the surface, midwater, and bottom water. Notably, both the strength of module-environment variable correlations and modularity values were lower in the bottom water microbial communities than in the surface and mesocosm communities (Figures 6A–C; Supplementary Table S4). This suggests reduced connectivity between the bottom microbial communities. In the surface and midwater layers, the structures of the different ecological network modules, predominantly composed of Bacteroidota, Proteobacteria, and Actinobacteria, were mainly regulated by pH, DO, and TN (Figures 6A,B; Supplementary Table S5). These findings are consistent with existing literature, indicating that pH variations can reshape competitive relationships among microbial populations and induce changes in nutrient availability, phylum composition, and genus-level abundance (Fierer and Jackson, 2006; Lauber et al., 2009; Zhang H. G. et al., 2021). Furthermore, only module 3 in the bottom-water network exhibited a significant correlation with the environmental variables (Figure 6C). Collectively, our results suggest that microbial networks with higher connectivity and compactness have greater potential to be influenced by environmental factors.

5 Conclusion

Using 16S rRNA high-throughput sequencing technology, this study comprehensively assessed the bacterioplankton diversity in Hulun Lake. The findings demonstrated that both exogenous inputs and endogenous releases exerted a significant influence on bacterioplankton community structure. Specifically, the relative abundance of Proteobacteria and Actinobacteria increased from the surface to the bottom layers of the lake. Redundancy analysis further confirmed that habitat conditions significantly affected bacterioplankton composition. Among the assessed environmental factors, TN, pH, and COD were identified as the key variables influencing bacterioplankton communities in the surface, midwater, and bottom layers, respectively. Symbiotic network analysis suggested distinct relationships with water properties. However, because the mesocosms were less subject to exogenous inputs and endogenous releases, their microorganisms tended to survive independently, exhibiting fewer symbiotic relationships. Nevertheless, this structure might have more abundant ecological functions. Through the Tax4Fun analysis, 23 potential nitrogen-related functional genes were identified in the bacterioplankton community. The most significant functional roles were observed in nitrate reduction and denitrification processes. The flexibility of surface planktonic bacterial communities for nitrogen fixation was driven by exogenous input, whereas endogenous release led to similar flexibility in nitrification processes within the bottom planktonic communities. These results indicate the need for further metagenomic studies to validate the function of these genes. Overall, this study provides crucial insights into the complexity and functionality of bacterioplankton communities in Hulun Lake and emphasizes the importance of managing both surface- and bottom-water ecosystems through comprehensive control of external inputs and internal releases to improve lake ecology.

Data availability statement

The original contributions presented in the study are included in the article/Supplementary material, further inquiries can be directed to the corresponding author.

Author contributions

YS: Writing – original draft. WL: Writing – review & editing. XG: Writing – original draft.

Funding

The author(s) declare financial support was received for the research, authorship, and/or publication of this article. This work was supported by the National Natural Fund (52160021), Inner Mongolia Autonomous Region Natural Science Fund (2021MS05043), Inner Mongolia Autonomous Region Science and Technology Tackling Project (2020GG0009), and Inner Mongolia Autonomous Region Major Science and Technology Projects (2020ZD0009).

Conflict of interest

The authors declare that the research was conducted in the absence of any commercial or financial relationships that could be construed as a potential conflict of interest.

Publisher's note

All claims expressed in this article are solely those of the authors and do not necessarily represent those of their affiliated organizations, or those of the publisher, the editors and the reviewers. Any product that may be evaluated in this article, or claim that may be made by its manufacturer, is not guaranteed or endorsed by the publisher.

Supplementary material

The Supplementary material for this article can be found online at: https://www.frontiersin.org/articles/10.3389/fmicb.2023.1305345/full#supplementary-material

References

Bertilsson, S., Eiler, A., Nordqvist, A., and Jørgensen, N. O. G. (2007). Links between bacterial production, amino-acid utilization and community composition in productive lakes. *ISME J.* 1, 532–544. doi: 10.1038/ismej.2007.64

Chen, J. Q., Wang, J., Wang, Q. W., Lv, J. M., Liu, X. M., Chen, J. S., et al. (2021). Common fate of sister lakes in Hulunbuir grassland: long-term harmful algal bloom crisis from multi-source remote sensing insights. *J. Hydrol.* 594:125970. doi: 10.1016/j.jhydrol.2021.125970

Chen, S. F., Zhou, Y. Q., Chen, Y. R., and Gu, J. (2018). fastp: An ultra-fast all-in-one FASTQ preprocessor. *Bioinformatics* 34, i884–i890. doi: 10.1093/bioinformatics/bty560

Christina, B., Michaela, S., Manfred, J., Vinay, P. R., and Jens, B. (2018). Synchrony of eukaryotic and prokaryotic planktonic communities in three seasonally sampled Austrian lakes. *Front. Microbiol.* 9:1290. doi: 10.3389/fmicb.2018.01290

Chuai, X., Chen, X., Yang, L., Zeng, J., Miao, A., and Zhao, H. (2012). Effects of climatic changes and anthropogenic activities on lake eutrophication in different ecoregions. *Int. J. Environ. Sci. Technol.* 9, 503–514. doi: 10.1007/s13762-012-0066-2

Chun, S. J., Cui, Y. S., Lee, J. J., Choi, I. C., Oh, H. M., and Ahn, C. Y. (2019). Network analysis reveals succession of Microcystis genotypes accompanying distinctive microbial modules with recurrent patterns. *Water Res.* 170:115326. doi: 10.1016/j.watres.2019.115326

de Menezes, A. B., Prendergast-Miller, M. T., Richardson, A. E., Toscas, P., Farrell, M., Macdonald, M. L., et al. (2015). Network analysis reveals that bacteria and fungi form modules that correlate independently with soil parameters. *Environ. Microbiol.* 17, 2677–2689. doi: 10.1111/1462-2920.12559

Dimitry, Y. S., Tom, B., Emily, D. M., Lex, O., Charlotte, D. V., and Gerard, M. (2014). Microbial diversity and biogeochemical cycling in soda lakes. *Extremophiles* 18, 791–809. doi: 10.1007/s00792-014-0670-9

Dong, Z. J., Liu, D. Y., Wang, Y. J., and Di, B. P. (2019). Temporal and spatial variations of coastal water quality in Sishili Bay, northern Yellow Sea of China. *Aquat. Ecosyst. Health Manag.* 22, 30–39. doi: 10.1080/14634988.2018.1525264

Dumbrell, A. J., Nelson, M., Helgason, T., Dytham, C., and Fitter, A. H. (2010). Relative roles of niche and neutral processes in structuring a soil microbial community. *ISME J.* 4, 337–345. doi: 10.1038/ismej.2009.122

Edgar, R. C. (2013). UPARSE: highly accurate OTU sequences from microbial amplicon reads. *Nat. Methods* 10, 996–998. doi: 10.1038/nmeth.2604

Fang, L., Chen, L., Liu, Y., Tao, W., Zhang, Z. Z., Liu, H. Y., et al. (2015). Planktonic and sedimentary bacterial diversity of Lake Sayram in summer. *Microbiology* 4, 814–825. doi: 10.1002/mbo3.281

Feng, B. W., Li, X. R., Wang, J. H., Hu, Z. Y., Meng, H., Xiang, L. Y., et al. (2009). Bacterial diversity of water and sediment in the Changjiang estuary and coastal area of the East China Sea. *FEMS Microbiol. Ecol.* 70, 236–248. doi: 10.1111/j.1574-6941.2009.00772.x

Fierer, N., and Jackson, R. B. (2006). The diversity and biogeography of soil bacterial communities. *Proc. Natl. Acad. Sci. U.S.A.* 103, 626–631. doi: 10.1073/pnas.0507535103

Fisher, M. M., Klug, J. L., Lauster, G., Newton, M., and Triplett, E. W. (2000). Effects of resources and trophic interactions on freshwater bacterioplankton diversity. *Microb. Ecol.* 40, 125–138. doi: 10.1007/s002480000049

Gao, N., Liang, Y. Y., Li, J., Cui, K., and Lu, W. X. (2022). Bacterial community composition and indicators of water quality in Caizi Lake, a typical Yangtze-connected freshwater lake. *FEMS Microbiol. Lett.* 369:fnac084. doi: 10.1093/femsle/fnac084

Glassman, S. I., Weihe, C., Li, J. H., Albright, M. B. N., Looby, C. I., Martiny, A. C., et al. (2018). Decomposition responses to climate depend on microbial community composition. *Proc. Natl. Acad. Sci. U. S. A.* 115, 11994–11999. doi: 10.1073/pnas.1811269115

Grover, J. P. (2017). Sink or swim? Vertical movement and nutrient storage in phytoplankton. *J. Theor. Biol.* 432, 38–48. doi: 10.1016/j.jtbi.2017.08.012

Gu, Z. Q., Liu, K. S., Pedersen, M. W., Wang, F., Chen, Y., Zeng, C., et al. (2020). Community assembly processes underlying the temporal dynamics of glacial stream and lake bacterial communities. *Sci. Total Environ.* 761:143178. doi: 10.1016/j.scitotenv.2020.143178

Huang, W., Chen, X., Wang, K., Chen, J. Y., Zheng, B. H., and Jiang, X. (2018). Comparison among the microbial communities in the lake, lake wetland, and estuary sediments of a plain river network. *Microbiology* 8:e00644. doi: 10.1002/mbo3.644

Jiao, S., Liu, Z. S., Lin, Y. B., Yang, J., Chen, W. M., and Wei, G. H. (2016). Bacterial communities in oil contaminated soils: biogeography and co-occurrence patterns. *Soil Boil. Biochem.* 98, 64–73. doi: 10.1016/j.soilbio.2016.04.005

Karpowicz, M., Rudczyk, E. J., Grabowska, M., and Karabin, J. E. (2012). *Assessment of trophic state of four lakes in the Suwaki Landscape Park (NE Poland) based on the summer phyto- and zooplankton in comparison with some physicochemical parameters*. Kraków: Institute of Botany Polish Academy of Sciences.

Khabouchi, I., Khadhar, S., Driouich Chaouachi, R., Chekirbene, A., Asia, L., and Doumenq, P. (2020). Study of organic pollution in superficial sediments of Meliane river catchment area: aliphatic and polycyclic aromatic hydrocarbons. *Environ. Monit. Assess.* 192:283. doi: 10.1007/s10661-020-8213-6

Kumar, A., Ng, D. H. P., Wu, Y. C., and Cao, B. (2019). Microbial community composition and putative biogeochemical functions in the sediment and water of tropical granite quarry lakes. *Microb. Ecol.* 77, 1–11. doi: 10.1007/s00248-018-1204-2

Lauber, C. L., Hamady, M., Knight, R., and Fierer, N. (2009). Pyrosequencing-based assessment of soil pH as a predictor of soil bacterial community structure at the continental scale. *Appl. Environ. Microbiol.* 75, 5111–5120. doi: 10.1128/AEM.00335-09

Liang, Y. T., Zhang, X., Zhou, J. Z., and Li, G. H. (2016). Long-term oil contamination increases deterministic assembly processes in soil microbes. *Ecol. Appl.* 25, 1235–1243. doi: 10.1890/14-1672.1

Li, H., Colica, G., Wu, P. P., Li, D. H., Rossi, F., de Philippis, R., et al. (2013). Shifting species interaction in soil microbial community and its influence on ecosystem functions modulating. *Microb. Ecol.* 65, 700–708. doi: 10.1007/s00248-012-0171-2

Li, S., Chen, J. P., Xiang, J., Pan, Y., Huang, Z. Y., and Wu, Y. L. (2019). Water level changes of Hulun Lake in Inner Mongolia derived from Jason satellite data. *J. Vis. Commun. Image Represent.* 58, 565–575. doi: 10.1016/j.jvcir.2018.12.031

Liu, K. S., Yao, T. D., Pearce, D. A., Jiao, N. Z., Zeng, Y. H., Guo, B. X., et al. (2021). Bacteria in the lakes of the Tibetan plateau and polar regions. *Sci. Total Environ.* 754:142248. doi: 10.1016/j.scitotenv.2020.142248

Li, Y. R., Meng, J., Zhang, C., Ji, S. P., Kong, Q., Wang, R. Q., et al. (2020). Bottom-up and top-down effects on phytoplankton communities in two freshwater lakes. *PLoS One* 15:e0231357. doi: 10.1371/journal.pone.0231357

Mago, T., and Salzberg, S. L. (2011). FLASH: fast length adjustment of short reads to improve genome assemblies. *Bioinformatics* 27, 2957–2963. doi: 10.1093/bioinformatics/btr507

Mesbah, N. M., Abou-El-Ela, S. H., and Wiegel, J. (2007). Novel and unexpected prokaryotic diversity in water and sediments of the alkaline, hypersaline lakes of the Wadi an natrun, Egypt. *Microb. Ecol.* 54, 598–617. doi: 10.1007/s00248-006-9193-y

Michael, H., and Jörg, L. (2008). Oxygen controls the phosphorus release from lake sediments - a long-lasting paradigm in limnology. *Internat. Rev. Hydrobiol.* 93, 415–432. doi: 10.1002/iroh.200711054

Mitchell, R. J., Hester, A. J., Campbell, C. D., Chapman, S. J., Cameron, C. M., Hewison, R. L., et al. (2010). Is vegetation composition or soil chemistry the best predictor of the soil microbial community? *Plant Soil* 333, 417–430. doi: 10.1007/s11104-010-0357-7

Nevers, M. B., Byappanahalli, M. N., Nakatsu, C. H., Kinzelman, J. L., Phanikumar, M. S., Shively, D. A., et al. (2020). Interaction of bacterial communities and indicators of water quality in shoreline sand, sediment, and water of Lake Michigan. *Water Res.* 178:115671. doi: 10.1016/j.watres.2020.115671

Newman, M. E. J. (2006). Modularity and community structure in networks. *Proc. Natl. Acad. Sci. U. S. A.* 103, 8577–8582. doi: 10.1073/pnas.0601602103

Newton, R. J., Jones, S. E., Eiler, A., McMahon, K. D., and Bertilsson, S. (2011). A guide to the natural history of freshwater lake bacteria. *Microbiol. Mol. Biol. Rev.* 75, 14–49. doi: 10.1128/MMBR.00028-10

Nikolai, S. J., and Dzialowski, A. R. (2014). Effects of internal phosphorus loading on nutrient limitation in a eutrophic reservoir. *Limnologica* 49, 33–41. doi: 10.1016/j.limno.2014.08.005

Perkins, T. L., Clements, K., Baas, J. H., Jago, C. F., Jones, D. L., Malham, S. K., et al. (2014). Sediment composition influences spatial variation in the abundance of human pathogen indicator bacteria within an estuarine environment. *PLoS One* 9:e112951. doi: 10.1371/journal.pone.0112951

Prober, S. M., and Wiehl, G. (2011). Resource heterogeneity and persistence of exotic annuals in long-ungrazed Mediterranean-climate woodlands. *Biol. Invasions* 13, 2009–2022. doi: 10.1007/s10530-011-0017-8

Quiza, L., Lalonde, I., Guertin, C., and Constant, P. (2014). Land-use influences the distribution and activity of high affinity CO-oxidizing bacteria associated to type I-coxL genotype in soil. *Front. Microbiol.* 5:271. doi: 10.3389/fmicb.2014.00271

Qu, J. Q., Zhang, Q. J., Zhang, N., Shen, L. X., and Liu, P. B. (2015). Microbial community diversity in water and sediment of an eutrophic Lake during harmful algal bloom using MiSeq Illumina technology. 2015 International Conference on Advances in Environment Research, Jeju.

Shang, Y. Q., Wu, X. Y., Wang, X. B., Wei, Q. G., Ma, S. C., Sun, G. L., et al. (2022). Factors affecting seasonal variation of microbial community structure in Hulun Lake, China. *Sci. Total Environ.* 805:150294. doi: 10.1016/j.scitotenv.2021.150294

Shang, Y. Q., Wu, X. Y., Wei, Q. G., Dou, H. S., Wang, X. B., Chen, J., et al. (2020). Total arsenic, pH, and sulfate are the Main environmental factors affecting the microbial ecology of the water and sediments in Hulun Lake, China. *Front. Microbiol.* 11:548607. doi: 10.3389/fmicb.2020.548607

Stackebrandt, E., and Goebel, B. M. (1994). Taxonomic note: a place for DNA-DNA reassociation and 16S rRNA sequence analysis in the present species definition in bacteriology. *Int. J. Syst. Bacteriol.* 44, 846–849. doi: 10.1099/00207713-44-4-846

Sun, Y., Li, X., Liu, J. J., Yao, Q., Jin, J., Liu, X. B., et al. (2019). Comparative analysis of bacterial community compositions between sediment and water in different types of wetlands of Northeast China. *J. Soils Sediments* 19, 3083–3097. doi: 10.1007/s11368-019-02301-x

Swift, M. J., Heal, O. W., and Anderson, J. M. (1979). Decomposition in terrestrial ecosystems. *Stud. Ecol.* 5, 2772–2774.

Tammert, H., Tertova, N., Kiprovskaja, J., Baty, F., Noges, T., and Kisand, V. (2015). Contrasting seasonal and interannual environmental drivers in bacterial communities within a large shallow lake: evidence from a seven year survey. *Aquat. Microb. Ecol.* 75, 43–54. doi: 10.3354/ame01744

van de Graaf, A. A., Mulder, A., de Bruijn, P., Jetten, M. S., Robertson, L. A., and Kuenen, J. G. (1995). Anaerobic oxidation of ammonium is a biologically mediated process. *Appl. Environ. Microbiol.* 61, 1246–1251. doi: 10.1128/aem.61.4.1246-1251.1995

Wahdan, S. F. M., Ji, L., Schädler, M., Wu, Y. T., Sansupa, C., Tanunchai, B., et al. (2023). Future climate conditions accelerate wheat straw decomposition alongside altered microbial community composition, assembly patterns, and interaction networks. *ISME J.* 17, 238–251. doi: 10.1038/s41396-022-01336-2

Walters, W., Hyde, E. R., Berg-Lyons, D., Ackermann, G., Humphrey, G., Parada, A., et al. (2016). Improved bacterial 16S rRNA gene (V4 and V4-5) and fungal internal transcribed spacer marker gene primers for microbial community surveys. *mSystems* 1, e00009–e00015. doi: 10.1128/mSystems.00009-15

Wang, L. H. (2006). Analysis on the aquatic environment and water quality condition of Lake Hulun. *J. Hulunbeier Univ.* 14, 5–7. doi: 1009-4601(2006)06-0005-03 (in Chinese).

Wang, Q., Garrity, G. M., Tiedje, J. M., and Cole, J. R. (2007). Naive Bayesian classifier for rapid assignment of rRNA sequences into the new bacterial taxonomy. *Appl. Environ. Microbiol.* 73, 5261–5267. doi: 10.1128/AEM.00062-07

Wang, Q. H., Li, Y., Liu, L., Cui, S. Z., Liu, X., Chen, F. Z., et al. (2023). Human impact on current environmental state in Chinese lakes. *J. Environ. Sci. (China)* 126, 297–307. doi: 10.1016/j.jes.2022.05.031

Wang, W. D., Liu, W. Y., Wu, D., Wang, X. X., and Zhu, G. B. (2018). Differentiation of nitrogen and microbial community in the littoral and limnetic sediments of a large shallow eutrophic lake (Chaohu Lake, China). *J. Soils Sediments* 19, 1005–1016. doi: 10.1007/s11368-018-2090-4

Wang, W. L., Li, W. J., Yan, Y., Liu, B., Wang, T. J., Mao, S. C., et al. (2020). Organic matter pollution during the spring thaw in Hulun lake basin: contribution of multiform human activities. *Bull. Environ. Contam. Toxicol.* 105, 307–316. doi: 10.1007/s00128-020-02911-z

Wang, Y. B., Hu, X. K., Sun, Y. Y., and Wang, C. X. (2020). Influence of the cold bottom water on taxonomic and functional composition and complexity of microbial communities in the southern Yellow Sea during the summer. *Sci. Total Environ.* 759:143496. doi: 10.1016/j.scitotenv.2020.143496

Wu, H. P., Hao, B. B., Cai, Y. P., Liu, G. H., and Xing, W. (2021). Effects of submerged vegetation on sediment nitrogen-cycling bacterial communities in Honghu Lake (China). *Sci. Total Environ.* 755:142541. doi: 10.1016/j.scitotenv.2020.142541

Xiong, J. B., Ye, X. S., Wang, K., Chen, H. P., Hu, C. J., Zhu, J. L., et al. (2014). Biogeography of the sediment bacterial community responds to a nitrogen pollution gradient in the East China Sea. *Appl. Environ. Microbiol.* 80, 1919–1925. doi: 10.1128/AEM.03731-13

Zhang, F. J., Xue, B., Yao, S. C., and Gui, Z. F. (2017). Organic carbon burial from multi-core records in Hulun Lake, the largest lake in northern China. *Quat. Int.* 475, 80–90. doi: 10.1016/j.quaint.2017.12.005

Zhang, H. G., Lyu, T., Liu, L. X., Hu, Z., and Pan, G. (2021). Exploring a multifunctional geoengineering material for eutrophication remediation: simultaneously control internal nutrient load and tackle hypoxia. *Chem. Eng. J.* 406:127206. doi: 10.1016/j.cej.2020.127206

Zhang, L., Shen, T. T., Cheng, Y., Zhao, T. T., Li, L., and Qi, P. F. (2020). Temporal and spatial variations in the bacterial community composition in Lake Bosten, a large, brackish lake in China. *Sci. Rep.* 10:304. doi: 10.1038/s41598-019-57238-5

Zhang, L. Y., Delgado-Baquerizo, M., Shi, Y., Liu, X., Yang, Y. F., and Chu, H. Y. (2021). Co-existing water and sediment bacteria are driven by contrasting environmental factors across glacier-fed aquatic systems. *Water Res.* 198:117139. doi: 10.1016/j.watres.2021.117139

Zhang, S. Y., Tsementzi, D., Hatt, J. K., Bivins, A., Khelurkar, N., Brown, J., et al. (2019). Intensive allochthonous inputs along the Ganges River and their effect on microbial community composition and dynamics. *Environ. Microbiol.* 21, 182–196. doi: 10.1111/1462-2920.14439

Zhang, W. Q., Jin, X., Di, Z. Z., Zhu, X. L., and Shan, B. Q. (2016). Heavy metals in surface sediments of the shallow lakes in eastern China: their relations with environmental factors and anthropogenic activities. *Environ. Sci. Pollut. Res. Int.* 23, 25364–25373. doi: 10.1007/s11356-016-7643-8

Zhang, Y. H., Yao, P., Sun, C., Li, S. Z., Shi, X. C., Zhang, X. H., et al. (2021). Vertical diversity and association pattern of total, abundant and rare microbial communities in deep-sea sediments. *Mol. Ecol.* 30, 2800–2816. doi: 10.1111/mec.15937

Zhao, H. Y., Li, C. C., Zhao, H. H., Tian, H. C., and Dou, Z. Q. (2007). The climate change and its effect on the water environment in the Hulun Lake wetland. *J. Glaciol. Geocryol.* 29, 795–801. doi: 10.1631/jzus.2007.A1858 (in Chinese).

Zhao, Y., Song, K. S., Wen, Z. D., Fang, C., Shang, Y. X., and Lv, L. L. (2017). Evaluation of CDOM sources and their links with water quality in the lakes of Northeast China using fluorescence spectroscopy. *J. Hydrol.* 550, 80–91. doi: 10.1016/j.jhydrol.2017.04.027

frontiers | Frontiers in Microbiology

TYPE Perspective
PUBLISHED 05 January 2024
DOI 10.3389/fmicb.2023.1320853

OPEN ACCESS

EDITED BY
Yongbin Li,
Dalian University of Technology, China

REVIEWED BY
Parul Chaudhary,
Graphic Era Hill University, India
Jai Prakash,
Babasaheb Bhimrao Ambedkar University, India

*CORRESPONDENCE
Xiaolin Jia
✉ 20110010@xijing.edu.cn
Xinping Zhang
✉ zhang_xinping@xaut.edu.cn
Haoming Chen
✉ chenhaoming89@hotmail.com

†These authors have contributed equally to this work

RECEIVED 13 October 2023
ACCEPTED 15 December 2023
PUBLISHED 05 January 2024

CITATION
Feng Y, He J, Zhang H, Jia X, Hu Y, Ye J, Gu X, Zhang X and Chen H (2024) Phosphate solubilizing microorganisms: a sustainability strategy to improve urban ecosystems. *Front. Microbiol.* 14:1320853. doi: 10.3389/fmicb.2023.1320853

Phosphate solubilizing microorganisms: a sustainability strategy to improve urban ecosystems

Yang Feng[1,2†], Jing He[1†], Hongchen Zhang[1], Xiaolin Jia[1,2*], Youning Hu[3], Jianqing Ye[1], Xinyuan Gu[1], Xinping Zhang[4*] and Haoming Chen[5*]

[1]School of Art and Design, Xijing University, Xi'an, China, [2]Shaanxi Provincial Research Center of Public Scientific Quality Development and Cultural and Creative Industry Development, Xi'an, China, [3]School of Biological and Environmental Engineering, Xi'an University, Xi'an, China, [4]School of Art and Design, Xi'an University of Technology, Xi'an, China, [5]School of Environmental and Biological Engineering, Nanjing University of Science and Technology, Nanjing, China

Intensification of urban construction has gradually destroyed human habitat ecosystems. Plants, which serve as the foundation of ecosystems, require green, low-cost, and effective technologies to sustain their growth in stressful environments. A total of 286 keywords and 10 clusters from the bibliometric analysis of 529 articles (1999–2023) indicate the increasing importance of research on microbial functionality in landscape ecosystems. Phosphate solubilizing microorganisms (PSMs) also improve plant disease resistance, adaptability, and survival. PSMs are widely used to promote plant growth and improve ecological quality. They can increase the availability of phosphorus in the soil and reduce the dependence of plants on chemical fertilizers. Microorganisms regulate phosphorus as key tools in landscape ecosystems. Most importantly, in urban and rural landscape practices, PSMs can be applied to green spaces, residential landscapes, road greening, and nursery planting, which play significant roles in improving vegetation coverage, enhancing plant resistance, improving environmental quality, and mitigating the heat island effect. PSMs are also helpful in restoring the ecological environment and biodiversity of polluted areas, such as brownfields, to provide residents with a more liveable living environment. Therefore, the multiple efficacies of PSM are expected to play increasingly important roles in the construction of urban and rural landscape ecosystems.

KEYWORDS

phosphate, landscape ecosystem, urban environmental, plants, soil nutrients

1 Introduction

1.1 Plants play a key role in landscape ecosystems

As the building blocks of ecosystems, plants convert solar energy into chemical energy through photosynthesis and absorb water and nutrients from the soil to create organic matter that supports life (Barrios et al., 2018). Meanwhile, the roots, leaves, and other organs of plants can not only absorb water and nutrients but also convert carbon dioxide into oxygen and release it into the atmosphere to regulate the air quality of the entire environment (Raven, 2022). Plants

have important physical and ecological functions in landscape ecosystems. For example, plant roots can hold soil particles and increase soil viscosity and stability to reduce soil and water loss and avoid natural disasters, such as landslides. Plants can also purify air by absorbing pollutants, capturing particles, and eliminating bacteria. Additionally, their roots can absorb nutrients and organic matter from the water, effectively mitigating water eutrophication and other environmental issues (Nowak et al., 2014; Bodnaruk et al., 2017). Additionally, plants provide habitats, food sources, and protection to maintain the diversity of plant and animal species within ecosystems (Maroyi, 2022). It should be emphasized that not only do the beautiful shapes and colors of plants have the ability to enhance emotions, but these natural esthetics can also have a positive impact on human health and well-being. As the basic components of landscape ecosystems, plants have a variety of interdependent ecological functions that play crucial roles in ecosystems. It is important for humans to make full use of plant resources to meet their own needs while simultaneously protecting and maintaining the ecological balance of ecosystems. Therefore, effective techniques (improvement, conservation, and restoration) are needed to ensure that plants continue to play an important and irreplaceable role in landscape ecosystems.

2 Microbial enhancement of P is a key mechanism for plant growth

2.1 Phosphorus is essential for plant growth and development

As a component of many important substances and structures, such as nuclear proteins, phospholipids and nucleic acids, in plant cells, phosphorus plays an important role in physiological and biochemical reactions during the whole life cycle of plants and is indispensable for plant growth and development (Han et al., 2022). However, most phosphorus in the soil exists in the form of insoluble inorganic phosphorus or organophosphorus, which is difficult for plants to absorb and use (Wang et al., 2021). Although humans use phosphorus fertilizers to meet plant demand for phosphorus, the problems caused by long-term use have not been effectively solved, such as a decline in soil fertility, deterioration of physical and chemical properties, a decrease in microbial diversity, and heavy metal pollution (Vassilev et al., 2006; Kalayu, 2019), which not only threaten human production, life, health, and well-being, but also interfere with the sustainable development of landscape ecosystems. We conducted a bibliometric analysis of 529 articles on the topics of P, microbial, urban, and landscape [retrieved string: TS = (phosphorus) AND TS = (bacteria OR fungi OR microorganisms) AND TS = (urban OR landscapes)]. The presence of terms such as "phosphate" "decomposition" "nutrient uptake" "enzyme activity" and "organic carbon" indicates that functional studies on microbial mineralization and activation of insoluble phosphorus (#4 cluster) and interaction with plant roots (#1, #6, and #8 clusters) are gradually taking a dominant position in research (Figure 1).

2.2 PSMs are promoters of plant growth

In addition to protecting and maintaining plant resources, it is important to protect the microbial community within ecosystems. PSMs were initially discovered in agri-environmental research as a class of microorganisms that benefit plant growth (Vassilev et al., 2006). PSMs can convert insoluble phosphorus in the soil into P, which can be absorbed and utilized by plants by relying on organic acids, phosphatases, and other products through their own metabolism or synergistic effects with other organisms (Chen et al., 2019). Existing research has identified PSMs as an effective alternative to agrochemicals in flower cultivation, and it has shown a positive impact on the quality and production of flower crops, such as roses, marigolds, carnations, and jasmine (Zaidi et al., 2016). PSMs can also improve the plant absorption of nitrogen, potassium, calcium, and other mineral nutrients, thereby promoting plant growth and development (Ogut et al., 2011). Furthermore, PSMs not only supply phosphorus but also offer the auxins indole-3-acetic acid (IAA), gibberellic acid (GA), and cytokinin (CTK) to enhance plant root growth and development in soil, thereby increasing the water and nutrient absorption efficiency of plant roots. Additionally, they release antibiotics and produce B vitamins that suppress plant pathogens (Gupta and Kumar, 2017). In recent years, an increasing body of research has demonstrated the practical value of PSMs in enhancing plant landscape ecology. In landscape ecosystems, the addition of PSM-rich organic fertilizers and microbial agents to the soil not only improves soil properties but also reduces plant dependence on chemical fertilizers (Timofeeva et al., 2022; Sarmah and Sarma, 2023). Therefore, PSMs have broad prospects for application in plant cultivation and maintenance.

3 PSMs are an effective strategy to prevent future deterioration of landscape ecosystems

In urban and rural environments, the most serious problems in landscape ecosystems are the heat island effect, soil compaction, salinization, and poor plant diversity. These problems not only lead to steep increases in planting and maintenance costs but also increase the risk of imbalance in landscape ecosystems. PSMs have attracted widespread attention from the community precisely for their advantages in enhancing plant drought resistance, salt alkalinity resistance and insect resistance (Kalayu, 2019; Jin et al., 2022; Hu and Chen, 2023). In particular, PSMs can break down and remove pollutants and other harmful chemicals (e.g., pesticides, antibiotics, and toxic heavy metals), which also play a vital role in the health and stability of ecosystems (Figure 2).

3.1 PSMs can enhance plant resistance in urban and rural environments

Drought often leads to slow plant growth and development, aggravates desertification trends in landscape ecosystems, and seriously affects the balance of the ecological environment, the survival of ornamental plants, and agricultural production. Under drought stress, plants wilt with closed stomata and exhibit photosynthesis inhibition. PSMs can enhance plant activity and nutrient uptake capacity, and improve plant tolerance under drought stress (Khoshmanzar et al., 2020). Soil compaction and salinization severely inhibit the respiration and growth of plant roots, thereby slowing the growth and development of seedlings (Zhang et al., 2022).

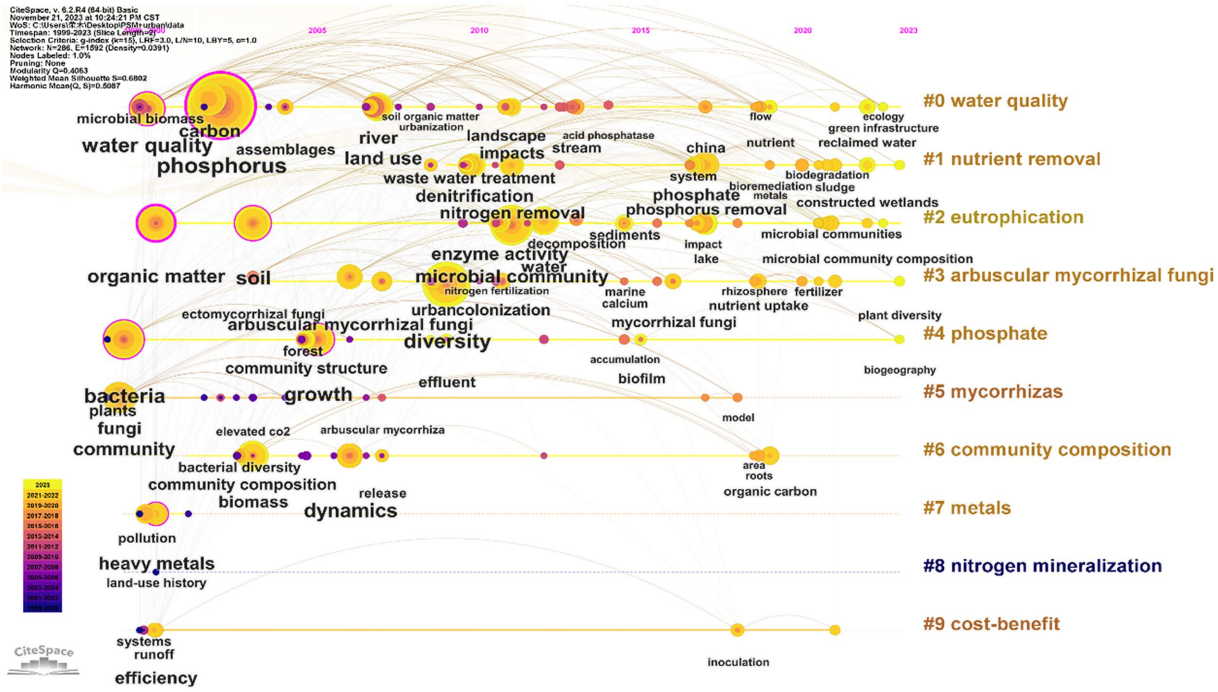

FIGURE 1
Keyword timeline clustering mapping based on CiteSpace.

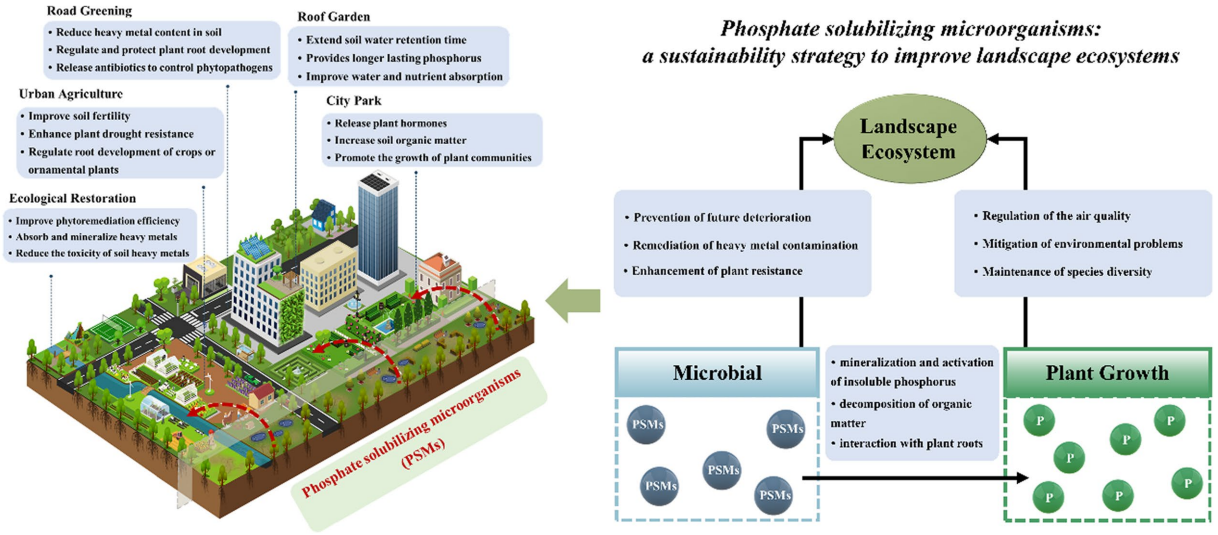

FIGURE 2
Schematic diagram of the mechanism by which phosphate-solubilizing microorganisms improve landscape ecosystem construction.

PSMs not only have strong saline-alkali tolerance but also enhance plant tolerance to saline-alkali stress (Jin et al., 2022). Studies have shown that PSMs can maintain the normal growth and metabolism of plants by controlling the production of osmotic adjustment substances and secondary metabolites (such as proline, soluble sugar, malondialdehyde, flavonoids and phenols) to balance the breakdown of reactive oxygen species in plants caused by drought, salinity and other stresses (Numan et al., 2018; Liang et al., 2019; Jin et al., 2022). Notably, some PSMs (*Aspergillus*, *Penicillium*, etc.) can eliminate the accumulation of reactive oxygen species by enhancing the activity of antioxidant enzymes in plants to reduce the damage caused by reactive oxygen species to plant cells (Li et al., 2017; Jin et al., 2022).

Most plants in urban and rural environments are artificially cultivated with a single plant diversity, serious diseases, and insect pests. Plant pests and diseases are primarily managed by chemicals. However, overuse of chemicals can lead to a range of environmental and social issues, including reduced plant yields, harm to animal ecosystems, and risks to human health. PSMs can improve the

disease resistance of plants and reduce the damage caused by pathogenic bacteria to plants, with good biological control effects (Kalayu, 2019; Tian et al., 2021). For example, PSMs can resist the invasion of pathogenic bacteria by producing active metabolites (cyclic dipeptides, quinazolinones, and alcohols, etc.). Meanwhile, PSMs can improve plant resistance to pests and diseases by increasing the activities of plant disease resistance-related defense enzymes (Rawat et al., 2021; Palmieri et al., 2022; Tyśkiewicz et al., 2022).

3.2 PSMs can repair heavy metal pollution in urban and rural soil

Heavy metal residues in the soil not only affect plant growth but also pose a serious threat to the health of urban and rural habitats. Studies have shown that PSMs have a good fixation effect on heavy metal ions, such as Cr^{6+}, Co^{2+}, Cd^{2+}, Zn^{2+}, Cu^{2+}, and Pb^{2+} in soil (Qian et al., 2019; Hu and Chen, 2023). PSMs can first dissolve insoluble phosphorus sources by releasing organic acids and enzymes and converting them to PO_4^{3-} which binds to heavy metals to form phosphate precipitates and can greatly reduce the amount of free heavy metal ions in the soil (Chen et al., 2023). Second, PSM can secrete organic acids, indoleacetic acids, iron carriers, and other substances with oxidizing or reducing properties, thereby altering the metal valence state and diminishing the toxicity of toxic metals (Lai et al., 2022; Yu et al., 2022).

In conclusion, PSMs contribute significantly to landscape ecosystems. They not only directly promote plant growth, but also contribute to the remediation of existing environmental pollution and ecosystem deficiencies. This remediation process has a positive impact on the quality of human habitats and plays a crucial role in maintaining ecosystem stability and health.

4 Discussion and perspectives

Microbial fertilizers and preparations with specific functions are less expensive, greener, and more sustainable than chemical and physical amendments in the construction of urban green spaces and public spaces. Compared to other functional microorganisms, PSMs have more important application value and the potential to improve the ecology of plant landscapes because they can improve crop growth in several ways. These include the secretion of hormones favorable to plant growth, enhancement of soil fast-acting phosphorus, potassium, and other nutrients, improvement of soil pore structure, and reduction of pollution stress in the soil. However, there are several limitations to the use of PSM in highly polluted urban environments. The activity of microorganisms is affected by environmental factors, such as pH, temperature, humidity, and oxygen, which can limit their biological functions. In addition, owing to the wide variety of PSM species, the tolerance and remediation capacities of different types of PSM for contamination vary. Therefore, long-term microbial remediation requires a continuous investment of time and resources to maintain microbial activity and monitor the effectiveness of remediation. In addition, introducing PSMs to target sites and maintaining their activity is challenging because there is a need to address new ecological issues that may arise from microbial introduction. In summary, the benefits and limitations of PSM applications in landscape ecosystems coexist, and their combination with other remediation strategies and technologies for integrated management should be the focus of future research.

Data availability statement

The original contributions presented in the study are included in the article/supplementary material, further inquiries can be directed to the corresponding authors.

Author contributions

YF: Investigation, Methodology, Writing – original draft. JH: Methodology, Writing – original draft. HZ: Methodology, Writing – original draft. XJ: Conceptualization, Writing – original draft. YH: Data curation, Writing – review & editing. JY: Methodology, Writing – original draft. XG: Methodology, Writing – original draft. XZ: Visualization, Writing – review & editing. HC: Supervision, Validation, Writing – review & editing.

Funding

The author(s) declare financial support was received for the research, authorship, and/or publication of this article. This study was supported by the Scientific Research Project of the Education Department of Shaanxi Provincial Government (grant no. 21JK0416), and the Xijing University Special Fund for High-level Talents (grant no. XJ23B02) to YF. This study was also supported by the National Social Science Fund Art Project (grant no. 20BH158) to XJ. This study was also supported by the Open Fund for Large Instrumentation of the Nanjing University of Science and Technology, Natural Science Foundation of Hebei Province (E2023519001) and the Postgraduate Research and Practice Innovation Program of Jiangsu Province (SJCX23_0125) to HC. This study was also supported by the Shaanxi Province Natural Science Basic Research Project (2019JQ-892) to YH.

Conflict of interest

The authors declare that the research was conducted in the absence of any commercial or financial relationships that could be construed as a potential conflict of interest.

Publisher's note

References

Barrios, E., Valencia, V., Jonsson, M., Brauman, A., Hairiah, K., Mortimer, P. E., et al. (2018). Contribution of trees to the conservation of biodiversity and ecosystem services in agricultural landscapes. *Int J Biodivers Sci Ecosyst Serv Manage* 14, 1–16. doi: 10.1080/21513732.2017.1399167

Bodnaruk, E. W., Kroll, C. N., Yang, Y., Hirabayashi, S., Nowak, D. J., and Endreny, T. A. (2017). Where to plant urban trees? A spatially explicit methodology to explore ecosystem service tradeoffs. *Landsc. Urban Plan.* 157, 457–467. doi: 10.1016/j.landurbplan.2016.08.016

Chen, H. M., Jiang, H. F., Nazhafati, M., Li, L. L., and Jiang, J. Y. (2023). Biochar: an effective measure to strengthen phosphate solubilizing microorganisms for remediation of heavy metal pollution in soil. *Front. Bioeng. Biotechnol.* 11:1127166. doi: 10.3389/fbioe.2023.1127166

Chen, H. M., Zhang, J. W., Tang, L. Y., Su, M., Tian, D., Zhang, L., et al. (2019). Enhanced Pb immobilization via the combination of biochar and phosphate solubilizing bacteria. *Environ. Int.* 127, 395–401. doi: 10.1016/j.envint.2019.03.068

Gupta, P., and Kumar, V. (2017). Value added phytoremediation of metal stressed soils using phosphate solubilizing microbial consortium. *World J. Microbiol. Biotechnol.* 33:9. doi: 10.1007/s11274-016-2176-3

Han, Y., White, P. J., and Cheng, L. (2022). Mechanisms for improving phosphorus utilization efficiency in plants. *Ann. Bot.* 129, 247–258. doi: 10.1093/aob/mcab145

Hu, X., and Chen, H. (2023). Phosphate solubilizing microorganism: a green measure to efectively control and regulate heavy metal pollution in agricultural soils. *Front. Microbiol.* 14:1193670. doi: 10.3389/fmicb.2023.1193670

Jin, F. Y., Hu, Q. L., Zhao, Y. X., Lin, X. Y., Zhang, J. F., Zhang, J. J., et al. (2022). Enhancing quinoa growth under severe saline-alkali stress by phosphate solubilizing microorganism *Penicillium funicuiosum* P 1. *PloS One* 17:e0273459. doi: 10.1371/journal.pone.0273459

Kalayu, G. (2019). Phosphate solubilizing microorganisms: promising approach as biofertilizers. *Int J Agron* 2019, 1–7. doi: 10.1155/2019/4917256

Khoshmanzar, E., Aliasgharzad, N., Neyshabouri, M. R., Khoshru, B., Arzanlou, M., and Lajayer, B. A. (2020). Effects of Trichoderma isolates on tomato growth and inducing its tolerance to water-deficit stress. *Int. J. Environ. Sci. Technol.* 17, 869–878. doi: 10.1007/s13762-019-02405-4

Lai, W. W., Wu, Y. Y., Zhang, C. N., Dilinuer, Y., Pasang, L., Lu, Y. Q., et al. (2022). Combination of biochar and phosphorus solubilizing bacteria to improve the stable form of toxic metal minerals and microbial abundance in lead/cadmium-contaminated soil. *Agronomy* 12:1003. doi: 10.3390/agronomy12051003

Li, X. N., Han, S. J., Wang, G. Y., Liu, X. Y., Amombo, E., Xie, Y., et al. (2017). The fungus aspergillus aculeatus enhances salt-stress tolerance, metabolite accumulation, and improves forage quality in perennial ryegrass. *Front. Microbiol.* 8:1664. doi: 10.3389/fmicb.2017.01664

Liang, S. C., Jiang, Y., Li, M. B., Zhu, W. X., Xu, N., and Zhang, H. H. (2019). Improving plant growth and alleviating photosynthetic inhibition from salt stress using AMF in alfalfa seedlings. *J. Plant Interact.* 14, 482–491. doi: 10.1080/17429145.2019.1662101

Maroyi, A. (2022). Traditional uses of wild and tended plants in maintaining ecosystem services in agricultural landscapes of the eastern Cape Province in South Africa. *J. Ethnobiol. Ethnomed.* 18:17. doi: 10.1186/s13002-022-00512-0

Nowak, D. J., Hirabayashi, S., Bodine, A., and Greenfield, E. (2014). Tree and forest effects on air quality and human health in the United States. *Environ. Pollut.* 193, 119–129. doi: 10.1016/j.envpol.2014.05.028

Numan, M., Bashir, S., Khan, Y., Mumtaz, R., Shinwari, Z. K., Khan, A. L., et al. (2018). Plant growth promoting bacteria as an alternative strategy for salt tolerance in plants: a review. *Microbiol. Res.* 209, 21–32. doi: 10.1016/j.micres.2018.02.003

Ogut, M., Er, F., and Neumann, G. (2011). Increased proton extrusion of wheat roots by inoculation with phosphorus solubilising microorganism. *Plant and Soil* 339, 285–297. doi: 10.1007/s11104-010-0578-9

Palmieri, D., Ianiri, G., Del Grosso, C., Barone, G., De Curtis, F., Castoria, R., et al. (2022). Advances and perspectives in the use of biocontrol agents against fungal plant diseases. *Horticulturae* 8:577. doi: 10.3390/horticulturae8070577

Qian, T. T., Yang, Q., Jun, D. C. F., Dong, F., and Zhou, Y. (2019). Transformation of phosphorus in sewage sludge biochar mediated by a phosphate-solubilizing microorganism. *Chem. Eng. J.* 359, 1573–1580. doi: 10.1016/j.cej.2018.11.015

Raven, J. A. (2022). Interactions between above and below ground plant structures: mechanisms and ecosystem services. *Front Agric Sci Engineer* 9, 197–213. doi: 10.15302/J-FASE-2021433

Rawat, P., Das, S., Shankhdhar, D., and Shankhdhar, S. C. (2021). Phosphate-solubilizing microorganisms: mechanism and their role in phosphate solubilization and uptake. *J. Soil Sci. Plant Nutr.* 21, 49–68. doi: 10.1007/s42729-020-00342-7

Sarmah, R., and Sarma, A. K. (2023). Phosphate solubilizing microorganisms: A review. *Commun. Soil Sci. Plant Anal.* 54, 1306–1315. doi: 10.1080/00103624.2022.2142238

Tian, J., Ge, F., Zhang, D. Y., Deng, S. Q., and Liu, X. W. (2021). Roles of phosphate solubilizing microorganisms from managing soil phosphorus deficiency to mediating biogeochemical P cycle. *Biology* 10:158. doi: 10.3390/biology10020158

Timofeeva, A., Galyamova, M., and Sedykh, S. (2022). Prospects for using phosphate-solubilizing microorganisms as natural fertilizers in agriculture. *Plan. Theory* 11:2119. doi: 10.3390/plants11162119

Tyśkiewicz, R., Nowak, A., Ozimek, E., and Jaroszuk-Ściseł, J. (2022). Trichoderma: the current status of its application in agriculture for the biocontrol of fungal phytopathogens and stimulation of plant growth. *Int. J. Mol. Sci.* 23:2329. doi: 10.3390/ijms23042329

Vassilev, N., Vassileva, M., and Nikolaeva, I. (2006). Simultaneous P-solubilizing and biocontrol activity of microorganisms: potentials and future trends. *Appl. Microbiol. Biotechnol.* 71, 137–144. doi: 10.1007/s00253-006-0380-z

Wang, L. J., Sheng, M. Y., Li, S., and Wu, J. (2021). Patterns and dynamics of plant diversity and soil physical-chemical properties of the karst rocky desertification ecosystem, SW China. *Pol. J. Environ. Stud.* 30, 1393–1408. doi: 10.15244/pjoes/124225

Yu, Z. C., Sun, M., Xiao, K. K., Ou, B., Liang, S., Hou, H. J., et al. (2022). Changes of phosphorus species during (hydro) thermal treatments of iron-rich sludge and their solubilization mediated by a phosphate solubilizing microorganism. *Sci. Total Environ.* 838:156612. doi: 10.1016/j.scitotenv.2022.156612

Zaidi, A., Khan, M. S., Ahmad, E., Saif, S., Rizvi, A., and Shahid, M. (2016). Growth stimulation and management of diseases of ornamental plants using phosphate solubilizing microorganisms: current perspective. *Acta Physiol. Plant.* 38:117. doi: 10.1007/s11738-016-2133-7

Zhang, K., Chang, L., Li, G., and Li, Y. (2022). Advances and future research in ecological stoichiometry under saline-alkali stress. *Environ. Sci. Pollut. Res.* 30, 5475–5486. doi: 10.1007/s11356-022-24293-x

frontiers | Frontiers in Microbiology

TYPE Original Research
PUBLISHED 20 March 2024
DOI 10.3389/fmicb.2024.1367062

OPEN ACCESS

EDITED BY
Yizhi Sheng,
China University of Geosciences, China

REVIEWED BY
Yuquan Wei,
China Agricultural University, China
Dongyi Guo,
Miami University, United States

*CORRESPONDENCE
Jianxin Wang
✉ jxwang@zjou.edu.cn

†These authors have contributed equally to this work and share first authorship

RECEIVED 08 January 2024
ACCEPTED 28 February 2024
PUBLISHED 20 March 2024

CITATION
Xian W-D, Chen J, Zheng Z, Ding J, Xi Y, Zhang Y, Qu W, Tang C, Li C, Liu X, Li W and Wang J (2024) Water masses influence the variation of microbial communities in the Yangtze River Estuary and its adjacent waters. *Front. Microbiol.* 15:1367062. doi: 10.3389/fmicb.2024.1367062

Water masses influence the variation of microbial communities in the Yangtze River Estuary and its adjacent waters

Wen-Dong Xian[1†], Jinhui Chen[1†], Zheng Zheng[1†], Junjie Ding[1], Yinli Xi[1], Yiying Zhang[1], Wu Qu[1], Chunyu Tang[1], Changlin Li[1], Xuezhu Liu[1], Wei Li[2] and Jianxin Wang[1*]

[1]Marine Microorganism Ecological & Application Lab, Marine Science and Technology College, Zhejiang Ocean University, Zhoushan, China, [2]College of Science, Shantou University, Shantou, China

The Yangtze River estuary (YRE) are strongly influenced by the Kuroshio and terrigenous input from rivers, leading to the formation of distinct water masses, however, there remains a limited understanding of the full extent of this influence. Here the variation of water masses and bacterial communities of 58 seawater samples from the YRE and its adjacent waters were investigated. Our findings suggested that there were 5 water masses in the studied area: Black stream (BS), coastal water in the East China Sea (CW), nearshore mixed water (NM), mixed water in the middle and deep layers of the East China Sea (MM), and deep water blocks in the middle of the East China Sea (DM). The CW mass harbors the highest alpha diversity across all layers, whereas the NM mass exhibits higher diversity in the surface layer but lower in the middle layers. *Proteobacteria* was the most abundant taxa in all water masses, apart from that, in the surface layer masses, *Cyanobacterium*, *Bacteroidota*, and *Actinobacteriota* were the highest proportion in CW, while *Bacteroidota* and *Actinobacteriota* were the highest proportion in NM and BS; in the middle layer, *Bacteroidota* and *Actinobacteriota* were dominant phylum in CW and BS masses, but *Cyanobacterium* was main phylum in NM mass; in the bottom layer, *Bacteroidota* and *Actinobacteriota* were the dominant phylum in CW, while *Marininimicrobia* was the dominated phylum in DM and MM masses. Network analysis suggests water masses have obvious influence on community topological characteristics, moreover, community assembly across masses also differ greatly. Taken together, these results emphasized the significant impact of water masses on the bacterial composition, topological characteristics and assembly process, which may provide a theoretical foundation for predicting alterations in microbial communities within estuarine ecosystems under the influence of water masses.

KEYWORDS

Yangtze river estuary, water masses, bacterial diversity, network topology, community assembly

1 Introduction

Microorganisms play a crucial role on biochemical cycling and serve as indicators of environmental conditions in marine ecosystems. Microorganisms can survive by gaining energies and nutrients from the geological materials and media (Dong et al., 2022), which including nutrient levels (Arrigo, 2005), oxygenation (Gómez-Plaza and Cano-López, 2011), temperature (Chwastowski et al., 2023), pollution (Rosenberg, 2012), carbon (Soong et al., 2020), nitrogen, carbon, sulfur, iron, and arsenic cycling (Chen et al., 2024). Their abundance and diversity provide valuable insights into nutrient concentrations, oxygen levels, and temperature variations across different oceanic regions (Bianchi et al., 2018). In addition, some microorganisms are particularly sensitive to pollutants, making them useful indicators of ecosystem health (Parmar et al., 2016), some microorganisms may be affected by changes in seawater pH and acidity, making them potential indicators of ocean acidification (Turley and Findlay, 2009a,b). They exhibit substantial abundance, extensive variety, remarkable susceptibility to environmental factors, and always interact with other organisms (Petsch et al., 2001; Torsvik et al., 2002). Additionally, they contribute to regulating marine climate change (Jiao and Azam, 2011) and essential for pollutes converting, nutrient and material circulation of the marine ecosystem, maintaining ecosystem health and alleviating environmental pressure (Zhang W.-C. et al., 2018).

In recent years, there has been a growing scientific interest in understanding the influence of ocean currents in shaping bacterial communities (Skarðhamar et al., 2007; Hsiao et al., 2011). Study by Baltar et al. suggests that hydrological characteristics play an important role in controlling microbial community structure (Baltar and Aristegui, 2017). The hydrological characteristics and distribution of water masses strongly support the idea that the East China Sea (ECS) is a hotspot for marine microbial life, as recently suggested by studies on bacterial, phytoplankton, and zooplankton community compositions (Hsieh et al., 2004; Zhou et al., 2021). The coastal current systems in the Yangtze River estuary (YRE) and its adjacent waters are primarily including the Yangtze River diluted water characterized by low salinity and rich nutrients, as well as the Taiwan warm current (a branch of the Kuroshio) with high salinity but low nutrient content (Li et al., 2014). The Kuroshio also plays a significant role in most hydrodynamic processes in the YRE and its adjacent waters, exerting an important impact on the regional ecological environment, local climate, hydrological conditions, and circulation structure (Guo et al., 2018). According to the conventional perspective (Qi, 2014), The ECS is primarily categorized into three major water systems: the coastal water system, the Kuroshio Water System, and the continental shelf mixed water system., owing to its unique geographical location and complex water systems, the YRE acts as a vital ecological barrier that purifies its flow towards the open sea (Jiang et al., 2017; Yang et al., 2022). The fluctuation process of the water masses in the ECS, the seasonal variation of Taiwan's warm water, the variability of the Kuroshio flow in the ECS, and the water exchange process on the continental shelf of the ECS influence marine environmental conditions, material transport dynamics, and energy transfer mechanisms within this region. Different water masses would create distinct physical and chemical environments, resulting in differences in microbial communities (Bardgett et al., 2008), however, research on the influence of water masses on the distribution patterns of estuarine microorganisms is limited. Since these ecosystems are typically affected by freshwater outflows and seawater intrusion, it can be hypothesized that the characteristics of the water mass have influences on the diversity of bacteria, species composition, network topology properties, keystone taxa composition, and community aggregation processes in the YRE.

To address the aforementioned hypothesis, we conducted investigations on distribution of water massed and variations of bacterial community based on 58 seawater samples collected from the YRE. 13 environmental factors, Illumina sequencing of bacterial 16S rRNA genes and network analysis were utilized to examine changes in bacterial community following 9 water masses across surface, middle and bottom layers.

2 Materials and methods

2.1 Sample collection and environmental factor measurement

Sampling of this study was conducted in August 2021 by the scientific research vessel "Zheyuke 2." A total of 58 seawater samples from the surface (depth of 1–2 m), middle (depth of 10–35 m), and bottom (within 5 m above the sediment) water columns were collected from 23 sampling stations along the YRE (Figure 1), Only stations with water depths exceeding 20 m were sampled for middle-layer water in this study. All samples were collected using Go-Flo® bottles equipped with conductivity-temperature-depth (CTD) sensors (Sea-Bird Electronics SBE 32). The *in situ* environmental parameters, including temperature, salinity, pH value, and dissolved oxygen (DO), were directly measured using the CTD sensors. The physical and chemical properties including nitrate (NO_3^-), nitrite (NO_2^-), chemical oxygen demand (COD), silicate (SiO_4^{2-}), phosphate (PO_4^{3-}), total alkalinity (Alk) concentration and chlorophyll a (Chl-a) were determined following the marine monitoring standards of China (Center, N.M.E.M, 2007), Ammonia nitrogen (NH_4^+) were analyzed using SmartChem automatic nutrition analyzer (Smartchem 200, Alliance, France). In detail, NO_3^- concentration was measured using copper cadmium column reduction method, the concentration of NO_2^- was measured using diazo coupling method, the potassium permanganate titration method was used to determine the COD concentration, the concentration of SiO_4^{2-} was measured using the silicon molybdenum blue method, the concentration of PO_4^{3-} was measured using the phosphorus molybdenum blue method, the total Alk concentration was measured using the pH potential drop method, the concentration of Chl a was determined using fluorescence spectrophotometry.

2.2 DNA extraction, sequencing, and amplicon analysis

Total DNA of each sample was extracted by the PowerSoil DNA isolation Kit (Mo bio, San Diego, CA, United States) according to the instructions. The quality of DNA was evaluated by 1% agarose gel electrophoresis and nanodrop 2000 (Thermo, Waltham, Ma, United States). The v4–v5 regions of the 16S rRNA gene were amplified using the primers 515F (5′-GTGCCAGCMGCGG-3′) and

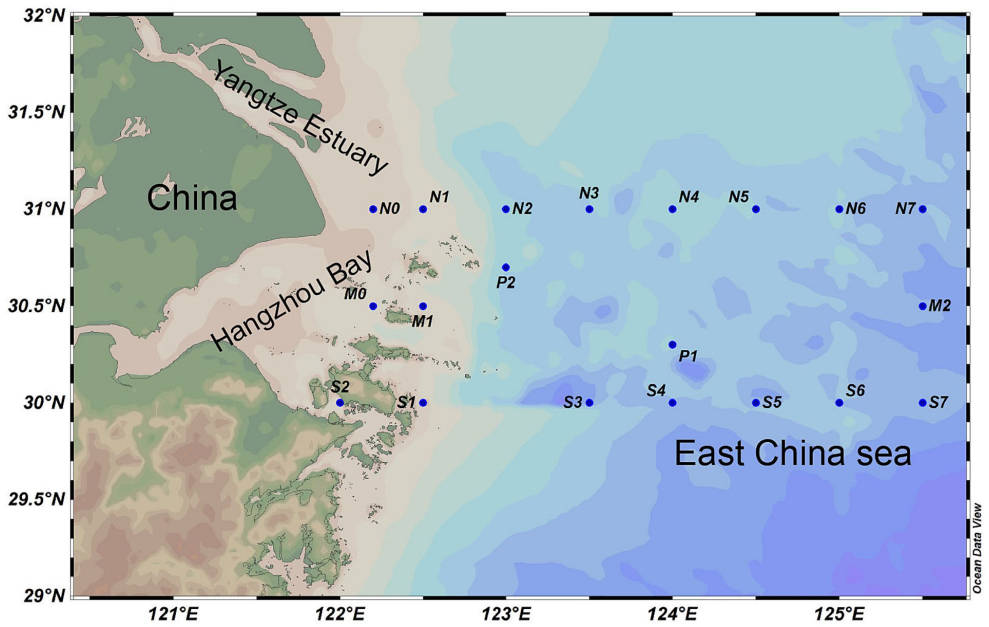

FIGURE 1
An overview of sampling sites. A total of 58 seawater samples were collected from 23 sampling stations along the YRE. The map was generated with the Ocean Data View (http://odv.awi.de).

907R (5′-CCGTCAATTCMTTRAGTTT-3′) (PCR instrument: abigeneamp® Model 9,700). The PCR products were purified with AxyPrepDNA gel recovery kit (Aisijin Biotechnology Co., Ltd.) for library construction, sequencing libraries were generated using Illumina HiSeq Platform, the library quality was assessed on NCBI database, high-throughput sequencing was performed by Majorbio Pharm Technology Co., Ltd. (Shanghai, China) on the Illumina miseq platform.

FLASH (fast length adjustment of short reads) was used to merge the original two terminal sequences (Chen et al., 2018). The original sequences of the paired-end sequencing were processed using the QIIME2 platform (Hall and Beiko, 2018). Primer excision and quality control were performed using vsearch (Rognes et al., 2016). Sequence analyses were performed by QIIME2 with open reference_otus.py, sequences with 97% similarity were assigned to the same ASVs (Caporaso et al., 2010). The SILVA database (v138) (Quast et al., 2012) was used to taxonomic annotation of each ASV based on the RDP classifier (Lan et al., 2012). The ASVs table was generated by mapping the primer removed reads to the representative sequences of ASVs.

2.3 Statistical analysis

The water masses in the continental shelf region usually tend to gather according to variations in both water temperature and salinity (Qiao et al., 2006; Li et al., 2018). Therefore, the "fpc" package in R was utilized to cluster the 58 samples into different groups based on their temperature and salinity (Li et al., 2018). Several packages in R software (Zhang et al., 2019) have been adopted to perform statistical analyses in this study. The "vegan" package (Edgar, 2010) was used for resampling, the "ggplot2" package (Oksanen et al., 2013) was used to generate all figures. "corrplot R" (Wei et al., 2017) package for calculating coefficients and the "picant" package (Wang et al., 2021) for estimation of diversity indices. The Wilcoxon test was used to check community variations between different groups in each water layer. The Bray Curtis distances were calculated using the package "vegan" (Edgar, 2010) with the relative counts of ASVs, and visualized using non metric multidimensional scale analysis (NMDS). Linear multivariate redundancy analysis (RDA) was used to analyze the correlation between bacterial community structure and environmental factors at the ASV level. Community composition maps were visualized using the package of "statnet" (Abdi and Williams, 2010) and "circlize" (Gu et al., 2014). To construct the ecological network of microbial community, we utilized the Conet algorithm in Cytoscape software (v3.9.1). Furthermore, we employed the "rnetcarto" (Doulcier and Stouffer, 2015) package to evaluate the intra-module connectivity (Zi) and inter-module connectivity (Pi) of microbial species, thus enabling the identification of keystone taxa within each community. Neutral models explore microbial taxa abundance through stochastic dispersal, random species formation, and ecological drift (Chen et al., 2019). R^2 indicates overall goodness of fit, while *m*-values represent community-level mobility. *Nm*-values result from multiplying metacommunity size (*N*) by *m*-values. They are used to analyze changes in community composition patterns visually (Zhou et al., 2010a,b).

3 Result

3.1 Identification of water masses

Samples of surface (20 water samples), middle (20 water samples) and bottom (18 water samples) seawater layers were divided into three categories, respectively (Figure 2). Then, to identify these categories of

10.3389/fmicb.2024.1367062

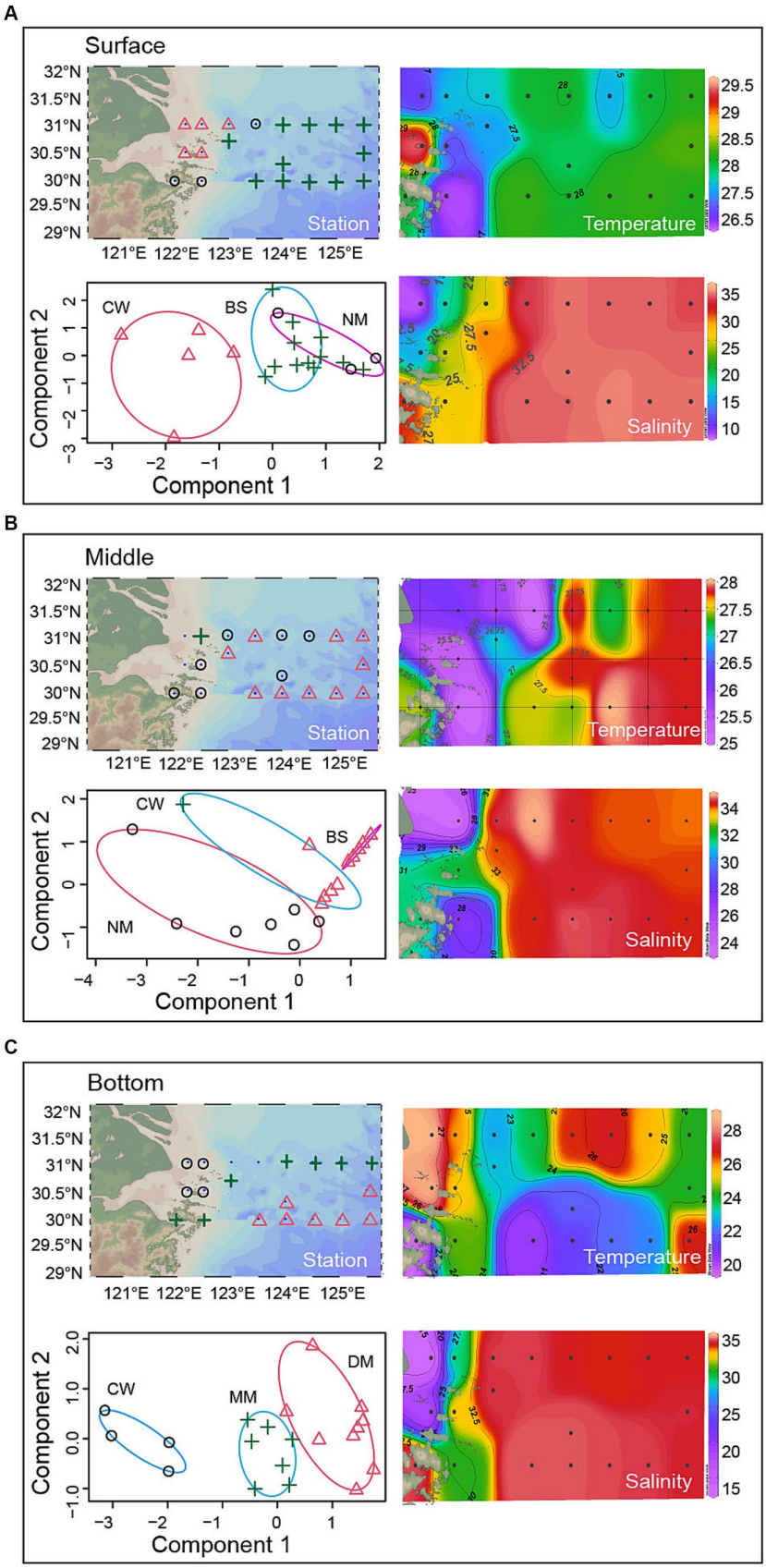

FIGURE 2
The distribution of water masses across the surface, middle and bottom layers.

TABLE 1 Characteristic values of water masses in the YRE and its adjacent waters (Pan et al., 2016).

Water masses	Temperature/°C	Salinity/PSU	Depth/m
coastal water in the East China Sea (CW)	26–28	10–30	0–10
Nearshore mixed water (NM)	25.4–27.6	30.6–32.8	0–20
Black stream (BS)	26.1–29.3	32.3–33.7	0–18
Deep water mass in the middle of the East China Sea (DM)	19.0–20.8	34.3–34.5	30-seabed
mixed water in the middle and deep of the East China Sea (MM)	21.9–22.8	34–34.1	30-seabed

water sample, the water characteristics was compared with a previous study (Table 1) (Pan et al., 2016). The results showed that the study area can be divided into Black Stream (BS) water mass, coastal water in the East China Sea (CW) water mass, nearshore mixed water (NM) water mass, middle deep mixed water in the East China Sea (MM) water mass, deep-water mass in the middle of East China Sea (DM). Finally, in the surface layer, M0, M1, N0, N1, and N2 were identified as CW mass (T: 26.80°C–29.60°C, S: 7.68–24.93 psu). M2, N4, N5, N6, N7, P1, P2, S3, S4, S5, S6, and S7 were identified as BS mass (T: 27.42°C–28.23°C, S: 32.63–33.53 psu). N3, S1, and S2 were identified as NM mass (T: 26.59°C–27.99°C, S: 25.61–32.48 psu). In the middle layer, N1 were identified as CW mass (T: 26.11°C, S: 24.96 psu). M2, N3, N6, N7, P2, S3, S4, S5, S6, and S7 were identified as NM mass (T: 25.31°C–28.01°C, S: 31.17–33.61 psu). M1, N2, N4, N5, P1, S1, and S2 were identified as BS mass (T: 25.25–28.01°C, S: 27.84–33.61 psu). In the bottom layer, N0, M0, N1, and M1 were identified as CW mass (T: 24.91°C–27.78°C, S: 13.62–32.52 psu). M2, N2, N3, P1, S3, S4, S5, S6, and S7 also were identified as CW mass (T: 20.85°C–26.08°C, S: 20.85°C–36.08°C, S: 20.62–32.52 psu). N2, N3, P1, S3, S4, S5, S6, and S7 were identified as DM mass (T: 20.85°C–26.08°C, S: 33.81–34.30 psu). N5, N6, N7, P2, S1, S2, and N4 were identified as MM mass (T: 20.03°C–26.20°C, S: 29.95–34.24 psu).

3.2 Bacterial diversity

The alpha diversity indices, including Chao1, Shannon index and ASVs Richness, were calculated among water masses (Figures 3A–I). The results indicate that, all three indices of CW mass community were highest across three layers. Additionally, significant differences ($p < 0.01$) in the Chao1, Shannon, and Richness index were observed between CW and BS mass in the surface seawater (Figures 3A–C). In the middle layer, differences ($p < 0.05$) were also observed among the Chao1, Shannon and Richness index between CW and BS mass (Figures 3D–F), moreover, the Shannon index and Richness index exhibit differences ($p < 0.05$) between BS and NM. In the bottom layer, significant differences ($p < 0.05$) of Chao1 and Richness index were observed across all water masses, the significant difference ($p < 0.05$) of Shannon was also observed between CW and DM mass community (Figures 3G–I).

To measure the differences in bacterial composition among samples, the beta diversity index was analyzed. The PCoA analysis based on the Mountford distance indicates a significant difference ($R^2 = 0.43–0.45$; $p < 0.05$) between bacterial communities among water masses within the same water layer (Figures 3J–L). In detail, the ANOSIM analysis revealed significant differences ($R^2 = 0.43$, $p = 0.005$) among CW, NM and BS masses in the surface layer (S-CW, S-NM, S-BS). Similarly, significant differences ($R^2 = 0.44$, $p < 0.005$) were observed among BS, CW, and NM masses in the middle layer (M-S, M-FE, M-M). Additionally, there were significant differences ($R^2 = 0.45$, $p < 0.001$) among MM, DM and CW masses in the bottom layer (M-MM, M-DM, M-CW).

We conducted redundancy analysis (RDA) to understand the relationship between microbial communities and environmental factors (Figure 4). The RDA results explained 67.2%, 53.7% and 64.1% of the variation in the surface, middle and bottom bacterial communities, respectively. The Mantel test revealed significant correlations between microbial communities in different layers and water masses with 13 environmental variables (Supplementary Table S2). The results indicated that COD, Chl a and NO_2^- were primary environmental factors significantly affecting community structure ($p < 0.05$). In the surface layer (Supplementary Table S2). In the middle layer, salinity, DO and temperature were identified as important environmental factors affecting community structure as well ($p < 0.05$) (Supplementary Table S2). In the bottom layer, COD, DO, Chl a, PO_4^{3-}, temperature, salinity, DIC were the main environmental factors affecting community structure ($p < 0.01$) (Supplementary Table S2).

3.3 Bacterial community composition across water masses

The distribution of bacterial phyla of different water masses at the surface, middle, and bottom layers were analyzed (Figure 5). *Proteobacteria* was detected as the dominant bacterial phylum across all nine water masses. In the surface seawater, *Cyanobacteria* exhibits the highest proportion in BS (25.73%), followed by NM (18.4%) and CW (10.44%), alongside *Bacteroidota* showing the highest proportion (34.05%) in NM, followed by CW (13.16%) and BS (8.69%). Notably, *Actinobacteriota* demonstrates varying proportions across 3 water masses, with BS having the highest proportion (12.56%). In contrast, CW displays higher proportions (15.05%) of other bacterial phyla compared to BS (7%) and NM (4.49%) (Figure 5A). In the middle layer, *Actinobacteriota* emerges as the second most abundant phylum, *Actinobacteriota* was found in all 3 water masses, with NM having the highest proportion (12.78%), followed by BS (9.81%) and CW (9.59%). The proportion of *Cyanobacteria* varies across CW, with CW showing a lower proportion (2%) compared to the NM (17.23%) and BS (4.41%), while the proportion of *Planctomycota* in CW (4.44%) was higher than NM (2.12%) and BS (3.5%), (Figure 5B). In the bottom seawater, the bacterial phyla with high abundance were *Bacteroidota*, *Actinobacteriota*, and *Marininimicrobia* (SAR406_clade). In CW, however, the proportion (1.41%) of *Marininimicrobia* (SAR406_clade) was lower compared to NM (3.2%) and BS (7.27%) (Figure 5C).

10.3389/fmicb.2024.1367062

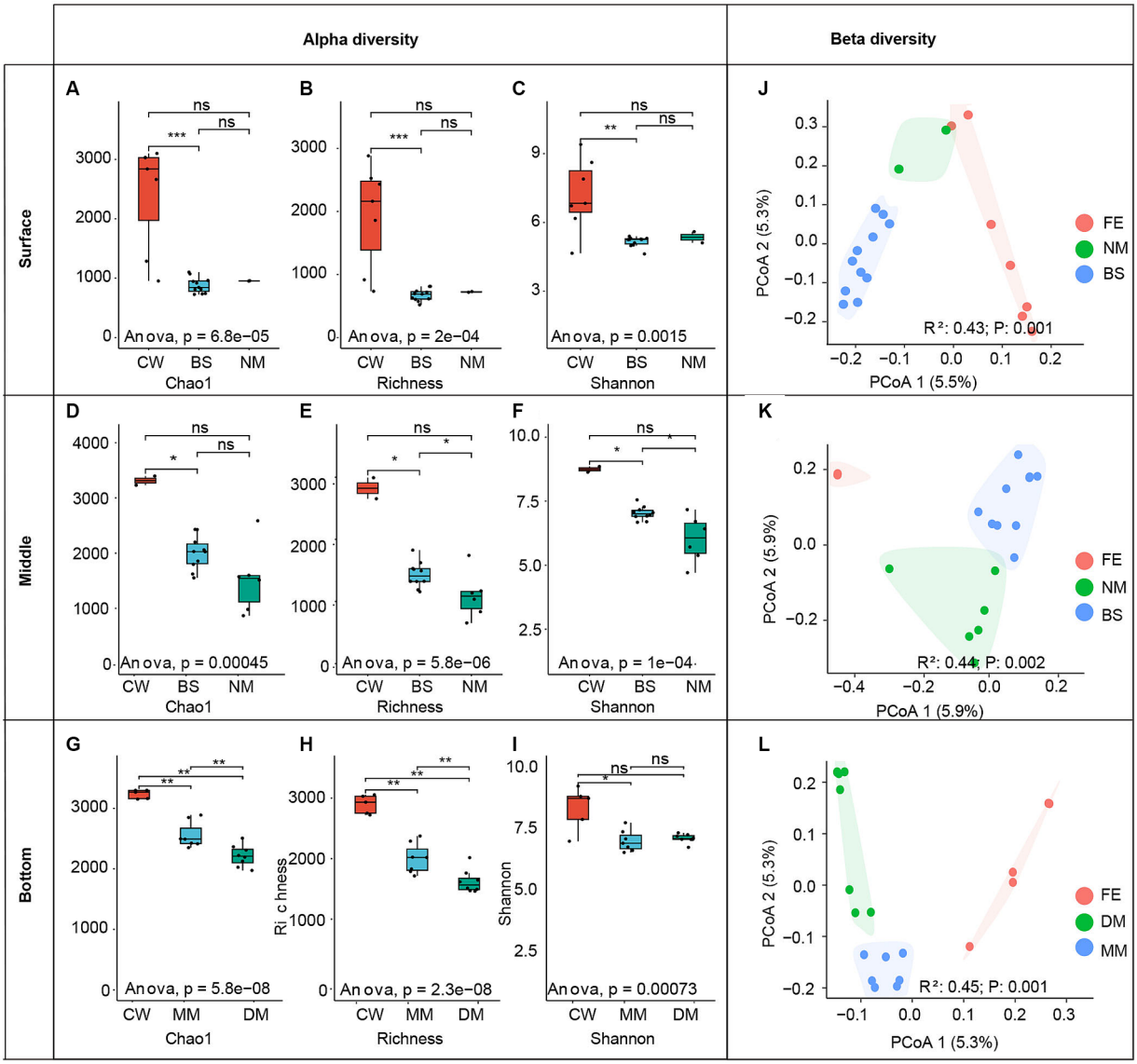

FIGURE 3
Left panel: alpha diversity indexes of different water layers (B, M, S). The group differences of Chao1 index **(A)**, richness index **(B)**, and Shannon index **(C)** of different water masses in surface **(A–C)**, meddle **(D–F)**, and bottom **(G–I)** seawater layers. Asterisks indicate the significance of the difference between the two groups ("***" indicates that the *p*-value is less than 0.001; "**" indicates that the *p*-value range is 0.001–0.01; "*" indicates that the *p*-value range is 0.01–0.05, "ns" indicates that the *p*-value is greater than 0.05). Right panel: principal coordinate analysis (PCoA) of bacterial communities based on Mountfort distance.

3.4 Topological characteristics and keystone taxa of bacteria across water masses

To compare the topological characteristics of microbial communities across different water masses, the ecological network was calculated (Table 2). The results of the topological properties were plotted in a columnar stacked graph (Figure 6). The nodes (1121), edges (102948), average degree (183.67), and density (0.16) of network in the S-CW were higher compared to those in other water masses. Moreover, the average path length is lower than that of other water masses. These findings indicate that the network size of this water mass is larger than other masses, with lower separation and higher connectivity. Apart from S-CW, the nodes and edges in the B-MM exhibit highest values compared to other water masses, indicating a larger network size in the B-MM. The average clustering coefficient and average path length in the M-BS were also higher than those of other water masses, suggesting lower separation and greater connectivity. Furthermore, the correlations between nodes across different water masses were predominantly characterized by positive correlations (76.66–96.1%).

In co-occurrence networks, different nodes represent various microbial species, and key species of the community can be identified based on the topological characteristics of the nodes. Node attribute types are typically classified into four categories: peripheral nodes ($Zi < 2.5$, $Pi < 0.62$), connector nodes ($Zi < 2.5$, $Pi \geq 0.62$), module hub nodes ($Zi \geq 2.5$, $Pi < 0.62$), and network hub nodes ($Zi \geq 2.5$, $Pi \geq 0.62$). According to previous research (Cox et al., 2016), nodes with $Zi \geq 2.5$ or $Pi \geq 0.62$ are defined as key species, based on their intra-module

10.3389/fmicb.2024.1367062

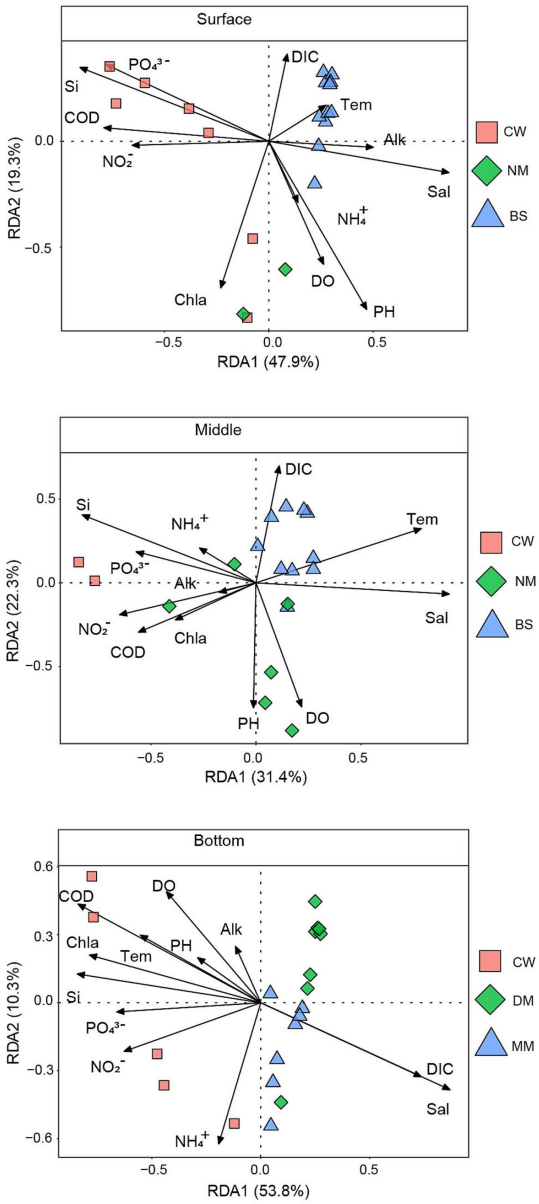

FIGURE 4
The relationship between environmental factors and the bacterial community.

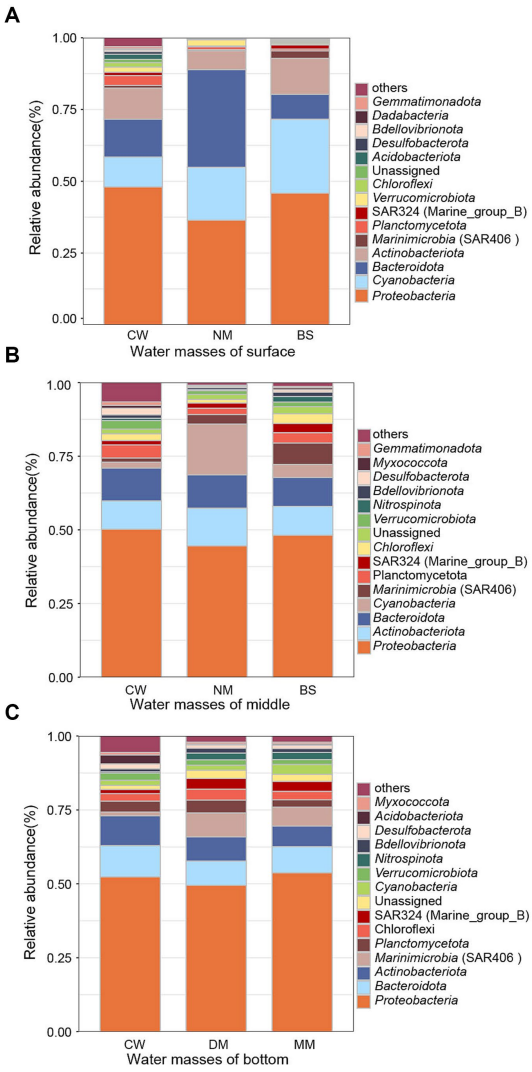

FIGURE 5
Bacterial community composition. The relative abundances of dominant bacterial phyla in surface **(A)**, middle **(B)**, and bottom **(C)** seawater community bacteria samples. Others indicate the other phyla except the top 15 in relative abundance in the total samples. BS (Black stream) water mass, CW (coastal water of the East China Sea) water mass, NM (nearshore mixed water) water mass, MM (middle deep mixed water in the East China Sea) water mass, DM (deep-water mass in the middle of the East China Sea) water mass.

connectivity (Zi) and inter-module connectivity (Pi) in the network. Generally, all three types of nodes, except for peripherals, are classified as key nodes (Deng et al., 2012). As depicted in Supplementary Figure S1, it was evident that S-CW exhibits the highest number of connectors, indicating a closer interaction between network modules in this water mass. Furthermore, there is only one modular hub in S-BS, M-BS, B-MM, and B-DM, whereas no modular hub was observed in S-CW and S-NM. This suggests a high degree of interconnections between species within each water mass. Figure 7 illustrates the composition of key species in bacterial communities at the phylum level across six water masses. The species composition of key species in S-CW was relatively complex, with the majority belonging to *Actinobacteriota* and *Bacteroidota* phyla. The key species in M-BS predominantly belong to *Nitrospinota*, while those in M-NM were mainly represented by *Planctomycota*. In B-DM, the majority of key species belong to *Marininimicrobia* (SAR406_clade), whereas most of the key species in B-MM belong to *Bacteroidota*.

3.5 Analysis of bacterial assembly process

The NCM analysis successfully captured a significant portion of the relationship between the occurrence frequency of ASVs and their mean relative abundances (Supplementary Figure S2; Figure 8). The results indicate that, compared to other water masses, the impact of stochastic processes has a greater influence on B-MM, M-CW, and S-NM, while M-NM and S-CW and S-BS were more influenced by deterministic processes. Additionally, species diffusion within communities in B-CW

TABLE 2 Coexistence network indicators of different water masses in the YRE and its adjacent waters.

Topological parameter	S-CW	S-BS	M-BS	B-DM	B-MM	M-NM
Nodes	1,121	305	546	995	1,378	417
Edges	102,948	388	645	1,534	2,432	1,140
positive correlation %	86.15	96.1	87.68	91.35	93.43	76.66
negative correlation %	13.85	3.9	12.32	8.65	6.57	23.34
Average degree	183.67	2.54	2.36	3.08	3.53	5.47
Density	0.16	0.01	0.01	0.01	0.01	0.01
Average clustering coefficient	0.69	0.36	2.27	0.68	0.80	0.84
Average path length	3.16	6.08	5.18	4.77	2.56	4.55
Network diameter	13	17	15	14	11	16
Modularity	0.20	0.87	0.86	0.97	0.75	0.92

S-CW, the surface layer (S) of coastal water mass in the East China Sea (CW); S-BS, the surface layer (S) of Black stream water mass (BS); M-BS, the surface layer (S) of Black stream water mass (BS); B-MD, the bottom layer (B) of deep water mass in the middle of the East China Sea mass (DM); B-MM, the bottom layer (B) of middle deep mixed water mass in the East China Sea (MM); M-NM, the middle layer (M) of nearshore mixed water mass (NM).

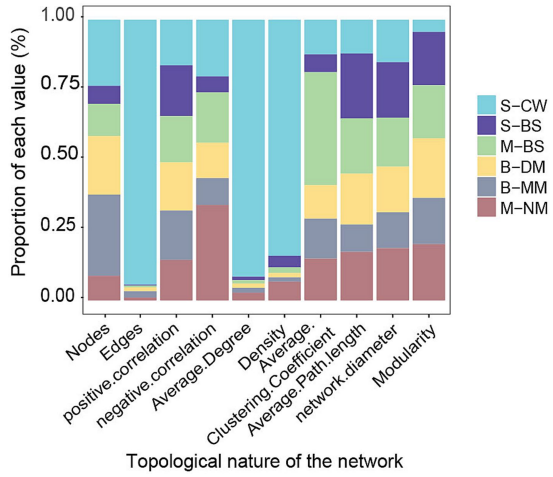

FIGURE 6
Coexistence network indicators of different water masses in the YRE and its adjacent waters.

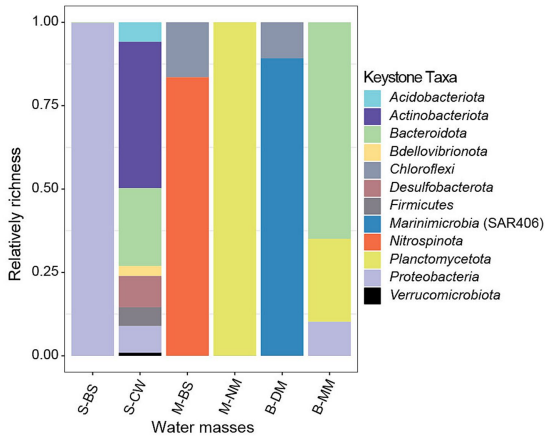

FIGURE 7
Keystone taxa composition of bacterial community.

and M-BS was more restricted compared to other water masses, whereas species in B-DM experience less constraint on diffusion.

4 Discussion

Water masses are commonly occurring in the estuarine environment, yet little is known about the influences on microbial community across the YRE ecosystems. In this study, we analyzed the bacterial diversity in various water masses occurred in the YRE and its adjacent waters. Across the studied area, five distinct water masses were identified. Significant differences of bacterial communities were observed when considering water masses on layers at different depths (Figures 3J–L), the great influence of dramatic changes in environmental gradients in a same water mass resulted in no apparent differences across all masses (Supplementary Figure S3), as a result, the communities in a mass were analyzed in surface, middle and bottom water layers.

4.1 Bacterial diversity and dominant taxa among water masses

The coastal current system in the YRE is primarily composed of Kuroshio, coastal, and continental shelf mixed water masses (Song, 2011). The Taiwan warm water mass, a branch of the Kuroshio, flows northward through the Taiwan Strait to the ECS, leading to an increase in both temperature and salinity within the sea water (Jan et al., 2002). The significant higher microbial diversity in CW water mass (Figure 3) may be attributed to warm temperature from Taiwan warm water mass and richer nutrients from coastal seawaters (Margesin et al., 2017). *Proteobacteria* was the dominant phylum in water masses at all layers, which consistent with previous results obtained from pure cultures in the YRE (He et al., 2013). In the surface seawater, except for *Proteobacteria* and *Cyanobacteria* in BS mass, *Bacteroidota* occupies the highest proportion compared to the other two water masses, followed by CW and NM. Freshwater from the Yangtze River influences the salinity and temperature (Ferrenberg et al., 2013), which may lead to a relatively low proportion of *Cyanobacteria* in the surface seawater masses. In

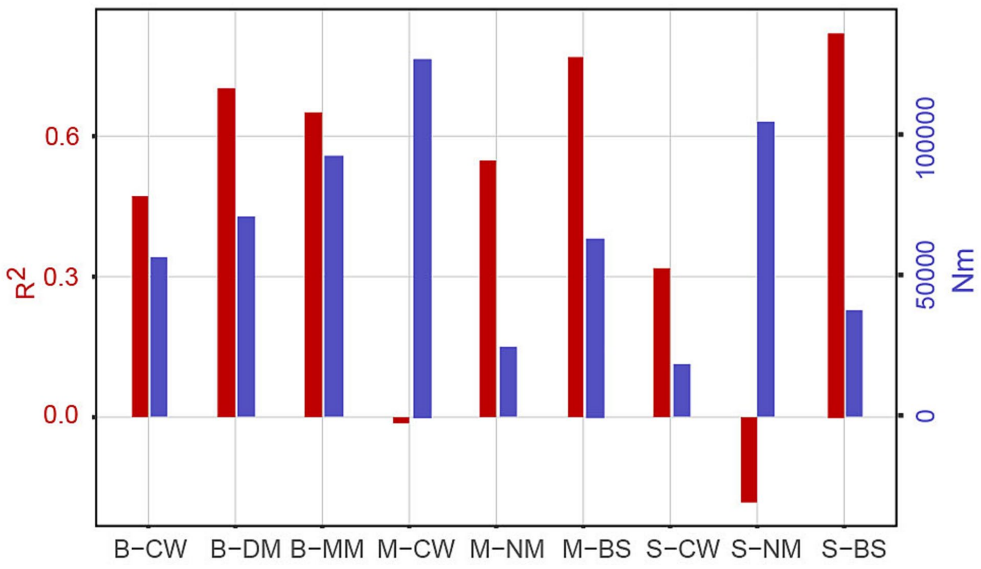

FIGURE 8
The neutral community model. Rsqr represents overall goodness of fit, *m*-value quantifies community level migration rate, and *Nm* value is the product of metacommunity size (*N*) and *m*-value. "Rsqr" commonly refers to *R*-squared, which is a statistical measure used to assess the goodness-of-fit of a regression equation to the observed data. *n* community ecology, "Nm" typically refers to the migration rate or population dispersal rate within a neutral model.

comparison, the distribution of *Actinobacteriota* varied across water masses, with CW exhibiting the highest proportion. This observation is consistent with previous research (Yang et al., 2023), which indicates a negative correlation between salinity levels and the abundance of *Actinobacteriota*. In the middle seawater, there was a significant difference in the proportion of *Cyanobacteria* among the various water masses. Specifically, the proportion of *Cyanobacteria* in CW was lower than that in the other two water masses, this finding contradicts previous research results, which claimed that *Cyanobacteria* were more likely to thrive in water with lower salinity (Śliwińska-Wilczewska et al., 2019). In the bottom seawater, *Bacteroidota*, *Actinobacteriota* and *Marinimicrobia* (SAR406_clade) account for a relatively high abundance, the proportion of *Marinimicrobia* (SAR406_clade) in CW was lower than that in the other two water masses, which is consistent with the previous study of the Pearl River estuary (Sang et al., 2022).

Temperature and salinity as crucial factors impacting the aggregation of bacterial communities in oceanic environments (Gilbert et al., 2009). Our findings with the RDA and Mantel analyses further revealed that salinity, temperature, COD, Chl a, and NO_2^- significantly influence the bacterial communities in the seawater masses. These findings suggests NO_2^- is another important environmental factor influencing bacterial diversities among water masses in the YRE.

4.2 Topological characteristics of networks and keystone taxa within different water masses

Network topological characteristics play the crucial role in evaluating the health of ecosystems and identifying potential targets for biotechnological interventions (Bull et al., 2000). In this study, the S-NM, M-CW, B-CW were omitted due to the limited samples. The correlations among microbes in different water masses were primarily characterized by positive relationship (Figure 8). However, the negative correlation ratio of M-NM and S-BS was slightly higher compared to other water masses in different layers, this suggests that the competition between species within these two water masses was greater than in other water masses. The S-CW and B-MM exhibit higher network connectivity, which indicates communities in these water mass possesses more complex inter-species interactions in comparison to other water masses. The bacterial networks within S-CW (Density = 0.164) and M-NM (Density = 0.013) were denser than other water masses, which suggest the more complex interactions, greater stability, and stronger stress resistance microbial community harbors in these water mass.

Among the different water masses, S-CW and B-MM exhibit relatively high network average and average clustering coefficients, as well as shorter average paths. These findings suggest that microbial communities residing within these two water masses possess enhanced connectivity and participate in more complex species interactions (Zhang B. et al., 2018; Yang et al., 2019). Therefore, the microbial communities in the S-CW and B-MM closely interact with each other and respond rapidly to external disturbances, but the community exhibits less stability. Conversely, the microbial communities in the middle and bottom seawater masses demonstrate a buffering effect on external disturbances, resulting in strong community stability. Furthermore, the bacterial community network in the S-CW and B-MM was more complex, indicating a closer association between the microbes (Yang et al., 2019). Additionally, the modularity parameters of the network diagrams in all water masses (except for CW) in this study were found to be greater than 0.4, This indicates that the overall topology of network in S-BS, M-BS, B-DM, B-MM, and M-NM exhibits a high level of modularity (Qin et al., 2021). Similar to other complex environments, such as networks constructed with soil (Williams et al., 2014), wetland sediments (Huang et al., 2019).

Keystone taxa are nodes that exhibit a high degree of connectivity within a network (Xian et al., 2020), these particular species hold a unique position within a microbial community, the absence of them impacts both the structure and function of microbial community (Modlmeier et al., 2014). In this study, keystone taxa mainly distributed in *Marinimicrobia*, *Planctomycetota*, *Bacteroidota*, *Nitrospinota*, and *Proteobacteria*. *Planctomycetota*, *Bacteroidetes*, the anaerobic planktonic bacteria within aquatic environments, serves as the main member responsible for the degradation of organic matter in the water column (Sun et al., 2021). Interestingly, *Proteobacteria* was the dominant phylum of in all water masses, but not the primary keystone taxa at phylum across water masses, and only identified as keystone taxa at phylum in three masses (S-BS, S-CW, and B-MM). The possible explanation was that the keystone taxa always not the dominant group (Cupit et al., 2019).

4.3 Assembly process of bacterial communities in different water masses

The neutral community model is commonly employed to assess the impacts of random diffusion and ecological drift on bacterial community assembly. In this model, R^2 represents the overall goodness of fit, *m*-value quantifies the community-level migration rate, and *Nm* value is the product of metacommunity size (*N*) and *m*-value. The *m*-value reflects the migration rate at the community level. A higher *m*-value indicates less restrictions on species diffusion within the entire community, while a lower *m*-value suggests higher constraint on species dispersal (Su et al., 2022). A higher R^2 value indicates a closer fit to the neutral model, suggesting that community assembly is predominantly influenced by stochastic processes rather than deterministic processes (Sloan et al., 2006). Using the neutral community model, we evaluated the differences in bacterial community assembly processes across various water masses within the YRE and adjacent environments.

The previous study conducted in the YRE claimed that stochastic processes dominate the assembly of bacterial communities (Shi et al., 2023). Despite the similar conclusion of B-MM and M-CW, the *Nm* value of M-NM, S-CW, and S-BS were less than 5,000 (the highest value in B-MM was 92,918) (Supplementary Figure S2), suggesting bacterial assembly process was not directly controlled by geographical niches in this zone. Instead, water mass dynamics strongly affect the assembly process of microorganisms in the same area. The YRE is eutrophic, and the availability of nutrients for planktonic microbes makes it compatible with nutrient-rich substrates, Besides the temperature and salt, differences of dissolved organic matter (Guo et al., 2018) and nutrient substrates (Catão et al., 2021) among masses may also influences the assembly process. Moreover, there exist unmeasured variables or factors that could potentially impact these dynamics, necessitating further investigation to elucidate their influence (Jiao and Lu, 2020).

5 Conclusion

This study investigated the effects of water masses on the variation of bacterial community in the YRE. The surveyed sea area was divided into five distinct water masses: Black Stream (BS) water mass, coastal water in the East China Sea (CW) water mass, nearshore mixed water (NM) water mass, middle deep mixed water in the East China Sea (MM) water mass, deep-water mass in the middle of the East China Sea (DM). In the surface layer, *Cyanobacteria* and *Bacteroidota* were the dominant phylum in BS water mass, while *Actinobacteriota* has the highest proportion in CW. In the middle seawater, the proportion of *Cyanobacteria* in CW was lower than that of the other two water masses, whereas the proportion of *Planctomycota* was higher. Additionally, the proportion of *Marininimicrobia* (SAR406_clade) in CW was lower than in the other two water masses. In the bottom seawater layer, the bacterial phyla with high abundance were *Bacteroidota*, *Actinobacteriota*, and *Marininimicrobia*. In CW, however, the proportion (1.41%) of *Marininimicrobia* (SAR406_clade) was lower compared to NM (3.2%) and BS (7.27%). The network analysis results suggested the interaction among bacterial communities in distinct water masses were primarily characterized by positive correlation. Both stochastic and deterministic processes influenced bacterial assembly processes among the diverse water masses.

Data availability statement

The datasets presented in this study can be found in online repositories. The names of the repository/repositories and accession number(s) can be found at: https://www.ncbi.nlm.nih.gov/sra/?term=PRJNA1000040.

Ethics statement

This article does not contain any studies involving to human participants or animals. Sample collection is following local regulations and is approved by management.

Author contributions

W-DX: Supervision, Validation, Writing – original draft, Writing – review & editing. JC: Investigation, Software, Writing – original draft. ZZ: Data curation, Investigation, Writing – review & editing. JD: Investigation, Software, Writing – review & editing. YX: Investigation, Writing – review & editing. YZ: Investigation, Methodology, Writing – review & editing. WQ: Methodology, Software, Writing – review & editing. CT: Methodology, Software, Writing – review & editing. CL: Writing – review & editing. XL: Data curation, Writing – review & editing. WL: Writing – review & editing. JW: Funding acquisition, Writing – review & editing, Conceptualization.

Funding

The author(s) declare that financial support was received for the research, authorship, and/or publication of this article. This work was funded by the Key R&D projects in Zhejiang Province (Grant Numbers: 2021C02047, 2022C02040, and 2023C03120), the Fundamental Research Fund for the Provincial Universities of Zhejiang (Grant Number: 2021JD003), the National Natural Science Foundation of China (Grant Number: Q20C060004), the Science and

Technology Program of Zhoushan (Grant Number: 2019C21011), the Research Project of Ecological Environment Protection and Restoration of Yangtze River in Zhoushan (Grant Number: 2019C21011), the Natural Science Foundation of Zhejiang Province (Grant Number: SZGXZS2020068), and the College Students' Innovative Entrepreneurial Training Plan Program (202110340009). The study was also supported by the Sophisticated Ocean Front and Fisheries Investigation (SOPHI) of Zhejiang Ocean University.

Conflict of interest

The authors declare that the research was conducted in the absence of any commercial or financial relationships that could be construed as a potential conflict of interest.

Publisher's note

Supplementary material

The Supplementary material for this article can be found online at: https://www.frontiersin.org/articles/10.3389/fmicb.2024.1367062/full#supplementary-material

References

Abdi, H., and Williams, L. (2010). Principal component analysis. *WIRES* 2, 433–459. doi: 10.1002/wics.101

Arrigo, K. R. (2005). Marine microorganisms and global nutrient cycles. *Nature* 437, 349–355. doi: 10.1038/nature04159

Baltar, F., and Aristegui, J. (2017). Fronts at the surface ocean can shape distinct regions of microbial activity and community assemblages down to the bathypelagic zone: the Azores front as a case study. *Front. Mar. Sci.* 4:e252. doi: 10.3389/fmars.2017.00252

Bardgett, R. D., Freeman, C., and Ostle, N. J. (2008). Microbial contributions to climate change through carbon cycle feedbacks. *ISME J.* 2, 805–814. doi: 10.1038/ismej.2008.58

Bianchi, T. S., Cui, X., Blair, N. E., Burdige, D. J., Eglinton, T. I., and Galy, V. (2018). Centers of organic carbon burial and oxidation at the land-ocean interface. *Org. Geochem.* 115, 138–155. doi: 10.1016/j.orggeochem.2017.09.008

Bull, A. T., Ward, A. C., and Goodfellow, M. (2000). Search and discovery strategies for biotechnology: the paradigm shift. *Microbiol. Mol. Biol. Rev.* 64, 573–606. doi: 10.1128/MMBR.64.3.573-606.2000

Caporaso, J. G., Kuczynski, J., Stombaugh, J., Bittinger, K., Bushman, F. D., Costello, E. K., et al. (2010). QIIME allows analysis of high-throughput community sequencing data. *Nat. Methods* 7, 335–336. doi: 10.1038/nmeth.f.303

Catão, C. P. E., Pollet, T., Garnier, C., Barry-Martinet, R., Rehel, K., Linossier, I., et al. (2021). Temperate and tropical coastal waters share relatively similar microbial biofilm communities while free-living or particle-attached communities are distinct. *Mol. Ecol.* 30, 2891–2904. doi: 10.1111/mec.15929

Center, N.M.E.M. (2007). The specification for marine monitoring. Part 4:seawater analysis(in Chinese). *General Administration of Quality Supervision, inspection and quarantine of the People's republic of China*

Chen, W., Ren, K., Isabwe, A., Chen, H., Liu, M., and Yang, J. (2019). Stochastic processes shape microeukaryotic community assembly in a subtropical river across wet and dry seasons. *Microbiome* 7, 1–16. doi: 10.1186/s40168-019-0749-8

Chen, X., Sheng, Y., Wang, G., Zhou, P., Liao, F., Mao, H., et al. (2024). Spatiotemporal successions of N, S, C, Fe, and as cycling genes in groundwater of a wetland ecosystem: enhanced heterogeneity in wet season. *Water Res.* 251:121105. doi: 10.1016/j.watres.2024.121105

Chen, S., Zhou, Y., Chen, Y., and Gu, J. (2018). Fastp: an ultra-fast all-in-one FASTQ preprocessor. *Bioinformatics* 34, i884–i890. doi: 10.1093/bioinformatics/bty560

Chwastowski, J., Wójcik, K., Kołoczek, H., Oszczęda, Z., Khachatryan, K., and Tomasik, P. (2023). Effect of water treatment with low-temperature and low-pressure glow plasma of low frequency on the growth of selected microorganisms. *Int. J. Food Prop.* 26, 502–510. doi: 10.1080/10942912.2023.2169708

Cox, F., Newsham, K. K., Bol, R., Dungait, J. A., and Robinson, C. H. (2016). Not poles apart: Antarctic soil fungal communities show similarities to those of the distant Arctic. *Ecol. Lett.* 19, 528–536. doi: 10.1111/ele.12587

Cupit, C., Lomstein, B. A., and Kjeldsen, K. U. (2019). Contrasting community composition of endospores and vegetative Firmicutes in a marine sediment suggests both endogenous and exogenous sources of endospore accumulation. *Environ. Microbiol. Rep.* 11, 352–360. doi: 10.1111/1758-2229.12679

Deng, Y., Jiang, Y.-H., Yang, Y., He, Z., Luo, F., and Zhou, J. (2012). Molecular ecological network analyses. *BMC Bioinformatics* 13, 1–20. doi: 10.1186/1471-2105-13-113

Dong, H., Huang, L., Zhao, L., Zeng, Q., Liu, X., Sheng, Y., et al. (2022). A critical review of mineral–microbe interaction and co-evolution: mechanisms and applications. *Natl. Sci. Rev.* 9:nwac128. doi: 10.1093/nsr/nwac128

Doulcier, G., and Stouffer, D. (2015). *Rnetcarto: fast network modularity and roles computation by simulated annealing. R package version 0.2 4*

Edgar, R. C. (2010). Search and clustering orders of magnitude faster than BLAST. *Bioinformatics* 26, 2460–2461. doi: 10.1093/bioinformatics/btq461

Ferrenberg, S., O'neill, S. P., Knelman, J. E., Todd, B., Duggan, S., Bradley, D., et al. (2013). Changes in assembly processes in soil bacterial communities following a wildfire disturbance. *ISME J.* 7, 1102–1111. doi: 10.1038/ismej.2013.11

Gilbert, J. A., Field, D., Swift, P., Newbold, L., Oliver, A., Smyth, T., et al. (2009). The seasonal structure of microbial communities in the Western English Channel. *Environ. Microbiol.* 11, 3132–3139. doi: 10.1111/j.1462-2920.2009.02017.x

Gómez-Plaza, E., and Cano-López, M. (2011). A review on micro-oxygenation of red wines: claims, benefits and the underlying chemistry. *Food Chem.* 125, 1131–1140. doi: 10.1016/j.foodchem.2010.10.034

Gu, Z., Gu, L., Eils, R., Schlesner, M., and Brors, B. (2014). Circlize implements and enhances circular visualization in R. *Bioinformatics* 30, 2811–2812. doi: 10.1093/bioinformatics/btu393

Guo, J.-Q., Liang, S.-K., Li, X.-J., Li, W., Wang, Y.-F., and Su, R.-G. (2018). Composition and bioavailability of dissolved organic matter in different water masses of the East China Sea. *Estuar. Coast. Shelf Sci.* 212, 189–202. doi: 10.1016/j.ecss.2018.07.009

Hall, M., and Beiko, R. G. (2018). 16S rRNA gene analysis with QIIME2. *Microbiome Anal. Methods Protocols* 1849, 113–129. doi: 10.1007/978-1-4939-8728-3_8

He, J., Liu, X., Zhao, R., Wu, F., and Wang, J. (2013). Diversity of cultured and uncultured bacteria in surface layer sediment from the East China Sea (in Chinese). *Biodivers. Sci.* 21, 28–37. doi: 10.3724/SP.J.1003.2013.10097

Hsiao, S.-H., Kâ, S., Fang, T.-H., and Hwang, J.-S. (2011). Zooplankton assemblages as indicators of seasonal changes in water masses in the boundary waters between the East China Sea and the Taiwan Strait. *Hydrobiologia* 666, 317–330. doi: 10.1007/s10750-011-0628-1

Hsieh, C.-H. H., Chiu, T.-S., and Shih, C.-T. (2004). Copepod diversity and composition as indicators of intrusion of the Kuroshio branch current into the northern Taiwan Strait in spring 2000. *Zool. Stud.* 43, 393–403.

Huang, W., Chen, X., Wang, K., Chen, J., Zheng, B., and Jiang, X. (2019). Comparison among the microbial communities in the lake, lake wetland, and estuary sediments of a plain river network. *Microbiology* 8:e00644. doi: 10.1002/mbo3.644

Jan, S., Wang, J., Chern, C.-S., and Chao, S.-Y. (2002). Seasonal variation of the circulation in the Taiwan Strait. *J. Mar. Syst.* 35, 249–268. doi: 10.1016/s0924-7963(02)00130-6

Jiang, X., Yao, L., Guo, L., Liu, G., and Liu, W. (2017). Multi-scale factors affecting composition, diversity, and abundance of sediment denitrifying microorganisms in Yangtze lakes. *Appl. Microbiol. Biotechnol.* 101, 8015–8027. doi: 10.1007/s00253-017-8537-5

Jiao, N., and Azam, F. (2011). Microbial carbon pump and its significance for carbon sequestration in the ocean. *Microb. Carbon Pump Ocean* 10, 43–45. doi: 10.1126/science.opms.sb0001

Jiao, S., and Lu, Y. (2020). Soil pH and temperature regulate assembly processes of abundant and rare bacterial communities in agricultural ecosystems. *Environ. Microbiol.* 22, 1052–1065. doi: 10.1111/1462-2920.14815

Lan, Y., Wang, Q., Cole, J. R., and Rosen, G. L. (2012). Using the RDP classifier to predict taxonomic novelty and reduce the search space for finding novel organisms. *PLoS One* 7:e32491. doi: 10.1371/journal.pone.0032491

Li, L., Ren, J.-L., Yan, Z., Liu, S.-M., Wu, Y., Zhou, F., et al. (2014). Behavior of arsenic in the coastal area of the Changjiang (Yangtze River) estuary: influences of water mass mixing, the spring bloom and hypoxia. *Cont. Shelf Res.* 80, 67–78. doi: 10.1016/j.csr.2014.02.021

Li, W., Wang, M., Pan, H., Burgaud, G., Liang, S., Guo, J., et al. (2018). Highlighting patterns of fungal diversity and composition shaped by ocean currents using the East China Sea as a model. *Mol. Ecol.* 27, 564–576. doi: 10.1111/mec.14440

Margesin, R., Siles, J. A., Cajthaml, T., Öhlinger, B., and Kistler, E. (2017). Microbiology meets archaeology: soil microbial communities reveal different human activities at archaic Monte Iato (sixth century BC). *Microb. Ecol.* 73, 925–938. doi: 10.1007/s00248-016-0904-8

Modlmeier, A. P., Keiser, C. N., Watters, J. V., Sih, A., and Pruitt, J. N. (2014). The keystone individual concept: an ecological and evolutionary overview. *Anim. Behav.* 89, 53–62. doi: 10.1016/j.anbehav.2013.12.020

Oksanen, J., Blanchet, F., Kindt, R., Legendre, P., Minchin, P., O'hara, R., et al. (2013). Package 'vegan'. Community ecology package, version 2. *Compreh. R Network (CRAN).* 8:9882. doi: 10.1038/s41598-018-27322-3

Pan, C., Gao, F., Li, Z., Li, J., and Chen, F. (2016). Water mass and temperature/salinity dailyvariation in east shallow-water area of Zhoushan (in Chinese). *J. Army Eng. Univ. PLA* 17, 296–302. doi: 10.12018/j.issn.1009-3443.20150710003

Parmar, T. K., Rawtani, D., and Agrawal, Y. K. (2016). Bioindicators: the natural indicator of environmental pollution. *Front. Life Sci.* 9, 110–118. doi: 10.1080/21553769.2016.1162753

Petsch, S., Eglinton, T., and Edwards, K. (2001). 14C-dead living biomass: evidence for microbial assimilation of ancient organic carbon during shale weathering. *Science* 292, 1127–1131. doi: 10.1126/science.1058332

Qi, J. (2014). *An estimation of water exchange between The East ChinaSea and Kuroshio (in Chinese). Doct of Physical Ocaenology* The University of Chinese Academy of Sciences.

Qiao, F., Yang, Y., Lü, X., Xia, C., Chen, X., Wang, B., et al. (2006). Coastal upwelling in the East China Sea in winter. *J. Geophys. Res.: Oceans* 54, 3988–3995. doi: 10.1029/2005jc003264

Qin, Y., Tang, Q., Lu, L., Wang, Y., Izaguirre, I., and Li, Z. (2021). Changes in planktonic and sediment bacterial communities under the highly regulated dam in the mid-part of the three gorges reservoir. *Appl. Microbiol. Biotechnol.* 105, 839–852. doi: 10.1007/s00253-020-11047-3

Quast, C., Pruesse, E., Yilmaz, P., Gerken, J., Schweer, T., Yarza, P., et al. (2012). The SILVA ribosomal RNA gene database project: improved data processing and web-based tools. *Nucleic Acids Res.* 41, D590–D596. doi: 10.1093/nar/gks1219

Rognes, T., Flouri, T., Nichols, B., Quince, C., and Mahé, F. (2016). VSEARCH: a versatile open source tool for metagenomics. *PeerJ* 4:e2584. doi: 10.7717/peerj.2584

Rosenberg, E. (2012). *Microorganisms to combat pollution*. Berlin: Springer Science & Business Media.

Sang, S., Huang, B., Wang, Y., Liu, H., Xu, L., and Zhang, J. (2022). Diversity and structure of prokaryotic microbial Community in Seawater Intrusion Aquifers and its Significance (in Chinese). *Res. Environ. Sci.* 35, 1458–1466. doi: 10.13198/j.issn.1001-6929.2022.03.28

Shi, J., Zuo, Y.-Q., Cao, P.-L., Fan, Y.-P., Wu, Q., and Wang, J.-X. (2023). The assembling of free-living and particle-attached archaea communities in the Changjiang river estuary in summer (in Chinese). *Oceanol. Limnologia Sinica* 54, 773–785. doi: 10.11693/hyhz20220800216

Skarðhamar, J., Slagstad, D., and Edvardsen, A. (2007). Plankton distributions related to hydrography and circulation dynamics on a narrow continental shelf off northern Norway. *Estuar. Coast. Shelf Sci.* 75, 381–392. doi: 10.1016/j.ecss.2007.05.044

Śliwińska-Wilczewska, S., Cieszyńska, A., Konik, M., Maculewicz, J., and Latała, A. (2019). Environmental drivers of bloom-forming cyanobacteria in the Baltic Sea: effects of salinity, temperature, and irradiance. *Estuar. Coast. Shelf Sci.* 219, 139–150. doi: 10.1016/j.ecss.2019.01.016

Sloan, W. T., Lunn, M., Woodcock, S., Head, I. M., Nee, S., and Curtis, T. P. (2006). Quantifying the roles of immigration and chance in shaping prokaryote community structure. *Environ. Microbiol.* 8, 732–740. doi: 10.1111/j.1462-2920.2005.00956.x

Song, J. (2011). *Biogeochemical processes of biogenic elements in China marginal seas* Springer Science & Business Media.

Soong, J. L., Fuchslueger, L., Marañon-Jimenez, S., Torn, M. S., Janssens, I. A., Penuelas, J., et al. (2020). Microbial carbon limitation: the need for integrating microorganisms into our understanding of ecosystem carbon cycling. *Glob. Chang. Biol.* 26, 1953–1961. doi: 10.1111/gcb.14962

Su, X., Yang, L., Yang, K., Tang, Y., Wen, T., Wang, Y., et al. (2022). Estuarine plastisphere as an overlooked source of N2O production. *Nat. Commun.* 13:e3884. doi: 10.1038/s41467-022-31584-x

Sun, C., Zeng, X., Li, G., Du, Y., Wang, Z., and Shao, Z. (2021). Diversity of anaerobic degrading bacteria for natural organic polymers in mangrove sediments and isolation of novel groups of bacteria (in Chinese). *Acta Microbiol Sin.* 61, 987–1001. doi: 10.13343/j.cnki.wsxb.20200715

Torsvik, V., Øvreås, L., and Thingstad, T. F. (2002). Prokaryotic diversity – magnitude, dynamics, and controlling factors. *Science* 296, 1064–1066. doi: 10.1126/science.1071698

Turley, C., and Findlay, H.S. (2009a). Chapter 21 – ocean acidification as an Indicator for climate change, *Climate change*, (Ed.) T.M. Letcher. Amsterdam: Elsevier, 367–390

Turley, C., and Findlay, H.S. (2009b). Ocean acidification as an indicator for climate change, *Climate change*. Elsevier, 367–390

Wang, Y., Dong, L., Zhang, M., Bai, X., Zhang, J., and Yu, X. (2021). Dynamic microbial network structure and assembly process in rhizosphere and bulk soils along a coniferous plantation chronosequence. *Research Square (Version 1)* 11:PPR426421. doi: 10.21203/rs.3.rs-1101835/v1

Wei, T., Simko, V., Levy, M., Xie, Y., Jin, Y., and Zemla, J. (2017). Package 'corrplot'. *Statistician* 56:e24

Williams, R. J., Howe, A., and Hofmockel, K. S. (2014). Demonstrating microbial co-occurrence pattern analyses within and between ecosystems. *Front. Microbiol.* 5:e358. doi: 10.3389/fmicb.2014.00358

Xian, W.-D., Salam, N., Li, M.-M., Zhou, E.-M., Yin, Y.-R., Liu, Z.-T., et al. (2020). Network-directed efficient isolation of previously uncultivated Chloroflexi and related bacteria in hot spring microbial mats. *NPJ Biofilms Microb* 6:e20. doi: 10.1038/s41522-020-0131-4

Yang, J., Chen, L., Yang, Y., Zhou, J., Shi, Y., Gao, Q., et al. (2022). Spatial-temporal niche of dominant zooplankton species in the Yangtze River estuary and adjacent waters in spring and summer (in Chinese). *J. Fishery Sci. China* 29, 1625–1635. doi: 10.12264/JFSC2022-0180

Yang, X., Dai, Z., Yuan, R., Guo, Z., Xi, H., He, Z., et al. (2023). Effects of salinity on assembly characteristics and function of microbial communities in the Phyllosphere and rhizosphere of salt-tolerant *Avicennia marina* mangrove species. *Microbiol. Spectrum* 11, e03000–e03022. doi: 10.1128/spectrum.03000-22

Yang, Y., Gao, Y., Huang, X., Ni, P., Wu, Y., Deng, Y., et al. (2019). Adaptive shifts of bacterioplankton communities in response to nitrogen enrichment in a highly polluted river. *Environ. Pollut.* 245, 290–299. doi: 10.1016/j.envpol.2018.11.002

Zhang, J., Liu, Y.-X., Zhang, N., Hu, B., Jin, T., Xu, H., et al. (2019). NRT1. 1B is associated with root microbiota composition and nitrogen use in field-grown rice. *Nat. Biotechnol.* 37, 676–684. doi: 10.1038/s41587-019-0104-4

Zhang, B., Zhang, J., Liu, Y., Shi, P., and Wei, G. (2018). Co-occurrence patterns of soybean rhizosphere microbiome at a continental scale. *Soil Biol. Biochem.* 118, 178–186. doi: 10.1016/j.soilbio.2017.12.011

Zhang, W.-C., Zhao, Y., Dong, Y., Zhao, L., Li, H.-B., and Xiao, T. (2018). Effects of temperature on the biological metabolism of microbial food web (in Chinese). *Mar. Sci.* 42, 137–145. doi: 10.11759/hykx20180723001

Zhou, J., Deng, Y., Luo, F., He, Z., Tu, Q., and Zhi, X. (2010a). Functional molecular ecological networks. *MBio* 1:e110. doi: 10.1128/mbio.00169-00110

Zhou, J., Deng, Y., Luo, F., He, Z., Tu, Q., and Zhi, X. (2010b). Functional molecular ecological networks. *MBio* 1:e10. doi: 10.1128/mBio.00169-10

Zhou, L., Wang, P., Huang, S., Li, Z., Gong, H., Huang, W., et al. (2021). Environmental filtering dominates bacterioplankton community assembly in a highly urbanized estuarine ecosystem. *Environ. Res.* 196:e110934. doi: 10.1016/j.envres.2021.110934

frontiers | Frontiers in Microbiology

TYPE Original Research
PUBLISHED 08 April 2024
DOI 10.3389/fmicb.2024.1383360

OPEN ACCESS

EDITED BY
Yongbin Li,
Dalian University of Technology, China

REVIEWED BY
Jiangxin Wang,
Shenzhen University, China
Azadeh Babaei,
Sharif University of Technology, Iran
Xiawei Peng,
Beijing Forestry University, China

*CORRESPONDENCE
Chunbo Hao
✉ chunbohao@cugb.edu.cn

RECEIVED 07 February 2024
ACCEPTED 25 March 2024
PUBLISHED 08 April 2024

CITATION
Zhan D, Liu Y, Yu N and Hao C (2024) Photosynthetic response of *Chlamydomonas reinhardtii* and *Chlamydomonas* sp. 1710 to zinc toxicity.
Front. Microbiol. 15:1383360.
doi: 10.3389/fmicb.2024.1383360

Photosynthetic response of *Chlamydomonas reinhardtii* and *Chlamydomonas* sp. 1710 to zinc toxicity

Di Zhan[1,2], Yue Liu[1,3], Na Yu[1,3] and Chunbo Hao[1,3]*

[1]Center for Geomicrobiology and Biogeochemistry Research, State Key Laboratory of Biogeology and Environmental Geology, China University of Geosciences, Beijing, China, [2]School of Earth Sciences and Resources, China University of Geosciences, Beijing, China, [3]School of Water Resources and Environment, China University of Geosciences, Beijing, China

Zinc (Zn) is an essential trace element but can lead to water contamination and ecological deterioration when present in excessive amounts. Therefore, investigating the photosynthetic response of microalgae to Zn stress is of great significance. In this study, we assessed the photosynthetic responses of neutrophilic *Chlamydomonas reinhardtii* and acidophilic *Chlamydomonas* sp. 1710 to Zn exposure for 96 h. The specific growth rate (μ), chlorophyll-a (Chl-a) content, and chlorophyll fluorescence parameters were determined. The results demonstrated that *Chlamydomonas* sp. 1710 was much more tolerant to Zn than *C. reinhardtii*, with the half-maximal inhibitory concentration (IC50) values of 225.4 mg/L and 23.4 mg/L, respectively. The μ and Chl-a content of *C. reinhardtii* decreased in the presence of 15 mg/L Zn, whereas those of *Chlamydomonas* sp. 1710 were unaffected by as high as 100 mg/L Zn. Chlorophyll fluorescence parameters indicated that the regulation of energy dissipation, including non-photochemical quenching, played a crucial role in Zn stress resistance for both *Chlamydomonas* strains. However, in the case of *C. reinhardtii*, non-photochemical quenching was inhibited by 5 mg/L Zn in the first 48 h, whereas for *Chlamydomonas* sp. 1710, it remained unaffected under 100 mg/L Zn. *Chlamydomonas* sp. 1710 also exhibited a 20 times stronger capacity for regulating the electron transfer rate than *C. reinhardtii* under Zn stress. The light energy utilization efficiency (α) of *Chlamydomonas* sp. 1710 had the most highly non-linear correlation with μ, indicating the energy utilization and regulation process of *Chlamydomonas* sp. 1710 was well protected under Zn stress. Collectively, our findings demonstrate that the photosystem of *Chlamydomonas* sp. 1710 is much more resilient and tolerant than that of *C. reinhardtii* under Zn stress.

KEYWORDS

zinc, *Chlamydomonas*, chlorophyll fluorescence parameters, non-photochemical quenching, rapid light curve, fast chlorophyll fluorescence induction curve

Highlights

- *Chlamydomonas* sp. 1710 is more Zn tolerant than *Chlamydomonas reinhardtii*.
- Non-photochemical quenching of *C. reinhardtii* was inhibited by 5 mg/L Zn, whereas that of *Chlamydomonas* sp. 1710 was stable under 100 mg/L.
- The electron transfer regulation of *Chlamydomonas* sp. 1710 was more effective than that of *C. reinhardtii* under Zn stress.
- The light energy utilization and regulation of *Chlamydomonas* sp. 1710 was well protected under Zn stress.

Introduction

Zinc (Zn) is the 24th most abundant element in the Earth's crust (Wong and Chau, 1990). As an essential trace element, Zn serves as a cofactor for numerous enzymes in various biological processes of plants, including photosynthesis (Broadley et al., 2007). However, excessive Zn can hinder the ability of plants to absorb other divalent metals, such as copper, iron, and calcium, leading to an imbalance of cellular redox processes, ultimately inhibiting photosynthesis (Broadley et al., 2007). Zn pollution mainly occurs in water bodies, originating primarily from industrial activities such as mining, metallurgy, and metal manufacturing. Acid mine drainage (AMD) is an important contributor to water contamination of Zn (Simate and Ndlovu, 2014; Jiang et al., 2023).

Microalgae are crucial components of aquatic environments, serving as primary producers to provide the basic nutrition for heterotrophic organisms (Rizwan et al., 2018). In recent decades, microalgae have garnered increasing attention due to their promising potential in biofuel, food manufacturing, and environmental industry (Spolaore et al., 2006; Zhu et al., 2022; Thanigaivel et al., 2023). *Chlamydomonas reinhardtii* (*C. reinhardtii*) has been widely used as a model organism for genetic and biochemical studies, with its typical habitat being freshwater environments with neutral to slightly alkaline pH optimum (Rochaix, 1995). However, acidophilic algae are the main photosynthetic organisms in AMD, and they contribute to removal of Zn from AMD through two main mechanisms: (1) accumulation of Zn by direct uptake or cohesion by secreting chelating agents such as organic acids and extracellular polymeric substances; (2) providing carbon sources for heterotrophic microorganisms able to increase the pH of the water body, such as sulfate-reducing bacteria, leading to Zn precipitation (Das et al., 2009; Mathimani et al., 2023). The removal of Zn by algae relies on their strong tolerance to Zn toxicity, and large amounts of biomass must be generated to maximize the bioremediation potential of algae. Therefore, photosynthesis, the most fundamental biological process in algae, should receive more attention.

The light energy absorbed by plants or algae has three main fates: (1) transformation into chemical energy through photosynthesis; (2) dissipation in the form of heat; (3) re-emission as fluorescence (i.e., chlorophyll fluorescence). Chlorophyll fluorescence is an important parameter measured in evaluating the physiological state of plants. The first chlorophyll fluorescence measurements were conducted in the 1960s, and this method achieved rapid development in the 1980s when pulse amplitude modulation technology was proposed (Schreiber et al., 1986). F_0 (initial fluorescence) and F_m (maximum fluorescence) are the two basic fluorescence parameters from which maximal photosystem II (PSII) quantum yield (F_v/F_m) is calculated (Kitajima and Butler, 1975; Genty et al., 1989; van Kooten and Snel, 1990). Furthermore, chlorophyll fluorescence parameters have evolved into several mainstream branches, including non-photochemical quenching (NPQ) parameters (Schreiber et al., 1986; Kramer et al., 2004), fast chlorophyll fluorescence induction curve (OJIP) parameters (Strasser et al., 2000), and rapid light curve (RLC) parameters (White and Critchley, 1999). Due to their convenience, reproducibility, sensitivity, and accuracy, chlorophyll fluorescence parameters are widely used to investigate photosynthetic responses to various stressors, such as heavy metals (Gebara et al., 2023), salinity (Guermazi et al., 2023), and heat stress (Liang et al., 2023).

Despite the wide utilization of NPQ, OJIP, and RLC parameters, previous studies have largely focused on only one of the aforementioned approaches (Marečková et al., 2019; Almeida et al., 2021; Gebara et al., 2023). Additionally, the temporal variations of these parameters are rarely accounted for, and few studies have compared the chlorophyll fluorescence characteristics across different algal species. In this study, quantum yield, the efficiency of the oxygen evolution complex (OEC), NPQ parameters, OJIP parameters, and RLC parameters were simultaneously used to evaluate the photosynthetic status of two *Chlamydomonas* strains, *C. reinhardtii* and *Chlamydomonas* sp. 1710, which are Zn-sensitive and Zn-tolerant, respectively. Additionally, we evaluated the growth and chlorophyll-a (Chl-a) content of the two *Chlamydomonas* strains. Principal components analysis (PCA), Pearson correlation, and linear/non-linear regression models were used to analyze the relationship between specific growth rate (μ), Chl-a content, and chlorophyll fluorescence parameters. Finally, the chlorophyll fluorescence parameters that were most suitable as indicators of growth and physiological response were identified for the two *Chlamydomonas* strains. Taken together, our findings provide comprehensive insights into the application of different chlorophyll fluorescence parameters for the evaluation of two different *Chlamydomonas* species under Zn stress.

Materials and methods

Algal cultures and Zn exposure

Chlamydomonas reinhardtii UTEX 90 was generously provided by the National Aquatic Germplasm Resource Bank of the Institute of Hydrobiology, Chinese Academy of Sciences (Wuhan, Hubei, China). *Chlamydomonas* sp. 1710 was isolated from the collected surface water of an AMD in Anhui Province, China. A photoautotrophic medium (1.89 mM $(NH_4)_2SO_4$, 2.03 mM $MgSO_4{\cdot}7H_2O$, 0.09 mM $CaCl_2$, 2.20 mM KH_2PO_4, 0.51 mM NaCl, 17.91 μM $FeSO_4{\cdot}7H_2O$, 7.72 μM $ZnSO_4{\cdot}5H_2O$, 46.26 μM H_3BO_3, 9.15 μM $MnCl_2{\cdot}4H_2O$, 1.61 μM $Na_2MoO_4{\cdot}2H_2O$, 0.17 μM $Co(NO_3)_2{\cdot}6H_2O$, 0.32 μM $CuSO_4{\cdot}5H_2O$, 26.86 μM $Na_2EDTA{\cdot}2H_2O$, 40.93 nM D-biotin, 7.38 nM cobalamin, 296.50 nM thiamine) was used. The pH was set to 3, the same as the original water sample, and the temperature was 25°C. 20 μL water sample was serially diluted (10^{-3}–10^{-6}) using sterile ddH_2O (18.20 MΩ·cm, Millipore Corporation, Bedford, MA) and inoculated onto agarose plates for two weeks. A single colony was picked and inoculated again onto plates. This procedure was repeated a few times to obtain pure isolate.

Both strains were cultivated in the photoautotrophic medium mentioned above. The pH of the culture medium was adjusted to their optimum (7.0 for *C. reinhardtii* and 3.0 for *Chlamydomonas* sp. 1710). Algal cultivation was conducted in custom-made glass tubes at 25°C. Prior to inoculation, the culture media were autoclaved for 20 min at 121°C. The growth of *Chlamydomonas* strains was monitored by measuring the optical density at 750 nm (OD_{750}). *Chlamydomonas* strains were maintained under white light (100 $\mu E{\cdot}m^{-2}{\cdot}s^{-1}$) and continuous air injection to reach an OD_{750} of 0.25, which indicated its logarithmic phase. Next, Zn exposure experiments were conducted in a 250 mL glass conical flask containing 100 mL *Chlamydomonas* culture (OD_{750} = 0.25). The Zn concentration range

was 0, 5, 15, 30 mg/L for *C. reinhardtii* and 0, 30, 100, 300, 600 mg/L for *Chlamydomonas* sp. 1710. The cells were exposed to Zn for a total of 96 h under 16:8 h (day:night) cycles of white light (100 $\mu E \cdot m^{-2} \cdot s^{-1}$) at 25°C, without air injection. The culture flasks were gently shaken every 12 h. Before use, all glassware was washed with neutral detergent and maintained in 1 M HNO_3 overnight. All cultures were prepared in triplicate.

Growth rate determination

OD_{750} is linearly correlated with algal biomass (Tang et al., 2011). Therefore, this parameter was used to determine the growth of *Chlamydomonas* strains in our study. The specific growth rate (μ) was calculated as follows:

$$\mu_{n-0} = \frac{\ln(N_b) - \ln(N_a)}{t_b - t_a}$$

where μ_{n-0} is the average specific growth rate within the time n, N_b is the OD_{750} at time b (t_b), and N_a is the OD_{750} at time a (t_a).

Chl-a content determination

Chl-a content was determined via the spectrometric method (Goodwin, 1965) at 24, 48, 72, 96 h. Briefly, a 2 mL sample of *Chlamydomonas* suspension was washed using 0.02 M phosphate buffered saline (pH 7.0), and centrifuged for 3 min at 8000 g and 25°C three times to eliminate any interference caused by acidity and Zn ions. The pellet was then extracted using 2 mL of 95% acetone combined with ultrasonication (75 W, 2 min). The extract was then centrifuged for 10 min at 16,000 g and 4°C. The absorbance of the supernatant was measured at 650 and 750 nm. Chl-a content (C_a) was calculated as follows:

$$C_a = 25.5 \times (A650 - A750)$$

where A650 and A750 represent the absorbance of supernatant at 650 nm and 750 nm, respectively.

Chlorophyll fluorescence measurements

The chlorophyll fluorescence parameters of *Chlamydomonas* sp. 1710 and *C. reinhardtii* exposed to Zn at 24, 48, 72 and 96 h were measured using an AquaPen-C 100 fluorometer (Photon Systems Instruments, Czech Republic) (Appendix 1). Two milliliters samples of *Chlamydomonas* cultures were kept in the dark at 25°C for at least 15 min to ensure that all PSII reaction centers were in an oxidized state. Prior to each measurement, the *Chlamydomonas* cultures were homogenized via gentle inversion.

To assess maximal PSII quantum yield (F_v/F_m) and the efficiency of the oxygen evolution complex (OEC), the samples were irradiated with a saturating light pulse (1,500 $\mu mol \cdot m^{-2} \cdot s^{-1}$) and the fluorescence intensity was recorded. The fluorescence intensity used to calculate effective PSII quantum yield [Y(II)] was obtained from NPQ test described below. To quantify NPQ parameters, the samples were exposed to continuous actinic light (100 $\mu mol \cdot m^{-2} \cdot s^{-1}$) and were irradiated 5 times with saturating light pulses (1,500 $\mu mol \cdot m^{-2} \cdot s^{-1}$) every 12 s. Afterwards, the actinic light was extinguished and the samples were exposed to three saturating light pulses (1,500 $\mu mol \cdot m^{-2} \cdot s^{-1}$) every 26 s.

For the RLC test, the samples were exposed to a series of actinic light intensities (i.e., 10, 20, 50, 100, 300, 500, 1,000 $\mu mol \cdot m^{-2} \cdot s^{-1}$), with each exposure lasting for 60 s. The samples were then irradiated with a saturating light pulse (1,500 $\mu mol \cdot m^{-2} \cdot s^{-1}$) at intervals determined by the shift in actinic light intensity, after which the relative photosynthetic electron transfer rate (ETR) under various light intensities of continuous illumination were obtained.

For the OJIP test, the cells were irradiated with 1,500 $\mu mol \cdot m^{-2} \cdot s^{-1}$ of blue light (450 nm) for 2 s to obtain a curve encompassing four typical phases: the start phase at 50 μs; the intermediate phases J and I at 2 ms and 30 ms, respectively; and the maximal phase P (equal to F_m at saturating light conditions). Following the above-described protocols, all relevant chlorophyll fluorescence parameters were measured or calculated.

Statistical analysis

One-way analysis of variance (ANOVA) with multiple comparison tests was used to identify statistically significant differences among the data under different Zn concentrations. A p-value < 0.05 was considered statistically significant. The statistical analyses were conducted using the GraphPad Prism 7.0 software (GraphPad, San Diego, USA).

The acquired data were processed via principal component analysis (PCA) using the OriginPro 2022 software (OriginLab Corporation, Northampton, MA) to resolve the collinearity of complex chlorophyll fluorescence-associated parameters (Wold et al., 1987), including μ, Chl-a content, maximal PSII quantum yield (F_v/F_m), efficiency of the oxygen-evolving complex (OEC), effective PSII quantum yield [Y(II)], coefficient of photochemical quenching (qP), non-photochemical quenching (NPQ), coefficient of photochemical quenching (qL), quantum yield of regulated energy dissipation [Y(NPQ)], quantum yield of nonregulated energy dissipation [Y(NO)], coefficient of non-photochemical quenching (qN), relative photochemical quenching [qP(rel)], relative non-photochemical quenching [qN(rel)], relative unquenched fluorescence [UQF(rel)], absorption flux per reaction center (ABS/RC), trapped energy flux per reaction center (TRo/RC), dissipated energy flux per reaction center (DIo/RC), electron transport flux per reaction center (ETo/RC), electron flux reducing end electron acceptors at the PSI acceptor side per reaction center (REo/RC), performance index for energy conservation from photons absorbed by PSII to the reduction of intersystem electron acceptors (PI_ABS), performance index for energy conservation from photons absorbed by PSII to the reduction of PSI and acceptors (PI_total), light energy utilization efficiency (α), and maximal relative photosynthetic electron transport rate (ETR_{max}). The obtained principal components (PCs) were used to resolve statistical models, in which the scores represent the distance from the PCs' origin to every data point, and the loadings represent the contributions of each parameter to each PC (Bro and Smilde, 2014).

Pearson correlation analysis was conducted to identify pairwise correlations between μ, Chl-a content, and all chlorophyll fluorescence parameters using the GraphPad Prism 7.0 software (GraphPad, San Diego, USA). Linear and non-linear regression analyses between μ, Chl-a content, and selected chlorophyll fluorescence parameters were determined with a variable slope model, using the least squares fitting method in the GraphPad Prism 7.0 software (GraphPad, San Diego, USA).

Results and discussion

Growth curves and Chl-a content

The impact of Zn on the growth of *C. reinhardtii* and *Chlamydomonas* sp. 1710 is illustrated in Figures 1A,B. These two species of *Chlamydomonas* exhibited different levels of tolerance toward Zn. 5 mg/L Zn did not exert any side effects on the growth of *C. reinhardtii*, whereas 15 mg/L and 30 mg/L Zn significantly inhibited its growth. In contrast, 30 mg/L and even 100 mg/L Zn did not inhibit the growth of *Chlamydomonas* sp. 1710. The half-maximal inhibitory concentrations (IC50) of *C. reinhardtii* and *Chlamydomonas* sp. 1710 were calculated to be 23.4 mg/L and 225.4 mg/L, respectively. These results aligned with previous comparative studies between acidophilic and neutrophilic algae, indicating *Chlamydomonas* sp. 1710 was more tolerant to Zn stress than *C. reinhardtii* (Abinandan et al., 2019; Mikulic and Beardall, 2021).

Chl-a is a pigment that plays an essential role in algal photosynthesis. The Chl-a content of both *Chlamydomonas* decreased under Zn stress (Figures 1C,D). However, Zn concentration as low as 5 mg/L significantly decreased the Chl-a content of *C. reinhardtii* (Figure 1C). In contrast, for *Chlamydomonas* sp. 1710, 30 and even 100 mg/L Zn did not have a significant inhibitory effect (Figure 1D). The result may be due to the fact that *Chlamydomonas* sp. 1710 had an inherently higher amount of Chl-a than *C. reinhardtii*, with 13.5 mg/L and 7.7 mg/L, respectively, under normal growth at 96 h (Figures 1C,D). This was consistent with previous studies (Pluciński et al., 2023). Furthermore, Zn-induced ROS would cause severe damage to Chl-a within cells (Dong et al., 2023; Pluciński et al., 2023), and *Chlamydomonas* sp. 1710 could have powerful antioxidant enzymes eliminating excessive ROS (del Carmen Romero-Cruz et al., 2024).

Quantum yield and OEC

Quantum yield is a measure of the number of useful products or events produced per absorbed photon during photosynthesis (Kitajima and Butler, 1975). This parameter represents the energy efficiency from absorbed photons to drive desired chemical or biological reactions. A quantum yield of 1.0 means that every absorbed photon is utilized to produce desired product or event. The maximal PSII quantum yield (F_v/F_m) refers to the maximum efficiency of converting light energy into chemical energy through the process of photochemical reactions (Kitajima and Butler, 1975). F_v/F_m typically cannot be reached, and the specific value of parameter is commonly used as an indicator of plant health. Effective PSII quantum yield [Y(II)] represents the authentic quantum conversion rate of algae under normal growth condition (Genty et al., 1989).

The quantum yield of both *C. reinhardtii* and *Chlamydomonas* sp. 1710 responded divergently to Zn exposure (Figures 2A–D). The F_v/F_m and Y(II) values of *C. reinhardtii* correlated negatively with Zn concentration, and their trends aligned with the growth curves presented in Figures 1A,B. Moreover, this negative correlation became more pronounced over time. In 96 h, F_v/F_m decreased from 0.68 at 0 mg/L Zn to 0.46 at 30 mg/L Zn. However, a concentration up to 300 mg/L did not have any inhibitory effect on the F_v/F_m and Y(II) of *Chlamydomonas* sp. 1710. This result indicated that the quantum yield of *C. reinhardtii* was inhibited by Zn, and the inhibition occurred at a concentration as low as 5 mg/L, whereas that of *Chlamydomonas* sp. 1710 could be stable up to 300 mg/L. The high stability of quantum yield to heavy metal stress was also reported in mercury-tolerant algae (Juneau et al., 2001).

The oxygen evolution complex is a protein complex located in the thylakoid membrane of the chloroplast, specifically within the PSII complex (Cady et al., 2008). This complex plays a crucial role in the light-dependent reactions of photosynthesis by facilitating the conversion of water molecules into molecular oxygen, protons, and electrons (Cady et al., 2008). OEC is defined by its ability to facilitate the process of oxygen evolution during photosynthesis (Maxwell and Johnson, 2000). For *C. reinhardtii*, the OEC exhibited a positive correlation with Zn concentration, and increased from 0.47 at 0 mg/L Zn to 1.17 at 30 mg/L Zn (Figure 2E). Conversely, the OEC of *Chlamydomonas* sp. 1710 remained unaffected at <300 mg/L Zn concentration but increased from 0.53 to 0.93 when the Zn concentration increased from 0 to 600 mg/L (Figure 2F). The variation trends of OEC were contrary to those of the quantum yield, which was consistent with their theoretical trends obtained via calculations, as well as the biological implications that the efficiency of light energy conversion was inhibited by a high level of Zn, thereby reinforcing the photo-oxidation of water (Kitajima and Butler, 1975; Kriedemann et al., 1985).

Both the quantum yield and OEC of *C. reinhardtii* and *Chlamydomonas* sp. 1710 exhibited divergent trends. For *C. reinhardtii*, the variations of F_v/F_m, Y(II), and OEC were consistent with those of the growth curves and Chl-a contents (Figures 1, 2). However, for *Chlamydomonas* sp. 1710, although algal growth was significantly inhibited by 300 mg/L Zn (Figure 1B), its F_v/F_m, Y(II) and OEC remained unaffected. This result suggests that low Zn concentrations can directly impair the photon conversion capacity of *C. reinhardtii*'s photosystem, hence suppressing its growth, whereas that of *Chlamydomonas* sp. 1710 could tolerate up to 300 mg/L Zn. Therefore, the observed variations in chlorophyll fluorescence parameters suggested that, unlike *C. reinhardtii*, *Chlamydomonas* sp. 1710 likely possesses important protective mechanisms for its photosystem, such as antioxidant enzymes and non-photochemical quenching (Pluciński et al., 2023; del Carmen Romero-Cruz et al., 2024).

NPQ parameters

In the past few decades, several NPQ parameters were proposed by different research groups, including coefficient of photochemical quenching (qP), coefficient of non-photochemical quenching (qN) (Schreiber et al., 1986), relative photochemical quenching [qP(rel)],

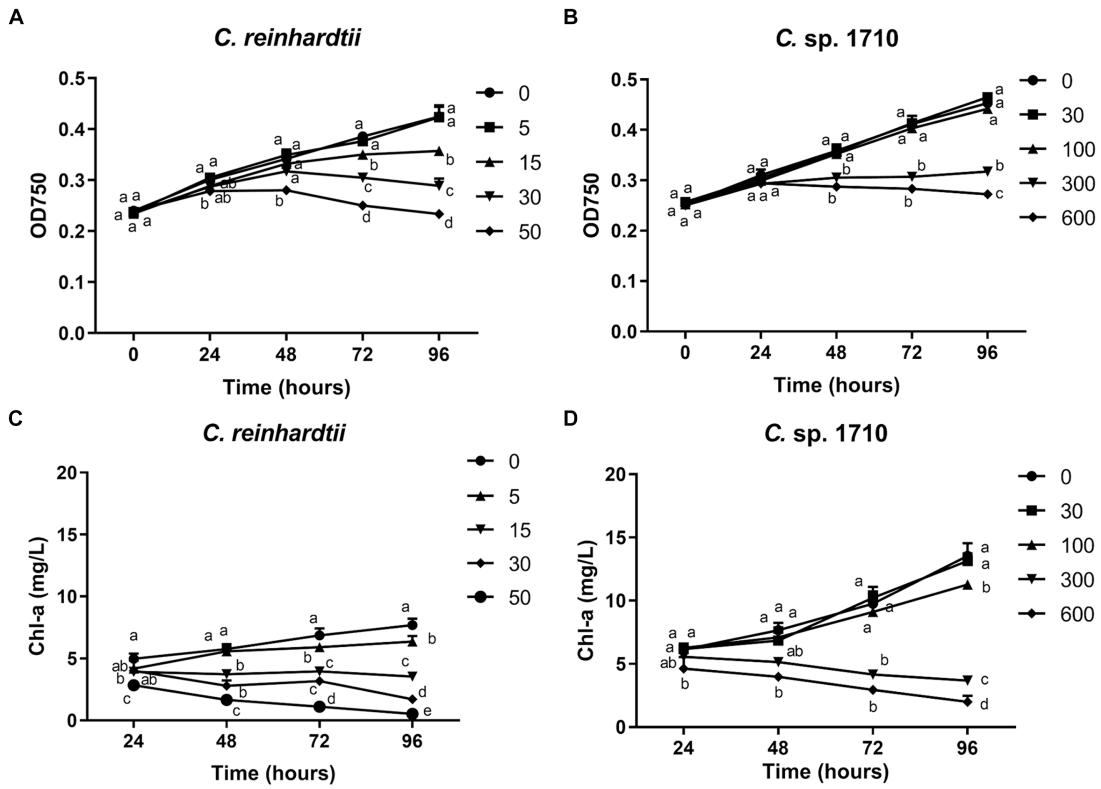

FIGURE 1
OD_{750} **(A,B)** and Chlorophyll a (Chl-a) content **(C,D)** of *C. reinhardtii* and *Chlamydomonas* sp. 1710 exposed to Zn (mg/L) for 96 h.

relative non-photochemical quenching [qN(rel)] (Buschmann, 1995), non-photochemical quenching (NPQ) (Bilger and Björkman, 1990), and coefficient of photochemical quenching (qL) (Kramer et al., 2004). Among these, qP, qP(rel), and qL represent photochemical quenching, whereas qN, qN(rel), and NPQ represent non-photochemical quenching. Photochemical quenching represents the energy transfer that occurs during photosynthesis (Ort and Baker, 2002), whereas non-photochemical quenching is an important regulation mechanism exhibited by plants in response to abiotic stress, involving the heat dissipation of light energy absorbed by light-harvesting antenna (Demmig-Adams et al., 2014). Furthermore, Y(NO) represents the passively dissipated energy in the form of heat and fluorescence, mainly due to closure of PSII reaction centers, which increases during photodamage (Klughammer and Schreiber, 2008). Y(NPQ) reflects the regulated energy dissipation through the non-photochemical quenching process. UQF(rel) represents the relative unquenched fluorescence mainly caused by closed PSII reaction centers (Juneau et al., 2005) and it usually increases with more severe stress (Ranjbarfordoei et al., 2006; Deblois et al., 2013).

qP, qP(rel), and qL exhibited very divergent trends for the two *Chlamydomonas* strains (Figures 3A,B; Supplementary Figures S1A–D). qL remained nearly constant across all Zn concentrations and exposure times for both *C. reinhardtii* and *Chlamydomonas* sp. 1710. Therefore, it may not be an appropriate parameter to evaluate the performance of the photosystem II for the two *Chlamydomonas* strains. However, qP(rel) and qP varied with Zn concentration and exposure time. In the first 48 h, the qP(rel) of *C. reinhardtii* increased slightly with increased Zn concentration (Figure 3A), indicating that Zn had no appreciable adverse effect on photosynthesis during this period. Subsequently, the qP(rel) of *C. reinhardtii* decreased with increased Zn concentration, except for 15 mg/L, where it was higher. In contrast, the qP(rel) of *Chlamydomonas* sp. 1710 was unchanged under 30 and 100 mg/L Zn but increased under 300 or 600 mg/L Zn (Figure 3B). The trends of qP were different from that of qP(rel). For *C. reinhardtii*, qP exhibited minimal changes at various Zn concentrations within the first 48 h (Supplementary Figure S1A) but decreased slightly as the Zn concentration increased after 72 h. Conversely, the qP of *Chlamydomonas* sp. 1710 remained unchanged during the initial 72 h even under a Zn concentration as high as 300 mg/L, and only decreased under 600 mg/L Zn at 96 h (Supplementary Figure S1B). This was consistent with previous studies (Baracho et al., 2019; Rocha et al., 2021) reporting that although the Chl-a content of both *C. reinhardtii* and *Chlamydomonas* sp. 1710 significantly decreased upon exposure to Zn, the residual Chl-a still possessed most photosynthetic functions. The results of qP(rel) and qP indicated that, being the most important cellular component of algae, the photosynthetic system would not be impaired primarily by heavy metals due to protective mechanisms, such as enzymatic and non-enzymatic antioxidants, as well as metal transporters (Candido and Lombardi, 2018; Leong and Chang, 2020).

qN, qN(rel), and NPQ exhibited highly similar trends in both *C. reinhardtii* and *Chlamydomonas* sp. 1710 (Figures 3C,D; Supplementary Figures S1E–H). Therefore, the discussion focused on the variations in qN. As a regulatory function, non-photochemical quenching was found to either increase (Nama et al., 2019; Rocha et al., 2021) or decrease (Almeida et al., 2021; Aparicio et al., 2022)

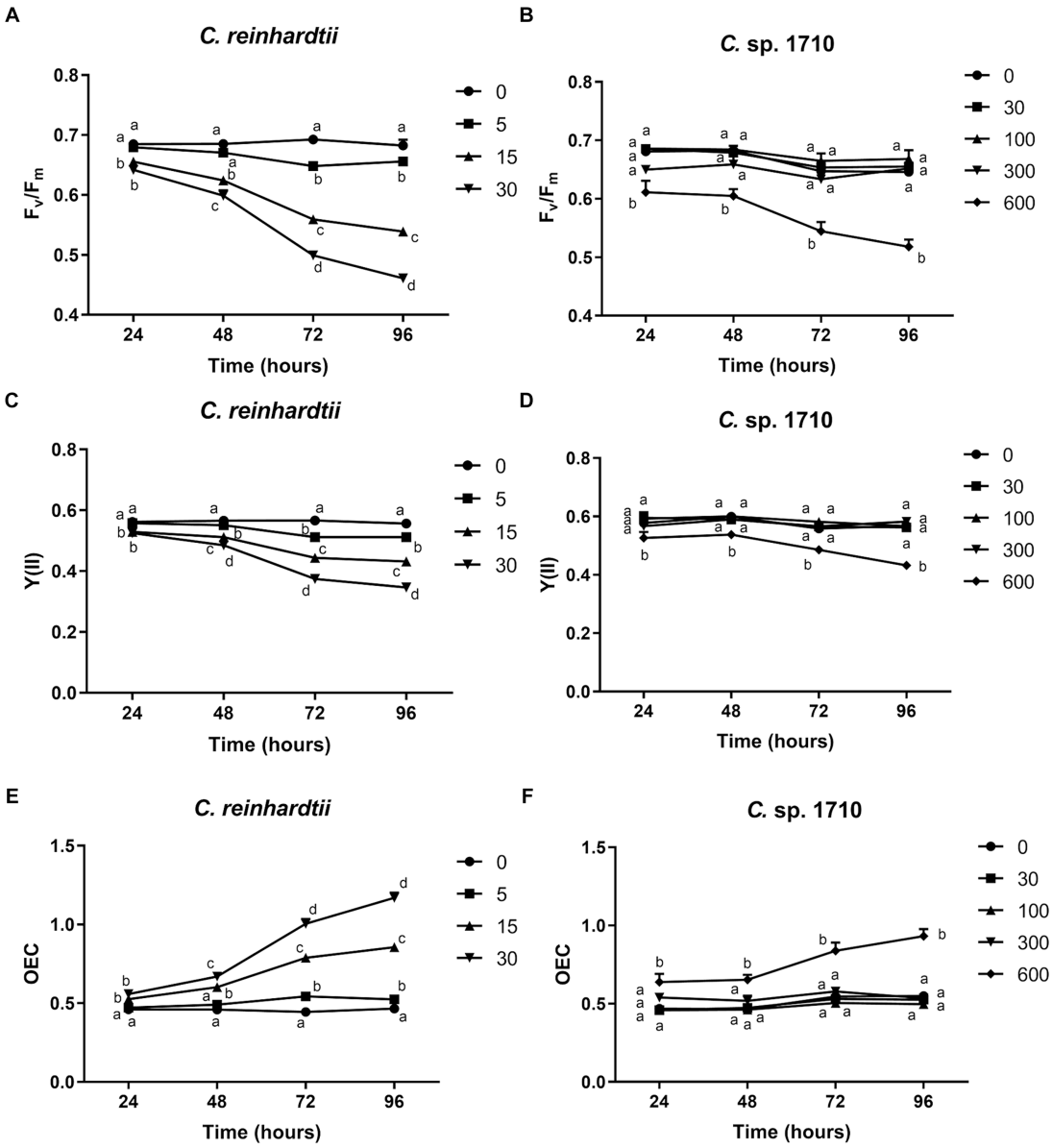

FIGURE 2
Maximal PSII quantum yield (F_v/F_m) **(A,B)**, effective PSII quantum yield [Y(II)] **(C,D)**, and OEC **(E,F)** of *C. reinhardtii* and *Chlamydomonas* sp. 1710 exposed to Zn (mg/L) for 96 h.

with increased concentration of toxic substances. This divergence may be due to the fact that most previous studies have only focused on a single time point without temporal trends. Additionally, previous studies have demonstrated that the mechanisms of non-photochemical quenching are distinct across algae, cyanobacteria, and plants, depending on different proteins and pigments (Giacometti and Morosinotto, 2013; Nowicka, 2020; Lu et al., 2022). In this study, non-photochemical quenching was simultaneously influenced by multiple factors including algae species, Zn concentration, and exposure time. Moreover, the responses of the two species of *Chlamydomonas* occurred at different times. Consistent with previous studies (Dewez et al., 2005), the qN of both *C. reinhardtii* and *Chlamydomonas* sp. 1710 were sensitive to Zn concentration. Under Zn stress, the qN of *C. reinhardtii* decreased from 0.3 to lower than 0.2 (Figure 3C) before 48 h but recovered afterwards. In contrast, under 30 and 100 mg/L, the qN of *Chlamydomonas* sp. 1710 increased from 0.05 to nearly 0.2 (Figure 3D) throughout the entire period. Therefore, non-photochemical quenching appeared to be delayed in *C. reinhardtii* under 5 mg/L Zn, whereas it was stable in *Chlamydomonas* sp. 1710 under 30 and 100 mg/L Zn. On the other hand, the growth of *C. reinhardtii* was unaffected by 5 mg/L Zn, and that of *Chlamydomonas* sp. 1710 also remained unaffected under 30 and 100 mg/L Zn. Consequently, non-photochemical quenching may serve as a crucial protective mechanism for both *C. reinhardtii* and *Chlamydomonas* sp. 1710 under Zn stress, which was consistent with previous studies (Gebara et al., 2023; Pluciński et al., 2023). However, *Chlamydomonas* sp. 1710 had a superior regulation of non-photochemical quenching compared to *C. reinhardtii* and other microalgae (Rocha et al., 2024).

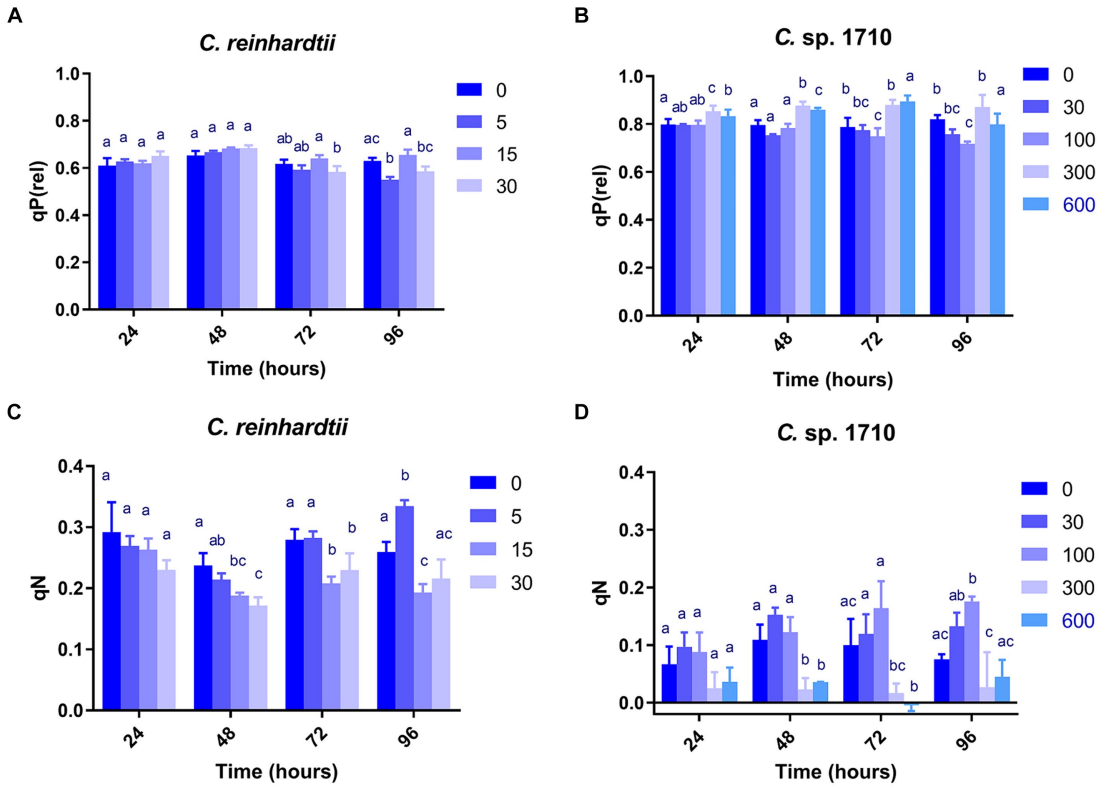

FIGURE 3
Relative photochemical quenching [qP(rel)] **(A,B)** and coefficient of non-photochemical quenching (qN) **(C,D)** of *C. reinhardtii* and *Chlamydomonas* sp. 1710 exposed to Zn (mg/L) for 96 h.

The Y(NO) of *C. reinhardtii* increased with both Zn concentration and exposure time (Figure 4A). The Y(NO) of *C. reinhardtii* was minimally affected at 5 mg/L Zn but increased to >0.5 at 30 mg/L. This indicates that for *C. reinhardtii*, the photosynthetic consumption and non-photochemical quenching were unable to offset the absorbed light energy under severe Zn stress (Sekulska-Nalewajko et al., 2019), resulting in light-induced impairment of the photosystem (Misra et al., 2012). In contrast, 30 and 100 mg/L Zn had negligible effects on the Y(NO) of *Chlamydomonas* sp. 1710, whereas its Y(NPQ) increased significantly (Figures 4B,D). This suggested that *Chlamydomonas* sp. 1710 exhibited robust energy regulation abilities under 30 or 100 mg/L Zn. The UQF(rel) of *C. reinhardtii* had a positive correlation with Zn concentration (Figure 4E), suggesting that Zn inhibited its cellular quenching regulation (Juneau et al., 2005). Conversely, the UQF(rel) of *Chlamydomonas* sp. 1710 was minimally influenced by Zn, indicating an excellent regulatory performance of *Chlamydomonas* sp. 1710 in response to Zn exposure. Interestingly, when combining Y(NO), Y(NPQ), and UQF(rel), *C. reinhardtii* and *Chlamydomonas* sp. 1710 had different photosynthetic responses to Zn, similar to the responses of different kinds of plants to biotic stress (Sekulska-Nalewajko et al., 2019). Under severe Zn stress, the Y(NO) and UQF(rel) of both *C. reinhardtii* and *Chlamydomonas* sp. 1710 increased, whereas Y(NPQ) decreased (Figure 4). However, both strains exhibited resilience to a slight Zn stress, albeit at different response rates. The Y(NO) and UQF(rel) of *C. reinhardtii* increased at 5 mg/L but returned to the baseline level at 96 h (Figures 4A,E). This was attributed to the fact that the Y(NPQ) of *C. reinhardtii* was inhibited before 48 h but began to recover afterwards (Figure 4C). Conversely, the Y(NPQ) of *Chlamydomonas* sp. 1710 immediately increased at 24 h (Figure 4D), whereas Y(NO) and UQF(rel) were maintained (Figures 4B,F). The results of *C. reinhardtii* aligned with previous studies, indicating increased unregulated energy dissipation under abiotic stress (Antunović Dunić et al., 2023; Pluciński et al., 2023). In contrast, *Chlamydomonas* sp. 1710 demonstrated a distinct response, showing superior energy regulation.

RLC parameters

RLC can be used to obtain the electron transport rate (ETR) of the photosystem of green algae under Zn stress, and to further calculate the light energy utilization efficiency (α) (Fu et al., 2012). The ETR of *C. reinhardtii* remained unaffected by Zn within the initial 48 h, but was inhibited significantly by 30 mg/L Zn after 72 h (Figure 5A; Supplementary Figures S2A,C,E). In contrast, for *Chlamydomonas* sp. 1710, the ETR was not inhibited until 96 h by 300 mg/L Zn (Figure 5B; Supplementary Figures S2B,D,F). The varying response patterns of the two *Chlamydomonas* strains did not align with their growth curves (Figures 1A,B). Their heavy metal sensitivity patterns were different from that of *Ankistrodesmus densus*, another green alga (Rocha et al., 2021). However, there were intriguing changes in the trend of ETR_{max}, with previous studies demonstrating that ETR_{max} has a good correlation with the growth and pigment content of algae (Bischof et al., 2000; Lüder et al., 2001).

10.3389/fmicb.2024.1383360

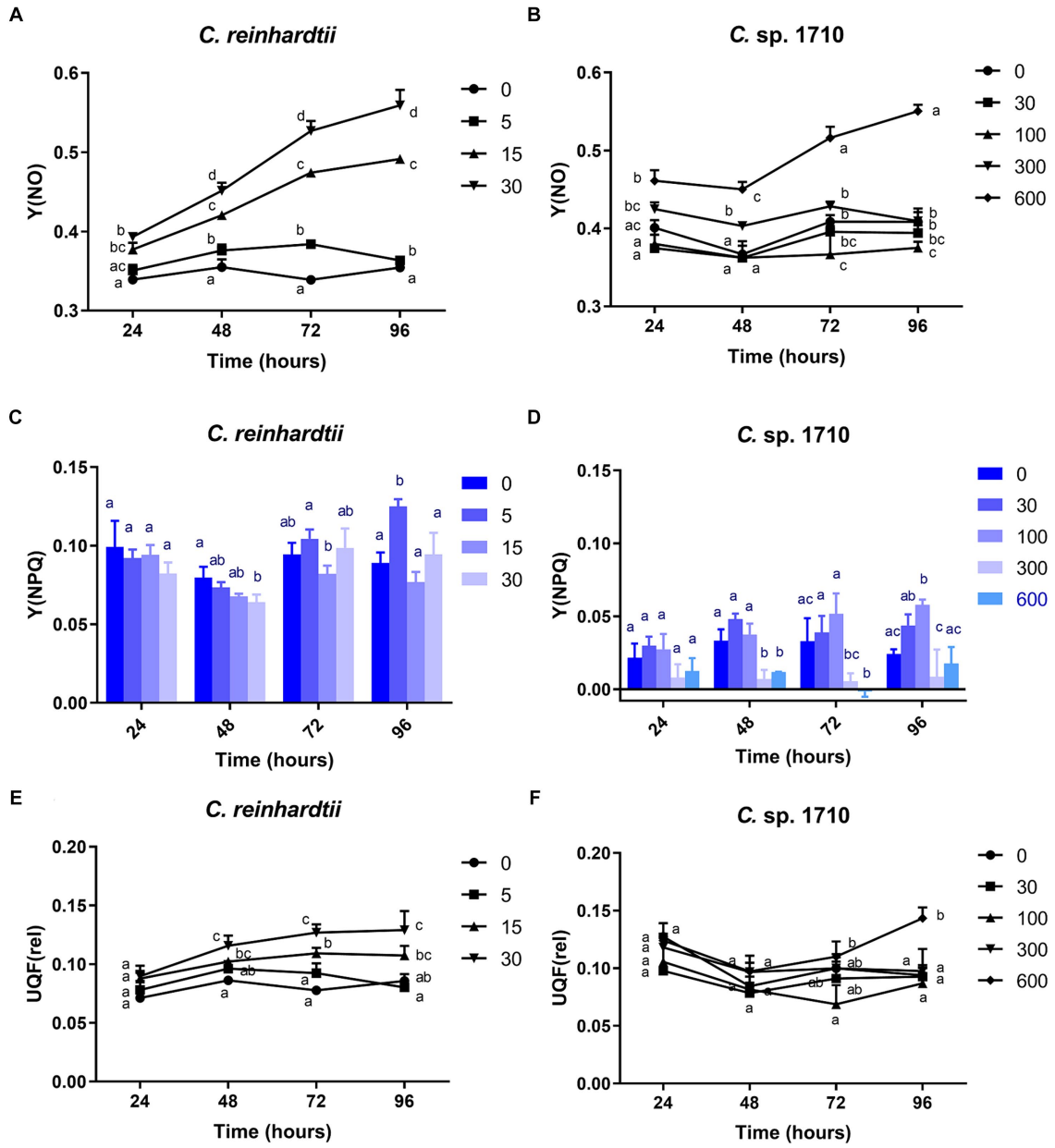

FIGURE 4
Quantum yield of nonregulated energy dissipation [Y(NO)] **(A,B)**, quantum yield of regulated energy dissipation (Y(NPQ)] **(C,D)**, and relative unquenched fluorescence [UQF(rel)] **(E,F)** of *C. reinhardtii* and *Chlamydomonas* sp. 1710 exposed to Zn (mg/L) for 96 h.

The ETR_{max} of *C. reinhardtii* decreased from 58 to 36.5 μmol electrons $m^{-2} \cdot s^{-1}$ when Zn concentration increased from 0 to 30 mg/L Zn at 96 h, but remained unchanged under 15 mg/L despite experiencing remarkable growth inhibition under this Zn level (Figure 5C). In contrast, the ETR_{max} of *Chlamydomonas* sp. 1710 was almost unaffected (Figure 5D). The fact that the cells maintained such a high electron transfer rate despite suppressed growth was rather intriguing. Here, we propose two potential explanations: (1) the electron transfer process was effectively protected by cellular regulation mechanisms including non-photochemical quenching or detoxification mechanisms (e.g., enzymatic and non-enzymatic removal of ROS impairing electron transfer) (Hasan et al., 2015; Rezayian et al., 2019); and (2) the high rate of electron transfer served as a protective mechanism (e.g., the enhancement of cyclic electron transfer protected the photosystem by promoting ATP synthesis) (Kalra et al., 2020). Therefore, the results indicated that both *Chlamydomonas* strains responded to Zn stress by maintaining a high electron transfer rate. However, the response of *Chlamydomonas* sp. 1710 was clearly superior given that its ETR_{max} was fairly high under 300 mg/L Zn, whereas that of *C. reinhardtii* was significantly inhibited by even 15 mg/L Zn. Notably, the trends of ETR_{max} were consistent with the growth curve for both *C. reinhardtii* and *Chlamydomonas* sp. 1710, indicating that under Zn stress, the growth of *Chlamydomonas* could be highly influenced by the electron transfer rate, and ETR_{max} could serve as a good growth rate indicator. The transition of ETR_{max} trend at approximately 48 h was also demonstrated by a previous

10.3389/fmicb.2024.1383360

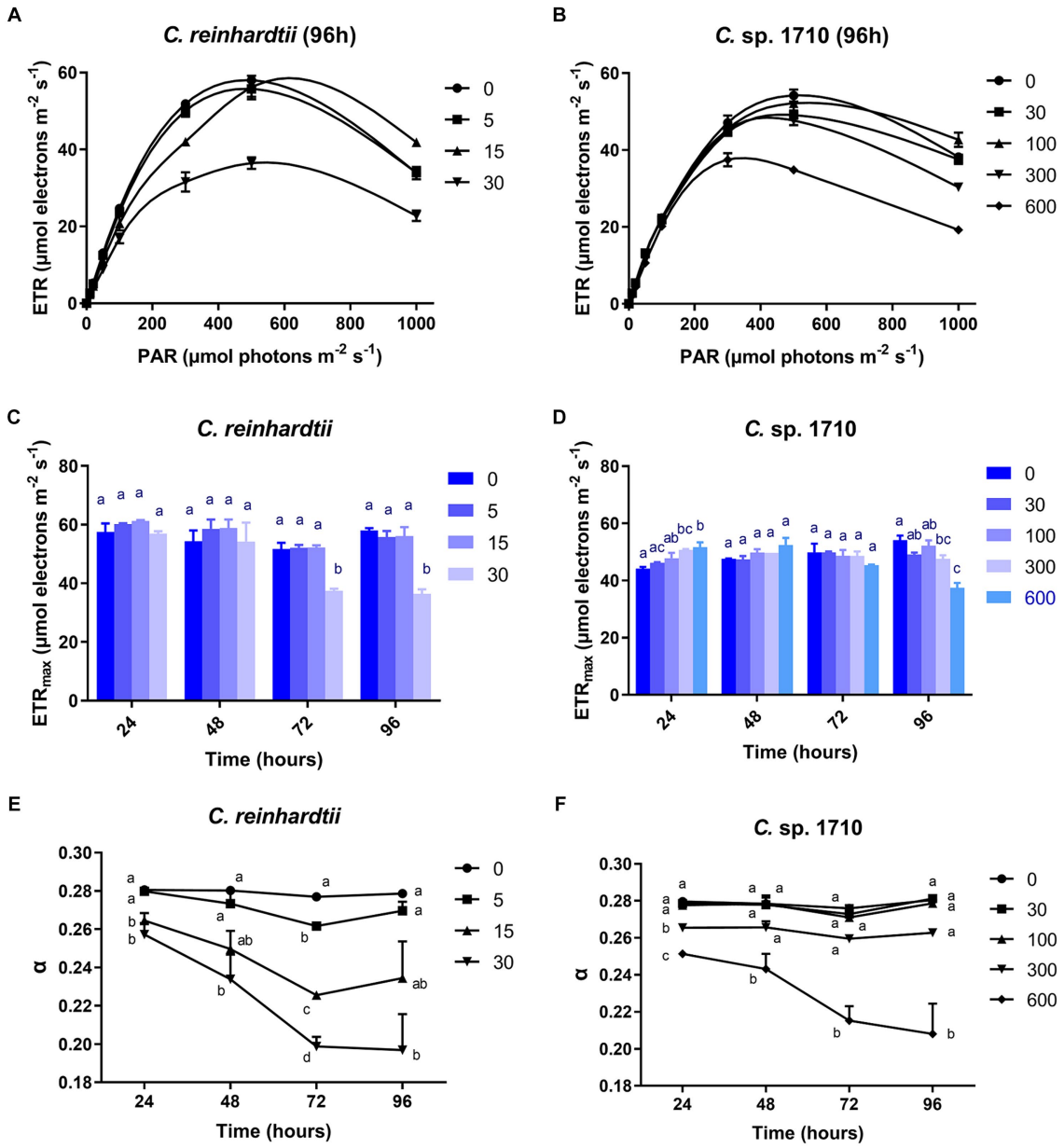

FIGURE 5
Rapid light curve (RLC) **(A,B)**, maximal relative photosynthetic electron transport rate (ETR_{max}) **(C,D)**, and light energy utilization efficiency (α) **(E,F)** of *C. reinhardtii* and *Chlamydomonas* sp. 1710 exposed to Zn (mg/L) for 96 h.

transcriptomic and metabolomic study of *Chlamydomonas* under heavy metal exposure (Jamers et al., 2013).

The light energy utilization efficiency (α) of *C. reinhardtii* was almost unaffected by 5 mg/L Zn, but decreased from 0.28 to 0.2 when Zn concentration increased from 0 to 30 mg/L (Figure 5E). In contrast, the α of *Chlamydomonas* sp. 1710 remained unchanged under 30 and 100 mg/L Zn (Figure 5F). The result indicated that compared to *C. reinhardtii*, *Chlamydomonas* sp. 1710 was more effective at regulating its light energy utilization. Notably, the trend of α was more consistent with that of the growth curve than any other examined parameters, indicating it had the potential to be the best indicative parameter of cell growth. This was in agreement with previous findings in *Chlorella*, another green alga species (Li et al., 2016).

OJIP parameters

The OJIP test provides insights into the electron flux among the different components of PSII by determining the transient fluorescence of several extremely short time points. Several parameters were derived in this study, including absorption flux per reaction center (ABS/RC), trapped energy flux per reaction center (TRo/RC), dissipated energy flux per reaction center (DIo/RC), electron transport flux per reaction center (ETo/RC), electron flux reducing end electron acceptors at the PSI acceptor side per reaction center (REo/RC), performance index for energy conservation from photons absorbed by PSII to the reduction of intersystem electron acceptors (PI_ABS) (Strasser et al., 2000, 2010).

ABS/RC is the average light energy absorbed by the PSII reaction center, and represents the effective antenna size of an active reaction center (Gomes et al., 2012). The increase in the size of light-harvesting antennae is an induced response under stress conditions that enables plants to compete for light energy (Negi et al., 2020). However, for algal populations, truncation of light-harvesting antennae is considered a very effective pathway for substantially enhancing photosynthetic efficiency and biomass yield (Negi et al., 2020; Kumar et al., 2021). The ABS/RC of *C. reinhardtii* had a positive correlation with Zn concentration, and increased from 2.35 to 4.36 when Zn concentration increased from 0 to 30 mg/L (Figure 6A), suggesting that Zn triggered an increase in the light energy absorbed per reaction center. In contrast, the ABS/RC of *Chlamydomonas* sp. 1710 maintained a fairly constant value under lower than 100 mg/L, but increased from 1.92 to 3.34 when Zn concentration increased from 0 to 600 mg/L (Figure 6B). This increase in the ABS/RC could be attributed to the increase in light-harvesting antennae or the reduction of cell concentration, thus decreasing the competition for light energy (Negi et al., 2020). Light saturation of the electron-transport system inevitably leads to the non-productive dissipation of excessive captured energy (Negi et al., 2020). Therefore, the DIo/RC of *C. reinhardtii* increased from 1.05 to 2.83 when Zn concentration increased from 0 to 30 mg/L, indicating a substantial dissipation of energy when exposed to Zn (Figure 6C). In contrast, The DIo/RC of

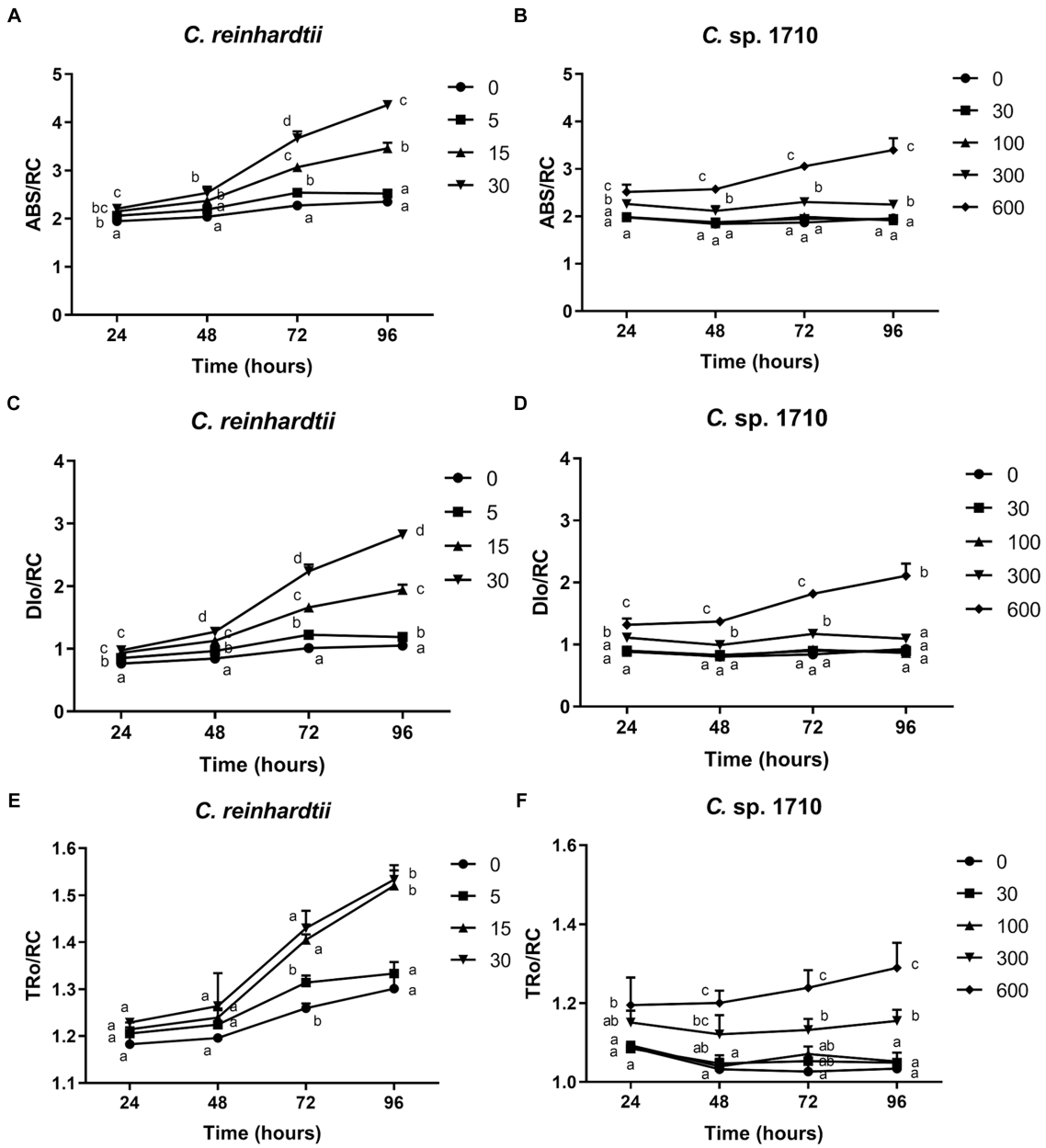

FIGURE 6
Absorption flux per reaction center (ABS/RC) **(A,B)**, trapped energy flux per reaction center (TRo/RC) **(C,D)**, and dissipated energy flux per reaction center (DIo/RC) **(E,F)** of *C. reinhardtii* and *Chlamydomonas* sp. 1710 exposed to Zn (mg/L) for 96 h.

Chlamydomonas sp. 1710 remained stable under lower than 300 mg/L, and increased from 0.87 to 2.11 when Zn concentration increased from 0 to 600 mg/L (Figure 6D). The TRo/RC of *C. reinhardtii* also increased with increased Zn concentration (Figure 6E), albeit to a lesser extent than the increase observed in ABS/RC and DIo/RC, owing to an enhanced passive energy acquisition (Li et al., 2018; Singh et al., 2022). Strikingly, although 5 mg/L slightly increased the ABS/RC and DIo/RC of *C. reinhardtii*, the TRo/RC remained largely unchanged (Figure 6E). This was consistent with previous studies (Liu et al., 2021; Antunović Dunić et al., 2023), indicating that the energy dissipation process offsets excess energy and effectively protected the photosystem complex. However, the TRo/RC of *C. reinhardtii* increased from 1.3 to 1.53 when Zn concentration increased from 0 to 30 mg/L (Figure 6E), showing that the energy dissipation was insufficient. Similar to DIo/RC, the TRo/RC of *Chlamydomonas* sp. 1710 remained unchanged at 30 and 100 mg/L throughout the entire 96 h, and increased from 1.03 to 1.29 when Zn concentration increased from 0 to 600 mg/L (Figure 6F). These results were highly consistent with the NPQ parameters, which demonstrated that energy dissipation, including non-photochemical quenching, were important for the energy regulation in the PSII of the two *Chlamydomonas*. However, the regulation of *Chlamydomonas* sp. 1710 was clearly more effective given that its trapped energy remained constant at Zn concentrations of up to 100 mg/L, whereas *C. reinhardtii* could only tolerate Zn concentrations of 5 mg/L or less.

The ETo/RC of both *C. reinhardtii* and *Chlamydomonas* sp. 1710 remained constant when exposed to various Zn concentrations (Figures 7A,B), indicating that the electron transport flux per active PSII was unaffected by Zn. In contrast, the result of REo/RC indicated that the electron transfer of *C. reinhardtii* and *Chlamydomonas* sp. 1710 had a different response from Q_A^- to final PSI acceptors per active PSII to Zn. The REo/RC of *C. reinhardtii* exhibited a negative correlation with Zn concentration throughout the entire experimental period (Figure 7C), indicating that the electron flux of *C. reinhardtii* from Q_A^- to the final PSI acceptors was inhibited by Zn (Kalaji et al., 2014). However, the REo/RC of *Chlamydomonas* sp. 1710 tended to increase with Zn concentration lower than 300 mg/L Zn, but decrease when Zn concentration was 600 mg/L (Figure 7D). This result indicated that slight Zn stress had no effect on the electron flux of *Chlamydomonas* sp. 1710 from Q_A^- to the final PSI acceptors, whereas severe Zn stress inhibited this process (Kalaji et al., 2014). This was consistent with previous research in which the PSI and PSII electron transport activities of acidophilic algae increased under suboptimal conditions (Gerloff-Elias et al., 2005), indicating that the PSI of *Chlamydomonas* sp. 1710 remained largely unaffected by 300 mg/L or lower concentrations of Zn (Kalaji et al., 2014). However, the photosynthetic electron transport chain of *C. reinhardtii* could be directly disrupted by heavy metals (Geoffroy et al., 2007; Aksmann et al., 2014). Heavy metals such as aluminum inhibit electron transport from PSII toward PSI of both acidophilic algae and neutrophilic algae, albeit at a lesser extent for acidophiles (Perreault et al., 2010). Therefore, the regulation of photosynthetic electron transfer may explain why *Chlamydomonas* sp. 1710 had a stronger tolerance toward Zn than *C. reinhardtii* (Cardol et al., 2011; Žuna Pfeiffer et al., 2018). A previous study demonstrated that extremophilic *Chlamydomonas* exhibited high cyclic electron flow under salinity stress, along with considerable changes in the expression of photosystem proteins (Kalra et al., 2020). Other mechanisms, such as chlororespiration and state transitions, may also participate in the stress adaptation of acidophilic algae (Gerloff-Elias et al., 2005).

PI_ABS is widely used to assess the response of plants to various types of stress, such as drought, extreme temperature, and nutrient deficiency (Stirbet et al., 2018). As illustrated in Figure 7E, the PI_ABS of *C. reinhardtii* exhibited a strong negative correlation with Zn concentration and decreased from 0.75 to 0.12 when Zn concentration increased from 0 to 30 mg/L, suggesting a direct impairment caused by Zn. In contrast, the PI_ABS of *Chlamydomonas* sp. 1710 was not affected in the same manner. Specifically, 30 and 100 mg/L Zn had no inhibitory effect on the PI_ABS of *Chlamydomonas* sp. 1710 (Figure 7F), indicating that *Chlamydomonas* sp. 1710 had a fairly high level of tolerance to Zn. However, the PI_ABS of *Chlamydomonas* sp. 1710 decreased from 0.79 to 0.16 when Zn concentration increased from 0 to 600 mg/L (Figure 7F). The changing trends of PI_ABS were strongly linked to those of μ, Chl-a content, and quantum yield, indicating that it could be a good parameter reflecting the physiological response of *Chlamydomonas* to Zn stress. Additionally, the result of PI_ABS was consistent with that of NPQ parameters, confirming that *C. reinhardtii* and *Chlamydomonas* sp. 1710 responded to Zn stress in different ways (Spoustová et al., 2013; Singh et al., 2015; Habibi, 2017).

Correlation between μ, Chl-a content, and chlorophyll fluorescence parameters

Due to the significant differences between various plant and algae species and despite the existence of numerous methods and parameters, a unified and widely applicable measurement and evaluation system for chlorophyll fluorescence has not been developed (Krause and Weis, 1991; Bussotti, 2004; Murchie and Lawson, 2013). Growth rate is the most intuitive and valuable index for evaluating the stress response of *Chlamydomonas* to Zn (Sunda and Huntsman, 1998). However, it is time-consuming and needs to be calculated based on the D-value of at least two time points. The impact of Zn on the growth of algae is regulated by various metabolic and resistant pathways of the algal cell (Esperanza et al., 2015), which cannot be represented by one indicator alone. Nevertheless, examining the relationship between growth rate and other parameters could offer valuable insights for identifying potential indicators of growth rate (Almeida et al., 2021). On the other hand, the level of damage caused by Zn and the underlying mechanisms vary depending on the plant species and the different components of the cells (Vaillant et al., 2005; Tsonev and Cebola Lidon, 2012; Szopiński et al., 2019). For example, Zn primarily affects the photosynthesis of *Triticum durum* by altering the electron transfer from Q_A to Q_B at the acceptor side of PSII (Paunov et al., 2018). To comprehensively evaluate the effect of Zn on the two *Chlamydomonas* species, PCA was conducted on μ, Chl-a content, and chlorophyll fluorescence parameters.

PCA was conducted to simplify the response patterns of *Chlamydomonas* upon exposure to Zn for 96 h (Figures 8A,B; Supplementary Figure S3). In the figure, each arrow represents a chlorophyll fluorescence parameter, whereas the circles represent the samples exposed to different Zn concentrations. The direction of the

10.3389/fmicb.2024.1383360

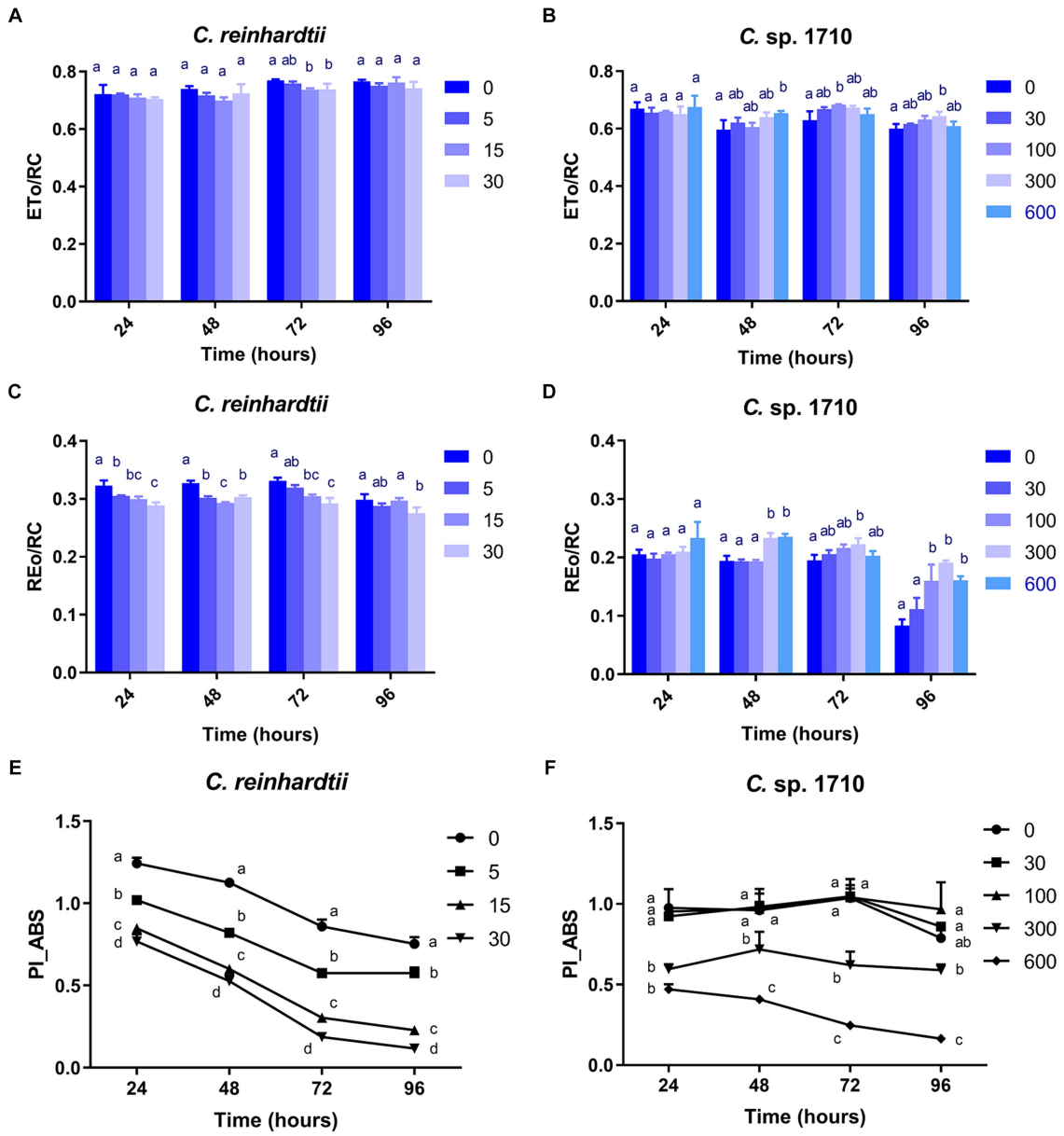

FIGURE 7
Electron transport flux per reaction center (ETo/RC) **(A,B)**, electron flux reducing end electron acceptors at the PSI acceptor side per reaction center (REo/RC) **(C,D)**, and performance index for energy conservation from photons absorbed by PSII to the reduction of intersystem electron acceptors (PI_ABS) **(E,F)** of *C. reinhardtii* and *Chlamydomonas* sp. 1710 exposed to Zn (mg/L) for 96 h.

arrows represents the trends of change for each parameter, whereas the arrow length represents the differences among the tested parameters (Machado et al., 2015). The PCA results also appeared to be time-dependent.

For *C. reinhardtii*, PC1 and PC2 explained 94.4% of the total data variance at 96 h. PC1, accounting for 72.3% of the data variance (eigenvalue 16.63), provided a clear distinction among the four Zn concentrations, which were distinctively distributed in four quadrants (Figure 8A). Similar trends were observed for *Chlamydomonas* sp. 1710. At 96 h, PC1 and PC2 explained 88.3% of the total data variance. The five concentrations were approximately distributed in separate quadrants, with 0, 300, and 600 mg/L being distributed in the fourth, third, and second quadrants, respectively, whereas both 30 and 100 mg/L were distributed in the first quadrant (Figure 8B).

Both the control groups (0 mg/L) of *C. reinhardtii* and *Chlamydomonas* sp. 1710 were positively correlated with ETo/RC, qP, Y(II), F_v/F_m, ETR_{max}, and α (Figures 8A,B). These parameters corresponded to the state of normal growth without stress. For *C. reinhardtii*, 5 mg/L was positively correlated with NPQ, Y(NPQ), qN, and qN(rel), whereas for *Chlamydomonas* sp. 1710, the concentrations were 30 and 100 mg/L (Figure 8A). This indicated that both *Chlamydomonas* strains responded to Zn toxicity via non-photochemical quenching and were able to retain a robust photosynthetic performance (Baracho et al., 2019; Rocha et al., 2021). For *C. reinhardtii*, 15 and 30 mg/L roughly correlated with

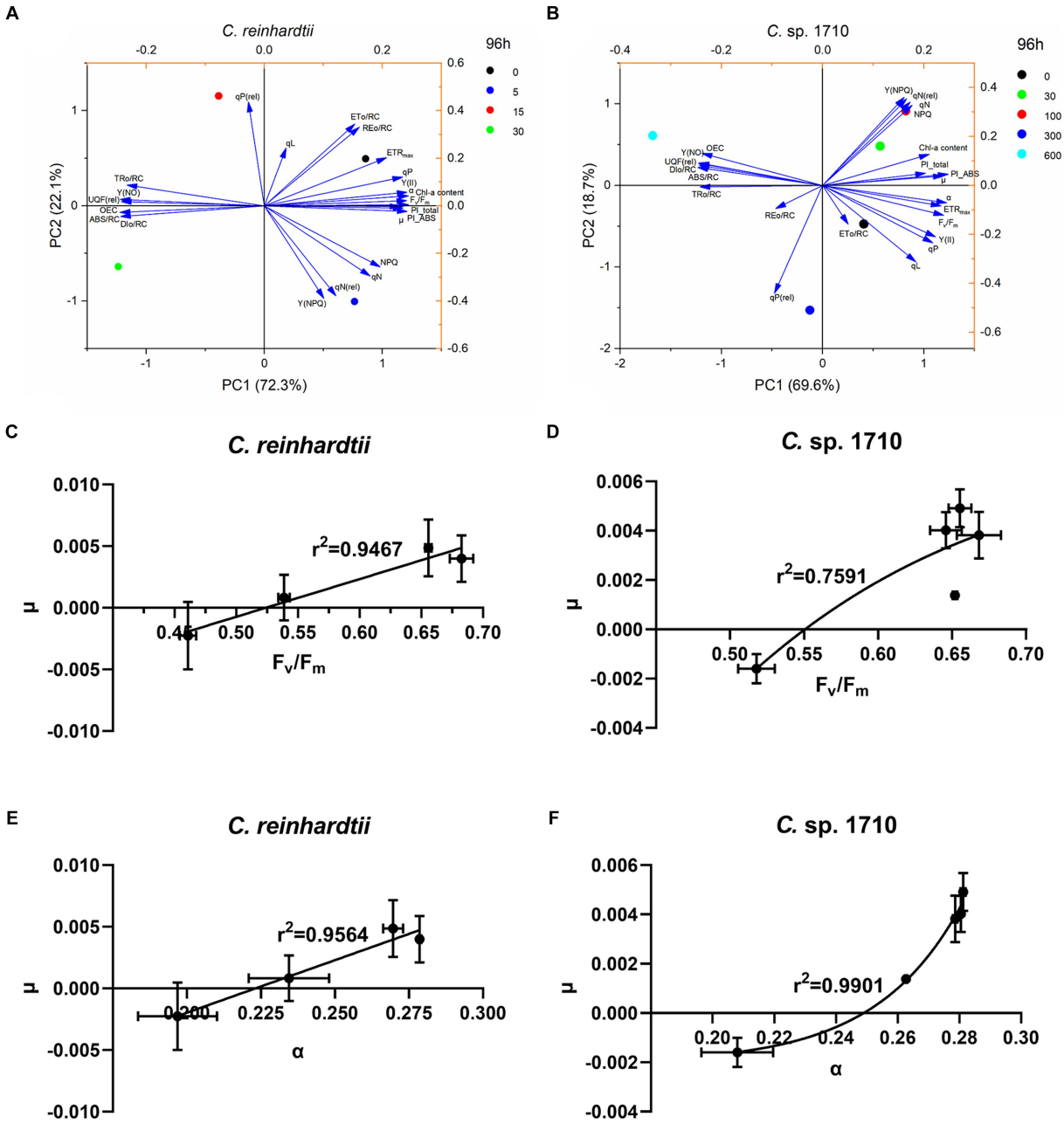

FIGURE 8
Principal component analysis (PCA) of the specific growth rate (μ), chlorophyll a (Chl-a) content, and chlorophyll fluorescence parameters **(A,B)**, regression models between maximal PSII quantum yield (F_v/F_m) and specific growth rate (μ) **(C,D)**, and regression models between light energy utilization efficiency (α) and μ **(E,F)** of *C. reinhardtii* and *Chlamydomonas* sp. 1710 exposed to Zn (mg/L) at 96 h.

OEC, Y(NO), UQF(rel), ABS/RC, TRo/RC, and DIo/RC, whereas for *Chlamydomonas* sp. 1710, 300 and 600 mg/L were more closely correlated with the aforementioned parameters (Figure 8B). Consistent with previous studies, these parameters were identified as the main indicators of severe Zn stress (Almeida et al., 2021; Antunović Dunić et al., 2023).

Supplementary Tables S1–S4 summarize the pairwise Pearson correlations of μ, Chl-a content, and all of the examined chlorophyll fluorescence parameters. For *C. reinhardtii*, α ($r^2 = 0.818$), F_v/F_m ($r^2 = 0.807$) and Y(II) ($r^2 = 0.792$) had a highly positive correlation with μ, whereas F_v/F_m ($r^2 = 0.990$), Y(II) ($r^2 = 0.987$), PI_ABS ($r^2 = 0.977$) and α ($r^2 = 0.939$) had an extremely significant positive correlation with Chl-a content. In contrast, ABS/RC ($r^2 = -0.836$), DIo/RC($r^2 = -0.831$), and OEC ($r^2 = -0.811$) had a negative correlation with μ, whereas OEC ($r^2 = -0.979$), Y(NO) ($r^2 = -0.977$), and ABS/RC ($r^2 = -0.971$) had an extremely significant negative correlation with Chl-a content. For *Chlamydomonas* sp. 1710, α ($r^2 = 0.927$) and PI_ABS ($r^2 = 0.912$) had an extremely significant positive correlation with μ, and PI_ABS ($r^2 = 0.834$) and α ($r^2 = 0.823$) also had a positive correlation with Chl-a content. In contrast, ABS/RC ($r^2 = -0.894$), TRo/RC ($r^2 = -0.928$), and DIo/RC ($r^2 = -0.882$) had a negative correlation with μ, and ABS/RC

($r^2 = -0.806$), TRo/RC ($r^2 = -0.902$) and DIo/RC ($r^2 = -0.777$) had a negative correlation with Chl-a content. These results were fairly consistent with the findings of previous studies (Almeida et al., 2021; Rocha et al., 2021).

F_v/F_m (Kitajima and Butler, 1975) and Y(II) (Genty et al., 1989) have been widely used to assess the photosynthetic function of plants for decades. In this study, these parameters were highly correlated with the μ of the green alga *C. reinhardtii*, which was consistent with previous research (Li et al., 2013). However, for *Chlamydomonas* sp. 1710, F_v/F_m and Y(II) were not the most correlated parameters with μ, substituted by α and PI_ABS, which were derived from RLC (Ralph and Gademann, 2005) and OJIP (Stirbet and Govindjee, 2011), respectively. These findings confirmed that the patterns of chlorophyll fluorescence parameters were species-specific.

Given that F_v/F_m, Y(II), and α had a strong correlation with μ in *C. reinhardtii*, whereas α and PI_ABS were strongly correlated with μ in *Chlamydomonas* sp. 1710, linear and non-linear regression models between these parameters and μ were constructed to determine which model and which chlorophyll fluorescence parameter was a better fit. For the *C. reinhardtii*, fine linear regression models were constructed, with the correlations of F_v/F_m ($r^2 = 0.9564$) and α ($r^2 = 0.9467$), with μ being better than those of Y(II) ($r^2 = 0.9074$) and PI_ABS ($r^2 = 0.826$) (Figures 8C–E; Supplementary Figures S4A,C). However, for the *Chlamydomonas* sp. 1710, good linear regression models between these chlorophyll fluorescence parameters and μ could not be constructed, whereas non-linear regression models were more applicable. Furthermore, α ($r^2 = 0.9901$) and PI_ABS ($r^2 = 0.9763$) clearly exhibited a stronger non-linear regression relationship with μ than F_v/F_m ($r^2 = 0.7591$) and Y(II) ($r^2 = 0.7542$) (Figure 8F; Supplementary Figures S4B,D). These results indicated that F_v/F_m and α were the optimal parameters reflecting the growth status of *C. reinhardtii*, whereas the growth of *Chlamydomonas* sp. 1710 was more accurately described by α and PI_ABS. Moreover, the growth rate of *Chlamydomonas* sp. 1710 was typically more consistent with the light energy utilization efficiency ($r^2 = 0.9901$) than the quantum yield ($r^2 = 0.7591$), suggesting that the energy utilization and regulation process of *Chlamydomonas* sp. 1710 was well protected under Zn stress. This aligns with the characteristics exhibited by salt-tolerant algae or cyanobacteria, which possess robust photoprotective mechanisms (Demmig-Adams et al., 2014; Liang et al., 2023). These data are also highly consistent with the result of OJIP parameters that the trapped photons of PSII of *Chlamydomonas* sp. 1710 were clearly lower than those of *C. reinhardtii*.

Potential implications of the tolerance of *Chlamydomonas* sp. 1710 to Zn manifested by photosynthetic response

Toxic heavy metals are abundant in acidic environments, and thus acidic wastewater endangers natural environments and human health (Simate and Ndlovu, 2014). In this study, Zn was used as a presentative heavy metal to investigate the photosynthetic response of two *Chlamydomonas* species. *Chlamydomonas* sp. *1710* thrives in acidic environments developed unique resistance mechanisms, including antioxidant enzymes and regulation of energy dissipation (Dong et al., 2022; Pluciński et al., 2023; del Carmen Romero-Cruz et al., 2024). The robust tolerance of *Chlamydomonas* sp. 1710 to heavy metals makes it an ideal candidate for addressing heavy metal pollution in acidic environments, such as acid mine drainage. The capability also carries economic benefits, as heavy metals accumulated in algal cells can be recovered, while algal biomass can be utilized for biofuel production (Pavithra et al., 2020; Chakravorty et al., 2023). Understanding the photosynthetic responses of *Chlamydomonas* sp. 1710 to heavy metals helps develop its potential for treating heavy metal pollution under optimized condition, such as adjusting the illumination to achieve appropriate light energy input under heavy metal stress (Ji et al., 2018; Zhao et al., 2023).

Conclusion

The *Chlamydomonas* sp. 1710 displayed a notably higher resistance to Zn-induced stress compared to the *C. reinhardtii*, as evidenced by a tenfold increase in the IC50 of Zn. The growth and Chl-a content of *C. reinhardtii* were inhibited by 15 mg/L Zn, whereas those of *Chlamydomonas* sp. 1710 was not affected by 100 mg/L Zn. The chlorophyll fluorescence parameters including NPQ, RLC, and OJIP were highly in agreement, indicating that, unlike *C. reinhardtii*, the photosystem of *Chlamydomonas* sp. 1710 possesses outstanding protection mechanisms. Non-photochemical quenching played a crucial role in the energy regulation of both *Chlamydomonas* strains under Zn stress. However, the non-photochemical quenching of *C. reinhardtii* was delayed in the initial 48 h by 15 mg/L Zn, and recovered at 72 h, whereas that of *Chlamydomonas* sp. 1710 remained stable throughout the entire Zn exposure process under 100 mg/L Zn. The quantum yield, light energy utilization efficiency (α), and PI_ABS of *C. reinhardtii* were inhibited by Zn, whereas the passively absorbed and dissipated energy and unregulated energy increased, and these effects could be observed when Zn concentration was only at 5 mg/L. However, although similar effects were exerted on *Chlamydomonas* sp. 1710 by Zn, they were negligible when the Zn concentration was 100 mg/L or lower. The electron flux from Q_A^- to the final PSI acceptor side of *Chlamydomonas* sp. 1710 was more resilient than that of *C. reinhardtii*. The varying trends of ETR_{max} in both the *Chlamydomonas* indicated that 48 h marked the beginning of the adaptation period under Zn stress. The high correlation between the light energy utilization efficiency and the growth rate of *Chlamydomonas* sp. 1710, along with its stable trapped photons of PSII, indicated its energy utilization and regulation process was well protected under Zn stress.

Data availability statement

The raw data supporting the conclusions of this article will be made available by the authors, without undue reservation.

Author contributions

DZ: Conceptualization, Data curation, Formal analysis, Investigation, Methodology, Validation, Writing – original draft,

Writing – review & editing. YL: Data curation, Investigation, Methodology, Writing – original draft. NY: Data curation, Investigation, Software, Writing – original draft. CH: Funding acquisition, Supervision, Writing – review & editing.

Funding

The author(s) declare that financial support was received for the research, authorship, and/or publication of this article. This work was supported by National Natural Science Foundation of China (92351303).

Acknowledgments

We are grateful to three reviewers who participated in the review and MJEditor (www.mjeditor.com) for its linguistic assistance during the preparation of this manuscript. This work was supported by the High-performance Computing Platform of China University of Geosciences Beijing.

Conflict of interest

The authors declare that the research was conducted in the absence of any commercial or financial relationships that could be construed as a potential conflict of interest.

Publisher's note

Supplementary material

The Supplementary material for this article can be found online at: https://www.frontiersin.org/articles/10.3389/fmicb.2024.1383360/full#supplementary-material

References

Abinandan, S., Subashchandrabose, S. R., Venkateswarlu, K., Perera, I. A., and Megharaj, M. (2019). Acid-tolerant microalgae can withstand higher concentrations of invasive cadmium and produce sustainable biomass and biodiesel at pH 3.5. *Bioresour. Technol.* 281, 469–473. doi: 10.1016/j.biortech.2019.03.001

Aksmann, A., Pokora, W., Baścik-Remisiewicz, A., Dettlaff-Pokora, A., Wielgomas, B., Dziadziuszko, M., et al. (2014). Time-dependent changes in antioxidative enzyme expression and photosynthetic activity of *Chlamydomonas reinhardtii* cells under acute exposure to cadmium and anthracene. *Ecotoxicol. Environ. Saf.* 110, 31–40. doi: 10.1016/j.ecoenv.2014.08.005

Almeida, A. C., Gomes, T., Lomba, J. A. B., and Lillicrap, A. (2021). Specific toxicity of azithromycin to the freshwater microalga Raphidocelis subcapitata. *Ecotoxicol. Environ. Saf.* 222:112553. doi: 10.1016/j.ecoenv.2021.112553

Antunović Dunić, J., Mlinarić, S., Pavlović, I., Lepeduš, H., and Salopek-Sondi, B. (2023). Comparative analysis of primary photosynthetic reactions assessed by OJIP kinetics in three Brassica crops after drought and recovery. *Appl. Sci.* 13:3078. doi: 10.3390/app13053078

Aparicio, S., Robles, Á., Ferrer, J., Seco, A., and Borrás Falomir, L. (2022). Assessing and modeling nitrite inhibition in microalgae-bacteria consortia for wastewater treatment by means of photo-respirometric and chlorophyll fluorescence techniques. *Sci. Total Environ.* 808:152128. doi: 10.1016/j.scitotenv.2021.152128

Baracho, D. H., Silva, J. C., and Lombardi, A. T. (2019). The effects of copper on photosynthesis and biomolecules yield in Chlorolobion braunii. *J. Phycol.* 55, 1335–1347. doi: 10.1111/jpy.12914

Bilger, W., and Björkman, O. (1990). Role of the xanthophyll cycle in photoprotection elucidated by measurements of light-induced absorbance changes, fluorescence and photosynthesis in leaves of *Hedera canariensis*. *Photosynth. Res.* 25, 173–185. doi: 10.1007/BF00033159

Bischof, K., Hanelt, D., and Wiencke, C. (2000). Effects of ultraviolet radiation on photosynthesis and related enzyme reactions of marine macroalgae. *Planta* 211, 555–562. doi: 10.1007/s004250000313

Bro, R., and Smilde, A. K. (2014). Principal component analysis. *Analytical methods* 6, 2812–2831. doi: 10.1039/C3AY41907J

Broadley, M. R., White, P. J., Hammond, J. P., Zelko, I., and Lux, A. (2007). Zinc in plants. *New Phytol.* 173, 677–702. doi: 10.1111/j.1469-8137.2007.01996.x

Buschmann, C. (1995). Variation of the quenching of chlorophyll fluorescence under different intensities of the actinic light in wildtype plants of tobacco and in an aurea mutant deficient of lightharvesting-complex. *J. Plant Physiol.* 145, 245–252. doi: 10.1016/S0176-1617(11)81884-5

Bussotti, F. (2004). Assessment of stress conditions in *Quercus ilex* L. leaves by O-J-I-P chlorophyll *a* fluorescence analysis. *Plant Biosyst.* 138, 101–109. doi: 10.1080/11263500412331283708

Cady, C. W., Crabtree, R. H., and Brudvig, G. W. (2008). Functional models for the oxygen-evolving complex of photosystem II. *Coord. Chem. Rev.* 252, 444–455. doi: 10.1016/j.ccr.2007.06.002

Candido, C., and Lombardi, A. T. (2018). The physiology of *Chlorella vulgaris* grown in conventional and biodigested treated vinasses. *Algal Res.* 30, 79–85. doi: 10.1016/j.algal.2018.01.005

Cardol, P., Forti, G., and Finazzi, G. (2011). Regulation of electron transport in microalgae. *Biochimica et Biophysica acta (BBA)* 1807, 912–918. doi: 10.1016/j.bbabio.2010.12.004

Chakravorty, M., Nanda, M., Bisht, B., Sharma, R., Kumar, S., Mishra, A., et al. (2023). Heavy metal tolerance in microalgae: detoxification mechanisms and applications. *Aquat. Toxicol.* 260:106555. doi: 10.1016/j.aquatox.2023.106555

Das, B. K., Roy, A., Singh, S., and Bhattacharya, J. (2009). Eukaryotes in acidic mine drainage environments: potential applications in bioremediation. *Rev. Environ. Sci. Biotechnol.* 8, 257–274. doi: 10.1007/s11157-009-9161-3

Deblois, C. P., Marchand, A., and Juneau, P. (2013). Comparison of photoacclimation in twelve freshwater photoautotrophs (chlorophyte, bacillaryophyte, cryptophyte and cyanophyte) isolated from a natural community. *PLoS One* 8:e57139. doi: 10.1371/journal.pone.0057139

del Carmen Romero-Cruz, M., Leon-Vaz, A., Giráldez, I., Vega, J. M., and Vigara, J. (2024). Effect of heavy metals on the antioxidant system of the acid-tolerant microalga Coccomyxa onubensis. *Algal Res.* 77:103337. doi: 10.1016/j.algal.2023.103337

Demmig-Adams, B., Garab, G., Adams Iii, W., and Govindjee. (2014). *Non-photochemical quenching and energy dissipation in plants, algae and Cyanobacteria*. Dordrecht: Springer Netherlands.

Dewez, D., Geoffroy, L., Vernet, G., and Popovic, R. (2005). Determination of photosynthetic and enzymatic biomarkers sensitivity used to evaluate toxic effects of copper and fludioxonil in alga *Scenedesmus obliquus*. *Aquat. Toxicol.* 74, 150–159. doi: 10.1016/j.aquatox.2005.05.007

Dong, H., Huang, L., Zhao, L., Zeng, Q., Liu, X., Sheng, Y., et al. (2022). A critical review of mineral–microbe interaction and co-evolution: mechanisms and applications. *Natl. Sci. Rev.* 9:nwac128. doi: 10.1093/nsr/nwac128

Dong, H., Zeng, Q., Sheng, Y., Chen, C., Yu, G., and Kappler, A. (2023). Coupled iron cycling and organic matter transformation across redox interfaces. *Nat. Rev. Earth Environ.* 4, 659–673. doi: 10.1038/s43017-023-00470-5

Esperanza, M., Cid, Á., Herrero, C., and Rioboo, C. (2015). Acute effects of a prooxidant herbicide on the microalga *Chlamydomonas reinhardtii*: screening cytotoxicity and genotoxicity endpoints. *Aquat. Toxicol.* 165, 210–221. doi: 10.1016/j.aquatox.2015.06.004

Fu, W., Li, P., and Wu, Y. (2012). Effects of different light intensities on chlorophyll fluorescence characteristics and yield in lettuce. *Sci. Hortic.* 135, 45–51. doi: 10.1016/j.scienta.2011.12.004

Gebara, R. C., de Alho, L. O. G., da Silva Mansano, A., Rocha, G. S., and da Melão, M. G. G. (2023). Single and combined effects of Zn and Al on photosystem II of the green microalgae Raphidocelis subcapitata assessed by pulse-amplitude modulated (PAM) fluorometry. *Aquat. Toxicol.* 254:106369. doi: 10.1016/j.aquatox.2022.106369

Genty, B., Briantais, J.-M., and Baker, N. R. (1989). The relationship between the quantum yield of photosynthetic electron transport and quenching of chlorophyll fluorescence. *Biochimica et Biophysica Acta (BBA)* 990, 87–92. doi: 10.1016/S0304-4165(89)80016-9

Geoffroy, L., Gilbin, R., Simon, O., Floriani, M., Adam, C., Pradines, C., et al. (2007). Effect of selenate on growth and photosynthesis of *Chlamydomonas reinhardtii*. *Aquat. Toxicol.* 83, 149–158. doi: 10.1016/j.aquatox.2007.04.001

Gerloff-Elias, A., Spijkerman, E., and Pröschold, T. (2005). Effect of external pH on the growth, photosynthesis and photosynthetic electron transport of *Chlamydomonas acidophila* Negoro, isolated from an extremely acidic lake (pH 2.6). *Plant Cell Environ.* 28, 1218–1229. doi: 10.1111/j.1365-3040.2005.01357.x

Giacometti, G. M., and Morosinotto, T. (2013). "Photoinhibition and photoprotection in plants, Algae, and Cyanobacteria" in *Encyclopedia of Biological Chemistry*, 482–487.

Gomes, M. T. G., da Luz, A. C., dos Santos, M. R., Batitucci, M., do Silva, D. M., and Falqueto, A. R. (2012). Drought tolerance of passion fruit plants assessed by the OJIP chlorophyll a fluorescence transient. *Sci. Hortic.* 142, 49–56. doi: 10.1016/j.scienta.2012.04.026

Goodwin, T. W. (1965). *Chemistry and biochemistry of plant pigments*.

Guermazi, W., Masmoudi, S., Trabelsi, N. A., Gammoudi, S., Ayadi, H., Morant-Manceau, A., et al. (2023). Physiological and biochemical responses in microalgae *Dunaliella salina*, Cylindrotheca closterium and Phormidium versicolor NCC466 exposed to high salinity and irradiation. *Life* 13:313. doi: 10.3390/life13020313

Habibi, G. (2017). Selenium ameliorates salinity stress in *Petroselinum crispum* by modulation of photosynthesis and by reducing shoot Na accumulation. *Russ. J. Plant Physiol.* 64, 368–374. doi: 10.1134/S1021443717030086

Hasan, K., Çevik, E., Sperling, E., Packer, M. A., Leech, D., and Gorton, L. (2015). Photoelectrochemical wiring of *Paulschulzia pseudovolvox* (algae) to osmium polymer modified electrodes for harnessing solar energy. *Adv. Energy Mater.* 5:1501100. doi: 10.1002/aenm.201501100

Jamers, A., Blust, R., De Coen, W., Griffin, J. L., and Jones, O. A. H. (2013). An omics based assessment of cadmium toxicity in the green alga *Chlamydomonas reinhardtii*. *Aquat. Toxicol.* 126, 355–364. doi: 10.1016/j.aquatox.2012.09.007

Ji, Y., Xie, X., and Wang, G. (2018). Effects of the heavy metal cadmium on photosynthetic activity and the xanthophyll cycle in *Phaeodactylum tricornutum*. *J. Ocean. Limnol.* 36, 2194–2201. doi: 10.1007/s00343-019-7160-y

Jiang, W., Meng, L., Liu, F., Sheng, Y., Chen, S., Yang, J., et al. (2023). Distribution, source investigation, and risk assessment of topsoil heavy metals in areas with intensive anthropogenic activities using the positive matrix factorization (PMF) model coupled with self-organizing map (SOM). *Environ. Geochem. Health* 45, 6353–6370. doi: 10.1007/s10653-023-01587-8

Juneau, P., Dewez, D., Matsui, S., Kim, S.-G., and Popovic, R. (2001). Evaluation of different algal species sensitivity to mercury and metolachlor by PAM-fluorometry. *Chemosphere* 45, 589–598. doi: 10.1016/S0045-6535(01)00034-0

Juneau, P., Green, B. R., and Harrison, P. J. (2005). Simulation of pulse-amplitude-modulated (PAM) fluorescence: limitations of some PAM-parameters in studying environmental stress effects. *Photosynt* 43, 75–83. doi: 10.1007/s11099-005-5083-7

Kalaji, H. M., Oukarroum, A., Alexandrov, V., Kouzmanova, M., Brestic, M., Zivcak, M., et al. (2014). Identification of nutrient deficiency in maize and tomato plants by in vivo chlorophyll a fluorescence measurements. *Plant Physiol. Biochem.* 81, 16–25. doi: 10.1016/j.plaphy.2014.03.029

Kalra, I., Wang, X., Cvetkovska, M., Jeong, J., McHargue, W., Zhang, R., et al. (2020). Chlamydomonas sp. UWO 241 exhibits high cyclic Electron flow and rewired metabolism under high salinity. *Plant Physiol.* 183, 588–601. doi: 10.1104/pp.19.01280

Kitajima, M., and Butler, W. L. (1975). Quenching of chlorophyll fluorescence and primary photochemistry in chloroplasts by dibromothymoquinone. *Biochim. Biophys. Acta* 376, 105–115. doi: 10.1016/0005-2728(75)90209-1

Klughammer, C., and Schreiber, U. (2008). Complementary PS II quantum yields calculated from simple fluorescence parameters measured by PAM fluorometry and the saturation pulse method. *PAM Appl. Notes* 1, 201–247.

Kramer, D. M., Johnson, G., Kiirats, O., and Edwards, G. E. (2004). New fluorescence parameters for the determination of QA redox state and excitation energy fluxes. *Photosynth. Res.* 79:209. doi: 10.1023/B:PRES.0000015391.99477.0d

Krause, G. H., and Weis, E. (1991). Chlorophyll fluorescence and photosynthesis: the basics. *Annu. Rev. Plant Physiol. Plant Mol. Biol.* 42, 313–349. doi: 10.1146/annurev.pp.42.060191.001525

Kriedemann, P. E., Graham, R. D., and Wiskich, J. T. (1985). Photosynthetic dysfunction and in vivo changes in chlorophyll a fluorescence from manganese-deficient wheat leaves. *Aust. J. Agric. Res.* 36, 157–169. doi: 10.1071/AR9850157

Kumar, V., Sharma, N., Jaiswal, K. K., Vlaskin, M. S., Nanda, M., Tripathi, M. K., et al. (2021). Microalgae with a truncated light-harvesting antenna to maximize photosynthetic efficiency and biomass productivity: recent advances and current challenges. *Process Biochem.* 104, 83–91. doi: 10.1016/j.procbio.2021.03.006

Leong, Y. K., and Chang, J.-S. (2020). Bioremediation of heavy metals using microalgae: recent advances and mechanisms. *Bioresour. Technol.* 303:122886. doi: 10.1016/j.biortech.2020.122886

Li, X., Li, W., Zhai, J., and Wei, H. (2018). Effect of nitrogen limitation on biochemical composition and photosynthetic performance for fed-batch mixotrophic cultivation of microalga Spirulina platensis. *Bioresour. Technol.* 263, 555–561. doi: 10.1016/j.biortech.2018.05.046

Li, M., Wan, C.-Y., Pan, X.-J., Zou, Y., Chi, S.-Y., and Chang, J.-B. (2013). Comparative study of stress by four heavy metals on Chlamydomonas reinhardtii and the potential application in bbe algae toximeter. *Fresenius Environ. Bull.* 22:1494. doi: 10.5555/20133219932

Li, T., Xu, J., Gao, B., Xiang, W., Li, A., and Zhang, C. (2016). Morphology, growth, biochemical composition and photosynthetic performance of *Chlorella vulgaris* (Trebouxiophyceae) under low and high nitrogen supplies. *Algal Res.* 16, 481–491. doi: 10.1016/j.algal.2016.04.008

Liang, M.-H., Dai, J.-L., Xie, S.-R., Wu, J.-X., Chen, H.-H., and Jiang, J.-G. (2023). Orange protein (DbOR) from the salt-tolerant green alga *Dunaliella bardawil* mediates photosynthesis against heat stress via interacting with DbPsbP1. *Algal Res.* 72:103105. doi: 10.1016/j.algal.2023.103105

Liu, M. S., Huang, X. H., Wang, R. J., Xu, H. Y., and Zhu, F. (2021). Inhibition of photosynthesis in Melia azedarach and *Ligustrum lucidum* induced by manganese toxicity using OJIP chlorophyll a fluorescence transient. *Photosynthetica* 59, 148–159. doi: 10.32615/ps.2021.006

Lu, D., Zhang, Y., Zhang, A., and Lu, C. (2022). Non-photochemical quenching: from light perception to photoprotective gene expression. *Int. J. Mol. Sci.* 23:687. doi: 10.3390/ijms23020687

Lüder, U., Knoetzel, J., and Wiencke, C. (2001). Acclimation of photosynthesis and pigments to seasonally changing light conditions in the endemic Antarctic red macroalga Palmaria decipiens. *Polar Biol.* 24, 598–603. doi: 10.1007/s003000100260

Machado, M. D., Lopes, A. R., and Soares, E. V. (2015). Responses of the alga *Pseudokirchneriella subcapitata* to long-term exposure to metal stress. *J. Hazard. Mater.* 296, 82–92. doi: 10.1016/j.jhazmat.2015.04.022

Marchetto, F., Santaeufemia, S., Lebiedzińska-Arciszewska, M., Śliwińska, M. A., Pich, M., Kurek, E., et al. (2023). Molecular mechanisms of heavy metal adaptation of an extremophilic red alga Cyanidioschyzon merolae. *bioRxiv*, 2023–2002. doi: 10.1101/2023.02.24.529964

Marečková, M., Barták, M., and Hájek, J. (2019). Temperature effects on photosynthetic performance of Antarctic lichen Dermatocarpon polyphyllizum: a chlorophyll fluorescence study. *Polar Biol.* 42, 685–701. doi: 10.1007/s00300-019-02464-w

Mathimani, T., Rene, E. R., Devanesan, S., and AlSalhi, M. S. (2023). Removal of zinc by Selenastrum sp. and simultaneous biodiesel production from metal-resistant biomass for energy and environmental sustainability. *Algal Res.*:103157. doi: 10.1016/j.algal.2023.103157

Maxwell, K., and Johnson, G. N. (2000). Chlorophyll fluorescence--a practical guide. *J. Exp. Bot.* 51, 659–668. doi: 10.1093/jexbot/51.345.659

Mikulic, P., and Beardall, J. (2014). Contrasting ecotoxicity effects of zinc on growth and photosynthesis in a neutrophilic alga (*Chlamydomonas reinhardtii*) and an extremophilic alga (*Cyanidium caldarium*). *Chemosphere* 112, 402–411. doi: 10.1016/j.chemosphere.2014.04.049

Mikulic, P., and Beardall, J. (2021). Oxidative and anti-oxidative responses to metal toxicity in an extremophilic alga (*Cyanidium caldarium*) and a neutrophilic alga (*Chlamydomonas reinhardtii*). *Phycologia* 60, 513–523. doi: 10.1080/00318884.2021.1984044

Misra, A. N., Misra, M., and Singh, R. (2012). Chlorophyll fluorescence in plant biology. *Biophysics* 7, 171–192. doi: 10.5772/35111

Murchie, E. H., and Lawson, T. (2013). Chlorophyll fluorescence analysis: a guide to good practice and understanding some new applications. *J. Exp. Bot.* 64, 3983–3998. doi: 10.1093/jxb/ert208

Nama, S., Madireddi, S. K., Yadav, R. M., and Subramanyam, R. (2019). Non-photochemical quenching-dependent acclimation and thylakoid organization of *Chlamydomonas reinhardtii* to high light stress. *Photosynth. Res.* 139, 387–400. doi: 10.1007/s11120-018-0551-7

Negi, S., Perrine, Z., Friedland, N., Kumar, A., Tokutsu, R., Minagawa, J., et al. (2020). Light regulation of light-harvesting antenna size substantially enhances photosynthetic efficiency and biomass yield in green algae†. *Plant J.* 103, 584–603. doi: 10.1111/tpj.14751

Nowicka, B. (2020). Practical aspects of the measurements of non-photochemical chlorophyll fluorescence quenching in green microalgae *Chlamydomonas reinhardtii* using open FluorCam. *Physiol. Plant.* 168, 617–629. doi: 10.1111/ppl.13003

Ort, D. R., and Baker, N. R. (2002). A photoprotective role for O2 as an alternative electron sink in photosynthesis? *Curr. Opin. Plant Biol.* 5, 193–198. doi: 10.1016/S1369-5266(02)00259-5

Oxborough, K., and Baker, N. R. (1997). Resolving chlorophyll a fluorescence images of photosynthetic efficiency into photochemical and non-photochemical

components - calculation of qP and Fv'/Fm' without measuring Fo'. *Photosynth. Res.* 54, 135–142. doi: 10.1023/A:1005936823310

Paunov, M., Koleva, L., Vassilev, A., Vangronsveld, J., and Goltsev, V. (2018). Effects of different metals on photosynthesis: cadmium and zinc affect chlorophyll fluorescence in durum wheat. *Int. J. Mol. Sci.* 19:787. doi: 10.3390/ijms19030787

Pavithra, K. G., Kumar, P. S., Jaikumar, V., Vardhan, K. H., and SundarRajan, P. (2020). Microalgae for biofuel production and removal of heavy metals: a review. *Environ. Chem. Lett.* 18, 1905–1923. doi: 10.1007/s10311-020-01046-1

Perreault, F., Dewez, D., Fortin, C., Juneau, P., Diallo, A., and Popovic, R. (2010). Effect of aluminum on cellular division and photosynthetic electron transport in Euglena gracilis and Chlamydomonas acidophila. *Environ. Toxicol. Chem.* 29, 887–892. doi: 10.1002/etc.109

Pluciński, B., Nowicka, B., Waloszek, A., Rutkowska, J., and Strzałka, K. (2023). The role of antioxidant response and nonphotochemical quenching of chlorophyll fluorescence in long-term adaptation to cu-induced stress in *Chlamydomonas reinhardtii*. *Environ. Sci. Pollut. Res.* 30, 67250–67262. doi: 10.1007/s11356-023-27175-y

Puente-Sánchez, F., Díaz, S., Penacho, V., Aguilera, A., and Olsson, S. (2018). Basis of genetic adaptation to heavy metal stress in the acidophilic green alga Chlamydomonas acidophila. *Aquat. Toxicol.* 200, 62–72. doi: 10.1016/j.aquatox.2018.04.020

Ralph, P. J., and Gademann, R. (2005). Rapid light curves: a powerful tool to assess photosynthetic activity. *Aquat. Bot.* 82, 222–237. doi: 10.1016/j.aquabot.2005.02.006

Ranjbarfordoei, A., Samson, R., and Van Damme, P. (2006). Chlorophyll fluorescence performance of sweet almond [*Prunus dulcis* (miller) D. Webb] in response to salinity stress induced by NaCl. *Photosynthetica* 44, 513–522. doi: 10.1007/s11099-006-0064-z

Rezayian, M., Niknam, V., and Ebrahimzadeh, H. (2019). Oxidative damage and antioxidative system in algae. *Toxicol. Rep.* 6, 1309–1313. doi: 10.1016/j.toxrep.2019.10.001

Rizwan, M., Mujtaba, G., Memon, S. A., Lee, K., and Rashid, N. (2018). Exploring the potential of microalgae for new biotechnology applications and beyond: A review. *Renew. Sust. Energ. Rev.* 92, 394–404. doi: 10.1016/j.rser.2018.04.034

Rocha, G. S., Lombardi, A. T., and Espíndola, E. L. G. (2021). Combination of P-limitation and cadmium in photosynthetic responses of the freshwater microalga Ankistrodesmus densus (Chlorophyceae). *Environ. Pollut.* 275:116673. doi: 10.1016/j.envpol.2021.116673

Rocha, G. S., Lopes, L. F. P., and Melão, M. G. G. (2024). Phosphorus limitation combined with aluminum triggers synergistic responses on the freshwater microalgae *Raphidocelis subcapitata* (Chlorophyceae). *Chemosphere* 352:141320. doi: 10.1016/j.chemosphere.2024.141320

Rochaix, J. D. (1995). *Chlamydomonas reinhardtii* as the photosynthetic yeast. *Annu. Rev. Genet.* 29, 209–230. doi: 10.1146/annurev.ge.29.120195.001233

Schreiber, U., Schliwa, U., and Bilger, W. (1986). Continuous recording of photochemical and non-photochemical chlorophyll fluorescence quenching with a new type of modulation fluorometer. *Photosynth. Res.* 10, 51–62. doi: 10.1007/BF00024185

Sekulska-Nalewajko, J., Kornaś, A., Gocławski, J., Miszalski, Z., and Kuźniak, E. (2019). Spatial referencing of chlorophyll fluorescence images for quantitative assessment of infection propagation in leaves demonstrated on the ice plant: Botrytis cinerea pathosystem. *Plant Methods* 15:18. doi: 10.1186/s13007-019-0401-4

Simate, G. S., and Ndlovu, S. (2014). Acid mine drainage: challenges and opportunities. *J. Environ. Chem. Eng.* 2, 1785–1803. doi: 10.1016/j.jece.2014.07.021

Singh, H., Kumar, D., and Soni, V. (2022). Performance of chlorophyll a fluorescence parameters in *Lemna minor* under heavy metal stress induced by various concentration of copper. *Sci. Rep.* 12:10620. doi: 10.1038/s41598-022-14985-2

Singh, M., Pratap Singh, V., Dubey, G., and Mohan Prasad, S. (2015). Exogenous proline application ameliorates toxic effects of arsenate in *Solanum melongena* L. seedlings. *Ecotoxicol. Environ. Saf.* 117, 164–173. doi: 10.1016/j.ecoenv.2015.03.021

Spolaore, P., Joannis-Cassan, C., Duran, E., and Isambert, A. (2006). Commercial applications of microalgae. *J. Biosci. Bioeng.* 101, 87–96. doi: 10.1263/jbb.101.87

Spoustová, P., Synková, H., Valcke, R., and Čeřovská, N. (2013). Chlorophyll a fluorescence as a tool for a study of the potato virus Y effects on photosynthesis of nontransgenic and transgenic Pssu-ipt tobacco. *Photosynt.* 51, 191–201. doi: 10.1007/s11099-013-0023-4

Stirbet, A., and Govindjee, G. (2011). On the relation between the Kautsky effect (chlorophyll a fluorescence induction) and photosystem II: basics and applications of the OJIP fluorescence transient. *J. Photochem. Photobiol. B* 104, 236–257. doi: 10.1016/j.jphotobiol.2010.12.010

Stirbet, A., Lazár, D., Kromdijk, J., and Govindjee, G. (2018). Chlorophyll a fluorescence induction: can just a one-second measurement be used to quantify abiotic stress responses? *Photosynt.* 56, 86–104. doi: 10.1007/s11099-018-0770-3

Strasser, R. J., Srivastava, A., and Tsimilli-Michael, M. (2000). The fluorescence transient as a tool to characterize and screen photosynthetic samples. *Probing Photosynthesis* 25, 445–483.

Strasser, R. J., Tsimilli-Michael, M., Qiang, S., and Goltsev, V. (2010). Simultaneous in vivo recording of prompt and delayed fluorescence and 820-nm reflection changes during drying and after rehydration of the resurrection plant *Haberlea rhodopensis*. *Biochim. Biophys. Acta* 1797, 1313–1326. doi: 10.1016/j.bbabio.2010.03.008

Sunda, W. G., and Huntsman, S. A. (1998). Interactions among Cu2+, Zn2+, and Mn2+ in controlling cellular Mn, Zn, and growth rate in the coastal alga Chlamydomonas. *Limnol. Oceanography* 43, 1055–1064. doi: 10.4319/lo.1998.43.6.1055

Szopiński, M., Sitko, K., Gieroń, Ż., Rusinowski, S., Corso, M., Hermans, C., et al. (2019). Toxic effects of Cd and Zn on the photosynthetic apparatus of the Arabidopsis halleri and *Arabidopsis arenosa* pseudo-metallophytes. *Front. Plant Sci.* 10:748. doi: 10.3389/fpls.2019.00748

Tang, D., Han, W., Li, P., Miao, X., and Zhong, J. (2011). CO2 biofixation and fatty acid composition of Scenedesmus obliquus and *Chlorella pyrenoidosa* in response to different CO2 levels. *Bioresour. Technol.* 102, 3071–3076. doi: 10.1016/j.biortech.2010.10.047

Thanigaivel, S., Rajendran, S., Gnanasekaran, L., Chew, K. W., Tran, D. T., Tran, H.-D., et al. (2023). Nanotechnology for improved production of algal biofuels: a review. *Environ. Chem. Lett.* 21, 821–837. doi: 10.1007/s10311-022-01529-3

Tsonev, T., and Cebola Lidon, F. J. (2012). Zinc in plants-an overview. *Emirates J. Food Agric.*:24.

Vaillant, N., Monnet, F., Hitmi, A., Sallanon, H., and Coudret, A. (2005). Comparative study of responses in four Datura species to a zinc stress. *Chemosphere* 59, 1005–1013. doi: 10.1016/j.chemosphere.2004.11.030

van Kooten, O., and Snel, J. F. (1990). The use of chlorophyll fluorescence nomenclature in plant stress physiology. *Photosynth. Res.* 25, 147–150. doi: 10.1007/BF00033156

White, A. J., and Critchley, C. (1999). Rapid light curves: A new fluorescence method to assess the state of the photosynthetic apparatus. *Photosynth. Res.* 59, 63–72. doi: 10.1023/A:1006188004189

Wold, S., Esbensen, K., and Geladi, P. (1987). Principal component analysis. *Chemom. Intell. Lab. Syst.* 2, 37–52. doi: 10.1016/0169-7439(87)80084-9

Wong, P. T. S., and Chau, Y. K. (1990). Zinc toxicity to freshwater algae. *Environ. Toxicol. Water Qual.* 5, 167–177. doi: 10.1002/tox.2540050205

Zhao, D., Cheah, W. Y., Lai, S. H., Ng, E.-P., Khoo, K. S., Show, P. L., et al. (2023). Symbiosis of microalgae and bacteria consortium for heavy metal remediation in wastewater. *J. Environ. Chem. Eng.* 11:109943. doi: 10.1016/j.jece.2023.109943

Zhu, Z., Sun, J., Fa, Y., Liu, X., and Lindblad, P. (2022). Enhancing microalgal lipid accumulation for biofuel production. *Front. Microbiol.* 13:1024441. doi: 10.3389/fmicb.2022.1024441

Žuna Pfeiffer, T., Štolfa Čamagajevac, I., Špoljarić Maronić, D., and Maksimović, I. (2018). Regulation of photosynthesis in algae under metal stress. *Environ. Photosynthesis Future Prospect Diverse*. doi: 10.1002/9781119501800.ch6

10.3389/fmicb.2024.1383360

Appendix

Parameter	Definition	Equation	Reference
F_0	Initial fluorescence	-	Kitajima and Butler (1975)
F_m	Maximum fluorescence	-	Kitajima and Butler (1975)
F_v/F_m	Maximal PSII quantum yield	$(F_m\text{-}F_0)/F_m$	Kitajima and Butler (1975)
OEC	Efficiency of the oxygen-evolving complex	$F_0/(F_m\text{-}F_0)$	Kriedemann et al. (1985)
Y(II)	Effective PSII quantum yield	$(F_m'\text{-}F)/F_m'$	Genty et al. (1989)
qP	Coefficient of photochemical quenching	$(F_m'\text{-}F)/(F_m'\text{-}F_0')$*	Schreiber et al. (1986)
NPQ	Non-photochemical quenching	$(F_m\text{-}F_m')/F_m'$	Bilger and Björkman (1990)
qL	Coefficient of photochemical quenching	$(F_m'\text{-}F)/(F_m'\text{-}F_0')\times F_0'/F = qP\times F_0'/F$*	Kramer et al. (2004)
Y(NPQ)	Quantum yield of regulated energy dissipation	$1 - Y(II) - 1/(NPQ + 1 + qL(F_m/F_0\text{-}1))$	Kramer et al. (2004)
Y(NO)	Quantum yield of nonregulated energy dissipation	$1/(NPQ + 1 + qL(F_m/F_0\text{-}1))$	Kramer et al. (2004)
qN	Coefficient of non-photochemical quenching	$(F_m\text{-}F_m')/(F_m\text{-}F_0')$*	Schreiber et al. (1986)
qP(rel)	Relative photochemical quenching	$(F_m'\text{-}F_t)/(F_m\text{-}F_0')$	Buschmann (1995)
qN(rel)	Relative non-photochemical quenching	$(F_m\text{-}F_m')/(F_m\text{-}F_0')$	Buschmann (1995)
UQF(rel)	Relative unquenched fluorescence	$(F_t\text{-}F_0')/(F_m\text{-}F_0')$	Juneau et al. (2005)
V_j	Relative variable fluorescence at the J-peak of OJIP curve	$(F_j\text{-}F_0)/(F_m\text{-}F_0)$	Strasser et al. (2000)
V_i	Relative variable fluorescence at the I-peak of OJIP curve	$(F_i\text{-}F_0)/(F_m\text{-}F_0)$	Strasser et al. (2000)
φ_{Po}	Maximum quantum yield of primary photochemistry (at $t = 0$)	$(F_m\text{-}F_0)/F_m$ (equal to F_v/F_m)	Strasser et al. (2000)
ψ_{Eo}	Probability (at $t = 0$) that a trapped exciton moves an electron into the electron transport chain beyond Q_A^-	$(1\text{-}V_j)$	Strasser et al. (2000)
δ_{Ro}	Efficiency/Probability with which an electron from the intersystem electron carriers moves to reduce end electron acceptors at the PS I acceptor side	$(1\text{-}V_i)/(1\text{-}V_j)$	Strasser et al. (2000)
M_0	Approximated initial slope (ms^{-1}) of the fluorescence transient normalized on the maximal variable fluorescence F_v	$4(F_{300}\text{-}F_0)/(F_m\text{-}F_0)$	Strasser et al. (2000)
ABS/RC	Absorption flux per reaction center	$M_0(1/V_j)(1/\varphi_{Po})$	Strasser et al. (2000)
TRo/RC	Trapped energy flux per reaction center	M_0/V_j	Strasser et al., 2000
ETo/RC	Electron transport flux per reaction center	$(M_0/V_j)\times\psi_{Eo}$	Strasser et al. (2000)
DIo/RC	Dissipated energy flux per reaction center	ABS/RC- TRo/RC	Strasser et al. (2000)
REo/RC	Electron flux reducing end electron acceptors at the PSI acceptor side per reaction center	$(M_0/V_j)\times(1\text{-}V_i)$	Strasser et al. (2010)
PI_ABS	Performance index for energy conservation from photons absorbed by PSII to the reduction of intersystem electron acceptors	$\frac{RC}{ABS}\times\frac{\varphi Po}{1-\varphi Po}\times\frac{\psi Eo}{1-\psi Eo}$	Strasser et al. (2010)
PI_total	Performance index for energy conservation from photons absorbed by PSII to the reduction of PSI and acceptors	$PI\_ABS\times\frac{\delta Ro}{1-\delta Ro}$	Strasser et al. (2010)
α	Light energy utilization efficiency	The initial slope of the ETR-PAR curve	Fu et al. (2012)
ETR	Relative photosynthetic electron transport rate	0.5 x Y(II) x PAR x I_A	Genty et al. (1989)
ETR_{max}	Maximal relative photosynthetic electron transport rate	Maximum of ETR	Genty et al. (1989)

*F_0' was calculated by: $F_0' = F_0/(Fv/Fm + F_0/Fm')$ (Oxborough and Baker, 1997).

frontiers | Frontiers in Microbiology

TYPE Original Research
PUBLISHED 10 April 2024
DOI 10.3389/fmicb.2024.1389954

OPEN ACCESS

EDITED BY
Xiangfeng Zeng,
Chinese Academy of Sciences (CAS), China

REVIEWED BY
Yongbin Li,
Dalian University of Technology, China
Yueyi Huang,
Chinese Academy of Agricultural Sciences (CAAS), China
Shanquan WANG,
Sun Yat-sen University, China

*CORRESPONDENCE
Hailiang Dong
✉ dongh@cugb.edu.cn

†These authors share co-lead authorship

RECEIVED 22 February 2024
ACCEPTED 27 March 2024
PUBLISHED 10 April 2024

CITATION
Li Y, Liu Y, Guo D and Dong H (2024) Differential degradation of petroleum hydrocarbons by *Shewanella putrefaciens* under aerobic and anaerobic conditions. *Front. Microbiol.* 15:1389954. doi: 10.3389/fmicb.2024.1389954

Differential degradation of petroleum hydrocarbons by *Shewanella putrefaciens* under aerobic and anaerobic conditions

Yang Li[1,2†], Yuan Liu[1,2†], Dongyi Guo[1] and Hailiang Dong[1,2*]

[1]Center for Geomicrobiology and Biogeochemistry Research, State Key Laboratory of Biogeology and Environmental Geology, China University of Geosciences, Beijing, China, [2]School of Earth Sciences and Resources, China University of Geosciences, Beijing, China

The complexity of crude oil composition, combined with the fluctuating oxygen level in contaminated environments, poses challenges for the bioremediation of oil pollutants, because of compound-specific microbial degradation of petroleum hydrocarbons under certain conditions. As a result, facultative bacteria capable of breaking down petroleum hydrocarbons under both aerobic and anaerobic conditions are presumably effective, however, this hypothesis has not been directly tested. In the current investigation, *Shewanella putrefaciens* CN32, a facultative anaerobic bacterium, was used to degrade petroleum hydrocarbons aerobically (using O_2 as an electron acceptor) and anaerobically (using Fe(III) as an electron acceptor). Under aerobic conditions, CN32 degraded more saturates ($65.65 \pm 0.01\%$) than aromatics ($43.86 \pm 0.03\%$), with the following order of degradation: dibenzofurans > *n*-alkanes > biphenyls > fluorenes > naphthalenes > alkylcyclohexanes > dibenzothiophenes > phenanthrenes. In contrast, under anaerobic conditions, CN32 exhibited a higher degradation of aromatics ($53.94 \pm 0.02\%$) than saturates ($23.36 \pm 0.01\%$), with the following order of degradation: dibenzofurans > fluorenes > biphenyls > naphthalenes > dibenzothiophenes > phenanthrenes > *n*-alkanes > alkylcyclohexanes. The upregulation of 4-hydroxy-3-polyprenylbenzoate decarboxylase (ubiD), which plays a crucial role in breaking down resistant aromatic compounds, was correlated with the anaerobic degradation of aromatics. At the molecular level, CN32 exhibited a higher efficiency in degrading *n*-alkanes with low and high carbon numbers relative to those with medium carbon chain lengths. In addition, the degradation of polycyclic aromatic hydrocarbons (PAHs) under both aerobic and anaerobic conditions became increasingly difficult with increased numbers of benzene rings and methyl groups. This study offers a potential solution for the development of targeted remediation of pollutants under oscillating redox conditions.

KEYWORDS

facultative bacteria, saturates, aromatics, aerobic degradation, anaerobic degradation

Highlights

- CN32 has the ability to degrade crude oil using both O_2 and Fe(III) as electron acceptors.
- CN32 promoted the breakdown of saturates under aerobic conditions.
- CN32 degraded aromatics more efficiently under anaerobic conditions.

1 Introduction

Petroleum hydrocarbons are complex mixtures consisting predominantly of saturates and aromatics (Strausz and Lown, 2003; Mbadinga et al., 2011; Liu et al., 2024). Over the last few decades, as the demand for petroleum products continues to rise, global oil production has surpassed 5 billion tons per year (BP, 2022). Every year, approximately 8 million tons of petroleum hydrocarbons pollute water and land as a result of exploration, production, storage, and transportation (Varjani, 2016). Petroleum compounds can be teratogenic, carcinogenic, and mutagenic, thus posing harm to both the ecological environment and human health (Khudur et al., 2019). For instance, 16 unbranched polycyclic aromatic hydrocarbons (PAHs) are listed as priority pollutants by the Environmental Protection Agency (EPA) of the United States (ATSDR, 2005). Bioremediation has emerged as a technology for removing petroleum pollutants from contaminated water, sediments, and soils because of its simplicity, cost-effectiveness, and environmental friendliness (Varjani, 2016; Khudur et al., 2019). Bacteria are more frequently and extensively employed as degraders compared to algae, fungi, and archaea (Brooijmans et al., 2009; Das and Chandran, 2011), because they can use petroleum hydrocarbons as the sole carbon and energy source (Mbadinga et al., 2011) when coupled with oxygen (Setti et al., 1993; Díaz et al., 2013), sulfate (Aeckersberg et al., 1991; Rueter et al., 1994), nitrate (Grishchenkov et al., 2000; Coates et al., 2001), and iron (Lovley et al., 1989; Anderson and Lovley, 1999; Liu et al., 2023a) as electron acceptors.

Compared with sulfate and nitrate, iron is more abundant in the crust [35% of the total mass of the Earth (Coey, 1980)], because they are present as both dissolved iron and solid forms in iron-bearing clay minerals and iron oxides in oxidized (Fe(III)) or reduced (Fe(II)) states (Davison, 1993; Weber et al., 2006; Dong et al., 2022). Bacteria play important roles in cycling iron between Fe(III) and Fe(II) (Dong et al., 2023b). For example, Fe(III)-reducing bacteria are found in oil-contaminated environments because of the presence of abundant oil compounds as electron donors (Martín-Gil et al., 2004; Kleemann and Meckenstock, 2011). Hence, Fe(III) can serve as the potential electron acceptor to couple with petroleum biodegradation (Lovley et al., 1989; Vodyanitskii, 2011; Liu et al., 2023a). Indeed, oil-contaminated sites often contain dissolved iron, with concentration levels ranging from 0.1 mM (Qian et al., 2018) to as high as 1 mM (Bennett et al., 1993). These high levels of dissolved iron may be a result of transformation of iron-bearing minerals through two mechanisms: (1) organic acids produced from microbial metabolism facilitate dissolution of iron-bearing minerals (Barth and Riis, 1992); (2) bio-reduction of Fe(III)-bearing minerals leads to reductive dissolution of iron-bearing minerals (Weber et al., 2006; Zeng et al., 2016, 2020). Furthermore, it may be feasible to amend dissolved iron for the purpose of degrading crude oil contamination (Yan et al., 2017; Zhang et al., 2021). However, the role of dissolved Fe(III) in oil degradation has not been fully studied, despite its higher bioavailability compared to iron-bearing minerals (Takahashi et al., 2011).

Oil-contaminated field sites encompass various environments with a range of oxygen levels, including aerobic surficial soil (Crowe and Smith, 2007), transition zones between aerobic and anaerobic settings such as water-bearing soil (Tong et al., 2016; Sheng et al., 2021b), and anaerobic habitats such as deep sea (Ma et al., 2021) and groundwater (Lovley and Lonergan, 1990; Sheng et al., 2016). Moreover, even in the same location, oxygen fugacity can change, leading to transition between aerobic and anaerobic conditions (Davison, 1993; Meckenstock and Mouttaki, 2011). However, previous studies have focused on biodegradation of oil compounds by the obligate bacteria under either aerobic or anaerobic conditions (Haritash and Kaushik, 2009; Xu et al., 2018), which prevents their applicability to oil-polluted environments with fluctuating oxygen conditions.

Facultative anaerobic bacteria exhibit higher adaptability to environmental changes compared to obligate bacteria (Cason et al., 2019). Several studies have shown that facultative anaerobes have the capability to biodegrade specific PAH compounds, such as phenanthrene, pyrene, and benzo[*a*]pyrene (BaP), under both aerobic and Fe(III) reduction conditions (Liang et al., 2014; Yan et al., 2017; Zhang et al., 2021). However, crude oil is a complex mixture of many different compounds with a wide range of solubilities. It has been challenging to find a bacterium capable of degrading a range of petroleum compounds under oscillating redox conditions. *Shewanella putrefaciens*, a representative typical facultative anaerobe, has demonstrated its capability to separately degrade dibenzothiophenes under aerobic conditions (Ansari et al., 2007) and petroleum hydrocarbons under anaerobic conditions (Liu et al., 2023a). Hence, *Shewanella putrefaciens* has the potential to degrade complex organic compounds of crude oil in both aerobic and anaerobic environments. However, its ability to degrade the same petroleum hydrocarbons under both aerobic and anaerobic conditions has not been demonstrated.

This study aimed to evaluate the biodegradation potential of complex oil compounds by facultative anaerobes using either O_2 or Fe(III) as the electron acceptor, employing *Shewanella putrefaciens* CN32 isolated from an anaerobic core sample 250 feet below the Morrison Formation in northwestern New Mexico (Zachara et al., 1998) as a model organism. Gas chromatography-mass spectrometer (GC–MS) was used to monitor changes in the concentration of oil compounds under two conditions. To unravel the biodegradation mechanism, quantitative reverse transcription polymerase chain reaction (RT-qPCR) was employed to examine the differential expression of specific genes responsible for biodegradation under both conditions. The findings of this study provide theoretical support for bioremediation of oil contamination. Moreover, this study sheds light on the significant role of facultative anaerobes in biogeochemical carbon and iron cycles under oxygen oscillating conditions.

2 Materials and methods

2.1 Preparation of crude oil, CN32 cells, and ferric citrate stock solution

A crude oil sample collected from the Changqing oilfield served as the substrate for the biodegradation experiments under aerobic and anaerobic conditions. CN32 cells were aerobically cultured in Luria-Bertani (LB) broth at pH 7.0. The culture was incubated at 30°C and agitated at 150 rpm in a constant temperature incubator (HZQ-X100, Suzhou Peiying Experimental Equipment Co., LTD, Suzhou, China). After reaching the logarithmic phase (approximately 16 h of growth), CN32 cells were centrifuged at 5,000 g for 5 min. The cells were then re-suspended in sterile bicarbonate buffer (consisting of 30 mM

$NaHCO_3$, 10 mM KCl, pH = 7.0) to remove residual LB medium. The centrifugation-resuspension process was repeated three times under either aerobic or anaerobic condition and the final cell pellet was re-suspended in the same buffer for the subsequent experiments. The aerobic experiment was conducted on a clean workbench (*VS*-1300 L-U, Suzhou Antai Air Technology Co., LTD, Suzhou, China). The anaerobic experiment was carried out inside an anaerobic chamber (filled with 98% N_2 and 2% H_2, Coy Laboratory Products, Grass Lake, Michigan). To prepare anoxic soluble Fe(III) stock solution, ferric citrate (>99%, Sigma) was dissolved in ddH_2O (18 MΩ cm) to achieve 100 mM concentration. The solution was sterilized by passing it through a 0.22 μm filter.

2.2 Biodegradation experiments

2.2.1 Aerobic experiment

Conical flasks (250 mL) were prepared, and 2 g of crude oil and 90 mL of basic medium (pH = 7.0) were added to the flasks. The concentration of crude oil, at 20 grams per liter, was much higher than those used in most studies (Wang et al., 2020; Liu et al., 2020a, 2023a). This higher concentration was chosen to represent a heavily polluted environment. The basic medium consisted of the following components: 3 g/L KNO_3, 2 g/L Na_2HPO_4, 2 g/L KH_2PO_4, 0.5 g/L $MgSO_4$, 0.5 g/L NaCl, 1 g/L NH_4Cl, and a 10 mL trace elements solution (Liu et al., 2020b). The trace element solution included the following components: 12 g/L $Na_2EDTA{\cdot}2H_2O$, 2 g/L NaOH, 1 g/L $CaCl_2$, 0.4 g/L $MnSO_4{\cdot}4H_2O$, 0.4 g/L $ZnSO_4{\cdot}7H2O$, 0.5 mL H_2SO_4 (98%), 10 g/L Na_2SO_4, 0.1 g/L $Na_2MoO_4{\cdot}2H_2O$, 2 g/L $FeSO_4{\cdot}7H_2O$, and 0.1 g/L $CuSO_4{\cdot}5H_2O$ (Liu et al., 2020b).

The prepared flasks containing the mixture of the crude oil and the basic medium were autoclaved (121°C for 30 min) (autoclave model: PHCbi MLLS-3718 L). After adding 10 mL cells (final concentration 10^8 CFU/mL), the flasks were aerobically incubated for 30 days at a temperature of 30°C and a speed of 150 rpm in an HZQ-X100 incubator. On day 16, new CN32 cells were introduced into flasks to maintain an adequate viable cell concentration. To establish an abiotic control, CN32 cells were replaced with sterilized distilled water (ddH_2O). All experiments were conducted in triplicates.

2.2.2 Anaerobic experiment

In the experimental setup, 150 mL serum bottles were used for the anaerobic degradation experiment. The serum bottles contained 20 g/L crude oil and 85 mL basic medium with a pH 6.9. The basic medium consisted of the following components: $NaHCO_3$ (2.5 g/L), $CaCl_2{\cdot}2H_2O$ (0.09 g/L), NH_4Cl (1.0 g/L), $MgCl_2{\cdot}6H_2O$ (0.2 g/L), NaCl (10 g/L), HEPES (7.2 g/L), K_2HPO_4 (36 mg/L), Na_2SO_4 (0.71 mg/L), and a trace mineral solution (10 mL). The trace mineral solution contained $FeCl_2{\cdot}4H_2O$ (0.2 g/L), $Na_2WO_4{\cdot}2H_2O$ (0.02 g/L), $MnCl_2{\cdot}4H_2O$ (0.1 g/L), $CoCl_2{\cdot}6H_2O$ (0.1 g/L), $ZnCl_2$ (0.05 g/L), $CuCl_2{\cdot}2H_2O$ (0.002 g/L), H_3BO_3 (0.005 g/L), $Na_2MoO_4{\cdot}2H_2O$ (0.01 g/L), Na_2SeO_3 (0.017 g/L), $NiCl_2{\cdot}6H_2O$ (0.024 g/L), and nitrilotriacetic acid (1.5 g/L) (Saito et al., 2016).

To create an anaerobic environment, the serum bottles were purged with anoxic N_2 to remove oxygen. After purging, the bottles were tightly sealed using a butyl rubber septum and an aluminum crimp. To ensure sterility, the sealed bottles were then autoclaved at a temperature of 121°C for 30 min. The serum bottles were prepared by combining 10 mL washed cells (at a final cell concentration approximately 10^8 CFU/mL) with 5 mL of ferric citrate solution (at a final concentration of 5 mM). The serum bottles were anaerobically incubated in the dark at 30°C and 150 rpm in an HZQ-X100 incubator for 30 days. On day 16, new CN32 cells were introduced into the serum bottles to maintain an adequate viable cell concentration. To establish an abiotic control, anoxic sterilized ddH_2O was used as a substitute for CN32 cells. All experiments were conducted in triplicates.

2.3 Analytical methods

2.3.1 Total Fe(II) and total Fe concentrations

Fe(II) concentration was measured to monitor Fe(III) reduction. Periodically, sub-samples (0.2 mL) were aseptically withdrawn from the serum bottles using sterile needles and syringes in an anaerobic chamber. The collected samples were then analyzed using the 1,10-phenanthroline method to determine the concentrations of total Fe(II) and total Fe (Amonette and Templeton, 1998). To determine the total Fe(II) content, a 0.2 mL of suspension sample was combined with 0.48 mL H_2SO_4 (3.6 N) in an Eppendorf tube. This mixture was then supplemented with 40 μL HF (40%, w/v) and 80 μL 1,10-phenanthroline reagent (10%, w/v). The tubes were then exposed to boiling at 100°C for 30 min and allowed to cool for 15 min at room temperature. Following these steps, 0.4 mL H_2BO_3 (5%, w/v) was added. Subsequently, 0.1 mL of the mixture was transferred to a separate tube containing 1 mL Na-citrate (1%, w/v). After reaction for 20 min, the total Fe(II) content was measured using a UV–Vis spectrophotometer (SHIMADZU2550, Japan) at 510 nm wavelength. To determine the total Fe concentration [Fe(III) and Fe(II)], the Fe(III) was first reduced to Fe(II) by adding hydroxylamine hydrochloride (10% in 1% Na-citrate, w/v). The extent of Fe(III) reduction was calculated using the following equation:

$$\mathrm{Fe(III)\ reduction\ extent}\,(\%) = \frac{\left(\mathrm{Fe(II)}_{\mathrm{total}} - \mathrm{Fe(II)}_{\mathrm{initial}}\right)}{\mathrm{Fe}_{\mathrm{total}}} * 100\%$$

2.3.2 Changes in petroleum hydrocarbons induced by O_2 and Fe(III) reduction

GC–MS was used to identify and quantify the changes in the composition of saturates and aromatics. The biodegraded oil samples that underwent 30-day degradation under aerobic and anaerobic conditions were labeled as A-30 and An-30, respectively. Following the 30-day biodegradation period, 30 mL dichloromethane was added to 10 mL suspension to extract the crude oil. A detailed extraction method was described previously (Liu et al., 2020b). The extracted oil was fractionated by column chromatography to collect saturates, aromatics, resins, and asphaltenes (Liu et al., 2020b). Saturates and aromatics from both A-30 and An-30 were analyzed using a GC–MS system (Agilent 6890/5975) (Supplementary material Text S1; Liu et al., 2020b). To enable semi-quantification of the saturated and aromatic fractions, deuterium nC_{24} (CAS: 16416–32-3; Chiron) and deuterium dibenzothiophene (CAS: 33262–29-2; Chiron) were used, respectively. For the *m*/*z* and abbreviations of the representative compound series, please refer to Liu et al. (2023a). The concentration (μg/g oil) and biodegradation ratio (%) of specific hydrocarbon

compounds were calculated using the following equations outlined in Liu et al. (2023a):

$$\frac{C_X}{C_I} = k * \frac{S_X}{S_I}\left(C_I = \frac{m_I}{m_0}\right);$$

$$\text{Biodegradation ratio}(\%) = \frac{C_0 - C_X}{C_0} * 100\%$$

where C_X and C_I are the concentrations (μg/g) of the compound in crude oil and the internal standard, respectively; S_X and S_I are the peak areas of each compound in crude oil and the internal standard, respectively; k is the response factor (assumed to be 1.0); m_I and m_0 represent the masses of the internal standard and oil samples, respectively; C_0 and C_X are the concentrations of the compounds in fresh and biodegraded crude oils (μg/g), respectively.

2.3.3 Quantitative reverse transcription polymerase chain reaction (RT-qPCT)

The 4-hydroxy-3-polyprenylbenzoate decarboxylase (ubiD) is present in the genome of the strain CN32 (Data from the NCBI database).[1] It is responsible for anaerobic carboxylation of benzene, naphthalene, and phenanthrene (Atashgahi et al., 2018; Koelschbach et al., 2019; Zhang et al., 2021), and it is also expressed in aerobic ubiquinone biosynthesis pathway in *Escherichia coli* (Arias-Cartin et al., 2023). Since the CN32 strain is facultative anaerobe, ubiD gene might play an unknown role for aromatic degradation under aerobic conditions. Therefore, ubiD was used to evaluate the degradation characteristics of aromatics under different conditions. RT-qPCR was employed to quantify the expression of the ubiD gene under aerobic and anaerobic conditions.

Specifically, total RNA of strain CN32 was extracted using UNIQ-10 column Trizol total RNA extraction kit (B511321, Shanghai Sangon Biological Engineering Technology & Services, Co., Ltd., China). The purity (OD_{260}/OD_{280}) and concentration (ng/μL) of the extracted RNA were determined by a microvolume UV–Vis spectrophotometer (SMA4000, Merinton Instrument Co., Ltd., Beijing, China) (Bezerra et al., 2019). The integrity of RNA was verified by detecting the 16S and 23S bands of rRNA in 1.5% (w/v) agarose gel stained with a nucleic acid dye (Bezerra et al., 2019).

Subsequently, RNA (~500 ng) was reverse-transcribed to cDNA using Random Primer p $(dN)_6$ (100 pmol) and Maxima Reverse Transcriptase (200 U; EP0743, Thermo Scientific, Wilmington, DE, United States). Primers of DNA amplification used for this study were designed in Primer Premier 5.0 based on a gene sequence obtained from the National Center for Biotechnology Information (NCBI) GenBank database. The primer sequences for the 16S rRNA gene were as follows: Forward - 5'-TTCAGTAGGGAGGAAAGGGTAA-3′ and Reverse - 5'-CCAGGGCTTTCACATCTCG-3′. For the ubiD gene, the primer sequences were: Forward - 5'-CGCCTGAGGGTTGTTCGT-3′ and Reverse - 5'-GCGGCAGTTCACATCTTCAT-3′. The primers were validated by q-PCR reactions using cDNA as the template.

qPCR reactions were carried out on a QuantStudio™1 Plus qPCR Detection System (Thermo Scientific, Wilmington, DE, USA). SYBR Green qPCR Master Mix (High Rox, B639273, ABI, USA) was used. The q-PCR program consisted of an initial denaturation step at 95°C for 3 min, followed by 45 cycles of amplification with denaturation at 95°C for 15 s and annealing/extension at 60°C for 30 s. Three biological replicates and three technical replicates were performed.

The 16S rRNA gene of the bacterial strain was utilized as a reference to normalize the expression of the target gene, ubiD. In brief, the threshold cycle (Ct) values for both the target (ubiD) and reference genes (16S rRNA) were obtained via qPCR across different samples. The expression of the target gene was then adjusted based on the Ct value of the reference gene (Sheng et al., 2023). The fold change in gene expression was determined using the $2^{-\Delta\Delta Ct}$ method, a well-established technique for relative quantification (Livak and Schmittgen, 2001; Vaishnav et al., 2022). Here, ΔCt refers to the Ct difference between the target gene (ubiD) and the reference gene (16S rRNA gene), while ΔΔCt calculates the ΔCt variation between the anaerobic and aerobic experimental groups.

3 Results

3.1 Overall degradation characteristics of petroleum hydrocarbons

The total ion chromatogram (TIC) of saturated hydrocarbons clearly illustrates the degradation of crude oil under both aerobic and anaerobic conditions (Figure 1). Notably, the TIC reveals a more pronounced degradation under aerobic condition than under anaerobic condition, based on a comparison of the peak height of the internal standard relative to all petroleum hydrocarbon compounds (Figure 1). Because pristane (Pr) and phytane (Ph) have been demonstrated to exhibit bio-resistance (Cabrerizo et al., 2016; Meng et al., 2021), the changes of nC_{17}/Pr and nC_{18}/Ph ratios should indicate biodegradation (Kennicutt II et al., 1987; Iheonye et al., 2019). Under aerobic condition, the nC_{17}/Pr and nC_{18}/Ph ratios decreased significantly from 2.73 ± 0.07 and 2.50 ± 0.05 to 0.60 ± 0.10 and 0.61 ± 0.10, respectively. However, under anaerobic condition, the nC_{17}/Pr and nC_{18}/Ph ratios only decreased to 2.58 ± 0.05 and 2.34 ± 0.04, respectively.

Under anaerobic conditions, the reduction of Fe(III) was coupled with biodegradation of petroleum compounds, reaching a reduction extent of 59.75 ± 0.05% by day 7 (Figure 2). The introduction of fresh CN32 cells on Day 16 led to a subsequent increase in the extent of bio-reduction to 82.82 ± 0.04% by day 30 (Figure 2).

The GC–MS semi-quantitative data were employed to characterize changes of concentrations (μg/g) and biodegradation ratios (%) of saturates (i.e., *n*-alkanes and alkylcyclohexane) and aromatics (i.e., PAHs with two and three benzene rings). Specifically, CN32 exhibited differential degradation of eight series of saturated and aromatic hydrocarbons under different conditions. Under aerobic condition, the degradation sequence followed the following order, based on the biodegradation ratio (in parentheses): dibenzofurans (83.11 ± 0.02%) > *n*-alkanes (71.26 ± 0.01%) > biphenyls (64.73 ± 0.02%) > fluorenes (64.48 ± 0.04%) > naphthalenes (63.36 ± 0.01%) > alkylcyclohexanes (52.28 ± 0.01%) > dibenzothiophenes (40.44 ± 0.04%) > phenanthrenes (33.15 ± 0.04%) (Figure 3). Under

1 https://www.ncbi.nlm.nih.gov/

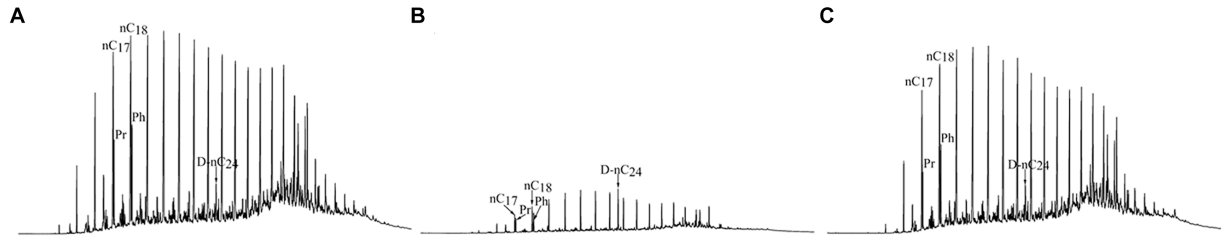

FIGURE 1
The total ion chromatograms (TICs) of saturates from control oil **(A)**, biodegraded oil after 30 days under aerobic condition **(B)**, and anaerobic condition **(C)**. Pr: pristane, Ph: phytane. Deuterium nC_{24} (D-nC_{24}) is used as an internal standard.

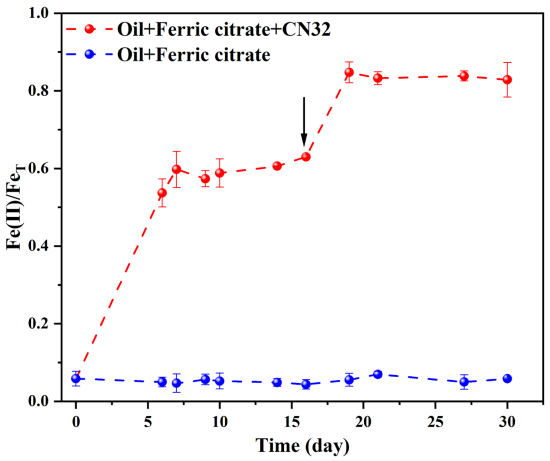

FIGURE 2
Time-course changes of Fe(II)/Fe_T by CN32 under anaerobic condition. The arrow denotes the time of injection of fresh CN32 cells (16 days).

anaerobic condition, the degradation sequence followed a different order: dibenzofurans (95.37 ± 0.02%) > fluorenes (84.87 ± 0.03%) > biphenyls (83.98 ± 0.02%) > naphthalenes (83.52 ± 0.01%) > dibenzothiophenes (41.35 ± 0.02%) > phenanthrenes (39.06 ± 0.02%) > *n*-alkanes (25.16 ± 0.01%) > alkylcyclohexanes (22.23 ± 0.00%) (Figure 3). These biodegradation patterns clearly indicate that saturates were more susceptible to degradation under aerobic condition than under anaerobic condition. In contrast, aromatics were more susceptible to degradation under anaerobic condition.

3.2 Degradation characteristics of saturated hydrocarbons

Saturates, mainly comprised of *n*-alkanes and alkylcyclohexanes (del Rio et al., 1994), were more effectively degraded under aerobic condition than under anaerobic condition (Figures 4A,B), consistent with the well-established understanding that aerobic degradation tends to be more efficient for degrading *n*-alkanes (Grishchenkov et al., 2000). The biodegradation ratios of alkylcyclohexanes (aerobic 52.28 ± 0.01%; anaerobic 22.23 ± 0.00%) were lower than those of *n*-alkanes (aerobic 71.26 ± 0.01%; anaerobic 25.16 ± 0.01%) (Figure 3). This result aligns with previous findings that alkylcyclohexanes are more resistant to biodegradation than *n*-alkanes (Kaplan et al., 1997). Some biomarkers, i.e., steranes and hopanes in saturated hydrocarbons (Fu and Sheng, 1989) were not degraded by CN32 (Figure S1 in Supplementary material). Under aerobic condition, the total content of *n*-alkanes decreased significantly from 85.02 mg/g in the abiotic control to 24.43 mg/g in the biotic treatment, representing a total degradation ratio of 71.26 ± 0.01% (Figure 3). Similarly, the total content of alkylcyclohexanes decreased from 7.79 mg/g in the abiotic control to 3.72 mg/g in the biotic treatment, indicating a total degradation ratio of 52.28 ± 0.01% (Figure 3).

At the molecular level, CN32 cells also exhibited higher biodegradation ratios of nC_{14}-nC_{37} compounds under aerobic condition than anaerobic condition (Figure 4C). Nevertheless, both conditions exhibited the following similar degradation patterns. First, nC_{14}, nC_{15}, and nC_{37} showed degradation ratios close to 100% (Figure 4C). Second, the biodegradation ratios of long- and short-chain *n*-alkanes were consistently higher compared to the *n*-alkanes of intermediate carbon chain length (Figures 4A,C). This trend was also observed in the degradation of nC_8-cHex-nC_{31}-cHex (Figures 4B,D).

3.3 Degradation characteristics of aromatic hydrocarbons

In contrast to the saturates, aromatic hydrocarbons present a significantly higher degradation efficiency by CN32 under anaerobic condition (53.94 ± 0.02%) compared to that in aerobic condition (43.86 ± 0.03%) (Table 1). The studied aromatics with two or three benzene rings showed clear degradation (Figure 3). In general, the concentration (μg/g) and biodegradation ratio (%) of PAHs decreased with the increasing number of benzene rings (Figures 3, 5, 6). Under aerobic condition, three-ring PAHs, such as phenanthrene, exhibited lower degradation ratios (33.15 ± 0.04%) than two-ring PAHs, including dibenzofurans (83.11 ± 0.02%), biphenyls (64.73 ± 0.02%), fluorenes (64.48 ± 0.04%), naphthalenes (63.36 ± 0.01%), and dibenzothiophenes (40.44 ± 0.04%) (Figure 3). Similarly, under anaerobic condition, three-ring PAHs showed lower degradation ratios (phenanthrene: 39.06 ± 0.02%) than two-ring PAHs (dibenzofurans: 95.37 ± 0.02%, fluorenes: 84.87 ± 0.03%, biphenyls: 83.98 ± 0.02%, naphthalenes: 83.52 ± 0.01%, and dibenzothiophenes: 41.35 ± 0.02%) (Figure 3). PAHs with more than three rings were not degraded under both aerobic and anaerobic conditions (Figure S2 in Supplementary material).

10.3389/fmicb.2024.1389954

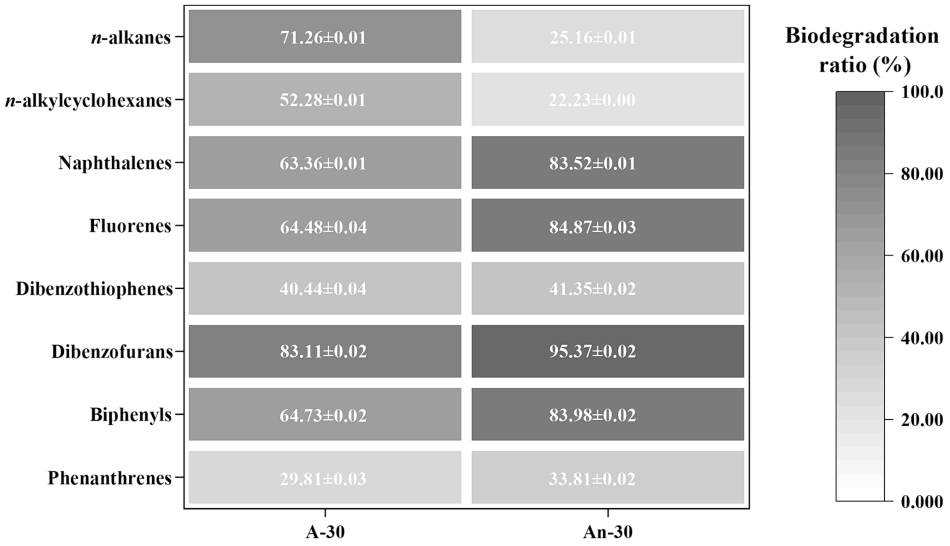

FIGURE 3
Biodegradation ratios (%) of eight classes of compounds in crude oil by CN32 under aerobic and anaerobic conditions. The saturated hydrocarbons include *n*-alkanes and *n*-alkylcyclohexanes. The aromatic hydrocarbons include two-ring PAHs (naphthalenes, fluorenes, dibenzothiophenes, dibenzofurans, and biphenyls) and three-ring PAHs (phenanthrenes).

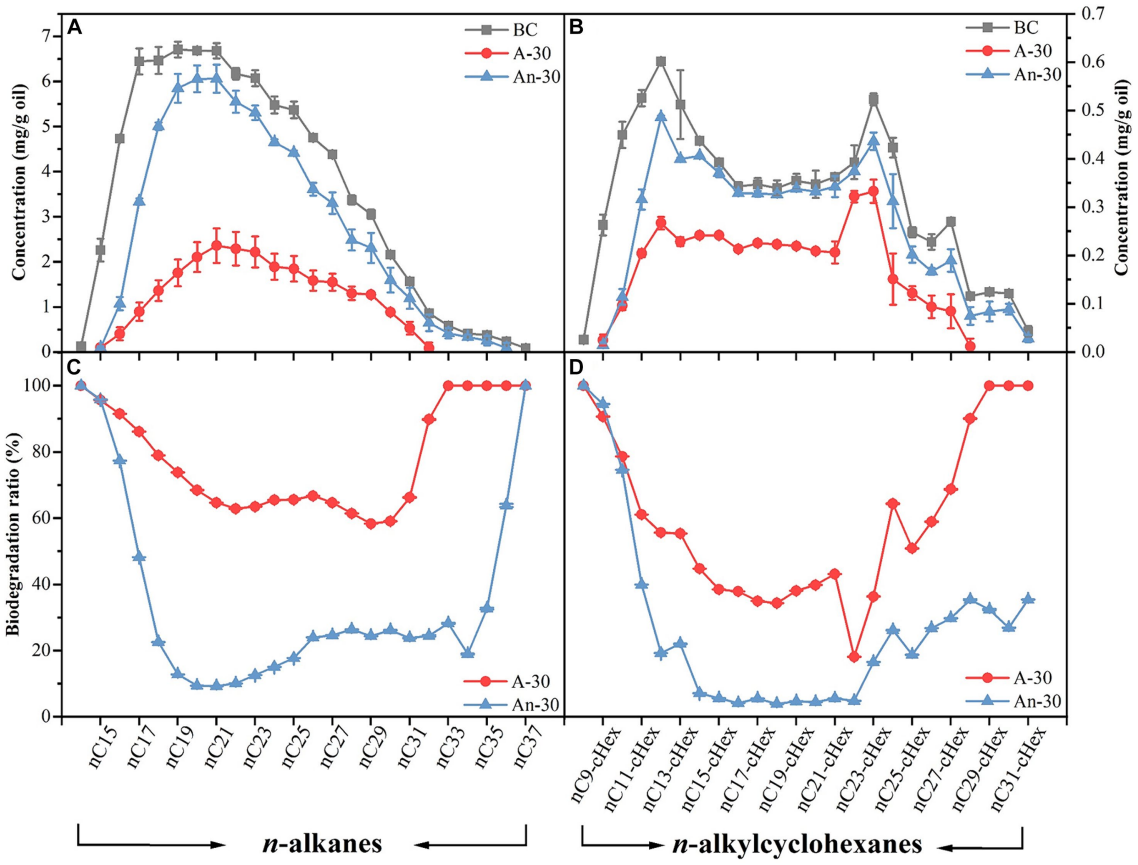

FIGURE 4
Concentration (mg/g) changes of saturated hydrocarbons due to aerobic (A-30) and anaerobic (An-30) biodegradation by CN32 for 30 days compared to the control oil (BC), including *n*-alkanes **(A)** (left axis) and *n*-alkylcyclohexanes **(B)** (right axis). Biodegradation ratios (%) of *n*-alkanes **(C)** and *n*-alkylcyclohexanes **(D)** under aerobic and anaerobic conditions.

10.3389/fmicb.2024.1389954

TABLE 1 The concentrations and biodegradation ratios of saturates (*n*-alkanes and *n*-alkylcyclohexanes) and aromatics (with two and three benzene rings) by *S. putrefaciens* CN32 under aerobic and anaerobic conditions.

Compound	Oil		A-30			An-30		
	Concentration (mg/g)	Stdev	Concentration (mg/g)	Stdev	Biodegradation ratio (%)	Stdev	Concentration (mg/g)	Stdev	Biodegradation ratio (%)	Stdev
Saturates	99.12	0.70	34.05	1.05	65.65	0.01	76.00	0.94	23.36	0.01
PAHs	2.02	0.03	1.14	0.05	43.86	0.03	0.93	0.04	53.94	0.02

Naphthalenes, a common type of PAHs, consist of various compounds such as dimethylnaphthalenes (DMNs), trimethylnaphthalenes (TMNs), tetramethylnaphthalenes (TeMNs), and pentamethylnaphthalenes (PMNs). While naphthalenes are generally considered to be less toxic compared to other PAHs, their high water solubility and volatility make them more available to receptors (Edwards, 1983). In contrast to saturated hydrocarbons, CN32 demonstrated a higher biodegradation ratio for naphthalenes (83.52 ± 0.01%) under anaerobic condition than under aerobic condition (63.36 ± 0.01%) (Figure 3). Furthermore, naphthalenes with more methyl groups were more resistant to degradation under both conditions (Figures 5A,E, 6). For example, the aerobic biodegradation ratio followed the order: DMNs, TMNs (75.31 ± 0.05% - 75.75 ± 0.02%) > TeMNs (59.28 ± 0.00%) > PMNs (43.05 ± 0.08%) (Figure 6). Similarly, the anaerobic biodegradation ratio followed the order: DMNs, TMNs (94.66 ± 0.01% - 96.91 ± 0.01%) > TeMNs (81.35 ± 0.02%) > PMNs (47.74 ± 0.05%) (Figure 6).

Methyl substitutions occur at its α(1, 4, 5, and 8) and β positions (2, 3, 6, and 7) of naphthalene structures (Liu et al., 2023b). The degradation ratio of alkylnaphthalenes is significantly influenced by the number of methyl substitutions in the ortho position. For instance, TeMNs with a single ortho substitution exhibited higher biodegradation ratios (aerobic: 57.49 ± 0.01% - 60.87 ± 0.01%; anaerobic: 80.87 ± 0.05% - 84.09 ± 0.06%) compared to those with two ortho substitutions (aerobic: 55.48 ± 0.01% - 58.52 ± 0.02%; anaerobic: 75.43 ± 0.02% - 79.48 ± 0.05%) (Figure 5E). The biodegradation efficiencies of PMNs with two ortho substitutions (aerobic: 41.76 ± 0.10% - 49.21 ± 0.09%; anaerobic: 50.84 ± 0.08% - 53.12 ± 0.07%) were higher than those of PMNs with three ortho substitutions (aerobic: 32.45 ± 0.15% - 42.79 ± 0.12%; anaerobic: 43.89 ± 0.07% - 46.23 ± 0.07%) (Figure 5E). Furthermore, the positions of methyl substitutions (i.e., α- or β-positions) influenced the biodegradation ratio. The biodegradation ratio of α,β,β-TMN (1,3,7-TMN; aerobic: 84.11 ± 0.11%, anaerobic: 97.72 ± 0.01%) > α,α,β-TMN (1,4,6 + 1,3,5-TMN; aerobic: 74.23 ± 0.03%, anaerobic: 97.16 ± 0.02%) (Figure 5E). The biodegradation ratio of α,α-DMN (1,8-DMN: aerobic: 71.61 ± 0.10%, anaerobic: 92.35 ± 0.01%) was the lowest among all other configurations (Figure 5E). These results indicate that the biodegradability of alkylnaphthalenes with methyl substitutions at the β position was higher than that with α substituent.

Fluorenes are classified as one of the 16 priority-controlled PAHs (Zhan et al., 2018). The average biodegradation ratio of fluorene series under anaerobic condition (84.87 ± 0.03%) was higher than that under aerobic condition (64.48 ± 0.04%) (Figures 3, 5B). The presence of methyl groups decreased the biodegradation ratio, with fluorene (F, aerobic 82.81 ± 0.07%; anaerobic 93.38 ± 0.01%) showing a higher biodegradation ratio than methylated fluorenes (MFs, aerobic 63.30 ± 0.02%; anaerobic 84.32 ± 0.03%) (Figures 5F, 6).

Thiophenes are a class of sulfur-containing heterocyclic aromatic hydrocarbons (Mezcua et al., 2008; Li et al., 2014). The biodegradation ratios of dibenzothiophenes (DBTs) by CN32 were slightly higher under anaerobic (41.35 ± 0.02%) condition than under aerobic condition (40.44 ± 0.04%) (Figures 3, 5B). Under both conditions, the biodegradation ratio of DBTs decreased as the number of methyl groups increased (Figures 5F, 6).

Dibenzofurans are a class of oxygen-containing heterocyclic aromatic hydrocarbons (Li et al., 2018). CN32 showed a higher degradation ratio

10.3389/fmicb.2024.1389954

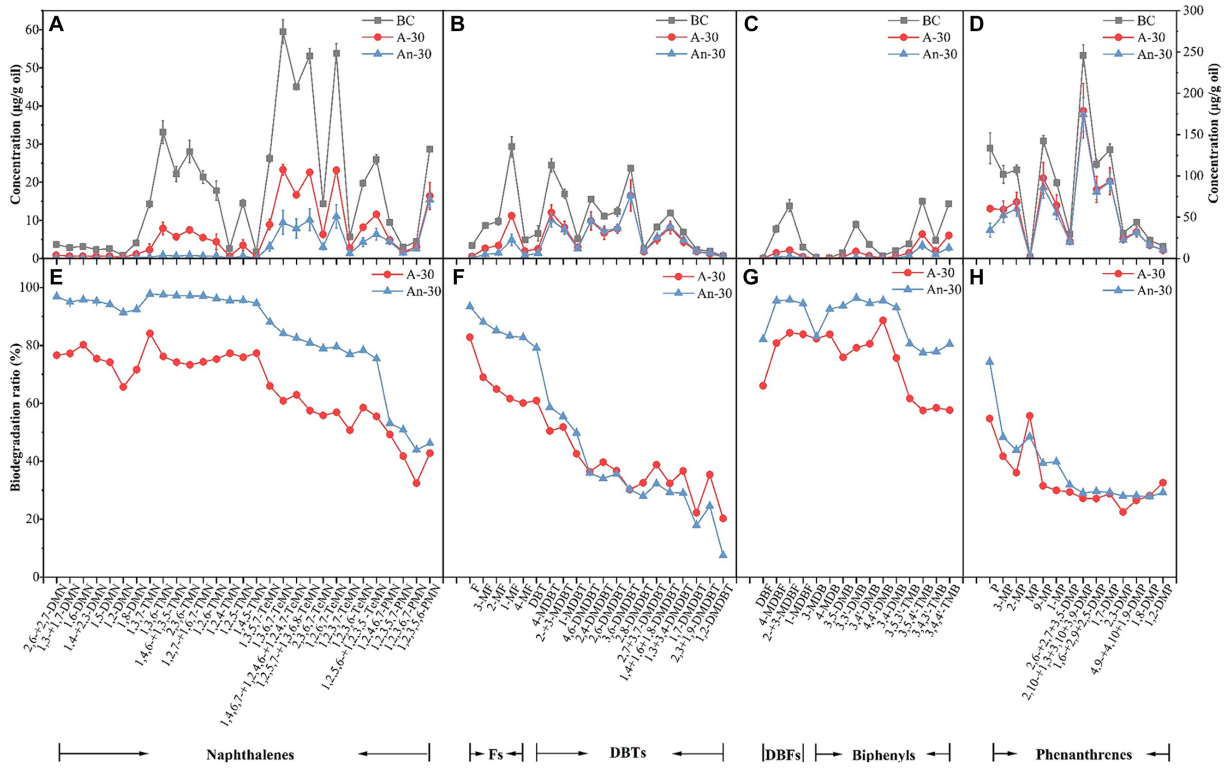

FIGURE 5
Concentration (μg/g) changes of aromatic hydrocarbons due to aerobic (A-30) and anaerobic (An-30) biodegradation by CN32 after 30 days relative to the control oil (BC), including naphthalenes **(A)**, fluorenes and dibenzothiophenes **(B)**, dibenzofurans and biphenyls **(C)**, and phenanthrenes **(D)**. Biodegradation ratios (%) of aromatic compounds under aerobic and anaerobic conditions **(E–H)**. **(A–C)** refers to the left axis, and (d) refers to the right axis.

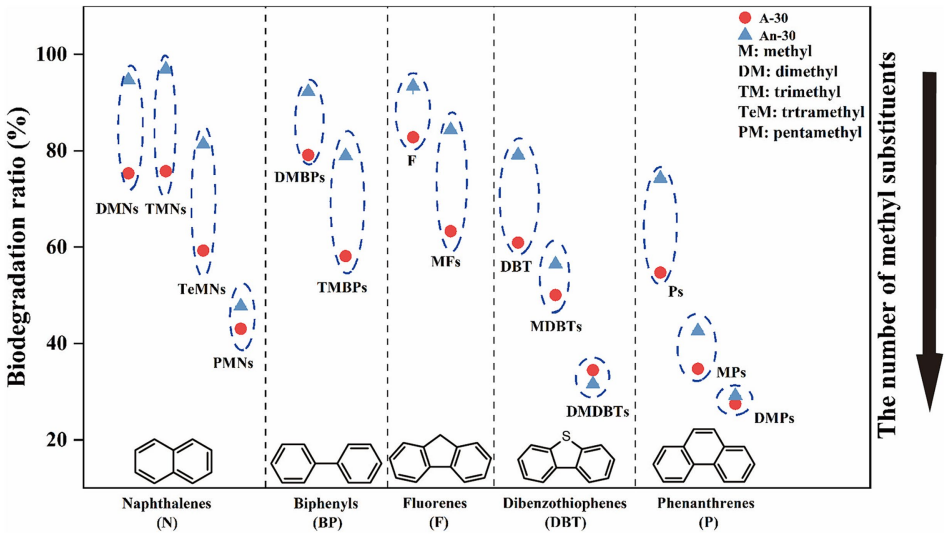

FIGURE 6
The relationship between the biodegradation ratio and the number of benzene rings and methyl substitutions in PAHs. The biodegradation order of compounds with different number of substitutions is as follow: DMNs, TMNs > TeMNs > PMNs; DMBPs > TMBPs; F > MFs; DBT > MDBTs > DMDBTs; P > MPs > DMPs.

of dibenzofurans (DBFs) under anaerobic condition (95.37 ± 0.02%) compared to aerobic condition (83.11 ± 0.02%) (Figure 3).

Biphenyls (BPs) are bicyclic PAHs composed of two benzene rings. Similar to other PAHs, CN32 showed a higher degradation ratio of BPs under anaerobic condition than under aerobic condition (Figures 3, 5C). Similarly, BPs with a higher number of methyl substitutions showed a lower biodegradation ratio. For example, DMBPs (containing two methyl groups) exhibited higher degradation

ratios compared to TMBPs (containing three methyl groups) (Figures 5G, 6).

The phenanthrene series contains three benzene rings (Wei et al., 2017), including phenanthrenes (Ps), methylphenanthrenes (MPs), and dimethylphenanthrenes (DMPs). Similarly to other PAHs, the degradation ratio of the phenanthrene series decreased as the number of methyl groups increased under both aerobic and anaerobic conditions (Figures 5D,H, 6), with P (aerobic 54.73 ± 0.06%; anaerobic 74.28 ± 0.05%) showing a higher biodegradation ratio than MPs (aerobic 34.75 ± 0.06%; anaerobic 42.60 ± 0.04%) and DMPs (aerobic 27.48 ± 0.06%; anaerobic 29.15 ± 0.04%) (Figures 5H, 6).

3.4 RT-qPCR results

The ratio of OD_{260} /OD_{280} of the extracted RNA was about 2.0 ± 0.1 (Table 2). Agarose gel electrophoresis showed clear bands of 23S and 16S subunits, indicating that the RNA was of high quality and did not degrade significantly. The samples exhibited Ct values below 35, and the melting curves for both the internal standard and the target genes showed a sole signal peak, providing clear evidence for a successful primer design. A nearly threefold increase in the relative expression levels of the ubiD gene was detected when CN32 was placed under anaerobic condition, as compared to aerobic conditions (Figure 7). The observed upregulation of the ubiD gene was consistent with the higher capacity of CN32 cells to break down aromatic compounds under anaerobic condition than under aerobic condition (Figure 3).

4 Discussion

4.1 Higher degradation of saturated hydrocarbons under aerobic condition than under anaerobic condition

The biodegradation ratio of *n*-alkanes by CN32 (71.26 ± 0.01%) under aerobic condition may be lower than those by obligately aerobic bacteria such as *Pseudomonas aeruginosa* XJ16 and *Bacillus cereus* XJ20 (98.2–98.8%) (Liu et al., 2020a). However, under anaerobic condition, the anaerobic biodegradation ratio of 25.16 ± 0.01% was much higher than ~7.5% achieved by an anaerobic community using Fe^{3+} as an electron acceptor over the same period (30 days) (Zhang et al., 2019). These unique capabilities expand the potential of CN32 for effective biodegradation of *n*-alkanes under a wide range of environmental conditions.

Bacterial utilization of *n*-alkanes is generally biased towards short carbon chain lengths under aerobic (Hasanuzzaman et al., 2007; Pasumarthi et al., 2013) and anaerobic condition (Rueter et al., 1994; Zhang et al., 2019). However, there are exceptions to this trend. For instance, *Acinetobacter lwoffii* XJ19 exhibited a higher capacity for biodegrading long-chain *n*-alkanes (> C_{28}, 56.8–74.5%) compared to nC_{15} - nC_{28} (9.1–55.8%) under aerobic condition (Liu et al., 2020a). Similarly, Cheng et al. (2019) reported the preferential degradation of long-chain *n*-alkanes (>nC_{19}) in heavy oil under methanogenic conditions. Therefore, the specific metabolic capability of bacteria plays a pivotal role in determining the efficiency of *n*-alkane degradation. CN32 demonstrated a remarkable ability of CN32 to degrade *n*-alkanes and alkylcyclohexanes with both short and long carbon chains under two conditions (Figure 3), which was first proposed. The presence of the alkB gene in the CN32 gene bank, as indicated by data from the NCBI database (see footnote 1), suggests its potential role in degrading *n*-alkanes with carbon numbers below 20 (Sierra-Garcia and de Oliveira, 2013). However, the genes responsible for biodegradation of long-chain *n*-alkanes, such as lutein-binding monooxygenase (almA; >nC_{32}) (Wentzel et al., 2007) and long-chain alkane monooxygenase (ladA; nC_{15}-nC_{36}) (Feng et al., 2007), are absent in the CN32 genome. Therefore, the specific genes accountable for the aerobic biodegradation of *n*-alkanes with carbon numbers above 20 remain unidentified. Consequently, the molecular mechanisms governing the biodegradation of *n*-alkanes with varying carbon numbers cannot be elucidated. Further investigations are imperative to pinpoint and characterize the specific genes and enzymes involved in biodegradation of these longer-chain *n*-alkanes by CN32.

4.2 Higher degradation of aromatic hydrocarbons under anaerobic condition than under aerobic condition

Anaerobic degradation of PAHs is generally considered slower than aerobic degradation (Widdel et al., 2006). For example, when using O_2 as an electron acceptor, a facultative bacterium completely degraded phenanthrene within 3 days, whereas when Fe(III) was used, it took 10 days to achieve complete degradation (Zhang et al., 2021). However, CN32 possesses a distinct ability to degrade PAHs more effectively under anaerobic condition than under aerobic condition (Figures 3, 5, 6). Grishchenkov et al. (2000) obtained similar conclusions when facultative nitrate-reducing bacteria were used to degrade PAHs with two rings (i.e., naphthalenes and fluorenes) under

TABLE 2 The concentration and OD value of RNA extracted from *S. putrefaciens* CN32.

Condition	ID	Sample type	SW (nm)	SW Abs	260 Abs (10 mm)	280 Abs (10 mm)	260/280	Conc. (ng/μl)
Aerobic	1–1	RNA	260	2.555	2.555	1.239	2.062	102.2
	1–2	RNA	260	2.535	2.535	1.23	2.062	101.4
	1–3	RNA	260	2.548	2.548	1.255	2.03	101.92
Anaerobic	2–1	RNA	260	5.462	5.462	2.85	1.916	218.48
	2–2	RNA	260	5.193	5.193	2.668	1.946	207.72
	2–3	RNA	260	5.067	5.067	2.638	1.921	202.68

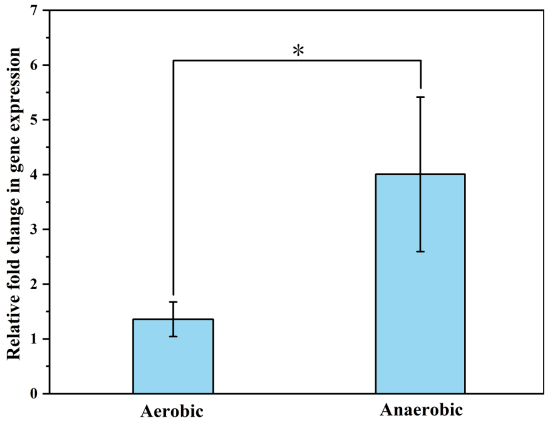

FIGURE 7
The expression of functional genes (ubiD) relevant to aromatic degradation by CN32 under aerobic and anaerobic conditions. 16S rRNA was used as a reference gene. *p* values from statistical analysis are shown with asterisks: <0.05, denoted by *.

both anaerobic and aerobic conditions. However, the study reported a significantly lower degradation ratio for two-ring PAHs, with the highest level not exceeding 23%, which stands in stark contrast to the remarkable ~84% degradation ratio observed in the current study (i.e., naphehalenes, fluorenes, Dibenzofurans, and biphenyls). In fact, the anaerobic degradation ratio achieved by CN32 surpassed many of the published degradation ratios for PAHs by anaerobic microorganisms under nitrate-, ferric-, sulfate-reducing, and methanogenic conditions (Grishchenkov et al., 2000; Rockne et al., 2000; Chang et al., 2006; Zhang et al., 2019). This underscores the significant potential of CN32 for petroleum degradation in anaerobic environments. With the ability to degrade PAHs using either O_2 or Fe(III) as electron acceptors, CN32 demonstrates a superior capability in utilizing different electron acceptors for PAH degradation.

The preferred degradation ability of CN32 under anaerobic condition can be attributed to the unique enzyme systems of this bacterium, because enzymes exhibit specificity for different compounds (Tani et al., 2001; Haritash and Kaushik, 2009; Sierra-Garcia and de Oliveira, 2013; Moreno and Rojo, 2017). Under anaerobic condition, the initial activation mechanisms of petroleum hydrocarbons include carboxylation (So et al., 2003), hydroxylation (Zhang et al., 2013), and fumarate addition (Wilkes et al., 2002). In the CN32 genome, there is a notable absence of conventional genes typically associated with fumarate addition (see footnote 1). However, our analysis reveals alternative mechanisms such as carboxylation, as evidenced by a significantly elevated expression of the ubiD gene (Figure 7). Indeed, a previous study by Zhang et al. (2021) demonstrated that carboxylation serves as the initial activation pathway for phenanthrene degradation under Fe(III)-reducing condition. Moreover, Atashgahi et al. (2018) and Koelschbach et al. (2019) reported the important role of ubiD-related carboxylases in the initial activation of benzene and naphthalene under nitrate- and sulfate-reducing conditions, respectively. These results suggest that carboxylation is a common activation pathway in anaerobic biodegradation of petroleum hydrocarbons. Furthermore, the CN32 genome harbors homologues of the benzoyl-CoA reductase (bamD) gene (Wischgoll et al., 2005) and the oxoenoyl-CoA hydrolase (bamA) gene (DiDonato Jr et al., 2010), suggesting their potential involvement in the reduction and cleavage of benzene rings during anaerobic degradation of PAHs. The synergy between the ubiD gene and the Bam system in CN32 may have enhanced its ability to effectively degrade PAHs under anaerobic conditions.

CN32 lacks genes encoding oxygenases for the hydroxylation and oxygenolytic ring cleavage of aromatic compounds under aerobic condition (Ghosal et al., 2016). Nevertheless, data from the KEGG database of degradation of aromatic compounds - *Shewanella putrefaciens* CN32 (https://www.kegg.jp/kegg-bin/show_pathway?spc01220) suggest possible involvement of dioxygenases in the degradation pathways of naphthalene, biphenyl, dibenzofuran, and phenanthrene under aerobic condition. Dioxygenases are recognized for their role in initiating the breakdown of aromatic rings (Bugg and Winfield, 1998). Remarkably, the complete genome of CN32 lacks typical genes associated with aerobic degradation of aromatic compounds, including those for naphthalene dioxygenase (NahAaAbAcAd) (Phale et al., 2019) and catechol 2,3-dioxygenase (C23O) (Fuentes et al., 2014). This leads us to conjecture that functionally analogous enzymes might be active within CN32, enabling it to metabolize aromatic compounds through alternate pathways. However, the specific genes and enzymes cannot be confirmed. Additional research is required to uncover the precise degradation genes and pathways utilized by CN32 for breaking down aromatic hydrocarbons under aerobic condition.

Besides the intrinsic biodegradability of CN32, the structure of the PAHs also exerts a significant influence on the degradation ratio. PAHs with three benzene rings (phenanthrenes) were less degraded compared to PAHs with two benzene rings under both conditions (Figures 3, 5, 6), and PAHs with more than three aromatic rings did not exhibit any significant biodegradation (Figure S2 in Supplementary material). Indeed, a previous study showed that PAHs with a higher number of aromatic rings exhibited increasing bio-resistance (George et al., 2002). The reason for this trend is that with the increasing number of benzene rings in PAHs, both the half-life times for PAH biodegradation and the resonance energy of their structures increase, which leads to their high thermodynamic stability and low bioavailability (Aronstein et al., 1991; Cerniglia, 1992; Morasch et al., 2011; Sharma et al., 2016). In addition, as the number of benzene rings and molecular weight of PAHs increase, the solubility of PAHs decreases, which leads to higher bio-resistance as well (Cerniglia, 1992; Dhar et al., 2020).

When the number of benzene rings is kept constant, PAHs were less degraded with the increased number of methyl groups (Figure 6). This matches what previous studies found, although they mainly focused on the specific compounds (Volkman et al., 1984; Chen et al., 2013) or specific environmental conditions (Liu et al., 2023b). In contrast, our study offers a comprehensive analysis of all series of dicyclic and tricyclic PHAs present in petroleum hydrocarbons, encompassing both aerobic and anaerobic conditions (Figure 6). The increased methyl substitutions may reduce the available sites for enzymatic activity, which in turn could diminish the biodegradation potential (Leblond et al., 2001). When the number of methyl groups remains constant, the position of these methyl becomes a crucial determinant of biodegradation ratios (Figures 5E-H). The presence of ortho substitutions introduces greater steric hindrance, consequently diminishing the biodegradation ratio (Liu et al., 2023b). Additionally, isomers featuring β-methyl substituents tend to undergo more rapid

degradation compared to those with α-methyl substituents (Raymond et al., 1967; Volkman et al., 1984). Our study aligns with these findings, as illustrated in Figure 5E. It's important to note that prior investigations exclusively focused on the aerobic degradation characteristics of alkylnaphthalenes (Raymond et al., 1967; Volkman et al., 1984; Liu et al., 2023b). In contrast, our study expands upon the understanding of alkylnaphthalenes degradation by examining its characteristics under anaerobic conditions.

4.3 Environmental implications

Facultative bacteria are commonly found and are prevalent in a wide range of environments (Table S1 in Supplementary material), because they adapt to diverse ecological niches (Tschech and Fuchs, 1987; Bae et al., 2006). These bacteria can thrive when oxygen is available and shift their metabolic pathways when oxygen becomes limited (Zhang et al., 2021). Thus, they contribute to the creation of biogeochemical gradients, such as redox gradients in sediments and water columns (Acosta-González and Marqués, 2016). Facultative bacteria are abundant in soil (Table S1 in Supplementary material), playing a crucial role in organic matter decomposition, element cycling, and the transformation of various compounds under changing oxygen conditions (McNally et al., 1998; Grishchenkov et al., 2000; Cason et al., 2019; Zuo et al., 2021; Sheng et al., 2021a; Dong et al., 2023a). In anaerobic environments, such as wetlands and sediments, facultative anaerobes can make up a substantial proportion of the microbial community (Bai et al., 2000; Zhu et al., 2011). In addition, ecosystems with fluctuating oxygen levels, like the water column in lakes and oceans, may have a significant presence of facultative bacteria (Haas et al., 2019). Some facultative bacteria are even found in extreme environments, such as hot springs, deep-sea hydrothermal vents, and acidic or alkaline environments (Raguénès et al., 1997; Pankratov et al., 2012; He et al., 2014; Mohr et al., 2018).

The versatility in adapting to changing conditions makes facultative bacteria valuable for breaking down complex molecules into simpler forms (McNally et al., 1998; Li et al., 2012; Zhang et al., 2021). As oxygen level decreases from the surface to subsurface environments, microorganisms can utilize iron-bearing minerals present in sediments as alternative electron acceptors for respiration (Favre et al., 2006; Han et al., 2020; Dong et al., 2022). Our results demonstrated that CN32 could utilize both O_2 and Fe(III) as electron acceptors for oil degradation, expanding its potential for remediating oil-contaminated sites in aerobic and anaerobic zones. Similarly, Pathiraja et al. (2019) revealed that the facultative bacterium *Lysinibacillus* sp. NP05 exhibited a superior ability of polychlorinated biphenyls (PCBs) degradation under two-stage anaerobic-aerobic conditions compared to constant aerobic (using O_2 as an electron acceptor) or anaerobic (using PCBs as an electron acceptor) conditions. Therefore, facultative bacteria like CN32 and NP05 could serve as effective alternatives to obligate bacteria for the degradation of organic pollutants under oscillating redox conditions. These findings highlight an advantage of facultative anaerobic bacteria in the continuous remediation of organic pollutants across diverse environments (Table S1 in Supplementary material).

We focused on the biodegradation of complex crude oil, in contrast to previous researches that primarily investigated the degradation of specific classes of petroleum hydrocarbons, such as phenanthrenes (Zhang et al., 2021), pyrene and benzo[*a*]pyrene (Liang et al., 2014; Yan et al., 2017), *n*-alkanes, naphthalenes, and fluorenes (Grishchenkov et al., 2000). Thus, this study provides valuable insights for developing targeted pollution remediation strategies by uncovering specific degradation capabilities of CN32 under different conditions. This bacterium can aerobically degrade *n*-alkane pollutants at the surface where oxygen is abundant. In the subsurface, where oxygen is limited but dissolved Fe(III), iron-bearing minerals, or iron (oxyhydr)oxides may be abundant, this bacterium switches to anaerobic degradation of aromatics. Thus, CN32 is a valuable microorganism for remediating oil pollutants in various environmental settings, including soil, groundwater, seafloor, and transitional zones between terrestrial and marine. The dual capabilities of CN32 to target both saturated and aromatic hydrocarbons under aerobic and anaerobic conditions highlight its versatility as a bioremediation agent for diverse hydrocarbon pollutants. Furthermore, it is also noteworthy that facultative bacteria have an advantage in pollutant degradation due to their ability to generate hydroxyl radicals through microbial-driven Fenton reaction, utilizing H_2O_2 generated during aerobic respiration or Fe(II) generated during anaerobic Fe(III) reduction (Sekar and DiChristina, 2014; Han et al., 2020, 2022). Hydroxyl radicals possess strong oxidizing capabilities and can chemically oxidize petroleum hydrocarbons (Tsai and Kao, 2009; Cheng et al., 2016). This approach not only offers a more cost-effective and environmentally friendly alternative to chemical Fenton reactions (Klečka and Gonsior, 1986; Stefan and Bolton, 1998), but also achieves faster degradation rates compared to traditional bioremediation methods (Shen et al., 2008; Kim et al., 2009). Therefore, the application potential of CN32 in this field can be further explored.

5 Conclusion

In this study, degradation of crude oil by a facultative anaerobic iron-reducing bacterium *S. putrefaciens* CN32 was investigated under aerobic and anaerobic conditions using O_2 and Fe(III) as electron acceptors. The results unveiled intriguing patterns, revealing that saturates were more susceptible to biodegradation under aerobic conditions, exhibiting a remarkable average biodegradation ratio of 65.65 ± 0.01%, higher than that of aromatics at 43.86 ± 0.03%. Notably, the degradation of saturated hydrocarbons displayed a complex pattern, with the biodegradation ratio initially decreasing and then increasing as the carbon chain length increased. Conversely, aromatics were more susceptible to biodegradation under anaerobic condition than under aerobic condition, due to the higher ubiD gene expression level under anaerobic condition. Furthermore, under anaerobic condition, CN32 demonstrated a preference for degrading aromatics (53.94 ± 0.02%) over saturates (23.36 ± 0.01%). Additionally, as the number of aromatic rings and methyl groups in PAHs increased, aromatic hydrocarbons became more resistant to biodegradation. These profound findings not only illuminate the intricate degradation pathways of crude oil by *S. putrefaciens* CN32, but also offer invaluable insights for the selection of microorganisms with specific fingerprint for targeted organic pollution remediation in both aerobic and anaerobic environments.

Data availability statement

The original contributions presented in the study are included in the article/Supplementary material, further inquiries can be directed to the corresponding author.

Author contributions

YaL: Data curation, Formal analysis, Investigation, Methodology, Visualization, Writing – original draft. YuL: Conceptualization, Data curation, Formal analysis, Funding acquisition, Methodology, Visualization, Writing – review & editing. DG: Visualization, Writing – review & editing. HD: Resources, Supervision, Writing – review & editing, Funding acquisition.

Funding

The author(s) declare that financial support was received for the research, authorship, and/or publication of this article. This research is financially supported by grants from the National Natural Science Foundation of China (NSFC-42102041), and China Postdoctoral Science Foundation (2021M692996).

Acknowledgments

The authors thank Lei Zhu and Shengbao Shi for their help on separation and detection of crude oil composition. The authors are grateful to three reviewers whose comments improved the quality of the manuscript. This work was supported by the High-performance Computing Platform of China University of Geosciences Beijing.

Conflict of interest

The authors declare that the research was conducted in the absence of any commercial or financial relationships that could be construed as a potential conflict of interest.

Publisher's note

All claims expressed in this article are solely those of the authors and do not necessarily represent those of their affiliated organizations, or those of the publisher, the editors and the reviewers. Any product that may be evaluated in this article, or claim that may be made by its manufacturer, is not guaranteed or endorsed by the publisher.

Supplementary material

The Supplementary material for this article can be found online at:https://www.frontiersin.org/articles/10.3389/fmicb.2024.1389954/full#supplementary-material

References

Acosta-González, A., and Marqués, S. (2016). Bacterial diversity in oil-polluted marine coastal sediments. *Curr. Opin. Biotechnol.* 38, 24–32. doi: 10.1016/j.copbio.2015.12.010

Aeckersberg, F., Bak, F., and Widdel, F. (1991). Anaerobic oxidation of saturated hydrobarbons to CO2 by a new type of sulfate-reducing bacterium. *Arch. Microbiol.* 156, 5–14. doi: 10.1007/BF00418180

Amonette, J. E., and Templeton, J. C. (1998). Improvements to the quantitative assay of nonrefractory minerals for Fe(II) and Total Fe using 1,10-Phenanthroline. *Clays Clay Miner.* 46, 51–62. doi: 10.1346/CCMN.1998.0460106

Anderson, R. T., and Lovley, D. R. (1999). Naphthalene and benzene degradation under Fe(III)-reducing conditions in petroleum-contaminated aquifers. *Biorem. J.* 3, 121–135. doi: 10.1080/10889869991219271

Ansari, F., Prayuenyong, P., and Tothill, I. E. (2007). Biodesulfurization of dibenzothiophene by *Shewanella putrefaciens* NCIMB 8768. *J. Biol. Phys. Chem.* 7, 75–78. doi: 10.4024/20708.jbpc.07.02

Arias-Cartin, R., Kazemzadeh Ferizhendi, K., Séchet, E., Pelosi, L., Loeuillet, C., Pierrel, F., et al. (2023). Role of the *Escherichia coli* ubiquinone-synthesizing UbiUVT pathway in adaptation to changing respiratory conditions. *MBio* 14, e03298–e03222. doi: 10.1128/mbio.03298-22

Aronstein, B. N., Calvillo, Y. M., and Alexander, M. (1991). Effect of surfactants at low concentrations on the desorption and biodegradation of sorbed aromatic compounds in soil. *Environ. Sci. Technol.* 25, 1728–1731. doi: 10.1021/es00022a008

Atashgahi, S., Hornung, B., Van Der Waals, M. J., Da Rocha, U. N., Hugenholtz, F., Nijsse, B., et al. (2018). A benzene-degrading nitrate-reducing microbial consortium displays aerobic and anaerobic benzene degradation pathways. *Sci. Rep.* 8, 4490–4412. doi: 10.1038/s41598-018-22617-x

ATSDR (2005). "Toxicology profile for polyaromatic hydrocarbons" in *ATSDR's toxicological profiles on CD-ROM* (Boca Raton, FL: CRC Press)

Bae, H.-S., Moe, W. M., Yan, J., Tiago, I., da Costa, M. S., and Rainey, F. A. (2006). *Propionicicella superfundia* gen. Nov., sp. nov., a chlorosolvent-tolerant propionate-forming, facultative anaerobic bacterium isolated from contaminated groundwater. *Syst. Appl. Microbiol.* 29, 404–413. doi: 10.1016/j.syapm.2005.11.004

Bai, Q., Gattinger, A., and Zelles, L. (2000). Characterization of microbial consortia in Paddy Rice soil by phospholipid analysis. *Microb. Ecol.* 39, 273–281. doi: 10.1007/s002480000020

Barth, T., and Riis, M. (1992). Interactions between organic acids anions in formation waters and reservoir mineral phases. *Org. Geochem.* 19, 455–482. doi: 10.1016/0146-6380(92)90012-M

Bennett, P. C., Siegel, D. E., Baedecker, M. J., and Hult, M. F. (1993). Crude oil in a shallow sand and gravel aquifer--l. hydrogeology and inorganic geochemistry. *Appl. Geochem.* 8, 529–549. doi: 10.1016/0883-2927(93)90012-6

Bezerra, D. S., Neves, B. G., Guedes, S. F., Regis, W. F. M., Stipp, R. N., and Rodrigues, L. K. A. (2019). Extraction and purification of RNA from human carious dentine: an approach to enable bacterial gene expression studies. *J. Health Biol. Sci.* 7, 145–151. doi: 10.12662/2317-3076jhbs

BP (2022). "*BP world energy statistical yearbook*". (London, UK: BP).

Brooijmans, R. J., Pastink, M. I., and Siezen, R. J. (2009). Hydrocarbon-degrading bacteria: the oil-spill clean-up crew. *Microb. Biotechnol.* 2, 587–594. doi: 10.1111/j.1751-7915.2009.00151.x

Bugg, T. D. H., and Winfield, C. J. (1998). Enzymatic cleavage of aromatic rings: mechanistic aspects of the catechol dioxygenases and later enzymes of bacterial oxidative cleavage pathways. *Nat. Prod. Rep.* 15, 513–530. doi: 10.1039/a815513y

Cabrerizo, A., Tejedo, P., Dachs, J., and Benayas, J. (2016). Anthropogenic and biogenic hydrocarbons in soils and vegetation from the South Shetland Islands (Antarctica). *Sci. Total Environ.* 569-570, 1500–1509. doi: 10.1016/j.scitotenv.2016.06.240

Cason, E. D., Vermeulen, J.-G., Müller, W. J., van Heerden, E., and Valverde, A. (2019). Aerobic and anaerobic enrichment cultures highlight the pivotal role of facultative anaerobes in soil hydrocarbon degradation. *J. Environ. Sci. Health* 54, 408–415. doi: 10.1080/10934529.2018.1558902

Cerniglia, C. E. (1992). Biodegradation of polycyclic aromatic hydrocarbons. *Biodegradation* 3, 351–368. doi: 10.1007/BF00129093

Chang, W., Um, Y., and Holoman, T. R. P. (2006). Polycyclic aromatic hydrocarbon (PAH) degradation coupled to methanogenesis. *Biotechnol. Lett.* 28, 425–430. doi: 10.1007/s10529-005-6073-3

Chen, J., Zhang, H., Huang, H., Li, X., Shi, S., Liu, F., et al. (2013). Impact of anaerobic biodegradation on alkylphenanthrenes in crude oil. *Org. Geochem.* 61, 6–14. doi: 10.1016/j.orggeochem.2013.05.003

Cheng, L., Shi, S., Yang, L., Zhang, Y., Dolfing, J., Sun, Y., et al. (2019). Preferential degradation of long-chain alkyl substituted hydrocarbons in heavy oil under methanogenic conditions. *Org. Geochem.* 138:103927. doi: 10.1016/j.orggeochem.2019.103927

Cheng, M., Zeng, G., Huang, D., Lai, C., Xu, P., Zhang, C., et al. (2016). Hydroxyl radicals based advanced oxidation processes (AOPs) for remediation of soils contaminated with organic compounds: a review. *Chem. Eng. J.* 284, 582–598. doi: 10.1016/j.cej.2015.09.001

Coates, J. D., Chakraborty, R., Lack, J. G., O'Connor, S. M., Cole, K. A., Bender, K. S., et al. (2001). Anaerobic benzene oxidation coupled to nitrate reduction in pure culture by two strains of Dechloromonas. *Nature* 411, 1039–1043. doi: 10.1038/35082545

Coey, J. M. D. (1980). Clay minerals and their transformations studied with nuclear techniques: the contribution of Mssbauer spectroscopy. *At. Energy Rev.* 18, 73–124.

Crowe, A. S., and Smith, J. E. (2007). Distribution and persistence of DDT in soil at a sand dune-marsh environment: point Pelee, Ontario Canada. *Canad. J. Soil Sci.* 87, 315–327. doi: 10.4141/s06-033

Das, N., and Chandran, P. (2011). Microbial degradation of petroleum hydrocarbon contaminants: an overview. *Biotechnol. Res. Int.* 2011, 1–13. doi: 10.4061/2011/941810

Davison, W. (1993). Iron and manganese in lakes. *Earth Sci. Rev.* 34, 119–163. doi: 10.1016/0012-8252(93)90029-7

del Rio, J. C., Garcia-Molla, J., Gonzalez-Vila, F. J., and Martin, F. (1994). Composition and origin of the aliphatic extractable hydrocarbons in the Puertollano (Spain) oil shale. *Org. Geochem.* 21, 897–909. doi: 10.1016/0146-6380(94)90049-3

Dhar, K., Subashchandrabose, S. R., Venkateswarlu, K., Krishnan, K., and Megharaj, M. (2020). Anaerobic microbial degradation of polycyclic aromatic hydrocarbons: a comprehensive review. *Rev. Environ. Contam. Toxicol.* 251, 25–108. doi: 10.1007/398_2019_29

Díaz, E., Jiménez, J. I., and Nogales, J. (2013). Aerobic degradation of aromatic compounds. *Curr. Opin. Biotechnol.* 24, 431–442. doi: 10.1016/j.copbio.2012.10.010

DiDonato, R. J. Jr., Young, N. D., Butler, J. E., Chin, K.-J., Hixson, K. K., Mouser, P., et al. (2010). Genome sequence of the deltaproteobacterial strain NaphS2 and analysis of differential gene expression during anaerobic growth on naphthalene. *PLoS One* 5:e14072. doi: 10.1371/journal.pone.0014072

Dong, H., Coffin, E. S., Sheng, Y., Duley, M. L., and Khalifa, Y. M. (2023a). Microbial reduction of Fe (III) in nontronite: role of biochar as a redox mediator. *Geochim. Cosmochim. Acta* 345, 102–116. doi: 10.1016/j.gca.2023.01.027

Dong, H., Huang, L., Zhao, L., Zeng, Q., Liu, X., Sheng, Y., et al. (2022). A critical review of mineral–microbe interaction and co-evolution: mechanisms and applications. *Natl. Sci. Rev.* 9:nwac128. doi: 10.1093/nsr/nwac128

Dong, H., Zeng, Q., Sheng, Y., Chen, C., Yu, G., and Kappler, A. (2023b). Coupled iron cycling and organic matter transformation across redox interfaces. *Nat. Rev. Earth Environ.* 4, 659–673. doi: 10.1038/s43017-023-00470-5

Edwards, N. T. (1983). Polycyclic aromatic hydrocarbons (PAH's) in the terrestrial environment—a review. *J. Environ. Qual.* 12, 427–441. doi: 10.2134/jeq1983.00472425001200040001x

Favre, F., Stucki, J. W., and Boivin, P. (2006). Redox properties of structural Fe in ferruginous smectite. A discussion of the standard potential and its environmental implications. *Clay Clay Miner.* 54, 466–472. doi: 10.1346/ccmn.2006.0540407

Feng, L., Wang, W., Cheng, J., Ren, Y., Zhao, G., Gao, C., et al. (2007). Genome and proteome of long-chain alkane degrading *Geobacillus thermodenitrificans* NG80-2 isolated from a deep-subsurface oil reservoir. *Proc. Natl. Acad. Sci. U.S.A.* 104, 5602–5607. doi: 10.1073/pnas.0609650104

Fu, J. M., and Sheng, G. Y. (1989). Biological marker composition of typical source rocks and related crude oils of terrestrial origin in the People's Republic of China: a review. *Appl. Geochem.* 4, 13–22. doi: 10.1016/0883-2927(89)90055-3

Fuentes, S., Méndez, V., Aguila, P., and Seeger, M. (2014). Bioremediation of petroleum hydrocarbons: catabolic genes, microbial communities, and applications. *Appl. Microbiol. Biotechnol.* 98, 4781–4794. doi: 10.1007/s00253-014-5684-9

George, S. C., Boreham, C. J., Minifie, S. A., and Teerman, S. C. (2002). The effect of minor to moderate biodegradation on C5 to C9 hydrocarbons in crude oils. *Org. Geochem.* 33, 1293–1317. doi: 10.1016/S0146-6380(02)00117-1

Ghosal, D., Ghosh, S., Dutta, T. K., and Ahn, Y. (2016). Current state of knowledge in microbial degradation of polycyclic aromatic hydrocarbons (PAHs): a review. *Front. Microbiol.* 7:369. doi: 10.3389/fmicb.2016.01369

Grishchenkov, V., Townsend, R., McDonald, T., Autenrieth, R., Bonner, J., and Boronin, A. (2000). Degradation of petroleum hydrocarbons by facultative anaerobic bacteria under aerobic and anaerobic conditions. *Process Biochem.* 35, 889–896. doi: 10.1016/s0032-9592(99)00145-4

Haas, S., Desai, D. K., LaRoche, J., Pawlowicz, R., and Wallace, D. W. R. (2019). Geomicrobiology of the carbon, nitrogen and Sulphur cycles in Powell Lake: a permanently stratified water column containing ancient seawater. *Environ. Microbiol.* 21, 3927–3952. doi: 10.1111/1462-2920.14743

Han, R., Lv, J., Huang, Z., Zhang, S., and Zhang, S. (2020). Pathway for the production of hydroxyl radicals during the Microbially mediated redox transformation of Iron (Oxyhydr)oxides. *Environ. Sci. Technol.* 54, 902–910. doi: 10.1021/acs.est.9b06220

Han, R., Wang, Z., Lv, J., Zhu, Z., Yu, G.-H., Li, G., et al. (2022). Multiple effects of humic components on Microbially mediated Iron redox processes and production of hydroxyl radicals. *Environ. Sci. Technol.* 56, 16419–16427. doi: 10.1021/acs.est.2c03799

Haritash, A., and Kaushik, C. (2009). Biodegradation aspects of polycyclic aromatic hydrocarbons (PAHs): a review. *J. Hazard. Mater.* 169, 1–15. doi: 10.1016/j.jhazmat.2009.03.137

Hasanuzzaman, M., Ueno, A., Ito, H., Ito, Y., Yamamoto, Y., Yumoto, I., et al. (2007). Degradation of long-chain n-alkanes (C36 and C40) by *Pseudomonas aeruginosa* strain WatG. *Int. Biodeterior. Biodegrad.* 59, 40–43. doi: 10.1016/j.ibiod.2006.07.010

He, Z., Li, S., Wang, L., and Zhong, H. (2014). Characterization of five chromium-removing Bacteria isolated from chromium-contaminated soil. *Water Air Soil Pollut.* 225:1904. doi: 10.1007/s11270-014-1904-2

Iheonye, C., Osuji, L. C., and Onyema, M. O. (2019). Petroleum contamination of Sombreiro River in Akuku-Toru local government area Rivers state, Nigeria, revealed by chemical fingerprinting of aliphatic hydrocarbons. *J. Appl. Sci. Environ. Manag.* 23, 805–809. doi: 10.4314/jasem.v23i5.5

Kaplan, I. R., Galperin, Y., Lu, S.-T., and Lee, R.-P. (1997). Forensic environmental geochemistry: differentiation of fuel-types, their sources and release time. *Org. Geochem.* 27, 289–317. doi: 10.1016/S0146-6380(97)87941-7

Kennicutt, M. C. II, Barker, C., Brooks, J. M., DeFreitas, D. A., and Zhu, G. H. (1987). Selected organic matter source indicators in the Orinoco Nile and Changjiang deltas. *Organ. Geochem.* 11, 41–51. doi: 10.1016/0146-6380(87)90050-7

Khudur, L. S., Shahsavari, E., Webster, G. T., Nugegoda, D., and Ball, A. S. (2019). The impact of lead co-contamination on ecotoxicity and the bacterial community during the bioremediation of total petroleum hydrocarbon-contaminated soils. *Environ. Pollut.* 253, 939–948. doi: 10.1016/j.envpol.2019.07.107

Kim, Y.-M., Jeon, J.-R., Murugesan, K., Kim, E.-J., and Chang, Y.-S. (2009). Biodegradation of 1, 4-dioxane and transformation of related cyclic compounds by a newly isolated Mycobacterium sp. PH-06. *Biodegradation* 20, 511–519. doi: 10.1007/s10532-008-9240-0

Klečka, G., and Gonsior, S. (1986). Removal of 1, 4-dioxane from wastewater. *J. Hazard. Mater.* 13, 161–168. doi: 10.1016/0304-3894(86)80016-4

Kleemann, R., and Meckenstock, R. U. (2011). Anaerobic naphthalene degradation by gram-positive, iron-reducing bacteria. *FEMS Microbiol. Ecol.* 78, 488–496. doi: 10.1111/j.1574-6941.2011.01193.x

Koelschbach, J., Mouttaki, H., Merl-Pham, J., Arnold, M., and Meckenstock, R. (2019). Identification of naphthalene carboxylase subunits of the sulfate-reducing culture N47. *Biodegradation* 30, 147–160. doi: 10.1007/s10532-019-09872-z

Leblond, J. D., Schultz, T. W., and Sayler, G. S. (2001). Observations on the preferential biodegradation of selected components of polyaromatic hydrocarbon mixtures. *Chemosphere* 42, 333–343. doi: 10.1016/S0045-6535(00)00161-2

Li, M., Liu, X., Wang, T., Jiang, W., Fang, R., Yang, L., et al. (2018). Fractionation of dibenzofurans during subsurface petroleum migration: based on molecular dynamics simulation and reservoir geochemistry. *Org. Geochem.* 115, 220–232. doi: 10.1016/j.orggeochem.2017.10.006

Li, L., Zhao, C. C., Liu, Q. Y., Zhang, Y. B., and Wang, L. (2014). Study on screening and degradation characteristics of moderately halophilic Bacteria degrading PASHs. *Chem. Bioeng.* 31, 44–47. doi: 10.3969/j.issn.1672-5425

Li, G., Zu, L., Wong, P.-K., Hui, X., Lu, Y., Xiong, J., et al. (2012). Biodegradation and detoxification of bisphenol a with one newly-isolated strain Bacillus sp. GZB: kinetics, mechanism and estrogenic transition. *Bioresour. Technol.* 114, 224–230. doi: 10.1016/j.biortech.2012.03.067

Liang, L., Song, X., Kong, J., Shen, C., Huang, T., and Hu, Z. (2014). Anaerobic biodegradation of high-molecular-weight polycyclic aromatic hydrocarbons by a facultative anaerobe Pseudomonas sp. JP1. *Biodegradation* 25, 825–833. doi: 10.1007/s10532-014-9702-5

Liu, Y., Shi, S., Zeng, Q., Li, Y., Chen, Y., Guo, D., et al. (2023a). Coupled reduction of structural Fe (III) in nontronite and oxidation of petroleum hydrocarbons. *Geochim. Cosmochim. Acta* 344, 103–121. doi: 10.1016/j.gca.2023.01.010

Liu, Y., Wan, Y. Y., Shi, S. B., and Zhang, Y. C. (2023b). Effect of methyl substituents on the biodegradation of two-ring polycyclic aromatic hydrocarbons in crude oil identified by aerobic biodegradation simulations. *J. Hazard. Mater. Adv.* 9:100239. doi: 10.1016/j.hazadv.2023.100239

Liu, Y., Wan, Y. Y., Wang, C., Ma, Z., Liu, X., and Li, S. (2020a). Biodegradation of n-alkanes in crude oil by three identified bacterial strains. *Fuel* 275:117897. doi: 10.1016/j.fuel.2020.117897

Liu, Y., Wan, Y. Y., Zhu, Y., Fei, C., Shen, Z., and Ying, Y. (2020b). Impact of biodegradation on polar compounds in crude oil: comparative simulation of

biodegradation from two aerobic bacteria using ultrahigh-resolution mass spectrometry. *Energy Fuel* 34, 5553–5565. doi: 10.1021/acs.energyfuels.0c00030

Liu, Y., Zhang, Y., Chen, G., Li, Y., Zeng, Q., Hu, J., et al. (2024). Molecular transformation of petroleum compounds by hydroxyl radicals produced upon oxidation of reduced nontronite. *Geochim. Cosmochim. Acta* 371, 31–51. doi: 10.1016/j.gca.2024.02.019

Livak, K. J., and Schmittgen, T. D. (2001). Analysis of relative gene expression data using real-time quantitative PCR and the 2− ΔΔCT method. *Methods* 25, 402–408. doi: 10.1006/meth.2001.1262

Lovley, D. R., Baedecker, M. J., Lonergan, D. J., Cozzarelli, I. M., Phillips, E. J., and Siegel, D. I. (1989). Oxidation of aromatic contaminants coupled to microbial iron reduction. *Nature* 339, 297–300. doi: 10.1038/339297a0

Lovley, D. R., and Lonergan, D. J. (1990). Anaerobic oxidation of toluene, phenol, and p-cresol by the dissimilatory iron-reducing organism, GS-15. *Appl. Environ. Microbiol.* 56, 1858–1864. doi: 10.1128/aem.56.6.1858-1864.1990

Ma, M., Gao, W., Li, Q., Han, B., Zhu, A., Yang, H., et al. (2021). Biodiversity and oil degradation capacity of oil-degrading bacteria isolated from deep-sea hydrothermal sediments of the south mid-Atlantic ridge. *Mar. Pollut. Bull.* 171:112770. doi: 10.1016/j.marpolbul.2021.112770

Martín-Gil, J., Ramos-Sánchez, M., and Martín-Gil, F. (2004). *Shewanella putrefaciens* in a fuel-in-water emulsion from the prestige oil spill. *Antonie Van Leeuwenhoek* 86, 283–285. doi: 10.1023/B:ANTO.0000047939.49597.eb

Mbadinga, S. M., Wang, L.-Y., Zhou, L., Liu, J.-F., Gu, J.-D., and Mu, B.-Z. (2011). Microbial communities involved in anaerobic degradation of alkanes. *Int. Biodeterior. Biodegradation* 65, 1–13. doi: 10.1016/j.ibiod.2010.11.009

McNally, D. L., Mihelcic, J. R., and Lueking, D. R. (1998). Biodegradation of three-and four-ring polycyclic aromatic hydrocarbons under aerobic and denitrifying conditions. *Environ. Sci. Technol.* 32, 2633–2639. doi: 10.1021/es980006c

Meckenstock, R. U., and Mouttaki, H. (2011). Anaerobic degradation of non-substituted aromatic hydrocarbons. *Curr. Opin. Biotechnol.* 22, 406–414. doi: 10.1016/j.copbio.2011.02.009

Meng, Q., Wang, X., Liao, Y., Lei, Y., Yin, J., Liu, P., et al. (2021). The effect of slight to moderate biodegradation on the shale soluble organic matter composition of the upper triassic Yanchang formation, Ordos Basin China. *Mar. Petrol. Geol.* 128:105021. doi: 10.1016/j.marpetgeo.2021.105021

Mezcua, M., Fernández-Alba, A. R., Boltes, K., Del Aguila, R. A., Leton, P., Rodríguez, A., et al. (2008). Determination of PASHs by various analytical techniques based on gas chromatography–mass spectrometry: application to a biodesulfurization process. *Talanta* 75, 1158–1166. doi: 10.1016/j.talanta.2008.01.034

Mohr, T., Aliyu, H., Küchlin, R., Polliack, S., Zwick, M., Neumann, A., et al. (2018). CO-dependent hydrogen production by the facultative anaerobe Parageobacillus thermoglucosidasius. *Microb. Cell Factories* 17:108. doi: 10.1186/s12934-018-0954-3

Morasch, B., Hunkeler, D., Zopfi, J., Temime, B., and Höhener, P. (2011). Intrinsic biodegradation potential of aromatic hydrocarbons in an alluvial aquifer – potentials and limits of signature metabolite analysis and two stable isotope-based techniques. *Water Res.* 45, 4459–4469. doi: 10.1016/j.watres.2011.05.040

Moreno, R., and Rojo, F. (2017). *Enzymes for aerobic degradation of alkanes in bacteria*. Berlin, Germany: Springer.

Pankratov, T. A., Kirsanova, L. A., Kaparullina, E. N., Kevbrin, V. V., and Dedysh, S. N. (2012). *Telmatobacter bradus* gen. Nov., sp. nov., a cellulolytic facultative anaerobe from subdivision 1 of the Acidobacteria, and emended description of *Acidobacterium capsulatum* Kishimoto et al. 1991. *Int. J. Syst. Evol. Microbiol.* 62, 430–437. doi: 10.1099/ijs.0.029629-0

Pasumarthi, R., Chandrasekaran, S., and Mutnuri, S. (2013). Biodegradation of crude oil by Pseudomonas aeruginosa and *Escherichia fergusonii* isolated from the Goan coast. *Mar. Pollut. Bull.* 76, 276–282. doi: 10.1016/j.marpolbul.2013.08.026

Pathiraja, G., Egodawatta, P., Goonetilleke, A., and Te'o, V. S. J. (2019). Solubilization and degradation of polychlorinated biphenyls (PCBs) by naturally occurring facultative anaerobic bacteria. *Sci. Total Environ.* 651, 2197–2207. doi: 10.1016/j.scitotenv.2018.10.127

Phale, P. S., Shah, B. A., and Malhotra, H. (2019). Variability in assembly of degradation operons for naphthalene and its derivative, carbaryl, suggests mobilization through horizontal gene transfer. *Genes* 10:569. doi: 10.3390/genes10080569

Qian, H., Zhang, Y. L., Wang, J. L., Si, C. Q., and Chen, Z. X. (2018). Characteristics of petroleum-contaminated groundwater during natural attenuation: a case study in Northeast China. *Environ. Monit. Assess.* 190, 80–11. doi: 10.1007/s10661-017-6449-6

Raguénès, G., Christen, R., Guezennec, J., Pignet, P., and Barbier, G. (1997). *Vibrio diabolicus* sp. nov., a new polysaccharide-secreting organism isolated from a deep-sea hydrothermal vent Polychaete annelid, Alvinella pompejana. *Int. J. Syst. Bacteriol.* 47, 989–995. doi: 10.1099/00207713-47-4-989

Raymond, R. L., Jamison, V. M., and Hudson, J. O. (1967). Microbial hydrocarbon co-oxidation: I. Oxidation of mono-and dicyclic hydrocarbons by soil isolates of the genus Nocardia. *Appl. Microbiol.* 15, 857–865. doi: 10.1128/am.15.4.857-865.1967

Rockne, K. J., Chee-Sanford, J. C., Sanford, R. A., Hedlund, B. P., Staley, J. T., and Strand, S. E. (2000). Anaerobic naphthalene degradation by microbial pure cultures under nitrate-reducing conditions. *Appl. Environ. Microbiol.* 66, 1595–1601. doi: 10.1128/AEM.66.4.1595-1601.2000

Rueter, P., Rabus, R., Wilkest, H., Aeckersberg, F., Rainey, F. A., Jannasch, H. W., et al. (1994). Anaerobic oxidation of hydrocarbons in crude oil by new types of sulphate-reducing bacteria. *Nature* 372, 455–458. doi: 10.1038/372455a0

Saito, J., Hashimoto, K., and Okamoto, A. (2016). Flavin as an indicator of the rate-limiting factor for microbial current production in *Shewanella oneidensis* MR-1. *Electrochim. Acta* 216, 261–265. doi: 10.1016/j.electacta.2016.09.002

Sekar, R., and DiChristina, T. J. (2014). Microbially driven Fenton reaction for degradation of the widespread environmental contaminant 1,4-dioxane. *Environ. Sci. Technol.* 48, 12858–12867. doi: 10.1021/es503454a

Setti, L., Lanzarini, G., Pifferi, P. G., and Spagna, G. (1993). Further research into the aerobic degradation of n-alkanes in a heavy oil by a pure culture of a Pseudomonas sp. *Chemosphere* 26, 1151–1157. doi: 10.1016/0045-6535(93)90202-G

Sharma, A., Singh, S. B., Sharma, R., Chaudhary, P., Pandey, A. K., Ansari, R., et al. (2016). Enhanced biodegradation of PAHs by microbial consortium with different amendment and their fate in in-situ condition. *J. Environ. Manag.* 181, 728–736. doi: 10.1016/j.jenvman.2016.08.024

Shen, W., Chen, H., and Pan, S. (2008). Anaerobic biodegradation of 1, 4-dioxane by sludge enriched with iron-reducing microorganisms. *Bioresour. Technol.* 99, 2483–2487. doi: 10.1016/j.biortech.2007.04.054

Sheng, Y., Baars, O., Guo, D., Whitham, J., Srivastava, S., Dong, H. J. E. S., et al. (2023). Mineral-bound trace metals as cofactors for anaerobic biological nitrogen fixation. *Environ. Sci. Technol.* 57, 7206–7216. doi: 10.1021/acs.est.3c01371

Sheng, Y., Dong, H., Kukkadapu, R. K., Ni, S., Zeng, Q., Hu, J., et al. (2021a). Lignin-enhanced reduction of structural Fe (III) in nontronite: dual roles of lignin as electron shuttle and donor. *Geochim. Cosmochim. Acta* 307, 1–21. doi: 10.1016/j.gca.2021.05.037

Sheng, Y., Liu, Y., Yang, J., Dong, H., Liu, B., Zhang, H., et al. (2021b). History of petroleum disturbance triggering the depth-resolved assembly process of microbial communities in the vadose zone. *J. Hazard. Mater.* 402:124060. doi: 10.1016/j.jhazmat.2020.124060

Sheng, Y., Tian, X., Wang, G., Hao, C., and Liu, F. (2016). Bacterial diversity and biogeochemical processes of oil-contaminated groundwater, Baoding North China. *Geomicrobiol. J.* 33, 537–551. doi: 10.1080/01490451.2015.1062061

Sierra-Garcia, I. N., and de Oliveira, V. M. (2013). Microbial hydrocarbon degradation: efforts to understand biodegradation in petroleum reservoirs. *Biodegrad. Eng. Technol.* 2011:810

So, C. M., Phelps, C. D., and Young, L. (2003). Anaerobic transformation of alkanes to fatty acids by a sulfate-reducing bacterium, strain Hxd3. *Appl. Environ. Microbiol.* 69, 3892–3900. doi: 10.1128/AEM.69.7.3892-3900.2003

Stefan, M. I., and Bolton, J. R. (1998). Mechanism of the degradation of 1, 4-dioxane in dilute aqueous solution using the UV/hydrogen peroxide process. *Environ. Sci. Technol.* 32, 1588–1595. doi: 10.1021/es970633m

Strausz, O.P., and Lown, E.M. (2003). *The chemistry of Alberta oil sands, bitumens and heavy oils*. Calgary: Alberta Energy Research Institute.

Takahashi, Y., Higashi, M., Furukawa, T., and Mitsunobu, S. (2011). Change of iron species and iron solubility in Asian dust during the long-range transport from western China to Japan. *Atmos. Chem. Phys.* 11, 11237–11252. doi: 10.5194/acp-11-11237-2011

Tani, A., Ishige, T., Sakai, Y., and Kato, N. (2001). Gene structures and regulation of the alkane hydroxylase complex in Acinetobacter sp. strain M-1. *J. Bacteriol.* 183, 1819–1823. doi: 10.1128/JB.183.5.1819-1823.2001

Tong, M., Yuan, S., Ma, S., Jin, M., Liu, D., Cheng, D., et al. (2016). Production of abundant hydroxyl radicals from oxygenation of subsurface sediments. *Environ. Sci. Technol.* 50, 214–221. doi: 10.1021/acs.est.5b04323

Tsai, T., and Kao, C. (2009). Treatment of petroleum-hydrocarbon contaminated soils using hydrogen peroxide oxidation catalyzed by waste basic oxygen furnace slag. *J. Hazard. Mater.* 170, 466–472. doi: 10.1016/j.jhazmat.2009.04.073

Tschech, A., and Fuchs, G. (1987). Anaerobic degradation of phenol by pure cultures of newly isolated denitrifying pseudomonads. *Arch. Microbiol.* 148, 213–217. doi: 10.1007/BF00414814

Vaishnav, E. D., de Boer, C. G., Molinet, J., Yassour, M., Fan, L., Adiconis, X., et al. (2022). The evolution, evolvability and engineering of gene regulatory DNA. *Nature* 603, 455–463. doi: 10.1038/s41586-022-04506-6

Varjani, S. J. (2016). Microbial degradation of petroleum hydrocarbons. *Bioresour. Technol.* 223, 277–286. doi: 10.1016/j.biortech.2016.10.037

Vodyanitskii, Y. N. (2011). Iron compounds and oil biodegradation in overmoistened contaminated soils: a review of publications. *Eurasian Soil Sci.* 44, 1250–1259. doi: 10.1134/S1064229311090171

Volkman, J. K., Alexander, R., Kagi, R. I., Rowland, S. J., and Sheppard, P. N. (1984). Biodegradation of aromatic hydrocarbons in crude oils from the Barrow sub-basin of Western Australia. *Org. Geochem.* 6, 619–632. doi: 10.1016/0146-6380(84)90084-6

Wang, X., Cai, T., Wen, W., Ai, J., Ai, J., Zhang, Z., et al. (2020). Surfactin for enhanced removal of aromatic hydrocarbons during biodegradation of crude oil. *Fuel* 267, 117272–117288. doi: 10.1016/j.fuel.2020.117272

Weber, K. A., Achenbach, L. A., and Coates, J. D. (2006). Microorganisms pumping iron: anaerobic microbial iron oxidation and reduction. *Nat. Rev. Microbiol.* 4, 752–764. doi: 10.1038/nrmicro1490

Wei, X., Hao, Y. Q., Li, G., Niu, S. L., Wang, S. H., and Zhao, H. X. (2017). Mechanism of Phenanthrene polluted soil by microbial remediation. *J. Microbiol.* 37, 114–124. doi: 10.3969/j.issn.1005-7021

Wentzel, A., Ellingsen, T. E., Kotlar, H.-K., Zotchev, S. B., and Throne-Holst, M. (2007). Bacterial metabolism of long-chain n-alkanes. *Appl. Microbiol. Biotechnol.* 76, 1209–1221. doi: 10.1007/s00253-007-1119-1

Widdel, F., Boetius, A., and Rabus, R. (2006). Anaerobic biodegradation of hydrocarbons including methane. *Prokaryotes* 2, 1028–1049. doi: 10.1007/0-387-30742-7_33

Wilkes, H., Rabus, R., Fischer, T., Armstroff, A., Behrends, A., and Widdel, F. (2002). Anaerobic degradation of n-hexane in a denitrifying bacterium: further degradation of the initial intermediate (1-methylpentyl) succinate via C-skeleton rearrangement. *Arch. Microbiol.* 177, 235–243. doi: 10.1007/s00203-001-0381-3

Wischgoll, S., Heintz, D., Peters, F., Erxleben, A., Sarnighausen, E., Reski, R., et al. (2005). Gene clusters involved in anaerobic benzoate degradation of *Geobacter metallireducens*. *Mol. Microbiol.* 58, 1238–1252. doi: 10.1111/j.1365-2958.2005.04909.x

Xu, X., Liu, W., Tian, S., Wang, W., Qi, Q., Jiang, P., et al. (2018). Petroleum hydrocarbon-degrading bacteria for the remediation of oil pollution under aerobic conditions: a perspective analysis. *Front. Microbiol.* 9:2885. doi: 10.3389/fmicb.2018.02885

Yan, Z., Zhang, Y., Wu, H., Yang, M., Zhang, H., Hao, Z., et al. (2017). Isolation and characterization of a bacterial strain Hydrogenophaga sp. PYR1 for anaerobic pyrene and benzo[a]pyrene biodegradation. *RSC Adv.* 7, 46690–46698. doi: 10.1039/c7ra09274a

Zachara, J. M., Fredrickson, J. K., Li, S. M., Kennedy, D. W., Smith, S. C., and Gassman, P. L. (1998). Bacterial reduction of crystalline Fe3+ oxides in single phase suspensions and subsurface materials. *Am. Mineral.* 83, 1426–1443. doi: 10.2138/am-1998-11-1232

Zeng, Q., Dong, H., Zhao, L., and Huang, Q. (2016). Preservation of organic matter in nontronite against iron redox cycling. *Am. Mineral.* 101, 120–133. doi: 10.2138/am-2016-5410

Zeng, Q., Huang, L., Ma, J., Zhu, Z., He, C., Shi, Q., et al. (2020). Bio-reduction of ferrihydrite-montmorillonite-organic matter complexes: effect of montmorillonite and fate of organic matter. *Geochim. Cosmochim. Acta* 276, 327–344. doi: 10.1016/j.gca.2020.03.011

Zhan, J., Liu, Y., Cheng, W., Zhang, A., Li, R., Li, X., et al. (2018). Remediation of soil contaminated by fluorene using needle-plate pulsed corona discharge plasma. *Chem. Eng. J.* 334, 2124–2133. doi: 10.1016/j.cej.2017.11.093

Zhang, Z., Guo, H., Sun, J., Gong, X., Wang, C., and Wang, H. (2021). Exploration of the biotransformation processes in the biodegradation of phenanthrene by a facultative anaerobe, strain PheF2, with Fe (III) or O2 as an electron acceptor. *Sci. Total Environ.* 750:142245. doi: 10.1016/j.scitotenv.2020.142245

Zhang, K., Hu, Z., Zeng, F., Yang, X., Wang, J., Jing, R., et al. (2019). Biodegradation of petroleum hydrocarbons and changes in microbial community structure in sediment under nitrate-, ferric-, sulfate-reducing and methanogenic conditions. *J. Environ. Manag.* 249:109425. doi: 10.1016/j.jenvman.2019.109425

Zhang, T., Tremblay, P. L., Chaurasia, A. K., Smith, J. A., Bain, T. S., and Lovley, D. R. (2013). Anaerobic benzene oxidation via phenol in *Geobacter metallireducens*. *Appl. Environ. Microbiol.* 79, 7800–7806. doi: 10.1128/AEM.03134-13

Zhu, Q., Ye, C., Li, C., Ke, L., and Zhao, X. (2011). Isolation and degradation effect of facultative anaerobic Flora with high efficiency organic matter biodegradation from near-shore wetland in Taihu Lake. *Res. Environ. Sci.* 24, 1129–1135. doi: 10.13198/j.res.2011.10.51.zhuqf.007

Zuo, H., Huang, L., Chu, R. K., Tolic, N., Washton, N., Zhu, Z., et al. (2021). Reduction of structural Fe(III) in nontronite by humic substances in the absence and presence of Shewanella putrefaciens and accompanying secondary mineralization. *Am. Mineral.* 106, 1957–1970. doi: 10.2138/am-2021-7828

frontiers | Frontiers in Microbiology

TYPE Original Research
PUBLISHED 10 May 2024
DOI 10.3389/fmicb.2024.1388973

OPEN ACCESS

EDITED BY
Linduo Zhao,
University of Illinois at Urbana-Champaign, United States

REVIEWED BY
Wen-Dong Xian,
Zhejiang Ocean University, China
Wei Li,
Lawrence Livermore National Laboratory (DOE), United States

*CORRESPONDENCE
Erin K. Field
✉ fielde14@ecu.edu

RECEIVED 20 February 2024
ACCEPTED 16 April 2024
PUBLISHED 10 May 2024

CITATION
Brooks CN and Field EK (2024) Microbial community response to hydrocarbon exposure in iron oxide mats: an environmental study.
Front. Microbiol. 15:1388973.
doi: 10.3389/fmicb.2024.1388973

Microbial community response to hydrocarbon exposure in iron oxide mats: an environmental study

Chequita N. Brooks[1,2] and Erin K. Field[1]*

[1]Department of Biology, East Carolina University, Greenville, NC, United States, [2]Louisiana Universities Marine Consortium, Chauvin, LA, United States

Hydrocarbon pollution is a widespread issue in both groundwater and surface-water systems; however, research on remediation at the interface of these two systems is limited. This interface is the oxic–anoxic boundary, where hydrocarbon pollutant from contaminated groundwaters flows into surface waters and iron mats are formed by microaerophilic iron-oxidizing bacteria. Iron mats are highly chemically adsorptive and host a diverse community of microbes. To elucidate the effect of hydrocarbon exposure on iron mat geochemistry and microbial community structure and function, we sampled iron mats both upstream and downstream from a leaking underground storage tank. Hydrocarbon-exposed iron mats had significantly higher concentrations of oxidized iron and significantly lower dissolved organic carbon and total dissolved phosphate than unexposed iron mats. A strong negative correlation between dissolved phosphate and benzene was observed in the hydrocarbon-exposed iron mats and water samples. There were positive correlations between iron and other hydrocarbons with benzene in the hydrocarbon-exposed iron mats, which was unique from water samples. The hydrocarbon-exposed iron mats represented two types, flocculent and seep, which had significantly different concentrations of iron, hydrocarbons, and phosphate, indicating that iron mat is also an important context in studies of freshwater mats. Using constrained ordination, we found the best predictors for community structure to be dissolved oxygen, pH, and benzene. Alpha diversity and evenness were significantly lower in hydrocarbon-exposed iron mats than unexposed mats. Using 16S rDNA amplicon sequences, we found evidence of three putative nitrate-reducing iron-oxidizing taxa in microaerophile-dominated iron mats (*Azospira, Paracoccus*, and *Thermomonas*). 16S rDNA amplicons also indicated the presence of taxa that are associated with hydrocarbon degradation. Benzene remediation-associated genes were found using metagenomic analysis both in exposed and unexposed iron mats. Furthermore, the results indicated that season (summer vs. spring) exacerbates the negative effect of hydrocarbon exposure on community diversity and evenness and led to the increased abundance of numerous OTUs. This study represents the first of its kind to attempt to understand how contaminant exposure, specifically hydrocarbons, influences the geochemistry and microbial community of freshwater iron mats and further develops our understanding of hydrocarbon remediation at the land–water interface.

KEYWORDS

iron mat, iron-oxidizing bacteria, hydrocarbons, microbial community, biogeochemistry

Introduction

Hydrocarbon pollution is an international issue from the Deepwater Horizon Oil Spill to 500,000+ underground storage tanks leaking oil into groundwaters (as of September 2020) (Meegoda and Hu, 2011; Office of Underground Storage Tanks, D.C., 2020). However, an effective and efficient clean-up method for these contaminants has yet to be developed. This is highly problematic, as groundwaters can release toxic hydrocarbons into public drinking water or aboveground recreational waterways. In turn, hydrocarbons, such as benzene, can be highly hazardous to human health, resulting in leukemia and anemia (Badham and Winn, 2007). To combat this long-standing public health crisis, there is a plethora of work focused on hydrocarbon biodegradation. Efforts have usually focused on benzene, as it is highly mobile in groundwater (Minetti et al., 2017) and resistant to oxidation and degradation (Johnson et al., 2003). Benzene biodegradation more readily occurs under aerobic conditions, and it occurs via well-studied pathways (Jindrová et al., 2002). However, the application of aerobic degradation pathways is limited as oxygen is quickly expended in the water column leading to anoxia in contaminated zones (Keller et al., 2018). Because it is not limited by oxygen dissolution in groundwater, anaerobic benzene degradation has also been a focus of research (Keller et al., 2018). Previous terrestrial studies have focused primarily on groundwater environments, but approaches that attempt to incorporate the oxic–anoxic boundary are notably limited (Bradley, 2012). In a study using beach sand from Pensacola Beach, FL, an oxic–anoxic incubation model was found to increase the efficacy of the aerobic hydrocarbon degradation, as aerobic bioremediation was bolstered by the byproducts of anaerobic metabolisms produced during anoxic periods (Karthikeyan et al., 2020). As "oxic" and "anoxic" conditions are concurrent in the iron mat, it is possible that similar bolstering of hydrocarbon degradation occurs over time within this microbial community. Furthermore, the oxic–anoxic boundary where groundwater meets surface water is the last stop prior to widespread contamination by hydrocarbons. In this way, iron mats could be considered the last chance for hydrocarbon remediation using microbial communities before it outspreads.

The use of microorganisms to degrade hydrocarbons does not come without other challenges. Hydrocarbons increase stress in the environment by leading to the production of reactive oxygen species, which can damage microbial DNA (Liu et al., 2019). This, in turn, can impact the structure of microbial communities exposed to hydrocarbons by decreasing community diversity (Maila et al., 2005; Máthé et al., 2012; Sun et al., 2013). In a study of cyanobacterial mats in Berre lagoon, France, hydrocarbon exposure decreased the influence of seasonality (Aubé et al., 2016) possibly due to the tendency for hydrocarbon-inundated communities to skew toward more extremophilic organisms (Paissé et al., 2008; Abed et al., 2014). Microbial communities exposed to hydrocarbon contamination can also decrease in alpha diversity as a result of the decreased probability of horizontal gene transfer compared with communities exposed to other contaminants, such as heavy metals or antibiotics (Máthé et al., 2012).

The microbial communities in freshwater iron mats are already exposed to high concentrations of heavy metals and increased environmental stress, since iron-oxyhydroxides (FeOOH) produced by iron-oxidizing bacteria (FeOB) adsorb heavy metals (Field et al., 2019; Li et al., 2020), aromatic carbons (Baskar et al., 2012), phosphorous (Takeda et al., 2010; Buliauskaitė et al., 2020), and hydrophilic pesticides (Søgaard et al., 2001) from the water column. These environmental contaminants can easily desorb from the FeOOH when environmental conditions lead to changes in pH, ionic strength, oxygen concentrations, or flow (Little et al., 2016), which may lead to acute stress in iron mat communities. Due to the adsorptive properties of biogenic FeOOH, iron mats have been suggested to be useful in removing benzene and other hydrocarbons from contaminated sites (Abbas et al., 2016; Brooks and Field, 2020). The chemical properties of iron mats are not the only source of potential for benzene removal. There have been multiple studies that show involvement in the biodegradation of benzene and other hydrocarbons from functional groups such as sulfate-reducing bacteria (SRB) (Edwards and Grbić-Galić, 1992; Chakraborty and Coates, 2004; Keller et al., 2018), iron-reducing bacteria (FeRB) (Lovley et al., 1996; Jahn et al., 2005; Tremblay and Zhang, 2020), and nitrate-reducing bacteria (NRB) (Coates et al., 2001; Fahy et al., 2008; Atashgahi et al., 2018), which have been previously identified in iron mats. If hydrocarbon-degrading organisms are present and active, the iron mat community could prove to be an invaluable resource in application of hydrocarbon remediation at the oxic–anoxic boundary. Here, we present study from *in situ* sampling of iron mats that have been chronically exposed to benzene contamination in Town Creek, Greenville, NC.

In this environmental study, we have paired geochemical and molecular data to establish a baseline understanding of how hydrocarbons impact iron mats. We present how the presence of hydrocarbons correlates with geochemical condition, microbial community structure, and microbial functional potential in iron mats. This study serves as the beginning of our understanding of how FeOB-driven communities respond to hydrocarbon exposure, which may lead to future advancement in hydrocarbon remediation at the oxic–anoxic interface.

Materials and methods

Site description, sample collection, and geochemical analyses

The creek site, Town Creek, Greenville, NC (Figure 1), is in a residential area and consists of a low-flow creek with high banks lined with riprap. Sampling of iron mats and water samples took place over four time points for 2 years in March of 2018 and July and August of 2019. Samples were collected from upstream, unexposed iron mats (U) and downstream, hydrocarbon-exposed iron mats (Da, Db). Samples for biological molecular analysis were collected aseptically and stored on ice until they were transported to the laboratory and stored at −80°C. Samples of iron mats were also processed via filtration in an acid-washed top-bottle filter using pre-ashed (500°C, 4 h) Whatman glass microfiber filters, Grade 934-AH (1.5 µm pore size, GE Healthcare Bio-Sciences, Marlborough, MA), and filtrates were stored on ice and transported to the laboratory where they were stored at −20°C until they could be analyzed. Sample analysis for phosphate, ammonia, nitrates/nitrites (SmartChem 170 and 200 Discrete Analyzer, Unity Scientific), and dissolved organic carbon (DOC) (TOC-LCPH/CPN PC-Controlled TOC Analyzer and ASI-L

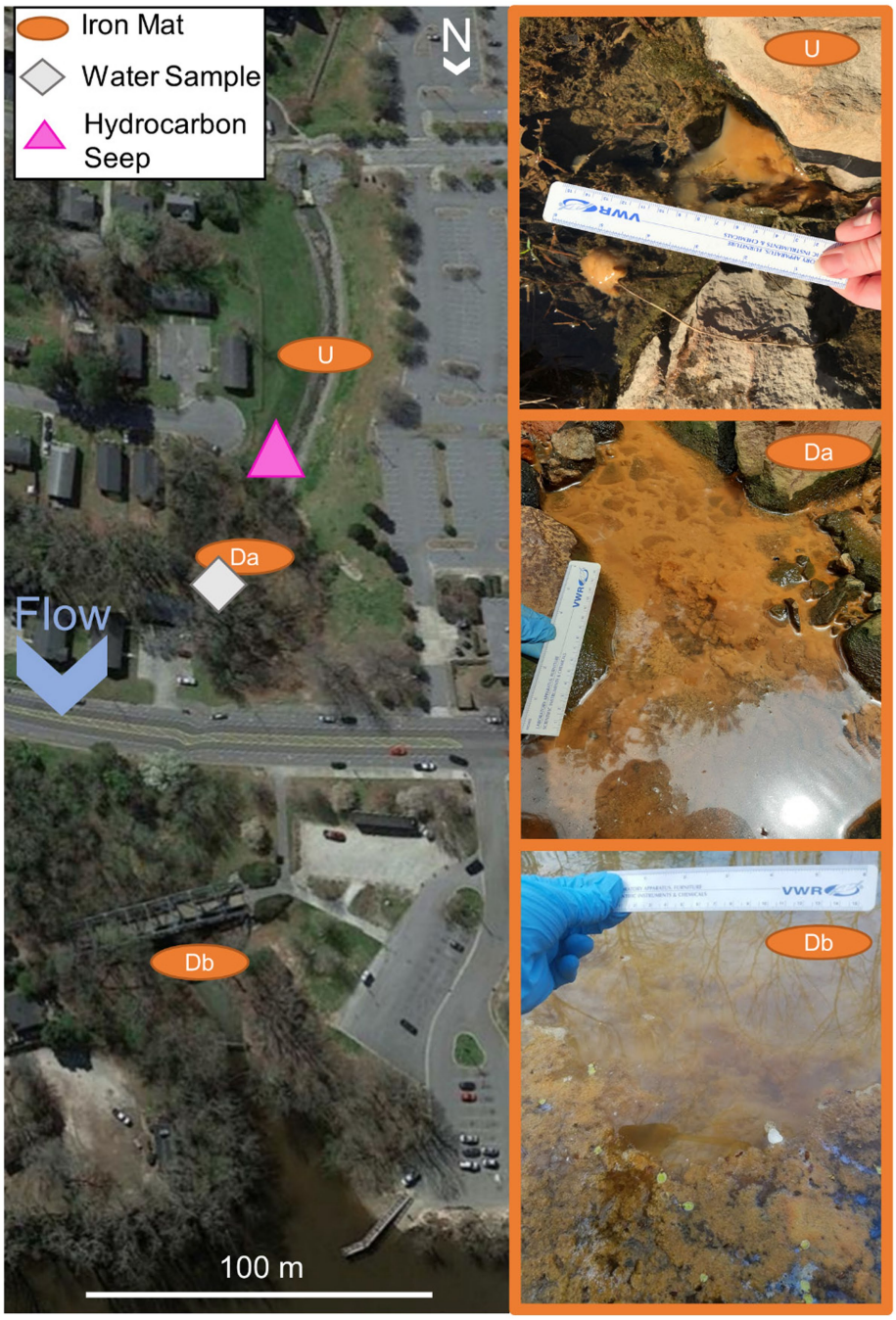

FIGURE 1
A map of Town Creek, Greenville, NC. Iron mat sampling locations indicated with orange ovals labeled with iron mat location ID: Upstream (U) unexposed, Downstream A (Da) hydrocarbon-exposed, or Downstream B (Db) hydrocarbon-exposed. The water sampling site (W) hydrocarbon-exposed is indicated by a gray diamond and was chosen so as to be as far across the creek cross-section from iron mat sample as possible to avoid confounding results. The hydrocarbon seeps are indicated by the pink triangle. Seep location based on the study by Humphrey et al. (2018). Map obtained from Google Earth Pro v. 7.3.3.7786 and modified with iron mat, benzene seep, and water sample locations and inset images.

Autosampler, Shimadzu Scientific Instruments, Inc.) was carried out by the Environmental Research Laboratory at East Carolina University, Greenville, NC. Iron mat was also collected in pre-treated bottles containing ascorbic acid provided by the Environment 1, Inc. lab in Greenville, NC. Immediately after collection, hydrochloric acid was added to the samples, and they were stored at 4°C until they were analyzed using the EPA method 602 (Warner et al., 1984). Measurements of total iron, oxidized iron (Fe^{3+}), and reduced iron (Fe^{2+}) for all sampling sites were conducted immediately followed by sampling using the ferrozine method (Lovley and Phillips, 1987). Measurements of pH, conductivity, dissolved oxygen, and water temperature were taken using a YSI Quatro Professional Plus (YSI Inc., Yellow Springs, OH).

DNA extraction, 16S rDNA sequencing, and phylogenetic analysis

The QIAGEN DNeasy PowerSoil Kit (Qiagen, Germantown, MD) was used according to the manufacturer's instructions for each mat sample with the following modifications: DNA was eluted in 60 µL and cell lysis occurred using a 10-min cycle in a Disruptor Genie (Scientific Industries, Inc., Bohemia, NY) set to maximum speed. 16S rDNA sequencing of the V4-V5 region was performed at the Comparative Genomics and Evolutionary Bioinformatics' Integrated Microbiome Resource (CGEB-IMR, Halifax, NS) using universal primers 515FB and 926R (Parada et al., 2016; Walters et al., 2016). Sequences were processed and annotated using mothur v. 1.44.1 (Schloss et al., 2009, 2011; Kozich et al., 2013) and the SILVA database v. 138.1 (Quast et al., 2013). The MiSeq SOP was accessed on 13 April 2020[1] and used to identify present taxa (97% OTU threshold). Further analyses were performed in R v. 3.5.2 using phyloseq v. 1.26.1 (McMurdie and Holmes, 2013) to import mothur data into R, perform quality checks, calculate alpha diversity indices, ordination, and calculate relative abundances. All samples were rarified to even depth (sample size of 6,883) based on the smallest sample with a set seed prior to alpha diversity and evenness calculations. The package microbiome v. 1.4.2 (Lahti et al., 2017) was used to convert data into a centered log ratio format for beta diversity indices and calculate Pielou's Evenness. Before calculating beta diversity indices, a centered log ratio was used to transform the count data into dominance of taxa compared with the geometric mean of all taxa on a log scale, and the principle coordinates analysis was performed using a redundancy analysis (RDA). The package vegan v. 2.5–6 (Oksanen et al., 2019) was used to convert phyloseq objects into Euclidean distance and beta dispersion and calculate statistics for the Canonical Correspondence Analysis (CCA). A permutation ANOVA (PERMANOVA) was used to test each of the margins (factors) (number of permutations = 9,999) for variance inflation factors, calculated using *vif.cca()*. CCA was chosen to show overall community structuring as it was most useful in building a model of community structuring in response to the numerous environmental factors measured. The package picante v. 1.8.2 (Kembel et al., 2010) was used to create a data frame with alpha diversity measurements. The package edgeR v. 3.24.3 (Robinson et al., 2009; McCarthy et al., 2012) was used to calculate the log-fold change (logFC) of OTUs between benzene exposed and unexposed sites. Phyloseq objects were converted to edgeR objects using the phyloseq extension accessed on 6 January 2020.[2] Samples were filtered for independence using a variance threshold set to $1e^{-7}$ prior to calculating logFC. Visuals were generated using ggplot2 v. 3.3.2 (Wickham, 2016), and relative abundances were converted to percentages for visualization using the package scales v. 1.1.1 (Wickham and Seidel, 2020). Color blind accessible palettes were applied to graphs using ggthemes v. 4.2.0 (Ichihara et al., 2008; Chang, 2013; Arnold, 2019).

1 https://mothur.org/wiki/miseq_sop/

2 https://joey711.github.io/phyloseq-extensions/edgeR.html

Metagenomic sequencing, assembly, and metagenomic-assembled genome annotation

DNA extraction methods for metagenomic sequencing were performed for 16S rDNA amplicon sequencing. Metagenomes were sequenced at CGEB-IMR using the Illumina Nextera Flex for the NextSeq at 3x depth paired-end reads. Sequence adapters were trimmed using TrimGalore v. 0.4.5 (Krueger, 2015), and sequence loss was assessed using FastQC v. 0.11.5 (Andrews, 2010). Reads were assembled using SPAdes v. 3.13.0 (Bankevich et al., 2012), and unpaired reads were preserved. Assembly quality was assessed using the MetaQUAST function in QUAST v. 5.0.2 (Gurevich et al., 2013) (Supplementary Table S5). Assemblies were binned into Metagenomic Assembled Genomes (MAGs) using MaxBin v. 2.2.7 (Wu et al., 2014), CONCOCT v. 1.0.0 (Alneberg et al., 2013), and Metabat2 v. 2.14 (Kang et al., 2019). All bins were aggregated using DAS Tool v. 1.1.2 (Sieber, 2017). The quality of each MAG was checked using the CheckM v. 1.0.18 (Parks et al., 2015) lineage-specific workflow (Supplementary File S3). Bin identities of MAGs (> 59% complete, < 10% contamination) were determined using MetaSanity v. 1.2.0 (Neely et al., 2020) PhyloSanity pipeline. MAG genome size and GC content were calculated using the RASTtk server (Aziz et al., 2008; Overbeek et al., 2014; Brettin et al., 2015) accessed on January 2021.

Assembled MAG FASTA files were imported into the online user interface for KBase (Arkin et al., 2018) on 28 December 2021. MAG classifications were verified using "Classify Microbes with GTDB-Tk – v.1.7.0" on 29 December 2021 (Chaumeil et al., 2020). MAG assemblies were annotated using "Annotate and Distill Assemblies with DRAM" on 19 May 2022 (Shaffer et al., 2020). Representative FeOB isolate genomes were sourced from NCBI on 21 February 2022. Assemblies were grouped in KBase using "Build AssemblySet – v1.0.1" and annotated with "Annotate and Distill Assemblies with DRAM" on 16 May 2022. Figures were compiled and edited in Vega-Lite (Satyanarayan et al., 2017). Representative FeOB assemblies chosen were BioProject: PRJNA32827 (*Gallionella capsiferriformans* ES-2 (b-proteobacteria)) (D. Emerson, unpublished), BioProject: PRJNA13615 (*Mariprofundus ferrooxydans* PV-1) (Emerson and Moyer Craig, 2002), BioProject: PRJNA56115 (*Leptothrix ochracea* L12) (E. Fleming, unpublished), BioProject: PRJNA224116 (*Ferriphaselus amnicola* strain OYT1 chromosome, complete genome) (S. Kato, unpublished), and BioProject: PRJNA542651 [*Mariprofundus erugo* (proteobacteria)] (Garrison et al., 2019).

Hidden Markov models

Assembled and unpaired reads from SPAdes were filtered to remove contigs with fewer than 500 base pairs using filter_contigs.py (accessed 2020 AUG 5; https://github.com/tinybio/filter_contigs) and was subsequently filtered for contigs that had at least 1.5x coverage using another python script (accessed 2020 AUG 5; https://microsizedmind.wordpress.com/2015/03/05/removing-small-low-coverage-contigs-from-a-spades-assembly/) (Gihawi et al., 2019). The remaining contigs were annotated by prokka v. 1.14.5 (Seemann, 2014) using the *--metagenome* flag. The UniProtKB database (accessed 2021 JAN 28; https://www.uniprot.org/) (Boutet et al., 2007) was used to find benzene-metabolism-related genes. The search term

"taxonomy:"Bacteria [2]" (benzene metabolism) AND reviewed: yes" was used, and the reviewed sequences were downloaded. Sequences for anaerobic benzene carboxylase (*ubiD*) (Atashgahi et al., 2018), periplasmic nitrate reductase (*napA*) (Schaedler et al., 2018), and aerobic toluene-4-monooxygenase (*tmoABCDEF*) (Atashgahi et al., 2018) were also retrieved from the database. As toluene-4-monooxygenase did not have a reviewed representative, the unreviewed sequences were used. Using MMseqs2 v. 12.113e3 (Steinegger and Söding, 2017), the sequences were collapsed using a 70% sequence identity cutoff to remove overrepresented protein sequences. The sequences were then aligned using Clustal Omega v. 1.2.4 (Sievers et al., 2011; Sievers and Higgins, 2017) and returned in Stockholm format using *--outfmt = st*. A hidden Markov model (HMM) was built from this file using the hmmbuild function of HMMER v. 3.2.1 (Eddy, 1998). The HMM was used to search the annotated contigs using the hmmsearch function of HMMER v. 3.2.1 (Eddy, 1998). Gene counts were normalized for total open reading frame number using OrfM v. 0.7.1 (Woodcroft et al., 2016). Assemblies were also analyzed for iron-cycling-related genes using FeGenie v. 1 (Garber et al., 2020). Assemblies were annotated using Prodigal v. 2.6.3 (Hyatt et al., 2010) contig_source *meta*. Gene counts were normalized using norm *y*.

Visuals for both HMM and FeGenie results were generated using ggplot2 v. 3.3.2 (Wickham, 2016), ggpubr v. 0.4.0 (Kassambara, 2020), and reshape v. 0.8.8 (Wickham, 2007). Gene count normalizations were converted to percentages for visualization using the package scales v. 1.1.1 (Wickham and Seidel, 2020). Color blind accessible palettes were applied to graphs using rcartocolor v. 2.0.0 (Nowosad, 2018).

Sequence data availability

The 16S rDNA amplicon sequences are available at NCBI BioSample accession numbers SAMN39732271, SAMN39732272, SAMN39732273, SAMN39732274, SAMN39732275, SAMN39732276, SAMN39732277, SAMN39732278, SAMN39732279, and SAMN39732280. The metagenomic sequences are available at NCBI BioProject PRJNA1072096 with BioSample accession numbers SAMN39944932, SAMN39944933, SAMN39944934, SAMN33944935, SAMN33944936, SAMN33944937, SAMN33944938, SAMN33944939, SAMN39944940, and SAMN39944941. The ".fasta" files for each MAG assembly are available at https://kbase.us/n/105846/210/ via static narrative.

Results

Site conditions

Samples were collected over four sampling trips from one iron mat upstream and two iron mats downstream of a leaking underground storage tank seepage site in Town Creek, Greenville, NC (Figure 1). The upstream mat (U) served as a reference (unexposed) iron mat community within the system that was not impacted by the leaking underground storage tanks. Downstream, hydrocarbon-exposed mats (Da and Db) and water samples (W) were collected. Samples were collected twice in spring, March 2018 (S1 and S2), as well as two sampling efforts in summer, July (S3) and August (S4), 2019, to gain a broader understanding of microbial community dynamics over time.

Geochemistry

Analytical measurements from the unexposed and hydrocarbon exposed mats are shown in Supplementary Table S1. Comparisons between hydrocarbon-exposed and hydrocarbon-unexposed iron mats were made using Wilcoxon Rank Sum Tests. Hydrocarbon-exposed mats had significantly higher concentrations of oxidized iron ($p = 0.043$) and salinity ($p = 0.014$) than unexposed mats (Figure 2). Unexposed mats had significantly higher concentrations of dissolved organic carbon ($p = 0.034$) and dissolved PO_4^{3-} ($p = 0.009$) (Figure 2). Comparisons between sampling seasons (spring vs. summer) were made using Wilcoxon Rank Sum Tests. Sampling season had a significant effect on water temperature (°C) ($p = 0.002$) and pH ($p = 0.004$) (Figure 3).

The hydrocarbon-exposed iron mats represented two previously observed mat types: flocculent and seep (Fleming et al., 2014). Flocculent mats are loosely associated and centimeters thick. Seep mats are densely associated and millimeters thick. All unexposed mats were seep mats and were not included in this statistical comparison due to their different geochemistry from exposed mats. Flocculent and seep mats had significantly different concentrations of reduced iron ($p = 0.044$), oxidized iron ($p = 0.44$), benzene ($p = 0.044$), ethylbenzene ($p = 0.044$), xylene ($p = 0.044$), and total dissolved PO_4^{3-} ($p = 0.027$) (Wilcoxon Rank Sum Tests; Figure 4). Compared with the exposed water samples, flocculent and seep mats had significantly different concentrations of reduced iron ($p = 0.044$, 0.000), oxidized iron ($p = 0.044$, 0.000), benzene ($p = 0.049$, 0.014), and dissolved nitrates and nitrites (NO_x^-) ($p = 0.044$, 0.024) (Wilcoxon Rank Sum Tests; Figure 4). Benzene concentrations were observed to be lower in the flocculent mats than seep mats or water samples, and flocculent mats had higher dissolved PO_4^{3-} concentrations than seep mats.

Of the analytes measured, concentration of dissolved phosphate (PO_4^{3-}) had the only significant negative correlation with the concentration of benzene (Pearson Correlation; $R^2 = 0.95$, $p = 1.6e^{-6}$; Figure 5A) and the hydrocarbon-exposed water samples ($R^2 = 0.58$, $p = 0.028$). In the hydrocarbon-exposed iron mats, the concentration of reduced iron ($R^2 = 0.46$, $p = 0.031$), oxidized iron ($R^2 = 0.56$, $p = 0.013$), ethylbenzene ($R^2 = 0.93$, $p = 5.4e^{-6}$), and xylene ($R^2 = 0.91$, $p = 2.2e^{-5}$) had significant positive correlations with the concentration of benzene (Figure 5). In the hydrocarbon-exposed water samples, the concentration of reduced iron ($R^2 = 0.58$, $p = 0.027$), ethylbenzene ($R^2 = 0.55$, $p = 0.035$), and total dissolved nitrogen ($R^2 = 0.57$, $p = 0.03$) had significant positive correlations with the concentration of benzene. In the hydrocarbon-exposed iron mats, PO_4^{3-} also had a significant negative correlation with oxidized iron ($R^2 = 0.71$, $p = 0.0021$), which was not observed in the hydrocarbon-exposed water samples ($R^2 = 0.24$, $p = 0.22$) or unexposed iron mats ($R^2 = 0.13$, $p = 0.38$).

Community richness, diversity, and structure

Bacterial community composition was determined using operational taxonomic unit (OTU) relative abundances and was compared between exposed and unexposed iron mats. The alpha

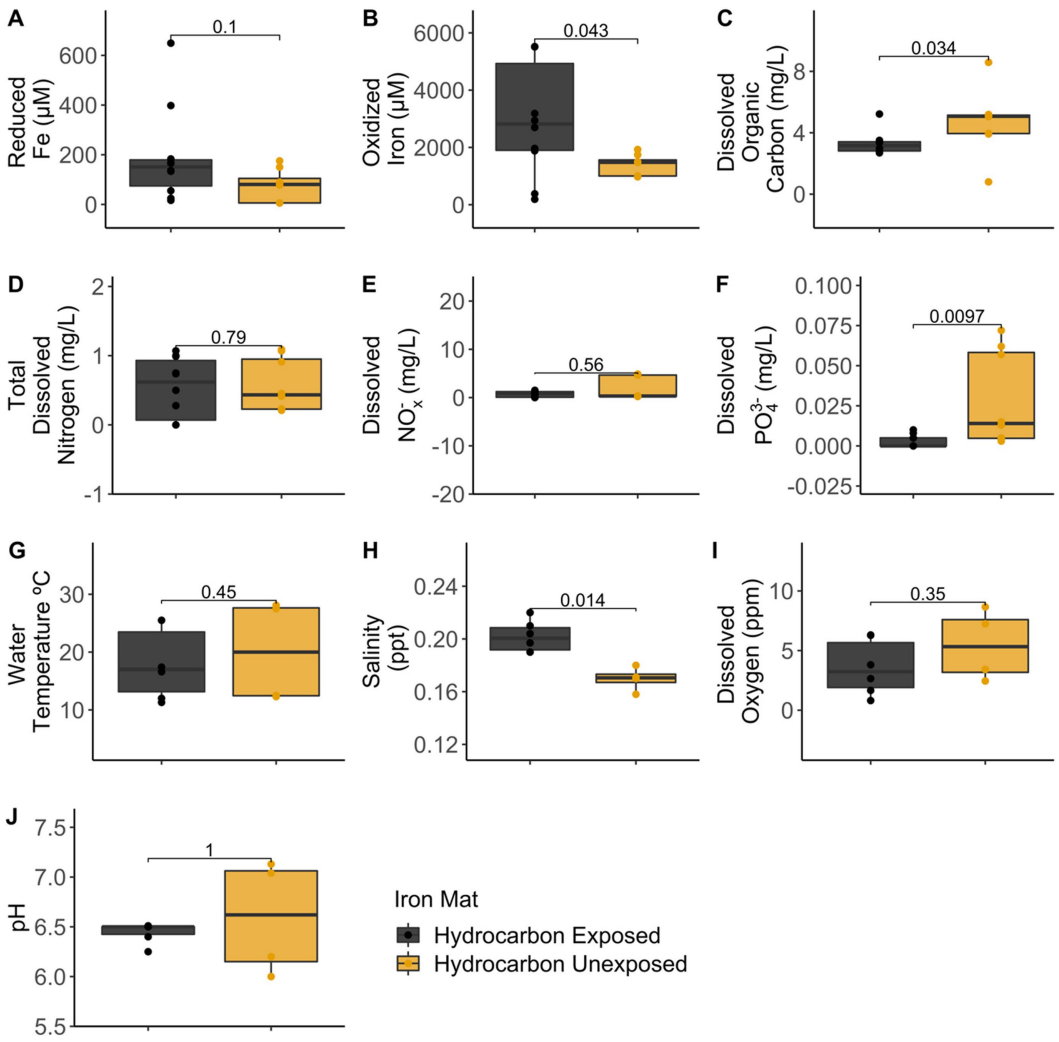

FIGURE 2
Comparisons between hydrocarbon-exposed (black) and unexposed (yellow) iron mats were made using Wilcoxon Rank Sum Tests for the measured analytes: **(A)** reduced iron (μM), **(B)** oxidized iron (μM), **(C)** dissolved organic carbon (mg/L), **(D)** total dissolved nitrogen (mg/L), **(E)** dissolved nitrates and nitrites (NO_x^-) (mg/L), **(F)** total dissolved phosphate (PO_4^{3-}) (mg/L), **(G)** water temperature (°C), **(H)** salinity (ppt), **(I)** dissolved oxygen (ppm), and **(J)** pH.

diversity indices (Supplementary Figure S1) and evenness index (Supplementary Figure S2) were significantly lower in exposed iron mats than unexposed iron mat microbial communities (e.g., Simpsons $U = 0$, $p = 0.01421$). Beta diversity did not significantly vary between exposed and unexposed iron mat microbial communities (ADONIS $R^2 = 0.12644$, $p = 0.234$, strata = hydrocarbon exposure). Across seasons (spring vs. summer), alpha diversity (Supplementary Figure S3) and evenness (Supplementary Figure S4) were not significantly different. However, when evenness was modeled for both season and hydrocarbon exposure as factors, it was significantly different between seasons ($F = 28.77$, $p = 0.001$) and hydrocarbon exposure ($F = 42.58$, $p = 0.0003$). Beta diversity was also significantly different in iron mat communities when season was used as the stratum (ADONIS $R^2 = 0.25$, $p = 0.004$, strata = season) (Supplementary Figure S5), and multiple OTUs were observed to be increased or decreased in abundance depending on season (Supplementary Figure S6).

The phylum Proteobacteria had the greatest relative abundance among exposed (average 85%) and unexposed (average 69%) iron mat microbial communities, followed by Bacteroidetes (average 10 and 19%, respectively) (Figure 6). OTUs of significantly higher abundance were found using a log-fold change (logFC) analysis and were classified to be in the phyla Proteobacteria, Bacteroidetes, and Cyanobacteria (Figure 7). There were 11 OTUs with increased abundance in the unexposed iron mat microbial communities and 12 OTUs with increased abundance in the hydrocarbon-exposed iron mat microbial communities. The most highly abundant OTUs in the unexposed iron mats were classified to belong to the family Chitinophagaceae and the genus *Emticicia* (family Spirosomaceae). The most highly abundant OTUs in the hydrocarbon-exposed iron mats were classified to belong to the family Methylococcaceae and the class Gammaproteobacteria.

Using a Canonical Correspondence Analysis (CCA), we observed that dissolved oxygen had the greatest statistical prediction power for community structure in the iron mats (PERMANOVA $F = 2.61$, $p = 0.0033$), followed by pH (PERMANOVA $F = 2.22$, $p = 0.0192$) and benzene concentration (PERMANOVA $F = 1.06$, $p = 0.4326$)

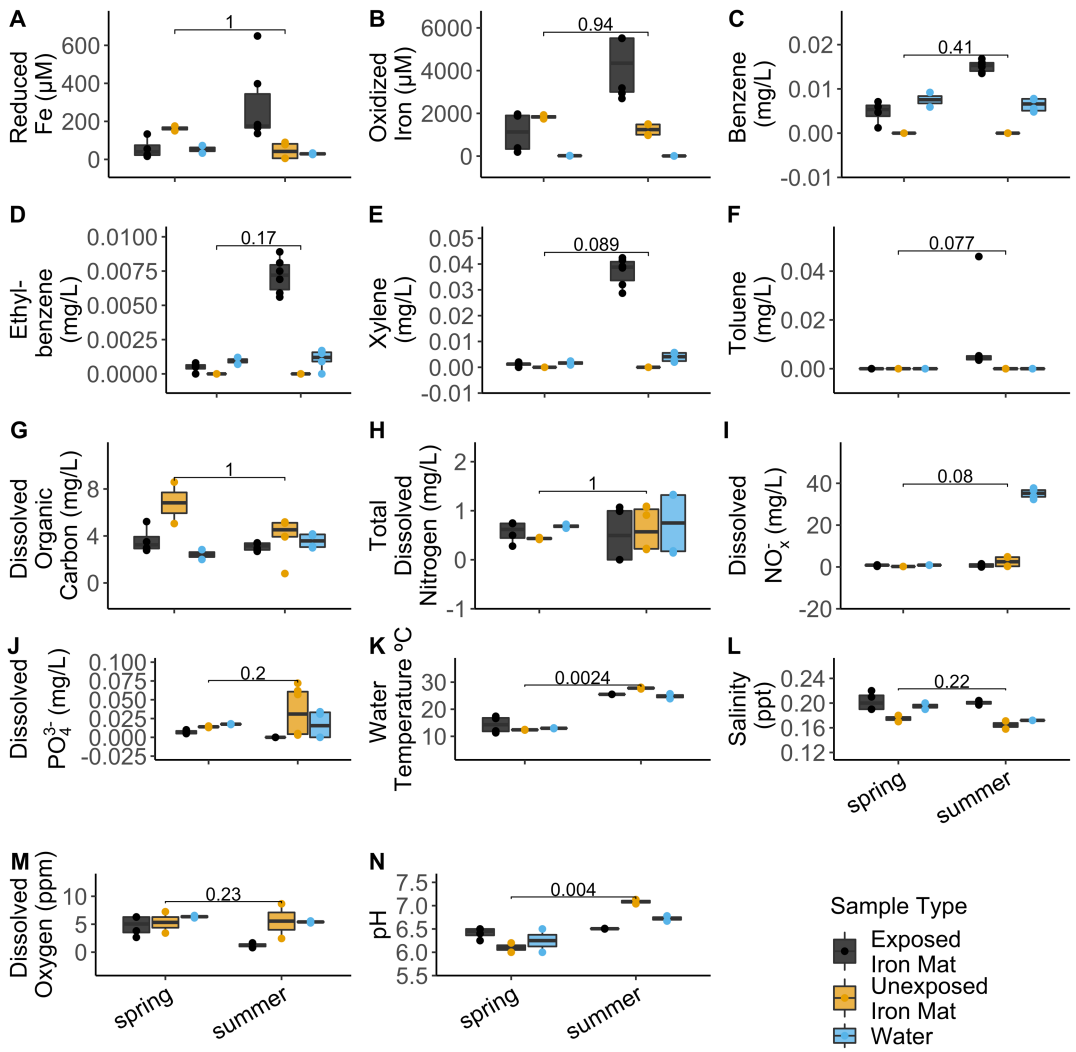

FIGURE 3
Comparisons for the measured analytes **(A)** reduced iron (µM), **(B)** oxidized iron (µM), **(C)** benzene (mg/L), **(D)** ethylbenzene (mg/L), **(E)** total xylenes (mg/L), **(F)** toluene (mg/L), **(G)** dissolved organic carbon (mg/L), **(H)** total dissolved nitrogen (mg/L), **(I)** dissolved nitrates and nitrites (NO_x^-) (mg/L), **(J)** total dissolved phosphate (PO_4^{3-}) (mg/L), **(K)** water temperature (°C), **(L)** salinity (ppt), **(M)** dissolved oxygen (ppm), and **(N)** pH between seasons (spring vs. summer) were made using Wilcoxon Rank Sum Tests. The results are displayed by sample type: hydrocarbon-exposed iron mat (black), unexposed iron mat (yellow), or hydrocarbon-exposed water sample (blue).

(Figure 8). The vertical axis, represented by dissolved oxygen and benzene, together rendered the greatest separation between microbial communities from each unique sample. This separation was more apparent in summer than spring samples.

Biogeochemical cycling potential—amplicon sequencing and metagenomes

The iron mat microbial community 16S amplicons were analyzed for taxa that potentially represent functional groups previously associated with iron mat biogeochemical cycling. These functional groups included iron-oxidizing bacteria, iron-reducing bacteria, sulfate-reducing bacteria, and nitrate-reducing bacteria. A special focus was also given to sequences that were classified as taxa that may be hydrocarbonoclastic bacteria (generally associated with the obligate use of hydrocarbons) or use benzene-degrading pathways.

Of the genera previously associated with microaerophilic iron-oxidation (Weiss et al., 2007; Fabisch et al., 2013; Kato et al., 2014; Fleming et al., 2018), only *Leptothrix* spp. were observed in the Town Creek iron mats by 16S rDNA amplicon sequence taxonomic classification (0.0095% relative abundance in hydrocarbon exposed mats, 0.0045% in unexposed mats). However, microscopy of iron mat samples revealed some FeOOH with a stalk morphology, which is associated with the stalk-forming *Gallionella* spp. (Fleming et al., 2014; Emerson et al., 2015; Gagen et al., 2018) These results, when paired, suggest that both stalk and sheath forming FeOB contribute to the production of iron mats in Town Creek.

Of the organisms that may play a role in anaerobic iron-oxidation, sequences for the putative nitrate-reducing iron-oxidizing bacteria in the genera *Acidovorax, Aquabacterium, Azospira, Paracoccus, Thermomonas,* and *Thiobacillus* (Hedrich et al., 2011) were recovered from both hydrocarbon-exposed and hydrocarbon-unexposed iron mats, with a higher relative abundance in hydrocarbon-exposed mats.

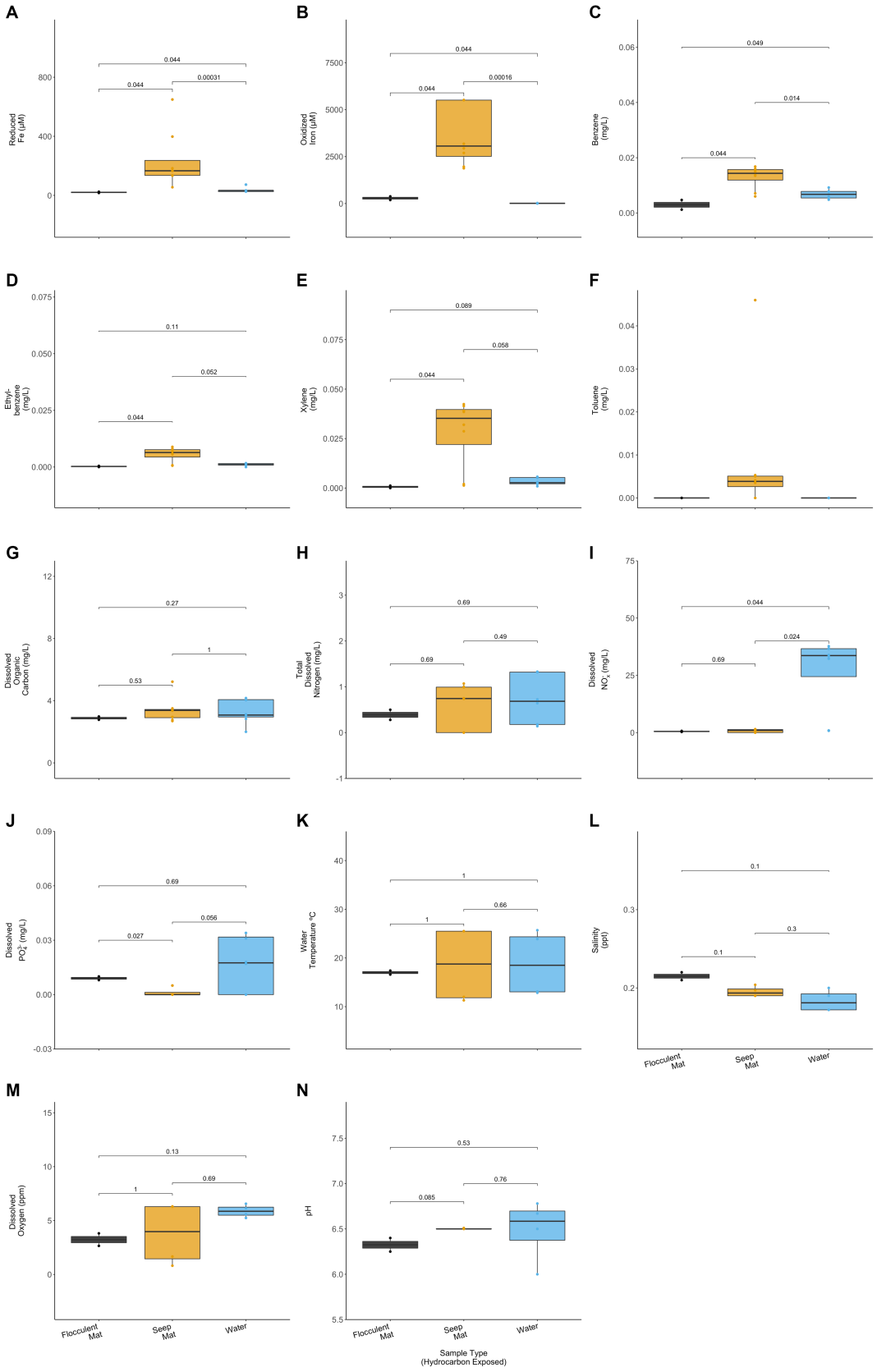

FIGURE 4
Hydrocarbon-exposed iron mats were designated to a mat type, either flocculent (black) or seep (yellow). Flocculent mats were in looser association and centimeters thick, whereas seep mats were denser and millimeters thick (Fleming et al., 2014). Mat types are plotted here with the hydrocarbon exposed water samples (blue) for **(A)** reduced iron (μM), **(B)** oxidized iron (μM), **(C)** benzene (mg/L), **(D)** ethylbenzene (mg/L), **(E)** total xylenes (mg/L),

(Continued)

FIGURE 4 (Continued)

(F) toluene (mg/L), **(G)** dissolved organic carbon (mg/L), **(H)** total dissolved nitrogen (mg/L), **(I)** nitrates and nitrites (NO_x^-) (mg/L), **(J)** total dissolved phosphate (PO_4^{3-}) (mg/L), **(K)** water temperature (°C), **(L)** salinity (ppt), **(M)** dissolved oxygen (ppm), and **(N)** pH. Only two of the sampled iron mats were classifiable as flocculent, and both were sampled in spring. *p*-values for comparisons were calculated using Wilcoxon Ranked Sum Tests.

Putative photoferrotrophic sequences were classified to the genera *Rhodobacter*, *Rhodomicrobium*, and *Rhodovulum* (Hedrich et al., 2011). These sequences had a higher relative abundance in unexposed iron mats.

On average, sequences classified as genera associated with FeRB (Supplementary Table S2) totaled 0.755 and 0.971% relative abundance of sequences from hydrocarbon-exposed and unexposed iron mats, respectively. Of these, the genus *Geobacter* has the potential to couple iron reduction with benzene degradation (Tremblay and Zhang, 2020) and represented an average of 0.56 and 0.74% relative abundance of hydrocarbon-exposed and unexposed iron mats, respectively. Sequences classified as genera associated with SRB (Supplementary Table S3), on average, 0.143 and 0.209% relative abundance of hydrocarbon-exposed and hydrocarbon-unexposed iron mats, respectively. Amplicon sequences were classified as the genus *Desulfobacula*, which may couple sulfate reduction with benzene degradation (Chakraborty and Coates, 2004), averaged 0.0026 and 0.0010% relative abundance of hydrocarbon-exposed and hydrocarbon-unexposed iron mats. Amplicon sequences classified as the genera *Hydrogenophaga* and *Dechloromonas*, which have the potential to couple nitrate reduction to benzene degradation (Coates et al., 2001; Fahy et al., 2006, 2008), were observed in hydrocarbon-exposed (average 5.27 and 0.16%, respectively) and hydrocarbon-unexposed (average 3.96 and 0.19%, respectively) iron mats. Only one genus of hydrocarbonoclast, *Planomicrobium,* was represented in classified amplicon sequences. *Planomicrobium* had a greater relative abundance in unexposed iron mat communities; however, they accounted for a very small relative abundance of these sequences (<0.0025%) from any sample.

Assembled contigs from the metagenomic sequences were assessed for quality (Supplementary Table S4) and then assigned functional potential using HMM analysis. There was no significant difference between hydrocarbon-exposed and unexposed sequences for iron-cycling (e.g., *cyc1, cyc2, mtrB, and mtoA*) or benzene-remediation (e.g., *napA, ubiA, fdnGHI, and pcrA*) gene sequence-normalized abundance (Supplementary Figures S7, S8).

Recovered MAGs

Twenty-nine MAGs were recovered from the iron mat samples (> 59% complete, < 10% contamination) (Supplementary File S3). Hydrocarbon exposure did not have an observable effect on genome size (unexposed average 2.57 ± [standard error = SE] 0.24 Mbp; hydrocarbon exposed average 2.61 ± SE 0.13 Mbp) or GC content (unexposed average 52.67 ± SE 4.68%; hydrocarbon exposed average 55.4 ± SE 2.17%). Greater taxonomic diversity in the MAGs was recovered from the unexposed iron mats, including two MAGS that were classified as the protist endosymbiont, *Phycorickettsia* spp. (Yurchenko et al., 2018). Seven MAGs (one unexposed/six hydrocarbon-exposed) were classified as belonging to the genus *Gallionella* (avgerage genome completeness 96%, contamination 2%). Eight MAGs (one unexposed/seven hydrocarbon-exposed) were classified as belonging to the family Burkholderiaceae (avgerage genome completeness 93%, contamination 3%). Seven of the eight Burkholderiaceae MAGs, excluding only MAG #13, had genomic evidence of iron oxidation genes (*cyc1*, *cyc2*, *mtrB*, and *mtoA*) based on the FeGenie analysis (Supplementary Table S5).

Whole genome representatives of FeOB from NCBI including *Mariprofundus ferrooxydans* PV-1, *Mariprofundus erugo*, *Gallionella capsiferriformans* ES-2, *Ferriphaselus amnicola*, and *Leptothrix ochracea* (Supplementary File S4) were annotated using DRAM, as well as the Burkholderiaceae family (Supplementary File S5) and *Gallionella* spp. (Supplementary File S6) MAGs. Of the isolated representatives of microaerophilic FeOB, *Leptothrix ochracea* was the most dissimilar, missing modules for the Entner-Doudoroff and reductive acetyl-CoA pathways, and ETC complexes NADH: quinone oxidoreductase, succinate dehydrogenase, and cytochrome bd ubiquinol oxidase. *L. ochracea* was also missing indicators of carbohydrate-active enzymes (CAZY), methanogenesis, and short-chain fatty acid metabolisms that were present in all other FeOB isolates. Of those MAGs assigned to the family Burkholderiaceae, MAG 26 was missing module for the Entner–Duodoroff and reductive acetyl-CoA pathways, as well as the CAZY, methanogenesis, and short-chain fatty acid metabolism indicators missing from the *L. ochracea* genome. All eight MAGs classified as Burkholderiaceae were missing from the ETC complex succinate dehydrogenase. Of the MAGs assigned to the genus Gallionella, all seven MAGs were missing modules for the Entner–Duodoroff pathway, as well as the ETC complexes for succinate dehydrogenase and cytochrome bd ubiquinol oxidase.

Discussion

This study of the freshwater iron mat system begins to address how contaminant hydrocarbon exposure influences geochemistry, microbial community structure, and potential microbial function. We found that hydrocarbon exposure had a significant effect on iron mat-oxidized iron, dissolved organic carbon, and dissolved PO_4^{3-}, independent of seasonal effects. Organic carbon concentration has been previously associated with *Leptothrix ochracea*-dominated iron mats (Fleming et al., 2014), such as those in Town Creek. The higher observed dissolved organic carbon in the unexposed iron mats helps to explain the higher number of recovered *Gallionella* spp. MAGs from the hydrocarbon exposed iron mats, where conditions likely were less favorable to *Leptothrix ochracea*.

Our amplicon sequencing results showed the presence of photoferrotrophs in the iron mats. The photoferrotrophs had a higher relative abundance in the unexposed iron mats, which may reflect the decreased irradiance in water exposed to hydrocarbons from the leaking underground storage tanks. In hydrocarbon-contaminated water, there was a thin sheen of both oxidized iron ("schwimmeisen")

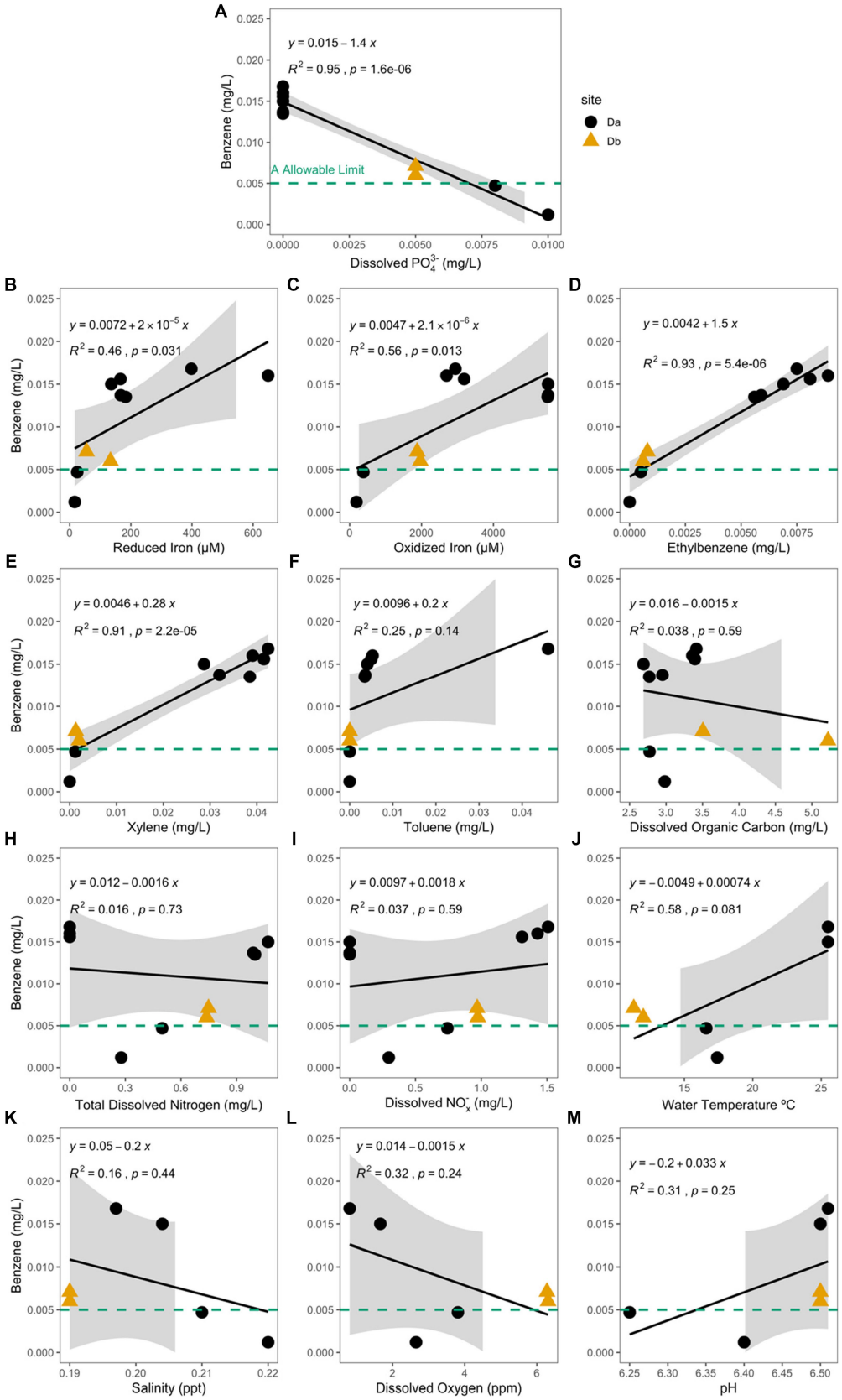

FIGURE 5
Benzene concentration (mg/L) at the hydrocarbon-exposed iron mat sampling sites, Da (black circle) and Db (yellow triangle) are plotted here against the measured analytes **(A)** total dissolved phosphate (PO_4^{3-}) (mg/L), **(B)** reduced iron (μM), **(C)** oxidized iron (μM), **(D)** ethylbenzene (mg/L), **(E)** total xylenes (mg/L), **(F)** toluene (mg/L), **(G)** dissolved organic carbon (mg/L), **(H)** total dissolved nitrogen (mg/L), **(I)** dissolved nitrates and nitrites (NO_x^-)

(Continued)

FIGURE 5 (Continued)

(mg/L), **(J)** water temperature (°C), **(K)** salinity (ppt), **(L)** dissolved oxygen (ppm), and **(M)** pH. The EPA allowable limit for benzene (0.005 mg/L) is designated by a green-dashed line in each panel. Db was only measured during the first two time points (S1 and S2). Correlation and significance were calculated using a standard linear model, and the calculated equation is included on each panel. PO_4^{3-} and benzene concentrations in the hydrocarbon-exposed iron mats have a significant negative correlation ($R^2 = 0.95$, $p = 1.6e^{-6}$), which is stronger than the correlation in the hydrocarbon-exposed water samples (not shown; $R^2 = 0.58$, $p = 0.028$).

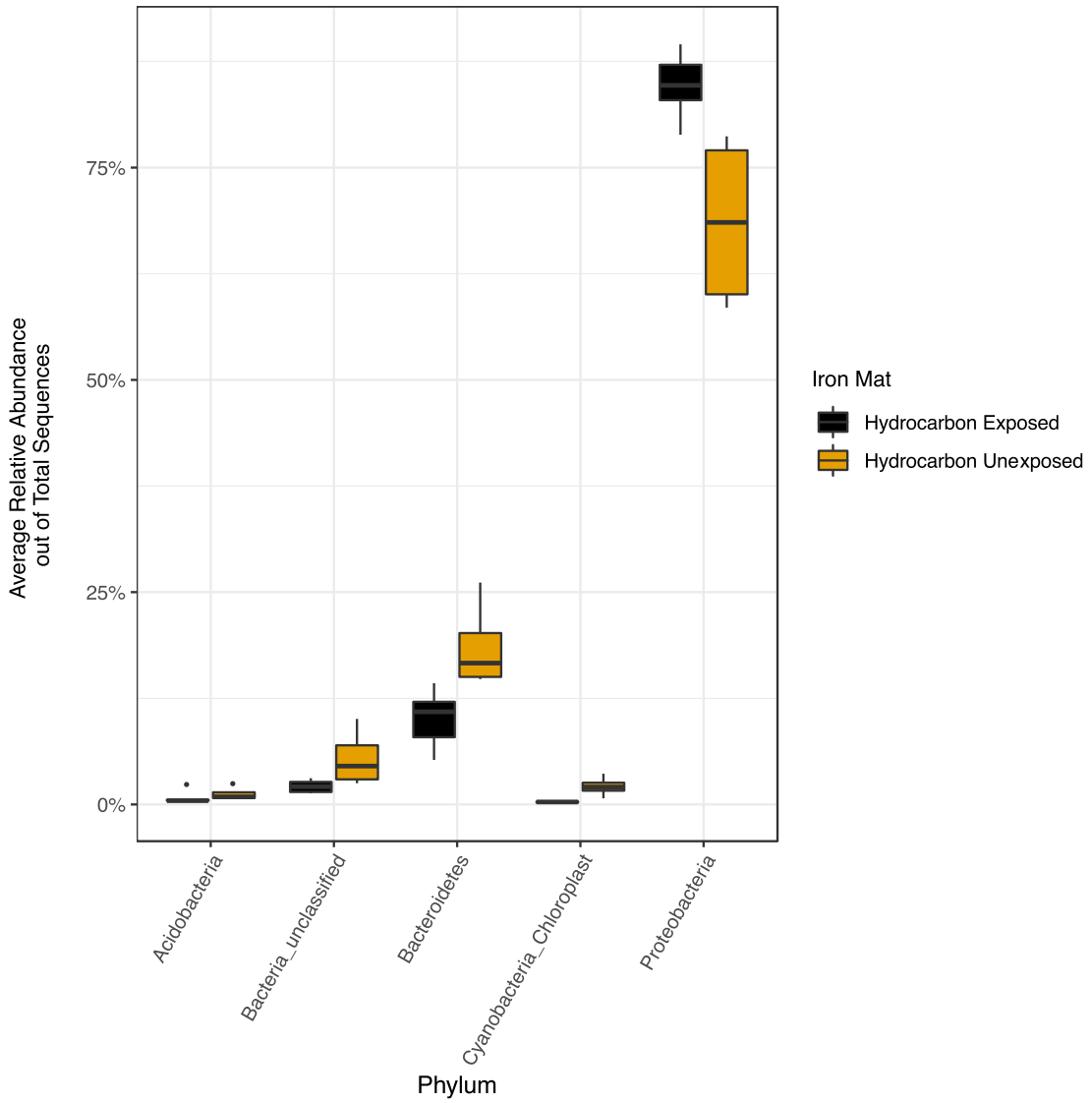

FIGURE 6
Relative abundances of phyla greater than 2 % were calculated out of total sequences for each sample and averaged by hydrocarbon exposure. Averages for present phyla are presented in yellow (unexposed) or black (hydrocarbon-exposed). The average relative abundance of all phyla except Proteobacteria are greater in unexposed samples. The increased relative abundance of Proteobacteria in the hydrocarbon-exposed iron mat microbial communities reflects the decreased overall diversity.

and oil floating on the top of the water, potentially decreasing niche suitability for phototrophic organisms. This was further supported as the logFC analysis suggested that Cyanobacteria were over-expressed in the unexposed iron mat microbial communities compared with the hydrocarbon-exposed communities.

The presence of nitrate-reducing iron-oxidizing taxa was also suggested by the amplicon sequencing results. Previously, three of these genera (*Azospira*, *Paracoccus*, and *Thermomonas*) have not been found to be present in freshwater iron mat microbial communities (Brooks and Field, 2020); however, *Azospira* has been identified previously in paddy soil (Li et al., 2016). These OTUs had higher relative abundances in the hydrocarbon-exposed iron mats. The exposed iron mats also had significantly lower NO_x^- concentrations than the exposed water samples. The lower concentration of NO_x^- did

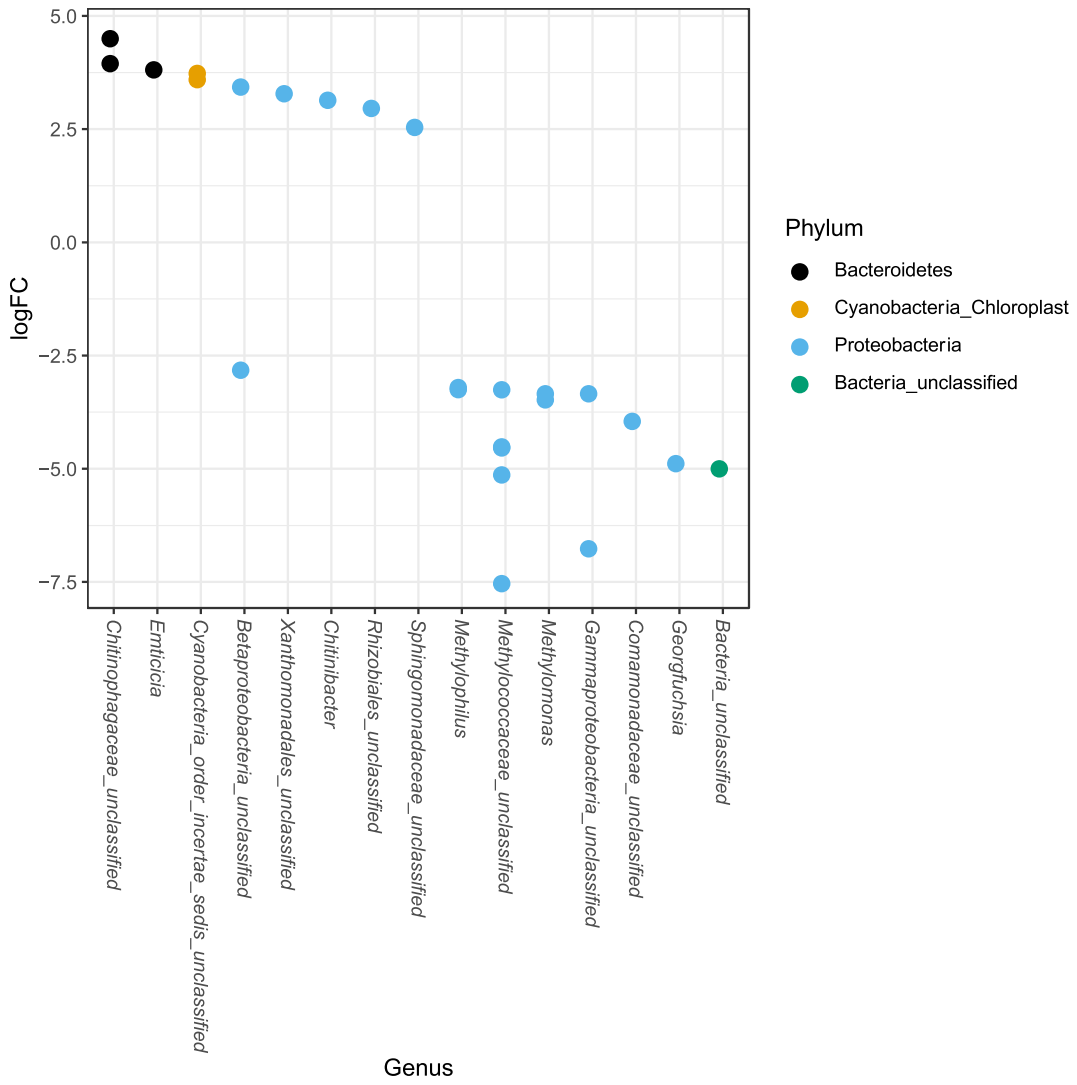

FIGURE 7
Differential abundances of taxa between upstream and downstream mats were calculated from an independently filtered data set. Genera with differential abundances with an alpha <0.05 were plotted. Each point on the plot represents a single OTU sequence. Points with a log-fold change greater than zero are of lower abundance in the hydrocarbon-exposed iron mat communities, whereas points with a log-fold change less than 0 are of increased abundance in hydrocarbon-exposed iron mat microbial communities relative to unexposed communities. The largest fold-changes were in OTUs in hydrocarbon-exposed communities and were observed in the highly represented phylum, Proteobacteria.

not have a significant correlation with any of the hydrocarbons measured. We hypothesize that active denitrification processes could be concentrated within the iron mats exposed to hydrocarbons. This may prove to be an important connection between the nitrogen cycle and freshwater iron mats, a connection that is only just being explored in marine iron mats (McAllister et al., 2021; Hribovšek et al., 2023). Alternatively, it has been observed in terrestrial samples that reduced iron reacts with nitrate to form $Fe(OH)_3$ and N_2O (Matus et al., 2019).

We observed a strong negative correlation between dissolved PO_4^{3-} and benzene in hydrocarbon exposed iron mats. This result, paired with significantly higher benzene concentrations in seep mats than the exposed water samples, suggests the differing geochemistry between iron mats and the surrounding water column likely influences hydrocarbon behavior. The concentration of dissolved PO_4^{3-} was also significantly greater in unexposed iron mats. Previously, FeOOH in iron mats has been demonstrated to adsorb phosphorous (Takeda et al., 2010; Buliauskaitė et al., 2020). We hypothesize that benzene and PO_4^{3-} interact antagonistically within the system, leading to competitive exclusion from the surface of FeOOH. Alternatively, the addition of phosphorous has been previously observed to increase microbial benzene removal (Xiong et al., 2012). Higher phosphorous concentrations may increase microbial scavenging of benzene, leading to a strong negative correlation. Further studies are needed to understand the negative correlation we observed between phosphate and benzene, and whether it is chemically, physically, or biologically driven. We recommend future experimental studies on the use of freshwater iron mats that killed controls with added phosphate, nitrates, and nitrites and organic carbon to better disentangle the chemical reactions in iron mat environments from biological reactions.

Alpha diversity and evenness were observed to be significantly lower in the hydrocarbon-exposed than unexposed iron mat microbial communities, which suggests that the within community diversity of

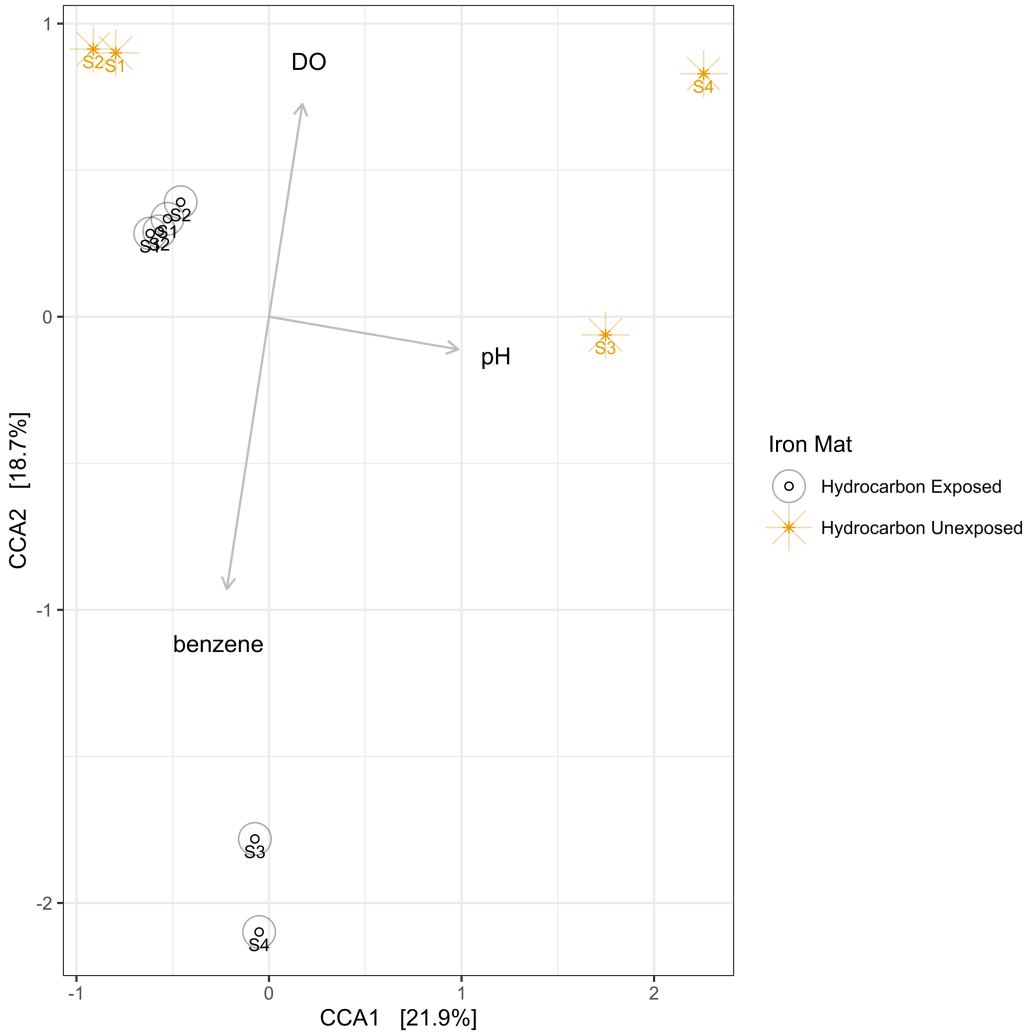

FIGURE 8
A canonical correspondence analysis (CCA) was used to calculate eigenvalues for the environmental conditions of iron mats. The overall model presented above is a good fit of the data (PERMANOVA $F = 1.95$, $p = 0.002$), and the variance inflation factor for each explanatory term is less than 3. The results indicate that the greatest effect on microbial community structure is from dissolved oxygen (DO; ppm), followed by pH and benzene concentration (mg/L). Sampling efforts (1–4) are labeled on each point.

iron mats is impacted by contaminant exposure. This is consistent with other oil-exposed microbial communities (Maila et al., 2005; Máthé et al., 2012). We also observed a potential interaction between season and hydrocarbon exposure. Evenness was higher in iron mat communities in summer compared with spring. A similar trend has been shown in riverine microbial communities to be associated with changes in flow resulting from seasonal precipitation differences (Luo et al., 2020) or hydrological factors, such as groundwater discharge (Valett et al., 1997). Seasonal differences have also been previously observed in the microbial communities of freshwater ion mats (Fleming et al., 2014). The Town Creek iron mat samples, however, did not have the confounding variable of dominant microaerophilic FeOB, which was observed in the previous study, to change with the seasons (Fleming et al., 2014). A previous study has found that the concentration and type of hydrocarbon present in watersheds in Mexico varied with season (spring and summer) are attributed to increased precipitation and motor traffic (Narciso-Ortiz et al., 2020). While we did not identify differences in the types of hydrocarbons present in the downstream mats by season, the concentrations of benzene, ethylbenzene, and xylenes were all higher in summer (0.015 ± 0.001 mg/L, 0.007 ± 0.000 mg/L, and 0.037 ± 0.005 mg/L) than spring (0.005 ± 0.003 mg/L, 0.000 ± 0.000 mg/L, and 0.001 ± 0.001 mg/L).

Both hydrocarbon-exposed and unexposed iron mat microbial communities were dominated by the phylum Proteobacteria. This is consistent with other studies of hydrocarbon-exposed microbial communities; however, the samples from previous studies tend to be dominated by Alphaproteobacteria (Saul et al., 2005; Zhao et al., 2020; Eze, 2021), whereas the iron mat sample 16S rDNA amplicon sequences (regardless of hydrocarbon exposure) were dominated by Betaproteobacteria (Supplementary Figure S9). The relative abundance of Betaproteobacteria, which may be associated with the degradation of lower molecular weight polycyclic aromatic hydrocarbons (Sun et al., 2019), was observed to be higher in hydrocarbon-exposed than in unexposed iron mats. These observations suggest that iron mat microbial community diversity and composition are impacted by exposure to hydrocarbons.

Only one genus of hydrocarbonoclast was observed at Town Creek: *Planomicrobium*. This is in agreement with previous findings in cyanobacterial mats that hydrocarbonoclastic genera are not good indicators of chronic hydrocarbon exposure; rather, they are cosmopolitan (Aubé et al., 2016). There was, however, a greater relative abundance of 16S rDNA amplicon OTUs associated with nitrate reduction-coupled benzene degradation (Coates et al., 2001; Fahy et al., 2006, 2008) in the hydrocarbon-exposed iron mats. Other OTUs classified as genera associated with iron reduction and sulfate reduction coupled to benzene degradation were observed in both hydrocarbon-exposed and unexposed iron mat microbial communities but at much lower relative abundances. These result in total represent possible connections between hydrocarbons and the nitrogen, iron, and sulfur cycles and suggest that the community within the iron mat could potentially contribute to bioremediation of benzene or other hydrocarbons. Freshwater iron mats have been previously hypothesized to connect the iron and sulfur cycles (Koeksoy et al., 2018; Brooks and Field, 2021); however, connections to the nitrogen cycle have not been previously proposed. Of interest, future studies would be whether microbial activity rates in the iron mat are the same when exposed to hydrocarbons, given the previously discussed loss of diversity.

Using a canonical correspondence analysis, it was observed that dissolved oxygen and pH were significantly correlated with microbial community structure. Iron mats are assemblages of microorganisms sensitive to oxygen conditions: microaerophiles, anaerobes, and aerobes. The microbial communities are therefore likely to be sensitive to changes in dissolved oxygen. Dissolved oxygen had a greater influence on community structure in the summer, reflecting a very low average dissolved oxygen concentration in hydrocarbon-exposed iron mats (average 2.0 ppm). Previous studies have shown that pH is a strong driver of community structure, even in communities exposed to polycyclic aromatic hydrocarbons (Wu et al., 2017). However, this result is somewhat surprising given that the pH of this data set only ranged from 6 to 7.13, which likely falls within the growth range of many microorganisms. Perhaps this result reflects the influence of pH on the biogeochemical cycles that were catalyzed or vice versa. It was also observed that functional potential, which was found using hidden Markov models for iron-cycling and benzene-remediation genes, did not significantly vary between hydrocarbon exposure states. This is inconsistent with a previous study of marine sediment core communities that find an increase in the potential of iron-cycling under hydrocarbon regimes (Zhao et al., 2020). In contrast, our results reflect iron-cycling as a key process in iron mats, which is unlikely to change under contaminant exposure. These results highlight that microbial communities exposed to contaminants are also under common selective pressures and reflect other environmental factors.

We were able to recover 29 MAGs from the iron mat microbial communities. MAGs are highly useful for linking geochemical cycles within a single taxon by identifying how they contribute holistically. MAGs have been found to be useful in identifying rare taxa from data sets that are not previously observed using 16S rDNA amplicon sequencing (Wilkins et al., 2019). None of the recovered MAGs were assigned to taxa known for hydrocarbon degradation. Seven MAGs (one unexposed/six hydrocarbon exposed) were classified to the genus of microaerophilic iron-oxidizing bacteria, *Gallionella*. The DRAM annotation of these MAGs was dissimilar to the annotation of the sequenced representative, *Gallionella capsiferriformans* ES-2. All seven MAGs were missing modules for the Entner–Duodoroff pathway (catabolizing glucose to pyruvate), as well as ETC complexes for succinate dehydrogenase (citric acid cycle/electron transport chain) and cytochrome bd ubiquinol oxidase (reduction of molecular oxygen). While it is possible that these modules are missing due to incomplete binning, previous study has demonstrated that MAGs with >90% completeness should be effective representation of organismal functions (Nelson et al., 2020). Two MAGs from the unexposed iron mat metagenomes were classified as the endosymbiont *Phycorickettsia* spp. The presence of these endosymbionts from MAGs indicates the putative presence of protists or other microeukaryotes in the upstream iron mats that would host these organisms, though studies of microeukaryotic members of the iron mat community are currently in need of further research (Brooks and Field, 2020).

This study aimed to pair geochemical and molecular data to develop an understanding of how contaminant exposure, specifically hydrocarbons, would impact freshwater iron mat geochemistry, microbial community structure, and microbial community function. We found significant effects of hydrocarbon exposure on iron mat geochemistry and microbial community diversity. We observed an especially interesting correlation between the concentrations of benzene and dissolved phosphate. We also observed key differences between iron mat types (seep vs. flocculent) in concentrations of reduced and oxidized iron, phosphate, and hydrocarbons. Our results suggested that some functional groups, detected using 16S rDNA amplicon sequencing, vary in the relative abundance correlated with hydrocarbon exposure. However, gene detection using hidden Markov models on metagenomic contigs did not demonstrate significant changes in iron-cycling or benzene-degrading functional potential. Previous research in other ecosystems has demonstrated links between community diversity shifts and changes in functional potential in microbial communities (Galand et al., 2018). We hypothesize that it may be possible to observe changes in activity in our system if alternative methods (i.e., direct microbial metabolism measurements or RT-qPCR) are applied in future studies. Additionally, increasing sequencing depth for future metagenomic analyses of these freshwater iron mats may also provide more functional data and help identify more differences between exposed and unexposed iron mat communities. However, these results are encouraging to research on iron mats, providing a good foundation, especially toward application in systems that are currently unbuffered from hydrocarbon pollution. With over 500,000 leaking storage tanks in the United States, it is inevitable that these pollutants will reach above ground reservoirs, where, as indicated here, the iron mat microbial community may be successfully applied at that oxic–anoxic interface.

Data availability statement

The 16S rDNA amplicon sequences are available at NCBI BioSample Accession numbers SAMN39732271, SAMN39732272, SAMN39732273, SAMN39732274, SAMN39732275, SAMN39732276, SAMN39732277, SAMN39732278, SAMN39732279, and SAMN39732280. The metagenomic sequences are available at NCBI BioProject PRJNA1072096 with BioSample Accession numbers SAMN39944932, SAMN39944933, SAMN39944934, SAMN33944935, SAMN33944936, SAMN33944937, SAMN33944938, SAMN33944939, SAMN39944940, and SAMN39944941. The ".fasta" files for each MAG

assembly is available at https://kbase.us/n/105846/210/ via static narrative.

Author contributions

CB: Conceptualization, Data curation, Formal analysis, Funding acquisition, Investigation, Methodology, Writing – original draft, Writing – review & editing. EF: Conceptualization, Formal analysis, Investigation, Methodology, Project administration, Writing – review & editing.

Funding

The author(s) declare financial support was received for the research, authorship, and/or publication of this article. Funding support was provided by the Graduate Women in Science National Fellowship Program and the Nell Mondy, Vessa Notchev, and Monique Braude Fellowship Funds to CB.

Acknowledgments

The authors would like to thank the members of the Field and Peralta Labs for assisting with field sampling. Part of the data presented in this manuscript can be found in the dissertation of CB (http://hdl.handle.net/10342/9128).

Conflict of interest

The authors declare that the research was conducted in the absence of any commercial or financial relationships that could be construed as a potential conflict of interest.

Publisher's note

Supplementary material

The Supplementary material for this article can be found online at: https://www.frontiersin.org/articles/10.3389/fmicb.2024.1388973/full#supplementary-material

References

Abbas, A., Abussaud, B. A., Ihsanullah, A.-B., Khraisheh, N. A. H., and Atieh, M. A. (2016). Benzene removal by Iron oxide nanoparticles decorated carbon nanotubes. *J. Nanomater.* 2016, 1–10. doi: 10.1155/2016/5654129

Abed, R. M. M., Al-Kharusi, S., Prigent, S., and Headley, T. (2014). Diversity, distribution and hydrocarbon biodegradation capabilities of microbial communities in oil-contaminated cyanobacterial Mats from a constructed wetland. *PLoS One* 9:e114570. doi: 10.1371/journal.pone.0114570

Alneberg, J., Bjarnason, B. S., De Bruijn, I., Schirmer, M., Quick, J., Ijaz, U. Z., et al. (2013). CONCOCT: Clustering contigs on coverage and composition. arXiv preprint arXiv:1312.4038.

Andrews, S. (2010). *FastQC: A quality control tool for high throughput sequence data*. Cambridge: Babraham Bioinformatics, Babraham Institute.

Arkin, A. P., Cottingham, R. W., Henry, C. S., Harris, N. L., Stevens, R. L., Maslov, S., et al. (2018). KBase: the United States Department of Energy Systems Biology Knowledgebase. *Nat. Biotechnol.* 36, 566–569. doi: 10.1038/nbt.4163

Arnold, J. B. (2019). Ggthemes: extra themes, scales and Geoms for 'ggplot2'. R package version 4.2.0.

Atashgahi, S., Hornung, B., Van Der Waals, M. J., Da Rocha, U. N., Hugenholtz, F., Nijsse, B., et al. (2018). A benzene-degrading nitrate-reducing microbial consortium displays aerobic and anaerobic benzene degradation pathways. *Sci. Rep.* 8:4490. doi: 10.1038/s41598-018-22617-x

Aubé, J., Senin, P., Pringault, O., Bonin, P., Deflandre, B., Bouchez, O., et al. (2016). The impact of long-term hydrocarbon exposure on the structure, activity, and biogeochemical functioning of microbial mats. *Mar. Pollut. Bull.* 111, 115–125. doi: 10.1016/j.marpolbul.2016.07.023

Aziz, R. K., Bartels, D., Best, A. A., Dejongh, M., Disz, T., Edwards, R. A., et al. (2008). The RAST server: rapid annotations using subsystems technology. *BMC Genomics* 9:75. doi: 10.1186/1471-2164-9-75

Badham, H. J., and Winn, L. M. (2007). Investigating the role of the aryl hydrocarbon receptor in benzene-initiated toxicity in vitro. *Toxicology* 229, 177–185. doi: 10.1016/j.tox.2006.10.021

Bankevich, A., Nurk, S., Antipov, D., Gurevich, A. A., Dvorkin, M., Kulikov, A. S., et al. (2012). SPAdes: a new genome assembly algorithm and its applications to single-cell sequencing. *J. Comput. Biol.* 19, 455–477. doi: 10.1089/cmb.2012.0021

Baskar, S., Baskar, R., Thorseth, I. H., Øvreås, L., and Pedersen, R. B. (2012). Microbially induced iron precipitation associated with a neutrophilic spring at Borra caves, Vishakhapatnam, India. *Astrobiology* 12, 327–346. doi: 10.1089/ast.2011.0672

Boutet, E., Lieberherr, D., Tognolli, M., Schneider, M., and Bairoch, A. (2007). "UniProtKB/Swiss-Prot: the manually annotated section of the UniProt KnowledgeBase" in *Plant bioinformatics*. ed. D. Edwards (Totowa, NJ: Humana Press), 89–112.

Bradley, P. M. (2012). Perils of categorical thinking: "Oxic/anoxic" conceptual model in environmental remediation. *Remediat. J.* 22, 9–18. doi: 10.1002/rem.21317

Brettin, T., Davis, J. J., Disz, T., Edwards, R. A., Gerdes, S., Olsen, G. J., et al. (2015). RASTtk: a modular and extensible implementation of the RAST algorithm for building custom annotation pipelines and annotating batches of genomes. *Sci. Rep.* 5:8365. doi: 10.1038/srep08365

Brooks, C. N. (2021). Bacteria of a feather floc together: Microbial interactions and function within iron-oxidizing bacterial communities. Doctoral dissertation, East Carolina University. Available at: http://hdl.handle.net/10342/9128

Brooks, C. N., and Field, E. K. (2020). Iron flocs and the three domains: microbial interactions in freshwater Iron Mats. *MBio* 11:e02720. doi: 10.1128/mbio.02720-20

Brooks, C. N., and Field, E. K. (2021). Orange leads to black: evaluating the efficacy of co-culturing iron-oxidizing and sulfate-reducing bacteria to discern ecological relationships. *Environ. Microbiol. Rep.* 13, 317–324. doi: 10.1111/1758-2229.12932

Buliauskaitė, R., Wilfert, P., Suresh Kumar, P., De Vet, W. W., Witkamp, G.-J., Korving, L., et al. (2020). Biogenic iron oxides for phosphate removal. *Environ. Technol.* 41, 260–266. doi: 10.1080/09593330.2018.1496147

Chakraborty, R., and Coates, J. D. (2004). Anaerobic degradation of monoaromatic hydrocarbons. *Appl. Microbiol. Biotechnol.* 64, 437–446. doi: 10.1007/s00253-003-1526-x

Chang, W. (2013). *R graphics cookbook: Practical recipes for visualizing data*. Beijing: O'Reilly Media.

Chaumeil, P.-A., Mussig, A. J., Hugenholtz, P., and Parks, D. H. (2020). GTDB-Tk: a toolkit to classify genomes with the genome taxonomy database. *Bioinformatics* 36, 1925–1927. doi: 10.1093/bioinformatics/btz848

Coates, J. D., Chakraborty, R., Lack, J. G., O'Connor, S. M., Cole, K. A., Bender, K. S., et al. (2001). Anaerobic benzene oxidation coupled to nitrate reduction in pure culture by two strains of Dechloromonas. *Nature* 411, 1039–1043. doi: 10.1038/35082545

Eddy, S. R. (1998). Profile hidden Markov models. *Bioinformatics* 14, 755–763. doi: 10.1093/bioinformatics/14.9.755

Edwards, E. A., and Grbić-Galić, D. (1992). Complete mineralization of benzene by aquifer microorganisms under strictly anaerobic conditions. *Appl. Environ. Microbiol.* 58, 2663–2666. doi: 10.1128/aem.58.8.2663-2666.1992

Emerson, D., and Moyer Craig, L. (2002). Neutrophilic Fe-oxidizing Bacteria are abundant at the Loihi seamount hydrothermal vents and play a major role in Fe oxide

deposition. *Appl. Environ. Microbiol.* 68, 3085–3093. doi: 10.1128/AEM.68.6.3085-3093.2002

Emerson, D., Scott, J. J., Benes, J., and Bowden, W. B. (2015). Microbial iron oxidation in the arctic tundra and its implications for biogeochemical cycling. *Appl. Environ. Microbiol.* 81, 8066–8075. doi: 10.1128/AEM.02832-15

Eze, M. O. (2021). Metagenome analysis of a hydrocarbon-degrading bacterial consortium reveals the specific roles of BTEX biodegraders. *Genes* 12:98. doi: 10.3390/genes12010098

Fabisch, M., Beulig, F., Akob, D. M., and Küsel, K. (2013). Surprising abundance of Gallionella-related iron oxidizers in creek sediments at pH 4.4 or at high heavy metal concentrations. *Front. Microbiol.* 4:390. doi: 10.3389/fmicb.2013.00390

Fahy, A., Ball, A. S., Lethbridge, G., Timmis, K. N., and McGenity, T. J. (2008). Isolation of alkali-tolerant benzene-degrading bacteria from a contaminated aquifer. *Lett. Appl. Microbiol.* 47, 60–66. doi: 10.1111/j.1472-765X.2008.02386.x

Fahy, A., McGenity, T. J., Timmis, K. N., and Ball, A. S. (2006). Heterogeneous aerobic benzene-degrading communities in oxygen-depleted groundwaters. *FEMS Microbiol. Ecol.* 58, 260–270. doi: 10.1111/j.1574-6941.2006.00162.x

Field, H. R., Whitaker, A. H., Henson, J. A., and Duckworth, O. W. (2019). Sorption of copper and phosphate to diverse biogenic iron (oxyhydr) oxide deposits. *Sci. Total Environ.* 697:134111. doi: 10.1016/j.scitotenv.2019.134111

Fleming, E. J., Cetinić, I., Chan, C. S., King, D. W., and Emerson, D. (2014). Ecological succession among iron-oxidizing bacteria. *ISME J.* 8, 804–815. doi: 10.1038/ismej.2013.197

Fleming, E. J., Woyke, T., Donatello, R. A., Kuypers, M. M. M., Sczyrba, A., Littmann, S., et al. (2018). Insights into the fundamental physiology of the uncultured Fe-oxidizing bacterium *Leptothrix ochracea*. *Appl. Environ. Microbiol.* 84, e02239–e02217. doi: 10.1128/AEM.02239-17

Gagen, E. J., Levett, A., Shuster, J., Fortin, D., Vasconcelos, P. M., and Southam, G. (2018). Microbial diversity in actively forming iron oxides from weathered banded iron formation systems. *Microbes Environ.* 33, 385–393. doi: 10.1264/jsme2.ME18019

Galand, P., Pereira, O., Hochart, C., Auguet, J. C., and Debroas, D. (2018). A strong link between marine microbial community composition and function challenges the idea of functional redundancy. *ISME J.* 12, 2470–2478. doi: 10.1038/s41396-018-0158-1

Garber, A. I., Nealson, K. H., Okamoto, A., Mcallister, S. M., Chan, C. S., Barco, R. A., et al. (2020). FeGenie: a comprehensive tool for the identification of Iron genes and Iron gene neighborhoods in genome and metagenome assemblies. *Front. Microbiol.* 11:37. doi: 10.3389/fmicb.2020.00037

Garrison, C. E., Price, K. A., and Field, E. K. (2019). Environmental evidence and genomic insight of Iron-oxidizing Bacteria preference towards more corrosion resistant stainless steel at higher salinities. *Appl. Environ. Microbiol.* 85:e00483-19. doi: 10.1128/AEM.00483-19

Gihawi, A., Rallapalli, G., Hurst, R., Cooper, C. S., Leggett, R. M., and Brewer, D. S. (2019). SEPATH: benchmarking the search for pathogens in human tissue whole genome sequence data leads to template pipelines. *Genome Biol.* 20:208. doi: 10.1186/s13059-019-1819-8

Gurevich, A., Saveliev, V., Vyahhi, N., and Tesler, G. (2013). QUAST: quality assessment tool for genome assemblies. *Bioinformatics* 29, 1072–1075. doi: 10.1093/bioinformatics/btt086

Hedrich, S., Schlömann, M., and Johnson, D. B. (2011). The iron-oxidizing proteobacteria. *Microbiology* 157, 1551–1564. doi: 10.1099/mic.0.045344-0

Hribovšek, P., Olesin Denny, E., Dahle, H., Mall, A., Øfstegaard Viflot, T., Boonnawa, C., et al. (2023). Putative novel hydrogen- and iron-oxidizing sheath-producing Zetaproteobacteria thrive at the Fåvne deep-sea hydrothermal vent field. *mSystems* 8, e0054323–e0000523. doi: 10.1128/msystems.00543-23

Humphrey, C., Blackmon, J., Kelley, T., Driscoll, M., and Iverson, G. (2018). Environmental health threats associated with drainage from a coastal urban watershed. *Environ. Nat. Resour.* 8, 52–60. doi: 10.5539/enrr.v8n1p52

Hyatt, D., Chen, G. L., Locascio, P. F., Land, M. L., Larimer, F. W., and Hauser, L. J. (2010). Prodigal: prokaryotic gene recognition and translation initiation site identification. *BMC Bioinform.* 11:119. doi: 10.1186/1471-2105-11-119

Ichihara, Y., Okabe, M., Iga, K., Tanaka, Y., Musha, K., and Ito, K. (2008). Color universal design: The selection of four easily distinguishable colors for all color vision types. Proceedings SPIE 6807, color Imaginging XIII: Processing, hardcopy, and applications.

Jahn, M. K., Haderlein, S. B., and Meckenstock, R. U. (2005). Anaerobic degradation of benzene, toluene, ethylbenzene, and o-xylene in sediment-free Iron-reducing enrichment cultures. *Appl. Environ. Microbiol.* 71, 3355–3358. doi: 10.1128/AEM.71.6.3355-3358.2005

Jindrová, E., Chocová, M., Demnerová, K., and Brenner, V. (2002). Bacterial aerobic degradation of benzene, toluene, ethylbenzene and xylene. *Folia Microbiol.* 47, 83–93. doi: 10.1007/BF02817664

Johnson, S. J., Woolhouse, K. J., Prommer, H., Barry, D. A., and Christofi, N. (2003). Contribution of anaerobic microbial activity to natural attenuation of benzene in groundwater. *Eng. Geol.* 70, 343–349. doi: 10.1016/S0013-7952(03)00102-9

Kang, D. D., Li, F., Kirton, E., Thomas, A., Egan, R., An, H., et al. (2019). MetaBAT 2: an adaptive binning algorithm for robust and efficient genome reconstruction from metagenome assemblies. *PeerJ* 7:e7359. doi: 10.7717/peerj.7359

Karthikeyan, S., Kim, M., Heritier-Robbins, P., Hatt, J. K., Spain, J. C., Overholt, W. A., et al. (2020). Integrated omics elucidate the mechanisms driving the rapid biodegradation of Deepwater horizon oil in intertidal sediments undergoing Oxic–anoxic cycles. *Environ. Sci. Technol.* 54, 10088–10099. doi: 10.1021/acs.est.0c02834

Kassambara, A. (2020). Ggpubr: 'ggplot2' based publication ready plots. R package version 0.4.0.

Kato, S., Krepski, S., Chan, C., Itoh, T., and Ohkuma, M. (2014). Ferriphaselus amnicola gen. Nov., sp. nov., a neutrophilic, stalk-forming, iron-oxidizing bacterium isolated from an iron-rich groundwater seep. *Int. J. Syst. Evol. Microbiol.* 64, 921–925. doi: 10.1099/ijs.0.058487-0

Keller, A. H., Kleinsteuber, S., and Vogt, C. (2018). Anaerobic benzene mineralization by nitrate-reducing and sulfate-reducing microbial consortia enriched from the same site: comparison of community composition and degradation characteristics. *Microb. Ecol.* 75, 941–953. doi: 10.1007/s00248-017-1100-1

Kembel, S. W., Cowan, P. D., Helmus, M. R., Cornwell, W. K., Morlon, H., Ackerly, D. D., et al. (2010). Picante: R tools for integrating phylogenies and ecology. *Bioinformatics* 26, 1463–1464. doi: 10.1093/bioinformatics/btq166

Koeksoy, E., Halama, M., Hagemann, N., Weigold, P. R., Laufer, K., Kleindienst, S., et al. (2018). A case study for late Archean and Proterozoic biogeochemical iron-and Sulphur cycling in a modern habitat—the Arvadi spring. *Geobiology* 16, 353–368. doi: 10.1111/gbi.12293

Kozich, J. J., Westcott, S. L., Baxter, N. T., Highlander, S. K., and Schloss, P. D. (2013). Development of a dual-index sequencing strategy and curation pipeline for analyzing amplicon sequence data on the MiSeq Illumina sequencing platform. *Appl. Environ. Microbiol.* 79, 5112–5120. doi: 10.1128/AEM.01043-13

Krueger, F. (2015). Trim Galore!: A wrapper around Cutadapt and FastQC to consistently apply adapter and quality trimming to FastQ files, with extra functionality for RRBS data, Babraham Institute. Available at: https://cir.nii.ac.jp/crid/1370294643762929691

Lahti, L., Shetty, S., Blake, T., and Salojarvi, J. (2017). Tools for microbiome analysis in R. 2.1.26.

Li, Y., Xu, Z., Wu, J., and Mo, P. (2020). Efficiency and mechanisms of antimony removal from wastewater using mixed cultures of iron-oxidizing bacteria and sulfate-reducing bacteria based on scrap iron. *Sep. Purif. Technol.* 246:116756. doi: 10.1016/j.seppur.2020.116756

Li, X., Zhang, W., Liu, T., Chen, L., Chen, P., and Li, F. (2016). Changes in the composition and diversity of microbial communities during anaerobic nitrate reduction and Fe(II) oxidation at circumneutral pH in paddy soil. *Soil Biol. Biochem.* 94, 70–79. doi: 10.1016/j.soilbio.2015.11.013

Little, B. J., Lee, J. S., and Gerke, T. L. (2016). The relationship between Iron oxides/Oxyhydroxides and toxic metal ions in drinking water distribution systems—a review. *Corrosion* 73, 138–143. doi: 10.5006/2162

Liu, X., Liu, M., Chen, X., Yang, Y., Hou, L., Wu, S., et al. (2019). Indigenous PAH degraders along the gradient of the Yangtze estuary of China: relationships with pollutants and their bioremediation implications. *Mar. Pollut. Bull.* 142, 419–427. doi: 10.1016/j.marpolbul.2019.03.064

Lovley, D. R., and Phillips, E. J. (1987). Rapid assay for microbially reducible ferric iron in aquatic sediments. *Appl. Environ. Microbiol.* 53, 1536–1540. doi: 10.1128/aem.53.7.1536-1540.1987

Lovley, D. R., Woodward, J. C., and Chapelle, F. H. (1996). Rapid anaerobic benzene oxidation with a variety of chelated Fe(III) forms. *Appl. Environ. Microbiol.* 62, 288–291. doi: 10.1128/aem.62.1.288-291.1996

Luo, X., Xiang, X., Yang, Y., Huang, G., Fu, K., Che, R., et al. (2020). Seasonal effects of river flow on microbial community coalescence and diversity in a riverine network. *FEMS Microbiol. Ecol.* 96:fiaa132. doi: 10.1093/femsec/fiaa132

Maila, M. P., Randima, P., Surridge, K., Drønen, K., and Cloete, T. E. (2005). Evaluation of microbial diversity of different soil layers at a contaminated diesel site. *Int. Biodeterior. Biodegradation* 55, 39–44. doi: 10.1016/j.ibiod.2004.06.012

Máthé, I., Benedek, T., Táncsics, A., Palatinszky, M., Lányi, S., and Márialigeti, K. (2012). Diversity, activity, antibiotic and heavy metal resistance of bacteria from petroleum hydrocarbon contaminated soils located in Harghita County (Romania). *Int. Biodeterior. Biodegradation* 73, 41–49. doi: 10.1016/j.ibiod.2012.05.018

Matus, F., Stock, S., Eschenbach, W., Dyckmans, J., Merino, C., Nájera, F., et al. (2019). Ferrous wheel hypothesis: abiotic nitrate incorporation into dissolved organic matter. *Geochim. Cosmochim. Acta* 245, 514–524. doi: 10.1016/j.gca.2018.11.020

McAllister, S. M., Vandzura, R., Keffer, J. L., Polson, S. W., and Chan, C. S. (2021). Aerobic and anaerobic iron oxidizers together drive denitrification and carbon cycling at marine iron-rich hydrothermal vents. *ISME J.* 15, 1271–1286. doi: 10.1038/s41396-020-00849-y

McCarthy, D. J., Chen, Y., and Smyth, G. K. (2012). Differential expression analysis of multifactor RNA-Seq experiments with respect to biological variation. *Nucleic Acids Res.* 40, 4288–4297. doi: 10.1093/nar/gks042

McMurdie, P. J., and Holmes, S. (2013). Phyloseq: an R package for reproducible interactive analysis and graphics of microbiome census data. *PLoS One* 8:e61217. doi: 10.1371/journal.pone.0061217

Meegoda, J. N., and Hu, L. (2011). A review of centrifugal testing of gasoline contamination and remediation. *Int. J. Environ. Res. Public Health* 8, 3496–3513. doi: 10.3390/ijerph8083496

Minetti, R. C. P., Macaño, H. R., Britch, J., and Allende, M. C. (2017). In situ chemical oxidation of BTEX and MTBE by ferrate: pH dependence and stability. *J. Hazard. Mater.* 324, 448–456. doi: 10.1016/j.jhazmat.2016.11.010

Narciso-Ortiz, L., Vargas-García, K. A., Vázquez-Larios, A. L., Quiñones-Muñoz, T. A., Hernández-Martínez, R., and Lizardi-Jiménez, M. A. (2020). Coral reefs and watersheds of the Gulf of Mexico in Veracruz: hydrocarbon pollution data and bioremediation proposal. *Reg. Stud. Mar. Sci.* 35:101155. doi: 10.1016/j.rsma.2020.101155

Neely, C. J., Graham, E. D., and Tully, B. J. (2020). MetaSanity: an integrated microbial genome evaluation and annotation pipeline. *Bioinformatics* 36, 4341–4344. doi: 10.1093/bioinformatics/btaa512

Nelson, W. C., Tully, B. J., and Mobberley, J. M. (2020). Biases in genome reconstruction from metagenomic data. *PeerJ* 8:e10119. doi: 10.7717/peerj.10119

Nowosad, J. (2018). 'CARTOColors' Palettes. R package version 2.0.0.

Office of Underground Storage Tanks, D.C. (2020). *Semiannual report of UST performance measures: End of fiscal year 2020 (October 1, 2019 – September 30, 2020)*. Washington, DC: U.S.E.P.A.

Oksanen, J., Guillame Blanchet, F., Friendly, M., Kindt, R., Legendre, P., et al. (2019). Vegan: community ecology package. R package version 2.5-6.

Overbeek, R., Olson, R., Pusch, G. D., Olsen, G. J., Davis, J. J., Disz, T., et al. (2014). The SEED and the rapid annotation of microbial genomes using subsystems technology (RAST). *Nucleic Acids Res.* 42, D206–D214. doi: 10.1093/nar/gkt1226

Paissé, S., Coulon, F., Goñi-Urriza, M., Peperzak, L., Mcgenity, T. J., and Duran, R. (2008). Structure of bacterial communities along a hydrocarbon contamination gradient in a coastal sediment. *FEMS Microbiol. Ecol.* 66, 295–305. doi: 10.1111/j.1574-6941.2008.00589.x

Parada, A. E., Needham, D. M., and Fuhrman, J. A. (2016). Every base matters: assessing small subunit rRNA primers for marine microbiomes with mock communities, time series and global field samples. *Environ. Microbiol.* 18, 1403–1414. doi: 10.1111/1462-2920.13023

Parks, D. H., Imelfort, M., Skennerton, C. T., Hugenholtz, P., and Tyson, G. W. (2015). CheckM: assessing the quality of microbial genomes recovered from isolates, single cells, and metagenomes. *Genome Res.* 25, 1043–1055. doi: 10.1101/gr.186072.114

Quast, C., Pruesse, E., Yilmaz, P., Gerken, J., Schweer, T., Yarza, P., et al. (2013). The SILVA ribosomal RNA gene database project: improved data processing and web-based tools. *Nucleic Acids Res.* 41, D590–D596. doi: 10.1093/nar/gks1219

Robinson, M. D., Mccarthy, D. J., and Smyth, G. K. (2009). edgeR: a Bioconductor package for differential expression analysis of digital gene expression data. *Bioinformatics* 26, 139–140. doi: 10.1093/bioinformatics/btp616

Satyanarayan, A., Moritz, D., Wongsuphasawat, K., and Heer, J. (2017). Vega-lite: a grammar of interactive graphics. *IEEE Trans. Vis. Comput. Graph.* 23, 341–350. doi: 10.1109/TVCG.2016.2599030

Saul, D. J., Aislabie, J. M., Brown, C. E., Harris, L., and Foght, J. M. (2005). Hydrocarbon contamination changes the bacterial diversity of soil from around Scott Base, Antarctica. *FEMS Microbiol. Ecol.* 53, 141–155. doi: 10.1016/j.femsec.2004.11.007

Schaedler, F., Lockwood, C., Lueder, U., Glombitza, C., Kappler, A., and Schmidt, C. (2018). Microbially mediated coupling of Fe and N cycles by nitrate-reducing Fe (II)-oxidizing bacteria in littoral freshwater sediments. *Appl. Environ. Microbiol.* 84, e02013–e02017. doi: 10.1128/AEM.02013-17

Schloss, P. D., Gevers, D., and Westcott, S. L. (2011). Reducing the effects of PCR amplification and sequencing artifacts on 16S rRNA-based studies. *PLoS One* 6:e27310. doi: 10.1371/journal.pone.0027310

Schloss, P. D., Westcott, S. L., Ryabin, T., Hall, J. R., Hartmann, M., Hollister, E. B., et al. (2009). Introducing mothur: open-source, platform-independent, community-supported software for describing and comparing microbial communities. *Appl. Environ. Microbiol.* 75, 7537–7541. doi: 10.1128/AEM.01541-09

Seemann, T. (2014). Prokka: rapid prokaryotic genome annotation. *Bioinformatics* 30, 2068–2069. doi: 10.1093/bioinformatics/btu153

Shaffer, M., Borton, M. A., McGivern, B. B., Zayed, A. A., La Rosa, S. L., Solden, L. M., et al. (2020). DRAM for distilling microbial metabolism to automate the curation of microbiome function. *Nucleic Acids Res.* 48, 8883–8900. doi: 10.1093/nar/gkaa621

Sieber, C. (2017). *Dereplication, aggregation and scoring tool (DAS tool) v1. 0*. Berkeley, CA: Lawrence Berkeley National Lab (LBNL).

Sievers, F., and Higgins, D. G. (2017). Clustal omega for making accurate alignments of many protein sequences. *Protein Sci.* 27, 135–145. doi: 10.1002/pro.3290

Sievers, F., Wilm, A., Dineen, D., Gibson, T. J., Karplus, K., Li, W., et al. (2011). Fast, scalable generation of high-quality protein multiple sequence alignments using Clustal omega. *Mol. Syst. Biol.* 7:539. doi: 10.1038/msb.2011.75

Søgaard, E. G., Aruna, R., Abraham-Peskir, J., and Koch, C. B. (2001). Conditions for biological precipitation of iron by *Gallionella ferruginea* in a slightly polluted ground water. *Appl. Geochem.* 16, 1129–1137. doi: 10.1016/S0883-2927(01)00014-2

Steinegger, M., and Söding, J. (2017). MMseqs2 enables sensitive protein sequence searching for the analysis of massive data sets. *Nat. Biotechnol.* 35, 1026–1028. doi: 10.1038/nbt.3988

Sun, X., Chu, L., Mercando, E., Romero, I., Hollander, D., and Kostka, J. E. (2019). Dispersant enhances hydrocarbon degradation and alters the structure of metabolically active microbial communities in shallow seawater from the northeastern Gulf of Mexico. *Front. Microbiol.* 10:2387. doi: 10.3389/fmicb.2019.02387

Sun, M. Y., Dafforn, K. A., Johnston, E. L., and Brown, M. V. (2013). Core sediment bacteria drive community response to anthropogenic contamination over multiple environmental gradients. *Environ. Microbiol.* 15, 2517–2531. doi: 10.1111/1462-2920.12133

Takeda, I., Somura, H., and Mori, Y. (2010). Recovery of phosphorus from natural water bodies using iron-oxidizing bacteria and woody biomass. *Ecol. Eng.* 36, 1064–1069. doi: 10.1016/j.ecoleng.2010.04.019

Tremblay, P., and Zhang, T. (2020). "Functional genomics of metal-reducing microbes degrading hydrocarbons" in *Anaerobic utilization of hydrocarbons, oils, and lipids. Handbook of Hydrocarbon and Lipid Microbiology*. ed. M. Boll (Heidelberg: Springer).

Valett, H. M., Dahm, C. N., Campana, M. E., Morrice, J. A., Baker, M. A., and Fellows, C. S. (1997). Hydrologic influences on groundwater-surface water ecotones: heterogeneity in nutrient composition and retention. *J. N. Am. Benthol. Soc.* 16, 239–247. doi: 10.2307/1468254

Walters, W., Hyde, E. R., Berg-Lyons, D., Ackermann, G., Humphrey, G., Parada, A., et al. (2016). Improved bacterial 16S rRNA gene (V4 and V4-5) and fungal internal transcribed spacer marker gene primers for microbial community surveys. *mSystems* 1, e00009–e00015. doi: 10.1128/msystems.00009-15

Warner, B., Finke, J., Gable, R., Strobel, J., and Snyder, A. (1984). *EPA (Environmental Protection Agency) method study 25, method 602, purgeable aromatics. Report for Sep 79-Dec 82*. Dayton, OH: Monsanto Co.

Weiss, J. V., Rentz, J. A., Plaia, T., Neubauer, S. C., Merrill-Floyd, M., Lilburn, T., et al. (2007). Characterization of neutrophilic Fe (II)-oxidizing bacteria isolated from the rhizosphere of wetland plants and description of Ferritrophicum radicicola gen. Nov. sp. nov., and Sideroxydans paludicola sp. nov. *Geomicrobiol J.* 24, 559–570. doi: 10.1080/01490450701670152

Wickham, H. (2007). Reshaping data with the reshape package. 21, 20.

Wickham, H. (2016). *ggplot2: Elegant graphics for data analysis*. New York: Springer-Verlag.

Wickham, H., and Seidel, D. (2020). Scales: scale functions for visualization. R package version 1.1.1.

Wilkins, L. G. E., Ettinger, C. L., Jospin, G., and Eisen, J. A. (2019). Metagenome-assembled genomes provide new insight into the microbial diversity of two thermal pools in Kamchatka, Russia. *Scientific Reports* 9:3059. doi: 10.1038/s41598-019-39576-6

Woodcroft, B. J., Boyd, J. A., and Tyson, G. W. (2016). OrfM: a fast open reading frame predictor for metagenomic data. *Bioinformatics* 32, 2702–2703. doi: 10.1093/bioinformatics/btw241

Wu, Y. W., Tang, Y. H., Tringe, S. G., Simmons, B. A., and Singer, S. W. (2014). MaxBin: an automated binning method to recover individual genomes from metagenomes using an expectation-maximization algorithm. *Microbiome* 2:26. doi: 10.1186/2049-2618-2-26

Wu, Y., Zeng, J., Zhu, Q., Zhang, Z., and Lin, X. (2017). pH is the primary determinant of the bacterial community structure in agricultural soils impacted by polycyclic aromatic hydrocarbon pollution. *Sci. Rep.* 7:40093. doi: 10.1038/srep40093

Xiong, W., Mathies, C., Bradshaw, K., Carlson, T., Tang, K., and Wang, Y. (2012). Benzene removal by a novel modification of enhanced anaerobic biostimulation. *Water Res.* 46, 4721–4731. doi: 10.1016/j.watres.2012.06.036

Yurchenko, T., Ševčíková, T., Přibyl, P., El Karkouri, K., Klimeš, V., Amaral, R., et al. (2018). A gene transfer event suggests a long-term partnership between eustigmatophyte algae and a novel lineage of endosymbiotic bacteria. *ISME J.* 12, 2163–2175. doi: 10.1038/s41396-018-0177-y

Zhao, R., Summers, Z. M., Christman, G. D., Yoshimura, K. M., and Biddle, J. F. (2020). Metagenomic views of microbial dynamics influenced by hydrocarbon seepage in sediments of the Gulf of Mexico. *Sci. Rep.* 10:5772. doi: 10.1038/s41598-020-62840-z

frontiers | Frontiers in Microbiology

TYPE Original Research
PUBLISHED 01 July 2024
DOI 10.3389/fmicb.2024.1423741

OPEN ACCESS

EDITED BY
Linduo Zhao,
University of Illinois at Urbana-Champaign, United States

REVIEWED BY
Wei Li,
Lawrence Livermore National Laboratory (DOE), United States
Amrik Bhattacharya,
Amity University, India

*CORRESPONDENCE
Loubna El Fels
✉ loubna.elfels@uca.ac.ma;
✉ loubna.elfels@gmail.com
Mohamed Hafidi
✉ hafidi@uca.ac.ma

RECEIVED 26 April 2024
ACCEPTED 03 June 2024
PUBLISHED 01 July 2024

CITATION
Aké AHJ, Rochdi N, Jemo M, Hafidi M, Ouhdouch Y and El Fels L (2024) Cr(VI) removal performance from wastewater by *microflora* isolated from tannery effluents in a semi-arid environment: a SEM, EDX, FTIR and zeta potential study.
Front. Microbiol. 15:1423741.
doi: 10.3389/fmicb.2024.1423741

Cr(VI) removal performance from wastewater by *microflora* isolated from tannery effluents in a semi-arid environment: a SEM, EDX, FTIR and zeta potential study

Aké Henri Joël Aké[1], Nabil Rochdi[2,3], Martin Jemo[4], Mohamed Hafidi[1,5]*, Yedir Ouhdouch[1,4] and Loubna El Fels[1]*

[1]Laboratory of Microbial Biotechnologies, Agrosciences and Environment, Labeled Research Unit-CNRST N°4, Faculty of Sciences Semlalia, Universiry Cadi Ayyad, Marrakesh, Morocco, [2]Laboratory of Innovative Materials, Energy and Sustainable Development (IMED-Lab), Cadi Ayyad University, Marrakesh, Morocco, [3]Department of Physics, Faculty of Sciences Semlalia, Cadi Ayyad University, Marrakesh, Morocco, [4]AgroBiosciences Program, College of Agriculture and Environmental Sciences, University Mohammed VI Polytechnic (UM6P), Ben Guerir, Morocco, [5]African Sustainable Agriculture Research Institute (ASARI), College of Agriculture and Environmental Sciences, University Mohammed VI Polytechnic (UM6P), Laâyoune, Morocco

Hexavalent chromium removal from the environment remains a crucial worldwide challenge. To address this issue, microbiological approaches are amongst the straightforward strategies that rely mainly on the bacteria's and fungi's survival mechanisms upon exposure to toxic metals, such as reduction, efflux system, uptake, and biosorption. In this work, scanning electron microscopy, energy-dispersive X-ray spectrophotometry, Fourier transform infrared spectroscopy, and zeta potential measurements were used to investigate the ability of chromium adsorption by *Bacillus licheniformis*, *Bacillus megaterium*, *Byssochlamys* sp., and *Candida maltosa* strains isolated from tannery wastewater. Scanning electron microscopy combined with energy dispersive X-ray spectroscopy revealed alterations in the cells treated with hexavalent chromium. When exposed to 50 mg/L Cr^{6+}, *Bacillus licheniformis* and *Candida maltosa* cells become rough, extracellular secretions are reduced in *Bacillus megaterium*, and *Byssochlamys* sp. cells are tightly bound and exhibit the greatest Cr weight percentage. In-depth analysis of Fourier transform infrared spectra of control and Cr-treated cells unveiled Cr-microbial interactions involving proteins, lipids, amino acids, and carbohydrates. These findings were supported by zeta potential measurements highlighting significant variations in charge after treatment with Cr(VI) with an adsorption limit of 100 mg/L Cr^{6+} for all the strains. *Byssochlamys* sp. showed the best performance in Cr adsorption, making it the most promising candidate for treating Cr-laden wastewater.

KEYWORDS

chromium bioremediation, scanning electron microscopy, energy-dispersive X-ray spectroscopy, Fourier transform infrared spectroscopy, zeta potential measurements

1 Introduction

Chromium (Cr) and its salts are involved in plenty of industrial processes, such as the manufacturing of paints, dyes, plastics, and stainless steel, the wood treatment, and the leather tanning. Unlike its trivalent form (Cr^{3+}), hexavalent chromium (Cr^{6+}) poses a serious environmental problem (Fu et al., 2021; Lara et al., 2021; Wang et al., 2022; Aguilar et al., 2023; Mohanty et al., 2023) and triggers harmful effects that make its elimination essential (Wang et al., 2021; Aké et al., 2022; Alharbi et al., 2022). Moreover, Cr^{6+} is found to be particularly hazardous to health (Tangahu et al., 2020; Aparicio et al., 2021) and responsible for dysfunction in living organisms (Tripathi et al., 2018; Chromikova et al., 2022). Hence, Cr^{6+} removal has become the focus of attention in health and safety projects (Tumolo et al., 2020; Anupong et al., 2022; Ariram et al., 2022).

Based on these considerations, it is obvious that substantial efforts were deployed toward building environmentally friendly solutions for the treatment of chromium (VI). In this context, researchers developed biological methods making use plants and microorganisms to detoxify the environment (Xia et al., 2019; Yasir et al., 2021). Bacteria and fungi repeatedly demonstrated their ability to resist or remove Cr^{6+} present in environmental or culture media (Chang et al., 2016; Kalsoom K. et al., 2021; Aké et al., 2023). Indeed, it has been shown that anaerobically or aerobically cultivated bacteria in laboratory can eliminate the synthetic Cr^{6+} contained in culture media via a number of mechanisms (Lin et al., 2020; Plestenjak et al., 2022). In an earlier work, we demonstrated the aerobic reduction of Cr^{6+} to trivalent chromium by cultures of *Bacillus licheniformis*, *Bacillus megaterium*, *Byssochlamys sp.*, and *Candida maltosa* strains isolated from tannery effluents (Aké et al., 2023). Similar reduction of Cr^{6+} to Cr^{3+} was observed for *Penicillium* sp. PL17, *Fusarium proliferatum* FBL1, *Aspergillus fumigatus* ML43, and *Rhizopus* sp. CUC23 (Bibi et al., 2018). The ability to reduce Cr^{6+} is one of the mechanisms of strain resistance to Cr (Aké et al., 2023) that include biosorption, bioaccumulation, biotransformation, and efflux systems (Gang et al., 2019; Xia et al., 2019; Ayele et al., 2021; Elahi et al., 2022; Plestenjak et al., 2022). Microorganisms can act as adsorbents, similar to carbon nanotubes, activated carbon, graphene oxide, polymers, clays, green slow-releasing denaturing colloidal substrates (such as gelatin, agar, and cane molasses), and their recently-used modifications (Sathvika et al., 2019). Once Cr^{6+} is in the vicinity of the cell, it can be attached (adsorption) to the cell's surface by specific molecules (COOH, NH_3^+, etc.) and subsequently reduced to Cr^{3+}. This reduction may be spontaneous or due to a cytochrome network in the cell wall (Thatoi et al., 2014; Upadhyay et al., 2017; Li et al., 2021; Mat Arisah et al., 2021). Chromium adsorption can be checked by measuring its content after the cell washing (exposure), allowing one to quantitatively assess the concentrations of adsorbed ionic species, especially Cr^{6+} and Cr^{3+} ions. On the other hand, the researchers can identify the families of molecules involved in the adsorption of Cr^{6+} using Fourier transform infrared spectroscopy (FTIR) analyses (Kaduková and Virčíková, 2005; Sharma et al., 2022). Besides adsorption on the cell surface, chromium can penetrate the microbial cell through sulfate and phosphate transporters (SO_4^{2-}, PO_4^{3-}), and Cr^{6+} can undergo enzymatic or non-enzymatic reduction (indirect reduction) inside the cell (Thatoi et al., 2014). The ability of microorganisms to adsorb Cr^{6+} and Cr^{3+} was also demonstrated using scanning electron microscopy (SEM) combined to energy dispersive X-ray spectroscopy (EDX) (Abo-Alkasem et al., 2022; Chromikova et al., 2022). At high concentrations, the authors found cellular modifications due to high Cr^{6+} concentrations (Abo-Alkasem et al., 2022; Chromikova et al., 2022). Therefore, the combination of FTIR and SEM-EDX analyses is a powerful tool to understand the Cr resistance mechanisms. While FTIR relies on the vibrational behavior of Cr-loaded cells to identify the chemical environments and involved functional groups, SEM and EDX provide an overview of the surface morphology and elemental contents in treated specimens. However, this approach is not sufficient since it does not provide insight into the electrical phenomena that occur between Cr molecules and ligands on the surface of microorganisms. The study of the electrical charges surrounding the cells enables a better understanding of the interactions between metals and microbial cells. To that end, zetametry is an effective tool to assess the electric charge that a particle, in suspension or in solution, acquires from the surrounding ion cloud using the potential difference between the particle-medium interfacial layer and the medium (the so-called zeta potential) (Samaké, 2008; Al-Jubory et al., 2020; Youssef et al., 2020). The combination of FTIR, SEM, EDX, and zetametry measurements has been used successfully in the study of Cd(II) biosorption by *Bacillus cereus* RC−1 cells, for instance (Huang et al., 2013) but not in a study of Cr^{6+} adsorption by bacteria and fungi.

Accordingly, the aim of the present work is to examine the potential of chromium (VI) adsorption and its biotransformation into chromium (III) using indigenous strains of *Bacillus licheniformis*, *Bacillus megaterium*, *Byssochlamys* sp., and *Candida maltosa* that were isolated from tannery effluents. SEM-EDX characterizations were carried out for the investigated biomasses to probe the modifications in morphology and chemical makeup after Cr loading. Similarly, FTIR characterizations were also performed to reveal the major vibrational alterations after treatment with chromium in order to incriminate the possible functional groups involved in the metal-microbial strain interactions. In this respect, we carried out in-depth analyses of vibrational modes in the investigated strains to provide a useful literature impetus about the infrared signature of investigated strains. Moreover, zeta potential characterizations were performed to assess the modifications in the electrical behavior of the strain environment upon Cr loading.

2 Materials and methods

2.1 Microorganism isolation

The raw tannery effluent was sampled from Bab Dbagh and the industrial district at Marrakech tannery manufacturing, which operates with chrome-tanning processes. *Bacillus licheniformis*, *Bacillus megaterium*, *Byssochlamys* sp., and *Candida maltosa* strains were isolated from tanneries effluents and identified using the previously reported molecular methods (Aké et al., 2023).

2.2 SEM-EDX analysis

Culture pellets were subjected to SEM and EDX characterizations in order to confirm Cr adsorption and to examine the impact of Cr on cell morphologies. The experimental procedure was similar to that applied by Karthik et al. (2017). After incubation for 96 h, the cells in 100-µL precultures with 0, 5, and 50 mg/L Cr^{6+} were harvested by centrifugation at 5000 rpm. After washing with a 0.1 mM phosphate buffer solution (pH 7) to remove the cells from the culture medium, the pellets were fixed overnight in 3% glutaraldehyde at 4 °C. Subsequent dehydration cycles using ethanol at different volume concentrations (20%, 40%, 60%, 80%, 90%, and 100%) were applied to the pellets treated with glutaraldehyde. The surface morphology and the chemical composition of dehydrated strains supported on carbon sheets were analyzed using a TESCAN VEGA 3 scanning electron microscope equipped with an energy-dispersive X-ray spectrometer. The SEM images were obtained by detecting the secondary electrons emitted by the samples when excited with a beam of 10 keV energy. The EDX spectra were recorded at a beam energy of 5 keV to detect the prominent Cr Lα radiation with an energy of about 0.57 keV. Further analyses were performed with a beam energy of 10 keV to check the detection of Cr Kα and Kβ characteristic lines located at 5.41 and 5.95 keV, respectively. Microbial cells cultured without Cr^{6+} were used as a control and are referred to as "native" hereafter.

2.3 FTIR analysis

In order to determine the impact of Cr^{6+} on the functional groups of the microbial cell surface, 100 µL of preculture (24 h) of each strain was introduced into Luria-Bertani (LB) broth containing 50 mg/L Cr^{6+} (30 °C, pH 7). At the same time, a control without Cr^{6+} was prepared for each strain. After 96 h incubation, the cells were then collected in 15 mL tubes and centrifuged at 5000 rpm (20 min, 4 °C). After that, the preparation procedure was performed according to the analytical method used by Maurya et al. (2022). The pellets were washed with a 0.1 mM phosphate buffer solution (pH 7) to remove to remove the cells from the culture medium, then freeze-dried using a Martin Christ Alpha 1-2 LO plus lyophilizer. A total 0.099 g of KBr powder was mixed with 0.001 g of each powder pellet obtained and grinded in a mortar. After mixing, the product was ground, homogenized, and then pressed into pellets using a compressor. The as-obtained pellets were introduced into a Bruker Vertex 70 FTIR spectrometer. Each IR spectrum was obtained by averaging 31 scans recorded in the 400–4000 cm^{-1} range with a wavenumber step of 2 cm^{-1}.

2.4 Zeta potential analysis

In order to understand the electrostatic interactions between the microbial cell and Cr^{6+}, the zeta potential measurements were carried out using a Malvern zetasizer ver. 7.12. To that end, a modified experiment derived from Beiranvand et al. (2022) was applied. Different concentrations of Cr^{6+}, namely 25, 50, 100, 250, 500, and 800 mg/L, were prepared in distilled water. The inoculum of each strain was added to each Cr^{6+} concentration (5 mL). Positive controls, i.e., solutions without inocula, were also prepared. The zeta potential was also measured in pure distilled water.

2.5 Statistical analysis

The experiments from the study were carried out in triplicate. The data obtained were statistically analyzed and are presented with the appropriate standard deviation. ANOVA tests were carried out to better understand the effect of the microbial strain treatments. *Post-hoc* tests were then applied to observe the significance between groups. The least significant differences among means were evaluated at the 5% significance level. IBM SPSS Statistics 25 was used for the statistical analysis of the data.

3 Results

3.1 SEM analysis

The SEM images of Figure 1 depict the morphologies of the *Bacillus licheniformis*, *Bacillus megaterium*, *Byssochlamys* sp., and *Candida maltosa* strains without Cr treatment (upper images) and after exposure to 5 and 50 mg/L of hexavalent chromium (middle and bottom images, respectively). These SEM images are displayed with the same magnifications to show specific features in structure of each sample.

In the case of the Cr^{6+}-free *Bacillus licheniformis* strains, the cells are smooth, compact, and firmly grouped in the form of asymmetric clusters (Figure 1A). In addition, the native cells are typically regular in shape, and their assembly gives rise to a domed structure with corrugations. After contact with 5 mg/L Cr^{6+}, the cells are still smooth and clustered, with a quite regular cell size. In other words, both of the native bacterial biomass and that exposed to 5 mg/L Cr^{6+} show similar cell surfaces. However, at 50 mg/L Cr^{6+}, the appearance of the bacterial biomass is altered and shows wrinkled, rough, and irregular clusters of less distinct cells, with possible extracellular secretions.

In contrast, the *Bacillus megaterium* strains do not show very distinct cell shapes, either in the absence or presence of Cr^{6+} (Figure 1B). The cells form aggregates with apparent depressions and exhibit a very compact texture with irregular edges that appear to be bound with an extracellular matrix. The visual examination of SEM images suggests a higher content of extracellular secretions in the control than in the strains grown at 5 and 50 mg/L Cr^{6+}.

For the *Byssochlamys* sp. strains (Figure 1C), the control and the strain loaded with 5 mg/L Cr^{6+} show the same appearance. Indeed, the cells appear smooth, less bound, and exhibit a few corrugations. In contrast, the strain cultured with 50 mg/L Cr^{6+} show a different topography since the cells are tightly bound and offer a compact space upon exposure to Cr^{6+}.

Similarly, the *Candida maltosa* control cells and those treated with 5 mg/L Cr^{6+} show a smooth outline morphology with visible depression regions (Figure 1D). The SEM image of native strains shows structures of a regular size in the 1–2 µm range, which

corresponds to the typical size of the *Candida maltosa* cells. However, at 5 mg/L Cr^{6+}, some cells are less visible and form irregular blocks. At a concentration of 50 mg/L Cr^{6+}, several cells had lose their initial structures and appear slightly rough and deformed.

3.2 EDX analysis

EDX analysis was performed to determine whether the microbial cell surfaces are capable of bio-adsorbing Cr. Figure 2 shows the EDX analysis of *Bacillus licheniformis*, *Bacillus megaterium*, *Byssochlamys* sp., and *Candida maltosa* strains grown without Cr treatment and after loading with 5 and 50 mg/L Cr^{6+}. The determined weight and atomic percentages of Cr (Cr wt.% and Cr at.%, respectively) are given in Table 1.

Besides the characteristic C K line (overlapping of the Kα and Kβ peaks) located at about 0.28 keV, the EDX spectra of all the control strains show no signature of the Cr Lα feature (at 0.57 keV) but the neighboring O K feature arising from the overlapping Kα and Kβ peaks (located at ~0.52 and 0.53 keV, respectively). The nitrogen signature (expected at 0.39 and 0.4 keV) is not discernible from the prominent carbon peak. Additional small peaks at energies consistent with the Kα and Kβ lines of Na (1.04 and 1.07 keV), Mg (1.25 and 1.3 keV), Al (1.49 and 1.55 keV), P (2.01 and 2.14 keV), and S (2.31 and 2.47 keV) are also observed. The presence of these peaks probably originates from compounds present in the cell wall.

In contrast, the biomasses that has grown in the Cr^{6+}-amended culture media show the abovementioned Cr peak (Cr Lα line at 0.57 keV). After treatment of the microorganisms with 5 mg/L Cr^{6+}, the EDX analyses reveal Cr weight percentages of 1.1, 0.52, 0.51, and 0.62 and atomic percentages of 0.30, 0.14, 0.13, and 0.17 for *Bacillus licheniformis*, *Bacillus megaterium*, *Byssochlamys* sp., and *Candida maltosa*, respectively. Nevertheless, chromium contents decrease in each strain after exposure to 50 mg/L Cr^{6+}; the Cr weight percentages were 0.29, 0.25, 0.35, and 0.23, and the Cr atomic percentages were 0.08, 0.07, 0.09, and 0.06 for *Bacillus*

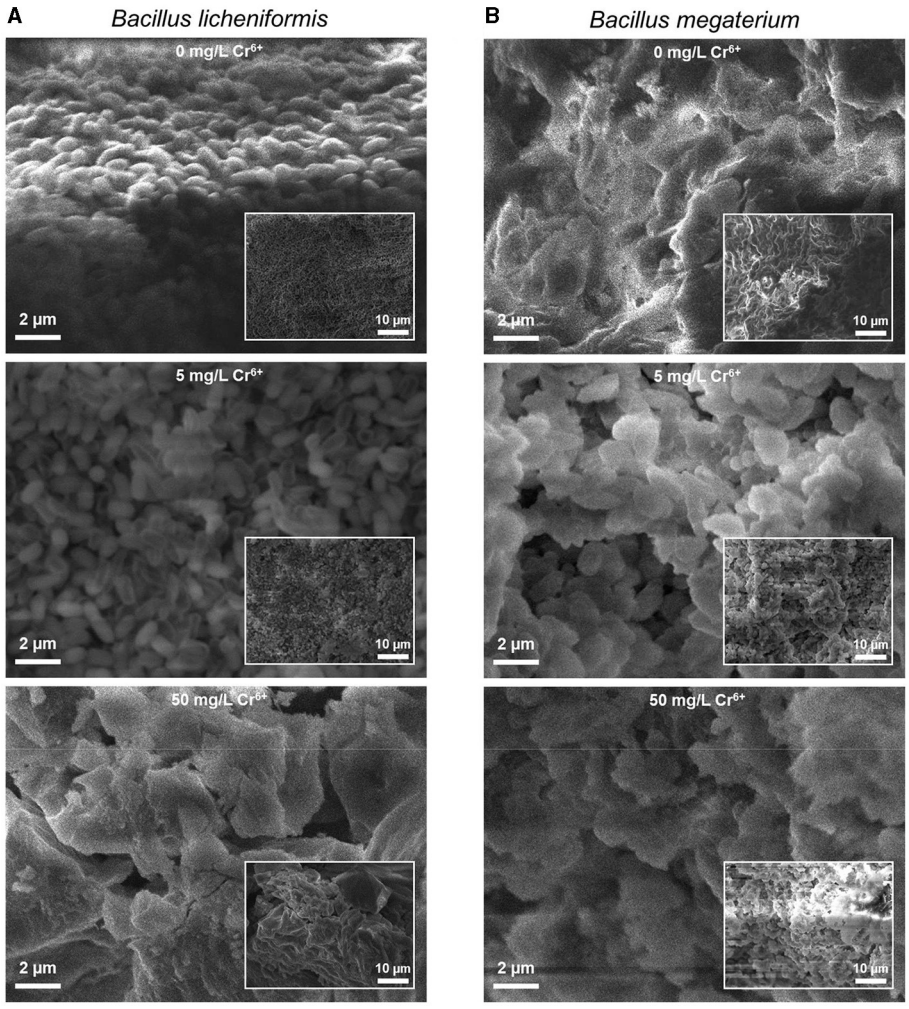

FIGURE 1
(Continued)

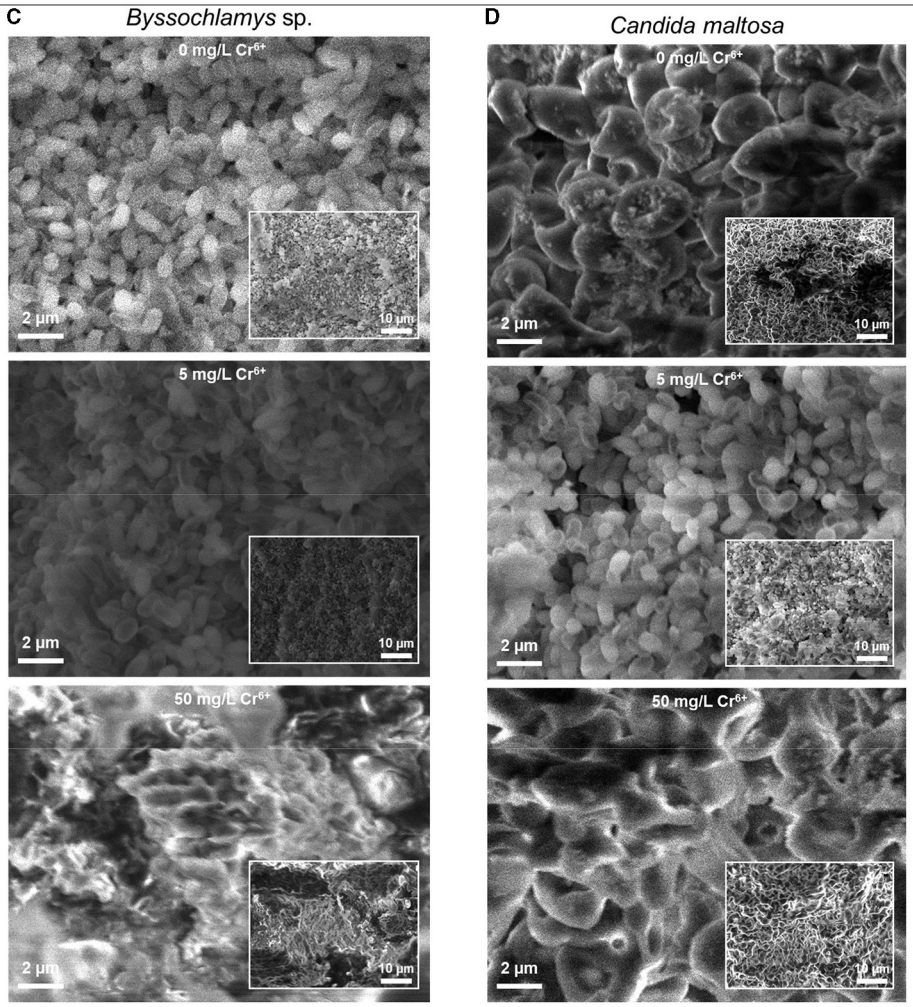

FIGURE 1 (Continued)
Secondary electron SEM images of the native (upper images) and treated strains with 5 (middle images) and 50 mg/L Cr^{6+} (bottom images) in LB medium for *Bacillus licheniformis* **(A)**, *Bacillus megaterium* **(B)**, *Byssochlamys* sp. **(C)**, and *Candida maltosa* **(D)** strains isolated from tannery effluents. The SEM images and the inset low-magnification secondary electron SEM images are displayed with the same scales for all the samples.

licheniformis, *Bacillus megaterium*, *Byssochlamys* sp., and *Candida maltosa*, respectively.

3.3 FTIR analysis

The FTIR spectra of the investigated strains consist of numerous overlapping bands, most of which are derived from protein, lipid, amino acid, and carbohydrate functional groups. Table 2 summarizes the prominent identified vibrations and corresponding assignments for the *Bacillus licheniformis*, *Bacillus megaterium*, *Byssochlamys* sp., and *Candida maltosa* specimens, before and after chromium loading.

As depicted in Figure 3, the FTIR spectrum of the native *Bacillus licheniformis* strains shows a prominent and asymmetric absorption band peaking at 3302 cm^{-1} due to protein and peptide N–H stretching (amide A band), which overlaps with a broad band related to O–H stretching from hydroxyl groups in carbohydrates (~3550–3150 cm^{-1}), along with the NH_3^+ asymmetric stretching band from amino acids (~3200–3000 cm^{-1}). Two strong secondary polyamide bands can be seen at ~1656 and 1546 cm^{-1}. The vibration at 1656 cm^{-1} is ascribed to the amide I band in α-helical structures (proteins and polypeptides), which is dominated by C=O stretching (Venyaminov and Kalnin, 1990b; Socrates, 2001). In this regard, it is noteworthy to mention that C=C stretching in lipid esters (expected at about 1650 cm^{-1}), β-type secondary structures of proteins (indiscernible features), along with CO_2^- and NH_3^+ vibrations in amino acids (around 1686 and 1636 cm^{-1}), may have contributed to the above-assigned amide I band (Venyaminov and Kalnin, 1990a,b; Naumann, 2000; Socrates, 2001). The band at 1546 cm^{-1} corresponds to the amide II band originating from in-plane N–H bending and C–N stretching and gives rise to an overtone feature, as shown by the shoulder around 3090 cm^{-1} (~3067 cm^{-1} as determined using the second derivative).

Moreover, the CH_3 and CH_2 functional groups (fatty acid chains in lipids) exhibit characteristic C–H asymmetric stretching vibrations at 2962 and 2929 cm^{-1}, respectively. The corresponding C–H asymmetric stretching vibrations were resolved into components at 2876 and 2852 cm^{-1}, respectively,

10.3389/fmicb.2024.1423741

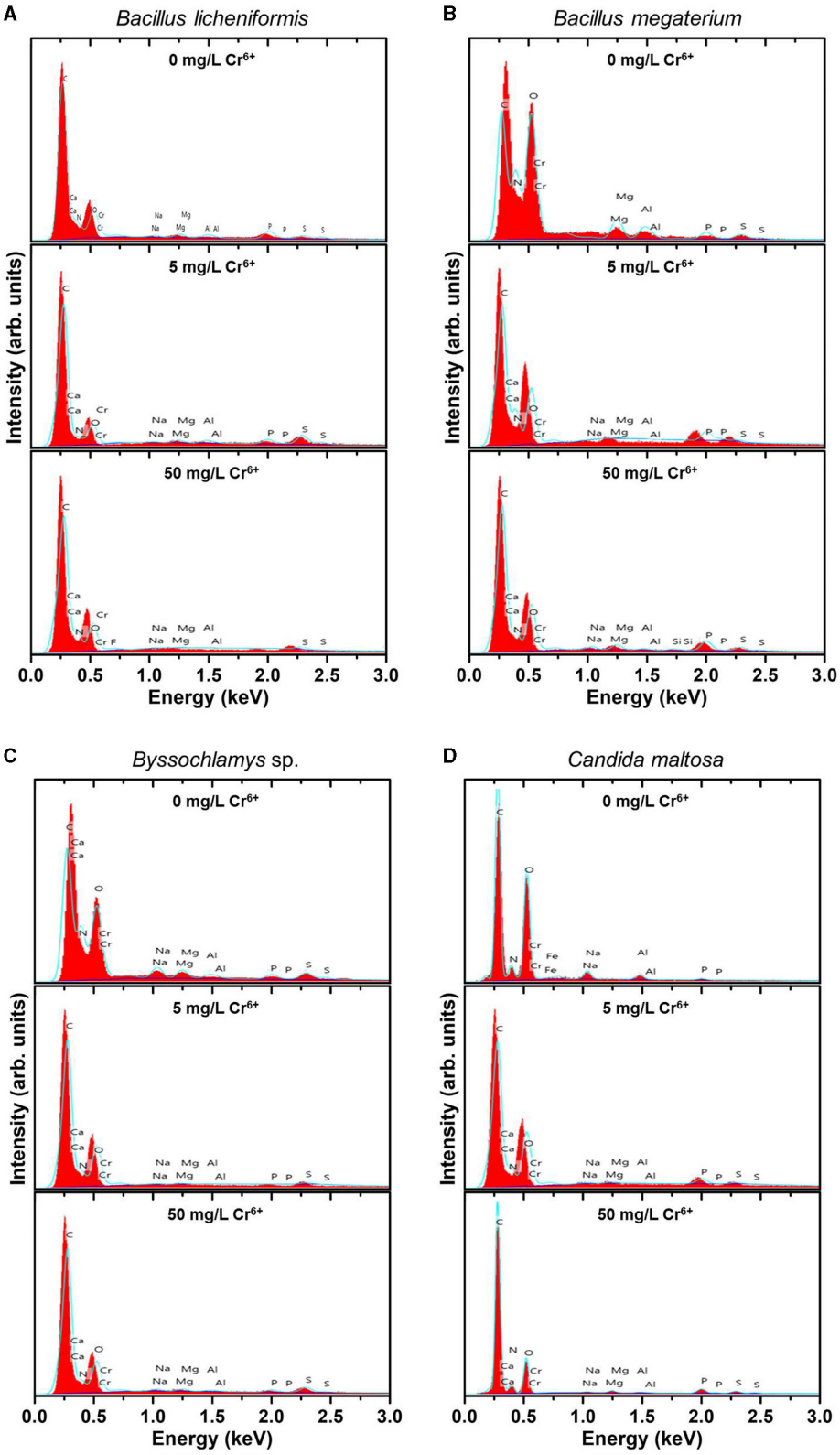

FIGURE 2
EDX spectra of the native (upper spectra) and treated strains with 5 mg/L Cr^{6+} (middle spectra) and 50 mg/L Cr^{6+} (bottom spectra) in LB medium for *Bacillus licheniformis* **(A)** *Bacillus megaterium* **(B)**, *Byssochlamys* sp. **(C)**, and *Candida maltosa* **(D)** strains isolated from tannery effluents.

TABLE 1 Weight and atomic percentages of *Bacillus licheniformis*, *Bacillus megaterium*, *Byssochlamys* sp., and *Candida maltosa* microbial biomasses before (0 mg/L Cr^{6+}) and after treatment with 5 and 50 mg/L Cr^{6+}.

Strain	Concentration (mg/L)	Cr contents	
		(wt.%)	(at.%)
Bacillus licheniformis	0	0.00	0.00
	5	1.10	0.30
	50	0.29	0.08
Bacillus megaterium	0	0.00	0.00
	5	0.52	0.14
	50	0.25	0.07
Byssochlamys sp.	0	0.00	0.00
	5	0.51	0.13
	50	0.35	0.09
Candida maltosa	0	0.00	0.00
	5	0.62	0.17
	50	0.23	0.06

yielding a single shoulder-like feature at about 2860 cm^{-1}. These aliphatic groups are also seen at 1444, 1386, and 723 cm^{-1}, corresponding to CH_2 deformation, CH_3 symmetric bending, and CH_2 rocking characteristic bands, respectively (Socrates, 2001). The FTIR spectra also display weak features corresponding to the amide III band in α-helical protein and peptide structures (caused by coupled C–N stretching and N–H bending) and the amide V band (originating from N–H bending), as shown by the shoulders at ~1275 and 726 cm^{-1}, respectively.

Characteristic bands of phosphodiester, free phosphate, and polysaccharide functional groups are found in the 1250–900 cm^{-1} region. Indeed, the bands at 1242 and 1110 cm^{-1} are attributed to the phosphodiester stretching modes, while the band at 1069 cm^{-1} refers to free phosphate ionic species. However, the latter is also consistent with the stretching of C–O and C–C bonds in polysaccharide rings and C–O–C bonds in lipids (Wilson et al., 2000; Socrates, 2001). Similarly, the band at 1156 cm^{-1} is consistent with C–O–C stretching in lipids, C–O stretching in monosaccharide compounds (such as glucose), and C–O–C stretching of the glycosidic link in polysaccharides (Naumann, 2000; Socrates, 2001). The bands at 765 and 920 cm^{-1} also refer to symmetric and asymmetric breathing of the pyranose ring in polysaccharide compounds (Copíková et al., 2001; Socrates, 2001). In this regard, the vibration at 886 cm^{-1} is characteristic of the anomer C–H deformation in carbohydrates and provides evidence of the major β-form of the polysaccharide pyranose rings (Socrates, 2001; Hong et al., 2021).

In the wavenumber range below 900 cm^{-1}, weak-to-medium intensity features are overlapped with a broad medium-to-strong band centered at roughly 660 cm^{-1}. The latter is typical of hydroxyl group O–H wagging, but it can also include contributions from other hydrogen-bonded groups, such as water O–H or amide N–H wagging motions. The presence of α-amino-acids (such as glutamic acid and alanine) in the *Bacillus licheniformis* spore is supported by features related to O–CO (bands at 659 and 618 cm^{-1}) and C–CO (shoulder at 531 cm^{-1}) deformation vibrations in α-aliphatic carboxylic acids in this spectral range (Hughes, 1968). The band at 439 cm^{-1} cannot be restrainedly assigned by cross-referencing with other bands and is not used in the discussion hereafter.

The FTIR spectrum of native *Bacillus licheniformis* also includes hidden vibrations, such as the band at 1749 cm^{-1} originating from C=O stretching of carboxylic groups (esters and fatty acids), the band at 1515 cm^{-1} related to C–C stretching in the tyrosine aromatic ring (side-chain vibration in amino acids), or the band at 1463 cm^{-1} due to methyl and methylene vibrations (Schmitt and Flemming, 1998; Socrates, 2001; Tremmel et al., 2005; El-Naggar et al., 2020).

The broad weak band at around 2120 cm^{-1}, which overlaps with the water scissoring and rocking vibrations, is related to amino acid NH_3^+ symmetric stretching (Socrates, 2001; Lasagabaster et al., 2006). Close to this band, the absorption features at 2375 and 2340 cm^{-1} correspond to asymmetric stretching of adsorbed and gaseous CO_2, respectively (Busca and Lorenzelli, 1982; Seiferth et al., 1999) and are most likely brought on by residual contamination.

The Cr(VI) treatment brings about the rise of the shoulder band (~964 cm^{-1}) and the shift (from 1069 to 1075 cm^{-1}) of the PO_3^{2-} symmetric and asymmetric stretching bands, respectively. Furthermore, the PO_2^- symmetric stretching band exhibits an increase in intensity along with a slight shift (from 1110 to 1113 cm^{-1}). These changes suggest that the phosphate-containing compounds are involved in the interaction with metal ions. This interaction yields the emergence of negative phosphoryl groups as a result of a deprotonation process. This is further supported by the partial vanishing and the shift (from 1033 to 1025 cm^{-1}) of the P–O–C stretching shoulder band. In addition, the increase of the PO_2^- band (~1110 cm^{-1}) is related to the observed weakening of the CH_3 stretching, as shown by the decrease in intensity of the band at 2929 cm^{-1} (with respect to the CH_2 band). This is also substantiated by the relative decrease of the CH_3 bending band (1386 cm^{-1}) with respect to the CH_3 deformation band (~1444 cm^{-1}) (Barkleit et al., 2011).

In contrast to *Bacillus licheniformis*, the high-frequency region in the native *Bacillus megaterium* spectrum (Figure 4) is dominated by the OH stretching band (3438 cm^{-1}) superimposed with the NH stretching band (shoulder at 3274 cm^{-1}). This is also visible at low frequencies, where the broad OH wagging (400–900 cm^{-1}) fully dominates the cluster of characteristic polysaccharide and amino acid absorption bands in this range. These intense OH vibrations probably stem from the monosaccharide content (mainly composed of D-glucose, D-xylose, D-galactose, and L-arabinose) in the *Bacillus megaterium* capsule (Cassity and Kolodziej, 1984). Additionally, the amide I and II bands appear at shifted positions (1641 and 1550 cm^{-1}, respectively) as a result of strong stretching of NH_3^+ and COO^- in amino acids (Venyaminov and Kalnin, 1990a). This is in agreement with the medium and broad band observed at 2120 cm^{-1} originating from NH_3^+ asymmetric stretching and the COO^- band at 1400 cm^{-1}. Therefore, a broad medium band arising from NH_3^+ symmetric stretching in the 2760–2530 cm^{-1} region could explain the weak

TABLE 2 Frequencies[a] and tentative assignment of prominent vibrational modes[b] in native and chromium(VI)-treated *Bacillus licheniformis, Bacillus megaterium*, *Byssochlamys sp.*, and *Candida maltosa* strains as identified from FTIR measurements.

B. licheniformis		*B. megaterium*		*Byssochlamys sp.*		*C. maltosa*		Assigned vibrations	Comments
Native	Treated	Native	Treated	Native	Treated	Native	Treated		
3761	3761	3755	3759	3755	3759	3756	3758	Water ν_{as}(O–H)	
–	–	3438 3435*	–	–	–	–	–	Carbohydrate ν(O–H)	
3302 3282*	3299 3282*	– 3274*	3299 3284*	3297 3279*	3298 3281*	3304 –	3304 –	Protein / peptide amide A ν(N–H)	Overlapped with hydroxyl group ν(O–H) and amino acid $\nu_{as}(-NH_3^+)$
– 3067*	– 3066*	– 3066*	3093 3067*	3094 3068*	– 3067*	– 3061*	– 3064*	First overtone of the amide II band	Also consistent with a polyglycine ν(N–H) band
2962 2964*	2963 2964*	2966 2963*	2961 2964*	2963 2965*	2962 2964*	2958 2965*	2958 2964*	Lipid / fatty acids $-CH_3$ ν_{as}(C–H)	
2929 2926*	2932 2928*	2933 2925*	2930 2926*	2934 2928*	2931 2927*	2928 2927*	2927 2925*	Lipid / polyglycine $>CH_2$ ν_{as}(C–H)	
– 2876*	– 2874*	– 2874*	– 2876*	2883 2874*	– 2875*	– 2877*	– 2877*	Lipid $-CH_3$ ν_s(C–H)	
2852*	2853*	2852*	2853*	2853*	2853*	2852*	2852*	Lipid / polyglycine $>CH_2$ ν_s(C–H)	
2375 2372*	2374 2372*	2373 2371*	2374 2371*	2373 2372*	2373 2371*	2372 2369*	2373 2370*	Physisorbed CO_2 $\nu_{as}(CO_2)$	Most likely a spurious band due to contamination with CO_2
2340 2341*	2339 2342*	2340 2342*	2340 2341*	2340 2341*	2341 2342*	2341 2340*	2341 2342*	Gaseous CO_2 $\nu_{as}(CO_2)$	Most likely a spurious band due to contamination with CO_2
–	–	2120	2128	2118	2129	2120	2124	Amino acid $\nu_{as}(-NH_3^+)$	Probably overlapped with Water sc(H_2O) and $\rho(H_2O)$
1749*	1747*	–	1746*	1746*	1744*	1747*	1748*	Lipid / amino acid ν(C=O)	
1686*	1689*	1684*	1689*	1693*	1690*	1697*	1691*	Polyglycine $\nu(CO_2^-)$	Also consistent with β-antiparallel pleated sheet protein / peptide amide I ν(C=O)
1656 1662*	1658 1662*	– 1660*	1657 1662*	1658 1662*	1656 1662*	1655 –	1657 1662*	α-helix protein / peptide amide I ν(C=O)	With smaller ν(C–N) and δ(N–H) contributions Probably overlapped with ester ν(C=C)
– 1636*	– 1635*	1641 1632*	– 1635*	–	1636*	–	–	Amino acid / polyglycine $\mu_{as}(NH_3^+)$	Also consistent with β-sheet protein / peptide amide I ν(C=O) and water δ(O–H)
–	–	–	–	1617*	–	1621*	1626*	Amino-/fatty acids $\nu_{as}(CO_2^-)$ and $\mu_{as}(-NH_3^+)$	
1573*	1572*	1568*	1574*	1573*	1574*	1572*	1572*	Polyglycine $\mu_{as}(NH_3^+)$	
1546 1544*	1544 1544*	1550 1546*	1546 1544*	1546 1544*	1546 1544*	1545 1544*	1545 1545*	α-helix protein / peptide amide II δ(N–H) and ν(C–N) Amino-/fatty acids $\nu_{as}(CO_2^-)$	Also consistent with amino acid $\mu(NH_2)$
1515*	1515*	1519*	1514*	1511*	1515*	1512*	1514*	Amino acid tyrosine ring vibration and $\mu_s(-NH_3^+)$	Also consistent with polyglycine μ(N–H)
1463*	1463*	1463*	1463*	1461*	1464*	1464*	1465*	Lipid $\delta_{as}(CH_3)$ and sc(CH_2)	
1444 1442*	1444 1442*	1446 1444*	1445 1443*	1444 1442*	1444 1442*	1447 1443*	1444 1443*	Lipid cyclohexyl (fatty acids) $\mu(CH_2)$	

(Continued)

TABLE 2 (Continued)

B. licheniformis		*B. megaterium*		*Byssochlamys sp.*		*C. maltosa*		Assigned vibrations	Comments
Native	Treated	Native	Treated	Native	Treated	Native	Treated		
–	–	1400 1404*	– 1401*	–	–	1398*	1401	Amino/fatty acids / Polyglycine $\nu_s(CO_2^-)$	
1386 1380*	1386 1378*	– 1380*	1386 1378*	1385 1376*	1386 1377*	1387 1376*	1385 1377*	Lipid $\delta_s(CH_3)$	Also consistent with Carbohydrate μ(CH)
1315 1314*	1314 1315*	1317 1320*	1316 1314*	1314 1314*	1315 1314*	1312 1313*	1314 1314*	Polysaccharide μ(OH)	Also consistent with amine $\tau(CH_2)$
1275 1279*	– 1280*	1280 1280*	1278 1280*	1276 1279*	1277 1280*	– 1280*	– 1280*	α-helix protein amide III ν(C–N) and δ(N–H)	With smaller ν(C=O) and δ(O=C–N) contributions
1242 1240*	1243 1237*	1245 1241*	1239 1240*	1243 1240*	1241 1238*	1242 1235*	1244 1237*	Phospholipid / phosphodiester $>PO_2^-$ ν_{as}(P=O)	
1156 1163*	– 1169*	1151 1160*	1159 1165*	1163 1165*	1160 1166*	– 1161*	– 1159*	Polysaccharide glycosidic link ν(C–O–C) Lipid ν_{as}(CO–O–C)	Also consistent with saccharide ν(C–C), secondary alcohol ν(C–O), and amino acid $\rho(NH_3^+)$
1110 1117*	1113 1115*	– 1120*	– 1118*	1111 1118*	1108 1118*	– 1118*	– 1111*	Phospholipid / phosphodiester $\nu_s(PO_2^-)$	Also consistent with saccharide secondary alcohol ν(C–O)
1069 1069*	1075 1068*	1071 1078*	1068 1065*	1069 1072*	1071 1067*	1073 1079*	1072 1077*	Polysaccharide ring ν(C–O) and ν(C–C) $ROPO_3^{2-}$ and $ROPO_3H^-$ compounds $\nu_{as}(PO_3^{2-})$	Also consistent with Lipid ν_s(CO–O–C)
1033*	1025*	1042*	–	1031*	1032*	–	–	Phospholipid ν_{as}(P–O–C)	Also consistent with saccharide primary alcohol ν(C–O)
–	–	–	1017*	1011*	1017*	1006*	1006*	Saccharide primary alcohol ν(C–O)	Also consistent with $\nu_s(PO_3^{2-})$ in $ROPO_3H^-$ compounds
– 963*	– 964*	979 976*	– 966*	– 966*	– 965*	– 967*	– 966*	$ROPO_3^{2-}$ compounds $\nu_s(PO_3^{2-})$ Polysaccharide β-pyranose ring vibration	May be overlapped with a weak lipid ν_{as}(C–N)
920 918*	919 919*	– 917*	923 919*	919 919*	920 919*	– 919*	916 918*	Polysaccharide pyranose O_{as}(ring)	
– 886*	– 887*	– –	– 891*	– 889*	– 890*	888 887*	889 888*	Polysaccharide β-pyranose μ(C–H) Amino acid ν_s(N–C–C)	
823 828*	– 827*	– –	826 829*	823 828*	824 829*	810 816*	811 814*	Phospholipid ν_{as}(P–O)	Probably overlapped with ω(O–H/N–H) bands
765 769*	764 768*	– 773*	766 770*	766 769*	766 769*	– 770*	– 768*	Polysaccharide pyranose O_s(ring)	Probably overlapped with ω(O–H/N–H) bands
723 730*	– 729*	–	724 730*	725 729*	725 729*	728*	728*	Lipid $>CH_2$ ρ(C–H)	May be overlapped with a weak protein amide V band due to δ(N–H) and ω(O–H/N–H) bands
701 701*	701 701*	697 701*	701 701*	701 701*	700 701*	700 701*	700 701*	Polyglycine $\rho(CH_2)$ and μ(N–H) Polysaccharide ν(ring)	Also consistent with out-of-plane μ(N–H) in hydrogen-bonded secondary amides and Probably overlapped with ω(O–H/N–H) bands
659 659*	658 659*	658 656*	659 659*	659 660*	660 660*	659 659*	659 659*	Fatty acid aliphatic carboxylic acid μ(O–CO)	Probably overlapped with ω(O–H/N–H) bands and the $\delta(CO_2)$ spurious band ($\sim$670 cm^{-1})

(Continued)

10.3389/fmicb.2024.1423741

TABLE 2 (Continued)

B. licheniformis		*B. megaterium*		*Byssochlamys sp.*		*C. maltosa*		Assigned vibrations	Comments
Native	Treated	Native	Treated	Native	Treated	Native	Treated		
618 620*	617 620*	621 619*	613 620*	621 622*	618 621*	607 603*/623*	615 618*	Fatty acid aliphatic carboxylic acid μ(O–CO)	Probably overlapped with ω(O–H/N–H) bands
531*	531*	–	528*	524*	525*	529*	530*	Amino / Fatty acid aliphatic carboxylic acid μ(C–CO)	Probably overlapped with ω(O–H/N–H) bands
439 431*	– 431*	– 428*	435 430*	434 429*	435 430*	– 431*	– 429*	–	Possibly secondary amine δ(C–N–C), α-aliphatic carboxylic acid μ(C–CO), aliphatic ether μ(C–O–C), or a band from Fatty acid alkyl esters

[a] Referring to the peak wavenumbers indicated in cm^{-1}. The given band positions were rounded to the nearest unit from the FTIR measurements performed with a wavenumber step of 1 cm^{-1}; hence, the accuracy of the band positions and shifts is 1 and 2 cm^{-1}, respectively. [b] ν, stretching; μ, deformation; δ, bending; sc, scissoring; ρ, rocking; o, breathing; ω, wagging; τ, twisting; s, symmetric; as, asymmetric. * Estimated band positions for shoulder, hidden (due to overlapping), and observed bands (for comparison) using second derivatives of FTIR spectra.

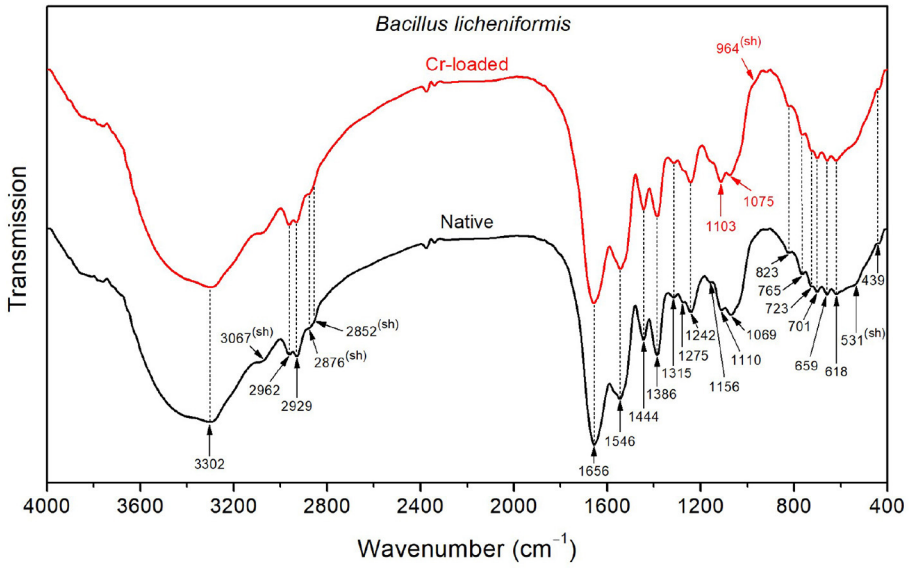

FIGURE 3
FTIR spectra of the *Bacillus licheniformis* bacterial strains before Cr loading (native) and after treatment with 50 mg/L Cr^{6+} (Cr-loaded).

intensity of CH_2 and CH_3 bands and shoulders observed at 2966, 2933, 2874, and 2852 cm^{-1}.

Upon exposure of the *Bacillus megaterium* strains to Cr(VI), the intense OH stretching band undergoes a significant decrease in intensity, revealing the underlying NH stretching band at 3299 cm^{-1}, which indicates that conformational changes occurred. Furthermore, the amide I and II bands appear at 1657 and 1546 cm^{-1}, indicating the decrease of the amino acid NH_3^+ and CO_2^- bands, as mentioned above. Accordingly, the CH_3 bending band appears at 1387 cm^{-1} as a result of the weakened CO_2^- symmetric stretching band. The emergence of a noticeable shoulder at 1748 cm^{-1} relative to C=O stretching in COOH functional groups also witnesses that the amino acids are involved in the interaction with chromium. The bands in the region below 900 cm^{-1} appear after chromium treatment as a result of the weakening of presumed OH wagging. However, the overall absorption in the 1800–900 cm^{-1} region increases after treatment with chromium, which could be tentatively assigned to the emergence of overtone features related to NH_2 wagging in the 900–400 cm^{-1} region.

As shown in Figure 5, the FTIR spectrum of the native *Byssochlamys* sp. strains exhibits typical vibrational bands as seen previously, including the overlapped OH and NH stretching bands peaking at 3297 cm^{-1}, CH_2 and CH_3 asymmetric stretching bands at 2963 and 2934 cm^{-1}, and the characteristic vibrations of carbohydrates and lipids in the 900–400 cm^{-1} spectral region (Table 2). The main specificities lie in the broadened amide bands at 1658 and 1546 cm^{-1}, most likely due to motions of the carboxylate and ammonium functional groups, as previously explained.

After treatment with chromium, the high-frequency OH stretching band (~3400 cm^{-1}) and the low-frequency OH wagging

10.3389/fmicb.2024.1423741

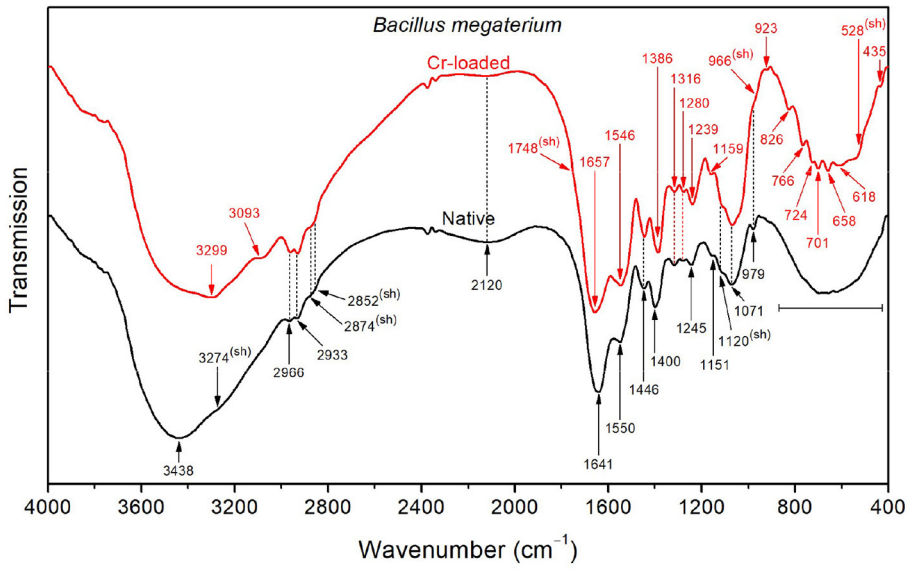

FIGURE 4
FTIR spectra of the native and Cr-treated (with 50 mg/L Cr^{6+}) *Bacillus megaterium* bacterial strains.

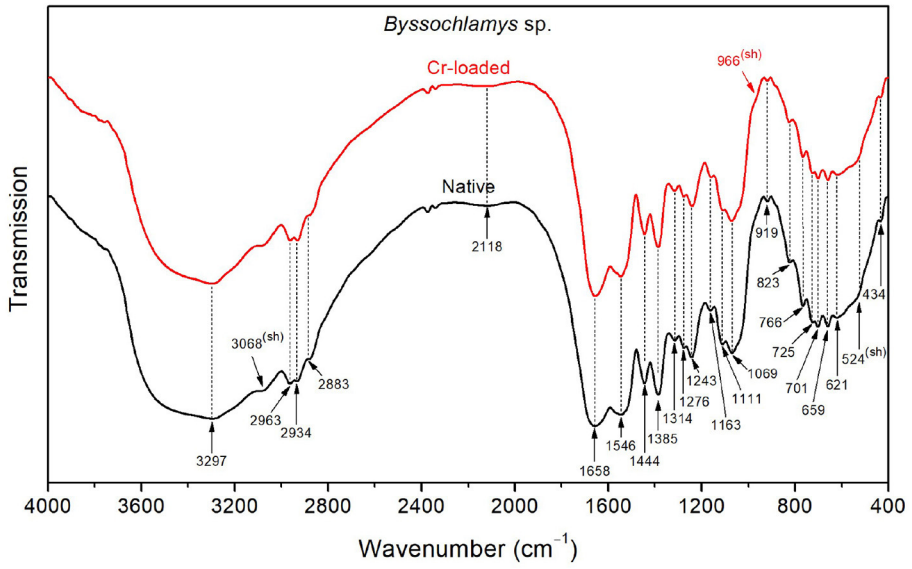

FIGURE 5
FTIR spectra of the *Byssochlamys* sp. strains before Cr loading (native) and after treatment with 50 mg/L Cr^{6+} (Cr-loaded).

band (900–400 cm^{-1}) slightly decreased in intensity. Additionally, the side of the amide I band toward low frequencies (i.e., lower than 1658 cm^{-1}) and that of the amide II band toward high frequencies (i.e., < 1546 cm^{-1}) become narrower, which indicates reduced contributions from the NH_3^+ asymmetric deformation (found at 1626 and 1572 cm^{-1} for the treated strains).

With respect to *Bacillus licheniformis*, the spectrum of the native *Candida maltosa* strains (Figure 6) exhibits an intense broad O–H stretching band in the region 3650–3550 cm^{-1}, along with a stronger O–H wagging in the region 900–400 cm^{-1}. This is likely to arise from the hydroxyl-rich glycosylphosphatidylinositol in the outer layer (mannose-containing compounds) and the polysaccharide-rich inner layer (β-glucan and chitin) in the cell wall of *Candida* strains (Chaffin et al., 1998; Kapteyn et al., 2000; Gow et al., 2011; Zvonarev et al., 2021). Accordingly, the methylene groups (abundant in the phospholipid tail of glycosylphosphatidylinositol) show a stronger absorption with respect to the methyl groups, as shown by the asymmetric stretching bands (2928 and 2958 cm^{-1}, respectively) and the sharpened shoulder band at 2852 cm^{-1} (i.e., at the position of symmetric stretching of CH_2). This is also consistent with the strong absorption in the spectral ranges 1200–950 cm^{-1} due to

10.3389/fmicb.2024.1423741

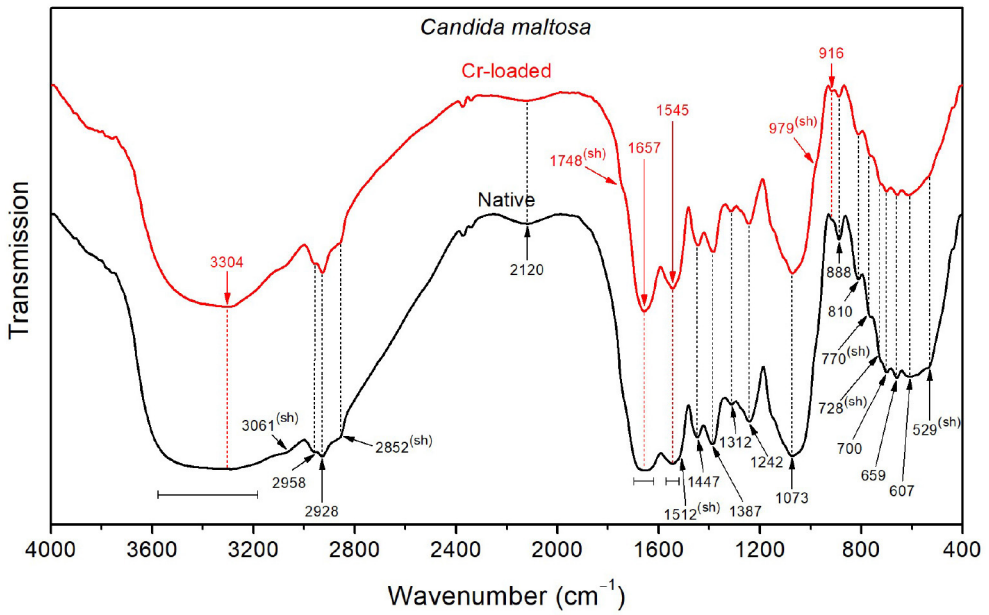

FIGURE 6
FTIR spectra of the *Candida maltosa* strains before Cr loading (native) and after treatment with 50 mg/L Cr^{6+} (Cr-loaded).

the C–O stretching in polysaccharide C–OH and C–O–C branches (mannans) and 1400–1300 cm^{-1} due to carbohydrate OH and CH deformation vibrations (see Table 2). Besides, the amide I band (~1655 cm^{-1}) is relatively broad, probably due to overlapping with the CO_2^- stretching features (~1697 and 1621 cm^{-1}).

The FTIR spectrum shows a decrease in the intensity of the OH stretching band after loading with Cr(VI), suggesting that hydroxyl groups may be involved in the interaction with metallic ions. In addition, the shoulder relative to C=O stretching of –COOH functional groups (~1748 cm^{-1}) becomes more noticeable after chromium treatment. The narrower amide I band (~1657 cm^{-1}) for the treated strain probably originates from the partial vanishing of the CO_2^- stretching modes, which were also shifted (from 1697 to 1691 cm^{-1} and from 1621 to 1626 cm^{-1}). The same effect can be seen for the amide II band (~1545 cm^{-1}), probably due to the decrease of NH_3^+ deformation vibrations, as shown by the softened shoulder band at 1512 cm^{-1}. This is further supported by the decrease in intensity of the NH_3^+ stretching band at 2120 cm^{-1} upon chromium treatment.

3.4 Zeta potential analysis

The zeta potential was measured for the four microbial strains in the absence and presence of different Cr^{6+} concentrations ranging from 25 to 800 mg/L (Table 3). Before contact with Cr^{6+}, the microbial strains show different zeta potentials of about −10.63 ± 0.38, −15.9 ± 1.39, −8.98 ± 0.40, and −10.15 ± 2.68 mV for *Bacillus licheniformis*, *Bacillus megaterium*, *Byssochlamys* sp., and *Candida maltosa*, respectively. These negative potential differences with respect to the medium are related to the amounts of negative charges present at the vicinity of the microorganisms before being brought into contact with Cr^{6+}.

After exposure to chromium, the zeta potential of *Bacillus licheniformis* strains undergoes a significant change from −10.63 ± 0.38 (0 mg/L Cr^{6+}) to −39.53 ± 1 mV (100 mg/L Cr^{6+}), indicating that the cells in contact with Cr^{6+} have experienced an increase in negative charge. As the Cr^{6+} concentration increases in *Bacillus licheniformis*, the zeta potentials are statistically identical up to 100 mg/L. The zeta potential reaches the highest value (−39.53 ± 1 mV) at 100 mg/L before decreasing beyond that.

For *Bacillus megaterium*, the zeta potential range from −15.3 ± 2.18 to −30.4 ± 1.51 mV for the investigated Cr^{6+} concentrations. Significant differences are also observed between the control and the strains treated with different concentrations of Cr^{6+} (from 25 to 250 mg/L).

The Cr^{6+}-treated *Byssochlamys* sp. show zeta potentials that are statistically different from those of the control. The zeta potentials are between −8.98 ± 0.40 and −20.7 ± 0.98 mV and correspond to the values for the Cr^{6+} concentrations of 0 and 50 mg/L. Statistically, the highest zeta potential values are −20.7 ± 0.98 and −20.53 ± 1.04 mV (50 and 100 mg/L of Cr^{6+}). In contrast, the lowest value is recorded for the control (−8.98 ± 0.40 mV).

Finally, zeta potentials that are statistically different from the control were recorded for the Cr^{6+}-treated *Candida maltosa* strains. This concerns the zeta potentials of treatments with 25, 50, 100, and 800 mg/L Cr^{6+}. The zeta potential values range from −10.15 ± 2.68 to −21.93 ± 2.08 mV (control and 100 mg/L Cr^{6+}).

4 Discussion

Biosorption (or bioadsorption) is a passive, rapid, and reversible physico-chemical phenomenon between a metal and

10.3389/fmicb.2024.1423741

TABLE 3 Zeta potential of *Bacillus licheniformis*, *Bacillus megaterium*, *Byssochlamys* sp., and *Candida maltosa* strains in the absence and presence of different concentrations of Cr^{6+}.

Cr^{6+} concentration (mg/L)	Zeta potential (mV)				
	Bacillus licheniformis	*Bacillus megaterium*	*Byssochlamys* sp.	*Candida maltosa*	Control
0	−10.63 ± 0.38^{c}	− 15.9 ± 1.39^{b}	− 8.98 ± 0.40^{c}	− 10.15 ± 2.68^{c}	− 12.15 ± 2.93^{cd}
25	− 26.53 ± 0.29^{b}	− 29.37 ± 0.55^{a}	− 18.33 ± 4.40^{ab}	− 13.63 ± 0.15^{bc}	− 17.07 ± 2.67^{bc}
50	− 24.37 ± 0.60^{b}	− 28.47 ± 0.38^{a}	− 20.7 ± 0.98^{a}	− 17.73 ± 1.08^{ab}	− 18.53 ± 0.06^{b}
100	− 39.53 ± 1^{a}	− 30.4 ± 1.51^{a}	− 20.53 ± 1.04^{a}	− 21.93 ± 2.08^{a}	− 35.3 ± 0.62^{a}
250	− 26.23 ± 1.10^{b}	− 22.33 ± 2.04^{ab}	− 13.70 ± 0.00^{abc}	− 10.78 ± 2.44^{c}	− 9.81 ± 2.39^{d}
500	− 22.7 ± 1.97^{b}	− 15.3 ± 2.18^{b}	− 16.07 ± 6.14^{abc}	− 11.29 ± 3.14^{c}	− 3.87 ± 1.05^{e}
800	− 25.37 ± 3^{b}	− 16.97 ± 8.36^{b}	− 12.23 ± 0.75^{bc}	− 12.13 ± 1.66^{bc}	− 3.75 ± 0.31^{e}

^{a,b,c,d,e}indicate statistically significant differences ($p < 0.05$) of the turkey test among different zeta potential values.

a biological material (biosorbent) (Fernandez et al., 2018). It independent from cell activity carried out by active or inactive microorganisms (Fernandez et al., 2018). This process was assessed using SEM-EDX, FTIR analysis, and zeta potential measurements. Adsorption relies on hexavalent (or trivalent chromium produced by hexavalent chromium reduction) binding through a number of molecules. Biosorption is also the passive immobilization of metals by biomass. Sorption mechanisms at the cell surface take place independently of the cell's metabolism. These mechanisms are based on physico-chemical interactions between the metal and functional groups in the cell wall (Kaduková and Virčíková, 2005).

4.1 SEM analysis

The morphology of the microbial strains analyzed by SEM showed different characteristics. The *Bacillus licheniformis* strains have a smooth surface in the control and after treatment with 5 mg/L Cr^{6+}. Similar results obtained by Hossan et al. (2020) showed that *Klebsiella* sp. have a smooth surface in the control cells. This smooth structure in untreated cells has also been observed in previous studies (Karthik et al., 2017; Bharagava and Mishra, 2018; Zhu et al., 2019; Kalola and Desai, 2020; Tan et al., 2020; Abo-Alkasem et al., 2022). Jobby et al. (2019), Selvakumar et al. (2021), and Su et al. (2021) demonstrated that the cells of *Sinorhizobium* sp. SAR1, *Bacillus vietnamensis*, *Bacillus lentus*, *Alcaligenes faecalis*, *Staphylococcus cohnii*, *Staphylococcus saprophyticus*, and *Rhodobacter sphaeroides* SC01 also have smooth surfaces in the absence of Cr^{6+}. Additionally, intact and regular cells of *Bacillus licheniformis* were observed in the absence of metal. This case is similar to that found by Sevak et al. (2023) in *Acinetobacter* sp. biomass. Hossan et al. (2020) observed depression in *Klebsiella* sp. treated with 100 mg/L Cr^{6+}. After exposure to 5 mg/L Cr^{6+}, the biomass of *Bacillus licheniformis* retains its smooth structure and the metal does not damage the cells, likely indicating the effective resistance of the cell at this concentration level. The wrinkles, rough clusters, irregular shapes, and possible production of extracellular substances in the biomass treated at higher concentrations (50 mg/L Cr^{6+}) revealed that the cells develops a strategy to circumvent the toxic effect of Cr^{6+}. Elahi et al. (2022) described wrinkles in *Bacillus cereus* strain b-525k after contact with 2 mM Cr^{6+}. Similarly, Hossan et al. (2020) reported ruptured surfaces in the biomass of *Klebsiella* sp. after treatment with Cr^{6+}.

The *Bacillus megaterium* cells were not individually distinguishable with and without Cr^{6+} in the medium. Hossan et al. (2020) noted a similar case in *Klebsiella* sp. control. In addition, the irregular appearance observed in *Bacillus megaterium* in media with or without Cr^{6+} is a common phenomenon in microorganisms. This could be due to the secretion of extracellular substances around the cells. These extracellular substances are probably reduced in cells grown at 50 mg/L Cr^{6+} because of the toxic effect of the metal and could be exopolysaccharides. These research findings are in accordance with earlier studies (Ozturk et al., 2009; Jobby et al., 2019).

The *Byssochlamys* sp. control biomass and that treated with 5 mg/L Cr^{6+} present identical aspects. The concentration of 5 mg/L Cr^{6+} shows no impact on the cells, which remain smooth and less bound. However, at 50 mg/L Cr^{6+}, the cells group together to provide a better Cr^{6+} adsorption surface. In this regard, Majumder et al. (2017) found ruptured surfaces with Cr^{6+} saturation on the biomass of *Arthrinium malaysianum*.

The *Candida maltosa* control cells and those treated with 5 mg/L Cr^{6+} appear in clusters with smooth outlines. However, at 5 mg/L Cr^{6+}, some cells are less visible and form irregular blocks. This phenomenon is thought to be due to the production of extracellular substances to resist the toxic effect of Cr^{6+}. At 50 mg/L Cr^{6+}, several cells are unable to retain their initial structures probably due to damaged cellular constituents of strains, as a result of the toxic effect of Cr^{6+} (Mat Arisah et al., 2021).

In the literature, some authors mentioned that wrinkles appeared on the biomass of *Aspergillus terricola* after treatment with Cr^{6+} (Mohamed et al., 2021). In the absence of Cr^{6+} in the medium, Dwivedi (2023) found that the hyphae of *Talaromyces pinophillus* are thin, rough, and loose. However, with Cr^{6+} stress, the hyphae are aggregated and dense. Similarly, Saranya et al. (2020) observed the same rough structures on *Trichoderma asperellum* after contact with Cr^{6+} and indicated the adsorption of Cr^{6+} and Cr^{3+}.

Majumder et al. (2017) showed that the cell surfaces are saturated by the toxic agent, and Mat Arisah et al. (2021) explain that the rough surfaces induced by Cr in the treatments are due to the adsorption of Cr^{6+}.

4.2 EDX analysis

EDX analysis showed the presence of peaks in all the biomasses stressed with Cr^{6+}. However, the biomasses not treated with Cr showed no chromium peaks. The appearance of Cr peaks in the biomasses treated with 5 and 50 mg/L Cr^{6+} indicates the presence of Cr bound to the cell surfaces of the strains (Karthik et al., 2017). The drop in the weight percentage of Cr is thought to be due to Cr toxicity, which damages parts of the cell surfaces (Su et al., 2021). Indeed, Cr is a metal capable of causing cell lysis and therefore bacteria and fungi could biosorb it. In this respect, Majumder et al. (2017) found that chromium could bind to the dried biomass of the fungus *Arthrinium malaysianum* (Cr peak detection). Similarly, Karthik et al. (2017) studied the ability of *Cellulosimicrobium funkei* strain AR6 to adsorb Cr at concentrations ranging from 100 to 250 µg/mL. They attributed the presence of Cr peaks to Cr^{3+} (reduction of Cr^{6+}) bound to cell surfaces. Kalola and Desai (2020) pointed out that Cr adsorption also occurs in *Halomonas* sp. DK4. Additionally, Cr-specific peaks were detected in *Bacillus vietnamensis, Bacillus lentus, Alcaligenes faecalis, Staphylococcus cohnii*, and *Staphylococcus saprophyticus* treated with 3400 mg/L Cr^{6+} (Selvakumar et al., 2021). Su et al. (2021) and Kalsoom A. et al. (2021) indicated that the presence of Cr peaks could be due to the complexation of Cr^{3+} ions with molecules located on the cell surface or the presence of reduced Cr^{3+} species precipitated on the outer surface of the strains. The peak observed by the scientists (Kalsoom A. et al., 2021) was in the biomass of *Staphylococcus simulans* treated with 1500 µg/mL Cr^{6+} (0.19 wt.% Cr).

The weight percentage of chromium detected in *Salipaludibacillus agaradhaerens* strain NRC-R stressed with 4 mM Cr^{6+} was 0.16 % (Abo-Alkasem et al., 2022). Moreover, Elahi et al. (2022) showed that adsorption is one of the detoxification mechanisms of *Bacillus cereus* b-525k.

Microcharacterization of *Cellulosimicrobium* sp. (SCRB10), *Bacillus* sp. CRB-B1, and *Klebsiella* sp. treated with 100, 150, and 100 mg/L Cr^{6+}, respectively, revealed Cr adsorption with weight percentages equivalent to 0.71, 3.54, and 6.02, respectively (Bharagava and Mishra, 2018; Hossan et al., 2020; Tan et al., 2020). These findings are in contrast with the results of some scientists showing that some strains do not adsorb Cr. For instance, Jobby et al. (2019) and Sevak et al. (2023) demonstrated that *Sinorhizobium* sp. SAR1 and *Acinetobacter junii* strain b2w do not adsorb Cr after contact with metal.

4.3 FTIR analysis

FTIR can be used to detect the functional groups that allow the adsorption of Cr. The chromium adsorption mechanism was carried out in a culture medium enriched with Cr^{6+} in order to identify the functional groups that appear only in the presence of Cr^{6+}. This gave us a clear understanding of Cr^{6+} bioremediation. The presence of other metals would have obscured this understanding.

Filamentous fungi are capable of adsorbing Cr^{6+} and this ability has been demonstrated by several researchers (Shroff and Vaidya, 2012; Majumder et al., 2017). The absorption peaks show molecules, such as NH, CH_3, CH_2, C=O, C=N, OH, PO^{2-}, P–O, and O–CO in *Bacillus licheniformis* control and exposed to Cr^{6+}. This suggests that these molecules are involved in the binding of Cr^{6+} or Cr^{3+} (Ayele et al., 2021; Su et al., 2021; Elahi et al., 2022). The peaks that remain at 3067, 1275, 1156, 1110, 1069, and 531 cm^{-1} and that corresponding to amide II, amide III, C–O–C, PO^{2-}, C–O, C–C, PO_3^{2-}, C–CO, or those that appear at 1075 cm^{-1} (C–O and C–C) and 964 cm^{-1} (PO_3^{2-}) highlight the strain resistance to metal (Su et al., 2021).

Functional groups, such as CH_3, CH_2, CH_3^+, hydroxide (OH), amide III, PO^{2-}, C–O, C–C, and PO_3^{2-} found on the cell surfaces of *Bacillus megaterium* biomasses grown in the absence and presence of Cr^{6+} are involved in the binding of Cr^{6+} and Cr^{3+} ions (Ayele et al., 2021; Su et al., 2021; Elahi et al., 2022). O–H (3438 cm^{-1}), amide A (3274 cm^{-1}), NH_3^+ (1641 cm^{-1}), N–H and C–N (1550 cm^{-1}), CO_2^- (1400 cm^{-1}), PO^{2-} (1245 cm^{-1}), and C–O–C (1151 cm^{-1}) were mainly identified on the control cells. These molecules play an important role in Cr resistance. In cells in contact with Cr^{6+}, amide A (3299 cm^{-1}), C=O (1748 cm^{-1}; 1657 cm^{-1}), CO_2^- (1546 cm^{-1}), CH_3 (1386 cm^{-1}), PO^{2-} (1239 cm^{-1}), C–O–C (1159 cm^{-1}), polysaccharide β-pyranose ring vibration (966 cm^{-1}), asymmetric breathing of polysaccharide pyranose (ring) (923 cm^{-1}), P–O (826 cm^{-1}), symmetric breathing of polysaccharide pyranose (766 cm^{-1}), C–H (724 cm^{-1}), CH_2 and N–H (701 cm^{-1}), O–CO (658 and 618 cm^{-1}), and C–CO (528 cm^{-1}) were found. This indicates that the strain increase its resistance to chromium by producing other molecules to adsorb metal ions.

Byssochlamys sp. cells bind Cr^{6+} and Cr^{3+} with amide A, CH_3, CH_2, OH, amide III, PO^{2-}, C–O–C, C–O, C–C, polysaccharide, P–O, N–H, N–H_2, O–CO, and C–CO (Ayele et al., 2021; Su et al., 2021; Elahi et al., 2022). It was observed that a peak at 3068 cm^{-1} indicates the presence of the amide II. In addition, polysaccharide β-pyranose ring vibration (966 cm^{-1}) detected in Cr^{6+}-treated cells suggests that the polysaccharide produced adsorbs Cr in its various forms (Karthik et al., 2017; Ayele et al., 2021; Su et al., 2021; Elahi et al., 2022).

On the other hand, CH_3, CH_2, NH_3^+, amide I, amide II, OH, PO^{2-}, C–O, C–C, polysaccharide, C–H, P–O, O–CO, and C–CO recorded on the *Candida maltosa* cell surface reveal their involvement in metal biding (Ayele et al., 2021; Su et al., 2021; Elahi et al., 2022). The *Candida maltosa* biomass control cells have cell surfaces composed of amide II (3061 cm^{-1}) and NH_3^+ (1512 cm^{-1}). In contrast, there was C=O (1748 cm^{-1}) and PO_3^{2-} (979 cm^{-1}) in the biomass treated with Cr^{6+}. The molecules produced during treatment are part of the strategy of resistance to the toxic metal.

The disappearance of certain functional groups observed at different frequencies is thought to be due to the toxic effect of Cr^{6+} (Karthik et al., 2017). The appearance of new functional groups in chromium-treated cells mean that the strain is setting up a resistance mechanism (Karthik et al., 2017; Princy et al., 2020). These molecules participate in the adsorption of Cr^{6+} and Cr^{3+} (Bharagava and Mishra, 2018). According to the results obtained, some functional groups remain after chromium treatment. This

phenomenon is in line with certain studies carried out by scientists. Bharagava and Mishra (2018) noted that before and after treatment, there is always an asymmetric stretching of proteins, polysaccharides, lipids, and nucleic acids. Fungal cell surfaces interact with Cr and functional groups on these surfaces include carboxyl (COOH), phosphate (PO_4^{3-}), amine ($-NH_2$), thiol (–SH), and hydroxyl (–OH) groups (García-Hernández et al., 2017). The distinctive peaks observed on the cell surfaces of cells exposed to Cr are common in many scientific papers. This reflects the ability of microbial strains to sequester chromium on their cell surfaces (Jobby et al., 2019; Kalsoom A. et al., 2021; Mat Arisah et al., 2021; Sharma et al., 2022).

Karthik et al. (2017) indicated that several functional groups such as, O–H, C–H, and C–O, are involved in metal-microbial interaction. Bharagava and Mishra (2018) pointed out that *Cellulosimicrobium* sp. cells sequester Cr on their surface using molecules with specific groups, such as alkene (C=C), carbonyl (C=O), nitro ($-NO_2$), carboxyl (–COOH), amines ($-NH_2$), and sulphonic ($-SO_3$).

It was revealed that amine (N–H), carboxyl (C=O), ether (C–O), alkyl halides (C–Cl, C–Br, and C–I), nitrile (C=N), and alkane (C–H) contribute to the retention of Cr on the cell surface of *Morganella morganii* (1Ab1) (Princy et al., 2020). Moreover, functional groups, such as O–H, N–H, C–HO, and C–O, were revealed on the *Exiguobacterium mexicanum* cell wall (Das et al., 2021).

Maurya et al. (2022) found –OH, $-CH_2$, –COOH, C=O, $-CH_3$, $-COO^-$, $-SO_3H$, S=O, C–OH, and C–O groups in *B. vallismortis*, *B. haynesii*, and *A. aquatilis* exposed to Cr^{6+}. In addition, *Acinetobacter junii* strain b2w was shown to make use of –OH, C–H, C=O, C–N, C–O, and C–N functional groups to bond Cr (Sevak et al., 2023).

Once Cr^{6+} is bound to cell surfaces, it is reduced to Cr^{3+}, which is less harmful. The microbial biomass can be recovered after centrifugation. The pellet was further washed with 1 mL of 10 mM EDTA solution for desorption of Cr from the cell surfaces. This method of decontamination is environmentally friendly. In addition, the biomass recovered can be used for another experiment in wastewater treatment.

4.4 Zeta potential analysis

Zeta potential analysis shows the different trends of charge present in tested microorganisms in the absence and presence of different hexavalent chromium concentrations. The presence of negative charges on cell surfaces is thought to be due to functional groups and that biosorption of Cr^{6+} modifies the zeta potential profiles. The attachment of chromium anion to cell surfaces leads to an accumulation of negative charges (Larson et al., 2023). The negative values of the zeta potentials confirm the accumulation of negative charges on the cell surfaces (Al-Jubory et al., 2020; El Malti et al., 2021). This observation suggests that electrostatic interactions play a role in metal adsorption. Modifications to the zeta potentials were observed by Huang et al. (2013), who indicated that the adsorption of cadmium (Cd) is due to electrostatic interactions. The authors found that living and dead *Bacillus cereus* RC−1 cells exhibit different zeta potentials in the presence of Cd(II). They noted that the negative charges on the surface of the dead cells are higher than those on the living cells. In this study, the negative charges varied from one strain to another. In *Bacillus licheniformis*, the highest negative charge of about −39.53 ± 1 mV was observed at 100 mg/L Cr^{6+}. In *Bacillus megaterium* and *Candida maltosa*, the highest negative charges recorded at 100 mg/L Cr^{6+} were −30.4 ± 1.51 and −21.93 ± 2.08 mV, respectively. In *Byssochlamys* sp., the highest negative charges were found at 50 and 100 mg/L Cr^{6+} of about −20.7 ± 0.98 and −20.53 ± 1.04 mV, respectively. The difference in absolute load values between the control and the Cr^{6+} concentrations (25 to 800 mg/L) were 15.90, 13.74, 28.90, 15.60, 12.07, and 14.74 for *Bacillus licheniformis*. The difference in absolute load values between the control and the 25 to 800 mg/L Cr^{6+} concentrations were 13.47, 12.57, 14.50, 6.43, −0.60, and 1.07 in *Bacillus megaterium*. Charge differences of 9.35, 11.72, 11.55, 4.72, 7.09, and 3.25 were found at concentration values ranging from 25 to 800 mg/L Cr^{6+} in *Byssochlamys* sp. The differences in absolute load values for Cr^{6+} concentrations ranging from 25 to 800 mg/L were 3.48, 7.58, 11.78, 0.63, 1.14, and 1.98 for *Candida maltosa*. These results show that the Cr adsorption limit for all strains is 100 mg/L.

In a previous study, Srinath et al. (2002) investigated the ability of *Bacillus megaterium* to adsorb Cr. They demonstrated that living and dead cells of this strain adsorb 15.7 and 30.7 mg Cr/g dry weight, respectively. In contrast, 23.8 and 39.9 mg Cr/g dry weight were observed as Cr adsorption values in living and dead *Bacillus coagulans* cells. Other studies have shown that bacteria, yeasts, and filamentous fungi are capable of adsorbing Cr (Quintelas et al., 2008; Ahluwalia, 2014; Dadrasnia et al., 2015; Iram et al., 2015; Chang et al., 2016; Vendruscolo et al., 2017). In addition, Kaduková and Virčíková (2005) showed that biosorption is possible with both living and dead microorganisms with, however, a promoted activity for dead cells. *Pseudomonas* strains are known to adsorb Cr^{6+}. It has been shown that *P. aeruginosa* 99, *P. stutzeri* T3, and *P. aeruginosa* 78 adsorb 22%, 14%, and 12% of 10 mg/L Cr onto the cell surfaces, respectively (Ozturk et al., 2012). The ability of a fungal consortium composed of *Cladosporeum perangustum* and *Penicillium commune* (isolated from tannery wastewater-contaminated soil), *Paecilomyces lilacinus*, and *Fusarium equiseti* (isolated from tannery sludge) to detoxify Cr^{6+}-laden wastewater was revealed by Sharma and Malaviya (2016). The fungi were able to remove 100% of the Cr^{6+}, with adsorption as the main mechanism. Singh et al. (2016) proved that *Aspergillus flavus* adsorb a maximum Cr^{6+} concentration equivalent to 16.1 mg/g. Bibi et al. (2018) mentioned that endophytic fungi could adsorb Cr^{6+} and act as fertilizers.

On the other hand, *Pseudomonas aeruginosa* RW9 was found to bind 0.46 mg/L Cr^{6+} to the cell surface (Mat Arisah et al., 2021). Other research works corroborate the results obtained in this study, i.e., the potential of fungi and bacteria in sequestering Cr on cell surfaces. Other microorganisms have been demonstrated to serve as effective agents in eliminating toxic metals. Additionally, Anupong et al. (2022) highlighted the ability of *Aspergillus flavus* DDN to eliminate the Cr contained in water contaminated by mine tailings. This ability was evidenced by a drop in Cr concentration from 3.1 ± 0.35 to 2.3 ± 0.74 mg/L mainly due to adsorption. Extracellular secretions are set up by the cell to prevent Cr from entering the cytoplasm. Samuel et al. (2021) indicated that biosorption depends on temperature, pH, biomass concentration, contact duration, and

initial metal concentration. Majumder et al. (2017) showed that Cr^{6+} biosorption is endothermic and entropy-driven.

5 Conclusion

Adsorption of Cr by *Bacillus licheniformis*, *Bacillus megaterium*, *Byssochlamys* sp., and *Candida maltosa* strains isolated from tannery effluents was investigated in this study. Scanning electron microscopy combined with energy-dispersive X-ray spectroscopy revealed Cr characteristic peaks in cells treated with Cr^{6+}. At 50 mg/L Cr^{6+}, *Bacillus licheniformis* and *Candida maltosa* cells are rough. Extracellular secretions are reduced in *Bacillus megaterium*, and *Byssochlamys* sp. cells are tightly bound. Adsorption of Cr by all strains was better at 5 mg/L than at 50 mg/L. At 50 mg/L Cr^{6+} in LB medium, Cr wt.% of *Bacillus licheniformis, Bacillus megaterium, Byssochlamys* sp., and *Candida maltosa* are 0.29, 0.25, 0.35, and 0.23, respectively. FTIR analysis revealed metal-microbial interactions. It was found that phosphoryl terminals contribute to the Cr adsorption mechanism of *Bacillus licheniformis* while the amino acid NH_3^+ and CO_2^- functional groups are involved in interaction of *Bacillus megaterium* strain with metal. Similarly, amino acid NH_3^+ infrared footprint show moderate changes in intensity and frequency, suggesting a possible contribution to the interaction between *Byssochlamys* sp. strains and metallic ions. The zeta potential analysis showed a variation in charges ranging from -10.63 ± 0.38 to -39.53 ± 1, -15.3 ± 2.18 to -30.4 ± 1.51, -8.98 ± 0.40 to -20.7 ± 0.98, and -10.15 ± 2.68 to -21.93 ± 2.08 for *Bacillus licheniformis*, *Bacillus megaterium*, *Byssochlamys* sp., and *Candida maltosa*. In addition, the zeta potential results indicated a Cr^{6+} adsorption limit of 100 mg/L for all strains. *Byssochlamys* sp. strain adsorb more Cr^{6+} at a concentration of 50 mg/L (0.35 wt.% Cr). It could therefore be used for the Cr bioremediation of tannery effluents. It is clear that in large-scale experiments, the adsorbed chromium can be recovered after washing the microbial cells, and the microbial biomass can act as a natural adsorbent. This green technology is highly advantageous.

Data availability statement

The datasets presented in this study can be found in online repositories. The names of the repository/repositories and accession number(s) can be found in the article/supplementary material.

Author contributions

AA: Data curation, Methodology, Writing—original draft, Writing—review & editing, Formal analysis. NR: Software, Formal analysis, Writing—original draft. MJ: Formal analysis, Writing—original draft. MH: Supervision, Investigation, Conceptualization, Writing—original draft, Writing—review & editing. YO: Methodology, Investigation, Formal analysis, Writing—original draft. LE: Supervision, Conceptualization, Methodology, Writing—original draft, Writing—review & editing.

Funding

The author(s) declare that no financial support was received for the research, authorship, and/or publication of this article.

Acknowledgments

We acknowledge the Centre d'Analyse et de Caractérisation (CAC) at the Cadi Ayyad Faculty in Marrakech for carrying out the SEM-EDX, FTIR, and zeta potential analyses. The authors would like to thank OCP Africa for its financial support through the project "Rhizobium" funded to Mohammed VI Polytechnic (U6MP).

Conflict of interest

The authors declare that the research was conducted in the absence of any commercial or financial relationships that could be construed as a potential conflict of interest.

Publisher's note

References

Abo-Alkasem, M. I., Maany, D. A., El-Abd, M. A., and Ibrahim, A. S. S. (2022). Bioreduction of hexavalent chromium by a novel haloalkaliphilic *Salipaludibacillus agaradhaerens* strain NRC-R isolated from hypersaline soda lakes. *3 Biotech* 12:17. doi: 10.1007/s13205-021-03082-2

Aguilar, M. V. M., Sasso, V. M., and Tabaldi, L. A. (2023). Handroanthus heptaphyllus as bioindicator of chromium-contaminated environments. *South Afr. J. Bot.* 155, 35–44. doi: 10.1016/j.sajb.2023.01.049

Ahluwalia (2014). Microbial removal of hexavalent chromium and scale up potential. *Int. J. Curr. Microbiol. App. Sci.* 3, 383–398. Available online at: http://www.ijcmas.com

Aké, A. H. J., Hafidi, M., Ouhdouch, Y., and El Fels, L. (2022). Physicochemical characterization and pollutant charge of industrial effluents from tanneries under semi-arid climate. *Desalin Water Treat* 260, 148–160. doi: 10.5004/dwt.2022.28431

Aké, A. H. J., Hafidi, M., Ouhdouch, Y., Jemo, M., Aziz, S., El Fels, L., et al. (2023). Microorganisms from tannery wastewater: Isolation and screening for potential chromium removal. *Environ. Technol. Innov.* 31:103167. doi: 10.1016/j.eti.2023.103167

Alharbi, T., Al-Kahtany, K., Nour, H. E., Giacobbe, S., and El-Sorogy, A. S. (2022). Contamination and health risk assessment of arsenic and chromium in coastal sediments of Al-Khobar area, Arabian Gulf, Saudi Arabia. *Mar. Pollut. Bull* 185:114255. doi: 10.1016/j.marpolbul.2022.114255

Al-Jubory, F. K., Mujtaba, I. M., and Abbas, A. S. (2020). Preparation and characterization of biodegradable crosslinked starch ester as adsorbent. Paper presented at the *2ND IConMEAS* 2019:170. doi: 10.1063/5.0000170

Anupong, W., Jutamas, K., On-Uma, R., Alshiekheid, M., Sabour, A., Krishnan, R., et al. (2022). Bioremediation competence of *Aspergillus flavus* DDN on pond water contaminated by mining activities. *Chemosphere* 304:135250. doi: 10.1016/j.chemosphere.2022.135250

Aparicio, J. D., Lacalle, R. G., Artetxe, U., Urionabarrenetxea, E., Becerril, J. M., Polti, M. A., et al. (2021). Successful remediation of soils with mixed contamination of chromium and lindane: Integration of biological and physico-chemical strategies. *Environ. Res.* 194:110666. doi: 10.1016/j.envres.2020.110666

Ariram, N., Pradeep, S., Sundaramoorthy, S., and Madhan, B. (2022). Single pot low float chromium tanning: cleaner pathway approach to environment friendly leather manufacturing. *Proc. Safety Environ. Prot.* 167, 434–442. doi: 10.1016/j.psep.2022.09.024

Ayele, A., Godeto, Y. G., and Zhang, Y. (2021). Bioremediation of chromium by microorganisms and its mechanisms related to functional groups. *J. Chem.* 2021, 1–21. doi: 10.1155/2021/7694157

Barkleit, A., Foerstendorf, H., Li, B., Rossberg, A., Moll, H., Bernhard, G., et al. (2011). Coordination of uranium(VI) with functional groups of bacterial lipopolysaccharide studied by EXAFS and FT-IR spectroscopy. *The Royal Soc. Chem.* 40, 9868–9876. doi: 10.1039/c1dt10546a

Beiranvand, M., Farhadi, S., and Mohammadi-Gholami, A. (2022). Adsorptive removal of tetracycline and ciprofloxacin drugs from water by using a magnetic rod-like hydroxyapatite and MIL-101(Fe) metal-organic framework nanocomposite. *RSC Adv.* 12, 34438–34453. doi: 10.1039/D2RA06213E

Bharagava, R. N., and Mishra, S. (2018). Hexavalent chromium reduction potential of *Cellulosimicrobium sp.* isolated from common effluent treatment plant of tannery industries. *Ecotoxicol. Environ. Saf.* 147, 102–109. doi: 10.1016/j.ecoenv.2017.08.040

Bibi, S., Hussain, A., Hamayun, M., Rahman, H., Iqbal, A., Shah, M., et al. (2018). Bioremediation of hexavalent chromium by endophytic fungi; safe and improved production of *Lactuca sativa* L. *Chemosphere* 211, 653–663. doi: 10.1016/j.chemosphere.2018.07.197

Busca, G., and Lorenzelli, V. (1982). Infrared spectroscopic identification of species arising from reactive adsorption of carbon oxides on metal oxide surfaces. *Mat. Chem.* 7, 89–126. doi: 10.1016/0390-6035(82)90059-1

Cassity, T. R., and Kolodziej, B. J. (1984). Isolation, partial characterization and utilization of a polysaccharide from *Bacillus megaterium* ATCC 19213. *J. Gen. Microbiol.* 130, 535–539. doi: 10.1099/00221287-130-3-535

Chaffin, W. L., López-Ribot, J. L., Casanova, M., Gozalbo, D., and Martínez, J. P. (1998). Cell wall and secreted proteins of *Candida albicans*: identification, function, and expression. *Microbiol. Mol. Biol. Rev.* 62, 130–180. doi: 10.1128/MMBR.62.1.130-180.1998

Chang, F., Tian, C., Liu, S., and Ni, J. (2016). Discrepant hexavalent chromium tolerance and detoxification by two strains of *Trichoderma asperellum* with high homology. *Chem. Eng. J.* 298, 75–81. doi: 10.1016/j.cej.2016.04.023

Chromikova, Z., Chovanova, R. K., Tamindzija, D., Bartova, B., Radnovic, D., Bernier-Latmani, R., et al. (2022). Implantation of *Bacillus pseudomycoides* chromate transporter increases chromate tolerance in *Bacillus subtilis*. *Front. Microbiol.* 13:842623. doi: 10.3389/fmicb.2022.842623

Copíková, J., Cerná, M., Novotná, M., Kaasová, J., and Synytsya, A. (2001). Application of FT-IR spectroscopy in detection of food hydrocolloids in confectionery jellies and food supplements. *Czech J. Food Sci.* 19, 51–56. doi: 10.17221/6575-CJFS

Dadrasnia, A., Chuan Wei, K. S., Shahsavari, N., Azirun, M. S., and Ismail, S. (2015). Biosorption potential of *Bacillus salmalaya* strain 139SI for removal of Cr(VI) from aqueous solution. *Int. J. Environ. Res. Public Health* 12, 15321–15338. doi: 10.3390/ijerph121214985

Das, S., Chandra Behera, B., Mohapatra, R. K., Pradhan, B., Sudarshan, M., Chakraborty, A., et al. (2021). Reduction of hexavalent chromium by *Exiguobacterium mexicanum* isolated from chromite mines soil. *Chemosphere* 282:131135. doi: 10.1016/j.chemosphere.2021.131135

Dwivedi, S. K. (2023). Hexavalent chromium (Cr+6) detoxification potential and stress response of fungus Talaromyces pinophillus isolated from tannery wastewater. *Environ. Adv.* 13:100417. doi: 10.1016/j.envadv.2023.100417

El Malti, W., Hamieh, M., Noaman, A., Nasser El-Dine, R., Hijazi, A., Al-Khatib, W., et al. (2021). Polyurethane loaded with vegetable activated carbon for heavy metals removal from water. *J. Ecol. Eng.* 22, 99–110. doi: 10.12911/22998993/141362

Elahi, A., Rehman, A., Zajif Hussain, S., Zulfiqar, S., and Shakoori, A. R. (2022). Isolation and characterization of a highly effective bacterium *Bacillus cereus* b-525k for hexavalent chromium detoxification. *Saudi J. Biol. Sci.* 29, 2878–2885. doi: 10.1016/j.sjbs.2022.01.027

El-Naggar, N. E., El-Khateeb, A. Y., Ghoniem, A. A., El-Hersh, M. S., and Saber, W. I. A. (2020). Innovative low-cost biosorption process of Cr(6+) by *Pseudomonas alcaliphila* NEWG-2. *Sci. Rep.* 10:14043. doi: 10.1038/s41598-020-70473-5

Fernandez, P. M., Vinarta, S. C., Bernal, A. R., Cruz, E. L., and Figueroa, L. I. C. (2018). Bioremediation strategies for chromium removal: current research, scale-up approach and future perspectives. *Chemosphere* 208, 139–148. doi: 10.1016/j.chemosphere.2018.05.166

Fu, L., Feng, A., Xiao, J., Wu, Q., Ye, Q., Peng, S., et al. (2021). Remediation of soil contaminated with high levels of hexavalent chromium by combined chemical-microbial reduction and stabilization. *J. Hazard Mater* 403:123847. doi: 10.1016/j.jhazmat.2020.123847

Gang, H., Xiao, C., Xiao, Y., Yan, W., Bai, R., Ding, R., et al. (2019). Proteomic analysis of the reduction and resistance mechanisms of *Shewanella oneidensis* MR-1 under long-term hexavalent chromium stress. *Environ. Int.* 127, 94–102. doi: 10.1016/j.envint.2019.03.016

García-Hernández, M. A., Villarreal-Chiu, J. F., and Garza-González, M. T. (2017). Metallophilic fungi research: an alternative for its use in the bioremediation of hexavalent chromium. *Int. J. Environ. Sci. Technol.* 14, 2023–2038. doi: 10.1007/s13762-017-1348-5

Gow, N. A., van de Veerdonk, F. L., Brown, A. J., and Netea, M. G. (2011). Candida albicans morphogenesis and host defence: discriminating invasion from colonization. *Nat. Rev. Microbiol.* 10, 112–122. doi: 10.1038/nrmicro2711

Hong, T., Yin, J. Y., Nie, S. P., and Xie, M. Y. (2021). Applications of infrared spectroscopy in polysaccharide structural analysis: progress, challenge and perspective. *Food Chem. X* 12:100168. doi: 10.1016/j.fochx.2021.100168

Hossan, S., Hossain, S., Islam, M. R., Kabir, M. H., Ali, S., Islam, M. S., et al. (2020). Bioremediation of hexavalent chromium by chromium resistant bacteria reduces phytotoxicity. *Int. J. Environ. Res. Public Health* 17:6013. doi: 10.3390/ijerph17176013

Huang, F., Dang, Z., Guo, C. L., Lu, G. N., Gu, R. R., Liu, H. J., et al. (2013). Biosorption of Cd(II) by live and dead cells of *Bacillus cereus* RC-1 isolated from cadmium-contaminated soil. *Colloids Surf B Biointerfaces* 107, 11–18. doi: 10.1016/j.colsurfb.2013.01.062

Hughes, R. C. (1968). The cell wall of *Bacillus licheniformis* N.C.T.C. 6346. Composition of the mucopeptide component. *Biochem J.* 106, 41–48. doi: 10.1042/bj1060041

Iram, S., Shabbir, R., Zafar, H., and Javaid, M. (2015). Biosorption and bioaccumulation of copper and lead by heavy metal-resistant fungal isolates. *Arab. J. Sci. Eng.* 40, 1867–1873. doi: 10.1007/s13369-015-1702-1

Jobby, R., Jha, P., Gupta, A., Gupte, A., and Desai, N. (2019). Biotransformation of chromium by root nodule bacteria *Sinorhizobium* sp. SAR1. *PLoS ONE* 14:e0219387. doi: 10.1371/journal.pone.0219387

Kaduková, J., and Virčíková, E. (2005). Comparison of differences between copper bioaccumulation and biosorption. *Environ. Int.* 31, 227–232. doi: 10.1016/j.envint.2004.09.020

Kalola, V., and Desai, C. (2020). Biosorption of Cr(VI) by *Halomonas* sp. DK4, a halotolerant bacterium isolated from chrome electroplating sludge. *Environ. Sci. Pollut. Res. Int.* 27, 27330–27344. doi: 10.1007/s11356-019-05942-0

Kalsoom, A., Batool, R., and Jamil, N. (2021). Highly Cr(vi)-tolerant Staphylococcus simulans assisting chromate evacuation from tannery effluent. *Green Proc. Synth.* 10, 295–308. doi: 10.1515/gps-2021-0027

Kalsoom, K., Batool, A., Din, G., Din, S. U., Jamil, J., Hasan, F., et al. (2021). Isolation and screening of chromium resistant bacteria from industrial waste for bioremediation purposes. *Braz. J. Biol.* 83:e242536. doi: 10.1590/1519-6984.242536

Kapteyn, J. C., Hoyer, L. L., Hecht, J. E., Müller, W. H., Andel, A., Verkleij, A. J., et al. (2000). The cell wall architecture of *Candida albicans* wild-type cells and cell wall-defective mutants. *Mol. Microbiol.* 35, 601–611. doi: 10.1046/j.1365-2958.2000.01729.x

Karthik, C., Ramkumar, V. S., Pugazhendhi, A., Gopalakrishnan, K., and Arulselvi, P. I. (2017). Biosorption and biotransformation of Cr(VI) by novel *Cellulosimicrobium funkei* strain AR6. *J Taiwan Inst. Chem. Eng.* 70, 282–290. doi: 10.1016/j.jtice.2016.11.006

Lara, P., Vega-Alvarado, L., Sahonero-Canavesi, D. X., Koenen, M., Villanueva, L., Riveros-Mckay, F., et al. (2021). Transcriptome analysis reveals Cr(VI) adaptation mechanisms in klebsiella sp. strain AqSCr. *Front. Microbiol.* 12:656589. doi: 10.3389/fmicb.2021.656589

Larson, S. L., Ballard, J. H., Runge, K. A., Zhang, H., Breland, B. R., Nick, Z. H., et al. (2023). Effects of aluminum ion on particle sizes and surface charges of exopolysaccharides from Rhizobium tropici and pH effects. *Rhizosphere* 26:100713. doi: 10.1016/j.rhisph.2023.100713

Lasagabaster, A., Abad, M. J., Barral, L., and Ares, A. (2006). FTIR study on the nature of water sorbed in polypropylene (PP)/ethylene alcohol vinyl (EVOH) films. *Eur. Polymer J.* 42, 3121–3132. doi: 10.1016/j.eurpolymj.2006.03.029

Li, J., Tang, C., Zhang, M., Fan, C., Guo, D., An, Q., et al. (2021). Exploring the Cr(VI) removal mechanism of *Sporosarcina saromensis* M52 from a genomic perspective. *Ecotoxicol. Environ. Saf.* 225:112767. doi: 10.1016/j.ecoenv.2021.112767

Lin, W. H., Chen, S. C., Chien, C. C., Tsang, D. C. W., Lo, K. H., Kao, C. M., et al. (2020). Application of enhanced bioreduction for hexavalent chromium-polluted groundwater cleanup: Microcosm and microbial diversity studies. *Environ. Res.* 184:109296. doi: 10.1016/j.envres.2020.109296

Majumder, R., Sheikh, L., Naskar, A., Vineeta, M. M., and Tripathy, S. (2017). Depletion of Cr(VI) from aqueous solution by heat dried biomass of a newly isolated fungus *Arthrinium malaysianum*: a mechanistic approach. *Sci. Rep.* 7:11254. doi: 10.1038/s41598-017-10160-0

Mat Arisah, F., Amir, A. F., Ramli, N., Ariffin, H., Maeda, T., Hassan, M. A., et al. (2021). Bacterial resistance against heavy metals in *Pseudomonas aeruginosa* RW9 involving hexavalent chromium removal. *Sustainability* 13:9797. doi: 10.3390/su13179797

Maurya, A., Kumar, P. S., and Raj, A. (2022). Characterization of biofilm formation and reduction of hexavalent chromium by bacteria isolated from tannery sludge. *Chemosphere* 286:131795. doi: 10.1016/j.chemosphere.2021.131795

Mohamed, L. A., Aniagor, C. O., and Hashem, A. (2021). Isotherms and kinetic modelling of mycoremediation of hexavalent chromium contaminated wastewater. *Cleaner Eng. Technol.* 4:100192. doi: 10.1016/j.clet.2021.100192

Mohanty, S., Benya, A., Hota, S., Kumar, M. S., and Singh, S. (2023). Eco-toxicity of hexavalent chromium and its adverse impact on environment and human health in Sukinda Valley of India: a review on pollution and prevention strategies. *Environ. Chem. Ecotoxicol.* 5, 46–54. doi: 10.1016/j.enceco.2023.01.002

Naumann, D. (2000). Infrared spectroscopy in microbiology. *Encycloped. Analyt. Chem*. 102:131. doi: 10.1002/9780470027318.a0117

Ozturk, S., Aslim, B., and Suludere, Z. (2009). Evaluation of chromium(VI) removal behaviour by two isolates of *Synechocystis* sp. in terms of exopolysaccharide (EPS) production and monomer composition. *Bioresour. Technol.* 100, 5588–5593. doi: 10.1016/j.biortech.2009.06.001

Ozturk, S., Kaya, T., Aslim, B., and Tan, S. (2012). Removal and reduction of chromium by *Pseudomonas spp*. and their correlation to rhamnolipid production. *J. Hazard Mater* 232, 64–69. doi: 10.1016/j.jhazmat.2012.06.038

Plestenjak, E., Kraigher, B., Leskovec, S., Mandic Mulec, I., Markovic, S., Scancar, J., et al. (2022). Reduction of hexavalent chromium using bacterial isolates and a microbial community enriched from tannery effluent. *Sci. Rep.* 12:20197. doi: 10.1038/s41598-022-24797-z

Princy, S., Sathish, S. S., Cibichakravarthy, B., and Prabagaran, S. R. (2020). Hexavalent chromium reduction by *Morganella morganii* (1Ab1) isolated from tannery effluent contaminated sites of Tamil Nadu, India. *Biocat. Agric. Biotechnol.* 23:101469. doi: 10.1016/j.bcab.2019.101469

Quintelas, C., Fernandes, B., Castro, J., Figueiredo, H., and Tavares, T. (2008). Biosorption of Cr(VI) by a Bacillus coagulans biofilm supported on granular activated carbon (GAC). *Chem. Eng. J.* 136, 195–203. doi: 10.1016/j.cej.2007.03.082

Samaké, D. (2008). *Traitement des eaux usées de tanneries à l'aide de matériaux à base d'argile*. Grenoble: Université Joseph-Fourier - Grenoble I,

Samuel, M. S., Selvarajan, E., Chidambaram, R., Patel, H., and Brindhadevi, K. (2021). Clean approach for chromium removal in aqueous environments and role of nanomaterials in bioremediation: Present research and future perspective. *Chemosphere* 284:131368. doi: 10.1016/j.chemosphere.2021.131368

Saranya, N., Suganya, E., Narayanasamy, S., Sivaprakasam, S., and Pandian, V. S. S., Selvaraj, R. (2020). 3-level Box–Behnkenoptimization of hexavalent chromium reduction by chromate resistant Trichoderma asperellum cells from simulated and industrial effluent. *Environ. Technol. Innov.* 19:101024. doi: 10.1016/j.eti.2020.101024

Sathvika, T., Balaji, S., Chandra, M., Soni, A., Rajesh, V., Rajesh, N., et al. (2019). A co-operative endeavor by nitrifying bacteria *Nitrosomonas* and Zirconium based metal organic framework to remove hexavalent chromium. *Chem. Eng. J.* 360, 879–889. doi: 10.1016/j.cej.2018.12.015

Schmitt, J., and Flemming, H. C. (1998). FTIR-spectroscopy in microbial and material analysis. *Int. Biodeterior. Biodegrad.* 41, 1–11. doi: 10.1016/S0964-8305(98)80002-4

Seiferth, O., Wolter, K., Dillmann, B., Klivenyi, G., Freund, H. J., Scarano, D., et al. (1999). IR investigations of CO_2 adsorption on chromia surfaces: Cr_2O_3 (0001)/Cr(110) versus polycrystalline α-Cr_2O_3. *Surf. Sci.* 421, 176–190. doi: 10.1016/S0039-6028(98)00857-7

Selvakumar, P., Subramanian, D., Natarajan, J., and Solai Ramatchandirane, P. (2021). Analysis of chromate transporters in bacterial species for Cr(VI) reduction isolated from tannery effluent contaminated site of Dindigul District, Tamil Nadu, India. *Geomicrobiol. J.* 38, 598–606. doi: 10.1080/01490451.2021.1906359

Sevak, P., Pushkar, B., and Mazumdar, S. (2023). Mechanistic evaluation of chromium bioremediation in *Acinetobacter junii* strain b2w: a proteomic approach. *J. Environ. Manage.* 328:116978. doi: 10.1016/j.jenvman.2022.116978

Sharma, P., Singh, S. P., Parakh, S. K., and Tong, Y. W. (2022). Health hazards of hexavalent chromium (Cr (VI)) and its microbial reduction. *Bioengineered* 13, 4923–4938. doi: 10.1080/21655979.2022.2037273

Sharma, S., and Malaviya, P. (2016). Bioremediation of tannery wastewater by chromium resistant novel fungal consortium. *Ecol. Eng.* 91, 419–425. doi: 10.1016/j.ecoleng.2016.03.005

Shroff, K. A., and Vaidya, V. K. (2012). Effect of pre-treatments on the biosorption of Chromium (VI) ions by the dead biomass of Rhizopus arrhizus. *J. Chem. Technol. Biotechnol.* 87, 294–304. doi: 10.1002/jctb.2715

Singh, R., Kumar, M., and Bishnoi, N. R. (2016). Development of biomaterial for chromium(VI) detoxification using *Aspergillus flavus* system supported with iron. *Ecol. Eng.* 91, 31–40. doi: 10.1016/j.ecoleng.2016.01.060

Socrates, G. (2001). *Infrared and Raman Characteristic Group Frequencies: Tables and Charts, 3rd Edn*. New York, NY: John Wiley and Sons Ltd.

Srinath, T., Verma, T., Ramteke, P. W., and Garg, S. K. (2002). Chromium (VI) biosorption and bioaccumulation by chromate resistant bacteria. *Chemosphere* 48, 427–435. doi: 10.1016/S0045-6535(02)00089-9

Su, Y. Q., Yuan, S., Guo, Y. C., Tan, Y. Y., Mao, H. T., Cao, Y., et al. (2021). Highly efficient and sustainable removal of Cr (VI) in aqueous solutions by photosynthetic bacteria supplemented with phosphor salts. *Chemosphere* 283:131031. doi: 10.1016/j.chemosphere.2021.131031

Tan, H., Wang, C., Zeng, G., Luo, Y., Li, H., Xu, H., et al. (2020). Bioreduction and biosorption of Cr(VI) by a novel *Bacillus* sp. CRB-B1 strain. *J. Hazard Mater* 386:121628. doi: 10.1016/j.jhazmat.2019.121628

Tangahu, B., Berlianto, M., and Kartika, A. A. (2020). Deconcentration of chromium contained in wastewater using a bacteria and microalgae consortia with a high rate algal reactor System. *J. Ecol. Eng.* 21, 272–284. doi: 10.12911/22998993/126878

Thatoi, H., Das, S., Mishra, J., Rath, B. P., and Das, N. (2014). Bacterial chromate reductase, a potential enzyme for bioremediation of hexavalent chromium: a review. *J. Environ. Manage.* 146, 383–399. doi: 10.1016/j.jenvman.2014.07.014

Tremmel, S., Beyermann, M., Oschkinat, H., Bienert, M., Naumann, D., Fabian, H., et al. (2005). 13C-labeled tyrosine residues as local IR probes for monitoring conformational changes in peptides and proteins. *Angew. Chem. Int. Ed. Engl.* 44, 4631–4635. doi: 10.1002/anie.200500547

Tripathi, M., Upadhyay, S. K., Kaur, M., and Kaur, K. (2018). Toxicity concerns of hexavalent chromium from tannery waste. *J. Biotechnol. Bioeng.* 2, 40–44. doi: 10.22259/2637-5362.0202007

Tumolo, M., Ancona, V., De Paola, D., Losacco, D., Campanale, C., Massarelli, C., et al. (2020). Chromium pollution in european water, sources, health risk, and remediation strategies: an overview. *Int. J. Environ. Res. Public Health* 17:438. doi: 10.3390/ijerph17155438

Upadhyay, N., Vishwakarma, K., Singh, J., Mishra, M., Kumar, V., Rani, R., et al. (2017). Tolerance and reduction of chromium(VI) by *Bacillus* sp. MNU16 isolated from contaminated coal mining soil. *Front. Plant Sci.* 8:778. doi: 10.3389/fpls.2017.00778

Vendruscolo, F., da Rocha Ferreira, G. L., and Antoniosi Filho, N. R. (2017). Biosorption of hexavalent chromium by microorganisms. *Int. Biodet. Biodegr.* 119, 87–95. doi: 10.1016/j.ibiod.2016.10.008

Venyaminov, S. Y., and Kalnin, N. N. (1990a). Quantitative IR spectrophotometry of peptide compounds in water (H_2O) solutions. I. Spectral parameters of amino acid residue absorption bands. *Biopolymers* 30, 1243–1257. doi: 10.1002/bip.360301309

Venyaminov, S. Y., and Kalnin, N. N. (1990b). Quantitative IR spectrophotometry of peptide compounds in water (H_2O) solutions. II. Amide absorption bands of polypeptides and fibrous proteins in α-, β-, and random coil conformations. *Biopolymers* 30, 1259–1271. doi: 10.1002/bip.360301310

Wang, Q., Song, X., Wei, C., Jin, P., Chen, X., Tang, Z., et al. (2022). In situ remediation of Cr(VI) contaminated groundwater by ZVI-PRB and the corresponding indigenous microbial community responses: a field-scale study. *Sci. Total Environ.* 805:150260. doi: 10.1016/j.scitotenv.2021.150260

Wang, Y., Liu, Y., Zheng, K., Xie, L., Ren, Q., Yang, Z., et al. (2021). The role of extracellular polymeric substances (EPS) in the reduction of Cr(VI) by Pannonibacter phragmitetus BB. *J. Environ. Chem. Eng.* 9:106163. doi: 10.1016/j.jece.2021.106163

Wilson, R. H., Smith, A. C., Kačuráková, M., Saunders, P. K., Wellner, N., Waldron, K. W., et al. (2000). The mechanical properties and molecular dynamics of plant cell wall polysaccharides studied by Fourier-transform infrared spectroscopy. *Plant Physiol.* 124, 397–405. doi: 10.1104/pp.124.1.397

Xia, S., Song, Z., Jeyakumar, P., Shaheen, S. M., Rinklebe, J., Ok, Y. S., et al. (2019). A critical review on bioremediation technologies for Cr(VI)-contaminated soils and wastewater. *Crit. Rev. Environ. Sci. Technol.* 49, 1027–1078. doi: 10.1080/10643389.2018.1564526

Yasir, M. W., Capozzi, S. L., Kjellerup, B. V., Mahmood, S., Mahmood, T., Khalid, A., et al. (2021). Simultaneous biotreatment of hexavalent chromium Cr(VI) and polychlorinated biphenyls (PCBs) by indigenous bacteria of Co-polluted wastewater. *Int. Biodet. Biodegr.* 161:105249. doi: 10.1016/j.ibiod.2021.105249

Youssef, M., Morin, A., Aubret, A., Sacanna, S., and Palacci, J. (2020). Rapid characterization of neutral polymer brush with a conventional zetameter and a variable pinch of salt. *Soft Matter* 16, 4274–4282. doi: 10.1039/C9SM01850F

Zhu, Y., Yan, J., Xia, L., Zhang, X., and Luo, L. (2019). Mechanisms of Cr(VI) reduction by *Bacillus* sp. CRB-1, a novel Cr(VI)-reducing bacterium isolated from tannery activated sludge. *Ecotoxicol. Environ. Saf.* 186:109792. doi: 10.1016/j.ecoenv.2019.109792

Zvonarev, A., Farofonova, V., Kulakovskaya, E., Kulakovskaya, T., Machulin, A., Sokolov, S., et al. (2021). Changes in cell wall structure and protein set in Candida maltosa grown on hexadecane. *Folia Microbiol.* 66, 247–253. doi: 10.1007/s12223-020-00840-2

frontiers | Frontiers in Microbiology

TYPE Mini Review
PUBLISHED 03 July 2024
DOI 10.3389/fmicb.2024.1430498

OPEN ACCESS

EDITED BY
Yizhi Sheng,
China University of Geosciences, China

REVIEWED BY
Dongyi Guo,
Miami University, United States
Michal Galamboš,
Comenius University, Slovakia

*CORRESPONDENCE
Qichao Zhang
✉ 263342066@qq.com
Yishan Jiang
✉ 276348088@qq.com
Feng Xiao
✉ 23458972@qq.com

RECEIVED 10 May 2024
ACCEPTED 21 June 2024
PUBLISHED 03 July 2024

CITATION
Wang T, Zhang Q, Qiao Y, Jiang Y, Xiao F, Duan J and Zhao X (2024) Research progress on microbial adsorption of radioactive nuclides in deep geological environments. *Front. Microbiol.* 15:1430498. doi: 10.3389/fmicb.2024.1430498

Research progress on microbial adsorption of radioactive nuclides in deep geological environments

Tianyu Wang[1,2], Qichao Zhang[1,3]*, Yanxin Qiao[2], Yishan Jiang[1]*, Feng Xiao[1]*, Jizhou Duan[3] and Xin Zhao[1]

[1]Navy Submarine Academy, Qingdao, China, [2]School of Materials Science and Engineering, Jiangsu University of Science and Technology, Zhenjiang, China, [3]CAS Key Laboratory of Marine Environment of Corrosion and Bio-Fouling, Institute of Oceanology, Chinese Academy of Sciences, Qingdao, China

Due to the development and utilization of nuclear energy, the safe disposal of nuclear waste needs to be urgently addressed. In recent years, the utilization of microorganisms' adsorption capacity to dispose of radioactive waste has received increasing attention. When compared with conventional disposal methods, microbial adsorption exhibits the characteristics of high efficiency, low cost, and no secondary pollution. In the long term, microbial biomass shows significant promise as specific chemical-binding agents. Optimization of biosorption conditions, identification of rare earth element binding sites, and studies on the sorption capacities of immobilized cells provide compelling reasons to consider biosorption for industrial applications in heavy metal removal from solutions. However, the interaction mechanism between microorganisms and radioactive nuclides is very complex. This mini-review briefly provides an overview of the preparation methods, factors affecting the adsorption capacity, and the mechanisms of microbial adsorbents.

KEYWORDS

microorganism, radioactive nuclides, nuclear waste, microbial adsorption, deep geological environments

1 Introduction

As a new generation of efficient energy, nuclear energy has the characteristics of low cost, small size, large heat, convenient transportation and cleanliness. However, with the rapid development of the nuclear energy industry, the problem of safe disposal of nuclear waste needs to be solved urgently. The nuclear waste mainly includes U, Am, Cs, Sr., Th and other radioactive nuclides, which usually exist in the form of ions and have strong migration ability. Its decay will cause radiation damage to organisms, and improper disposal will seriously threaten the living environment of human beings (Qiao et al., 2024). At present, the main dispose method for radioactive nuclides is solidification treatment, which is to fix the radioactive nuclides in a stable solid medium, so that the radioactive material can be transformed into a solidified body that is easy to transport, store and operate (Galamboš et al., 2011; Ighalo et al., 2024). The solidified body is then packed into a metal disposal container and buried deep in an underground repository, allowing it to decay naturally and be permanently isolated from the human living environment. However, the presence of aggressive anions in the underground repository environment can cause corrosion of the metal containers, which in severe cases can lead to failure and eventual leakage of the nuclear waste inside.

As early as the 1940s, it was observed that some microorganisms have a special affinity for metal ions (Rushhoft, 1949). Since then, the research on the recovery of precious metals by microorganisms has attracted the attention of foreign scholars and gradually entered the practical industrial application. Adsorption is regarded as one of the most efficient methods for removing U (VI) from wastewater due to its high efficiency, affordability, and simplicity (Zein et al., 2023; Ahmadi et al., 2024). It also abides by the ideals of sustainable development and green chemistry and has rapid adsorption kinetics, a large amount of adsorption capacity, and strong adsorption–desorption performance (Meng et al., 2019; Ramli et al., 2023). Through the adsorption, transformation and fixation of radioactive nuclides by microorganisms, the original curing method has been broken through to a certain extent. This method has the characteristics of low investment, low energy consumption and high efficiency, no secondary pollution, and can even effectively recycle some nuclides (Kim and Park, 2001; Dong et al., 2004; Kleinübing et al., 2011). In nature, microorganisms are not only widely distributed and diverse, but also multiply quickly, have small size, large specific surface area and have strong adaptability. There are dozens of microbial species that adsorb and enrich radioactive nuclides, mainly including bacteria, fungi and algae.

2 Preparations of biosorbent

Excellent stability, low toxicity, great selectivity, and high affinity are requirements for effective adsorbents. The secret to enhancing adsorption performance is to increase the adsorbent's adsorption capacity through some kind of preparation technique of modification/treatment (Umeh et al., 2023; Ighalo, 2024). After selecting a suitable microbial producer, it is also necessary to predispose the microorganisms to improve their adaptability to the environment and make them have a better adsorption effect on radioactive nuclides. At present, the main methods used include: chemical method, physical method, immobilization, inorganic salt activation, etc., or modern technological means such as protein modification and genetic modification are used to dispose cells at the molecular level (Choi and Yun, 2004). The main purpose of which is to deprotonate the surface of the adsorbent and activate the adsorption site, so as to improve the chemical properties of the adsorbent. The summary of the preparations of biosorbent is shown in Table 1, which introduce some methods and effects about different preparations of biosorbents.

2.1 Physical and chemical methods

Chemical pretreatment can enhance the selectivity and adsorption efficiency of the biosorbents. All biological moieties including bacteria, fungi, algae, plants, and animal biomass, as well as derived products such as chitosan, have the capability of microbial adsorption. Specific functional groups present on the cell surface, such as carboxyl, amine, hydroxyl, phosphate, and sulfhydryl groups, interact with the metal and lead to the sorption of metals (Banala et al., 2021). Alkali dispose can increase the adsorption site of the adsorbent and expose additional functional groups (Brierley, 1990). The system can also be alkalized, and the buffer media can no longer be added in subsequent steps, thus simplifying the process and making it easy to industrialize. Liao et al. compared the U (VI) adsorption capacities of a PMBC-based adsorbent. They discovered that pretreatment with potassium permanganate significantly increased the capacity of biochar to adsorb U(VI) (979.3 mg/g) by activating many groups on the material's surface (Liao et al., 2022). Xiong et al. (2022) used HAP aerogels with strong chemical bonding between phosphate and U(VI) to maximize the adsorption capacity, achieving an adsorption efficiency of 99.4% for U(VI) at pH 4.0 and 25°C, with an adsorption capacity of 2087.6 mg/g. Juan and Liyu (1999) showed that the adsorption capacity of white-rot-fungus disposed with 0.1 mol/L NaOH for Pb increased significantly, reaching 23.66 mg/g. They believe the reason is that NaOH can dissolve impurities on the cell that are not conducive to adsorption and neutralize H^+, exposing more active binding sites on the cell and increasing the adsorption capacity. *P. laminosum* Sampedro et al. (1995) disposed *S. cerevisiae* with 1 mol/L HNO_3 did not significantly improve its adsorption capacity, while disposed with 1 mol/L NaOH, the adsorption capacity of *S. cerevisiae* increased by 5 ~ 30%.

Physical pretreatment refers to a variety of physical ways to make microorganisms produce changes conducive to adsorption, including drying, grinding, radiation and other methods. Domesticated under Sr.(II) stress promoted the microbial adsorption ability of *B. pumilus* to Sr.(II), and the microbial adsorption efficiency increased from 46.09 to 94.69%. At a lower initial concentration, the living bacteria had the ability to resist the microbial adsorption of Sr.(II) (Dai et al., 2020). Suslov et al. (2004) isolated a series of *S. cerevisiae* from extreme environments, cultured the *S. cerevisiae* on 0.1 mol/L Sr. medium, and found that its accumulation efficiency of Sr. could reach 80%. Mingxue (2011) used Sr. for stress induced domestication after radiation pretreatment of *S. cerevisiae*, and found that the Sr. removal rate of disposed *S. cerevisiae* reached 95% in simulated low-level waste solution. They used the accelerator to domesticate and select 8 strains of *S. cerevisiae* with high tolerance to U and Sr. by pulsed X-ray irradiation and stress induction. The results indicated that *S. cerevisiae* cells can tolerate irradiation with high doses of pulsed X-rays. After domestication, they have strong tolerance to U and Sr., and the adsorption rate of U and Sr. can reach 90% (Liu et al., 2016).

2.2 Immobilize microorganism technology

The disadvantages of free and suspended microorganisms are fine particle and low mechanical strength, which can be overcome by solidified cells. Immobilize biotechnology refers to the process of solidifying cells in a free state by physical or chemical methods. At present, the main methods used are physical adsorption, embedding in agar, embedding in sodium alginate-gelatin and embedding in polyacrylamide gel. Compared with the conventional methods of microbial adsorption of radioactive nuclides, solidified microorganisms have advantages in mechanical strength, chemical stability, physical form, mass transfer permeability, resistance to degradation, and reuse in addition to high adsorption rate and large adsorption capacity. At present, solidified microorganisms are mainly applied to dispose the wastewater contaminated by heavy metals and organic matter, while relatively little research has been done on disposing radioactive waste (Xueqin et al., 2006; Yujian and Hongyu, 2006).

As shown in Figure 1A, the adsorption rate of uncured *S. cerevisiae* decreased with the increase of strontium concentration, and the adsorption rate was close to 90% when the strontium concentration was

TABLE 1 Summary of the preparations of biosorbent.

Preperations	Methods	Effects
Physical and chemical methods	➢ Chemical methods(NaOH, HNO3, et al.) ➢ Physical methods(dry, grind, radiate, et al.)	✓ The adsorption capacity of *S. cerevisiae* disposed with NaOH increased by 5 ~ 30% ✓ HNO_3 did not significantly improve its adsorption capacity ✓ The Sr. removal rate of disposed *S. cerevisiae* reached 95%
Immobilize microorganism technology	➢ Physical adsorption ➢ Embedding in agar ➢ Embedding in sodium alginate-gelatin ➢ Embedding in polyacrylamide gel	✓ Improve mechanical strength, chemical stability, physical form, mass transfer permeability, resistance to degradation ✓ Reuse in addition to high adsorption rate and large adsorption capacity.
Genetic engineering	➢ Create radiation-resistant microorganisms (*D. radiodurans*, et al.) ➢ Recombinant genetic engineering (constructe *D. radiodurans* containing phoN gene encoding nonspecific acid phosphatase) ➢ Radiation resistance gene: recA ➢ Damage-repair gene: pprA	✓ *D. radiodurans* is extremely tolerant to ionizing radiation, ultraviolet radiation, et al. ✓ The new E-coli using pprA gene had better oxidation resistance ✓ *D. radiodurans*' recA can make DNA repair faster and more efficient

10 mg/L. Figure 1B shows the curve of strontium adsorption rate of immobilized *S. cerevisiae* with time. The adsorption rate increased rapidly at the beginning and reached the maximum at 8 h, which was mainly because the adsorption of strontium ions by calcium alginate particles. After that, due to the shedding of surface particles, the adsorption rate decreased temporarily. As the *S. cerevisiae* began to participate in the adsorption, the whole process entered the second stage, and the adsorption equilibrium was reached after 20 h. Rome and Gadd (1991) used *S. cerevisiae* fixed in calcium alginate particles to carry out ion removal experiments. The results showed that the immobilized *S. cerevisiae* cells exhibited better adsorption effect than free cells.

Macaskie and Dean (1989) successfully fixed a strain of *Citrobacter* to remove radioactive U and Pb by using gel embedding method and glass spirochetes adsorption method. The results showed that the removal rates of U and Pb reached 99 and 94%, respectively. Akhtar et al. (2009) solidified *Trichoderma harzianum* with calcium alginate and found that the solidified *Trichoderma harzianum* had better stability. The adsorption column equipped with 1.5 g calcium alginate immobilized particles could purify 8.5 L of U solution (25 mg/L), and the adsorbed U could be eluted with 0.1 mol/L HNO3. The elution rate was 98.1% ~ 99.3%. The above results indicate that solidify microbial cells can improve their adsorption effect and play a better role in environmental pollution control.

2.3 Genetic engineering

In recent years, the use of gene modification to dispose microorganisms has attracted extensive attention from scholars. Because the radioactivity of radioactive nuclides may have an effect on the microorganism, and even lead to a decrease in its adsorption capacity. Currently, *D. radiodurans* is widely studied at home and abroad. Studies have shown that *D. radiodurans* is extremely tolerant to extreme environments such as ionizing radiation, ultraviolet radiation and oxidation resistance. And can avoid death or mutagenic changes under acute gamma irradiation exceeding 15 KGy. Moreover, it can grow continuously under chronic gamma irradiation (60Gy/h), and its growth rate and expression of cloned genes are not affected by irradiation (Jianlong, 2004).

In terms of construction and application of genetically engineered bacteria, Appukuttan et al. (2006) constructed a strain of *D. radiodurans* containing phoN gene encoding nonspecific acid phosphatase. The recombinant genetically engineered bacteria precipitated 90% of U from 0.8 mM acid solution within 6 h. RecA is one of the radiation-resistant genes cloned from *D. radiodurans*. Compared with *E. coli's* recA, recA is more likely to bind DSBs (double-stranded DNA fragments), which can make DNA repair faster and more efficient. Other studies found that recA of E.coli could not compensate for the absence of recA of *D. radiodurans*, indicating that recA of *D. radiodurans* had a unique and extraordinary anti-radiation DNA repair function (Bonacossa de Almeida et al., 2002; Haruta et al., 2003). Disruption of recX (dr1310) in *D. radiodurans* using targeted mutagenesis method enhanced its ROS scavenging activity, and recX overexpression in this bacterium repressed its antioxidant activity significantly (Sheng et al., 2005).

Satoh et al. (2002) found a damage repair gene pprA in DR, and the study found that the deletion of this gene would lead to the decline of radiation resistance. The pprA protein has DNA-binding activity and plays an important role in non-homologous DNA recombination repair independent of recA pathway. At the same time, Kota and Misra (2006) constructed a new E-coli using pprA gene. Compared with ordinary *E. coli*, the newly constructed strain had better oxidation resistance.

3 Affected factors of microbial adsorption

The adsorption behavior of radioactive nuclides by microorganisms is influenced by numerous physical and chemical factors. It includes the physical and chemical properties of the biosorbent and the adsorbed ion itself. As well as various environmental conditions, such as pH, time, temperature, etc. Simultaneously, it is also impacted by the physiological conditions of the microorganisms themselves, including bacterial activity and concentration.

3.1 pH

The pH of the aqueous solution is the main factor affecting the saturated adsorption amount due to the competitive adsorption effect between H^+ and the adsorbed cations. The competitive adsorption

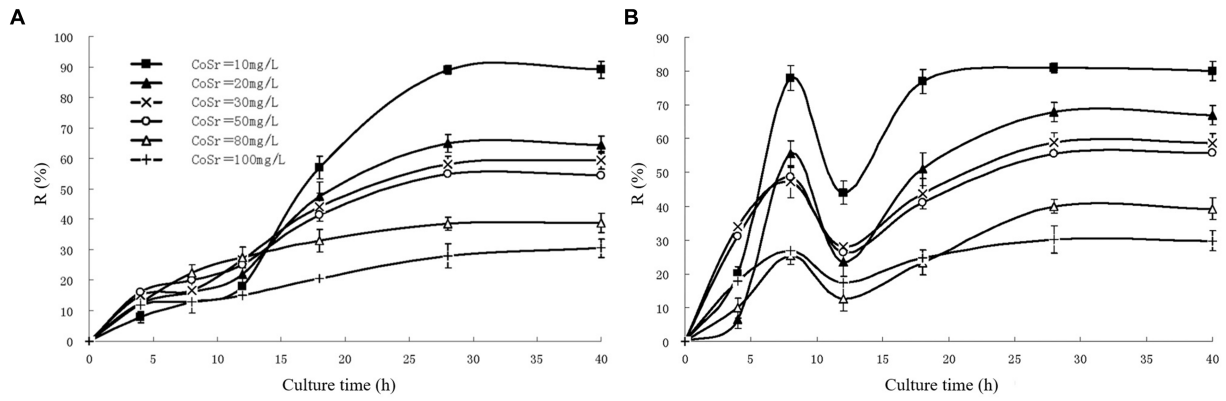

FIGURE 1
The adsorption rate of strontium by cerevisia particles **(A)** unsolidified **(B)** solidified (Mingxue, 2011).

effect means that when systemic pH is low, H_3O^+ occupies a large number of adsorption active sites, preventing the cation from contacting with the adsorption active sites. As a result, the adsorption capacity decreases Many studies have shown that when the pH fluctuates within a certain range, the adsorption amount will change with the pH value. But it will not be a simple linear relationship.

The effectiveness of the adsorbent's active sites is often diminished by cations with large radii and high valence states, which lowers the adsorbent's efficiency for adsorbing U(VI) (Ding et al., 2021). HCP adsorbents containing carboxyl and amino groups, according to Bai et al. (2020), primarily rely on inner-sphere surface complexation rather than ion exchange, indicating that strong ionic strength has little bearing on uranium adsorption onto polymers. Brady et al. (1994) showed that the optimum pH for Cu^{2+} adsorption by *S. cerevisiae* was 5 ~ 9, and that adsorption of Cu^{2+} was reduced under any limiting conditions, especially at low pH. Dhami et al. (1998) used R. Arrhizus to adsorb radioactive nuclides, and found that the pH of Am, Ce, Pu, Eu and Zr reached 2.0 when the maximum adsorption capacity was reached. With the increase of pH, the adsorption capacity of U and Pu increases, and the maximum value is reached when the pH is 6 ~ 7. And then the adsorption decreased gradually when the pH continued to increase. Kazy et al. (2009) adsorbed U and Th with Pseudomonas, it was found that the maximum adsorption capacity reached 150 mg/L when the pH reached 4.0, because $Th_2(OH)_2$ and other polymers were formed to improve the adsorption capacity of element Th. Because U is a univalent polymer, UO_2 will be formed when pH = 2.0, so that the adsorption capacity of U can reach a maximum of 400 mg/L.

3.2 Temperature

Temperature has an effect on the growth of microorganisms and can influence the adsorption of metals by affecting the metabolic activity of the microorganisms, the thermodynamic force of group adsorption and the heat capacity of adsorption. For active microorganisms, it is at the right temperature that their own metabolism can be optimized. However, for dead organisms, the effect of temperature is not significant. For some biosorbents, temperature is an important factor, but generally not as significant as pH. And the effect on different microorganisms or adsorbed metal ions is different.

In the adsorption of U and Th with R. Arrhizus Tsezos and Volesky (1981) found that the amount of U and Th adsorbed increased only slightly when the temperature was increased from 5°C to 40°C. In contrast, in the range between 2°C and 7°C, the adsorption of U by K. marxianus MB3 increased sharply with increasing temperature (Bustard et al., 1997). Some studies have also shown that the effect of temperature on adsorption is also related to pH and equilibrium concentration. Cossich et al. (2002) found that the adsorption capacity of *Sargassum* sp. for Cr at pH = 3.0 had a definite increase when the temperature was changed from 30°C to 40°C. At pH = 4.0 and high equilibrium concentrations, there was a significant increase in the adsorption capacity with the change in temperature, which did not occur at low equilibrium concentrations. In general, the effect of temperature on adsorption is not obvious. But in practical applications, considering the factors of operating costs and operating environment, it is also necessary to choose the appropriate temperature.

3.3 Time

Adsorption time is also an important factor that affecting the efficiency of metal adsorption by microorganisms. A long enough time is required during the adsorption process for the adsorption to reach equilibrium, thus effectively adsorbing or removing metal ions. Generally, it requires 2 ~ 4 h or longer to reach adsorption equilibrium. Scholars generally believe that the adsorption of metal ions by biomaterials can be divided into two stages. The first stage is the fast adsorption stage, which usually reaches about 70% of the final adsorption amount in a few minutes; the second stage is the slow adsorption stage, which often takes several hours or more to reach the final adsorption amount. The former is a rapid surface adsorption, while the latter often involves the transformation of metal ions to the cell, controlled by intracellular metabolism and cell diffusion processes (Ning, 2006).

Kazy et al. (2009) adsorbed U and Th with Pseudomonas and found that the adsorption equilibrium was reached within 2 ~ 4 h. The maximum adsorption was 500 mg/L and 170 mg/L, respectively. Nakajima and Tsuruta (2004) isolated *Lactobacillus* sp. from U mines can clear 2,200 μmol/g of U within 1 h. Khani et al. (2008) investigated the adsorption of *Catenella repens* at low pH and showed that *Catenella repens* could adsorb 90% of U within 30 min and reach

equilibrium at 45 min with adsorption of up to 303 mg/g. Shunzhong et al. (2003) studied the adsorption of ^{241}Am by R. Arrhizus and the results showed that the adsorption rate reached 69.7% at 15 min and 93.8% at 60 min, after which the adsorption rate increased slowly and reached an equilibrium of about 97% by 2 h.

3.4 Bacterial concentration

In practical application, the amount of microorganisms placed and its cost-effectiveness should also be taken into account while achieving the role of removing radioactive nuclides. Overseas researchers choose live and dead Pseudomonas to adsorb U and Th, and found that the adsorption rate is proportional to the concentration of the bacterium in the concentration of 0.2 ~ 3.0 mg/L. And the adsorption rate is 100% when the concentration of the bacterium reaches 3 mg (Andres et al., 1993). When studying the adsorption capacity of microorganisms to U Takehiko (2004) found that actinomycetes had the strongest ability, and the most prominent stem cells were Streptomyces levoris, which could adsorb U by 380 μmol/g.

In addition, it will also affect its adsorption capacity whether the microorganism is alive. There is a bioaccumulation process in the adsorption of living cells. However, in the actual adsorption process, the adsorption capacity of living cells is not higher than that of dead cells due to the participation of the energy metabolism system (Golab et al., 1991). Ling et al. (2001) studied the adsorption capacity of Cu^{2+}, Pb^{2+}, Ni^{2+}, Zn^{2+}, Ag^{+} and Cd^{2+} by living and dead organisms of *Prorocentrum micans*. The experiment showed that after 30 min adsorption of metal ion mixture by *Prorocentrum micans*, the concentration of each ion decreased significantly and reached equilibrium. The living and dead *Prorocentrum micans* have similar adsorption capacity for these six metal ions. The results showed that living *S. horneri* biomass was effective at scavenging Sr., Co, and Mn from seawater in both mono-and multi-nuclide contamination scenarios. Notably, the removal efficiency of *S. horneri* was found to be in the following order: Mn > Co > Sr (Wang et al., 2021).

3.5 Microorganisms in a radioactive environment

The presence of radionuclides results in the accumulation of significant amounts of radioactive materials within living organisms, leading to the degradation of cellular structures and vital biological molecules such as proteins and DNA. For instance, magnetic bacteria, which orient themselves by sensing the geomagnetic field, may suffer disrupted migration due to radioactive disturbances, thereby impacting the availability and ecological equilibrium of other organisms within the food chain. Consequently, organisms may experience impaired physiological functions, disrupted hormonal balance, reduced immunity, and potential reproductive failure and genetic mutations. Radioactive substances accumulate in the food chain in a cascading manner: initially contaminating microorganisms are ingested by herbivores and subsequently transferred to predators through predatory interactions.

However, less is known about microorganisms in the nuclear environment. An understanding of the microbial communities in the nuclear environment has been developed through microbial distribution studies at uranium mines, high and low volume liquid waste storage tanks, reactors, and nuclear waste repositories. It has been found that a large number of microorganisms, including bacteria and fungi, grow in the nuclear environment. Microbial taxa were analyzed in sediments from the leachate area of the United States Department of Energy's Nuclear Waste Storage Site (NWSS) in Washington State. The sediments were contaminated by a waste tank constructed in 1962 to store high concentrations of alkali, nitric acid, aluminum, chromium, Cs-137, and Tc-99 waste streams. The study isolated viable microorganisms from 11 of the 16 samples, but cell counts were low, with a maximum of only 10^4 clones forming units per gram of sample. *Arthrobacter* was the most abundant, with distribution in all samples. Other microorganisms with high G + C content such as *Rhodococcus* and Nocaedia were also present (Mingxue, 2011). In addition, Ruggiero et al. studied the effect of the toxicity of actinides, metal ions, etc. on *D. radiodurans* and *Pseudomonas putida*. It was found that Pu(IV), U(VI) and Np(V) inhibited the growth of *D. radiodurans* at concentrations of 5.2, 2.5 and 2.1 mM, respectively; and inhibited the growth of *Pseudomonas putida* at concentrations of.

Some microbes hold abilities to reduce/oxidize metals, such as U, Cr, Pb, etc. Lovley et al. (1991) first reported that the Fe (III)-reducing bacteria *G. metallireducens* and *S. oneidensis* could gain energy by reducing U(VI) for anaerobic growth, demonstrating that microorganisms are capable of heterogeneously reducing U(VI). On this basis, a large number of studies have utilized the reduction of microorganisms to immobilize radionuclides such as uranium *in situ*, thereby realizing the control of nuclide migration at uranium-contaminated sites.

4 Mechanisms of interaction between biosorbents and radioactive nuclides

Figure 2 illustrates the interaction between microorganisms and radioactive nuclides. Bacterial resistance mechanisms include efflux and enzymatic detoxification, which have the potential to release intracellular toxic metals, e.g., Hg(II) reduction to Hg(0) (Osman and Cavet, 2008). Bacterial plasmids and chromosomes contain resistance genes to a variety of toxic metals, including Ag^{+}, AsO_2^{-}, Cd^{2+}, Co^{2+}, CrO_4^{2-}, Cu^{2+}, etc. The sequences of these genes have been determined and resistance mechanisms have been proposed. Metal concentrations in fungal cells are also affected by translocation regulation and compartmentalization, including exocytosis mechanisms and internal compartmentalization. Microorganisms also synthesize metal-binding peptides and proteins, such as metallothioneins and phytochelatins, which balance metal ions and influence toxic responses (Eide, 2000; Avery, 2001). In eukaryotes, intracellular partitioning also plays an important role in tolerance. The study of resistance in bacteria and fungi is important for understanding how microorganisms respond to toxic metals and other antibiotics in the environment.

Based on the diverse modes of interaction, the process of metal ion absorption by organisms can be primarily divided into two stages: (i) adsorption of metal ions on the cell surface: passive adsorption facilitated by extracellular polymers and functional groups on the cell wall to metal ions. It is characterized by rapid, reversible, and independent of energy metabolism (ii) active adsorption involving living cells: mainly encompasses the influence of substances generated during microbial metabolism and activities of biological macromolecules on nuclide adsorption, leading to intracellular accumulation. Theoretically, living cells should exhibit higher

adsorption capacity than dead cells. However, due to high concentrations of heavy metal ions inhibiting biological cell metabolism, the second stage of living cell adsorption becomes sluggish. Consequently, in practical adsorption processes where energy metabolism systems are involved, the adsorption capacity of living cells does not surpass that of dead cells. As research progresses further in this field, it has been discovered that biological adsorption results from a combination of multiple mechanisms rather than a single mechanism alone. So far, the following adsorption mechanisms have been generally accepted by scholars at home and abroad.

4.1 Extracellular deposition

Popa et al. (2003) studied the adsorption of U by cerevisiae, they found that U attachments appeared on the surface of cerevisiae through SEM. During the process of adsorption of U by *Pseudomonas fluorescens*, it was also found that the complexes formed by U covered the whole surface of the cells and were a complex of membrane-peptidoglycan-plasmalemma, consisting of plate U mineralized particles with the shape of 10 nm ~ 1 μm. Strandberg et al. (1981) studied the adsorption of U by *S. cerevisiae* and *Pseudomonas aeruginosa* cells, they found that U was deposited on the cell surface in the shape of acicular fiber layer. At the same time, it was found that U entered the cell very fast (10s), which may have nothing to do with cell metabolism. Microorganisms can also precipitate nuclides by producing ligands such as PO_3^{3-}, SO_4^{2-}, CO_3^{2-} and OH^-. Microorganisms effectively remove the nuclides by producing a high concentration of ligands around the cell, thereby forming a precipitated nucleation site around the cell. Among them, the precipitation of nuclides by phosphate production by Serratia is the most widely studied (Pattanapipitpaisal et al., 2002). Glycerol-2-phosphate is produced by phospholipase hydrolysis to produce inorganic phosphate (Yong et al., 2004), which can form cell-bound metal phosphate with heavy metal ions, thus achieving the purpose of removing nuclides. Sheng et al. (2022) explores the extent to which interaction with primary silicates and secondary minerals affects the activity and longevity of a model soil enzyme β-glucosidase (BG). In Sheng et al.'s (2023) study, the bioavailability of mineral-bound Mo, V, and Fe was determined by incubating an obligately anaerobic diazotroph *Clostridium kluyveri* with Mo-, V-, and Fe-bearing minerals (molybdenite, cavansite, and ferrihydrite, respectively) and basalt under diazotrophic conditions. They found that as a result of microbial weathering, mineral surface chemistry significantly changed, likely due to surface coating by microbial exudates for metal extraction.

4.2 Extracellular complexation

The cell wall is also a major accumulation site for metal ions. The surface structure of bacterial cell wall is mainly composed of polysaccharides, protein and chitin. N, O, S atoms of hydroxy, carboxyl, phosphoryl and acylamino in the surface structure can be used as coordination atoms to coordinate with radionuclide ions. It has been reported that Zn and Pb can form complexes with phosphoryl and carboxyl groups on the surface of *P. chrysogenum*. Anions (EDTA, SO_4^{2-}, $C1^-$, PO_4^{3-}, etc.) appearing in the solution can compete with cells to form complexes of heavy metal cations. Thereby reducing the adsorption amount of metal ions, which can also reflect the existence of the complexation mechanism from another aspect (Can and Jianlong, 2006). A few studies have shown that uranyl ions mainly interact with carboxyl and phosphoryl groups in adsorption process (Renshaw et al., 2007). Merroun et al. (2005) studied the adsorption of *Bacillus sphaericus* JG-A12 on uranyl ion. They found that U can interact with S-layer. XAS results show that uranyl ion forms a binary complex with carboxyl group and a unary complex with phosphoryl group. So that U accumulates in a dense way on the cell surface. *S. cerevisiae* exhibits good performance in the enrichment of uranium and strontium with as high as almost 90% microbial adsorption efficiency. The results demonstrate that adsorbed uranium and strontium precipitates can be transformed into authenite and strontium sulfate on cell surface. The final state of uranium is mainly in form of UP_2O_7, while the final state of Sr.(II) is mainly in form of $SrSO_4$ after ashing (Zhou et al., 2022). Recently, marine yeast Yarrowia lipolytica has been explored for uranyl removal (Kolhe et al., 2020).

4.3 Intracellular enrichment

Since they studied the adsorption of Sr. by cerevisiae Avery and Tobin (1992) found that adding glucose could stimulate Sr. absorption, and they believed that glucose might promote the synthesis and activity of transporters on the cell membrane. Sr^{2+} internal flow and H^+ outflow occurred when glucose was added 1 ~ 2 min later, and Sr^{2+} was enriched in the cellular vacuole and other locations. However more studies have found that intracellular accumulation is often unrelated to metabolism. For example Volesky and May-Phillips (1995) and Renshaw et al. (2007) found that U could accumulate both inside and outside cerevisiae cells and eventually form aciculr crystals. They believe that this process has nothing to do with metabolism and is mainly because the high osmotic pressure that U forms on the cell membrane. It is worth mentioning that some microorganisms do not die when they are enriched in U intracellularly. For example, *Arthrobacter ilicis*, a bacterium isolated from acidic U contaminated soil, can form U precipitation in the intracellularly, which is related to

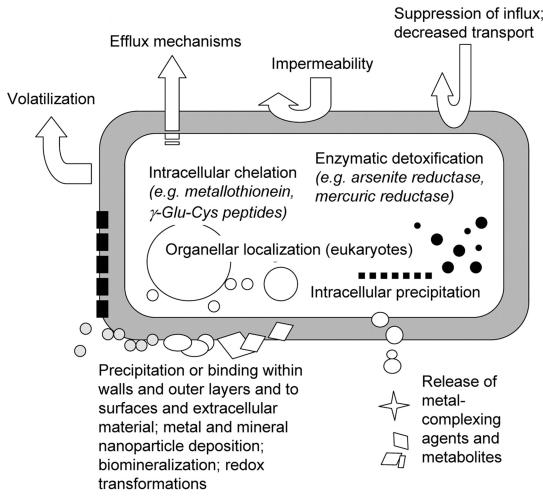

FIGURE 2
Mechanisms of microorganism adsorption (Gadd, 2010).

polyphosphate particles. Researchers believe that this intracellular precipitation is a detoxification mechanism of microorganisms (Yohey and Jillian, 2004). In addition, other studies have shown that the accumulation of Pu in cells is metabolically dependent, and this process depends on the iron transport system to form the U (IV)-desferrioxamine B complex (John et al., 2001).

5 Conclusion and outlook

Given the extensive research conducted in recent years, microorganisms have demonstrated significant potential as adsorbents. Moreover, the utilization of microorganisms for radionuclide treatment has gained widespread acceptance. In comparison to conventional solidification, this approach offers notable advantages in terms of both cost-effectiveness and efficiency, particularly when addressing nuclear wastewater. However, several challenges still need to be addressed, including:

1 Adsorption is a preferred technology for the removal of U(VI) from the aqueous phase. Super adsorbents have been shown to have an adsorption capacity of >1,000 mg/g. Additionally, the adsorbent can be degraded and recycled. If the source of the adsorbent is environmentally friendly, then it can also be considered an environmentally friendly process. The main challenge in this application is the scalability of the technology. To achieve high throughput, a column adsorption configuration is required, and the adsorbent must be able to be reused many times before it permanently loses its adsorption capacity. This is particularly important for expensive engineered adsorbent materials. We suggest that further investigation into adsorption studies be conducted. The radiation resistance and adsorption capacity of microorganisms cannot be simultaneously achieved, which is currently the most intractable problem;
2 Following the recovery of the adsorbent, it can be remediated using biological remediation techniques. However, biological remediation techniques is highly sensitive to pH and temperature, and therefore requires very close monitoring of parameters. Given that biological remediation techniques is relatively less efficient than other high-capacity processes, further research is needed in this area;
3 There is a possibility of process automation. The automation of the microorganism treatment process and the adsorption process can provide strong supporting conditions for microorganism adsorption to be implemented on a large scale;
4 Modern science and technology are being applied. For example, the adsorption mechanism has been further studied by means of FTIR spectroscopy and isotope tracing methods. Additionally, genetic engineering technology is used to achieve precise transformation of microorganisms.

Furthermore, it was observed that membrane filtration and ion exchange are the most promising processes for this application. Membrane processes have the advantage of high throughput, although they do present a challenge in terms of fouling. In addition to its high pH sensitivity, ion exchange does not present any significant challenges in terms of its application.

Author contributions

TW: Writing – original draft. QZ: Supervision, Writing – review & editing, Writing – original draft. YQ: Writing – review & editing. YJ: Supervision, Writing – review & editing. FX: Supervision, Writing – review & editing. JD: Writing – review & editing. XZ: Resources, Writing – review & editing.

Funding

The author(s) declare financial support was received for the research, authorship, and/or publication of this article. This work was financially supported by the Natural Science Foundation of Shandong Province under grant no. ZR2022QE131.

Conflict of interest

The authors declare that the research was conducted in the absence of any commercial or financial relationships that could be construed as a potential conflict of interest.

Publisher's note

References

Ahmadi, S., Ghosh, S., Malloum, A., Sillanpää, M., Igwegbe, C. A., Ovuoraye, P. E., et al. (2024). Amoxicillin adsorption from aqueous solution by magnetite iron nanoparticles: molecular modelling and simulation. *Indian Chem. Eng.* 66, 1–14. doi: 10.1080/00194506.2023.2234908

Akhtar, K., Khalid, A. M., Akhtar, M. W., and Ghauri, M. A. (2009). Removal and recovery of uranium from aqueous solutions by ca-alginate immobilized Trichoderma harzianum. *Bioresour. Technol.* 100, 4551–4558. doi: 10.1016/j.biortech.2009.03.073

Andres, Y., MacCordick, H. J., and Hubert, J.-C. (1993). Adsorption of several actinide (Th, U) and lanthanide (La, Eu, Yb) ions by *Mycobacterium smegmatis*. *Eur. J. Appl. Microbiol. Biotechnol.* 39, 413–417. doi: 10.1007/BF00192103

Appukuttan, D., Rao, A. S., and Apte, S. K. (2006). Engineering of *Deinococcus radiodurans* R1 for bioprecipitation of uranium from dilute nuclear waste. *Appl. Environ. Microbiol.* 72, 7873–7878. doi: 10.1128/AEM.01362-06

Avery, S. V. (2001). Metal toxicity in yeasts and the role of oxidative stress. *Adv. Appl. Microbiol.* 49, 111–142. doi: 10.1016/s0065-2164(01)49011-3

Avery, S. V., and Tobin, J. M. (1992). Mechanisms of strontium uptake by laboratory and brewing strains of *Saccharomyces cerevisiae*. *Appl. Environ. Microbiol.* 58, 3883–3889. doi: 10.1128/AEM.58.12.3883-3889.1992

Bai, J., Ma, X., Yan, H., Zhu, J., Wang, K., and Wang, J. (2020). A novel functional porous organic polymer for the removal of uranium from wastewater. *Microporous Mesoporous Mater.* 306:110441. doi: 10.1016/j.micromeso.2020.110441

Banala, U. K., Das, N. P. I., and Toleti, S. R. (2021). Microbial interactions with uranium: towards an effective bioremediation approach. *Environ. Technol. Innov.* 21:101254. doi: 10.1016/j.eti.2020.101254

Bonacossa de Almeida, C., Coste, G., Sommer, S., and Bailone, A. (2002). Quantification of RecA protein in *Deinococcus radiodurans* reveals involvement of RecA, but not LexA, in its regulation. *Mol. Biol. Rep.* 268, 28–41. doi: 10.1007/s00438-002-0718-x

Brady, D., Stoll, A., and Duncan, J. R. (1994). Biosorptton of heavy metal cations by non-viable yeast biomass. *Environ. Technol. Lett.* 15, 429–438. doi: 10.1080/09593339409385447

Brierley, C. L. (1990). Bioremediation of metal-contaminated surface and groundwaters. *Geomicrobiol J.* 8, 201–223. doi: 10.1080/01490459009377894

Bustard, M., Donnellan, N., Rollan, A., and Mchale, A. P. (1997). Studies on the biosorption of uranium by a thermotolerant, ethanol-producing strain of *Kluyveromyces marxianus*. *Bioprocess Eng.* 17, 45–50. doi: 10.1007/PL00008955

Can, C., and Jianlong, W. (2006). Review on biosorption of heavy metal by *Saccharomyces cerevisiae*. *China Biotechnol.* 26, 69–76. doi: 10.3969/j.issn.1671-8135.2006.01.015

Choi, S. B., and Yun, Y. S. (2004). Lead biosorption by waste biomass of *Corynebacterium glutamicum* generated from lysine fermentation process. *Biotechnol. Lett.* 26, 331–336. doi: 10.1023/B:BILE.0000015453.20708.fc

Cossich, E. S., Tavares, C. R. G., and Ravagnani, T. M. K. (2002). Biosorption of chromium(III) by *Sargassum* sp. biomass. *Electron. J. Biotechnol.* 10, 129–138. doi: 10.1023/B:ADSO.0000039868.02942.47

Dai, Q., Zhang, T., Zhao, Y., Li, Q., Dong, F., and Jiang, C. (2020). Potentiality of living *Bacillus pumilus* SWU7-1 in biosorption of strontium radionuclide. *Chemosphere* 260:127559. doi: 10.1016/j.chemosphere.2020.127559

Dhami, P. S., Gopalakrishnan, V., Kannan, R., Ramanujam, A., and Udupa, S. R. (1998). Biosorption of radionuclides by *Rhizopus arrhizus*. *Biotechnol. Lett.* 20, 225–228. doi: 10.1023/A:1005313532334

Ding, L., Liao, J., and Zhang, Y. (2021). Adsorption performance and mechanism of Al2O3 aerogels towards aqueous U(VI) using template synthesis technology. *Colloids Surf. A Physicochem. Eng. Asp.* 612:125980. doi: 10.1016/j.colsurfa.2020.125980

Dong, Z., Kuanliang, L., Houjun, K., Yibei, F., and Zhengkun, S. (2004). Thermodynamics analysis of Uranium's chemical Species, Migration and deposition in groundwater of a certain place. *J. Nuclear Radiochem.* 26:5. doi: 10.3969/j.issn.0253-9950.2004.01.009

Eide, D. (2000). Metal ion transport in eukaryotic microorganisms: insights from *Saccharomyces cerevisiae*. *Adv. Microb. Physiol.* 43, 1–38. doi: 10.1016/S0065-2911(00)43001-8

Gadd, M. G. (2010). Metals, minerals and microbes: geomicrobiology and bioremediation. *Microbiology* 156, 609–643. doi: 10.1099/mic.0.037143-0

Galamboš, M., Rosskopfová, O., Kufčáková, J., and Rajec, P. (2011). Utilization of Slovak bentonites in deposition of high-level radioactive waste and spent nuclear fuel. *J. Radioanal. Nucl. Chem.* 288, 765–777. doi: 10.1007/s10967-011-0987-0

Golab, Z., Orlowska, B., and Smith, R. W. (1991). Biosorption of lead and uranium by Streptomyces sp. *Water Air Soil Pollut.* 60, 99–106. doi: 10.1007/BF00293968

Haruta, N., Yu, X., Yang, S., Egelman, E. H., and Cox, M. M. (2003). A DNA pairing-enhanced conformation of bacterial RecA proteins. *J. Biol. Chem.* 278, 52710–52723. doi: 10.1074/jbc.M308563200

Ighalo, J. O. (2024). Biowastes and derived green sorbents for water decontamination: insights on thermochemical conversion strategies. *Curr. Opin. Green Sustain. Chem.* 45:100880. doi: 10.1016/j.cogsc.2024.100880

Ighalo, J. O., Chen, Z., Ohoro, C. R., Oniye, M., Igwegbe, C. A., Elimhingbovo, I., et al. (2024). A review of remediation technologies for uranium-contaminated water. *Chemosphere* 352:141322. doi: 10.1016/j.chemosphere.2024.141322

Jianlong, W. (2004). Engineered radiation-resistant bacteria and their application in bioremediation of radioactive wastes-contaminated environment. *J. Radiat. Res. Radiat. Proc.* 22:4. doi: 10.3969/j.issn.1000-3436.2004.05.001

John, S. G., Ruggiero, C. E., Hersman, L. E., Tung, C. S., and Neu, M. P. (2001). Siderophore mediated Plutonium accumulation by *Microbacterium flavescens* (JG-9). *Environ. Sci. Technol.* 35, 2942–2948. doi: 10.1021/es010590g

Juan, W., and Liyu, H. (1999). Study on adsorption of lead by white rot fungus. *Acta Microbiol Sin.* 42, 691–698. doi: 10.1007/s00226-008-0180-y

Kazy, S. K., D'Souza, S. F., and Sar, P. (2009). Uranium and thorium sequestration by a Pseudomonas sp.: mechanism and chemical characterization. *J. Hazard. Mater.* 163, 65–72. doi: 10.1016/j.jhazmat.2008.06.076

Khani, M. H., Keshtkar, A. R., Ghannadi, M., and Pahlavanzadeh, H. (2008). Equilibrium, kinetic and thermodynamic study of the biosorption of uranium onto *Cystoseria indica* algae. *J. Hazard. Mater.* 150, 612–618. doi: 10.1016/j.jhazmat.2007.05.010

Kim, D. S., and Park, B. Y. (2001). Effects on the removal of Pb2+ from aqueous solution by crab shell. *J. Chem. Technol. Biotechnol.* 76, 1179–1184. doi: 10.1002/jctb.505

Kleinübing, S. J., Silva, E. A. D., Silva, M. G. C. D., and Guibal, E. (2011). Equilibrium of cu(II) and Ni(II) biosorption by marine alga *Sargassum filipendula* in a dynamic system: competitiveness and selectivity. *Bioresour Technol.* 102, 4610–4617. doi: 10.1016/j.biortech.2010.12.049

Kolhe, N., Zinjarde, S., and Acharya, C. (2020). Impact of uranium exposure on marine yeast, *Yarrowia lipolytica*: insights into the yeast strategies to withstand uranium stress. *J. Hazard. Mater.* 381:121226. doi: 10.1016/j.jhazmat.2019.121226

Kota, S., and Misra, H. S. (2006). PprA: a protein implicated in radioresistance of *Deinococcus radiodurans* stimulates catalase activity in *Escherichia coli*. *Appl. Microbiol. Biotechnol.* 72, 790–796. doi: 10.1007/s00253-006-0340-7

Liao, J., Ding, L., Zhang, Y., and Zhu, W. (2022). Efficient removal of uranium from wastewater using pig manure biochar: understanding adsorption and binding mechanisms. *J. Hazard. Mater.* 423:127190. doi: 10.1016/j.jhazmat.2021.127190

Ling, Z., Pinghe, Y., Qiming, Y. U., and Yuzao, Q. (2001). Bioaccumulation mechanism of red tide alga *Prorocentrum micans* for heavy metal ions. *Environ. Sci.* 22, 42–45. doi: 10.3321/j.issn:0250-3301.2001.04.010

Liu, M., Dong, F., Zhang, W., Nie, X., Sun, S., Wei, H., et al. (2016). Programmed gradient descent biosorption of strontium ions by *Saccaromyces cerevisiae* and ashing analysis: a decrement solution for nuclide and heavy metal disposal. *J. Hazard. Mater.* 314, 295–303. doi: 10.1016/j.jhazmat.2016.04.049

Lovley, D. R., Phillips, E. J. P., Gorby, Y. A., and Landa, E. R. (1991). Microbial reduction of uranium. *Nature* 350, 413–416. doi: 10.1038/350413a0

Macaskie, L. E., and Dean, A. C. (1989). Microbial metabolism, desolubilization, and deposition of heavy metals: metal uptake by immobilized cells and application to the detoxification of liquid wastes. *Adv. Biotechnol. Process.* 12, 159–201

Meng, J., Lin, X., Li, H., Zhang, Y., Zhou, J., Chen, Y., et al. (2019). Adsorption capacity of kelp-like electrospun nanofibers immobilized with bayberry tannin for uranium(vi) extraction from seawater. *RSC Adv.* 9, 8091–8103. doi: 10.1039/C8RA09297D

Merroun, M. L., Raff, J., Rossberg, A., Hennig, C., Reich, T., and Selenska-Pobell, S. (2005). Complexation of uranium by cells and S-layer sheets of *Bacillus sphaericus* JG-A12. *Appl. Environ. Microbiol.* 71, 5532–5543. doi: 10.1128/aem.71.9.5532-5543.2005

Mingxue, L. (2011). *Studies on microorganism - strontium*, Uranium Interactions and Mechanisms. University of Electronic Science and Technology of China.

Nakajima, A., and Tsuruta, T. (2004). Competitive biosorption of thorium and uranium by *Micrococcus luteus*. *J. Radioanal. Nuclear Chem.* 260, 13–18. doi: 10.1023/B:JRNC.0000027055.16768.1e

Ning, L. (2006). Biosorption behaviour and mechanism of ^{241}Am by microorganisms. Chengdu, China: Sichuan University.

Osman, D., and Cavet, J. S. (2008). Copper homeostasis in bacteria. *Adv. Appl. Microbiol.* 65, 217–247. doi: 10.1016/s0065-2164(08)00608-4

Pattanapipitpaisal, P., Mabbett, A. N., Finlay, J. A., Beswick, A. J., Paterson-Beedle, M., Essa, A., et al. (2002). Reduction of Cr(VI) and bioaccumulation of chromium by gram positive and gram negative microorganisms not previously exposed to Cr-stress. *Environ. Technol. Lett.* 23, 731–745. doi: 10.1080/09593332308618367

Popa, K., Cecal, A., Drochioiu, G., Pui, A., and Humelnicu, D. (2003). *Saccharomyces cerevisiae* as uranium bioaccumulating material: the influence of contact time, pH and anion nature. *Nukleonika* 200, 121–125.

Qiao, Y., Wang, T., Chen, Z., Wang, J., Li, C., and Chen, J. (2024). Corrosion techniques and strategies for used fuel containers with copper corrosion barriers under deep geological disposal conditions: a literature review. *Int. J. Miner. Metall. Mater.* 2024:2949. doi: 10.1007/s12613-024-2949-x

Ramli, N. N., Kurniawan, S. B., Ighalo, J. O., Mohd Said, N. S., Marsidi, N., Buhari, J., et al. (2023). A review of the treatment technologies for hexavalent chromium contaminated water. *Biometals* 36, 1189–1219. doi: 10.1007/s10534-023-00512-x

Renshaw, J. C., Lloyd, J. R., and Livens, F. R. (2007). Microbial interactions with actinides and long-lived fission products. *C. R. Chim.* 10, 1067–1077. doi: 10.1016/j.crci.2007.02.013

Rome, L. D., and Gadd, G. M. (1991). Use of pelleted and immobilized yeast and fungal biomass for heavy metal and radionuclide recovery. *J. Ind. Microbiol. Biotechnol.* 7, 97–104. doi: 10.1007/BF01576071

Rushhoft, C. C. (1949). The possibilities of disposal of radioactive wastes by biological treatment methods. *Sew. Work. J.* 21, 877–883. doi: 10.2307/25031145

Sampedro, M. A., Blanco, A., Llama, M. J., and Serra, J. L. (1995). Sorption of heavy metals to *Phormidium laminosum* biomass. *Biotechnol. Appl. Biochem.* 22, 355–366.

Satoh, K., Narumi, I., Kikuchi, M., Kitayama, S., Yanagisawa, T., Yamamoto, K., et al. (2002). Characterization of RecA424 and RecA670 proteins from *Deinococcus radiodurans*. *J. Biochem.* 131, 121–129. doi: 10.1093/oxfordjournals.jbchem.a003066

Sheng, Y., Baars, O., Guo, D., Whitham, J., Srivastava, S., and Dong, H. (2023). Mineral-bound trace metals as cofactors for anaerobic biological nitrogen fixation. *Environ. Sci. Technol.* 57, 7206–7216. doi: 10.1021/acs.est.3c01371

Sheng, Y., Dong, H., Coffin, E., Myrold, D., and Kleber, M. (2022). The important role of enzyme adsorbing capacity of soil minerals in regulating β-glucosidase activity. *Geophys. Res. Lett.* 49:e2021GL097556. doi: 10.1029/2021GL097556

Sheng, D., Gao, G., Tian, B., Xu, Z., Zheng, Z., and Hua, Y. (2005). RecX is involved in antioxidant mechanisms of the radioresistant bacterium *Deinococcus radiodurans*. *FEMS Microbiol. Lett.* 244, 251–257. doi: 10.1016/j.femsle.2005.01.051

Shunzhong, L., Ning, L., Yuanyou, Y., Taiming, Z., Jiannan, J., and Xinfeng, H. (2003). Biosorption of ^{241}Am by Candida sp. *Nuclear Tech.* 91, 315–318. doi: 10.1524/ract.91.6.315.20024

Strandberg, G. W., Ii, S. E. S., and Parrott, J. R. (1981). Microbial cells as biosorbents for heavy metals: accumulation of uranium by Saccharomyces cerevisiae and *Pseudomonas aeruginosa*. *Appl. Environ. Microbiol.* 41, 237–245. doi: 10.1128/aem.41.1.237-245.1981

Suslov, A. V., Suslova, I. N., Bagiian, G. A., Davydenko, S. G., and Iarovo, B. F. (2004). Isolation and investigation of natural yeast strains resistant to heavy metal salts and radionuclides. *Radiats. Biol. Radioecol.* 44, 574–578.

Takehiko, T. (2004). Adsorption of uranium from acidic solution by microbes and effect of thorium on uranium adsorption by *Streptomyces levoris* (environmental biotechnology). *J. Biosci. Bioeng.* 97, 275–277. doi: 10.1016/s1389-1723(04)70203-0

Tsezos, M., and Volesky, B. (1981). Biosorption of uranium and thorium. *Biotechnol. Bioeng.* 23, 583–604. doi: 10.1002/bit.260230309

Umeh, C. T., Akinyele, A. B., Okoye, N. H., Emmanuel, S. S., Iwuozor, K. O., Oyekunle, I. P., et al. (2023). Recent approach in the application of nanoadsorbents for malachite green (MG) dye uptake from contaminated water: a critical review. *Environ. Nanotechnol. Monit. Manage.* 20:100891. doi: 10.1016/j.enmm.2023.100891

Volesky, B., and May-Phillips, H. A. (1995). Biosorption of heavy metals by *Saccharomyces cerevisiae*. *Appl. Microbiol. Biotechnol.* 42, 797–806. doi: 10.1007/bf00171964

Wang, X., Shan, T., and Pang, S. (2021). Removal of Sr, co, and Mn from seawater by *Sargassum horneri* in mono- and multi-nuclide contamination scenarios. *J. Appl. Phycol.* 33, 2587–2596. doi: 10.1007/s10811-021-02477-1

Xiong, T., Li, Q., Liao, J., Zhang, Y., and Zhu, W. (2022). Highly enhanced adsorption performance to uranium(VI) by facile synthesized hydroxyapatite aerogel. *J. Hazard. Mater.* 423:127184. doi: 10.1016/j.jhazmat.2021.127184

Xueqin, X., Xiaoming, L., Qi, Y., Guangming, Z., and Ke, J. (2006). Immobilized microorganism technology and its application in heavy metal wastewater treatment. *Chin. J. Environ. Eng.* 7, 99–105.

Yohey, S., and Jillian, F. B. (2004). Resistance to, and accumulation of, uranium by Bacteria from a uranium-contaminated site. *Geomicrobiol J.* 21, 113–121. doi: 10.1080/01490450490266361

Yong, P., Macaskie, L. E., Sammons, R. L., and Marquis, P. M. (2004). Synthesis of nanophase hydroxyapatite by a *Serratia* sp. from waste-water containing inorganic phosphate. *Biotechnol. Lett.* 26, 1723–1730. doi: 10.1007/s10529-004-3744-4

Yujian, W., and Hongyu, L. (2006). Advances in immobilized microorganism and It's research on waste water treatment. *Biotechnology* 1112, 425–434. doi: 10.1196/annals.1415.028

Zein, R., Hevira, L., Zilfa, R., Fauzia, S., and Ighalo, J. O. (2023). The improvement of indigo carmine dye adsorption by *Terminalia catappa* shell modified with broiler egg white. *Biomass Convers. Biorefinery* 13, 13795–13812. doi: 10.1007/s13399-021-02290-3

Zhou, L., Dong, F., Dai, Q., Liu, M., Zhang, W., and Zhang, Y. (2022). Transformation of radionuclide occurrence state in uranium and strontium recycling by *Saccharomyces cerevisiae*. *J. Radioanal. Nucl. Chem.* 331, 2621–2629. doi: 10.1007/s10967-022-08308-y

frontiers | Frontiers in Microbiology

TYPE Original Research
PUBLISHED 29 August 2024
DOI 10.3389/fmicb.2024.1463665

OPEN ACCESS

EDITED BY
Anhuai Lu,
Peking University, China

REVIEWED BY
Moushumi Hazra,
University of Nebraska-Lincoln, United States
Wen-Dong Xian,
Zhejiang Ocean University, China

*CORRESPONDENCE
Nuan Yang
✉ yangnuan@xust.edu.cn
Enke Hou
✉ houek@xust.edu.cn

RECEIVED 12 July 2024
ACCEPTED 19 August 2024
PUBLISHED 29 August 2024

CITATION
Guo L, Chen X, Sheng Y, Yang N, Hou E and Fang H (2024) Impact of soil fissure status on microbial community in mining-disturbed area, the northern Shaanxi province. *Front. Microbiol.* 15:1463665. doi: 10.3389/fmicb.2024.1463665

Impact of soil fissure status on microbial community in mining-disturbed area, the northern Shaanxi province

Liang Guo[1], Xianglong Chen[2], Yizhi Sheng[2], Nuan Yang[1]*, Enke Hou[1]* and Haisong Fang[1]

[1]College of Geology and Environment, Xi'an University of Science and Technology, Xi'an, China, [2]State Key Laboratory of Biogeology and Environmental Geology & MOE Key Laboratory of Groundwater Circulation and Environment Evolution, China University of Geosciences, Beijing, China

Mining disturbance has great impacts on soil physicochemical factors, causing notable differences between pre-mining and after-mining conditions, and between coal mining areas and non-mined areas. However, little is known about whether the fissure statuses induced by mining activities affect the edaphic factors and how soil microbial communities respond to these fissure development states. In this study, we systematically investigated the edaphic factors and microbial communities in a mining disturbance area exhibiting the full development status of soil fissures, where the sampling sites were divided into soil fissure development and closure zones. Microbial alpha-and beta-diversity, correlation coefficient matrix, non-metric multi-dimensional scaling, principal co-ordinates analysis, mantel test, and microbial co-occurrence network were employed to elucidate variations, correlations, and interactions between edaphic factors and microbial communities under the two different soil fissure states. Results suggested that soil physicochemical properties were significantly affected by fissure states, showing an increasing trend in soil moisture content and soil nutrients. The associations among edaphic factors have weakened during the soil fissure development process. Soil microbial communities showed different compositions and the underlying influential mechanisms between two soil fissure states. Soil moisture content, pH, particle compositions, organic matter, and heavy metals largely affected microbial communities. Rare species were vulnerable to mining disturbance and were keystone taxa that reinforced the overall interconnections of the soil microbial community (e.g., *Nordella*, *Sphingomonas*, *Massilia*, and *Rubritepida*). Our study revealed the impacts of distinct fissure states on the soil physicochemical properties and microbial communities, and the edaphic conditions showed key contributions to the soil microbial communities, particularly the abundance and ecological roles of rare species.

KEYWORDS

microbial community, soil biodiversity, mining disturbance, soil fissure, co-occurrence network

1 Introduction

China's energy supply heavily relies on coal resources, although vigorously advocating the "two-carbon policy" in recent years. The Ordos Plateau and its adjacent areas had been bearing tremendous shallow-buried coal deposits and became one of the most important coal-producing areas in China. However, the development of the coal mining industry has resulted in soil fissures, land subsidence, degradation, etc. in mining disturbance areas (Liu et al., 2015; Wang G. et al., 2017; Yang et al., 2019), and further causing countless losses, severe anthropogenic geological disasters. Mining fissures are categorized into three types: tensile fissures, collapse fissures, and sliding fissures. The dynamic characteristics of mining-induced fissures undergo a development cycle of fissure-expansion-closure (Liu et al., 2019; Kang et al., 2023). Ground fissures showed an inverse C-shape feature and developed in advance of the coal seam working face excavation, and then distributed in the "O" form on the boundary of the working face after subsidence stabilized (Hou et al., 2022).

The emergence of soil fissures has a profound influence on the ecological environment and soil physicochemical factors (Liu et al., 2019). Mining activities significantly altered soil organic matter (SOM), total nitrogen (TN), and available phosphorus (AP). Upon mining disturbances, SOM, TN, and AP typically decreased by 35.49, 23.56, and 38.06%, respectively, compared to the pre-mining topsoil (Wang et al., 2021). Other lowered indicators included soil moisture content, soil clay content, and available potassium (Luo et al., 2019; Ma et al., 2019). Moreover, in the vertical profile of the mining disturbance area, most soil parameters (e.g., SOM, AP) were lower than those in the nonmined area at all depths. In contrast, these indicators showed an opposite trend in the nonmined area with increasing depth, indicating that mining activities altered the vertical distribution of edaphic factors (Shi et al., 2017). However, in other cases, soil nutrients (e.g., TP, TN) showed an increasing trend with the development of soil fissures (Peng et al., 2020; Long et al., 2022).

Soil microorganisms are ubiquitously present in soil and have tight correlations with their environment and nutrient levels (Chapman et al., 2018). Therefore, soil microbial communities are highly susceptible to the changing environment in mining disturbance areas. Compared to non-mined sites, soil microbial community structure and diversity in the coal mining area would be impaired and significantly influenced by soil properties (Ezeokoli et al., 2019; Yuan et al., 2022). Under the mining disturbance conditions, soil pH was deemed as one of the most influential factors for shaping microbial diversity, taxonomic composition, and ecological distribution, especially along the mining disturbance gradient (Xiao et al., 2021a). Additionally, other factors influencing soil bacterial community included conductivity (EC), soil moisture content, soil depth, nutrient concentrations, etc. (Banning et al., 2012; Guo et al., 2021; Sheng et al., 2021b). Mining activities have been shown to reduce soil microbial abundance and diversity (Shi et al., 2017). There were also concerns regarding the recovery of the soil environment and microbial communities after mining activity ceased and the duration required for recovery. While soil pH, moisture content, nutrients, and heavy metals were stabilized and reconnected with microbial communities after soil restoration, no matter the positive or negative restoration processes, these attributes rarely return to their original levels, even after decades of restoration efforts (Banning et al., 2012; de Quadros et al., 2016).

In all, there remains a substantial knowledge gap regarding whether the different fissure states induced by mining activities have an impact on soil microbial communities, and how the edaphic factors and microbial communities co-varied during the different fissure development states. Therefore, based on field investigation findings, we selected a shallow-buried coal seam located in the Shaanxi Province, known for its extensively developed soil fissures. An integrated approach combining soil edaphic and microbial community analysis was employed to elucidate soil physicochemical variables and microbial community variation, as well as the correlation between the soil edaphic factors and microbial communities under different soil fissure states. Soil physicochemical properties, including size distribution of soil particles, inorganic variables, organic components, and heavy metals, were determined to decipher soil edaphic conditions in mining disturbance areas. Soil bacteria and archaea communities were analyzed using high-throughput sequencing of the 16S rRNA gene. This study aimed to uncover the variations and interconnections of the edaphic condition and microbial community across distinct soil fissure states.

2 Materials and methods

2.1 Site description

The study area is located at the junction of Shaanxi and Inner Mongolia Provinces, northeast of the Yushenfu mining area, one of the most coal production fields in China. This area is characterized by a temperate semi-arid continental monsoon climate with dryness, low precipitations, and meteorological disasters. The annual temperature is approximately 6.6°C, while the annual precipitation ranges from 109 mm to 819 mm, and 76% of total precipitation is concentrated from June to September (Xiao et al., 2020). In contrast, the annual evaporation is seven times greater than the rainfall. This vast deficit between precipitation and evaporation has led to the scarcity of regional water resources and fragile ecological environments. Soil texture is dominated by aeolian sandy soil and loess, characterized by poor structure, low fertility, and low resistance to erosion (Hou et al., 2022). Therefore, surface soil is sensitive to mining disturbance, and fissures are extensively developed. The sampling site was chosen at one of the most productive coal mines, the Ningtiaota coalfield, with flat topography in the Yushenfu mining area (Huang et al., 2018). In this area, the active mining depth of the Ningtiaota coalfield is less than 200 m, causing surface fissures to reach the topsoil directly. Due to shallow-buried coal seams and large coal yields, two different types of soil fissures developed: fissure development state and fissure closure state (Hou et al., 2022).

2.2 Sampling method and soil edaphic properties measurement

Soil sampling sites were strategically chosen based on the field investigations during September 2021, with sampling points distributed across the soil fissure development and closure areas of the coal mine (Figure 1; Supplementary Figure S1). A total of 12 sampling points were selected based on the soil fissure states, of which half were distributed at the soil fissure development zone (FDZ, including

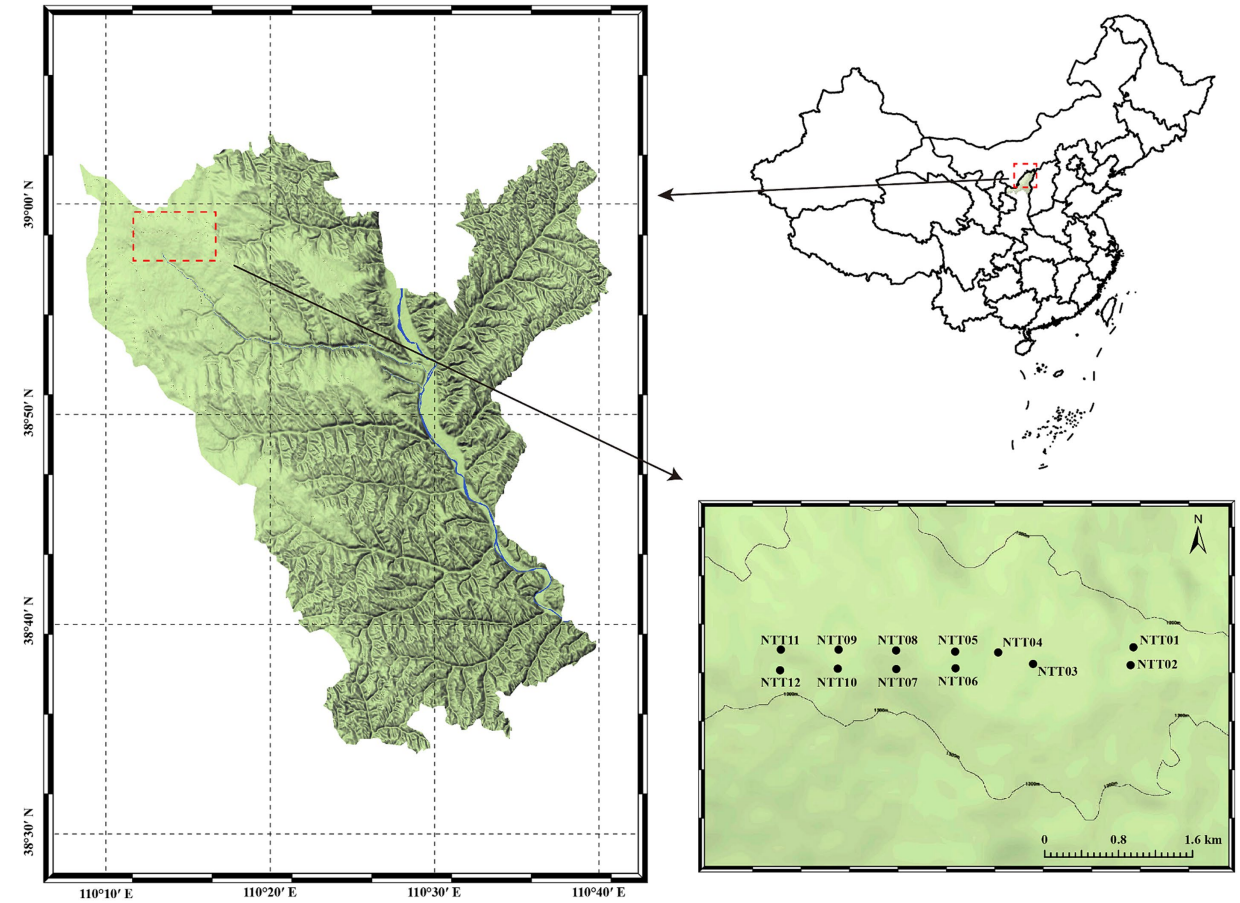

FIGURE 1
Simplified topographical map of the study area and sampling locations.

NTT02, NTT03, NTT06, NTT07, NTT10, and NTT12), and the other half were distributed at the soil fissure closure zone (FCZ, including NTT01, NTT04, NTT05, NTT08, NTT09, and NTT11). Soil samples were collected 10 cm below the surface to avoid interference of potential surface pollutants. For each sample, five replicates were uniformly collected within a 1 m radius and mixed to effectively form one soil sample based on the five-point sampling method (Deng et al., 2013). Each collected sample was split into two parts for physicochemical and biological analysis. For the edaphic factors determination, rocks and roots were removed from the soil samples, which were then air-dried and sieved through a 0.25 mm sieve before the measurements (Xin et al., 2016). Soil samples for microbial analysis were collected by sterile shovel, stored in dry ice immediately in the field, and transported into the laboratory within 48 days for further DNA extraction (Sheng et al., 2021b). All samples were preserved under 4°C before being transported to the laboratory within 48 h.

Soil samples were analyzed for a variety of geochemical parameters. Soil pH and electrical conductivity (EC) were tested using a glass electrode in water (1:2.5 and 1:5 soil/water ratio, respectively). Soil texture, soil moisture content (SMC), cation exchange capacity (CEC), total phosphorus (TP), available phosphorus (AP), total potassium (TK), and available potassium (AK) were determined by standard methods (Lu, 1999). The soil organic carbon (SOC) content was measured using the dichromate oxidation method (Kalembasa and Jenkinson, 1973). Total carbon (TC) and dissolved organic carbon (DOC) content were measured by the total organic carbon analyzer (TOC-V Series SSM-5000A). Soil microbial biomass carbon (MBC) and nitrogen (MBN) were determined by the chloroform fumigation-extraction method, which is the most common technique for measuring microbial biomass elements (Cleveland and Liptzin, 2007). Heavy metals, including cadmium (Cd), iron (Fe), copper (Cu), manganese (Mn), and chromium (Cr), were estimated by atomic absorption spectrometry (McLaughlin et al., 2000; Tüzen, 2003). Hydride generation atomic fluorescence detection measured total arsenic (As) in soil samples (Shi et al., 2003). Total nitrogen (TN) was measured by the Kjeldahl method, and ammonium nitrogen (NH_4-N) and nitrate nitrogen (NO_3-N) were determined by extracting fresh soil with 1 mol/L KCl for 30 min and were analyzed using an autoanalyzer. Alkali-hydrolyzable nitrogen (AHN) was regarded as soil-available nitrogen and determined by the diffusion-absorption method (Zhang et al., 2018; Xiao et al., 2019). Nitrite nitrogen (NO_2-N) was analyzed colorimetrically by extraction method with potassium chloride (KCl, 1 mol/L) solution (Dai et al., 2020). Humus substance (Humus) and its fractions [humin (Hm), humic acid (HA), and fulvic acid (FA)] were determined based on the standard protocols after extraction with a mix of sodium hydroxide (0.1 mol/L) and sodium pyrophosphate (0.1 mol/L) (Sheng et al., 2021b).

2.3 Soil DNA extraction and microbial high-throughput sequencing

Soil genomic DNA was extracted using the FastDNA Spin Kit (MP Biomedicals™, Fisher Scientific, United States) according to the manufacturer's instructions. Amplification of partial hypervariable 16S rRNA gene was performed by using bacterial primer pairs 338F (5′-ACTCCTACGGGAGGCAGCAG-3′)/806R (5′-GGACTACH VGGGTWTCTAAT-3′) for V3–V4 region (Liu et al., 2020), and archaeal primer pairs 524F10extF (5′-TGYCAGCCGCCGCGG TAA-3′)/Arch958RmodR (5′-YCCGGCGTTGAVTCCAATT-3′) for V4–V5 region (Liu et al., 2016). Bacterial and archaeal soil genomic DNA was amplified by PCR which consisted of an initial denaturation step (94°C) for 5 min, followed by 30 cycles of 94°C (1 min), 64°C (1 min), and 72°C (1 min), and a final 10 min elongation (72°C) (Sheng et al., 2021b). After PCR, 16S rRNA amplicons were extracted from 2% agarose gels and purified using the AxyPrep DNA Gel Extraction Kit (Axygen Biosciences, United States) and quantified by a fluorescent quantitation system (QuantiFluor™-ST, Promega, United States) according to the manufacturer's instructions. Purified amplicons were pooled in equimolar and paired-end sequenced on an Illumina MiSeq platform. The raw reads were deposited into the NCBI Sequence Read Archive (SRA) database (Accession Number: SRP503985).

2.4 Data statistics and bioinformatics analysis

Totally 542,868 bacterial raw reads and 684,944 archaeal raw reads were produced for all samples, and the rarefaction curve showed that the numbers of observed operational taxonomic units (OTU) were close to saturation, indicating a sufficient sequencing depth (Sheng et al., 2016). The sequencing quality controlling of raw reads was conducted by removing low-quality reads using the QIIME pipeline as previously described (Caporaso et al., 2010; Guo et al., 2022). Operational taxonomic units (OTUs) were clustered using UPARSE based on the 97% similarity criteria (Edgar, 2013). The taxonomy of each OTUs was analyzed according to the SILVA (SSU115) database (Wang et al., 2007). Representative OTUs were also blasted against the NCBI taxonomic database[1] to acquire a more reliable taxonomic resolution for further analysis. Alpha-and beta-microbial diversity were calculated within QIIME, and microbial beta-diversity was conducted by Bray–Curtis metrics based on pairwise distance values (Guo et al., 2022).

The correlation between edaphic factors was measured by the Pearson correlation coefficient. Mantel test was used to evaluate the correlation between soil physicochemical properties and microbial communities. To avoid the bias induced by different units of edaphic factors, soil datasets were scaled before calculating. Pearson correlation analysis and Mantel test were performed and visualized by using "vegan," and "LinkET" packages in R. Non-metric multi-dimensional scaling (NMDS) and principal co-ordinates analysis (PCoA) were conducted to evaluate the similarity of microbial communities in soil samples. Other statistical analyses, e.g., one-way analysis of variance (ANOVA), and analysis of similarity (ANOSIM) with 9,999 permutations were conducted by using SPSS 19.0 (IBM Company, 2010). Redundancy analysis (RDA, lengths of gradient ≤3.0) was implemented with the forward selection of variables in Canoco 5.0, and the contribution of each edaphic factor to microbial beta diversity and associated statistical tests were calculated. To estimate microbial species co-occurrence patterns, distance-based microbial networks were constructed with those microbial taxa (OTU level) with >50% presence at each sample by the Spearman correlation matrix of pairwise associations among the OTUs (Sheng et al., 2021c). The network topological indices [e.g., nodes, links, average degree (avgK), average clustering coefficient (avgCC), average path distance (GD), within-module connectivity (Zi), and among-module connectivity (Pi)] were calculated to describe the properties of the networks and the network was visualized by the Gephi 0.9.2 as previously described (Deng et al., 2012).

3 Results

3.1 Impact of fissure status on soil physicochemical properties

The size distribution of soil particles in the study area predominantly consisted of fine sand and silt, with relatively low proportions of clay and coarse sand (Table 1). The content of fine sand in the fissure closure zone (FCZ, 64.8 ± 3.0%) was slightly lower than that in the fissure development zone (FDZ, 67.9 ± 4.0%). In contrast, the contents of silt and clay in the FCZ group were higher than those in FDZ, with silt at 21.85 ± 2.24% and clay at 12.0 ± 0.7% % in FCZ, compared to 20.43 ± 2.9% and 10.2 ± 1.4% in FDZ. Coarse sand, the largest particle in soil, was less than 2% in both FCZ and FDZ groups. Soil pH exhibited minor variations, ranging from 7.95 to 9.05 with an average of 8.6, indicating an alkaline nature. EC and SMC exhibited significant variations. The FCZ group displayed lower EC (41.1 ± 5.6 μs/cm) and SMC (4.77 ± 0.26%) compared to the FDZ group (53.2 ± 3.6 μs/cm and 5.71 ± 0.22%, respectively).

Soil carbon, nitrogen, and organic matter were significantly affected by variations in soil fissure status induced by mining disturbance (Table 1 and Supplementary Figure S2). In FCZ, TC, MBC, and DOC were significantly lower than those in FDZ ($p < 0.05$). Specifically, TC was 17.34 ± 1.44 g/kg in FCZ compared to 22.32 ± 1.13 g/kg in FDZ, MBC was 53.4 ± 4.84 mg/kg in FCZ versus 80.5 ± 9.76 mg/kg in FDZ, and DOC was 55.96 ± 2.81 mg/kg in FCZ compared to 67.51 ± 1.64 mg/kg in FDZ, indicating declines of 22.3, 33.7, and 17.1%, respectively. Furthermore, compared with the FDZ region, the contents of SOC (4.33 ± 0.59 g/kg and 4.46 ± 0.28 g/kg), Humus (1.01 ± 0.1 g/kg and 1.15 ± 0.06 g/kg), and HA (0.68 ± 0.08 g/kg and 0.85 ± 0.09 g/kg) decreased in FCZ, accounting for reductions of 2.9, 11.8, and 20.69%, respectively. Hm, the largest fraction of molecules remained stable in both sampling regions (3.31 ± 0.49 g/kg and 3.31 ± 0.24 g/kg). While most organic matter decreased in FCZ, FA increased from 0.29 ± 0.06 g/kg in FDZ to 0.33 ± 0.03 g/kg in FCZ, an increase of 14.27%. NO_3-N, MBN, and AHN in FCZ also decreased significantly compared with those in FDZ. NO_3-N content dropped from 4.65 ± 0.41 mg/kg in FDZ to 2.36 ± 0.28 mg/kg in FCZ, MBN from 8.76 ± 1.32 mg/kg to 5.55 ± 0.67 mg/kg, and AHN from

1 https://blast.ncbi.nlm.nih.gov/Blast.cgi

10.3389/fmicb.2024.1463665

TABLE 1 Soil edaphic factors between soil fissure development and closure zone.

Variables	Unit	FCZ	FDZ	Variance
Clay	<0.002 mm	12.02 ± 0.69	10.19 ± 1.36	17.99%
Silt	0.002–0.02 mm	21.85 ± 2.24	20.43 ± 2.9	6.93%
Fine sand	0.02–0.2 mm	64.79 ± 3.02	67.93 ± 4.0	−4.62%
Coarse sand	0.2–2 mm	1.34 ± 0.43	1.45 ± 0.35	−7.55%
pH		8.50 ± 0.17	8.73 ± 0.08	−2.69%
Electrical conductivity (EC)	μs/cm	41.1 ± 5.62	53.23 ± 3.63	−22.79%
Soil moisture content (SMC)	%	4.78 ± 0.26	5.71 ± 0.22	−16.43%
Cation exchange capacity (CEC)	cmol/kg	5.17 ± 0.56	5.60 ± 0.38	−7.52%
Total nitrogen (TN)	g/kg	0.39 ± 0.05	0.42 ± 0.02	−4.91%
Microbial biomass nitrogen (MBN)	mg/kg	5.55 ± 0.67	8.76 ± 1.32	−36.71%
Nitrate nitrogen (NO_3-N)	mg/kg	2.36 ± 0.28	4.65 ± 0.41	−49.21%
Ammonium nitrogen (NH_4-N)	mg/kg	0.49 ± 0.05	0.52 ± 0.06	−6.29%
Nitrite nitrogen (NO_2-N)	mg/kg	0.03 ± 0.004	0.03 ± 0.001	9.30%
Alkali-hydrolyzable nitrogen (AHN)	mg/kg	23.92 ± 1.84	28.88 ± 1.33	−17.19%
Total carbon (TC)	g/kg	17.34 ± 1.44	22.32 ± 1.13	−22.28%
Microbial biomass carbon (MBC)	mg/kg	53.40 ± 4.84	80.50 ± 9.76	−33.67%
Dissolved organic carbon (DOC)	mg/kg	55.96 ± 2.81	67.51 ± 1.64	−17.11%
Soil organic carbon (SOC)	g/kg	4.33 ± 0.59	4.46 ± 0.28	−2.94%
Humus substance (Humus)	g/kg	1.01 ± 0.1	1.15 ± 0.06	−11.76%
Humic acid (HA)	g/kg	0.68 ± 0.08	0.85 ± 0.09	−20.69%
Humin (Hm)	g/kg	3.31 ± 0.49	3.31 ± 0.24	0.12%
Fulvic acid (FA)	g/kg	0.33 ± 0.03	0.29 ± 0.06	14.27%
Copper (Cu)	mg/kg	5.06 ± 0.55	5.33 ± 0.45	−5.06%
Manganese (Mn)	g/kg	0.25 ± 0.02	0.23 ± 0.01	6.18%
Cadmium (Cd)	mg/kg	0.11 ± 0.02	0.08 ± 0.02	36.50%
Chromium (Cr)	mg/kg	20.62 ± 1.67	17.35 ± 1.35	18.84%
Iron (Fe)	g/kg	22.38 ± 1.51	20.12 ± 1.05	11.22%
Arsenic (As)	mg/kg	5.33 ± 0.67	5.57 ± 0.38	−4.33%
Total phosphorus (TP)	g/kg	0.32 ± 0.02	0.35 ± 0.02	−8.39%
Total potassium (TK)	g/kg	20.43 ± 0.21	20.51 ± 0.22	−0.40%
Available phosphorus (AP)	mg/kg	0.98 ± 0.17	1.27 ± 0.24	−22.71%
Available potassium (AK)	mg/kg	58.5 ± 5.04	72.67 ± 7.36	−19.50%

Statistical value "variance" represented the changes of soil physicochemical variables in the soil fissure closure zone (FCZ) in relative to the soil fissure development zone (FDZ). The reference value referred to the edaphic factors in FDZ.

28.88 ± 1.33 mg/kg to 23.92 ± 1.84 mg/kg, representing reductions of 49.2, 36.6, and 17.3%, respectively. The contents of AK and AP in FCZ were 58.5 ± 5.0 mg/kg and 1.0 ± 0.2 mg/kg, whereas these were 72.7 ± 7.4 mg/kg and 1.3 ± 0.2 mg/kg in FDZ, representing decreases of 19.5 and 22.7%, respectively. Similarly, compared with FDZ, there was an overall reduction of 8.4% in TP and 0.4% in total potassium (TK) in FCZ. However, heavy metals had higher contents in FCZ compared to FDZ, including Cd (0.11 ± 0.02 mg/kg and 0.08 ± 0.02 mg/kg), Cr (20.62 ± 1.67 mg/kg and 17.35 ± 1.35 mg/kg), Fe (22.38 ± 1.51 g/kg and 20.12 ± 1.05 g/kg), and Mn (0.23 ± 0.02 g/kg and 0.23 ± 0.01 g/kg). These variables increased by 36.5% for Cd, 18.84% for Cr, 11.22 for Fe, and 6.18% for Mn. Conversely, only Cu (5.06 ± 0.55 mg/kg and 5.33 ± 0.45 mg/kg) and As (5.33 ± 0.67 mg/kg and 5.57 ± 0.38 mg/kg) in FCZ had lower contents than that of FDZ, the declines accounted for 5.06 and 4.33%, respectively. To sum up, soil nutrients decreased but metals generally increased from FDZ to FCZ.

In the study area, the correlations between the edaphic factors in FCZ differed significantly from those in FDZ (Figures 2A,B). The heatmap results revealed that edaphic factors had high-level associations in FCZ and the coefficient was generally greater than that in FDZ. Only CEC and TN had significant positive correlations with heavy metals (such as Cu, Mn, Cr, Fe, and As), and the correlation between heavy metals strengthened in FDZ. The results clearly showed that the relationship among soil physicochemical properties significantly deteriorated during the development process of soil fissures in the study area. Notably, the size distribution of soil particles

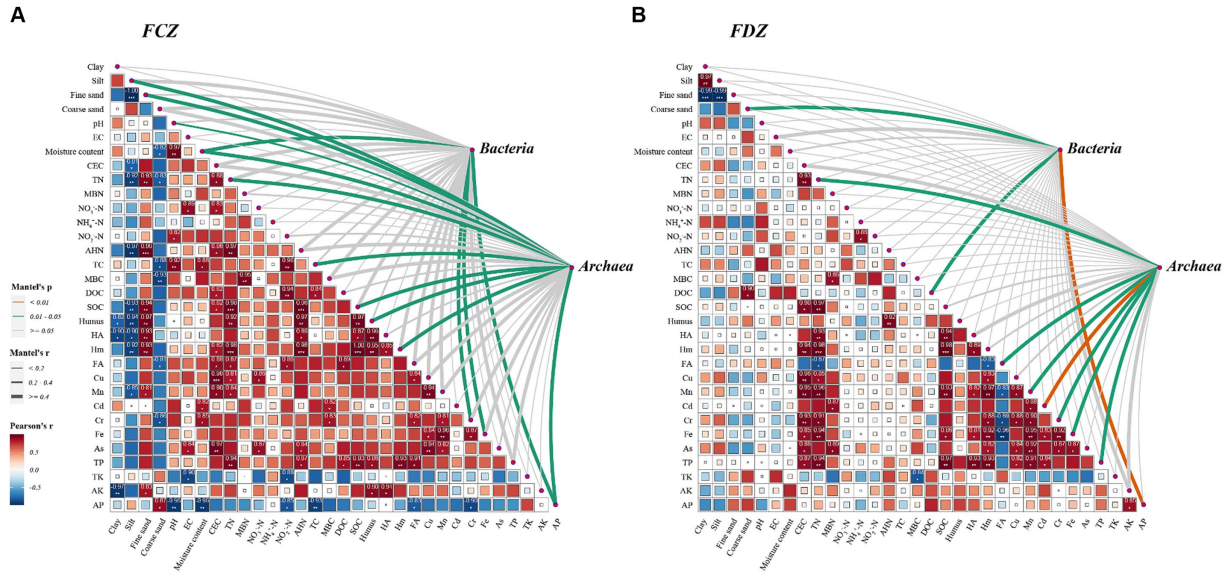

FIGURE 2
Pearson correlation matrix of the edaphic factors, and the correlation between microbial community composition and the edaphic factors using the Mantel test. **(A)** Pearson and Mantel results in the FCZ. **(B)** Pearson and Mantel results in the FDZ. $*p < 0.05$, $**p < 0.01$, and $***p < 0.001$. The strength of the correlation is represented by the thickness of the lines, and the significance p-values are annotated with colors (yellow: $p < 0.01$; green: $p < 0.05$; gray: $p > 0.05$).

was significantly correlated with soil physicochemical components in FCZ (Figure 2A). Clay and silt, which are smaller diameter particles, had a negative correlation with organic components (including SOC, Humus, HA, and Hm), AHN, CEC, and Mn, while fine sand particles with larger diameter showed a significant positive correlation with above-mentioned factors. Coarse sand was not significantly correlated with these variables but was negatively correlated with SMC, TC, MBC, and FA. This is a solid dataset indicating that the soil physicochemical properties were significantly affected by the different fissure states caused by mining disturbance, resulting in significant divergence in their co-appearance and correlations.

3.2 Soil microbial composition variations under two stages of fissure conditions

According to the results of microbial high-throughput sequencing, a total of 486,595 bacterial sequences and 607,615 archaeal sequences were obtained, with the number of valid archaeal sequences surpassing that of bacterial sequences, indicating a substantial and non-neglectable archaea community harbored in the soils. This study evaluated the microbial community's richness, diversity, and evenness using the microbial alpha diversity index (Table 2). The Sobs and Chao indexes represent the observed and theoretical values of microbial richness, which had an average value of 2,563 and 3,170 for the bacteria community and 254 and 366 for the archaea community, indicating a higher microbial richness level of the bacteria community than the archaea community. The Shannon and the Simpson indexes represent the diversity of microbial communities. The bacterial community showed higher diversity levels than the archaea community, as the average values were 6.5 and 0.0035 for the bacteria community and 2.1 and 0.17 for the archaea community. The evenness of the bacterial community ranged from 0.25 to 0.29, while that of the archaeal community ranged from 0.02 to 0.04, suggesting that the archaea community was less evenly distributed.

The archaea communities' composition was simple and homogeneous (Figure 3A and Supplementary Table S1). *Nitrososphaeria* class, the most broadly distributed chemolithoautotrophy of Archaea and known for its capacity of aerobic oxidation of ammonia (Kerou et al., 2016), had an overwhelming abundance of more than 95% in all soil samples. At the genus taxonomic level, 72.04% ± 1.6% archaea lineages belonged to the genus *Nitrososphaera*, while 17.52% ± 0.9% archaea were identified as Candidatus *Nitrososphaera*, genetically similar to those of the *Nitrososphaera* genus. Additionally, 8.17% ± 1.4% of archaea belonged to an unclassified genus, Candidatus *Nitrocosmicus*. The aforementioned archaea showed no significant difference between the FDZ and FCZ groups ($p > 0.05$), indicating that mining disturbance has a relatively minor impact on the distribution of dominant archaea. Correspondingly, *Methanomassiliicoccus* (0.9% ± 0.2%) and numerous rare species (classified as "others" in this study) with relative abundances less than 1% showed significant differences between the two distinct sampling regions ($p < 0.05$), indicating mining disturbance has a greater impact on rare species within the archaea community.

The bacteria community was more complex and divergent compared to the archaea community. Due to many bacterial sequences not matching to the database at the genus taxonomic level, the bacteria composition was analyzed at the class taxonomic level (Figure 3B and Supplementary Table S2). No single bacterial lineage exceeded 25% relative abundance within the bacterial community. The most abundant bacteria, *Actinomycetes*, had an average abundance of 20.0% ± 0.6% across all soil samples, with small variations among sampling points. *Thermoleophilia*, *Alphaproteobacteria*, and *Vicinamibacteria* maintained relative abundances of around 10%, with

TABLE 2 The alpha diversity estimators from the soil bacteria and archaea communities.

SampleID	Coverage		Sobs		Chao		Shannon		Simpson		Heip	
	Bacteria	Archaea	Bacteria	Archaea	Bacteria	Archaea	Bacteria	Archaea	Bacteria	Archaea	Bacteria	Archaea
NTT01	98.5%	99.8%	2,393	209	2,926	272	6.40	1.89	0.005	0.247	0.25	0.03
NTT02	98.4%	99.8%	2,635	240	3,186	330	6.53	2.21	0.004	0.158	0.26	0.03
NTT03	98.0%	99.8%	2,633	271	3,279	424	6.56	2.11	0.003	0.165	0.27	0.03
NTT04	98.0%	99.8%	2,712	258	3,270	332	6.64	2.25	0.003	0.135	0.28	0.03
NTT05	97.7%	99.6%	2,579	246	3,272	447	6.56	2.20	0.004	0.142	0.27	0.03
NTT06	97.8%	99.8%	2,624	392	3,296	414	6.64	2.41	0.003	0.137	0.29	0.03
NTT07	98.2%	99.8%	2,630	214	3,070	282	6.61	2.25	0.003	0.144	0.28	0.04
NTT08	97.9%	99.8%	2,408	165	3,089	251	6.56	1.87	0.003	0.204	0.29	0.03
NTT09	97.2%	99.8%	2,465	243	3,268	350	6.57	2.04	0.003	0.169	0.29	0.03
NTT10	98.4%	99.8%	2,731	248	3,300	423	6.51	2.15	0.004	0.151	0.25	0.03
NTT11	98.0%	99.8%	2,488	286	3,077	406	6.51	2.01	0.004	0.173	0.27	0.02
NTT12	98.2%	99.7%	2,460	279	3,009	458	6.54	1.86	0.003	0.214	0.28	0.02

average values of 11.79% ± 0.5, 11.75% ± 0.6, and 9.46% ± 1.1%. *Blastocatellia*, *Dehalococcoidia*, *Gemmatimonadetes*, *Chloroflexia*, *Gammaproteobacteria*, and *Bacilli* were all top 10 abundant bacteria, with abundances of 5.46% ± 0.5, 4.77% ± 0.3, 3.92% ± 0.2, 3.84% ± 0.2, 3.67% ± 0.2, and 3.36% ± 0.5%, respectively. Furthermore, *Rubrobacteria*, *Acidimicrobiia*, *Methylomirabilia*, *Bacteroidia*, *Bacillota sensu stricto incertae sedis*, and *Anaerolineae* exceeded 1% of bacteria community. Similar to archaeal community, there was no significant difference ($p > 0.05$) in the relative abundances of bacteria above 1% between FDZ and FCZ, while some rare species (e.g., *Rhodothermia*, no-ranked *Armatimonadota*, and no-ranked *Bacteroidota*) exhibited significant differences ($p < 0.05$) between the two different regions.

3.3 Microbial beta diversity characteristics under different soil fissure stages

Soil microorganisms play a vital role in maintaining the surface ecological environment and geochemical elements cycling, especially in ecologically vulnerable areas. Dry climate, scarce rainfall, and extensive coal mining activities in the study area destroyed the original structures and stresses of soil and rock and further exacerbated the vulnerability of the surface ecological environment. To quantitatively describe variations in microbial community compositions and how they respond to the mining activities, microbial beta-diversity analysis was employed. Microbial beta-diversity of the archaea and bacteria communities was analyzed by NMDS and PCoA methods, and both analyses were conducted at the same taxonomic level to ensure the consistency and comparability of the results.

Briefly, the stress values of NMDS results for the microbial communities were less than or close to 0.05, and the explanatory degree of the first two components (PC1 and PC2) in PCoA results exceeded 70%. This indicated high representativeness, allowing for a quantitative description of microbial composition characteristics (Figure 4). The distribution of the archaeal community was scattered with no obvious clustering between samples, primarily following the direction of the horizontal axis on the biplots (Figures 4A,B). Rare species could be the main attributions for the scattered pattern since significant variations observed in the rare species among the archaeal communities. Additionally, the archaeal communities collected from FDZ and FCZ overlapped on the biplot. The archaeal communities in FDZ showed more scattered distribution compared to that of FCZ on the plot, indicating more pronounced differences. Comparatively, the distribution of the bacterial community on the biplots appeared to be more clustered compared to the archaea community (Figures 4C,D), indicating a higher similarity in bacteria community compositions. In the biplot, samples from FDZ were generally distributed along the horizontal axis while those from FCZ were distributed along the vertical axis, hinting that the bacteria communities in FDZ and FCZ regions were influenced by distinct dominant factors.

Mining activities lead to significant changes in soil physicochemical properties due to soil fissure development and the subsequent closure. From the results of microbial beta diversity, the impact of mining disturbances on bacteria communities was more profound than that of archaea communities. Although the distribution characteristics of the two bacteria community subgroups on the biplot were different, the overall beta diversity differences between FCZ and FDZ were not significantly greater than within-group differences

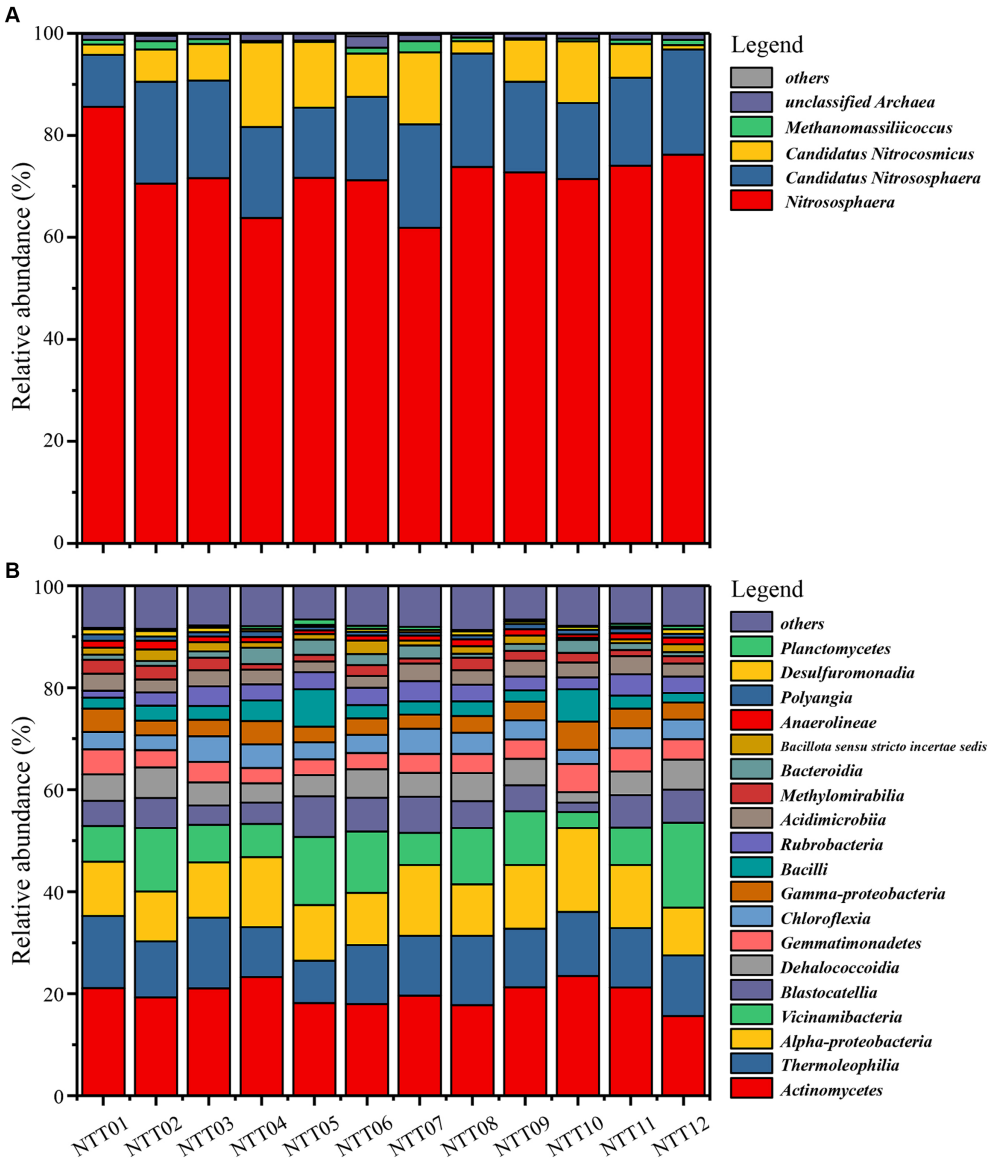

FIGURE 3
Microbial community compositions in the mining disturbance areas. **(A)** Archaea community at the genus taxonomic level. **(B)** Bacteria community at the class taxonomic level.

(ANOSIM, $p > 0.05$), reflecting the complexity of soil microbial communities.

3.4 Relationships between the edaphic factors and soil microbial community

In the present study, under the two different fissure statuses, the interactions between various environmental indicators and soil bacteria and archaea communities were determined by the Mantel test (Figure 2). Results showed that the bacteria community was significantly correlated with SMC, Cr, Fe, and AP, while the archaea community was strongly correlated with soil particle compositions (including silt and fine sand particles), pH, SMC, TN, TC, DOC, Hm, HA, Cr, Fe, and AP in the FCZ subregion (Figure 2A). In contrast, three environmental variables including coarse sand composition, DOC, and AP were significantly associated with the bacteria community in the FDZ region. At the same time, TN, FA, Mn, Cd, Cr, Fe, and TP likely impacted the archaea community due to significant correlations (Figure 2B). Archaea communities showed stronger interactions with environmental variables than bacteria communities under both stages of soil fissures, in terms of the number of associated environmental variables. This result indicated that the impact on archaeal communities may be more significant and far-reaching, despite variations in soil physicochemical properties caused by mining disturbances. Furthermore, for both bacterial and archaeal communities, the number and strength of significant correlations with environmental variables were fewer and weaker in the FDZ region than in the FCZ region, suggesting that the associations between microorganisms and soil environments deteriorated during the

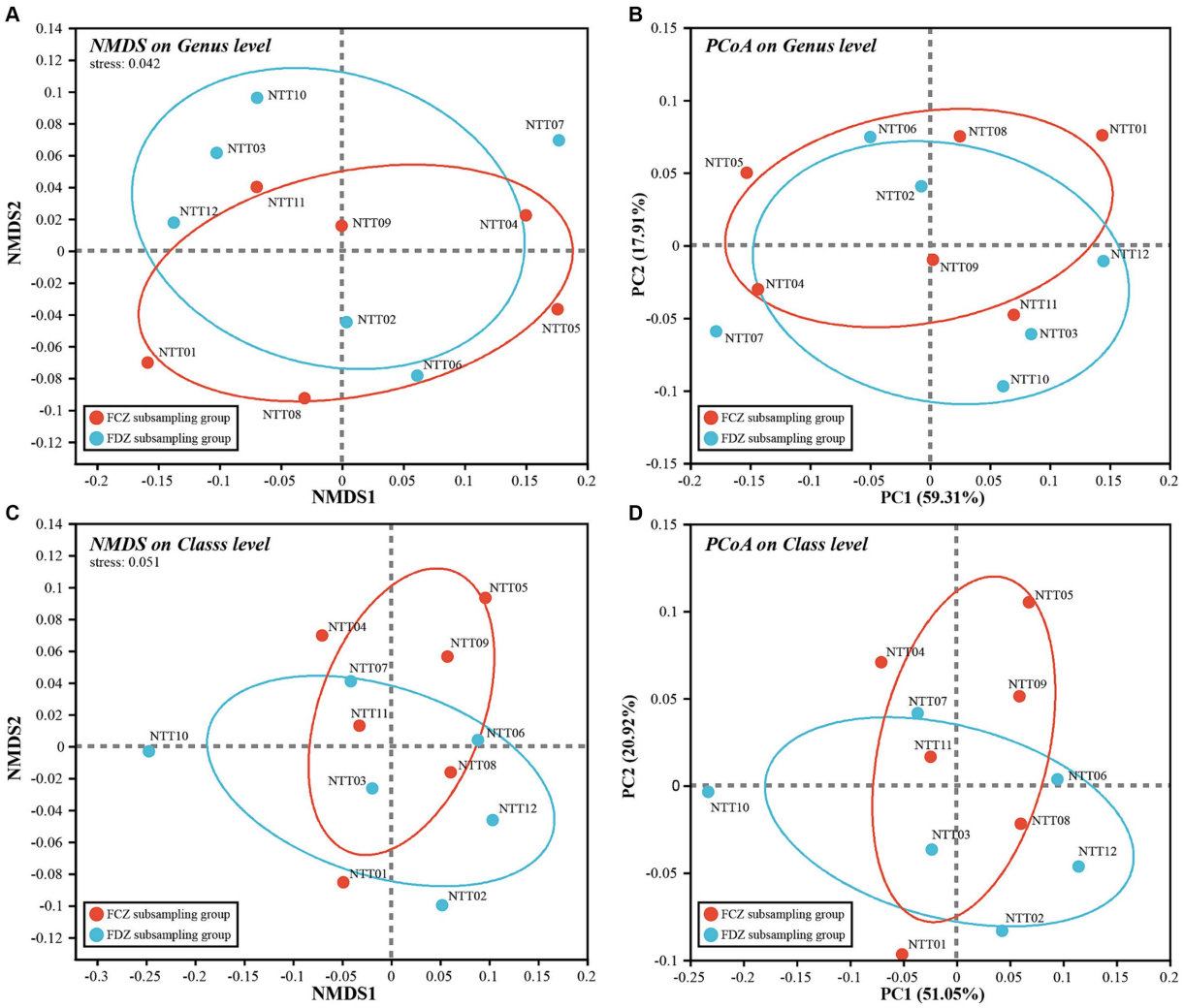

FIGURE 4
NMDS and PCoA biplot of **(A,B)** archaea community and **(C,D)** bacteria community, respectively.

development of soil fissure, consistent with the observed deterioration in correlations among edaphic factors.

In this study, a total of 32 soil physicochemical variables were measured. However, collinearity among these parameters could obstruct the accuracy of analyses regarding the relationship between environmental conditions and soil microbial communities. To address this, a collinearity test was conducted, and 10 parameters were selected, including SMC, EC, MBN, NO_3-N, DOC, FA, Cr, Fe, TK, and AP. The two-dimensional ordination plot generated by RDA results showed that the top two components accounted for more than 50% of the overall community variance (Figure 5). Edaphic factors had different impacts on bacteria and archaea communities in FCZ and FDZ. Fe, SMC, and AP had significant impacts on the bacteria community ($p < 0.05$), explaining total variances of 17.8, 17, and 12%, respectively (Figure 5A and Supplementary Table S3). MBN also accounted for a high level of explanatory degree (12.2%). In addition, the explanations of EC and FA were greater than 5%. In the FCZ subgroup, the edaphic factors, including Fe, Cd, MBN, FA, DOC, and NO_3-N, showed strong influences on bacterial communities. Among these factors, Fe, DOC, and MBN exhibited greater contributions. In the FDZ subregion, the direction of SMC, EC, AP, and TK were the main influential factors. The influence of the physicochemical factors on the archaea community was also depicted by the RDA biplot (Figure 5B and Supplementary Table S4). The impact of SMC, FA, and Cd on the archaea community was significant ($p < 0.05$) and these three environmental factors collectively explained 53.8% of the overall community variations, with individual contributions of 25.6, 19.1, and 13.6%, respectively. Additionally, NO_3-N, Fe, DOC, and EC accounted for 9.3, 8.9, 7.9, and 5.5% of the overall community variance. In the FCZ subsampling area, SMC, DOC, NO_3-N, EC, AP, and MBN exhibited strong influences on the soil archaea communities, and SMC had the greatest contribution. In contrast, in the FDZ, FA, Cd, and Fe presented a high correlation with the archaea community, and FA and Cd significantly correlated with archaea communities ($p < 0.05$).

3.5 Impacts of fissure conditions on microbial co-occurrence network

Soil microbial co-occurrence networks were used to explore the interactions among soil microorganisms in the FCZ and FDZ

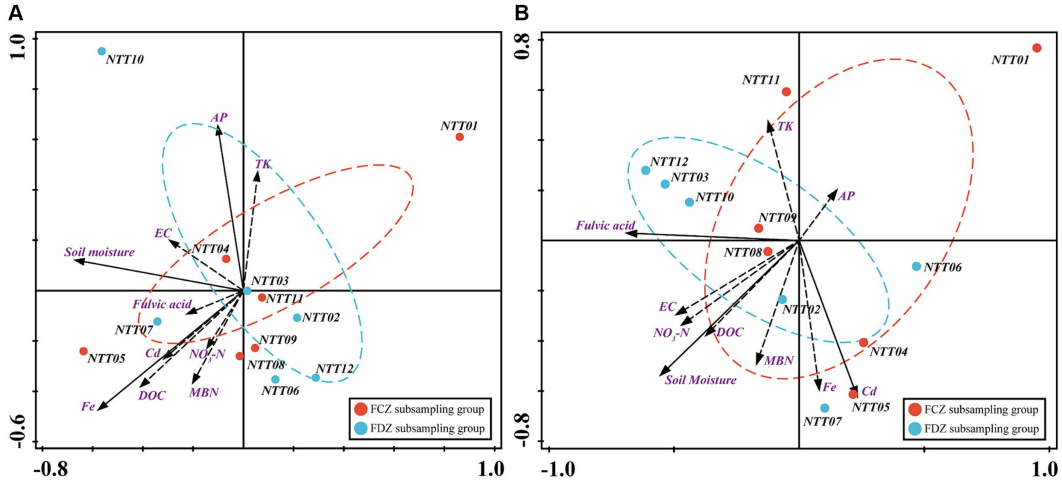

FIGURE 5
Drivers of microbial community composition. Redundancy analysis (RDA) between **(A)** bacteria community and **(B)** archaea community indicating the relationship between the edaphic factors and microbial communities at the OTU taxonomic level.

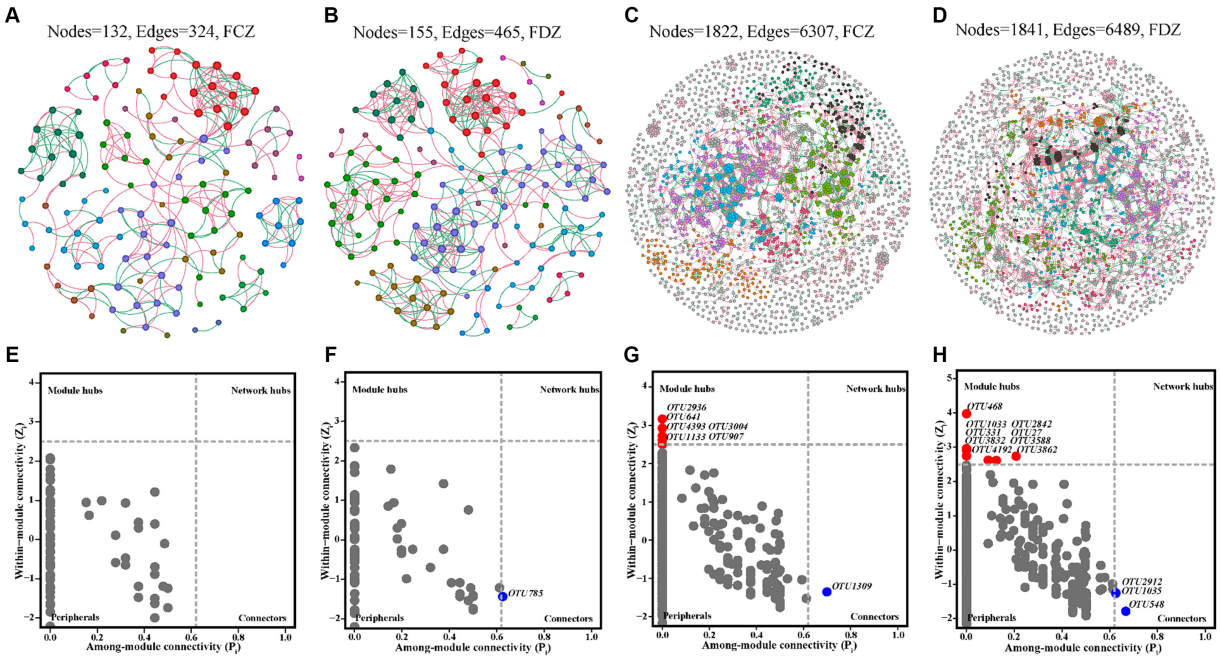

FIGURE 6
Microbial co-occurrence networks of archaea community in **(A)** FCZ, **(B)** FDZ, and bacteria community in **(C)** FCZ, **(D)** FDZ, respectively. The corresponding results about the roles of nodes in co-occurrence networks as indicated by their values of within-module connectivity (Zi) and among-module connectivity (Pi) of archaea community in **(E)** FCZ, **(F)** FDZ, and bacteria community in **(G)** FCZ, **(H)** FDZ.

subregions. No significant difference in the number of nodes, edges, and avgK of the bacterial community co-occurrence network was observed under the two different stages of soil fissure (Figures 6A–D and Table 3). Briefly, the number of microbial co-occurrence network nodes, edges and avgK of the bacteria communities in FCZ was 1,822, 6,307, and 6.923. Correspondingly, the number of nodes, edges, and avgK of the bacteria communities in FDZ was 1,841, 6,489, and 7.049. However, as for the archaeal communities, significant difference was observed. The microbial co-occurrence network of archaea communities in FDZ had more interactions than those in FCZ, in terms of the number of nodes (155 in FDZ, 132 in FCZ), edges (465 in FDZ, 324 in FCZ), and avgK (6 in FDZ, 4.909 in FCZ). In addition, soil microbial co-occurrence network in FDZ had closer interactions than FCZ based on the GD values (Bacteria: 14.053 in FDZ, 15.006 in FCZ; Archaea: 6.623 in FDZ, 7.394 in FCZ; Table 3). Stronger internal microbial interactions reflected the variations of the external soil environment. The correlation analysis and Mantel result both suggested that the associations among the edaphic factors deteriorated

TABLE 3 The microbial co-occurrence network topological parameters between the two soil fissure states.

Topological parameter	Bacteria		Archaea	
	FCZ	FDZ	FCZ	FDZ
Nodes	1,822	1,841	132	155
Edges	6,307	6,489	324	465
Average path distances (GD)	15.006	14.053	7.394	6.623
Positive edge ratios	56.48%	58.90%	59.26%	55.70%
Average degree (avgK)	6.923	7.049	4.909	6.000
Average clustering coefficient (avgCC)	0.537	0.529	0.569	0.591
Centralization of degree (CD)	0.012	0.016	0.054	0.045
Module	145	143	14	13
Modularity	0.847	0.836	0.796	0.776
Peripheral species	1,815	1,829	132	154
Connector hubs	1	3	0	1
Module hubs	6	9	0	0

during the development of soil fissures, which may be the main reason for the changes in the microbial co-occurrence network.

The positive edge ratios in the co-occurrence networks of both bacterial and archaeal communities were relatively low, ranging from 55.7 to 59.26% in both FCZ and FDZ groups. This indicated interspecific competitive (or antagonistic) interactions were notable under the situation of soil disturbed by mining disturbances, regardless of whether the fissures were in development or developed state. According to Zi and Pi values, most nodes in the co-occurrence networks were peripheral (Figures 6E–H), and the number of modules of the bacterial communities (145 in FCZ, 143 in FDZ) was much higher than that of the archaeal communities (14 in FCZ, 13 in FDZ), suggesting greater abundance and complexity in bacterial communities. Soil bacteria networks had only 1 connector hub and 6 module hubs in FCZ, but those from FDZ had up to 3 connector hubs and 9 module hubs. The co-occurrence network of archaeal communities showed similar characteristics: archaeal networks had zero connector hubs or module hubs in FCZ, while the FDZ region had 1 connector hub but zero module hubs. These results indicated that soil microbial communities had more complex and interactive compositions under the soil fissures development states. Rare species constituted module hubs and connectors (Figures 6E–H), highlighting their keystone roles in microbial co-occurrence networks.

4 Discussion

4.1 Impacts of the fissure status on edaphic factors

Coal mining activities have changed the stability of geological structures, especially soil fissures that occurred in the topsoil layer (Liu et al., 2019; Yang et al., 2019). Generally speaking, soil fissures experience two distinct stages: fissure development and subsequent fissure closure (Kang et al., 2023). Previous studies have shown that mining activities disturbed soil physicochemical conditions and nutrient levels to varying degrees (Ma et al., 2019; Wang et al., 2021). Lots of effort paid attention to whether and to what extent mining disturbance changes soil conditions. However, little is known about whether the fissure statuses induced by mining activities affect the edaphic factors and how soil microbial communities respond to these fissure development states. Here, a shallow buried coal mining area was selected to investigate whether the fissure status impacts soil physicochemical characteristics. In this area, according to the accurate locations of active mining panels and surface soil conditions, two states of soil fissures were identified. Almost all organic matters (e.g., MBC, MBN, DOC, AHN, and HA), SMC, AK, AP, pH, and CEC, had lower contents in the soil fissure closure zone (FCZ). This result differed from some previous studies showing that the nutrients were depleted upon fissure development (Ma et al., 2019; Wang et al., 2021). In addition, heavy metals and fine soil particles including clay and silt were enriched in FCZ (Table 1). The increase of soil fissures altered the size distribution of soil particles during soil fissure development. Clay and silt, the smaller particles in soil compositions, had lower contents in FDZ (Table 1), which might be the result of the enhanced small-sized particle's downward movement under the increase of soil fissure space and connectivity (Wang et al., 2021).

The expansion of soil fissures would reduce the tortuosity of the water flow path to promote vertical movement of the water and result in increasing infiltration (Karacan and Goodman, 2009; Bi et al., 2014), leading to an enhancement of the effective downward flow and increase in soil moisture content (Zang et al., 2012; Wang J. et al., 2017). The contents of soil physicochemical properties, except for heavy metals, increased to a certain extent with the increasing soil moisture content in FDZ (Table 1), due to the enhanced dissolution of soluble substances in topsoil and accumulated in the subsoil (Zhu et al., 2020). In addition, lower contents of heavy metals (e.g., Mn, Cd, Cr, and Fe) in FDZ were probably due to high adsorption or binding capacity with dissolved organic matter (Ponizovsky et al., 2006; Liu et al., 2021) and microbial weathering or reductive dissolution of metals into the mobilized forms (Sheng et al., 2021a, 2023a).

However, despite these increased nutrients in FDZ, the connections among soil physicochemical properties in this area were damaged by the process of the fissure development, weakening the relationships among factors (Wang et al., 2021; Zhang et al., 2022). Soil physicochemical variables in FCZ had high-level correlations, with greater coefficients than FDZ. The size distribution of soil particles strengthened in correlations with soil physicochemical components in FCZ, especially

having a significant relationship with organic matters (such as AHN, HA, and Humus). This phenomenon hinted that the associations of soil physicochemical properties were recovered as the process of the soil fissures closed. This result was similar to the previous research illustrating that mining disturbance significantly reduced TN, NO_3-N, and TC contents in the soil, and the correlations of soil variables were generally recovered after the mining activities ceased (Ngugi et al., 2018).

4.2 Soil fissure status affects microbial diversity, composition, and their co-occurrence

Soil nutrients, SMC, and inorganic properties were significantly altered in the mining disturbance area, leading to a large differentiation of soil microbial biomass, community structure, and their activities (Huang et al., 2015; Guo et al., 2021; Sheng et al., 2022; Sheng et al., 2023b). The dominant viewpoint held that surface subsidence reduced microbial richness and diversity of the soil microbial community. For instance, the relative abundance of predominant microbial lineages, such as *Pseudomonas*, *Gemmatimonas*, *Arthrobacter*, *Aciditerrimonas*, *Gaiella*, and *Sphingomonas* in the mining area decreased significantly (Shi et al., 2017; Wang et al., 2023). In addition, mining disturbance changed the soil microbial co-occurrence network, and the phylogenetic community assembly mechanism differed between mining-disturbed and non-disturbed areas (Ma et al., 2023; Wang et al., 2023). However, whether and how the soil microbial community's diversity, composition, and interaction changed under the different soil fissure states induced by mining disturbance still lacked evidence and remained unclear.

In this research, we investigated soil microbial communities under the two states of soil fissure. The archaeal community was solely composed of *Nitrososphaeria* which had a predominant abundance exceeding 95% in FCZ and FDZ. For the bacterial community, *Actinomycetes*, *Thermoleophilia*, *Alphaproteobacteria*, and *Vicinamibacteria* were dominant bacteria members with an average abundance exceeding 10% across all soil samples, with some variations between FCZ and FDZ (Figure 3 and Supplementary Tables S1, S2). Although there were little variations from the perspective of dominant microbial community composition, this study reported a distinct composition of rare species (e.g., *Methanomassiliicoccus*, *Rhodothermia*, *Armatimonadota*) between FCZ and FDZ, as well as the microbial co-occurrence network were connected by rare species (Figure 6).

Microbial communities had close correlations with soil environment conditions, including different fissure states induced by mining disturbance (Poncelet et al., 2014; Shi et al., 2017). The distribution of microbial communities in FDZ and FCZ regions showed independent vertical characteristics, revealing that the edaphic factors had varying degrees of impact on bacterial and archaeal communities in soils at two different stages of soil fissures (Figures 4, 5). During the soil fissure development process in the present study, the original porosity and structure were destroyed and the relatively close correlations among soil edaphic factors were weakened, except for heavy metals. As a result, the archaeal community showed a high correlation with organic matters in the FCZ area, and transformed to the correlations with heavy metals in the FDZ region (Figure 5B). The bacteria community showed similar features and had much lower correlations with soil physicochemical conditions in the FDZ area (Figure 5A). When the external environment changes, microorganisms tend to strengthen internal connections in response to environmental variations (Lu et al., 2022). The soil microbial co-occurrence network depicted a more complex and interactive microbial network in the FDZ region, with the soil bacterial co-occurrence network having three connector hubs and nine module hubs in FDZ and lowered to one connector hub and six module hubs in FCZ. Similar characteristics were also observed in the archaeal network, which had one connector hub in FDZ but none in FCZ (Table 3). The results showed that the relationship between soil microorganisms and the environment is destroyed in the process of developing fissures.

Not only was the microbial community affected by mining activities, but the soil microbial diversity and biomass of the restored mining area also significantly differed from that in the undisturbed area (de Quadros et al., 2016). Over time, the bacterial communities on restored sites became progressively more similar to those of nonmined analog sites (Ngugi et al., 2018). However, some findings also argued that the microbial composition and abundance of the restoration site still had significant differences with the undisturbed area after a long period of restoration time (de Quadros et al., 2016; Du et al., 2021). In this research, the process of soil fissure closure was similar to the restoration sites (Ngugi et al., 2018). As the soil fissure closed, the disturbed correlations among soil physicochemical variables reconnected, showing higher and more significant correlations compared to those in FDZ (Figure 2). Correspondingly, the bacterial and archaeal communities in FCZ showed closer correlations with soil environmental parameters compared with the microbial communities in FDZ, both in terms of the number of significantly correlated variables and the value of their correlation coefficient (Figure 2). The compositions and variations of soil microbial community and microbial-soil interactions were largely attributed to the continuity of the soil environment, as well as the correlations among physicochemical variables (e.g., soil organic matter), which is conducive to the establishment of stable microbial communities (Guo et al., 2021; Luo et al., 2019).

4.3 Rare species of soil microbial community are vulnerable to mining disturbance

It is generally believed that when the environment changes, the main manifestations of microbial community variation are changes in dominant species or functional genes, especially in environments such as soil and groundwater. Soil edaphic factors, such as pH, salinity, SMC, organic matter, etc., showed high attributes in shaping microbial diversity, taxonomic composition, and functional groups (Ezeokoli et al., 2019; Guo et al., 2021; Xiao et al., 2021a). In consideration of soil fissure stages in mining disturbance areas, in the present study, we observed a significant variation occurring in rare species, instead of dominant microorganisms as the previous research reported (Xiao et al., 2021a). Archaeal lineage (e.g., *Methanomassiliicoccus*) and bacterial members (e.g., *Rhodothermia*, *Armatimonadota*) were significantly different between FCZ and FDZ ($p < 0.05$). Rare species with an abundance of less than 1% accounted for the main inter-group differences, indicating that mining disturbances have a greater impact

on rare species. Previous studies have illustrated that rare species play an over-proportional role and might be a hidden driver in biogeochemical cycles (Jousset et al., 2017). Both common and rare species could contribute to soil ecological function. Dominant species make persistent, unique contributions to functional diversity, while rare species play key roles in changing environments (Chapman et al., 2018; Liang et al., 2020). Thus, it is vital to account for the abundance and diversity of rare species when interpreting their contributions to the entire microbial community diversity and variation in different soil fissure states.

The microbial co-occurrence network proved that rare species occupied an important soil ecological position in the study area, as the module hubs and connectors were composed of rare species rather than common species. In addition, rare species reinforced the overall interconnections of the soil microbial community. According to the compositions of connector hubs or module hubs, rare species such as *Nordella*, unclassified species of *Chloroflexia*, and *Acidimicrobiia* were connector hubs in microbial co-occurrence networks. As for module hubs, they were largely composed of rare species *Sphingomonas*, *Massilia*, *Candidatus Alysiosphaera*, *Rubritepida*, and other unclassified rare lineages (Figures 6E–H). These rare species connected microbial symbionts and provided habitat complexity in the view of co-occurrence relationships. Abundant taxa have been reported more sensitive to ecological disturbance situations, showing significant variation between non-disturbed and disturbed areas (Yuan et al., 2022). Two different soil fissure states induced by mining activities significantly impacted the edaphic factors and the microbial community (Figure 7). Compared with abundant species, rare species of soil microbial community were vulnerable to mining disturbance, as illustrated by microbial composition and co-occurrence network. Soil fissure states had a great impact on the soil edaphic factors and deteriorated the correlation between these variables in the process of soil fissure development, except for the correlation between heavy metals (Figure 6). Among these factors, soil moisture content was the most influential edaphic factor attributed to microbial variations (Figure 5). Controlled by the distinct states of soil fissures, the edaphic conditions showed key attributions to microbial communities, particularly affecting the abundance and ecological roles of rare species (Xiao et al., 2021b).

5 Conclusion

The effects of soil fissure status on the microbial community have been thoroughly investigated in a representative mining disturbance area. Here, we presented a novel insight into soil microbial community characteristics and variations under distinct soil fissure states through multiple statistical and bioinformatic approaches. Distinct soil fissure states significantly impacted the edaphic factors, especially in soil moisture content and organic matter. Soil microbial communities showed different structures under the two different fissure states, and the soil moisture content, pH, particle compositions, organic matter, and heavy metals contributed to the variation of microbial communities. Rare species of soil microbial community were vulnerable to mining disturbance and played keystone roles in the soil microbial community (e.g., *Nordella*, *Sphingomonas*, *Massilia*, and *Rubritepida*). Our work highlighted the impacts of soil fissure states on soil physicochemical properties and microbial communities, and expanded our knowledge of the effects of mining activities on the edaphic factors and microbial communities. In addition, future works should pay more attention to microbial function and metabolism (e.g., metagenomics, metatranscriptomics) under mining-disturbed conditions.

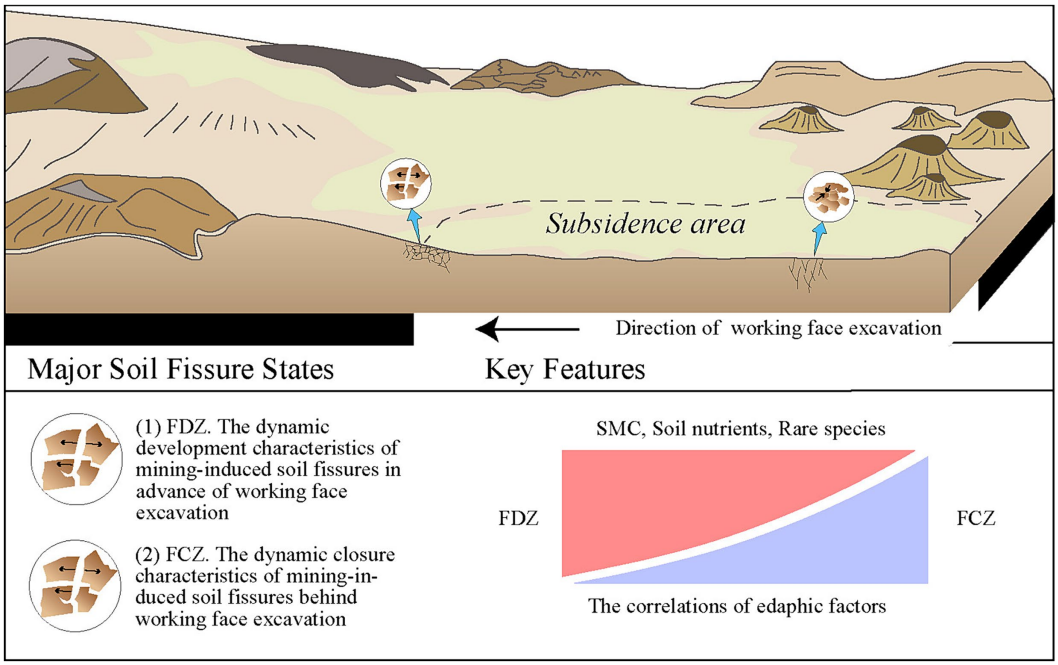

FIGURE 7
Conceptual map of the impacts of mining disturbance on soil edaphic factors and microbial community. Two different soil fissure states induced by mining activities significantly impacted the edaphic factors and the microbial community, especially in rare species.

Data availability statement

The original contributions presented in the study are included in the article/Supplementary material, further inquiries can be directed to the corresponding authors.

Author contributions

LG: Formal analysis, Funding acquisition, Investigation, Methodology, Software, Visualization, Writing – original draft, Writing – review & editing. XC: Investigation, Software, Visualization, Writing – review & editing. YS: Conceptualization, Data curation, Methodology, Writing – review & editing. NY: Funding acquisition, Investigation, Methodology, Resources, Writing – review & editing. EH: Conceptualization, Funding acquisition, Methodology, Project administration, Writing – review & editing. HF: Software, Visualization, Writing – review & editing.

Funding

The author(s) declare that financial support was received for the research, authorship, and/or publication of this article. This work was financially supported by grants from the National Natural Science Foundation of China (42107101), the China Postdoctoral Science Foundation (2022MD723822), the Natural Science Basic Research Program of Shaanxi Province (2023-JC-QN-0317), and the Outstanding Youth Science Fund of Xi'an University of Science and Technology.

Acknowledgments

The authors sincerely thank Yizhi Sheng for the valuable discussion and Fu Liao, Shen Qu, Chenyu Wang, and Fengxia Liu for their assistance during the field investigation and sampling collection.

Conflict of interest

The authors declare that the research was conducted in the absence of any commercial or financial relationships that could be construed as a potential conflict of interest.

The author(s) declared that they were an editorial board member of Frontiers, at the time of submission. This had no impact on the peer review process and the final decision.

Publisher's note

Supplementary material

The Supplementary material for this article can be found online at: https://www.frontiersin.org/articles/10.3389/fmicb.2024.1463665/full#supplementary-material

References

Banning, N. C., Lalor, B. M., Cookson, W. R., Grigg, A. H., and Murphy, D. V. (2012). Analysis of soil microbial community level physiological profiles in native and post-mining rehabilitation forest: which substrates discriminate? *Appl. Soil Ecol.* 56, 27–34. doi: 10.1016/j.apsoil.2012.01.009

Bi, Y., Zou, H., and Zhu, C. (2014). Dynamic monitoring of soil bulk density and infiltration rate during coal mining in sandy land with different vegetation. *Int. J. Coal Sci. Technol.* 1, 198–206. doi: 10.1007/s40789-014-0025-2

Caporaso, J. G., Kuczynski, J., Stombaugh, J., Bittinger, K., Bushman, F. D., Costello, E. K., et al. (2010). QIIME allows analysis of high-throughput community sequencing data. *Nat. Methods* 7, 335–336. doi: 10.1038/nmeth.f.303

Chapman, A. S. A., Tunnicliffe, V., and Bates, A. E. (2018). Both rare and common species make unique contributions to functional diversity in an ecosystem unaffected by human activities. *Divers. Distrib.* 24, 568–578. doi: 10.1111/ddi.12712

Cleveland, C. C., and Liptzin, D. (2007). C:N:P stoichiometry in soil: is there a "Redfield ratio" for the microbial biomass? *Biogeochemistry* 85, 235–252. doi: 10.1007/s10533-007-9132-0

Dai, S., Wen, T., Cai, Z., and Zhang, J. (2020). Dynamics of nitrite in acidic soil during extraction with potassium chloride studied using ^{15}N tracing. *Rapid Commun. Mass Spectrom.* 34:e8746. doi: 10.1002/rcm.8746

de Quadros, P. D., Zhalnina, K., Davis-Richardson, A. G., Drew, J. C., Menezes, F. B., de Oliveira Camargo, F. A., et al. (2016). Coal mining practices reduce the microbial biomass, richness and diversity of soil. *Appl. Soil Ecol.* 98, 195–203. doi: 10.1016/j.apsoil.2015.10.016

Deng, Y., Jiang, Y. H., Yang, Y., He, Z., Luo, F., and Zhou, J. (2012). Molecular ecological network analyses. *BMC Bioinformatics* 13:113. doi: 10.1186/1471-2105-13-113

Deng, L., Wang, K. B., Chen, M. L., Shangguan, Z. P., and Sweeney, S. (2013). Soil organic carbon storage capacity positively related to forest succession on the Loess Plateau, China. *Catena* 110, 1–7. doi: 10.1016/j.catena.2013.06.016

Du, H., Wang, S., Nie, W., and Song, S. (2021). Soil properties and bacterial community dynamics in a coal mining subsidence area: active versus passive revegetation. *J. Soil Sci. Plant Nutr.* 21, 2573–2585. doi: 10.1007/s42729-021-00548-3

Edgar, R. C. (2013). UPARSE: highly accurate OTU sequences from microbial amplicon reads. *Nat. Methods* 10, 996–998. doi: 10.1038/nmeth.2604

Ezeokoli, O. T., Mashigo, S. K., Paterson, D. G., Bezuidenhout, C. C., and Adeleke, R. A. (2019). Microbial community structure and relationship with physicochemical properties of soil stockpiles in selected South African opencast coal mines. *Soil Sci. Plant Nutr.* 65, 332–341. doi: 10.1080/00380768.2019.1621667

Guo, L., Xie, Q., Sheng, Y., Wang, G., Jiang, W., Tong, X., et al. (2022). Co-variation of hydrochemistry, inorganic nitrogen, and microbial community composition along groundwater flowpath: a case study in Linzhou-Anyang area, Southern North China plain. *Appl. Geochem.* 140:105296. doi: 10.1016/j.apgeochem.2022.105296

Guo, J., Zhang, Y., Huang, H., and Yang, F. (2021). Deciphering soil bacterial community structure in subsidence area caused by underground coal mining in arid and semiarid area. *Appl. Soil Ecol.* 163:103916. doi: 10.1016/j.apsoil.2021.103916

Hou, E., Xie, X., Feng, D., Chen, Q., Che, X., and Hou, P. (2022). Laws and prevention methods of ground cracks in shallow coal seam mining. *Coal Geol. Explor.* 50, 30–40. doi: 10.12363/issn.1001-1986.22.05.0427 (in Chinese)

Huang, Y., Tian, F., Wang, Y., Wang, M., and Hu, Z. (2015). Effect of coal mining on vegetation disturbance and associated carbon loss. *Environ. Earth Sci.* 73, 2329–2342. doi: 10.1007/s12665-014-3584-z

Huang, X., Wang, G., Liang, X., Cui, L., Ma, L., and Xu, Q. (2018). Hydrochemical and stable isotope (δD and $\delta^{18}O$) characteristics of groundwater and hydrogeochemical processes in the Ningtiaota coalfield, Northwest China. *Mine Water Environ.* 37, 119–136. doi: 10.1007/s10230-017-0477-x

Jousset, A., Bienhold, C., Chatzinotas, A., Gallien, L., Gobet, A., Kurm, V., et al. (2017). Where less may be more: how the rare biosphere pulls ecosystems strings. *ISME J.* 11, 853–862. doi: 10.1038/ismej.2016.174

Kalembasa, S. J., and Jenkinson, D. S. (1973). A comparative study of titrimetric and gravimetric methods for the determination of organic carbon in soil. *J. Sci. Food Agric.* 24, 1085–1090. doi: 10.1002/jsfa.2740240910

Kang, H., Gao, F., Xu, G., and Ren, H. (2023). Mechanical behaviors of coal measures and ground control technologies for China's deep coal mines—a review. *J. Rock Mech. Geotech. Eng.* 15, 37–65. doi: 10.1016/j.jrmge.2022.11.004

Karacan, C. Ö., and Goodman, G. (2009). Hydraulic conductivity changes and influencing factors in longwall overburden determined by slug tests in gob gas ventholes. *Int. J. Rock Mech. Min. Sci.* 46, 1162–1174. doi: 10.1016/j.ijrmms.2009.02.005

Kerou, M., Eloy Alves, R. J., and Schleper, C. (2016). "Nitrososphaeria" in Bergey's manual of systematics of archaea and bacteria. eds. M. E. Trujillo, S. Dedysh, P. DeVos, B. Hedlund, P. Kämpfer and F. A. Raineyet al. (John Wiley & Sons, Inc.), 1–8.

Liang, Y., Xiao, X., Nuccio, E. E., Yuan, M., Zhang, N., Xue, K., et al. (2020). Differentiation strategies of soil rare and abundant microbial taxa in response to changing climatic regimes. *Environ. Microbiol.* 22, 1327–1340. doi: 10.1111/1462-2920.14945

Liu, H., Deng, K., Lei, S., and Bian, Z. (2015). Mechanism of formation of sliding ground fissure in loess hilly areas caused by underground mining. *Int. J. Min. Sci. Technol.* 25, 553–558. doi: 10.1016/j.ijmst.2015.05.006

Liu, H., Deng, K., Zhu, X., and Jiang, C. (2019). Effects of mining speed on the developmental features of mining-induced ground fissures. *Bull. Eng. Geol. Environ.* 78, 6297–6309. doi: 10.1007/s10064-019-01532-z

Liu, M., Han, X., Liu, C., Guo, L., Ding, H., and Lang, Y. (2021). Differences in the spectroscopic characteristics of wetland dissolved organic matter binding with Fe^{3+}, Cu^{2+}, Cd^{2+}, Cr^{3+} and Zn^{2+}. *Sci. Total Environ.* 800:149476. doi: 10.1016/j.scitotenv.2021.149476

Liu, C., Li, H., Zhang, Y., Si, D., and Chen, Q. (2016). Evolution of microbial community along with increasing solid concentration during high-solids anaerobic digestion of sewage sludge. *Bioresour. Technol.* 216, 87–94. doi: 10.1016/j.biortech.2016.05.048

Liu, Y., Sheng, Y., Feng, C., Chen, N., and Liu, T. (2020). Distinct functional microbial communities mediating the heterotrophic denitrification in response to the excessive Fe(II) stress in groundwater under wheat-rice stone and rock phosphate amendments. *Environ. Res.* 185:109391. doi: 10.1016/j.envres.2020.109391

Long, L., Liu, Y., Chen, X., Guo, J., Li, X., Guo, Y., et al. (2022). Analysis of spatial variability and influencing factors of soil nutrients in western China: a case study of the Daliuta mining area. *Sustainability* 14:2793. doi: 10.3390/su14052793

Lu, R. (1999). Soil agricultural chemical analysis. Nanjing, China: China Agricultural Science and Technology Press in Chinese.

Lu, M., Wang, X., Li, H., Jiao, J. J., Luo, X., Luo, M., et al. (2022). Microbial community assembly and co-occurrence relationship in sediments of the river-dominated estuary and the adjacent shelf in the wet season. *Environ. Pollut.* 308:119572. doi: 10.1016/j.envpol.2022.119572

Luo, Z., Ma, J., Chen, F., Li, X., Hou, H., and Zhang, S. (2019). Cracks reinforce the interactions among soil bacterial communities in the coal mining area of Loess Plateau, China. *Int. J. Environ. Res. Public Health* 16:4892. doi: 10.3390/ijerph16244892

Ma, X., Qu, H., Liao, S., Yuan, D., Yu, J., Li, J., et al. (2023). Changes in assembly processes and differential responses of soil microbial communities during mining disturbance in mining reclamation and surrounding grassland. *Catena* 231:107332. doi: 10.1016/j.catena.2023.107332

Ma, K., Zhang, Y., Ruan, M., Guo, J., and Chai, T. (2019). Land subsidence in a coal mining area reduced soil fertility and led to soil degradation in arid and semi-arid regions. *Int. J. Environ. Res. Public Health* 16:3929. doi: 10.3390/ijerph16203929

McLaughlin, M. J., Zarcinas, B. A., Stevens, D. P., and Cook, N. (2000). Soil testing for heavy metals. *Commun. Soil Sci. Plant Anal.* 31, 1661–1700. doi: 10.1080/00103620009370531

Ngugi, M. R., Dennis, P. G., Neldner, V. J., Doley, D., Fechner, N., and McElnea, A. (2018). Open-cut mining impacts on soil abiotic and bacterial community properties as shown by restoration chronosequence. *Restor. Ecol.* 26, 839–850. doi: 10.1111/rec.12631

Peng, X., Wang, X., Dai, Q., Ding, G., and Li, C. (2020). Soil structure and nutrient contents in underground fissures in a rock-mantled slope in the karst rocky desertification area. *Environ. Earth Sci.* 79:3. doi: 10.1007/s12665-019-8708-z

Poncelet, D. M., Cavender, N., Cutright, T. J., and Senko, J. M. (2014). An assessment of microbial communities associated with surface mining-disturbed overburden. *Environ. Monit. Assess.* 186, 1917–1929. doi: 10.1007/s10661-013-3505-8

Ponizovsky, A. A., Metzler, D. M., Allen, H. E., and Ackerman, A. J. (2006). The effect of moisture content on the release of organic matter and copper to soil solutions. *Geoderma* 135, 204–215. doi: 10.1016/j.geoderma.2005.12.004

Sheng, Y., Baars, O., Guo, D., Whitham, J., Srivastava, S., and Dong, H. (2023a). Mineral-bound trace metals as cofactors for anaerobic biological nitrogen fixation. *Environ. Sci. Technol.* 57, 7206–7216. doi: 10.1021/acs.est.3c01371

Sheng, Y., Bibby, K., Grettenberger, C., Kaley, B., Macalady, J. L., Wang, G., et al. (2016). Geochemical and temporal influences on the enrichment of acidophilic iron-oxidizing bacterial communities. *Appl. Environ. Microbiol.* 82, 3611–3621. doi: 10.1128/aem.00917-16

Sheng, Y., Dong, H., Coffin, E., Myrold, D., and Kleber, M. (2022). The important role of enzyme adsorbing capacity of soil minerals in regulating β-glucosidase activity. *Geophys. Res. Lett.* 49:e2021GL097556. doi: 10.1029/2021GL097556

Sheng, Y., Dong, H., Kukkadapu, R. K., Ni, S., Zeng, Q., Hu, J., et al. (2021a). Lignin-enhanced reduction of structural Fe(III) in nontronite: dual roles of lignin as electron shuttle and donor. *Geochim. Cosmochim. Acta* 307, 1–21. doi: 10.1016/j.gca.2021.05.037

Sheng, Y., Hu, J., Kukkadapu, R., Guo, D., Zeng, Q., and Dong, H. (2023b). Inhibition of extracellular enzyme activity by reactive oxygen species upon oxygenation of reduced iron-bearing minerals. *Environ. Sci. Technol.* 57, 3425–3433. doi: 10.1021/acs.est.2c09634

Sheng, Y., Li, G., Dong, H., Liu, Y., Ma, L., Yang, M., et al. (2021b). Distinct assembly processes shape bacterial communities along unsaturated, groundwater fluctuated, and saturated zones. *Sci. Total Environ.* 761:143303. doi: 10.1016/j.scitotenv.2020.143303

Sheng, Y., Liu, Y., Yang, J., Dong, H., Liu, B., Zhang, H., et al. (2021c). History of petroleum disturbance triggering the depth-resolved assembly process of microbial communities in the vadose zone. *J. Hazard. Mater.* 402:124060. doi: 10.1016/j.jhazmat.2020.124060

Shi, J., Tang, Z., Jin, Z., Chi, Q., He, B., and Jiang, G. (2003). Determination of As(III) and As(V) in soils using sequential extraction combined with flow injection hydride generation atomic fluorescence detection. *Anal. Chim. Acta* 477, 139–147. doi: 10.1016/S0003-2670(02)01402-2

Shi, P., Zhang, Y., Hu, Z., Ma, K., Wang, H., and Chai, T. (2017). The response of soil bacterial communities to mining subsidence in the west China aeolian sand area. *Appl. Soil Ecol.* 121, 1–10. doi: 10.1016/j.apsoil.2017.09.020

Tüzen, M. (2003). Determination of heavy metals in soil, mushroom and plant samples by atomic absorption spectrometry. *Microchem. J.* 74, 289–297. doi: 10.1016/S0026-265X(03)00035-3

Wang, Q., Garrity, G. M., Tiedje, J. M., and Cole, J. R. (2007). Naïve Bayesian classifier for rapid assignment of rRNA sequences into the new bacterial taxonomy. *Appl. Environ. Microbiol.* 73, 5261–5267. doi: 10.1128/AEM.00062-07

Wang, H., Liu, H., Yang, T., Lv, G., Li, W., Chen, Y., et al. (2023). Mechanisms underlying the succession of plant rhizosphere microbial community structure and function in an alpine open-pit coal mining disturbance zone. *J. Environ. Manag.* 325:116571. doi: 10.1016/j.jenvman.2022.116571

Wang, J., Wang, P., Qin, Q., and Wang, H. (2017). The effects of land subsidence and rehabilitation on soil hydraulic properties in a mining area in the Loess Plateau of China. *Catena* 159, 51–59. doi: 10.1016/j.catena.2017.08.001

Wang, Z., Wang, G., Wang, C., Wang, X., Li, M., and Ren, T. (2021). Effect of environmental factors on soil nutrient loss under conditions of mining disturbance in a coalfield. *Forest* 12:1370. doi: 10.3390/f12101370

Wang, G., Wu, M., Wang, R., Xu, H., and Song, X. (2017). Height of the mining-induced fractured zone above a coal face. *Eng. Geol.* 216, 140–152. doi: 10.1016/j.enggeo.2016.11.024

Xiao, L., Bi, Y., Du, S., Wang, Y., and Guo, C. (2019). Effects of re-vegetation type and arbuscular mycorrhizal fungal inoculation on soil enzyme activities and microbial biomass in coal mining subsidence areas of Northern China. *Catena* 177, 202–209. doi: 10.1016/j.catena.2019.02.019

Xiao, E., Ning, Z., Xiao, T., Sun, W., and Jiang, S. (2021a). Soil bacterial community functions and distribution after mining disturbance. *Soil Biol. Biochem.* 157:108232. doi: 10.1016/j.soilbio.2021.108232

Xiao, E., Wang, Y., Xiao, T., Sun, W., Deng, J., Jiang, S., et al. (2021b). Microbial community responses to land-use types and its ecological roles in mining area. *Sci. Total Environ.* 775:145753. doi: 10.1016/j.scitotenv.2021.145753

Xiao, W., Zhang, W., Ye, Y., Lv, X., and Yang, W. (2020). Is underground coal mining causing land degradation and significantly damaging ecosystems in semi-arid areas? A study from an ecological capital perspective. *Land Degrad. Dev.* 31, 1969–1989. doi: 10.1002/ldr.3570

Xin, Z., Qin, Y., and Yu, X. (2016). Spatial variability in soil organic carbon and its influencing factors in a hilly watershed of the Loess Plateau, China. *Catena* 137, 660–669. doi: 10.1016/j.catena.2015.01.028

Yang, X., Wen, G., Dai, L., Sun, H., and Li, X. (2019). Ground subsidence and surface cracks evolution from shallow-buried close-distance multi-seam mining: a case study in Bulianta coal mine. *Rock Mech. Rock. Eng.* 52, 2835–2852. doi: 10.1007/s00603-018-1726-4

Yuan, Q., Wang, P., Wang, X., Hu, B., Liu, S., and Ma, J. (2022). Abundant microbial communities act as more sensitive bio-indicators for ecological evaluation of copper mine contamination than rare taxa in river sediments. *Environ. Pollut.* 305:119310. doi: 10.1016/j.envpol.2022.119310

Zang, Y., Ding, G., and Gao, Y. (2012). Effects of coal mining subsidence on infiltration into unsaturated soils in sand drift area. *Adv. Water Sci.* 23, 757–768. in Chinese. doi: 10.14042/j.cnki.32.1309.2012.06.001

Zhang, K., Yang, K., Wu, X., Bai, L., Zhao, J., and Zheng, X. (2022). Effects of underground coal mining on soil spatial water content distribution and plant growth type in Northwest China. *ACS Omega* 7, 18688–18698. doi: 10.1021/acsomega.2c01369

Zhang, X., Zhu, A., Xin, X., Yang, W., Zhang, J., and Ding, S. (2018). Tillage and residue management for long-term wheat-maize cropping in the North China Plain: I. Crop yield and integrated soil fertility index. *Field Crop Res.* 221, 157–165. doi: 10.1016/j.fcr.2018.02.025

Zhu, M., Kong, F., Li, Y., Li, M., Zhang, J., and Xi, M. (2020). Effects of moisture and salinity on soil dissolved organic matter and ecological risk of coastal wetland. *Environ. Res.* 187:109659. doi: 10.1016/j.envres.2020.109659

Frontiers in Microbiology

Explores the habitable world and the potential of microbial life

The largest and most cited microbiology journal which advances our understanding of the role microbes play in addressing global challenges such as healthcare, food security, and climate change.

Discover the latest Research Topics

See more →

Frontiers

Avenue du Tribunal-Fédéral 34
1005 Lausanne, Switzerland
frontiersin.org

Contact us

+41 (0)21 510 17 00
frontiersin.org/about/contact